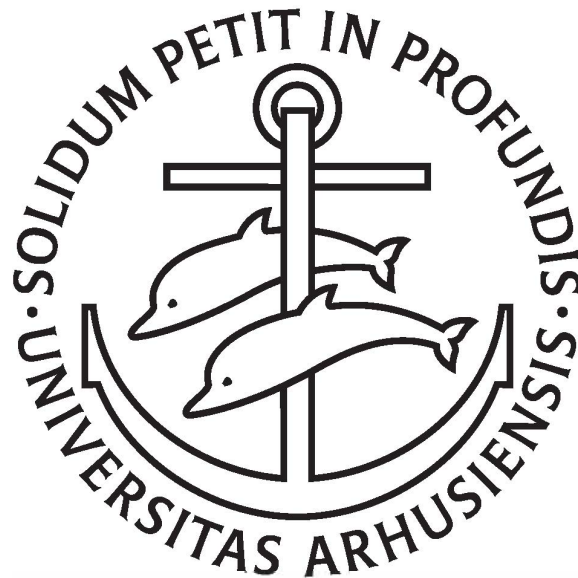


CONTROL OF RESIDENTIAL SPACE HEATING FOR DEMAND RESPONSE USING GREY-BOX MODELS

PhD Thesis



Rasmus Elbæk Hedegaard

Graduate School of Science and Technology

Aarhus University

November 2018

**CONTROL OF RESIDENTIAL SPACE HEATING FOR DEMAND RESPONSE
USING GREY-BOX MODELS**

PhD Thesis

This thesis is submitted in partial fulfilment of the requirements for the degree of PhD at the Graduate School of Science and Technology at Aarhus University.

ISBN: 978-87-7507-447-1

DOI: 10.7146/aul.317.215

Copyright © 2018 by Rasmus Elbæk Hedegaard

All right reserved. The content of this thesis is freely available, but publication (with reference) may only be pursued due to agreement with the author. Except where otherwise indicated, the content is produced by the author.

Supervisor:

Steffen Petersen, Associate Professor, Department of Engineering, Aarhus University

Assessment Committee:

Henrik Madsen, Professor and Head of section, Technical University of Denmark (DTU)

Laurent Georges, Associate Professor, Norwegian University of Science and Technology (NTNU)

Anders Bentien (Chair), Associate Professor, Department of Engineering, Aarhus University (AU)

Aarhus University

Graduate School of Science and Technology

Nordre Ringgade 1

DK-8000 Aarhus C

<http://phd.au.dk/graduate-schools/scienceandtechnology/>



AARHUS
UNIVERSITY
SCIENCE AND TECHNOLOGY

*Dedicated to Mille, our son Alfred
and his future siblings.*

ABSTRACT

Certain advanced control schemes are capable of making a part of the thermostatic loads of space heating in buildings flexible, thereby enabling buildings to engage in so-called *demand response*. It has been suggested that this flexible consumption may be a valuable asset in future energy systems where conventional fossil fuel-based energy production have been partially replaced by intermittent energy production from renewable energy sources. Model predictive control (MPC) is a control scheme that relies on a model of the building to predict the future impact on the temperature conditions in the building of both control decisions (space heating) and phenomena outside the influence of the control scheme (e.g. weather conditions). MPC has become one of the most frequently used control schemes in studies investigating the potential for engaging buildings in demand response. While research has indicated MPC to have many useful applications in buildings, several challenges still inhibit its adoption in practice. A significant challenge related to MPC implementation lies in obtaining the required model of the building, which is often derived from measurements of the temperature and heating consumption. Furthermore, studies have indicated that, although demand response in buildings could contribute to the task of balancing supply and demand, suitable tariff structures that incentivize consumers to engage in DR are lacking. The main goal of this work is to contribute with research that addresses these issues. This thesis is divided into two parts.

The first part of the thesis explores ways of simplifying the task of obtaining the building model that is required for implementation of MPC. Studies that explore practical ways of obtaining the measurement data needed for model identification are presented together with a study evaluating the suitedness of different low-order model structures that are suited for control-purposes.

The second part of the thesis presents research on the potential of utilizing buildings for demand response. First, two studies explore and evaluate suitable incentive mechanisms for demand response by implementing an MPC scheme in a multi-apartment building block. These studies evaluate two proposed incentive mechanisms as well as the impact of building characteristics and MPC scheme implementation. Finally, a methodology for bottom-up modelling of entire urban areas is presented, and proved capable of predicting the aggregated energy demand of urban areas. The models resulting from the methodology are then applied in an analysis on demand response.

RESUMÉ

En del af energiforbruget som går til opvarmning af bygninger kan gøres fleksibelt ved hjælp af avancerede kontrolmetoder. Dette gør bygninger i stand til at deltage i såkaldt *demand response* – et begreb som dækker over energiforbrugere, der er i stand til at tilpasse deres forbrug til energisystemets behov. Flere studier har indikeret at dette koncept til dels kan afhjælpe nogle af de udfordringer som er forbundet med at basere en større del af vores energisystem på vedvarende energi kilder med fluktuerende produktion. *Model predictive control* (MPC) er en af de kontrolmetoder der anvendes til at styre opvarmningen af vores bygninger og dermed skabe gøre en del af dette forbrug fleksibelt. I praksis sker dette ved eksempelvis at forvarme bygningen (og dens masse) inden perioder med højt energiforbrug (spidslast) eller lav energiproduktion, således at forbruget i bygningen under spidslasten kan sænkes uden at gå på kompromis med indeklimaet. MPC bruger en termisk model af bygningen til at forudsige den fremtidige effekt af både eget varmeforbrug, men også af andre fænomener (fx vejrforhold) som kan have en indflydelse på bygningens varmebalance. Denne model bliver typisk kalibreret ved brug af måledata af temperaturforhold og energiforbrug i bygningen. Til trods for at forskning har påvist flere fordele ved denne kontrol metode, har flere udfordringer forbundet med metoden betydet at den endnu ikke er anvendt i bygninger i praksis. Blandt disse er udfordringen det kan være at opsætte en model af bygningen der er tilpas nøjagtig til brug i MPC. Ligeledes er en mangel på økonomiske incitamenter der skal få forbrugere til at deltage i *demand response* et problem. Målet med denne afhandlingen er at adressere nogle af disse problemstillinger. Afhandlingen er derfor inddelt i to dele.

Den første del udforsker metoder hvormed udfordringen der ligger i modelleringen af bygninger som er nødvendig for MPC implementering. Forskningen præsenteret i denne del undersøger metoder hvormed måledata til bygnings modellering kan erhverves på praktiske måder. Derudover præsenteres en evaluering af forskellige typer af modeller.

Den anden del udforsker mulige tilgange til etablering af de økonomiske incitamenter der skal få forbrugere til at deltage i *demand response*. Først præsenteres studier som tager udgangspunkt i en enkelt bygning. Dernæst præsenteres en udviklet metode som muliggør modellering af bygninger i større bolig områder. Metoden bruges til at opsætte modeller af et boligområde i Aarhus, og vises at være i stand til at forudsige forbruget af boligområdet med høj præcision. De resulterende modeller anvendes til sidst i et studie af *demand response* på større skala.

ACKNOWLEDGEMENTS

First, I would like to thank my supervisor Steffen Petersen, not only for his guidance during my pursuit of the PhD degree, but also for making this endeavour possible in the first place. I would also like to express my gratitude towards the following contributors for their financial support of the project: Graduate School of Science and Technology at Aarhus University; the project ‘READY.dk’ financed by the Danish energy R&D program ForskEl; and finally the project ‘READY’ financed by the 7th EU Framework Program (FP7-Energy project reference: 609127).

I would also like to thank my fellow colleagues and PhD-students at the institute: Theis Friis Pedersen, Martin Heine Kristensen and Michael Dahl Knudsen for their invaluable support and participation in fruitful discussions, development of ideas and academic collaborations. In particular, I thank them for making my time as a PhD student an exciting time which I will look back upon with fond memories.

Finally, I thank my beloved Mille and the rest of my family for their interest in my research, for their acceptance of a sometimes-skewed work/life balance and for the support that they have selflessly given along the way.

Thank you.

PREFACE

This thesis is the result of a 3-year PhD fellowship at the Graduate School of Science and Technology at Aarhus University, where I was enrolled from August 2015 to November 2018 under the supervision of Assistant Professor Steffen Petersen. The thesis is the result of my own work and includes nothing, which is the outcome of work done in collaboration except where specifically indicated in the text. It has not been previously submitted, in part or in whole, to any university of institution for any degree, diploma, or other qualification.

The thesis is a collection of papers that have either been published in high-ranking international journals or published in conference proceedings. The majority of studies to which I have contributed were conducted in collaboration with not only my supervisor, Steffen Petersen, but also my fellow PhD students at the Indoor Climate and Energy research group at Aarhus University. This thesis is comprised of the studies in which I have assumed a major role.

This thesis is submitted for the Danish degree of PhD in partial fulfilment and conformity with the requirements of the GSST Rules and Regulations and the Ministerial Order on the PhD Degree Programme.

Rasmus Elbæk Hedegaard
Aarhus University, 13 November 2018

This published version of the thesis contains the published manuscript of the paper “*Bottom-up modelling methodology for urban-scale analysis of residential space heating demand response*”, which in the originally submitted thesis was still a submitted draft. Other than the layout of the article, the published version contains a few minor changes that resulted from the peer-review process. The original version of the thesis is available upon request. Similarly, the paper “*The effect of including hydronic radiator dynamics in model predictive control of space heating*” was replaced with the published layout - in this case only a cosmetic change.

Rasmus Elbæk Hedegaard Aarhus
University, 26 March 2019

PUBLICATION LIST

The following is a list of the published research to which I have contributed. The publications are divided into primary and secondary publications. The papers that constitute the main body of this thesis are referred to as primary publications. These are publications where I have assumed a central role in conceiving the study, conducting the analysis and the writing (an exception for the latter is paper P1). The secondary research articles are not featured directly in this thesis – either because they are less relevant to the objectives of the thesis, or because I have only assumed a minor role in the work involved. These publications are instead appended to the thesis. References to articles I have co-authored within the thesis is done in parenthesis, e.g. (P1).

PRIMARY PUBLICATIONS

PUBLICATIONS IN JOURNALS

- P1 Theis Heidmann Pedersen, Rasmus Elbæk Hedegaard, Steffen Petersen. 'Space heating demand response potential of retrofitted residential apartment blocks', *Energy and Buildings*, vol. 141, pp. 158-166, Apr. 2017.
- P2 Rasmus Elbæk Hedegaard, Theis Heidmann Pedersen, Steffen Petersen. 'Multi-market demand response using economic model predictive control of space heating in residential buildings', *Energy and Buildings*, vol. 150, pp. 253-261, Sep. 2017.
- P3 Rasmus Elbæk Hedegaard, Theis Heidmann Pedersen, Michael Dahl Knudsen, Steffen Petersen. 'Towards practical model predictive control of residential space heating: Eliminating the need for weather measurements', *Energy and Buildings*, vol. 170, pp. 206-216, July 2018.
- P4 Rasmus Elbæk Hedegaard, Martin Heine Kristensen, Theis Heidmann Pedersen, Steffen Petersen. "Bottom-up modelling methodology for urban-scale analysis of residential space heating demand response," *Applied Energy*, vol. 242, pp. 181-204, May 2019.

CONFERENCE PUBLICATIONS

- P5 Rasmus Elbæk Hedegaard, Theis Heidmann Pedersen, Michael Dahl Knudsen, Steffen Petersen. 'Identifying a Comfortable Excitation Signal for Generating Building Models for Model Predictive Control: A Simulation Study', in *CLIMA 2016: Proceedings of the 12th REHVA World Congress: vol. 10*, May 2016, Aalborg University, Aalborg, Denmark.
- P6 Rasmus Elbæk Hedegaard, Steffen Petersen. 'Evaluation of grey-box model parameter estimates intended for thermal characterization of buildings', *Energy Procedia*, vol. 132, pp. 982-987, June 2017. Special issue: 11th Nordic Symposium on Building Physics, NSB2017, 11-14 June 2017, Trondheim, Norway.

SECONDARY PUBLICATIONS

PUBLICATIONS IN JOURNALS

- S1 Martin Heine Kristensen, Rasmus Elbæk Hedegaard, Steffen Petersen. "Hierarchical calibration of archetypes for urban building energy modeling," *Energy and Buildings*, vol. 175, pp. 219-234, Sep. 2018.
- S2 Theis Heidmann Pedersen, Rasmus Elbæk Hedegaard, Kristian Fogh Kristensen, Benjamin Gadgaard, Steffen Petersen. "The effect of including hydronic radiator dynamics in model predictive control of space heating," *Energy and Buildings*, vol. 183, pp. 772-784, Jan. 2018.

CONFERENCE PUBLICATIONS

- S3 Michael Dahl Knudsen, Rasmus Elbæk Hedegaard, Theis Heidmann Pedersen, Steffen Petersen. 'Model Predictive Control of Space Heating and the Impact of Taxes on Demand Response: A Simulation Study', in *CLIMA 2016: Proceedings of the 12th REHVA World Congress: vol. 10*, May 2016, Aalborg University, Aalborg, Denmark.
- S4 Theis Heidmann Pedersen, Michael Dahl Knudsen, Rasmus Elbæk Hedegaard, Steffen Petersen. 'Handling Stochastic Occupancy in an Economic Model Predictive Control Framework for Heating System Operation in Dwellings', in *CLIMA 2016: Proceedings of the 12th REHVA World Congress: vol. 10*, May 2016, Aalborg University, Aalborg, Denmark.
- S5 Theis Heidmann Pedersen, Rasmus Elbæk Hedegaard, Michael Dahl Knudsen, Steffen Petersen. 'Comparison of centralized and decentralized model predictive control in a building retrofit scenario', *Energy Procedia*, vol. 122, pp. 979-984, Sep. 2017. Special issue: CISBAT 2017 International Conference, 6-8 September 2017, Lausanne, Switzerland.
- S6 Theis Heidmann Pedersen, Michael Dahl Knudsen, Rasmus Elbæk Hedegaard, Steffen Petersen. 'Handling thermal comfort in economic model predictive control schemes for demand response', *Energy Procedia*, vol. 122, pp. 985-990, Sep. 2017. Special issue: CISBAT 2017 International Conference, 6-8 September 2017, Lausanne, Switzerland.
- S7 Michael Dahl Knudsen, Theis Heidmann Pedersen, Rasmus Elbæk Hedegaard, Steffen Petersen. 'System identification of thermal building models for demand response - A practical approach', *Energy Procedia*, vol. 122, pp. 937-942, Sep. 2017. Special issue: CISBAT 2017 International Conference, 6-8 September 2017, Lausanne, Switzerland.
- S8 Martin Heine Kristensen, Rasmus Elbæk Hedegaard, Steffen Petersen. 'Urban-scale dynamic building energy modeling and prediction using hierarchical archetypes: A case study of two Danish towns', in *Proceedings of BSO 2018: 4th Building Simulation and Optimization Conference*, Cambridge, UK, pp. 348-349.

CONTENTS

1 INTRODUCTION.....	1
1.1 BACKGROUND AND PROBLEM STATEMENT.....	1
1.2 SCOPE OF THIS WORK.....	8
1.3 THESIS OUTLINE.....	14
PART I MODELLING RESIDENTIAL BUILDINGS.....	15
2 MODELLING APPROACH	17
2.1 DATA-DRIVEN MODELLING.....	18
3 EXPERIMENT DESIGN.....	23
3.1 PAPER: IDENTIFYING A COMFORTABLE EXCITATION SIGNAL FOR GENERATING BUILDING MODELS FOR MODEL PREDICTIVE CONTROL: A SIMULATION STUDY (P5).....	27
3.2 EPILOGUE.....	35
4 MODEL STRUCTURE SELECTION	37
4.1 PAPER: EVALUATION OF GREY-BOX MODEL PARAMETER ESTIMATES INTENDED FOR THERMAL CHARACTERIZATION OF BUILDINGS (P6)	39
4.2 EXTENSION TO PAPER	45
4.3 EPILOGUE.....	51
5 PRACTICAL DATA ACQUISITION	57
5.1 PAPER: TOWARDS PRACTICAL MODEL PREDICTIVE CONTROL OF RESIDENTIAL SPACE HEATING – ELIMINATING THE NEED FOR WEATHER MEASUREMENTS (P3).....	59
5.2 EPILOGUE.....	71
PART II DEMAND RESPONSE IN RESIDENTIAL SPACE HEATING.....	73
6 DEMAND RESPONSE – THEN AND NOW	75
7 IMPACT OF BUILDING CHARACTERISTICS.....	79
7.1 PAPER: SPACE HEATING DEMAND RESPONSE POTENTIAL OF RETROFITTED RESIDENTIAL APARTMENT BLOCKS (P1).....	81
7.2 EPILOGUE.....	90
8 MULTI-MARKET APPROACH.....	93
8.1 PAPER: MULTI-MARKET DEMAND RESPONSE USING ECONOMIC MODEL PREDICTIVE CONTROL OF SPACE HEATING IN RESIDENTIAL BUILDINGS (P2)	95
8.2 EPILOGUE.....	104
9 URBAN-SCALE ANALYSIS	107
9.1 PAPER: BOTTOM-UP MODELLING METHODOLOGY FOR URBAN-SCALE ANALYSIS OF RESIDENTIAL SPACE HEATING DEMAND RESPONSE (P4).....	109
9.2 EPILOGUE.....	133
10 CONCLUSIONS.....	137
10.1 MAIN FINDINGS.....	137
10.2 FUTURE WORK	140
11 REFERENCES	143
12 APPENDICES.....	149

LIST OF APPENDICES

APPENDIX 1 PAPER: HIERARCHICAL CALIBRATION OF ARCHETYPES FOR URBAN BUILDING ENERGY MODELING (S1).....	150
APPENDIX 2 PAPER: THE EFFECT OF INCLUDING HYDRONIC RADIATOR DYNAMICS IN MODEL PREDICTIVE CONTROL OF SPACE HEATING (S2).....	167
APPENDIX 3 PAPER: MODEL PREDICTIVE CONTROL OF SPACE HEATING AND THE IMPACT OF TAXES ON DEMAND RESPONSE: A SIMULATION STUDY (S3)	181
APPENDIX 4 PAPER: HANDLING STOCHASTIC OCCUPANCY IN AN ECONOMIC MODEL PREDICTIVE CONTROL FRAMEWORK FOR HEATING SYSTEM OPERATION IN DWELLINGS (S4).....	193
APPENDIX 5 PAPER: COMPARISON OF CENTRALIZED AND DECENTRALIZED MODEL PREDICTIVE CONTROL IN A BUILDING RETROFIT SCENARIO (S5).....	205
APPENDIX 6 PAPER: HANDLING THERMAL COMFORT IN ECONOMIC MODEL PREDICTIVE CONTROL SCHEMES FOR DEMAND RESPONSE (S6)	212
APPENDIX 7 PAPER: SYSTEM IDENTIFICATION OF THERMAL BUILDING MODELS FOR DEMAND RESPONSE – A PRACTICAL APPROACH (S7).....	219
APPENDIX 8 PAPER: URBAN-SCALE DYNAMIC BUILDING ENERGY MODELING AND PREDICTION USING HIERARCHICAL ARCHETYPES: A CASE STUDY OF TWO DANISH TOWNS (S8).....	226

LIST OF ABBREVIATIONS AND ACRONYMS

MPC	Model predictive control
DR	Demand response
DSM	Demand side management
EPBD	Energy Performance of Buildings Directive
nZEB	Nearly zero-energy buildings
BR	Building regulations
DK1	Market region on the Nordpool spot market (Western Denmark)
STES	Structural thermal energy storage
BEM	Building energy model
PE	Prediction error (method)
SID	Subspace Identification (method)
PRBS	Pseudo-random binary sequence
SNR	Signal-to-noise ratio
RTP	Real-time prices
FERC	Federal Energy Regulatory Commission
PH	Passive house
MAP	Maximum a posteriori
IEA EBC	International Energy Agency Energy in Buildings and Communities programme

1 INTRODUCTION

1.1 Background and problem statement

The increasing evidence of climate change has prompted the beginning of a shift towards an energy system powered by renewable energy production rather than conventional production based on burning fossil fuels. These efforts are accompanied by an ambition to increase the sustainability of almost every aspect of our daily lives – this includes an increased focus on recycling and the development of more energy efficient cars, electronics and appliances. Buildings, which account for nearly 40% of the energy consumption in Europe [1], are also facing increasingly steep requirements for energy efficiency through national or European building regulations (BR). Despite these efforts, the data on the final energy use of the building sector reported by Eurostat, the EU entity providing statistical information, shows no clear tendency of decreasing consumption levels [2]. Similar trends are reported by studies concerned with nations outside the EU [3]. Possible reasons for this lack of progress in the building sector are a growth in population and thus also in the number of buildings; the increasing number of energy consuming devices in our society; and occupants trading in the energy efficiency increases gained from building retrofits for increased comfort (the so-called *rebound effect*).

The EU introduced its first directive on the energy performance of buildings in 2002 [4], which required the energy performance calculation in the BR of its member states to not only consider

thermal insulation levels, but take all factors that influence the energy consumption in a building into account. These factors included the impact of the building design and furthermore allowed on-site renewable energy production to offset consumption in the calculation. In Denmark, this resulted in a new calculation method being implemented in the national BR in 2006, along with a forecast of the BR requirements being further tightened in 2010 and 2015 – each time by approximately 25% of the 2006 baseline level. The 2010 revision of the EU’s Energy Performance of Buildings Directive (EPBD) [5] introduced a requirement for its member states to ensure buildings built after 2020 to be *nearly net zero-energy buildings* (nZEB). This led to the voluntary ‘Building Class 2020’ being introduced in the Danish BR in 2010 [6]. This building class further tightened the energy requirements with 25% of the 2006 baseline (now 75% in total), and constituted the Danish nZEB definition, which was to become mandatory in 2020. Since then, ‘Building Class 2020’ has faced criticism from the construction industry because of the diminishing returns associated with passive energy efficiency measures: *The last millimetre of insulation is not as effective as the first*. Because of these diminishing returns, it was argued that ‘Building Class 2020’ constituted a *de facto* requirement for on-site renewable production for buildings to be able to comply. Furthermore, a recent review of ‘Building Class 2020’ indicated that implementing it as a mandatory requirement would not be economically feasible – neither in societal terms nor for consumers [7]. This has led to ‘Building Class 2020’ being replaced by the ‘Low-Energy Building Class’ [8], which features slightly lower requirements for energy efficiency and remains a voluntary class even after 2020. This development indicates that the current levels of regulatory requirements for energy efficiency have reached a point where further tightening them would require new technological development.

In parallel to this development on the demand side, the production of electricity from renewable energy sources in the EU has seen a steady increase for almost two decades, as indicated by the upper part of Figure 1. In 2016, energy production from wind and solar in the current 28 member states of the EU reached levels more than 18 times higher than the production recorded in 2000 [9]. In contrast, the total energy production in the EU only saw an 8 % increase in the same period [10]. These developments indicate that both the demand side and the supply side are currently undergoing a transition towards higher energy efficiency and more renewable energy production. However, this transition brings about new challenges that need to be addressed as the penetration of renewable energy in the system increases. Solar and wind energy, which are among the types of renewable energy production that have seen the highest growth in recent years, depend entirely

on weather phenomena and are therefore characterized by a high degree of intermittency. This intermittency complicates the task of maintaining a balance between supply and demand in the energy system.

An example of this issue is given in the lower part of Figure 1, which shows wind power production together with the annual number of hours that saw negative electricity prices for the Nord Pool electricity market region of Western Denmark (DK1) [11]. This region is characterized by a high share of electricity production from intermittent wind power [12]. The data indicates a clear tendency of increased intermittent production from wind turbines leading to an increase in the number of hours where the region experienced negative electricity prices. The Pearson correlation between the two data series supports this with a strong correlation of 0.90 ($p=0.00216$). Negative electricity prices occur when there are no buyers for the excess production, which may happen when the interconnectors between different market regions are congested, or at times when neighbouring market regions are also experiencing excess production.

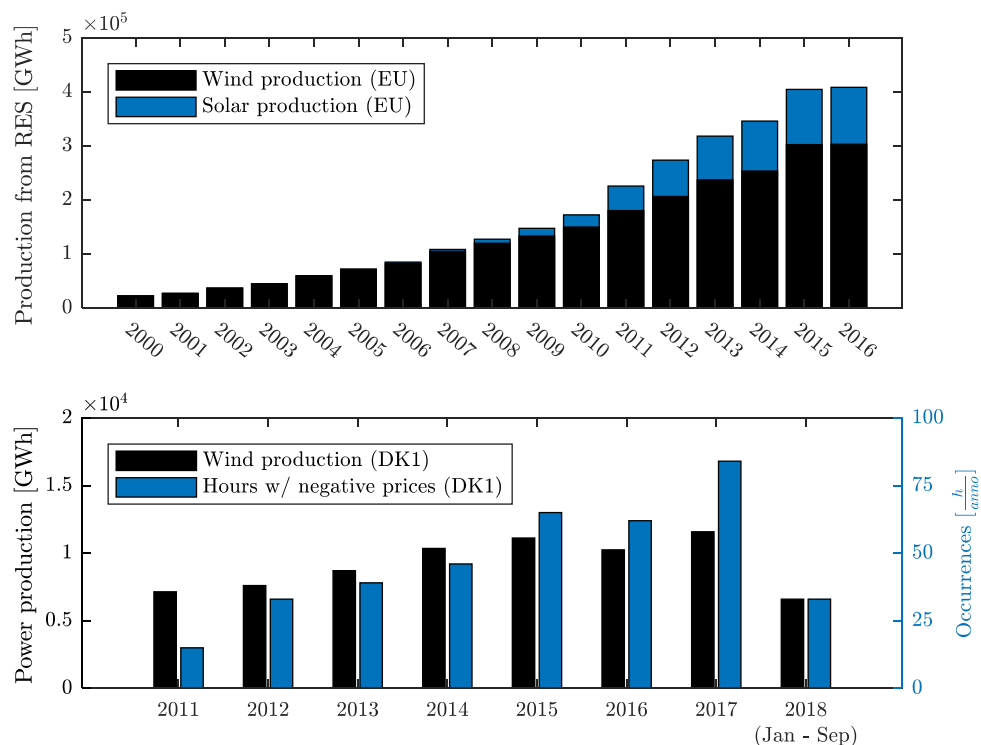


Figure 1 Top) The combined power production from renewable energy sources in the 28 EU member states, source: Eurostat. Bottom) Relationship between wind power production and the occurrence of negative prices in the DK1 day-ahead market region (source: Energinet).

Traditionally, imbalances between supply and demand have been addressed by adjusting the output of dispatchable generation units such as combined heat and power plants, or by using interconnectors between different regions to resolve balancing issues through import and export. However, as the number of dispatchable power plants declines and the RES-based production in all market regions increases, these conventional approaches may no longer be sufficient for maintaining a balanced energy system. The practice of allowing local renewable production to offset consumption in the calculation method used to evaluate the energy efficiency of a building may further complicate things. Recent research has indicated that nZEB buildings, despite having a near-zero impact on the grid on an annual basis, are characterized by a significant mismatch between the times at which energy is produced and consumed locally [13–14]. In practice, this imbalance is handled by exporting excess production to the grid and importing electricity in times of insufficient local production – thus using the electricity grid as a virtual energy storage. As a result, despite what the zero-energy label suggests, these buildings are not highly autonomous from the rest of the energy system. On the contrary, this two-way interaction with the grid may result in nZEB buildings contributing negatively to the balancing issue already at hand [15].

These challenges suggest that the conventional load-driven structure of energy-systems may not be ideal for system configurations with a high penetration of RES-based production. This has led to the proposal of complementing the efforts towards energy efficiency, more renewable production, and strengthened energy import and export capabilities with the implementation of so-called *smart grids* [16]. The main attribute that separates smart grids from conventional electricity grids is that smart grids can utilize information and communication technology to integrate the actions of all parties connected to it in an intelligently manner, thereby increasing the efficiency of the energy system as a whole. One of the key characteristics of smart grids is that the task of maintaining a balance between supply and demand is not only addressed through supply-side initiatives but also through demand side initiatives. This increases the ability of individual regions to absorb the fluctuations of renewable production themselves, thus maximizing the utilization of RES while avoiding production curtailment. While the smart grid concept relates purely to electricity grids, which arguably face the largest challenges in terms of RES-based production and balancing, Lund et al. [17] argue that there may be several benefits to be gained from taking a *smart energy systems* approach rather than focusing efforts on individual energy sectors. A closer integration between electricity grids and other energy system sectors such

as the district heating networks may reveal synergies that benefit all sides. As such, several aspects of smart grids may also be relevant for other energy sectors.

The notion of adapting demand to the benefit of the energy system is generally denoted *demand response* (DR). The share of consumption that may be adapted without a significant degradation of the consumer experience is referred to as *flexible consumption*. Because of the significant energy consumption that takes place in buildings, many researchers have considered them suitable candidates for DR initiatives, see e.g. [3, 18–19]. A similar point of view is found in the recent 2018 amendments of the EPBD (Directive 2018/844/EU), which states that the Union by end of 2019 shall have adopted a common scheme for rating the *smart readiness* of buildings [20]. The directive further elaborates on this term by defining it as the ability of a building or building unit to adapt its operation to the needs of occupants or the grid.

Several energy-consuming processes in buildings may be adapted in this way and are therefore considered partially flexible. These processes include the operation of certain appliances (e.g. dishwashers and washing machines) and the charging of electrical vehicles or domestic hot water tanks [21–22]. Flexible loads may be scheduled to take place at times which benefit the grid, e.g. at times of sufficient or excessive energy production from renewables or at times of otherwise low grid load. Another approach is to adapt the more continuous thermostatic loads for space heating and cooling of buildings. The approach is often referred to as structural thermal energy storage (STES), as it utilizes the inherent thermal capacity of massive structural elements in buildings as a means of storage. The way that energy is stored in this approach depends on how the particular heating system interacts with the thermal mass of the building. Some heating systems are designed to act directly on the thermal mass of the building through thermal activation of building components (e.g. underfloor heating), while other systems use convectors or radiators to dissipate most of their heat output into the air of the building. Figure 2 presents an illustration of a heating strategy that utilizes the thermal mass of a building by engaging in preheating in order to reduce consumption during peak periods.

The task of utilizing STES to generate flexible demand in practice is characterized by several challenges. One of these is that there are certain limitations as to how large (and how fast) the temperature fluctuations used to enable energy storage may be, before the occupants of the building begin to feel thermal discomfort. Therefore, utilization of STES requires the occupants of the building to indicate what level of comfort they consider acceptable, e.g. in the form of a

temperature comfort-band as indicated in Figure 2. Furthermore, since the process of storing heat in structural mass is not lossless, a key aspect of effective utilization of this storage method is the task of determining the exact intensity and duration of a temperature-increase that results in the right amount of energy being stored. Doing so with sufficient accuracy involves accounting for the current thermal state of the building as well as external influences that affect the building in the near future. Model predictive control (MPC) is a control scheme that utilizes a building energy model (BEM) to address all of these concerns.

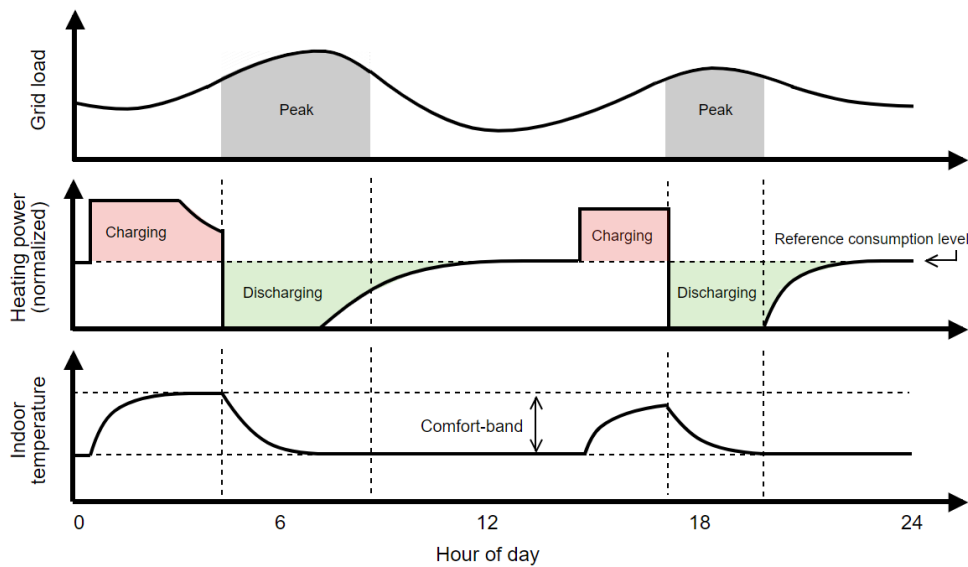


Figure 2 Principle in utilizing the structural thermal energy storage for demand response. Adapted from (P4).

MPC schemes determine the optimal control strategy for a given process by solving an optimization problem. This process involves using a model of the process in combination with forecasts to predict the impact of phenomena outside the influence of the control scheme. In a building-control context, a dynamic model of the thermal dynamics of a building is used to account for the impact of e.g. weather conditions and occupancy-related internal heat gains. These influences are incorporated in the optimization problem solved by the control unit to ensure that the obtained control strategy accounts for them. Furthermore, the optimization routine that serves as the foundation of the control scheme allows for the inclusion of explicit constraints relevant to the particular process. While incorporating system-related constraints such as the maximum power output of a HVAC system is straightforward for any control scheme, the use of a BEM as an integrated part of the control scheme allows the optimization problem to include comfort-related constraints as well. These may represent an allowed range of temperatures or an upper

bound of the temperature rate-of-change. Solving the optimization problem yields the control strategy that is optimal in terms of a predefined objective function and constraints. The objective function may reflect the objectives of the building owner or the utility company supplying the building with energy. Typically used objectives minimize the overall energy consumption or economic costs of operating the building – while others maximize the share of the consumed energy that is produced from renewable energy sources. The functions that describe these objectives may be readily adapted as circumstances change and new control behaviour is desired. This, together with the ability of MPC to explicitly handle constraints related to the operation of the building, has resulted in MPC becoming the most frequently used control strategy for research on *smart buildings* [23]. In spite of several advantages of utilizing MPC for DR purposes in buildings, several factors still hindered progress towards realizing these potentials in actual buildings at the time when the work presented in this thesis was conducted – and still do.

Among these factors are several challenges related to implementing MPC in buildings in a cost-effective and reliable way. MPC is an advanced control scheme requiring a significant amount of technical infrastructure in order to function; both in terms of the sensors needed in the building and in terms of the infrastructure used to communicate with external entities. Examples of the latter are weather services providing the weather forecasts to be used in the optimization, but also utility companies who broadcast time-varying energy prices or engage in DR coordination by other means. Although the need for a complex technical infrastructure seems highly inhibitive for the viability of MPC schemes, several factors indicate otherwise: the recent EU Directive 2018/844 directly underlines the importance of establishing high-capacity communication networks for smart homes [20], thus suggesting that standardized solutions for facilitating such communication may be rolled out in the future. Furthermore, Killian and Kozek [24] argue that the increasing adoption of home automation systems is likely to reduce or eliminate many of the expenses related to establishing the internal infrastructure required in the buildings, since many of the sensors needed for MPC are typically already a part of such systems. Another and more urgent issue, however, is the task of obtaining a BEM that is a sufficiently accurate representation of the building to be used in MPC schemes. Obtaining the BEM is generally considered the most challenging aspect of implementing model-based control schemes in practice, because the diversity of buildings has hindered the development of standardized modelling methods, thus resulting in this process being both expensive and time-consuming while also requiring some level of expert knowledge [23–25].

In addition to the challenging aspects related to the practical implementation of MPC, Cutter et al. [26] consider one of the greatest barriers for utilization of DR in general to be the lack of appropriate market structures to support it. The authors argue that many of the requirements that apply to participants in conventional power markets may render the balancing power achievable through DR unable to compete with that of conventional combustion turbine plants. Similarly, Ma et al. [27] describe how a tendency toward continued use of rules and definitions of the conventional bulk power system may inhibit potential providers of DR from participating in the markets. In this regard, the authors mention requirements for the minimum bidding amounts (energy quantities) that may enter the balancing markets as well as requirements related to the technical infrastructure needed to coordinate/facilitate DR as examples of inhibiting regulatory structures. Finally, O’Connell et al. [28] point to the lack of transparency in current tariff structures as a barrier, especially for residential customers, who are unable to respond to variations in electricity production prices if these variations are not reflected in their utility expenses directly.

1.2 Scope of this work

The topic of this thesis is the utilization of buildings as flexible resources that may be used to address some of the challenges related with the transition to an energy system powered by intermittent renewable energy sources. The aim of the presented work is to contribute with research addressing some of the specific challenges of the previous section that inhibit utilization of buildings for DR in practice. This section is devoted to limiting the scope of the thesis within this relatively broad setting, and condensing the observations presented so far into a set of explicit research objectives.

As consumers are not obligated through rules and regulations to participate in DR activities, the potential of DR is determined entirely by the willingness of consumers to adapt their consumption – and hence the convenience at which they may do so. In this regard, the approach of manipulating thermostatic loads for utilize STES separates itself from many other sources of flexible consumption, because the level of participation may be seen as a continuous variable. Continuous, in this sense, refers to the fact that the level of degradation of the consumer experience is entirely up to the consumers themselves. As such, the more sensitive consumer who is still willing to participate in DR may specify a stricter set of constraints, e.g. a smaller range of allowable temperatures, at the cost of a corresponding reduction in the economic incentive provided by the utility company. This is in contrast to the type of DR originating from many of today’s marketed

smart appliances, which often have a binary ‘either/or’ characteristic to them, where consumers on a day-to-day basis have to decide whether e.g. a postponement of running the dishwasher is acceptable to them. Compared to DR gained from thermostatic loads, I consider these types of *discrete* sources of DR much more likely of being perceived as inconvenient by consumers, and thereby in themselves constitute a hindrance for the utilization of DR in general. This belief, together with my background in civil engineering and building physics, has resulted in the scope of this work being limited to DR initiatives based on the utilization of STES.

Furthermore, while essentially all buildings in which the thermal environment is conditioned through space heating or cooling may be utilized for DR, this work focuses on residential buildings for a number of reasons. With the residential building sector accounting for 25% of final energy use in the EU, whereof approximately two-thirds is used for space heating in the north and west regions of the EU [1, 29], the theoretical potential for DR in residential buildings is enormous. Furthermore, due to the fact that DR based on STES can be tailored to fit the personal preferences of consumers, residential buildings may be the ideal setting for such initiatives. Finally, the more lenient attitude towards indoor climate control that has traditionally applied to residential buildings may result in increased thermal comfort being experienced by occupants as more advanced control schemes are implemented. This may increase the willingness of consumers to allow for controlled temperature fluctuations used to enable DR, both benefitting the grid and generating economic incentives for the building owners.

These observations have led to the scope of the thesis being limited to the utilization of STES for DR purposes in residential buildings. Considering the challenges outlined in this thesis so far, two relevant areas requiring further research emerge: *modelling residential buildings* and *demand response in residential space heating*.

Part I: Modelling residential buildings

Building energy modelling is a field of research that has been gaining interest due to the many possible applications of building energy models. These include model-assisted design, control, commissioning, fault detection and energy labelling. In rough terms, setting up a building model generally amounts to selecting a suitable model structure and identifying its parameters from relevant information about the building. In purely physics-based modelling approaches, building models are derived from information on specific buildings (e.g. construction plans or energy performance certificates) or, alternatively, information about buildings in general (e.g. typical geometry and materials). Statistical methods, on the other hand, rely on measurements to derive models. This data describes the influence of various factors such as weather conditions (inputs) on the indoor temperature or the heating demand of the building (inputs or outputs). While the latter often result in highly accurate building energy models that are suitable for control-purposes, data-driven modelling approaches are characterized by several challenges.

One of these challenges is the data acquisition itself, where the sensor equipment needed to measure weather conditions constitutes an economic and practical barrier for residential applications. Another challenge is ensuring that the data has a set of properties that makes it suited for dynamic modelling. To achieve this, data is often collected by conducting experiments in the building that are designed with this particular goal in mind. These experiments typically involve imposing a series of temperature fluctuations (excitation) on the building to reveal its dynamic properties. In many cases, increasing the amplitude of these fluctuations results in better data, since the dynamic characteristics of the building are exposed more clearly, while the effects of noise or disturbances are reduced. High-quality data not only allows for more precise parameter estimates, but also allows the modeller to work with more complex model structures with a higher number of parameters. In this regard, the challenge with residential buildings is that these buildings are rarely vacant for extended periods. Due to comfort considerations, the presence of occupants limits how large these fluctuations may be. At the same time, occupants may affect the heat balance of the building in ways that are difficult to account for in the measured data. As such, occupants simultaneously introduce noise in the measurement data and limit the precautions that can be taken to address such noise. The choice of model structure thus becomes a trade-off between increasing the model complexity to achieve a better representation of the physical phenomena that take place in the building, or decreasing model complexity to ensure that the model parameters can be identified from the measured data.

These challenges have been condensed into the following set of explicit research objectives. Each objective is addressed in one or more of the primary or secondary publications of this thesis, which are stated in the parentheses following each objective.

- 1.1** Investigate how to design excitation experiments with special attention to the trade-off between the conflicting objectives of maintaining a comfortable indoor climate during experiments and obtaining building models of high quality. (P5, S7)
- 1.2** Identify low-complexity model structures capable of describing the thermodynamic characteristics and behaviour of buildings when identified using typical measurement data. (P6)
- 1.3** Identify practical methods for obtaining (or avoiding) weather measurements intended for control-oriented modelling of buildings. (P3)

Part II: Demand response in residential space heating

Several studies have investigated leveraging structural thermal energy storage (STES) in buildings for DR purposes. An example of a study applying MPC in buildings is that of Široký et al. [30], who implemented an MPC scheme in a university building to lower energy consumption while improving comfort levels. Another application was presented by Ma et al. [31], who in a simulation-based study involving a commercial building showed that MPC was superior to other rule-based control schemes in terms of generating economic savings under time-varying energy prices. Oldewurtel et al. [32] used a mixed objective function considering both electricity prices and the grid load for MPC in an office building.

In the current body of research, only a few studies investigating the potential of engaging residential buildings in STES-driven demand response applications were identified. Reynders et al. [14] investigated the ability of rule-based control schemes (both non-predictive and predictive) to improve the temporal match between local energy production and consumption. This work was further expanded Reynders' doctoral thesis [33], in which he presented a fundamental analysis of the potential for utilizing STES and the impact of certain building characteristics. One of the conclusions drawn in this work was that the efficiency at which STES in buildings may be utilized depends not only on the available thermal mass, but also on the energy efficiency of the envelope. Other studies have investigated the performance of MPC in achieving economic or societal objectives: Halvgaard et al. [34] demonstrated the use of MPC for exploiting the thermal mass of a residential building equipped with underfloor heating, and achieved 25-35% economic savings by adapting the heating strategy to the time-varying electricity prices from the Nord Pool day-ahead electricity market. The authors furthermore argued that, since electricity prices are correlated with the amount of renewable production from e.g. wind turbines, MPC could essentially be used to store cheap renewable energy in the thermal mass of buildings. Knudsen and Petersen [35] argued that such a relationship between energy prices and the source of its production cannot always be assumed, and demonstrated the ability of an MPC scheme controlling the space heating in a dormitory apartment to handle a multi-purpose objective function, which considered both the electricity prices and the carbon-dioxide intensity associated with the electricity production. Depending on the chosen weighing between the objectives of reducing costs and reducing CO₂ emissions, the change in economic costs compared to a baseline ranged from approximately +6% (higher costs) to -15% (savings). Similarly, the change in CO₂ emissions ranged from +6% to -8%. In general, studies report significant differences in the

potential of utilizing MPC in buildings. Most likely, the building characteristics identified by Reynders [33], which were found to influence the effectiveness at which buildings may engage in DR, are among the main causes of discrepancies between studies. Another possibility is differences in the prices used to evaluate these potentials.

The scarcity of studies on DR in residential buildings calls for further research on the potential benefits of utilizing this source of flexible consumption. Furthermore, previous research has indicated that the energy performance of buildings affects their ability to engage in DR. However, research on how these relationships affect the control actions of MPC schemes is lacking. Finally, several studies have used the time-varying prices from electricity wholesale markets to set up objectives concerned with minimizing the costs of operating a building. However, research has indicated that wholesale market prices may not truly reflect the actual needs of the grid [32, 35]. Therefore, further research exploring alternative incentive mechanisms is needed. These gaps in current knowledge have led to the formulation of four explicit research objectives:

- 2.1** Investigate the influence of building energy efficiency on the potential for utilizing the structural thermal mass for residential demand response through model predictive control. (P1, P2)
- 2.2** Identify the impact of heat exchange between adjacent zones on the performance of centralized and decentralized control schemes. (P1, S5)
- 2.3** Explore and evaluate existing and new market structures on their ability to incentivize residential DR that generates societal or grid-related benefits. (S3, P1, P2, P5)
- 2.4** Investigate how the demand response potential in individual buildings translates to a scenario of large-scale utilization. (P5)

1.3 Thesis outline

The format of this thesis is based on the two research areas identified in the previous section:

Part I: Modelling residential buildings

Part II: Demand response in residential space heating

Each part begins with an introductory chapter, which is followed by three chapters presenting research related to the objectives defined in section 1.2. These chapters are comprised of a short motivation of the study that is presented, the paper itself and finally a section discussing the analysis and main findings in the context of the objectives of this thesis. In a few cases, additional results that were either left out of the published paper or obtained since the publication are also provided. The thesis is concluded with a unifying summary of the main findings together with suggestions for future work.

PART I
MODELLING RESIDENTIAL
BUILDINGS

2 MODELLING APPROACH

The process of modelling any physical system involves a series of choices being made by the modeller. Among the most significant, is the choice between the physics-based and statistics-based modelling approaches. Physics-based modelling, which is also referred to as *white-box* modelling, relies on knowledge about the characteristics of the system and the physical phenomena affecting it to set up a model. Detailed building energy performance simulation tools such as EnergyPlus, BSim, IDA-ICE and TRNSYS Type56 are examples of white-box modelling tools. These tools have an emphasis on detail, and achieve it through a deterministic modelling approach that is heavily reliant on user-specified inputs describing the building. This approach allows them to be used for detailed analysis of buildings that have not yet been built, and so-called model-assisted building design where models are used actively in the design phase of a building project. An issue associated with this approach is that the high complexity of these models makes them unfit for control purposes, since the modelling approach requires a level of detail that is rarely available. This typically necessitates a significant amount of assumptions being made in setting up the model, which may be based on default values described in modelling standards or on the subjective experience of the modeller. Such assumptions inevitably affect the accuracy of the resulting models, thereby limiting their use for control purposes. Even if a high level of detail is available, several factors during the building construction and operational phases may still cause discrepancies between the theoretical (*as-ordered*) and actual (*as-built*) energy performance of the building. A way of improving the accuracy of such models is to calibrate them using measured data. However, even if an acceptable level of accuracy may be achieved in this way, the complexity of the models itself renders them unfit for many control purposes due to the significant computational work involved in simulating them [25, 36].

The requirement for accuracy and computationally fast simulations has led to this work focusing on modelling approaches that rely on measured data to obtain simple models that are suited for control purposes. Before any analysis is presented, the following chapter provides a brief description of some of the modelling-related choices that have applied to the majority of the conducted work.

2.1 Data-driven modelling

The field of system identification is concerned with the practice of developing mathematical models of real-world phenomena using data. This data consists of measurements of phenomena (inputs) affecting a given system, and the corresponding change in the state of the system (outputs). The combination of these measurements describes the input-output relationships that are characteristic of the modelled system. The objective of the modelling process is to identify a model which, when exposed to the measured inputs, replicates the measured output of the true system with sufficient accuracy. System identification is a mature field of research in which several methods for deriving models from measured data have been developed. Among these, some of the more intuitive techniques are those belonging to the family of prediction error (PE) methods [37]. The basic principle of PE methods is to parameterize a given model in terms of a finite number of parameters. The parameter identification then becomes an optimization problem with the objective of minimizing some measure of the error between the output of the model and the measured output of the true system, which is a function of model parameters. The basic principle of PE methods is depicted in Figure 3.

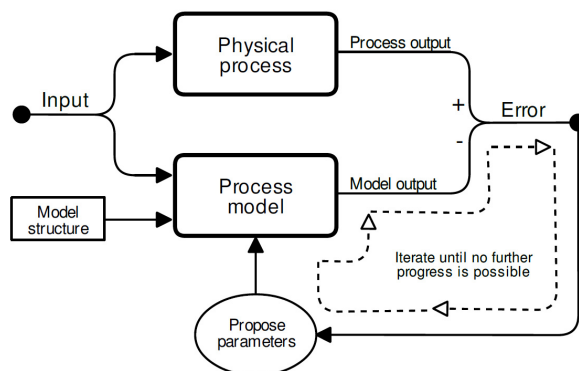


Figure 3 The principle of the family of prediction error methods in system identification.

STATISTICS- AND PHYSICS-BASED MODELLING

A family of methods that is frequently used as an alternative to the PE methods are the purely data-driven subspace identification (SID) methods, which rely on projections of the input-output data to determine the optimal state vector, from which the system matrices (model) can be extracted [38]. One of the significant advantages of SID methods is that the model parameters are identified in a non-iterative fashion and are hence easily computed. This is only the case for a small subset of models when using the PE methods. The system matrices obtained through SID

are freely parameterized, meaning that no a-priori structure may be imposed on them. An advantage associated with this is that models may be derived with minimum effort and knowledge about the system. On the other hand, a drawback of free parameterization is that the parameters of the obtained models have no physical meaning. Furthermore, the disregard of the physical characteristics of the modelled system results in a heavy reliance on the measured data to reveal the internal workings of the system. Naturally, this results in strict requirements for the quality of the data, but also has the consequence that these models generally have poor extrapolation capabilities – i.e. the ability of the model to describe the behaviour of the system under other conditions than those present in the training data [36]. The lack of parameter interpretability in models obtained through SID methods has earned them the label *black-box models*.

One of the key differences between the SID and PE methods is the fact that only the latter allows for the use of structured models, as also suggested by Figure 3 [36]. This allows the modeller to base the structure of the model on knowledge about the physical phenomena affecting the system – e.g. the laws of thermodynamics. Thereby, the modelling principles of the aforementioned white-box approach are mixed those of the statistical methods, which is why these models are referred to as *grey-box models*. The use of structured models is the main driver of both the advantages and disadvantages of PE methods when compared to SID methods. Using a physics-based model structure often reduces the number of parameters of the model when compared to its black-box counterpart, thereby in many cases simplifying the task of identifying the parameter values from data. Another advantage is that the parameters become physically interpretable, thus allowing the modeller to not only incorporate knowledge about the modelled system through the specification of the model structure itself, but also by constraining or guiding the parameter identification. This may be done by fixing certain parameters whose values are known with sufficient certainty, or by specifying the likelihood of a given parameter assuming a given value. As stated by Tangirala [36], incorporating a model structure also reduces the sensitivity of the parameter identification to the quality of the input-output data;

‘... a practical benefit of working with grey-box models is that the prior knowledge significantly lowers the burden of persistent excitation or information requirements in input-output data that is normally required for black-box identification’ – Arun K. Tangirala

A final advantage of the PE method is its ability to identify parameters from input-output data captured under closed-loop control, and therefore contain a high level of feedback [37]. The prevalence of closed-loop control in buildings could pose an issue for the correlation, spectral analysis and subspace identification methods, since they are more sensitive to data containing feedback [39].

CHALLENGES IN GREY-BOX MODELLING

The perhaps most significant drawback of the PE method is that it typically involves an iterative identification approach rather than the non-iterative approaches applied in SID methods. In almost all cases, the optimization problem of minimizing the prediction error as a function of model parameters is non-linear in nature. In these cases, there is no guarantee of the applied optimization routine finding the set of parameters associated with the global minimum of the chosen *error criterion* – i.e. the function that maps a sequence of prediction errors to the scalar that is minimized during the parameter identification. This issue becomes more significant as the size and complexity of the model structure increases. Therefore, increasing the complexity of a model structure may allow it to represent the dynamics of the modelled system more accurately, but it may also render the optimization routine unable to identify a suitable set of parameters. A term denoting the ability to identify the parameters from data is *identifiability*. The trade-off between model complexity and parameter identifiability constitutes one of the most challenging aspects of grey-box modelling.

Clearly, both the black-box and grey-box modelling approaches have their own merits. In the context of buildings, however, I consider the advantages of the PE methods to outweigh the added efforts related to the proposal of model structures and the added computational work in identifying their parameters. The primary reason for this is the requirements for data-quality that are associated with black-box modelling. Usually, input-output data is obtained through measurement experiments that are designed to yield as informative data as possible. In the context of buildings, such experiments usually involve exciting the building by imposing temperature fluctuations through the heating system. However, several factors may inhibit the generation of highly informative data in buildings. These include the lack of control over certain inputs (weather phenomena, occupancy-related heat gains) and the high costs (both in economic and comfort terms) associated with measurement experiments. Therefore, the *prediction error method* and physics-based grey-box model structures were used in the modelling work of this thesis.

CHOICE OF ERROR CRITERION

A significant choice related to PE methods is the choice of error criterion. The classical PE method minimize some measure or norm of the one-step-ahead prediction errors of a model using an either predefined or identified noise model. This approach yields models ideal for e.g. set point tracking and other applications that benefit from short-term predictions. Furthermore, Zhao et al. [40] argue that the one-step-ahead approach is optimal if the prediction errors are mainly driven by stochastic noise in the data originating from disturbances acting on the system. Whenever long-range predictions are desirable, several studies have suggested that minimizing the *k-step-ahead* (or *multi-step-ahead*) prediction error is more appropriate [41, 42]. The underlying notion is that the simultaneous identification of the deterministic model (in our context; the building model) and the stochastic model (noise model) in the one-step-ahead approach produces a potentially biased estimate of the plant model. This biased plant-model is optimal when used in combination with the identified noise model to make predictions. However, since the input to the noise-model is the previous prediction errors, it cannot be used in long-range predictions. Therefore, in this setting, a biased plant model would perform worse than an unbiased plant model which was identified either without a stochastic noise model (Output Error model), or with a noise model but using a *k-step-ahead* error criterion. Here, the latter ensures that more emphasis is put on the deterministic model than the noise model, thus increasing the accuracy of long-range predictions.

The connection between the *k-step-ahead* error criterion and the long-range predictive performance have led to identification methods using this criterion being referred to as control-relevant identification or, in the context of MPC, MPC-relevant identification. The modelling conducted in this thesis uses an infinite-step-ahead error criterion (also denoted *simulation error*), essentially putting full emphasis on the plant model estimate. For applications where a noise model is desired, the parameters of the noise model were identified independently – i.e. after the parameters of the plant model had been identified.

USE OF BUILDING ANALOGUES

Finally, although research concerned with modelling the thermodynamic behaviour of buildings should ideally be based on experimental data captured in actual buildings, the majority of the analysis contained in this thesis is based on simulations. The main reason for this is that several of the thesis objectives (of both Parts I and II) call for comparative analyses that require a proposed set of methods (e.g. experiment design or control schemes) to be evaluated under

identical boundary conditions. Changing weather conditions, for instance, make such analyses difficult to conduct in real buildings. Instead, in the majority of the conducted research, detailed building models are used as analogues for real buildings to retain as much of the complexity of real buildings as possible, while still allowing repeated and identical evaluation of modelling and control-related methods. The building energy performance simulation tool EnergyPlus [43], developed by the U.S. Department of Energy, was used for this purpose. EnergyPlus simulates the thermal conditions inside buildings down to a temporal resolution of one minute, and uses detailed algorithms to describe the thermodynamic phenomena that take place in buildings. The Building Controls Virtual Test Bed [44] software allows the EnergyPlus to be coupled with programming engines such as MATLAB [45]. This approach of simulating two separate pieces of software simultaneously and exchanging information between them is referred to as co-simulation. This simulation method constitutes a versatile framework for evaluating a wide range of the aspects related to building modelling and control.

The following chapters each present a research paper that addresses one of the research objectives related to the first part of this thesis. Each chapter provides a brief motivation for the study, before the paper is presented in full in its own separate section. Finally, each chapter contains an epilogue in which the main findings of each paper are discussed in the context of the objectives of the thesis.

3 EXPERIMENT DESIGN

A prerequisite for the ability to identify the parameters of models describing any given system (including buildings) from measured input-output data is that the data is *informative* [37]. Data can be regarded as informative if it reveals all relevant properties of a given system and allows the modelling procedure to distinguish between any two candidate models. *Experiment design* is concerned with ensuring that the measured data is sufficiently informative to identify the type of model that is desired. Assuming that other basic prerequisites are met (e.g. that all relevant inputs are measured), experiments are designed with two important attributes of the resulting input-output data in mind: the *frequency content* and *signal-to-noise ratio* of the data.

FREQUENCY CONTENT

The frequency content of an input signal is the instrument used to reveal the dynamic properties of the system. The more frequencies with sufficient power contained in the input signal, the more clearly can the resulting input-output data reveal the differences between two similar candidate models. A lack of power in a certain frequency band of an input signal may render it unable to reveal certain dynamics of the system. A way to ensure sufficient frequency content is to choose an input signal with a flat frequency spectrum – e.g. a signal of pure white noise. However, a more frequently used type of input signal is pseudo-random binary sequence (PRBS) signals, which can be generated in a way that ensures they have white noise-like properties – power in essentially all frequencies. Signals that by default carry information in all frequencies may be manipulated to put emphasis on certain parts of the frequency spectrum, which is advantageous whenever the relevant dynamics of the modelled system are confined to a certain frequency range. For instance, Rivera et al. [46] proposed a set of guidelines for constructing suitable PRBS signals through utilizing prior estimates of the dominant time-constants of the modelled system. This is particularly useful in the context of buildings, where the time constant of the room air may be in the order of minutes, while the heavy structural components may have time-constants spanning upwards of days. Figure 4 depicts a PRBS signal and its frequency power spectrum generated

using this approach¹. The PRBS signal carries information across the entire frequency band that was specified as relevant when designing the signal.

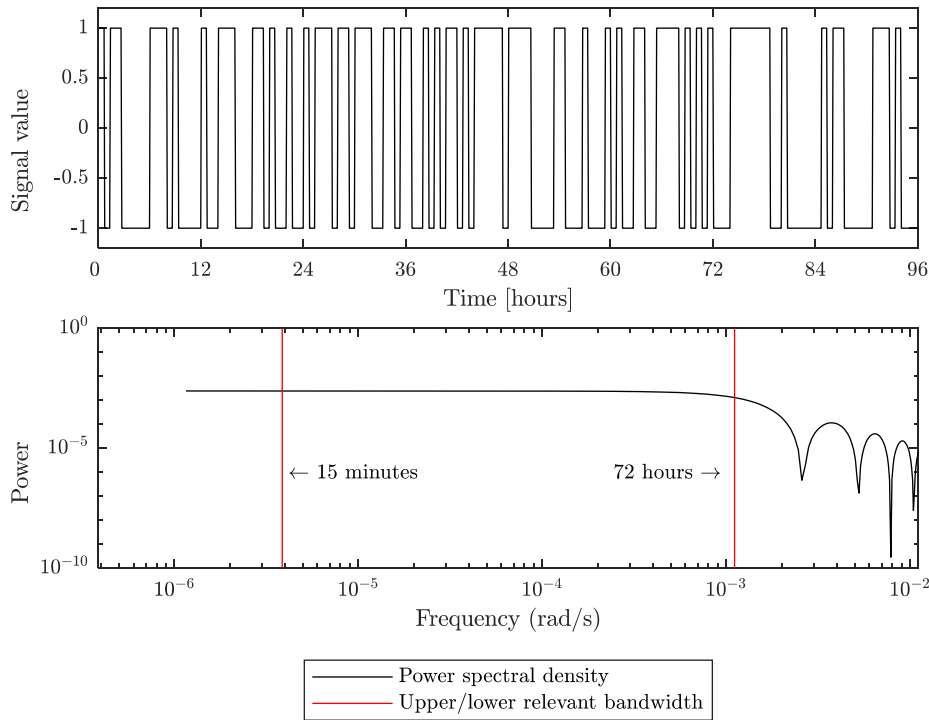


Figure 4 Full-length PRBS signal and its power spectrum. Relevant bandwidth as per [46, 47]. Only part of the signal is shown – length of full signal is approx. 28 days.

SIGNAL-TO-NOISE RATIO

The second prerequisite for informative data is a suitable signal-to-noise ratio (SNR). This ratio describes the strength of the input signal (determined by signal amplitude) relative to the amount of noise present in the data. Noise, in this context, may originate from the sensor equipment itself or from unmeasured phenomena acting on the system. The higher the SNR, the easier it is to differentiate between measured output effects resulting from the inputs and those driven by noise. A low SNR can result in the in a high uncertainty associated with identified the parameter estimates. In more severe cases, the noise in the data may be so dominant that the relationship between inputs and outputs cannot be identified; thereby resulting in a model that describes the true system poorly.

¹ Signal generated for a system with low and high time-constants of 30 minutes and 3 days, respectively. User design input was selected as $\alpha = 2$ and $\beta = 1$, see [46].

The maximum input power that can be exerted on a system, and thereby the achievable SNR, may be limited by a variety of considerations that depend on the specific system in question. An example of this is a desire to maintain the state of the system within a certain range – e.g. within typical operating conditions or to ensure that the system remains in a regime in which it can be approximated by a linear model [48]. Another reason may simply be that it is expensive or impossible to manipulate an input to achieve a certain level of power. A building-related example of the latter could be the maximum power output of the heating system that is used to excite the building. In cases where such limitations exist, the type of signals that are imposed during measurement experiments are often chosen with the *crest factor* in mind. The crest factor (C_r) describes the ratio between the peak amplitude and the root mean square of a given signal (u) [36], and is defined by Eq. (3.1).

$$C_r = \frac{\max_t(u(t) - \bar{u}(t))}{\lim_{n \rightarrow \infty} \frac{1}{N} \sqrt{\sum_{t=1}^N u^2(t)}} \quad (3.1)$$

In a more applied sense, the crest factor describes the input power obtainable through a given signal confined to a certain maximum amplitude – the lower the crest factor the higher the power (variance). PRBS signals also excel in this sense, since these signals are characterized by the lowest possible crest factor. From a theoretical standpoint, these properties of PRBS signals make them ideal for (linear) building modelling applications, where the presence of occupants poses a significant challenge to the efforts of ensuring a high SNR. The reason for this is that occupants limit the input power due to comfort considerations, and at the same time generate noise through their metabolism and other activities that affect the heat balance of the building such as venting or use of appliances.

Because of these observations, thesis objective **1.1** is concerned with the question of whether a sufficiently high SNR can be achieved in occupied buildings without causing the occupants to feel thermal discomfort. The paper in the following section presents an analysis of this topic. Due to significant differences in the layout of this thesis and the conference proceedings in which the paper was published, the paper is reproduced here in a format more in line with the rest of this thesis.

Identifying a Comfortable Excitation Signal for Generating Building Models for Model Predictive Control: A Simulation Study

Rasmus Elbæk Hedegaard^{#1}, Theis Heidmann Pedersen^{#2}

Michael Dahl Knudsen^{#3}, Steffen Petersen^{#4}

[#]Department of Engineering, Aarhus University
Inge Lehmanns Gade 10, 8000 Aarhus C, Denmark

¹ reh@eng.au.dk, ² thp@eng.au.dk ³ mdk@eng.au.dk, ⁴ stp@eng.au.dk

Abstract

Model predictive control (MPC) uses mathematical models of the building to plan HVAC operation. One way of obtaining models is to use statistical methods to derive models from building measurement data. This data is typically collected through excitation experiments that impose temperature fluctuations on the building to reveal information on the buildings thermal dynamics. This paper investigated the trade-off between occupant comfort during excitation experiments and the quality of the resulting model. The results showed no clear tendency of higher model quality with increasing experiment strength. Implementation of models with varying accuracy in an MPC algorithm showed similar heating patterns and achieved cost savings during operation. None of the experiments violated the comfort requirements which indicate that expedient grey-box models for MPC can be obtained without annoying occupants when generating data for calibration of the model.

Keywords - Model Predictive Control, Building models, Occupancy comfort, Excitation signals.

1 Introduction

In the pursuit of increasing energy efficiency and flexibility, a number of model-based control schemes are beginning to emerge in building automation. One of the most prevailing approaches is model predictive control (MPC). An important part of MPC algorithms is the mathematical building model which is used to predict how the building response to stimuli such as changing weather conditions, internal heat loads and the operation of the heating, ventilation and air conditioning (HVAC) system [1] [2]. While these building models can be derived based on knowledge of physics, a more common approach is to derive models using statistical methods. Such methods, also referred to as *system identification*, are either used to calibrate grey-box models or to create black-box models to reproduce the behavior of the system being modelled [3]. Statistical approaches to building modelling rely on measurement data from the actual building to estimate (black-box) or fine-tune (grey-box) the model parameters. To obtain this data, an experiment that imposes temperature fluctuations on the actual building is carried out. The general theory is that these fluctuations must excite the system in question to a degree that data reveals the dynamic properties of the system [4]. As stated in [5], fitting models intuitively amounts to explaining variations in the output of the system. This task becomes increasingly difficult as the ratio between the known signal and the unknown noise decreases. This is probably why previous experiments exited buildings with temperature fluctuations far beyond normal indoor environment conditions [6] [7]. Such experiments are, however, infeasible if complex model-aided HVAC controls are ever to enter the residential building sector since the extreme indoor climate would force occupants to leave their homes during experiments. The aim of this study is to investigate whether suitable models for MPC can be obtained through low thermal comfort-impacting experiments.

2 Methods

The following sections present the methodology used to generate and evaluate results as well as important assumptions regarding model structure, input design and the presence of noise. Overall, the study is based on the co-simulation principle. The actual building is modelled in EnergyPlus [8] while a MATLAB program handles the MPC operation of the heater in the EnergyPlus model. The two programs are coupled with the Building Controls Virtual Test Bed [9].

2.1 Model structure

The model used in this study can be categorised as grey-box models. Grey-box models are characterized by having a predefined structure of physically meaningful parameters, such as the U-value of the building envelope or the g-value of the windows. These parameters are coupled with the principles of thermal dynamics to derive differential equations that describe the temperature conditions in the building, and thus how the building responds to the operation of HVAC-equipment, occupants and weather conditions. The model structure used in this study has two lumped capacities: one for the room air and one for the building construction. The model takes solar heat gains, outdoor temperature and heating from the HVAC system as input. Fig. 1 depicts the used model structure, which is a modification of the model presented in [10].

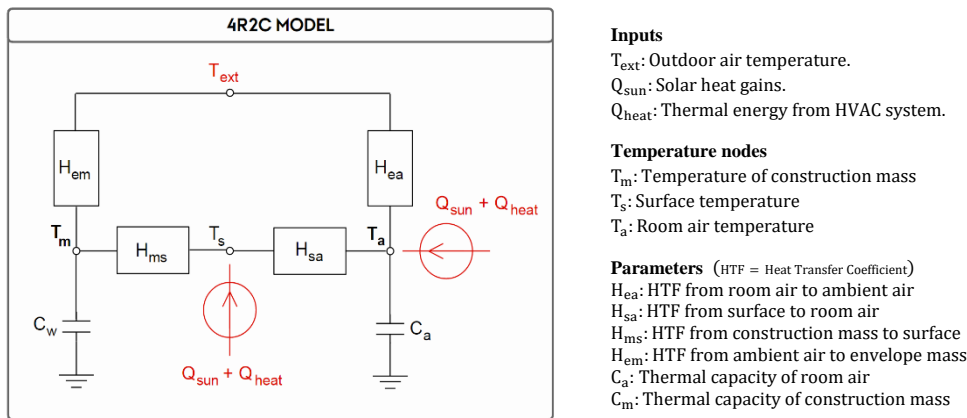


Fig. 1 Model structure and coefficient nomenclature.

With the model structure being fixed, the task of the system identification process is to determine the values of the coefficients in the model.

2.2 Artificial noise generation

Excitation experiments are carried out to lower the impact of noise on the system identification process. This study would therefore not be meaningful unless there is some noise involved. A simple method for generating random noise in an expected occupancy-related heat load profile in a building is therefore developed. The noise is generated in two steps:

- The times at which occupants arrive or leave home are randomized using the uniform distribution. Uncertainty varies depending on time-of-day with occupant arrival in afternoons being characterized by the highest uncertainty.
- Random fluctuations are added to emulate the opening of windows and use of electronic equipment. The fluctuations are created using a combination of a random walk and a moving average filter.

Fig. 2 shows an example of how the noise model affects a static occupancy profile. It is clear how the developed noise model retains some of the occupancy patterns that is expected to occur in residential buildings, but alters both the duration and times at which heat loads occur.

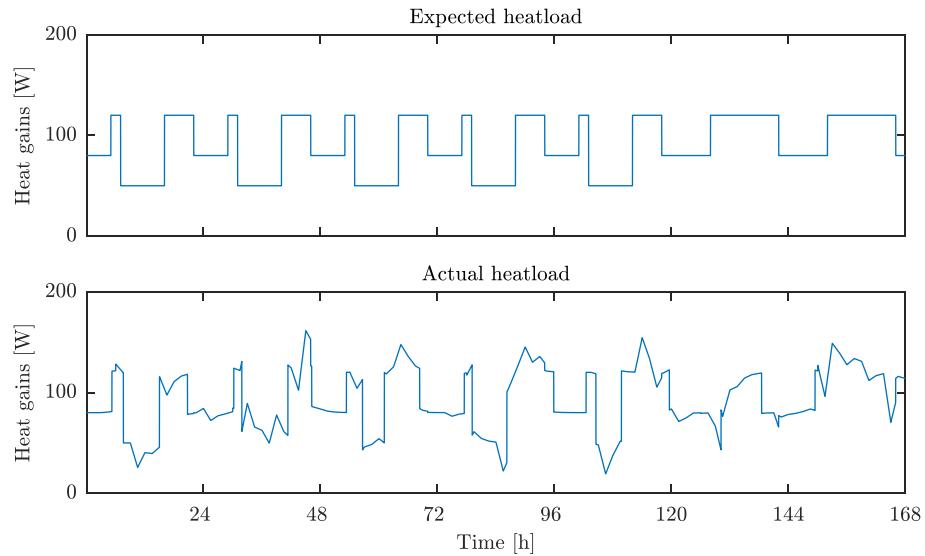


Fig. 2 Top: Expected heat load based on 24-hour static schedules. Bottom: Actual heat load, i.e. noise added to the static profile using the developed noise generator.

In this study, a total of five different noise sequences were generated and used in simulations to ensure that conclusions are not based on mere coincidence generated with the noise model. The actual heat load (Fig. 2, bottom) is the one used in the EnergyPlus simulation to represent the actual heat load in the building.

2.3 Experimental Design

The design of the excitation sequence is based on the methodology for designing common input signals in multivariable systems presented by Gaikwad and Rivera [11]. Buildings are good examples of such systems since room air and furniture are characterized by relatively low time constants while the buildings thermal mass can have a time constant spanning over several days. The type of input sequence chosen for this study is the pseudo random binary signal (PRBS). The PRBS signal has advantages that makes it a widely used for excitation experiments. First of all, since PRBS signals are deterministic, they can be designed specifically to fit the system to be identified in terms of the frequency content [11]. Furthermore, PRBS signals are persistently exciting which means that they excite the system on many different frequencies [4]. Because of this, even the properties of complex systems containing several different time constants can be identified. The user-specified parameters of the signal design process are shown in Table 1. For the remaining steps of the signal design process, see the original paper [11].

Table 1. Design values used in the design of the input signals

α -value: Determines signal high-frequency content.	0.25	[-]
β -value: Determines signal low-frequency content.	3	[-]
Sampling time (simulation timestep)	60	[s]
Lowest (fastest) time constant	6	[min]
Highest (slowest) time constant	160	[h]

In the following, the term *experiment strength* will refer to the size of heating fluctuations occurring during the experiment. Four different input signals with identical mean heat

loads are generated. The upper and lower bound of each excitation signal and their respective signal-to-noise ratio are shown in Table 2.

Table 2. Experiment designs. Mean value of all experiments is 120 W. SNR-values are calculated using the normalized signal (PRBS+Expected occupancy) and the noise (Expected occupancy-Actual occupancy).

Experiment	PRBS 1	PRBS 2	PRBS 3	PRBS 4
Heating load bounds [W]	90 – 150	60 – 180	30 – 210	0 – 240
Signal-to-noise ratio [dB]	3.4	7.7	10.8	13.2

2.4 System Identification Methodology

The process of estimating the parameters of the grey-box model is carried out using the System Identification Toolbox in MATLAB. Fig. 3 gives an overview of the methodology to generate data and identify models used in this study.

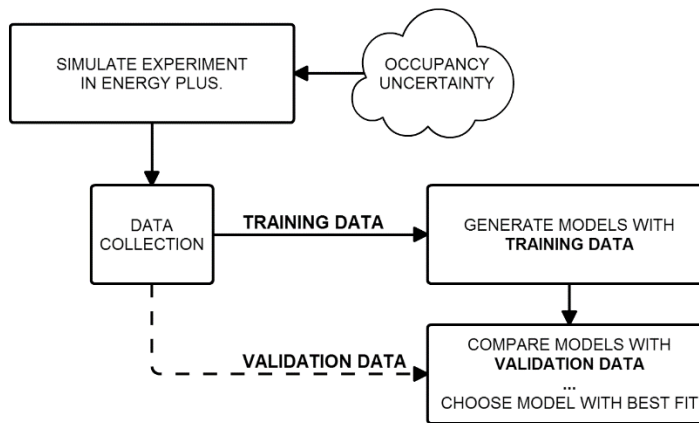


Fig. 3. System identification methodology (Hold-out cross-validation).

The method uses one subset of the data to train several models, while the other is used to validate model performance and find the best model. This approach is often referred to as hold-out cross-validation. In this study, five models are identified with each experiment. Both data subsets are affected by the presented noise model.

2.5 Case Building

The analysis is carried out on a dorm apartment built according to the Danish low-energy 2015 building standard. The apartment has a 2.55 m² south facing window with a U-value of 1.1 W/(m²K). One façade is facing the outside, while all other room boundaries are considered adiabatic. The heat source is an electric radiator. As seen in Table 3, the apartment is characterized by heavy construction elements, most of which consist of concrete. The EnergyPlus model was created by Knudsen in [12].

Table 3. Construction elements and material properties used in the EnergyPlus model [12].

	Material	Thickness [m]	Resistance [m ² K/W]	Capacity [kJ/(m ³ K)]
External wall	Concrete (ext.)	0.100	0.09	736
	Insulation	0.250	6.76	52
	Concrete (int.)	0.200	0.18	736
Internal wall	Concrete	0.180	0.16	736
Ceiling/ Floor	Wood floor	0.025	0.17	991
	Air space	0.050	0.10	
	Concrete	0.220	0.20	736

3 Results and Discussion

This section presents the results from the model fitting process using the different PRBS signals and how they affect thermal comfort, model quality, and model effectiveness in relation to MPC.

3.1 Occupant Comfort During Experiments

For simplicity, this section only evaluates the impact on comfort of the low-strength *PRBS1* experiment and the high-strength *PRBS4* experiment. Fig. 4 shows the amplitude of the excitation signals and their impact on room air and operative temperatures, respectively.

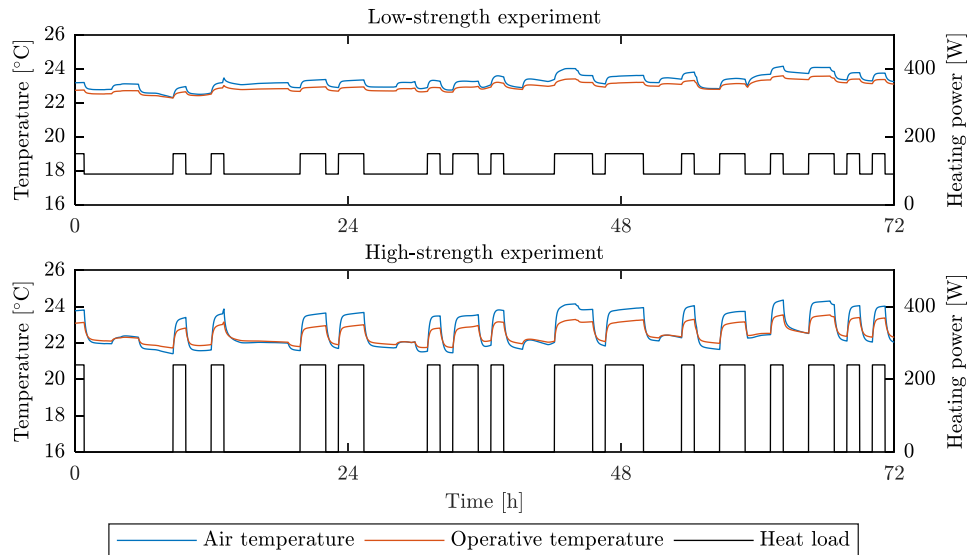


Fig. 4 Comparison of low- and high-strength experiments. Top: PRBS1, Bottom: PRBS4.

Fig. 4 shows how both experiments keep the temperature levels within the typical thermal comfort boundaries used in buildings (20-26 °C). It is thus not the temperature itself that may give rise to occupant discomfort but rather the rate of change of the temperature as the heating power fluctuates.

Several studies have been carried out to determine the impact of transient thermal conditions in the indoor environment, but with contradicting conclusions [13]. ASHRAE requirements for the maximum allowable rate of change of operative temperatures [14] are used in this study, see Table 4. The 15 minute-requirement is considered to be the strictest of the requirements during PRBS experiments. This is because the PRBS signal essentially produces series of step responses with short but high temperature rate of change. Inspection of the simulation data, however, revealed that the high-strength experiment only comes close to violating the 15-minute requirement with a maximum rate-of-change of 0.94 °C.

Table 4. ASHRAE requirements on thermal drifts and ramps compared to experiment data.

Duration of temperature increase	0.25 h	0.5 h	1.0 h	2.0 h	4.0 h
ASHRAE limits [K]	1.10	1.70	2.20	2.80	3.30
PRBS1 max rate-of-change [K]	0.39	0.57	0.68	0.80	0.88
PRBS4 max rate-of-change [K]	0.94	1.24	1.4	1.49	1.51

As mentioned in section 2.5, the dormitory apartment consists of heavy construction elements, which effectively dampens the temperature fluctuations. The same experiment may impact light-weight buildings more severely.

The results presented here should be interpreted in light of the assumptions that typically apply to the use of building performance simulation programs: The source of heat is modelled as a fully convective source of heat, and the heat is assumed to be distributed evenly throughout the whole apartment. In actual buildings both the radiative and convective contributions from radiators will affect the near vicinity more than more distant parts of the room. Whether this effect is enough to cause discomfort is not treated in this study.

3.2 Model Quality

Model quality is evaluated through the commonly used normalized root mean square error (NRMSE) goodness-of-fit metric. Prior to the analysis two new terms are introduced; the *realistic fit* and *benchmark*. Fig. 5 clarifies the terminology and can be seen as an extension to the methodology depicted on Fig. 3.

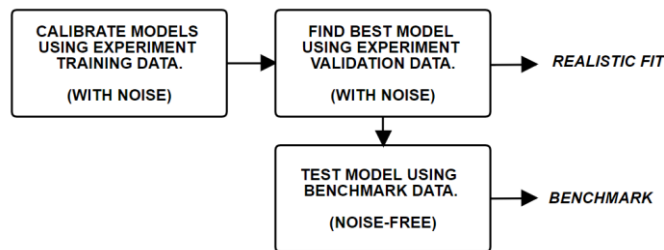


Fig. 5 Methodology of assessing model quality

The *realistic fit* is the only of the two measures of model quality that can be obtained in real-world applications. The data used to calculate the *benchmark fit* does not stem from the experiments simulated, but a noise-free simulation of the EnergyPlus building using several different excitation signals as well as periods of constant heat load. The dataset were designed to expose the models to both high-frequency and low-frequency signals to thoroughly test the models.

Six different occupancy profiles were used in the simulation. All of them are based on the same expected occupancy profile, but five of them have been altered by the noise model (see section 2.2). For each occupancy profile, four different experiments were carried out and used to identify models. The NRMSE-fits of the resulting models on experiment and benchmark data respectively are shown on Fig. 6.

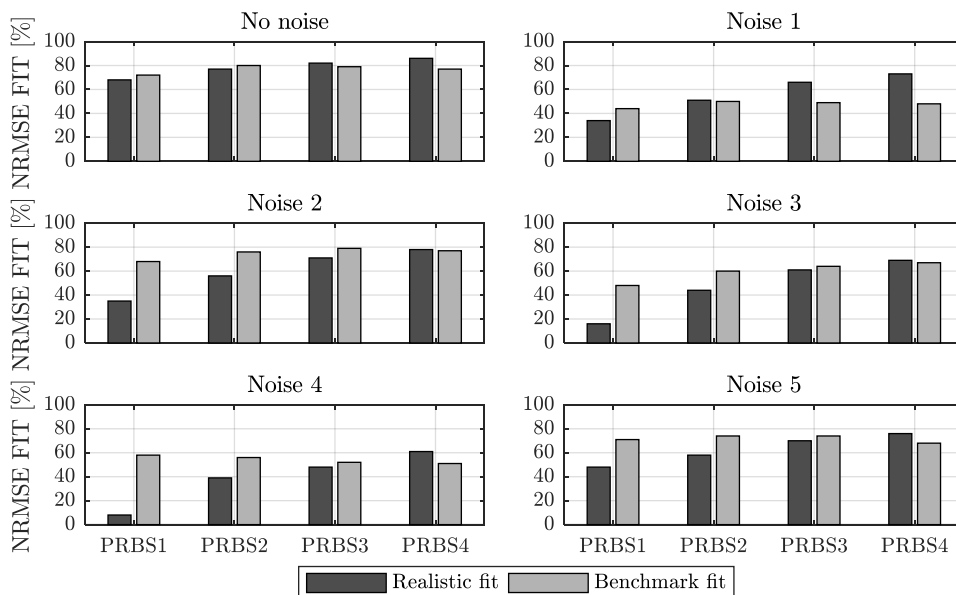


Fig. 6 Comparison of model accuracy on different noise realizations. Prediction horizon: infinite

The *realistic fits* show a clear tendency of model quality improvements as the experiment strength is increased. The benchmark fits, which are much better estimates of model quality, showed that only in a few cases the increased experiment strength actually provided better circumstances for deriving models. During identification using one of the occupancy profiles the benchmark fits were even seen to decrease with experiment strength – despite the *realistic fit*-values indicating the opposite. The decline in benchmark fit is most likely a coincidence but the result is still highly relevant in this discussion as it highlights the fact that using normalized fits during model validation should be carried out with caution.

The NRMSE-fit, or other normalized fit metrics, are often used as they give a dimensionless rating of model accuracy which is easily interpreted. Furthermore, it seems logical to view model residuals in the context of how large of an interval the data spans. The use of such fit metrics, however, becomes problematic when they are used as a basis for designing experiments. This is because using normalized fits essentially favours highly fluctuating experiments because of the way it is calculated [15] – a tendency clearly shown in the results presented here. This characteristic of the NRMSE-fit means that it could easily be interpreted as incentive for increasing the strength of the experiments more than needed. Based on the tendencies of model-fits seen in Fig. 6, low-strength experiments – which are less likely to introduce occupant discomfort – may be sufficient to derive suitable building models.

3.3 Model Effectiveness

In this analysis, a selection of the models estimated in section 3.2 was tested as part of an economic MPC algorithm to investigate the control scheme’s robustness to model inaccuracies. The effectiveness of a model is evaluated as the MPC’s ability to generate savings by exploiting varying electricity prices compared to a traditional PID controller, and ability to maintain room air temperature above a specified set point of 21 °C.

The Nord Pool electricity spot price [16] is used as the cost of space heating. The MPC prediction horizon is six days and the time step is one hour. A Kalman filter is used to introduce feedback in the control scheme. Danish design weather data is used in the simulation [17]. Table 5 presents the results from a 45-day simulation using three of the models generated in the last section. The MPC algorithm used is further presented in [12].

Table 5. Model performance as part of an MPC algorithm. Fits on noise-free benchmark data.

Realistic/Benchmark fits	Time below 21 °C	Min./Mean temp.	Cost reduction
27 / 52%	1.55%	20.94 / 22.42 °C	7.75%
46 / 66%	26.40%	20.49 / 22.22 °C	9.22%
77 / 81%	4.87%	20.80 / 22.39 °C	8.15%

It is seen that the model fit value says very little about whether a model is sufficiently accurate to carry out MPC. Visual inspection of model fits during system identification showed that all of the models were able to describe the building’s dynamic behavior reasonable well, but that lower-fitting models had a tendency of slowly diverging from the measurement data. In such scenarios, state estimators such as the Kalman Filter becomes very useful as they keep track of inconsistencies between the temperatures of the model and measurements in the buildings and applies corrections. This ensures that each prediction carried out during MPC operation has a reasonable set of initial conditions which is vital for efficient model-aided control.

The results in Table 5 shows that the model with 66 % fit on benchmark data caused small but frequent violations of the prescribed temperature set point, which in term resulted in higher savings on space heating. These differences are, however, considered to be

relatively low – just as the comfort violations are considered to be of too small magnitude and/or duration to be considered critical.

4 Conclusion

This simulation-based study investigated the necessity for conducting high-strength excitation experiments to derive models suited for model predictive control of heating systems in buildings. Mathematical models were identified using data from the simulated experiments. No clear tendency of better model fits with increasing experiment strength was found which suggests that the quality of measurement data was sufficient in all of the experiments. The NRMSE fit, however, was unable to indicate this, as fit values of low-strength experiments were found to be much lower than those achieved using high-strength experiments. This suggests a pitfall in system identification that may lead to experiments being designed with unnecessarily high temperature fluctuations. All models performed satisfactory in terms of thermal comfort but due to general simplifications made in building performance simulation programs, further research on this topic is needed (e.g. physical experiments in climate chambers). Finally, simulations where low-fit models were used to perform economic MPC showed the control scheme to be robust to model inaccuracies both in terms of the achieved cost savings and in terms of maintaining the prescribed set point. Depending on how realistically the noise model developed in this study reproduced the disturbances occurring in actual buildings, these results suggest that sufficiently accurate models can be derived from relatively subtle excitation experiments. Future research could be to investigate performance of other building scenarios, and carry out similar analysis using an actual building instead of an EnergyPlus model.

5 References

- [1] S. Prívvara, J. Cigler, Z. Vána, F. Oldewurtel, C. Sagerschnig, E. Záčeková. Building modeling as a crucial part for building predictive control. *Energy and Buildings* 56 (2013) 8-22.
- [2] Y.-G. Xi, D.-W. Li, S. Lin. Model Predictive Control - Status and Challenges. *Acta Automatica Sinica* 39(3) (2013) 222 - 236.
- [3] A. Afram, F. Janabi-Sharif. Review of modeling methods for HVAC systems. *Applied Thermal Engineering* 67 (2014) 507-519.
- [4] L. Ljung. *System Identification - Theory for the user*, 2nd edition, New Jersey (USA): Prentice Hall PTR, 1999.
- [5] A. K. Tangirala. *Principles of System Identification - Theory and Practice*, Boca Raton: CRC Press, 2015.
- [6] P. Bacher, H. Madsen. Identifying suitable models for the heat dynamics of buildings. *Energy and Buildings* 43 (2011) 1511-1522.
- [7] G. Fraisse, C. Viardot, O. Lafabrie, G. Achard. Development of simplified and accurate building model based on electrical analogy. *Energy and Buildings* 34 (2002) 1017-1031.
- [8] U. S. Department of Energy. EnergyPlus.net [Online]. Available: <https://energyplus.net/>. [Visited 29 01 2016].
- [9] M. Wetter. Co-simulation of building energy and control systems with the Building Controls Virtual Test Bed. *Journal of Building Performance Simulation* 4(3) (2001) 185-203.
- [10] T. R. Nielsen. Simple tool to evaluate energy demand and indoor environment in the early stages of building design. *Solar Energy* 78 (2005) 73-83.
- [11] S. V. Gaikwad, D. E. Rivera. *Control-Relevant Input Signal Design for Multivariable System Identification: Application to High-Purity Distillation*. San Francisco, 1996.
- [12] M. D. Knudsen, R. E. Hedegaard, T. H. Pedersen, S. Petersen. Model Predictive Control of Space Heating and the Impact of Electricity Taxes on Demand Response: A Simulation Study. In *Clima 2016 Conference*, Aalborg, Denmark, May 22-25 2016.
- [13] J. L. M. Hensen. Literature review on thermal comfort in transient conditions. *Building and Environment* 25(4) (1990) 309 - 316.
- [14] ASHRAE. *Standard 55-2010: Thermal Environmental Conditions for Human Occupancy*. ASHRAE, Atlanta, 2010.
- [15] Mathworks. Compare function. [Online]. Available: <http://se.mathworks.com/help/ident/ref/compare.html>. [Visited 31 01 2016].
- [16] Nord Pool. Day-Ahead Market Elspot. [Online]. Available: <http://www.nordpoolspot.com/TAS/Day-ahead-market-Elspot>. [Visited 24 01 2016].
- [17] U.S. Department of Energy. Copenhagen Weather Data download [Online]. Available: https://energyplus.net/weather-location/europe_wmo_region_6/DNK//DNK_Copenhagen.061800_IWEC. [Visited 29 01 2016].

3.2 Epilogue

The purpose of this analysis was to investigate the trade-off between the conflicting objectives of maintaining a comfortable indoor environment during experiments and obtaining models of sufficient accuracy. While all experiments used a PRBS input signal, the amplitude of the signal was varied between experiments to generate data with different signal-to-noise ratios. Each experiment was repeated multiple times under different realizations of noise generated with a simple occupancy model, and models were identified using the obtained input-output data. The quality of these models was evaluated both on their predictive capabilities using validation data, and on their impact on the performance of an economic MPC scheme. The results indicated no clear tendency for the model quality to improve when the amplitude of the PRBS signals was increased. Furthermore, the MPC scheme was found to be relatively robust to model deficiencies, since acceptable performance was achieved even when it was implemented using the poorest performing model. Further inspection of the results suggested that the nature of the prediction errors in an MPC context could be even more important than the size of the prediction errors.

The term *model quality* used in the paper is clearly a broad term that covers a wide range of model deficiencies. These deficiencies may affect the ability of the model to describe the thermodynamic characteristics of buildings under steady-state or dynamic conditions. A steady-state prediction bias results in a prediction error that grows as the prediction horizon increases. On the other hand, a poor estimate of the dynamic properties of the building affects the ability of the model to describe dynamic transitions as well as its ability to account for thermal energy being stored and discharged from the thermal mass of the building. In the context of MPC schemes, a steady-state prediction bias is less problematic than a poor representation of dynamic properties. This is because Kalman filters [49] are typically used in MPC schemes to continuously estimate the current state of the model using measurements from the building. Since this feedback does not allow the state of the model to *drift away* from the state of the actual building, it ensures that the predictions made by the control scheme are always made with a reasonable initial state of the model. This, in turn, ensures that the short-term prediction errors are kept to a minimum. The differences in the impact of these two types of model deficiencies were not treated further in the analysis. Therefore, a more detailed analysis on how such deficiencies impact the control performance of MPC schemes, and how they may be addressed through experiment design, are considered relevant topics of future research.

In a more recent study (S7) on experiment design, we investigated through a similar analysis whether the PRBS signal used in the experiments here could be substituted with a signal that was more representative of MPC operation. One of the guiding principles of experiment design is that the resulting input-output data should reflect the conditions under which the model is to be used in its intended application [48]. Therefore, we proposed simply implementing an MPC scheme with an un-calibrated model, and generating the input-output data by allowing the MPC scheme to impose temperature fluctuations by engaging in load shifting. An advantage of the MPC data was that the temperature fluctuations imposed on the building were less frequent than in the PRBS-approach, and therefore considered less likely to cause occupant discomfort during the initial experiment period. The analysis showed that the models obtained from the MPC data performed similarly to models generated by an experiment in which a PRBS signal were used.

The fact that both of these studies relied purely on simulations and therefore applied several assumptions, calls for further research to assess the generality of the conclusions drawn. In addition to the assumed occupancy model, the most significant assumptions were the assumption of adiabatic internal walls; a fully mixed indoor air temperature distribution; and finally, the use of transmitted solar heat gains instead of a more realistic input such as measurements of global radiation on a horizontal plane. With these assumptions in mind, the analyses of both studies indicate that models of sufficient accuracy can be obtained from input-output data created under conditions that do not impose significant discomfort on occupants. The analysis presented in the following chapter applies this result in a comparative evaluation of the suitability of different grey-box model structures.

4 MODEL STRUCTURE SELECTION

Grey-box models representing the thermodynamic behaviour of buildings typically model these phenomena as a network of resistances, capacities, energy sources and energy sinks. Because they primarily consist of these components, these models are often referred to as *RC models* or *RC networks*. Usually, a lumped parameter approach is used to reduce the order of these models, which eases both the task of identifying the parameters of the model and simulating it. The optimal complexity of a particular RC-model may vary significantly depending on the intended application of the model. In the simplest models, a thermal capacity and resistance may represent an entire thermal zone, while more detailed models use multiple resistances and capacities to represent individual structural components alone. The choice of complexity (order, layout) of an RC model affects both the identifiability of model parameters, their interpretability, and the predictive performance of the model itself.

Only a few studies comparing several model structures were identified in previous literature: Reynders et al. [50] evaluated RC-models of varying complexity in terms of their predictive performance and their ability to produce accurate estimates of building characteristics through system identification techniques. The authors concluded that models of low orders (2nd and 3rd order) resulted in high uncertainties associated with the parameter estimates, and therefore preferred 4th and 5th order models instead. Harb et al. [51] presented a similar analysis in which models ranging from 1st to 3rd order were evaluated. In this case, the authors found the 2nd order model superior to the other models investigated. Finally, Bacher and Madsen [52] applied a forward modelling approach and likelihood ratio tests to identify suitable model structures. The approach indicated that expanding the model structure from the initial 1st order model resulted in statistically significant improvements until a 4th order model was reached. Furthermore, residual analysis and the physical meaningfulness of parameter estimates indicated that models of 3rd order and above were preferable.

In addition to the many case-specific details which inevitably differ between such studies, possible reasons for the discrepancies between the conclusions drawn in previous work are differences in the used input-output data as well as differences in the layout of the RC components of each of the evaluated model structures. In terms of data, Reynders et al. [50] used data simulated with detailed building energy models to avoid the inevitable uncertainties and noise associated with measurements from actual buildings, while both Harb et al. [51] and Bacher and Madsen [52] used data measured in actual buildings. Furthermore, only the forward modelling method applied in [52] explicitly addressed the possibility of the drawn conclusions being affected by the chosen layouts of the proposed RC-networks. Due to the discrepancies between the conclusions drawn in previous studies, additional research aimed at identifying suitable grey-box model structures for modelling the thermodynamic characteristics and behaviour of buildings is needed.

The following paper presents an evaluation of four simple grey-box model structures, and constitutes the published research of this thesis that contributes to research objective **1.2**. Due to paper size limitations, several relevant details were left out. These are laid out in the section following the article itself.



Available online at www.sciencedirect.com

ScienceDirect

Energy Procedia 132 (2017) 982–987

Energy

Procedia

www.elsevier.com/locate/procedia

11th Nordic Symposium on Building Physics, NSB2017, 11-14 June 2017, Trondheim, Norway

Evaluation of Grey-Box Model Parameter Estimates Intended for Thermal Characterization of Buildings

Rasmus Elbæk Hedegaard^{a*}, Steffen Petersen^a

^a*Department of Engineering, Aarhus University, Inge Lehmanns Gade 10, 8000 Aarhus C, Denmark*

Abstract

The ability to obtain reliable estimates the actual thermal characteristics of whole buildings through fitting dynamical resistance-capacitance grey-box models to measurement data was investigated. The actual total heat loss coefficient was identified with a maximum deviation of 4% for all the evaluated model structures. The best performing models tended to overestimate the effective thermal mass by 10-32 % compared to the Effective Thickness Method of ISO 13786. The results also indicated that identifying the distribution of the total heat loss into transmission and infiltration heat losses is unlikely to be achieved from typical building measurement data.

© 2017 The Authors. Published by Elsevier Ltd.

Peer-review under responsibility of the organizing committee of the 11th Nordic Symposium on Building Physics.

Keywords: System Identification; Building thermal characterization; Model structure selection; Identifiability analysis; Estimation of heat losses.

1. Introduction

Estimation of actual thermodynamic characteristics of real buildings is relevant for many purposes, e.g. for energy labelling and verification of the desired effect of energy saving measures in new as well as renovated buildings. Several methods for this purpose already exist, which in general can be characterized as 1) local methods focusing on individual building components, and 2) methods that seek to characterize the building as a whole. Standardized local methods for characterizing the performance of building envelope walls are specified in ISO 9869-1:2014 [1]. These methods rely on measurements of the internal and external temperature conditions and heat flux, usually measured at the internal surface of the component. The ISO standard presents both a quasi-stationary method and a dynamic

* Corresponding author. Tel.: +45 61707378.

E-mail address: reh@eng.au.dk

method; however, a recent study suggests that the dynamic method gives better estimates of the U-value when compared to theoretical values [2]. Whole-building thermal characteristics can be inferred through co-heating tests which rely on linear regression and measurement data from the building under quasi-stationary heat loss conditions to provide reliable estimates of the whole-building heat transfer coefficient [3]. A limitation of co-heating tests is the neglect of dynamic characteristics. Another more practical limitation is the need of a fairly long measurement periods; the recommended duration of co-heating experiments as specified in IEA EBC Annex 58 is 2-4 weeks [4], while a recent study concluded that newer and more insulated buildings need up to eight weeks [5]. Everett [6] list other factors that complicate the analysis such as solar gains, varying air infiltration rate, ground floor losses and shared walls. Dynamic methods have also been proposed for whole-building characterization. A common approach is to model the dynamic heat transfer in the building as resistance-capacitance (RC) networks and then fit the model parameters to experimental data. This approach is in many aspects opposite from the quasi-stationary co-heating test. A major difference is that instead of seeking stationary conditions, emphasis is put on exciting the building during the measurement campaign to reveal the transient thermodynamic behaviour in the measurement data. Studies have previously evaluated the use of different RC models for data-based whole-building characterization. Reynders et al. [7] evaluated RC models of different complexity ranging between first order and fifth order models, and came to multiple conclusions: Low-order models (third order and below) were concluded to be too simple to obtain reliable estimates while fourth and fifth order models were found to be of sufficient complexity, but came with the significant price of needing heat flux measurements in addition to temperature measurements in order to be identified. Harb et al. [8] evaluated low-order RC-models on their ability to give acceptable estimates and predictive performance without any prior knowledge of the building. Two models included in the analysis showed reasonable predictive performance, while only a second order model yielded parameter estimates considered plausible by the authors. Thus, the studies of Reynders et al. [7] and Harb et al. [8] present significantly different answers to the question of which type of reduced-order RC model structure that is suitable for data-based characterization of the thermal characteristics of buildings. The discrepancies between the two conclusions could potentially be caused by identifiability issues during the selection of model structures.

On this background, the goal of this study is to derive model structures that only rely on temperature measurements to identify the building dynamics and quantify various characteristics relating to the thermodynamic behaviour of buildings. To further improve the robustness and practical application of such models, special attention is devoted to evaluating simple models that reduce potential identifiability issues.

2. Method

The goal of this study is to identify robust model structures suitable for characterization of the thermal characteristics of real buildings. Simulations are used to ensure the availability of high-quality data. The simulation platform consists of the building performance simulation program EnergyPlus and MATLAB, coupled via the Building Controls Virtual Test Bed [9]. Two geometrically different apartments are modelled in EnergyPlus, and data collected from the thermal zones and environment is used to identify models with the MATLAB System Identification Toolbox. The two apartments are 93 m² and 50 m², respectively. Further details on the two case apartments are provided in ref. [10]. The model structures included in the analysis undergo identifiability analysis using MATLAB and DAISY [11]. The following sections provide more details on the method used.

2.1. Reference estimates

The thermal characteristics of the apartments are estimated through widely used methods defined in standards and compared to the estimates resulting from using different model structures. Heat losses expressed as heat transfer coefficients (equivalent to UA-values) are calculated from material properties, construction element composition and standard values for internal and external surface resistances as specified in ISO 6946 [12]. Infiltration heat loss is calculated directly from zone volume and air change rate. Heat loss through windows are calculated using the U-value for the entire window component as calculated by Window 7.4 [13], which was used to model the windows in the EnergyPlus model. The effective thermal capacity is estimated using the Effective Thickness Method of ISO 13786 Annex A [14]. Despite the fact that the heating system during the experiment period introduced smaller temperature

fluctuations in the building, the period of variation defined in the standard is chosen to be 24 hours because the data spans several days and therefore include a natural day-night variation. The total thermal mass capacity is calculated as half the thickness of symmetrical internal walls separating thermal zones and all mass before the first layer of insulating material in other parts of construction parts. In addition to the abovementioned characteristics, it is interesting to evaluate whether dynamic modelling can distinguish between infiltration and transmission heat losses. If the environment surrounding the building gets colder these heat losses will naturally increase. For the opaque parts of the envelope, this increase in transmission heat loss is delayed as the envelope components with high thermal inertia cool down. Infiltration, on the other hand, is not characterized by any significant thermal inertia, and can thus be considered instantaneous. These differences in how changing weather conditions affect the measurements makes it, at least in theory, possible to distinguish between the two heat loss mechanics. Windows, however, complicate this task. On one hand, the thermal mass of the window is small compared to the rest of the envelope, which is why windows are typically modelled without mass in building energy performance simulation tools such as EnergyPlus [15]. Consequently, there is no delay as for the opaque (heavy) envelope components. The inner glass pane absorbs heat through long-wave radiation and convection. The convective part affects the room air temperature directly, and is thus often assumed to be a part of the infiltration rather than transmission heat loss. The radiative part receives a net gain of heat from other surfaces inside the zone, thereby affecting the temperature of the thermal mass. This part of the heat loss is therefore assumed to exhibit some of the same inertia as transmission losses. Following this distinction, the question is how to distribute the total heat loss through windows onto these two heat loss mechanics and thereby determine the equivalent transmission and infiltration heat loss coefficients of the system that include the contribution to heat loss from windows. In this paper, we assume this distribution corresponds to the fractions of convective and radiative heat transfer coefficients of uncoated soda lime glass as defined in EN 673 [16]. It is noted that this assumption does not affect the modelling procedure as it is only used to derive the reference measurements used for comparison. The calculated thermal characteristics of the apartments are shown in Table 1.

Table 1 White-box estimates of thermal characteristics

		Large apartment		Small apartment	
Capacities	Air capacity	2.93E+05	J/K	1.57E+05	J/K
	Total interior mass capacity	1.49E+07	J/K	7.89E+06	J/K
	Effective mass capacity (ISO 13786)	1.26E+07	J/K	6.71E+06	J/K
Heat loss coefficients	Envelope (opaque parts)	22.7	W/K	6.4	W/K
	Windows	49.9	W/K	35.8	W/K
	Infiltration	40.7	W/K	21.8	W/K
	Total heat loss	113.3	W/K	64.1	W/K
Equivalent heat loss	Transmission	49.30	W/K	25.52	W/K
	Infiltration	64.03	W/K	38.57	W/K

The dynamic characteristics such as the thermal inertia of the heavy elements in the building is also relevant to identify. From a comfort point of view, the thermal mass can reduce temperature fluctuations caused by internal or external gains throughout the day. Furthermore, the thermal inertia is also directly linked to the potential for storing energy in the building, which ties into research on the flexibility of buildings and demand response. However, since the active thermal capacity is not a static parameter in the same way as the resistance of most building components can be assumed to be, a methodology for comparing the ISO 13786 estimates with the RC-estimates is needed. One approach is to compare the capacity estimates of the model to the reference value directly. This method, however, seems impractical since the layout of resistances and capacitances in the model affects the estimates of the capacities significantly. Instead, the time constants of the models are used to calculate an effective mass using the assumptions of the lumped capacitance approach, where the estimate of the thermal mass is obtained by multiplying the time constant with the total heat loss coefficient. The capacitance estimate of the air-node is not sensitive to the specific model layout, and is thus compared directly to the reference value. In practice, this estimate will also contain the capacitance of the heating system and furniture, but this influence is outside the scope of this study. Finally, it should be noted that the estimate of the small capacity will rely on the chosen sampling time.

2.2. Model structures

EN ISO 13790 suggests a single-capacity RC-model in the simple hourly method for calculating the heating and cooling needs of buildings [17]. However, this study does not include single-state models for several reasons. While the assumptions of the ISO 13790 model related to the temperature of the zone air may be sufficiently accurate when estimating energy performance under fairly constant temperature conditions, it is not sufficient in the case of changing set points and fluctuating heating output. A sudden step in heating power from fast-response systems such as radiators and convectors will result in an initial fast temperature increase as the air heats up followed by a slower response as the capacity of the construction is activated. A single state model is unable to predict or simulate the combined response from these very different capacities. Finally, first-order models have been shown to have too low predictive performance [7]. For these reasons, this study investigated a simple second-order model which was expanded upon using a forward modelling approach. The resulting model structures are depicted in Figure 1.

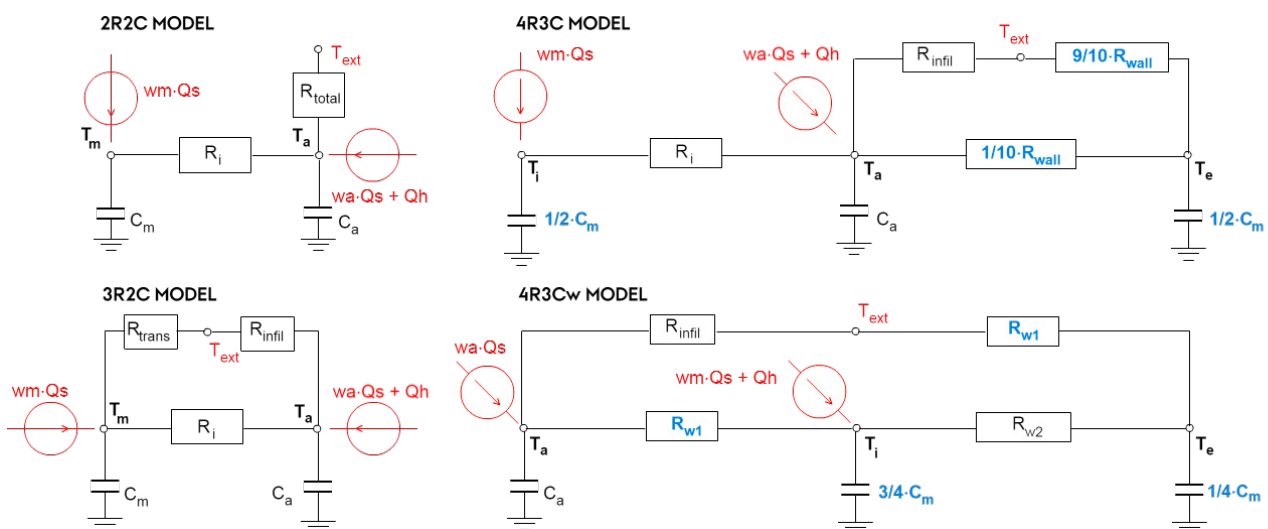


Figure 1 Model structures depicted as RC-networks. Red text denotes inputs, blue highlights the assumptions made for third order models.

The initial model (2R2C in Figure 1) is a modified version of the model presented in ref. [18], which was initially intended for white-box simulation. The modification was to replace an algebraic equation describing the surface temperature in the original model with a single resistance to reduce the number of parameters and thereby improve the identifiability of the model. The proposed 3R2C model extends the modified 2R2C model by adding a transmission heat loss directly from the thermal mass to the exterior. The 3R2C model was finally expanded into two third-order models: The 4R3C model contains an interior capacity representing internal elements that only interact with the zone air. In the 4R3Cw model the third thermal mass node is placed in the envelope in an attempt to better model the distribution of capacity in the envelope. The heating system was assumed to be fully convective in all models, which matches the heating system modelled in EnergyPlus. However, the two third order models required further assumptions to be introduced in order to reduce identifiability issues: In the 4R3C model, where the mass capacity is separated in internal capacity and envelope capacity, two dependencies between parameters were introduced to ensure identifiability. These dependencies were 1) an equal distribution of the thermal mass between the interior and envelope nodes, and 2) that 90 % of the envelope resistance is placed on the cold side of the envelope capacity node. Assumption 2 draws on the assumption that only the capacity on the warm side of the insulation layer will significantly add to the efficient thermal capacity. In the 4R3Cw model, where the envelope contains two states, assumptions were again made both with respect to the distribution of resistance and thermal mass: 1) The internal mass node contains the majority (75%) of total thermal mass, as it represents all mass on the warm side of the insulation layer and 2) the resistance is assumed to be symmetrically distributed around the insulation layer, corresponding to a ‘sandwich-type’ envelope. This assumption is considered likely in apartment blocks and less likely in buildings where the envelope also contains ground floor and roof constructions.

3. Results

The four model structures were used to estimate the thermal characteristics of the two apartments using two weeks' worth of measurements with a 1-minute sample rate. To investigate the consistency of the estimates across different weather conditions, data from four of the coldest months were used (Nov–Feb). The estimates were normalized against the reference values from Table 1 to ease the model comparison. Figure 2 depicts the estimates of all model structures using data from each of the four months. The red line denotes the reference values.

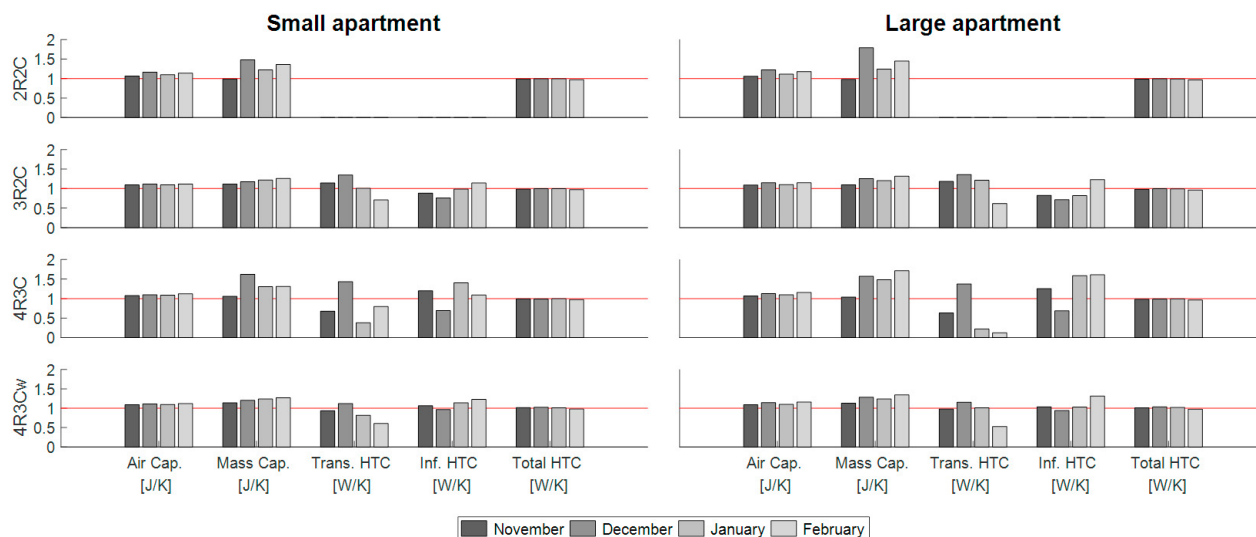


Figure 2 Comparison of normalized parameter estimates. Red line denotes the reference value of the characteristics.

The results show that all model structures yielded accurate and consistent estimates of the short time constant (air cap.) and the overall heat loss coefficient (total HTC). The 2R2C model is not capable of providing estimates of the individual heat loss coefficients due to its structure. It is also clear that this simple model together with the 4R3C model lack the consistency and accuracy of the other two models, and are therefore not suitable for thermodynamic characterization purposes. The 3R2C and the 4R3Cw models showed very similar estimates of all characteristics, with decent accuracy and consistency across all datasets. Both models tended to slightly overestimate the effective thermal mass by 10–32%. Upon closer inspection of the results, the 4R3Cw model outperformed the 3R2C model in terms of the average deviation seen over all parameters and all data sets. The third-order model deviated on average 8% and 7% on the small and large apartment, respectively. With the second order model the deviations were 13% and 17%, respectively. Despite decent accuracy on average, the estimates of the individual heat loss components exhibit the by far highest inconsistency across all models, thus suggesting that these are difficult to reliably estimate.

4. Discussion

The 4R3Cw model showed slightly better performance than the second order model 3R2C. This performance was gained through the added complexity of the model, which came at the price of introducing interdependency assumptions between some of the parameters of the model. The question is then whether these assumptions hold for other types of building models and, more importantly, for real buildings. The assumption concerning the distribution of capacities in the 4R3Cw model is considered to some extent to be case-specific. Future work could therefore be to carry out a sensitivity analysis of the assumptions, e.g. for several different building compositions, before such assumptions can be assumed reasonable for a wider range of buildings. The models estimated the thermal capacitance higher than the reference value calculated with a simplified (yet impractical) method described in ISO 13786. It remains to be concluded which of the two approaches – data-based identification or calculation – yields the most accurate or useful result. Finally, Gaspar et al. [2] concluded that dynamic local characterization methods outperformed the static ones. An in-depth comparison of the co-heating test and the dynamic RC-model approach should therefore be conducted to determine whether the same applies to whole-building characterization methods.

5. Conclusion

This paper presented an evaluation of four different RC-model structures intended for data-based estimation of the thermal characteristics of buildings. The four model structures were evaluated in a comparative analysis, where estimates from each model were compared to estimates from calculation methods described in relevant standards. The results indicated that both second order and third order models, depending on their RC-network structure, are capable of yielding consistent estimates of the short time constant (zone air, furniture), the effective thermal mass and the total heat loss coefficient. Individual estimates of infiltration and transmission heat losses were found to be highly inconsistent across all models, with deviations as high as 47% even for the better performing models.

The 3R2C model is considered to be the most practically viable model structure for characterization purposes over the third order models because of 1) the additional assumptions needed to make consistent estimates with the investigated third order models, and 2) the relatively low performance increase gained by introducing the extra state.

Acknowledgements

The research was conducted as part of the ‘Resource Efficient Cities Implementing Advanced Smart City Solutions’ (READY) financed by the 7th EU Framework Programme (FP7-Energy project reference: 609127) and the project “READY.dk” financed by the Danish Energy Research and Development program ForskEl.

References

- [1] European Committee for Standardization, ISO 9869-1:2014 - Thermal insulation -- Building elements -- In-situ measurement of thermal resistance and thermal transmittance -- Part 1: Heat flow meter method, European Committee for Standardization, Brussels, 2014.
- [2] K. Gaspar, M. Casals and M. Gangolells, A comparison of standardized calculation methods for in situ measurements of facades U-value, *Energy and Buildings* 130 (2016) 592-599.
- [3] G. Bauwens and S. Roels, Co-heating test: A state-of-the-art, *Energy and Buildings* 82 (2014) 163-172.
- [4] A. Janssens, International Energy Agency, EBC Annex 58: Reliable building energy performance characterisation based on full scale dynamic measurements, KU Leuven, Leuven, 2016.
- [5] D. K. Alexander and H. G. Jenkins, The validity and reliability of co-heating tests made on highly insulated dwellings, *Energy Procedia* 78 (2015) 1732-1737.
- [6] R. Everett, Rapid Thermal Calibration of Houses, Technical report, Open University Energy Research Group, Milton Keynes, 1985.
- [7] G. Reynders, J. Diriken and D. Saelens, Quality of grey-box models and identified parameters as function of the accuracy of input and observation signals, *Energy and Buildings* 82 (2014) 263-274.
- [8] H. Harb, N. Boyanov, L. Hernandez, R. Streblow and D. Müller, Development and validation of grey-box models for forecasting the thermal response of occupied buildings, *Energy and Buildings* 117 (2016) 199-207.
- [9] Lawrence Berkeley National Laboratory, Buildings Control Virtual Test Bed - BCVTB (1.4.0), [Online].
- [10] T. H. Pedersen, R. E. Hedegaard, S. Petersen, Space heating demand response potential of retrofitted residential apartment blocks, *Energy and Buildings* 141 (2017) 158–166.
- [11] G. Bellu, M. P. Saccomani, S. Audoly and L. D’Angiò, DAISY: A new software tool to test global identifiability of biological and physiological systems, *Computer Methods and Programs in Biomedicine* 88 (2007) 52-61.
- [12] European Committee for Standardization, EN ISO 6946:2007 - Building components and building elements -- Thermal resistance and thermal transmittance -- Calculation method, European Committee for Standardization, Brussels, 2007.
- [13] Berkeley Lab WINDOW v7.4.8.0, 2016. [Online]. Available: https://windows.lbl.gov/software/window/7/index_7_4_8.html.
- [14] European Committee for Standardization, ISO 13786:2007 - Thermal performance of building components - dynamic thermal characteristics, European Committee for Standardization, Brussels, 2007.
- [15] U.S. Department of Energy, EnergyPlus Documentation: Engineering Reference, 2016.
- [16] DS/EN 673: Glass in building - Determination of thermal transmittance (U-value) - Calculation method, Dansk Standard, Charlottenlund, 2011.
- [17] European Committee for Standardization, DS EN/ISO 13790:2008 - Energy performance of buildings -- Calculation of energy use for space heating and cooling, European Committee for Standardization, Brussels, 2008-05-23.
- [18] T. R. Nielsen, Simple tool to evaluate energy demand and indoor environment in the early stages of building design, *Solar Energy* 78 (2005) 73-83.

4.2 Extension to paper

The analysis used an EnergyPlus model as an analogue for an actual building. This has both advantages and disadvantages: the main disadvantage is that even detailed building models to some extent simplify the complex phenomena occurring in actual buildings, thus inevitably reducing the trustworthiness of the results. A clear advantage, however, is that simulations allow us to know the exact composition of materials and the geometry of the building, thus allowing a fair comparison of the *true* characteristics of the building, and those indicated by identified RC models. Two apartments of different sizes were used to evaluate the sensitivity of the conclusions to geometric properties such as footprint area, window area and the ratio between floor area and envelope surface area. Figure 5 depicts the floor plans of the two apartments that were modelled with EnergyPlus.

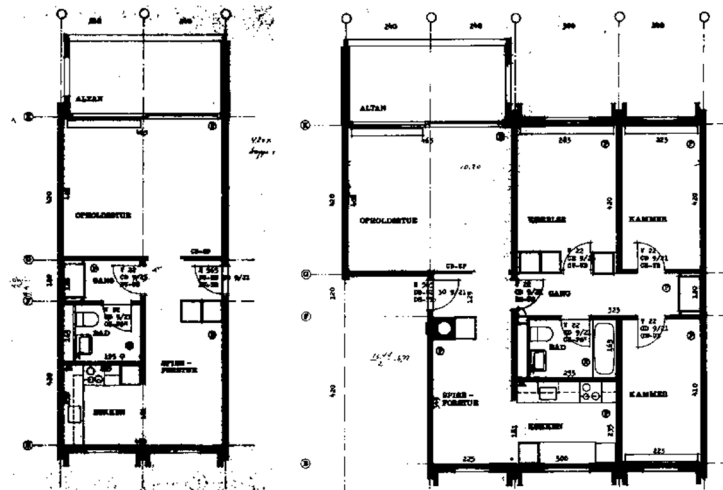


Figure 5 Layout of the two apartments modelled in EnergyPlus

A closed-loop experiment using a conventional PI control scheme was simulated in each apartment to generate informative input-output data. The experiment imposed excitation on the apartments by letting the heating set points follow a PRBS signal alternating between a set point of 20 °C and 23 °C. In order to evaluate the consistency of the parameter estimates obtained with each model structure, an experiment was simulated during the first three weeks of each month from November to February. The temporal resolution of the data used in the analysis to identify the models was 60 seconds. Furthermore, to keep the results as clear as possible, the analysis used the actual solar heat gains extracted from EnergyPlus. Figure 6 depicts (in hourly resolution) one of the input-output datasets captured in the large apartment.

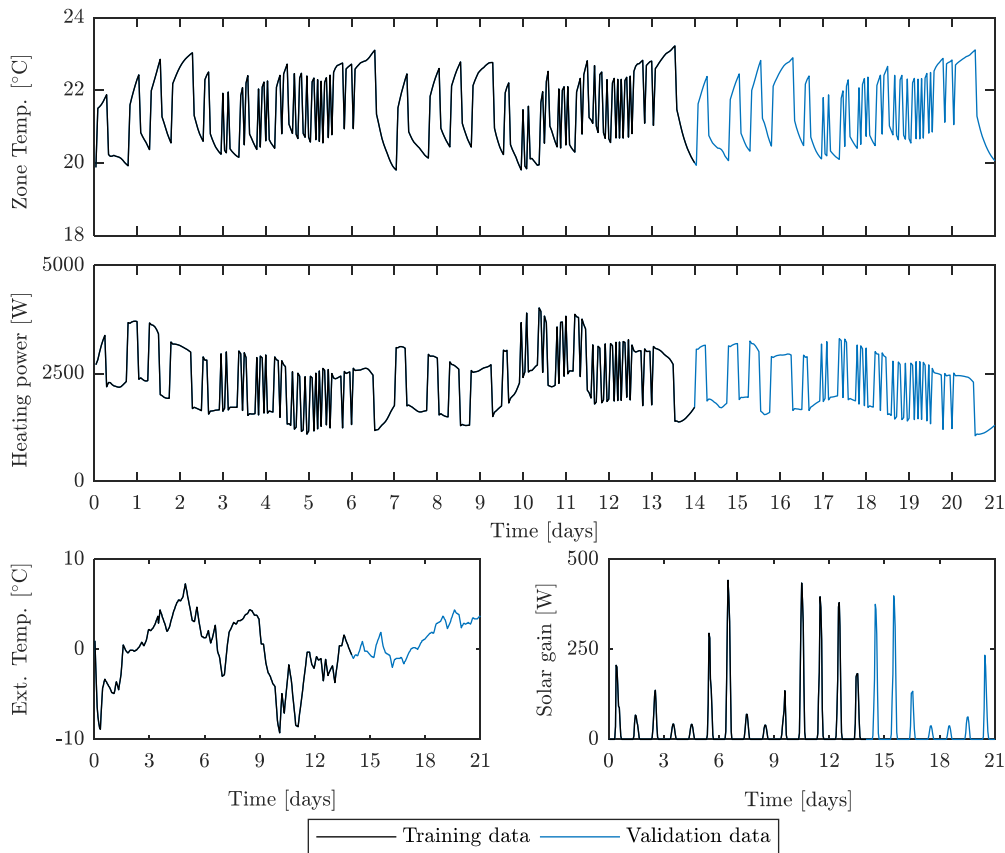


Figure 6 The Input-output used for parameter identification. The data was simulated with an EnergyPlus model containing two apartments. For readability, the data is here presented as hourly values.

As stated in the paper, the four model structures resulted from a forward modelling approach initiated with a 2R2C model structure. The forward modelling approach was guided by an evaluation of the identifiability of each proposed model structure. The structural identifiability of each model structure was first assessed with the DAISY (differential algebra for identifiability of systems) software [53]. Once structural identifiability was ensured, the practical identifiability of the models was assessed by initiating several parameter identification runs from randomized starting points in the parameter space. If the majority of these runs converged to the same optimum, the model was considered practically identifiable. In the case of the two third order models, practical identifiability was first achieved when the parameter-interdependencies outlined in the paper were introduced. The four resulting model structures were all concluded to be structurally identifiable, as well as practically identifiable with the input-output data used in the analysis.

A set of models were identified for each combination of model structure and dataset. The criterion minimized in the identification process was the simulated prediction errors (i.e. infinite-step-ahead predictions). All but the best-performing model of each model-set were discarded. The resulting models were then evaluated on their parameter estimates (documented in the paper), and on their predictive performance on the validation data depicted in Figure 6. The initial state of the models used in the simulation of the validation dataset was estimated from the training dataset. Figure 7 presents the performance of the models identified with each model structure using data from the large apartment.

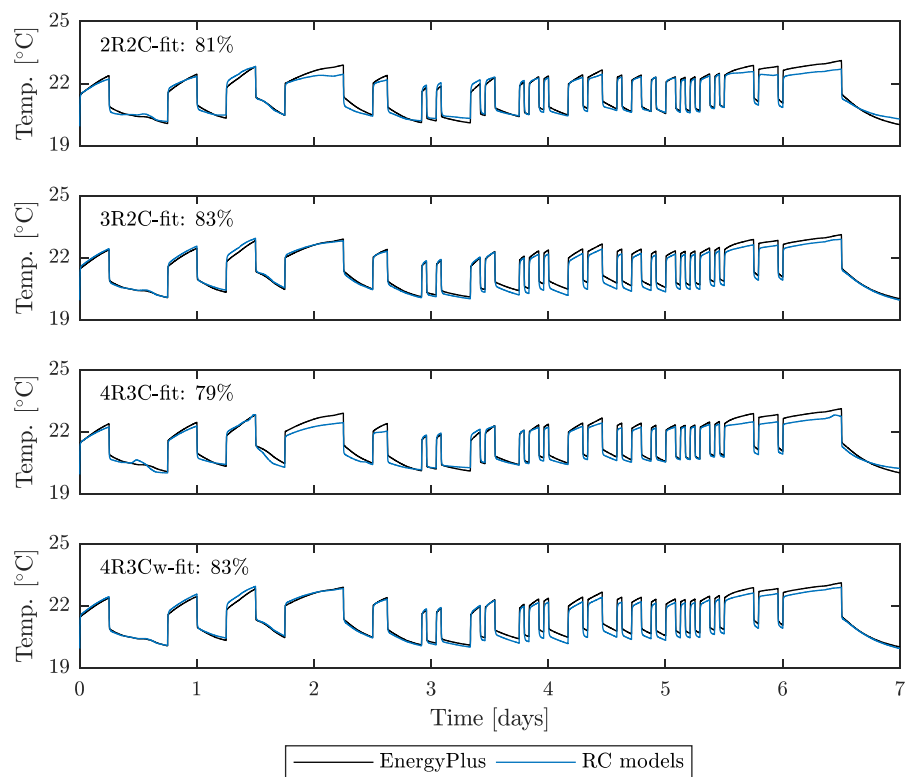


Figure 7 Predictive performance of identified models on the December dataset (large apartment). Each plot depicts the best-performing model obtained with a given model structure. The indicated fit-values are the NRMSE-fits.

The NRMSE fit was the metric that was used to quantify the predictive performance of the models. The NRMSE is defined according to Eq. (4.1), in which \mathbf{y} is a vector of measurements, $\bar{\mathbf{y}}$ is the mean of the measurements, $\hat{\mathbf{y}}$ is the vector of simulated model output and $\|\cdot\|$ is the 2-norm of a vector.

$$NRMSE = 100 \cdot \left(1 - \frac{\|\mathbf{y} - \hat{\mathbf{y}}\|}{\|\mathbf{y} - \bar{\mathbf{y}}\|} \right) \quad (4.1)$$

Comparison of the simulated and measured time series of Figure 7 show that the models are capable of describing the thermodynamic phenomena of the more complex EnergyPlus model with a high accuracy. A similar multi-step-ahead predictive was found also found for the datasets not depicted here. The similarities between the predictive performances of the models also meant that this aspect did not affect the conclusions drawn in the paper.

Finally, the analysis presented so far featured two assumptions, whose potential impact was considered worth investigating further: 1) an unusually high temporal resolution of the data (1-minute resolution), and 2) the use of the actual solar heat gains transmitted through the windows of the apartments. These assumptions were originally introduced to ensure that the conclusions related to the suitedness of the model structures were not affected by our ability to handle solar heat gains or our beliefs related to the availability of data. To evaluate whether these assumptions had a significant effect on the results, the entire analysis was also conducted two additional times, each time with one of these assumptions addressed.

SENSITIVITY ANALYSIS

This subsection presents the results achieved by conducting the analysis presented in the paper, but using 1) an hourly temporal resolution (instead of 1-minute), and 2) the horizontal global radiation (instead of the transmitted solar heat gains). The latter is of particular interest since using of anything but the *transmitted solar heat gains* results in the need for an additional parameter describing the *actual* or *equivalent* window areas (sometimes referred to as the solar aperture). Figure 8 presents these results for the 3R2C model structure only, since these results were representative for the tendencies observed in all model structures. For ease of comparison, the results published in the paper are reproduced as well.

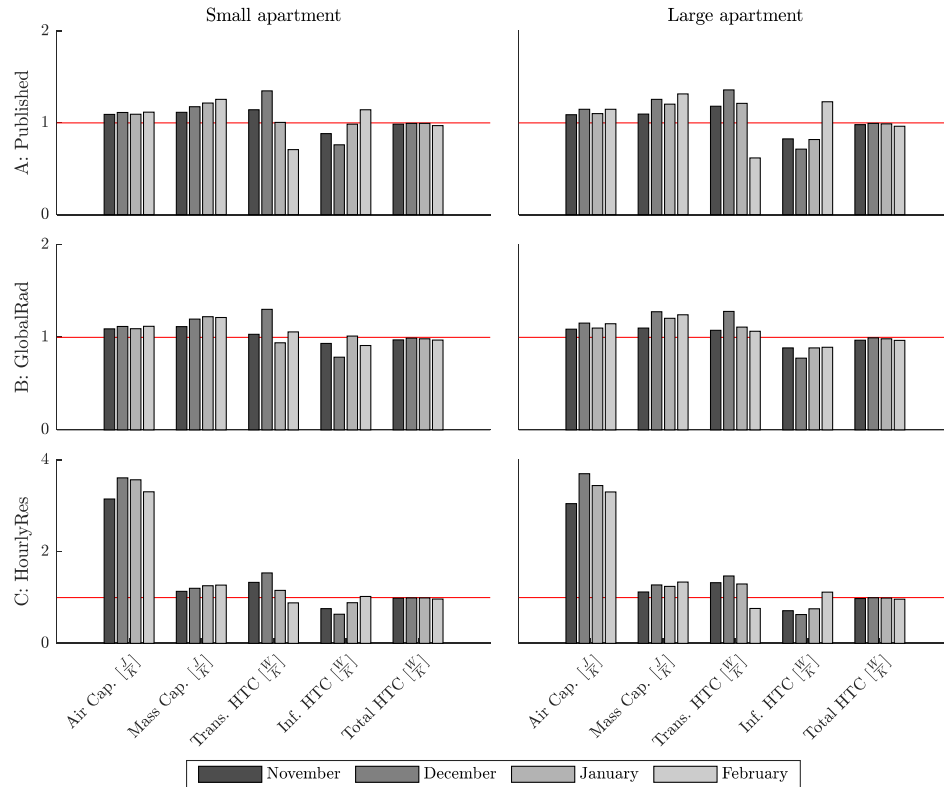


Figure 8 Evaluation of the sensitivity of parameter estimates to the assumptions drawn in the initial analysis. Normalized parameter values relative to their white-box estimate (red line). Rows 1, 2 and 3 present the estimates obtained with data using 1) transmitted solar data with 1-minute resolution (from the paper), 2) global radiation with 1-minute resolution, and 3) transmitted solar with hourly resolution.

The results of the sensitivity analysis indicated that using measurements of the global radiation did not affect the interpretability of the identified model parameters, which in general were similar to those presented in paper. Reducing the sampling rate to hourly measurements resulted in a loss of information in relation to the thermal capacity of the zone air, leading to inaccurate estimates of this parameter. In actual buildings, this parameter will also contain contributions from the heating system and furniture, which could reduce this issue by slowing down the dynamic temperature response. The reduced resolution did not affect the estimates of the remaining parameters. Neither in terms of the predictive performance of the models did the assumptions have a significant impact, as clear from the relatively similar NRMSE fits achieved for the model structures using each of the three datasets depicted on Figure 9.

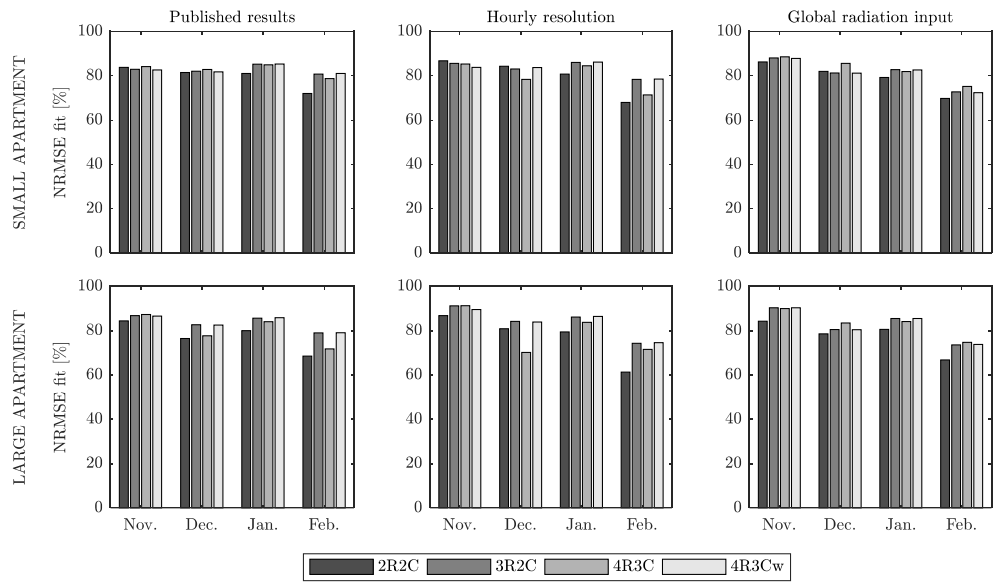


Figure 9 Impact of the used dataset on the NRMSE fits of the resulting models evaluated on the validation data. The top/bottom row presents results for the small/large apartment, while each column refers to the dataset (published, hourly or global radiation) used for identifying model parameter.

4.3 Epilogue

The purpose of the analysis presented in this chapter was to identify RC model structures capable of describing the thermodynamic characteristics and behaviour of buildings when identified using typical measurement data. The analysis indicated that the 3R2C model structure offered a good trade-off between model complexity and performance. Furthermore, two models of second- and third order, respectively, were found capable of identifying the thermal capacity of the indoor air and the effective thermal capacity of the structural building components with sufficient accuracy. While all of the investigated model structures were capable of identifying the overall heat loss coefficient of each apartment, none of them yielded consistent estimates of the transmission and infiltration heat loss components. Since this was not possible even under the idealized conditions of this analysis, obtaining estimates of the individual heat loss components in this way is not considered possible in practice.

Identifiability issues were encountered when extending the model from a second-order to a third-order model. While the proposed layout of the models undoubtedly has some influence in this regard, the primary cause of the identifiability issues was considered to be the growth in the number of model parameters associated with increasing the model order. Doing so required the introduction of not only additional resistance and capacity parameters, but also parameters describing the distribution of heat gains – e.g. from solar or the heating system. Two ways of addressing identifiability issues are to 1) extend the dataset with additional measurements, or 2) reduce the number of free parameters by either fixing certain parameters or introducing parameter interdependencies. Identifiability issues with model structures of order three and above were also identified in the study of Reynders et al. [54]. Here, the authors addressed these issues by extending the training data with heat flux measurements, while acknowledging the difficulty of obtaining such measurements in practice. Therefore, we instead addressed identifiability issues by imposing assumptions that simplified the parameterization of the model structure. Despite these efforts, the analysis did not indicate any significant benefits from choosing one of the third-order models over the 3R2C model, thus leading to differences in the conclusions drawn in the study of Reynders et al., for example, and in the present study.

The analysis indicated that all of the evaluated model structures described the thermodynamic behaviour of the apartments with a level of accuracy considered sufficient for MPC purposes. While the application of grey-box models in control does not necessarily require that model

parameters be physically interpretable, the ability to characterize the thermodynamic properties of buildings through dynamic building energy modelling has several other interesting applications. These include identification of relevant retrofit strategies, building commissioning, HVAC fault detection and energy labelling. Therefore, it is worth discussing potential causes of the discrepancies between the conclusions drawn in previous studies and those drawn here.

DISCUSSION OF DISCREPANCIES

One of the possible explanations that come to mind relates to the simplifications involved when using models from detailed building energy modelling tools (e.g. EnergyPlus) as analogues for actual buildings. These simplifications typically include assumptions of a fully mixed air temperature distribution and uniform surface temperatures. However, since the study of Reynders et al. applied similar assumptions, the use of these tools alone cannot be considered the cause of differences in the drawn conclusions. This is supported by the fact that both of the studies conducted by Harb et al. [51] and Bacher and Madsen [52] used data from real buildings, yet still reached different conclusions. A possible explanation for the discrepancy between these two studies is that only Bacher and Madsen imposed excitation on the building during the measurement period, while Harb et al. relied on consumption data from normal operation.

Another hypothesis, which seems more consistent with the methods applied by different studies, is that the discrepancies may be related to differences between studies in the error criterion used for parameter identification. Both the present study and the study of Harb et al. concluded that second-order models were preferable - both in terms of predictive capability and the physical interpretability of the parameter estimates. Another similarity between these studies is their use of the simulation error (infinite-step-ahead) as the error criterion. In contrast, the studies by Reynders et al. as well as the study by Bacher and Madsen relied on one-step-ahead prediction errors, and concluded that higher-order models were preferable. It therefore seems worthwhile to investigate whether the choice of error criterion itself is the cause of the discrepancies in the drawn conclusions. From my point of view, there are both advantages but also potential issues associated with using the one-step-ahead error criterion for the thermodynamic characterization of buildings. A potential issue is the inevitable effect on the parameter estimates of the deterministic model (the building model) that originates from the simultaneous tuning the deterministic and stochastic

(noise model) components of the model. As noted by Ljung [48], it seems more natural (from a physical point of view) to identify these models separately².

THE INFLUENCE OF THE ERROR CRITERION

In the context of thermodynamic characterization, intuition would suggest that if we wish to interpret the parameters of the deterministic part of a given model as estimates of the characteristics of the actual system, we would also want such a model to be characterized by high simulation performance – i.e. be somewhat independent of the noise-model.

This, in turn, would suggest the simulation error criterion to be an appropriate choice for this application. However, this reasoning is flawed in cases where significant levels of noise from unmeasured disturbances have corrupted the input-output data. A good example of such a disturbance in buildings is the presence of occupants, whose stochastic behaviour and use of appliances may have a significant effect on the thermal state of the building. In this case, a parameter identification method relying on the simulation error criterion would inevitably incorporate these effects into the estimates of the deterministic part of the model. This would be less of an issue for parameter identification methods relying on the one-step-ahead error criterion, since the effects of such disturbances would (at least partially) be absorbed by the noise model. A similar point is made by Zhao et al. [40], who state that the multi-step-ahead error criterion is preferable when prediction errors are dominated by a model bias (under-modelling), while the one-step-ahead criterion is preferable in the presence of significant disturbances.

To further investigate these effects, the parameters of each model structure (2R2C, 3R2C, 4R3C and 4R3Cw) were identified using the same noise-free data as was used in the original analysis, but using the one-step-ahead error criterion instead. Equations (4.2a) and (4.2b) present the *innovations form* of a state-space model [48].

$$\mathbf{x}_{k+1} = \mathbf{A}\mathbf{x}_k + \mathbf{B}\mathbf{u}_k + \mathbf{K}\mathbf{e}_k \quad (4.2a)$$

$$\mathbf{y}_k = \mathbf{C}\mathbf{x}_k + \mathbf{D}\mathbf{u}_k + \mathbf{e}_k \quad (4.2b)$$

In these equations, the subscripts refer to the time-increment in a given simulation, \mathbf{x} is a vector of model states, \mathbf{u} is a vector of inputs, and \mathbf{e}_k is the unpredictable prediction errors (or *model residuals*) that are assumed to follow a Gaussian white-noise process. The matrices \mathbf{A} , \mathbf{B} , \mathbf{C} and

² Section ‘Output Error Model Structure’ in ‘*System Identification – Theory for the User*’, 2nd edition.

\mathbf{D} describe the characteristics of the modelled system – here in discrete form. Finally, \mathbf{K} is the *Kalman gain* that scales the impact of the prediction errors, \mathbf{e}_k . The magnitude of the Kalman gain is derived from the system matrices and assumed uncertainties related to the measurements and the prediction of the states, respectively.

The difference between the *simulation* and *one-step-ahead* error criteria lies in whether the current (or past) prediction error is used for predicting the future state of the model. More formally, an *Equation Error model* (implying a k -step-ahead error criterion, here with $k = 1$) is achieved by setting the \mathbf{K} in Eq. (4.2a) equal to the *Kalman gain*, while an *Output Error model* (implying the *infinite*-step-ahead error criterion, or *simulation*) is achieved by setting \mathbf{K} to zero. The terms *Output Error model* and *Equation Error model* refer to the fact that the prediction error only enters the *output*, i.e. Eq. (4.2b), in the case of the former, while for the latter it also enters the *equation* that predicts the future state of the model, i.e. Eq. (4.2a). The impact of the choice of error criterion on the parameter estimates is depicted on Figure 10.

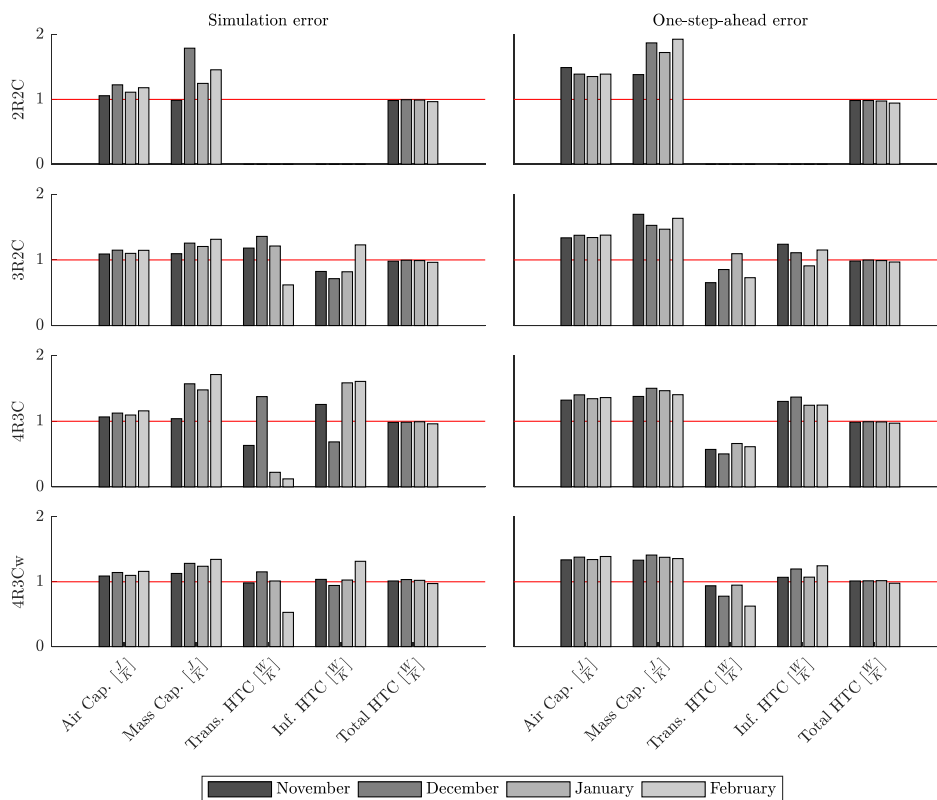


Figure 10 The impact of identification error criterion on parameter estimates.

Comparison of the results depicted in Figure 10 shows that the choice of error criterion did not affect the estimates of the total heat transfer coefficient of the building. On the other hand, a tendency of higher estimates of the thermal capacities associated with the one-step-ahead error criterion is seen. Especially the capacity of the air volume was estimated higher for this criterion consistently across all model structures. For the 3R2C model, the one-step-ahead error criterion led to significantly higher estimates of the thermal capacity mass: the maximum overshoot was 32% and 70% for the simulation and one-step-ahead error criteria, respectively. This tendency was less pronounced for the results of the 4R3Cw model – the other of the four models that was concluded in the paper to yield consistent estimates.

This investigation of the influence of the choice of error criterion indicated that it does affect the estimates of model parameter and thereby potentially their interpretability. While these results are merely a preliminary analysis, they indicate that this choice in modelling may be one of the causes of the discrepancies found in the conclusions of studies that compare several model structures.

Most theoretical work on the subject of the consistency of parameter estimates (e.g. [36], chapter 21.3) assumes that the deterministic model structure (i.e. the building model) matches the true system. Since this is never the case in practice (and, in particular for reduced-order models), it is difficult to apply the results of such theoretical analysis to our context. In this preliminary analysis, I used noise-free EnergyPlus simulation data to compare the two error criteria, which arguably favours the simulation error criterion. The one-step-ahead error criterion may prove more appropriate when using more realistic datasets characterized by noise from unmeasured disturbances. It would therefore be interesting to investigate whether a compromise between the two extreme error criteria (one-step-ahead and infinite-step-ahead) would produce the best results in practice. For instance, a k -step-ahead criterion could be applied, where k could be chosen with regard of the dynamics of the modelled system or the characteristics of the noise acting on the system. Other approaches, suggested in previous studies include combining the one-step-ahead and simulation errors in a single weighted error criterion [55], or relying solely on the one-step-ahead criterion but penalizing the size of the state correction that is applied in that process [56]. This topic has not been investigated further in this thesis, but is considered a relevant topic for future research.

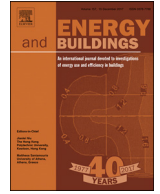
In the following chapter, the 3R2C model structure is used to investigate whether the implementation of MPC schemes can be simplified by applying weather forecasts in a way that may make weather measurements unnecessary.

5 PRACTICAL DATA ACQUISITION

The task of obtaining a model that describes the thermodynamic properties of a given building is widely considered to be the most challenging aspect of implementing MPC schemes in buildings [24, 25]. In this context, one of the practical challenges is that the sensor equipment needed to obtain the input-output dataset used in system identification is typically not present in residential buildings, and would therefore constitute an expense associated with the modelling effort. Therefore, it is relevant to investigate whether any of these sensors can be omitted without significantly affecting the performance of the resulting MPC scheme. Especially sensors measuring weather conditions would be beneficial to avoid in MPC applications, since the control scheme during the operational phase use weather *forecasts* – and not measurements. A potential issue of using weather measurements for identifying the building model is that there might be a bias between these measurements and the forecasts obtained from a given meteorological model. This bias carries through to the predictions made with the model in the operation of the MPC scheme, thus potentially reducing the performance of the control scheme. Gyalistras et al. [57] addressed this issue by bias-correcting forecasts using local observations. A relevant question, however, is whether this issue can be avoided entirely by identifying models using weather data derived from forecasts instead of relying on weather measurements. If sufficiently accurate models can be obtained in this way, this approach has two advantages:

1. The bias in model predictions resulting from the use of weather data from multiple sources is eliminated. Furthermore, a potential bias between the actual weather at the site of the building and the weather indicated by forecasts is automatically absorbed in the parameters of the model during system identification.
2. The sensor array dedicated to measuring weather conditions can be avoided, thereby simplifying the technical infrastructure needed to implement MPC schemes.

The following paper presents an analysis of the viability of this proposed MPC implementation approach – thereby constituting the research efforts that addresses thesis objective **1.3**.



Towards practical model predictive control of residential space heating: Eliminating the need for weather measurements

Rasmus Elbæk Hedegaard*, Theis Heidmann Pedersen, Michael Dahl Knudsen, Steffen Petersen

Department of Engineering, Aarhus University, Inge Lehmanns Gade 10, Aarhus C 8000, Denmark

ARTICLE INFO

Article history:

Received 30 November 2017

Revised 6 February 2018

Accepted 11 April 2018

Available online 17 April 2018

ABSTRACT

Model-based control schemes such as model predictive control (MPC) can assist smart-energy systems in achieving higher efficiency and utilization of renewable energy sources. A practical barrier for deploying such control schemes for space heating of residential buildings is the costs related to obtaining the weather data measurements needed for identifying a model that describes the dynamic behaviour of the building. Therefore, this paper reports on a simulation-based study investigating whether there is a significant impact on the performance of MPC schemes when substituting these weather measurements with data from meteorological weather services. Since access to weather forecasts is necessary during the operation of the MPC scheme, this implementation approach draws on data already available to remove the need for weather measurements. The results indicated that this approach only led to a minor performance impact in that heating savings were reduced by 4% while comfort violations increased by less than 0.1 Kh per day on average. The results thereby suggest that the use of data from meteorological forecast services for model identification may constitute a cost-efficient alternative to on-site or near-by weather measurements.

© 2018 Elsevier B.V. All rights reserved.

1. Introduction

There is an increasing interest in the use of model predictive control (MPC) of building systems due to its potential for synergy with smart grids [1] and its potential for improving the energy performance of building HVAC systems and occupant comfort [2]. Several theoretical studies have indicated that MPC schemes are able to exploit the thermal storage capacity of building structures to provide price-based demand response to reduce the total operating costs [3–5] and to facilitate incentive-based demand response programs [6–7]. However, there are a number of practical challenges currently preventing MPC from being widely deployed in practice: an MPC scheme utilizes a mathematical model of the thermodynamic behaviour of the building together with forecasts of weather and potential internal loads to determine the optimal strategy for operating the building's HVAC systems. One of these challenges is the effort needed to obtain a suitable building model [8].

The data required for obtaining building models suitable for MPC is time series with measurements of indoor air temperature, energy use for HVAC and local weather conditions (solar radiation and external temperature). The same measurements are needed

during the operational phase of the MPC scheme, along with the weather forecasts needed for predicting the influence of weather on the building. In some cases additional factors such as internal heat gains, wind speed and direction may improve the performance of the MPC scheme. With regard to MPC of residential buildings, Killian and Kozek [1] note that home automation systems and advances in wireless technology have provided practical and flexible means for collecting data needed for MPC, but these technologies are an extra cost if they are not already present in residential buildings. However, while there are currently no alternatives to acquiring sensors for measuring indoor air temperature and energy use, there might be alternatives that could eliminate the need for sensors measuring weather data.

Conventional ways of collecting weather data for estimating a building model for MPC are to install a weather station at the site of the building or to rely on data from nearby public weather stations. All other things being equal, the advantage of on-site weather stations over nearby measurements is that the resulting measurements reflect the weather conditions that the building is exposed to, thus providing optimal conditions for obtaining a good building model. However, the benefit of on-site measurements comes at the cost of installing and maintaining an external array of sensors. Relying on data from nearby public weather stations eliminates these expenses, but introduces a risk of discrepancies between the measurements and the actual weather conditions

* Corresponding author.

E-mail address: reh@eng.au.dk (R.E. Hedegaard).

Table 1
Scenarios for weather data sources.

Scenario	Data for model identification	Forecast data for MPC
PB	On-site measurements	Perfect forecasts
A1	On-site measurements	Corrected forecasts using on-site measurements
A2	Public measurements	Raw or corrected forecasts using public measurements
A3	Forecast data	Uncorrected forecasts

at the site of the building, which may affect the quality of the obtained model. In both cases, the MPC scheme would require continuous access to weather measurements to be able to bias-correct weather forecasts. This is assumed to be unproblematic with on-site sensors, while the access to online measurements from public weather stations may depend on the specific setup.

To overcome the practical and economic disadvantages related to the two different ways of obtaining measured weather data, we propose utilizing forecast data from the weather forecast service used to facilitate the MPC scheme as a substitute for weather measurements during model identification. If this approach is viable, one practical barrier for deploying MPC, i.e. the costs of on-site or public weather data measurements, is eliminated. In this paper, we therefore present a simulation-based study comparing MPC performance when using measured weather data from on-site and nearby weather stations, respectively, and weather forecasts for generating the building model required for MPC of space heating.

Section 2 describes the prerequisites for the analysis including the used methods, data and the case study itself. The results are presented in Section 3 and discussed in Section 4. Finally, the overall conclusions of the study are drawn in Section 5.

2. Method

The presented study was based on simulations to enable comparison of how different types of weather data affect the qual-

ity of obtained control-oriented models and subsequently the performance of MPC schemes. The influence of occupants and internal heat gains were considered outside the scope of the analysis to ensure clearly interpretable results. A case building was modelled in EnergyPlus (EP) [9], while the MPC scheme was implemented in MATLAB [10]. The connection between the MPC scheme and EP was facilitated with the Building Controls Virtual Test Bed (BCVTB) [11]. This setup was used to investigate the performance of MPC schemes with different implementation approaches in the case building. Table 1 outlines three scenarios (denoted A1–A3) which rely on different sources of weather data for the implementation and operation of the MPC scheme.

All scenarios make use of the same case building (EP model) and the same actual weather conditions at the site of the building (EP weather file). The differences between scenarios are the data for identifying the control-oriented models used in the MPC, and whether there is access to online measurements during operation. Here, the latter affects the ability of the controller to use bias-correction algorithms to further improve the accuracy of forecasts from weather services – a process which requires local measurements (see Section 2.5 for further details).

In addition to scenarios A1–A3, a performance bound (PB) scenario using perfect weather forecasts was included as a benchmark enabling comparison of the realizable potentials to the theoretical potentials often reported in studies. Each implementation approach was evaluated in terms of the predictive performance of the re-

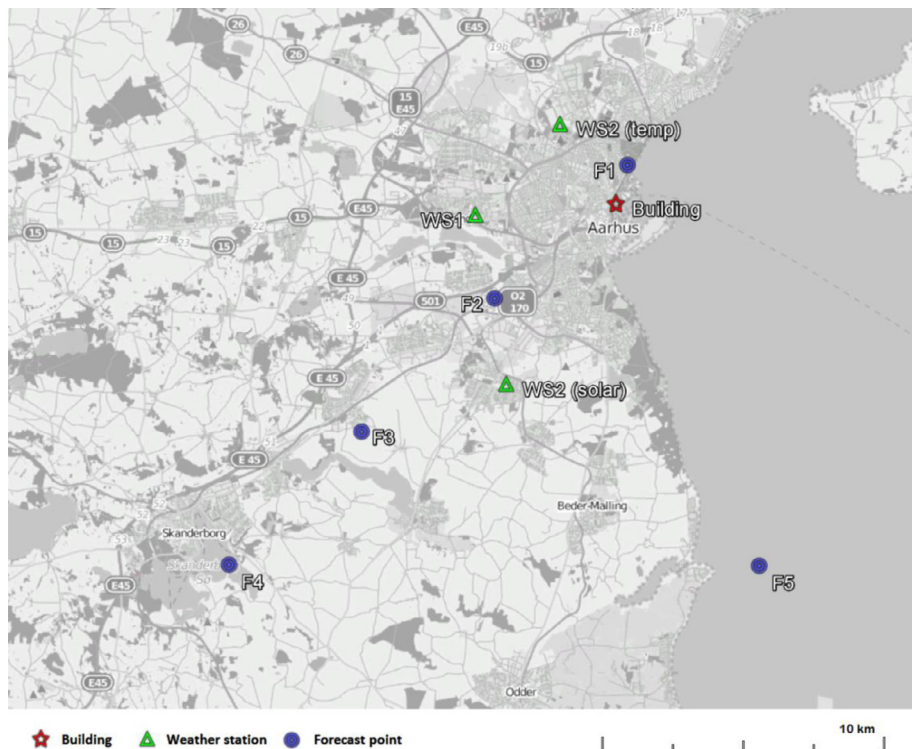


Fig. 1. Map showing the location of the building, weather stations and forecast points.

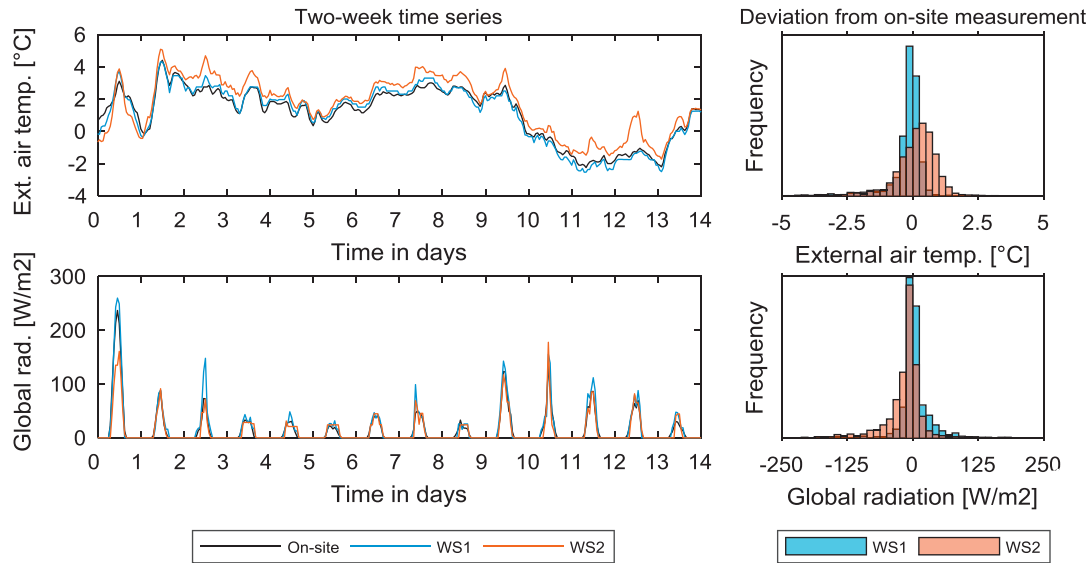


Fig. 2. Comparison of on-site measurements and the two weather stations.

sulting building models and the performance of these models once implemented in a MPC scheme.

The following sections present the weather data used in the analysis, the EP case building model, the grey-box model used for the MPC, the formulation of the MPC problem, and finally the method used to bias-correct forecasts in the simulations where this is relevant.

2.1. Weather data and control configurations

The weather data used for model calibration in scenario PB and A1 were measurements from a Delta-T GP1 weather station (accuracy: temp. ± 0.3 °C, global rad $\pm 5\%$) located on an unshaded roof top at the site of the case building in the city of Aarhus, Denmark (labelled 'Building' in Fig. 1).

Model identification in scenario A2 was run for two sets of measurements from public weather stations (WS) located within 10 km from the building: WS1 is a complete weather station while WS2 is a combination of measurements from two different loca-

tions (see Fig. 1). Fig. 2 depicts time series of a two-week period of the measurements from the on-site sensors and the two weather stations together with histograms of the deviations between on-site observations and WS1 and WS2, respectively, for the entire simulation period.

Model identification for scenario A3 was carried out using five sets of weather forecasts generated for locations between 1.6 km and 22 km from the building. All forecasts were provided by the Danish Meteorological Institute (DMI) and were generated with the HIRLAM ensemble-based meteorological model at a spatial resolution of 5 km [12]. The forecasts used for this study were taken as the average of the ensemble-set consisting of 25 forecasts for each location. Fig. 3 presents time series and deviations for three out of the five forecast locations used in this study. New forecasts were available every six hours, meaning that time series were created by consecutively combining the first six hours of each forecast. Consequently, only the part of the forecast with a short lead-time is used, thus minimizing forecast errors. The histograms of the temperature deviations show that the bias and spread of forecast er-

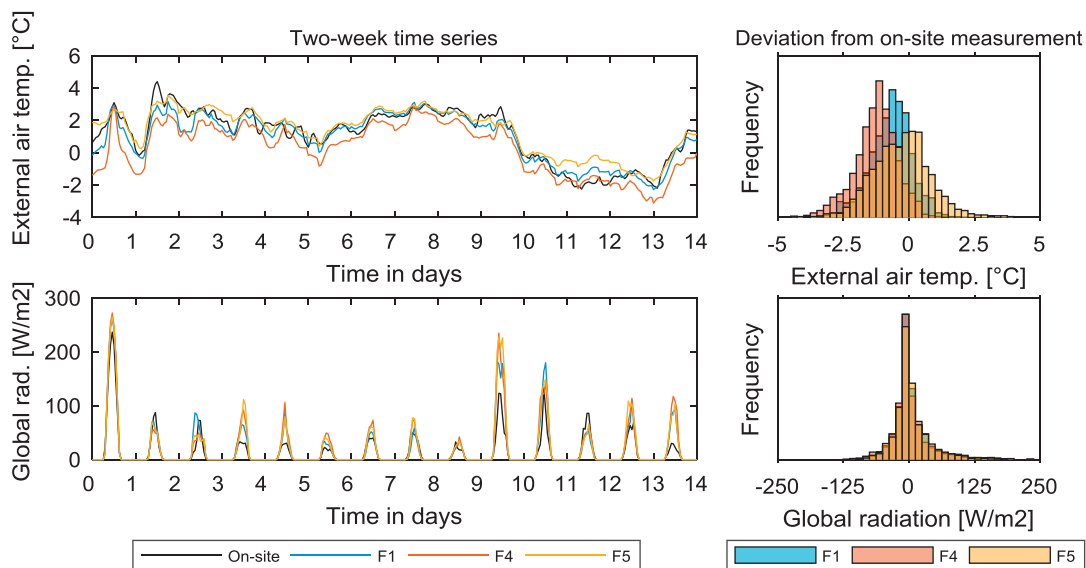


Fig. 3. Comparison of on-site measurements and forecast time-series for a period of two weeks.

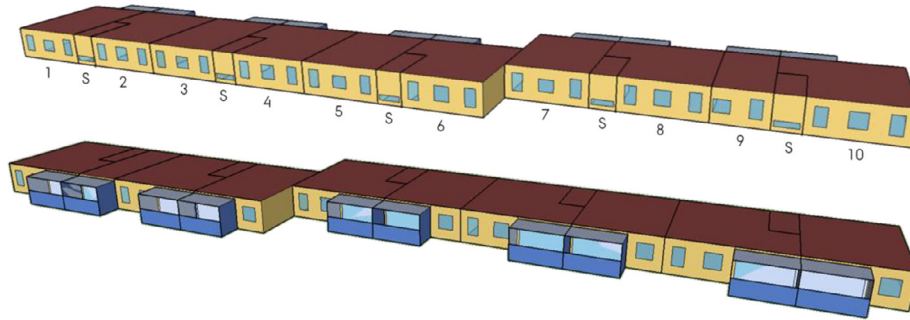


Fig. 4. Geometry of the 10-apartment building (3rd floor) used in the case study. Top: East façade. Bottom: West façade. (Illustration from [4]).

rors strongly depend on the forecast point. Libonati et al. [13] list factors contributing to systematic forecast errors as discrepancies of the meteorological model in topological heights and specification of surface-related parameters such as the soil-reflectivity. Furthermore, forecast accuracy is influenced by the spatial resolution of the meteorological model. Therefore, this study features forecasts from five different forecast points: F1–F4 were chosen because of their distance from the building while the last point (F5) was included due to its location slightly off-coast (see Fig. 1). The first four forecasts (F1–F4) differed primarily in the size of the systematic bias, while the off-coast point (F5) was characterized by a broader and less systematic distribution of forecast-errors. To give an indication of this, Fig. 3 presents the forecast error histograms of the forecast point closest (F1) and furthest (F4) from the building, as well as the off-coast forecast location (F5).

The weather data from both measurements and forecasts were time series with hourly values of incident global radiation [W/m^2] and external air temperature [$^{\circ}\text{C}$] from 1 December 2016 to 28 February 2017.

2.2. Case building

The EP model described by Pedersen et al [4] was used as case building. The model represents the thermal behaviour of ten energy-retrofitted residential apartments located on the third floor of an unobstructed four-story typical Danish pre-fabricated concrete building from the 1970'ies. Fig. 4 depicts a sketch of the east/west-oriented building facades. The energy efficiency of the case study building is indicated in Fig. 8 (result section). A detailed description of the construction components and HVAC systems used in the model is available in [4]. It is noted that the apartments were assumed heated by fully convective electrical baseboard heaters, and that internal loads from people and plug loads are left out to make results easier to interpret.

The building is modelled as 15 individual thermal zones: 10 apartments and 5 stairwells. Floors and ceilings were modelled as adiabatic zone boundaries while interior walls allowed heat transfer between both zones and the stairwells which were kept at a minimum temperature of 15°C . Simulations were carried out using a weather file populated with weather measurements from the site of the building. Dew-point temperature was approximated according to ref. [14] and the direct and indirect components of the measured global radiation were approximated according to ref. [15]. The time step used in the EP model was 1 min..

2.3. Grey-box model for MPC

The MPC scheme applied in this study relied on a grey-box model to represent the thermodynamics of each apartment in the EP building model. Whether the choice of a particular grey-box model structure is appropriate depends significantly on the in-

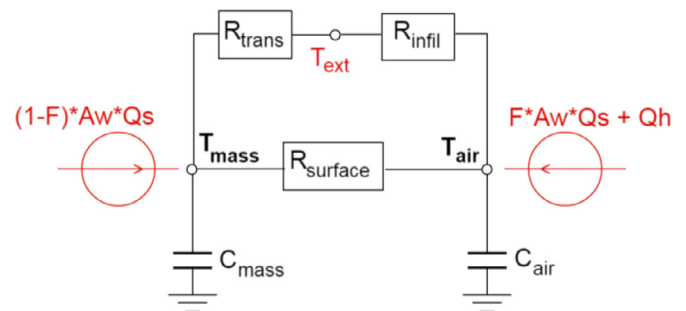


Fig. 5. RC-network of the physics-based 3R2C-model used in the MPC scheme of each apartment.

tended application of the model. An important trade-off to consider when choosing a model structure is that, while more complex models in principle are able to describe the physics of the system more accurately, the added complexity also makes the parameters of the model increasingly difficult to estimate from measured data. Fig. 5 shows the rather simple model structure chosen for the MPC scheme in this study. This choice was based on results from a previous study [16] in which this structure was found to be robust for identifying the thermal behaviour and characteristics of buildings when compared to other model structures of similar complexity.

The resistances of the model structure (R) represent the interior surface resistance and the resistances for transmission and infiltration heat losses, respectively. The capacities (C) are the lumped thermal capacities of the indoor air and building components, respectively. The temperature nodes of the model are denoted by T . F is a dimensionless factor determining distribution of solar heat gains between the internal air and construction components while A_w is the solar aperture equivalent to the area of horizontally placed windows with perfect transmittance. The inputs of the model (in red) are the external air temperature, T_{ext} , the global solar radiation, Q_s , and the heating power, Q_h .

A grey-box model for each apartment was calibrated using hourly values of energy consumption and indoor air temperature obtained from a simulation of the multi-zone EP model using a weather file containing the measurements taken at the site of the building. These measurements were combined with weather data from one of the three scenarios listed in Table 1. While some model parameters can be identified using data measured during steady-state conditions in the building, steady-state data is insufficient for identifying other parameters that describe the dynamic behaviour of the building. In Fig. 5, this especially applies to the thermal capacities of the model. Therefore, a series of temperature fluctuations were imposed on the EP model to create data suitable for dynamic modelling. The necessary excitation was evaluated by observing at the convergence of the parameter estimates when re-

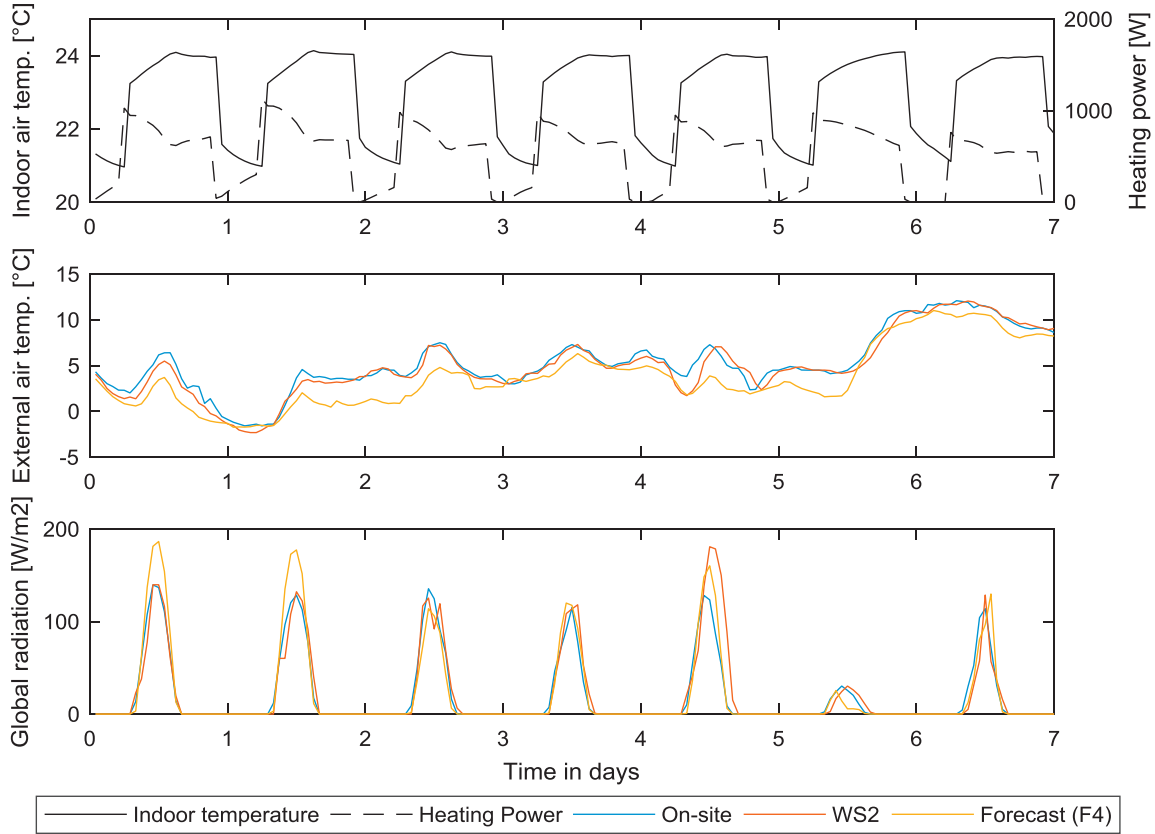


Fig. 6. One week of the hourly data used to identify grey-box models with three different sources for weather measurements.

peating the process multiple times with different initial conditions. The relatively simple model structure meant that suitable convergence of the parameter estimates was achieved using a simple excitation signal based on a night-setback of three degrees. However, this signal may not be sufficient for identification of models with stochastic occupancy.

Data from a period of two weeks was used as training data to identify models, while a third week was used for validation (cross-validation). The parameters in the grey-box models were identified using the gradient-based *greyest* function available in MATLAB's System Identification Toolbox [17]. Fig. 6 depicts a part of the data series used in the model identification process. Each data set used to train models consisted of indoor air temperature and heating power from the EP model (identical across all scenarios) and weather measurements specific to the scenario being evaluated.

To increase the robustness of the analysis, models of the ten apartments were identified using data from five different periods. This was done for each of the eight sources of weather data (i.e. F1–F5, WS1, WS2 and the on-site weather station) resulting in 400 RC-models of apartments to be evaluated as part of the control scheme of their respective scenarios. Because of this relatively large number of models, it was decided to keep the number of weather inputs at a minimum to ease the task of identifying the models. This was done by using the global radiation directly, instead of projecting it onto vertical surfaces in the four cardinal directions as suggested by Reynders et al. [18].

2.4. Model predictive control scheme

The MPC scheme used to operate the space heating of each apartment in the EP model was a so-called Economic Model Predictive Control (E-MPC) scheme, where the optimal sequence of control actions was determined by solving the optimization prob-

lem defined by Eq. 1a–g. A decentralized MPC scheme in which each apartment has its own control unit was chosen since previous studies indicated that decentralized schemes have similar performance to the more complicated centralized control schemes in terms of implementation [4,19]. The control objective was to minimize the total operational cost while maintaining room temperatures within a predefined comfort interval.

$$\underset{u}{\text{minimize}} \sum_{k=1}^N c_k^T \cdot u_k \quad (1a)$$

$$\text{subject to } x_k = \mathbf{A}x_{k-1} + \mathbf{B}u_{k-1} + \mathbf{E}d_{k-1} \quad (1b)$$

$$y_k = \mathbf{C}x_k \quad (1c)$$

$$0 \leq u_k \leq P_{\max} \quad (1d)$$

$$T_{\min,k} \leq y_k \leq T_{\max,k} \quad (1e)$$

$$\Delta T_{\min,k} \leq \frac{\Delta y_k}{\Delta t} \leq \Delta T_{\max,k} \quad (1f)$$

$$x_{0|k} = x_{0|k-1} + \mathbf{K} \cdot (y_{\text{measured}} - \mathbf{C} \cdot x_{0|k-1}) \quad (1g)$$

The objective function (1a) describes the price of implementing the full extent of the control sequence, u , under a forecasted sequence of time varying prices, c . The length of the sequence depends on the chosen prediction horizon, N . The building dynamics governed by the grey-box model is specified in (1b), while (1c) relates the states of the model to the indoor air temperature. The maximum available heating power is defined by (1d), and was in

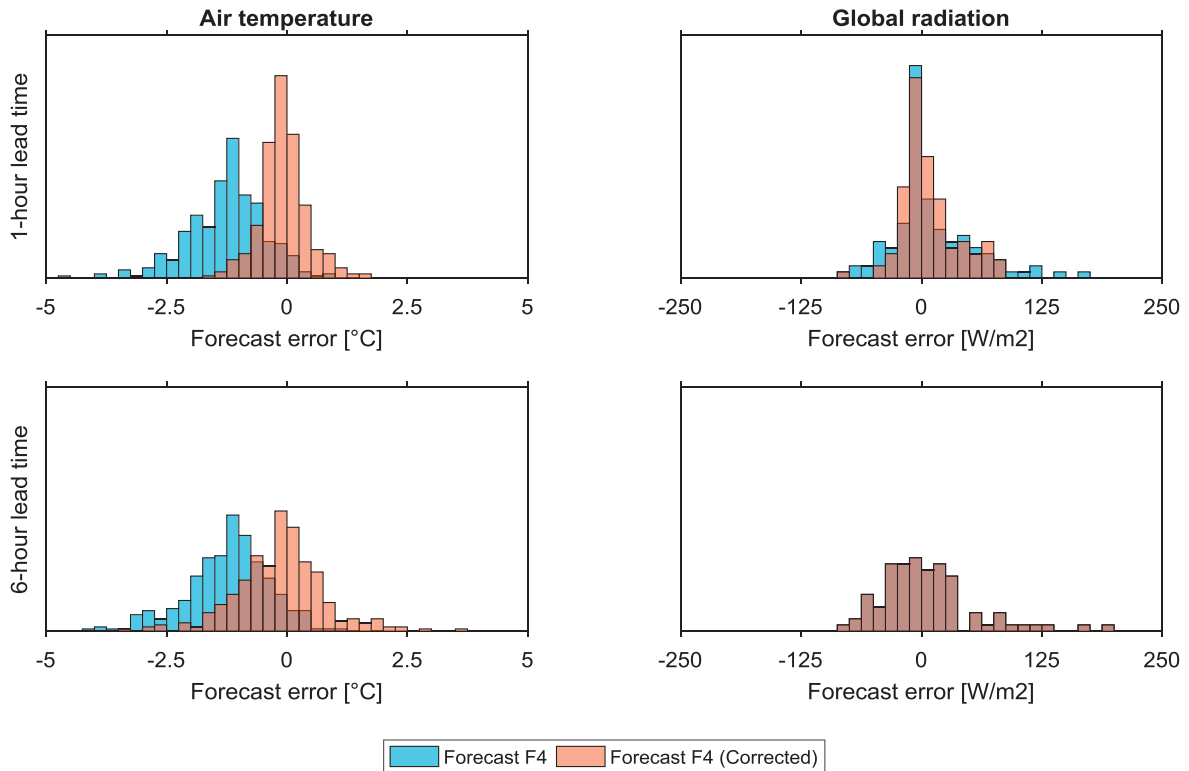


Fig. 7. Impact of forecast bias corrections of air temperature and global solar radiation on short-term forecast errors. Top: 1 h lead time. Bottom: 6 h lead time.

this study assumed to be 50 W/m^2 . The temperature interval in which thermal comfort was assumed was defined by (1e) as $20\text{--}24 \text{ }^\circ\text{C}$ for all apartments corresponding to thermal comfort class II in EN 15251 [20]. Temperatures outside of this range were considered comfort violations which were attributed a significant penalty in the optimization problem, such that the controller at all times tried to maintain temperatures within the specified temperature interval. Eq. (1f) constrained the temporal temperature gradient to not surpass the recommendation of $2.1 \text{ }^\circ\text{C/h}$ by ASHRAE [21]. Finally, Eq. (1g) used measurements to update the states of the model with a Kalman filter. Here, $x_{0|k-1}$ and y_k were the predicted and measured temperature in the building, respectively, while \mathbf{K} was the Kalman gain.

The implementation of the E-MPC scheme was based on the receding horizon principle [2], where an optimization problem was solved at a frequency depending on the time-resolution of the control unit. In this study a control frequency of one hour was used. The optimal sequence of control actions, u , was determined for a prediction horizon of 24 h. Only the first action of the sequence was implemented in the EP building, after which a new optimization problem was solved using updated weather forecasts and energy prices. The price signal used in the optimization problem of the control scheme was the historic whole-sale electricity price for the period (spot-market) excluding taxes, which were obtained from the Danish transmission system operator Energinet [22]. Consequently, the reported results should be interpreted as a way of comparing the performance of the MPC using different weather data sources rather than an indication of the actual obtainable savings in practice.

2.5. Bias-correction of weather forecasts

The presence of systematic biases in weather forecasts has resulted in the development of several methods for improving the accuracy of forecasts by using local measurements. Several studies

have used a Kalman filter for this purpose [13,23–24]. In the context of MPC of buildings, Gyalistras et al. [25] implemented a bias correction in the MPC scheme of an office building and found that performance varied between forecasts of different weather phenomena. The bias correction performed well when correcting forecasts of the outdoor air temperature (20–30% RMSE improvement), while the correction for some periods made the forecasts of global radiation worse by increasing the variability of the forecast errors. Gyalistras et al. [25] concluded the latter to be related to the use of a constant noise variance ratio for the Kalman filter and suggested that use of time-varying noise variance ratios could potentially address the issue.

Due to these findings, a bias-correction scheme was also implemented in this study to fully include the added value of having measurements available in the MPC operational phase. The correction scheme was used in all simulations of the A1 scenario and in half of the simulations from the A2 scenario, which was evaluated both with and without bias-correction (see Table 1). As elaborated on in Section 3.2, the simulations of the presented case study were limited to winter months. It is therefore considered unlikely that a time-varying and adaptive correction scheme would have a significant effect on the results, since one of the main strengths of these schemes is the ability to adapt to seasonal changes in the bias. Because of this, and to avoid issues with the tuning parameters as in [25], a time-invariant correction scheme based on the Kalman update equation was chosen. The correction scheme was defined by Eq. 2a and b.

$$\epsilon_0 = T_0^{\text{OBS}} - T_0^{\text{F}} \quad (2a)$$

$$T_i^{\text{F}*} = T_i^{\text{F}} + K_f \cdot \epsilon_0 \cdot e^{b \cdot i} \quad \forall i = 0, \dots, N-1 \quad (2b)$$

Eq. 2a defines the forecast error (ϵ_0) calculated as the difference between the observation (T_0^{OBS}) and the forecasted value (T_0^{F}). The correction was then applied as defined in Eq. 2b, which is a modification of the update equation of the Kalman filter. Here, the

size of the correction is determined by the forecast error (ϵ_0) and a time-invariant gain (K_f). Furthermore, it was decided to let the correction decay as the lead time (denoted i) of the forecasted value increased (i.e. $b < 0$). The length of the forecasts (N) matches the prediction horizon of the MPC scheme described in Section 2.4. The decay was included to reflect the fact that the information provided by the observation diminishes over time. Therefore, the correction is applied to the first hour of the forecast in full effect, after which the size of the correction decays as a function of the lead time. The outline of the correction scheme is based on the external air temperature forecasts. For the correction of solar radiation, the correction scheme was slightly adapted to ensure corrections that would not result in negative solar radiation in the forecasts. To ensure a well-performing correction scheme suitable for the purposes of the case study, the gain (K_f) of the correction and the rate-of-decay (b) were optimized using forecasts and weather measurements from the simulated period itself. The objective of the optimization was to minimize the sum of forecast errors throughout the forecast. In practice, a similar scheme could be used to obtain an adaptive correction similar to the Kalman filter-based methods. The gain (K_f) was fixed at 1 and 0.6 for the correction of air temperature and global radiation, while the corresponding rates of decay (b) were fixed at 0.02 and 0.04, respectively. The introduction of the decay slightly increased the performance of the correction scheme despite the fact that the relatively small rates of decay for both parameters indicated that the information provided by the observations only diminished rather slowly. The impact of the correction scheme on one of the forecast series is presented in Fig. 7. The bias correction was highly efficient in removing the systematic biases of the air temperature forecasts. The forecast errors of the global radiation, however, were characterized by an insignificant bias and relatively high variability; the latter makes it difficult to achieve reliable estimates of the forecast error which resulted in the correction scheme generally applying smaller corrections.

3. Results

The effect of using the different weather data sources outlined in Table 1 were evaluated in terms of model quality as well as the performance of the models when used for MPC.

3.1. Quality of the models

The quality of the identified models using the different weather data sources was evaluated on the training and validation data, respectively, using the normalized root mean square error (NRMSE) as the performance metric:

$$NRMSE = 100 \cdot \left(1 - \frac{\|y - \hat{y}\|}{\|y - \bar{y}\|} \right) \quad (3)$$

where y is the measured zone temperature, \hat{y} is the simulated temperature of the identified model and \bar{y} is the average of the measured zone temperature time series. The metric thus relates the size of the prediction errors to the variability of the air temperature measurements. The resulting NRMSE-fit percentages are directly comparable since only the weather inputs of the model (external temperature and solar radiation) varied between control configurations, whereas the temperature measurements from the EP model (i.e. y and \bar{y}) were identical across all datasets.

Table 2 lists the average NRMSE-fit percentage for the apartment models, where the entries of each row describe 50 models (10 apartments, modelled with data from five different periods). As expected, models identified using forecast data tended to be characterized by lower NRMSE-fits than the models identified using measured weather data. On-site measurements led to the highest fits on both training and validation data, while models identified

Table 2

Average NRMSE-fit percentages for the ten apartment models for all data sources.

Weather data		Model NRMSE-fit [%]			
		Training data		Validation data	
Weather data source		Average	Std. dev.	Average fit	Std. dev.
Forecast data	F1	82.2	0.3	75.3	0.6
	F2	81.7	1.7	75.1	0.5
	F3	82.1	0.7	75.1	0.6
	F4	82.0	0.4	73.7	0.8
	F5	75.8	7.3	69.0	2.0
WS data	WS1	86.2	0.4	82.5	1.4
	WS2	83.6	1.0	75.2	1.6
On-site data		90.4	0.4	87.6	0.9

using forecasts from F5 achieved the lowest fits on average; most likely caused by the wider distribution of forecast errors of the F5-forecasts (see Fig. 3). While use of the data from WS1 resulted in models nearly on par with those derived from on-site measurements, the models identified with WS2 data generally resulted in models of similar quality to those derived with forecast data. Fig. 8 shows the impact of the biased weather data on the estimates of the overall heat loss coefficients and the solar apertures for the 400 apartment models identified.

The results presented on Fig. 8 suggests a relation between the bias of a given weather measurement, and the corresponding parameter estimate obtained in the physics based state space model: A biased estimate of the external air temperature affects the estimates of the overall heat loss coefficient, where negative biases (temperature measurement colder than actual conditions) generally resulted in lower estimates of the heat loss coefficients and vice versa. Similarly, negatively biased global radiation (WS2) data was compensated for through higher estimates of the solar aperture (equivalent window area).

These tendencies support the notion that RC-models can only be trusted to predict accurately when the predictions are made using weather data with a bias similar to that of the data initially used to train the models. This is the reason it makes sense to bias-correct forecasts using measurements from the same sensors that were used in the initial model identification. The alternative of doing so is to use the forecasts directly in both phases (i.e. for identification and prediction), as proposed in the A3 scenario, whereby any discrepancy between data sources is removed entirely if the bias can be assumed stationary.

3.2. MPC performance

The differences in model quality indicated in Table 2 may affect the ability of the E-MPC scheme to maintain temperatures within the specified comfort bounds as well as the potential for generating cost savings. Therefore, we also evaluated the performance of the models when used for E-MPC as described in Section 2.4 over a three month simulation period covering a typical Danish heating season (1 December 2016–28 February 2017). Two E-MPC performance metrics were used: the achieved economic savings and the extent of thermal comfort violations. Savings were defined as the reduction in space heating costs obtained by E-MPC when compared to the space heating costs of a reference simulation in which the air temperature was maintained at the lower bound of the comfort range. Comfort violations were quantified as the number of degree-hours where the indoor air temperature was outside the comfort bounds. Both metrics are necessary to obtain a fair performance evaluation, since e.g. frequent violations of the lower set point lowers the overall consumption thereby giving the appearance of high savings. Fig. 9 depicts indoor air temperature and heating consumption data from three scenarios together with on-

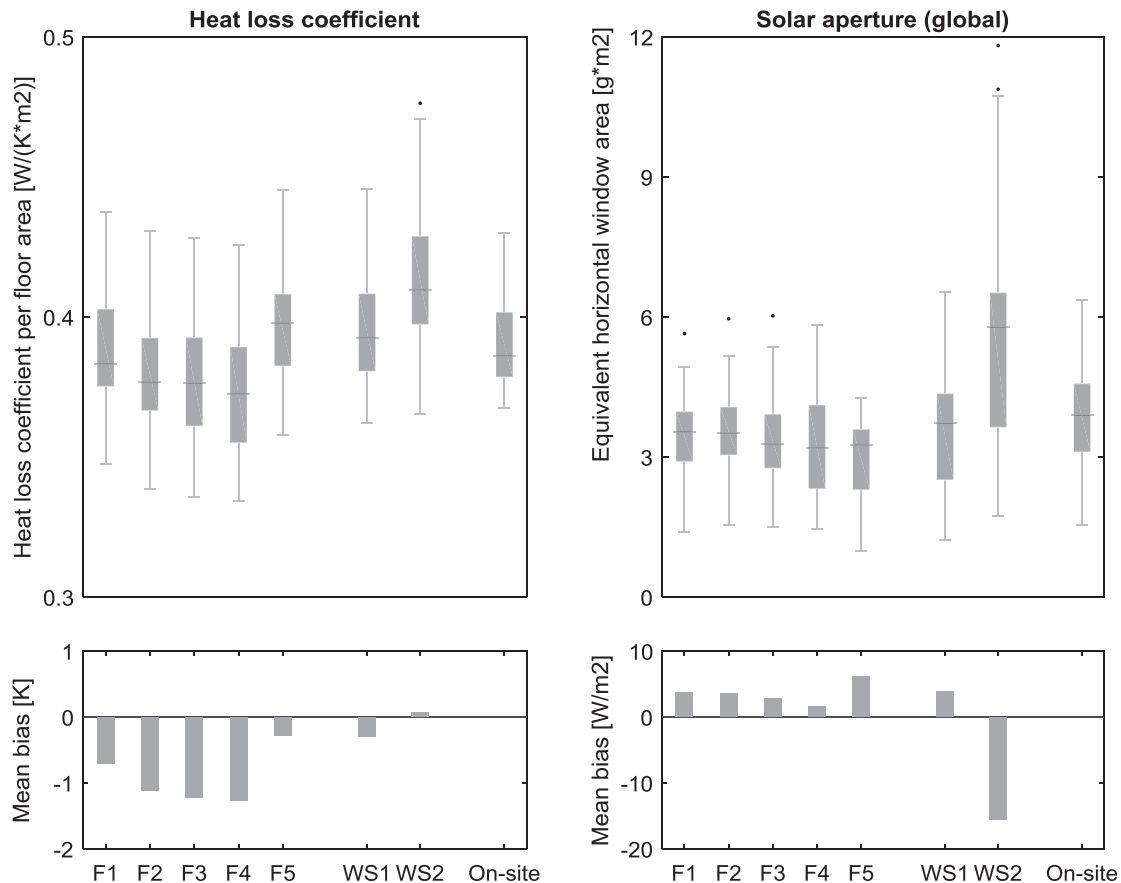


Fig. 8. Parameter estimates across grey-box models identified using data from different sources.

site weather conditions and the utility price signal used for the optimization in the E-MPC scheme. Three time-series were selected to aid the interpretation of the overall results: 1) a simulation from the performance bound scenario with low comfort violations and relatively high cost savings, 2) the simulation that led to the highest comfort violations from scenario A2, and 3) a simulation from scenario A3 with average performance in both metrics.

The pattern of the energy consumption and the time-varying energy price indicate the general mechanism of the E-MPC scheme in all scenarios; space heating consumption was increased whenever fluctuations in the price encouraged it (i.e. during low price periods or just before a high price period).

The simulation from scenario A2(WS2) was the least capable of maintaining temperatures above the specified lower limit of 20 °C. The time-series also indicate that the comfort violations typically occur during hours of high global radiation. This can be attributed to the tendency of WS2 data leading to the solar aperture being overestimated for some of the identified models, see Fig. 8. In addition to this, the model used in the depicted WS2 simulation also seemed to describe the dynamics of the building inadequately, which at several points throughout the simulation led to control actions significantly different than those made in the more similar simulations of the PB and A3 scenarios.

Fig. 10 presents the MPC performance (energy savings and comfort violations) of each scenario using forecast data from each of the five forecast locations shown in Fig. 1. The models used in scenario A3 were identified using forecast data obtained at the same point as the forecasts used in the operational phase, while models used in scenarios A1 and A2 were identified using measured weather data. Scenario A2 was simulated twice using data from WS1 and WS2, where each simulation was carried out using raw

and corrected forecasts. Finally, the PB is depicted as a single boxplot bar since only one forecast series was used (perfect forecasts). The horizontal red line in the second box plot denotes the number of degree hours that correspond to a 1-degree violation occurring in 5% of the dwelling's time-of-use (assumed 24/7), in accordance with EN 15,251 [18].

Each boxplots contains results from the 50 MPC simulations (ten apartments each simulated five times with different RC models as per Section 2.3). The horizontal line of each box indicates the median while the box itself contains simulation results within the first and third quartile (also referred to as the interquartile range or IQR), while the whiskers contain the remaining results. The size of the whiskers were limited to 1.5 times the IQR, while points residing outside these limits were regarded as outliers.

The vast majority of MPC simulation results indicated savings in the range of approx. 9–12% compared to the costs of the reference case (PI control). The highest energy savings were not achieved by the PB, but by scenario A1 which, on the other hand, had almost twice as many comfort violations as the PB. The energy savings achieved in scenarios A2 and A3 tended to be slightly lower and characterized by higher variability than those obtained in the A1 and PB scenarios. Here, especially the energy savings in scenario A3 using forecasts from location F5 stood out with higher variation between simulations.

The majority of scenarios led to rather similar magnitudes of comfort violations (approx. 40–50 Kh) with fewer violations for the PB scenario and more frequent violations for the A2(WS2) scenario. The A2(WS2) simulations were also characterized by a significant number of outliers in both directions which most likely is linked to the large spread in parameter estimates apparent from Fig. 8. The outliers with high comfort violations were the only results indicat-

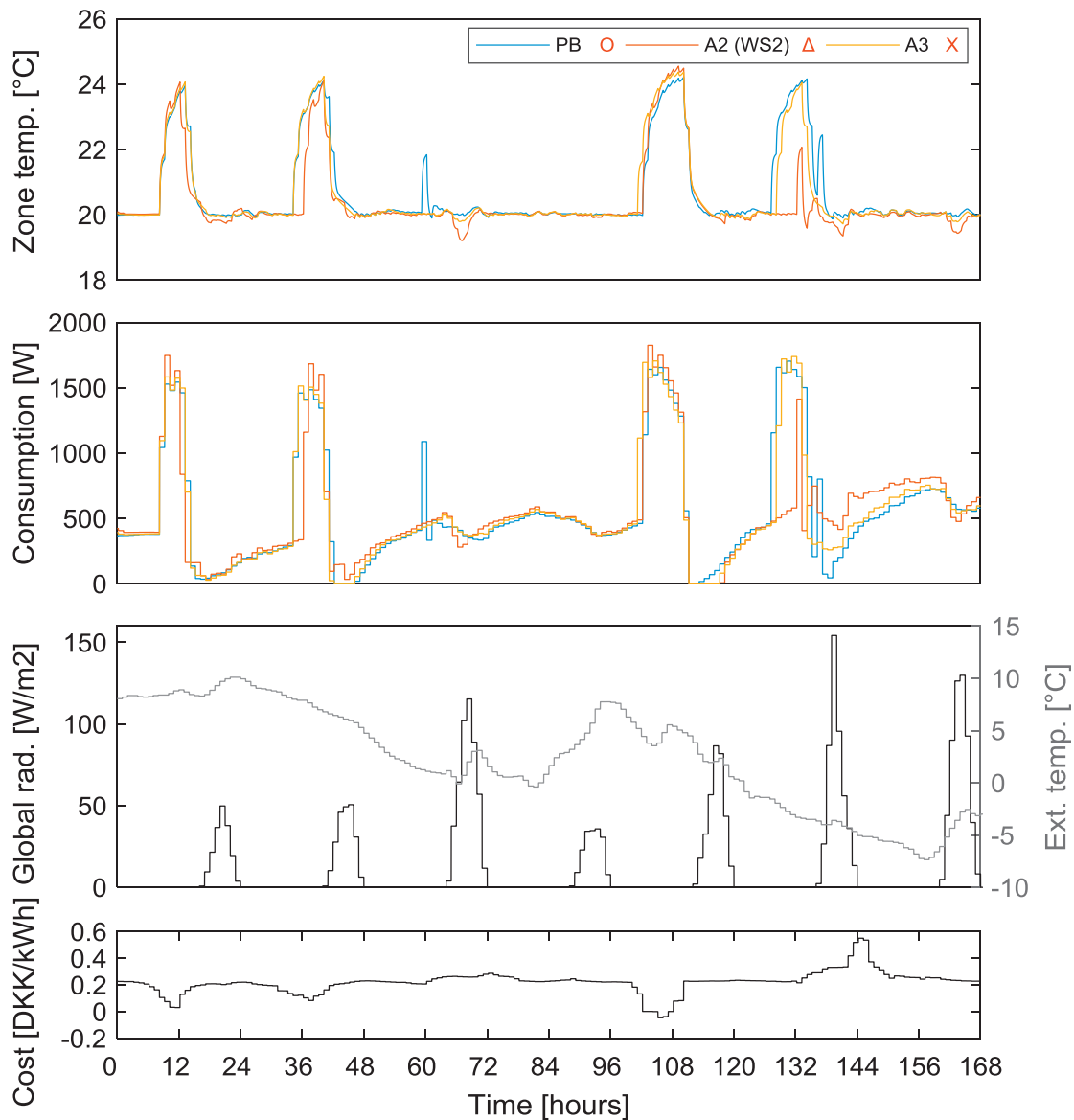


Fig. 9. Simulation data from an apartment controlled by the E-MPC-scheme for three weather source data scenarios. The red symbols in the legend refer to the results of Fig. 10. (For interpretation of the references to color in this figure legend, the reader is referred to the web version of this article.)

ing poorer performance than the guidelines specified in EN 15,251 [18].

Finally, the bias-correction of incoming weather forecasts in the A2 scenarios only led to an insignificant increase in average savings (<0.2%). The reduction of comfort violations for the A2(WS1) scenarios were also insignificant due to the fairly low bias of the measurements from WS1. However, the bias correction of the more biased WS2 measurements reduced comfort violations by 11% because the effect of the positively biased measurements from WS2 was amplified by the mainly negatively biased forecast series.

4. Discussion

The variability of the results within each of the scenarios shown in Fig. 10 can be caused by either varying accuracy of the sources of weather data between the five periods, or that the actual weather conditions during some periods was less suited for dynamic modelling. An example of the latter could be extended periods of cloudy weather with low solar heat gains. The impact of these factors can likely be addressed through frequent recalibration

of the control models; we consider this a topic for future studies. Similarly, the impact of neglecting occupants and the internal heat gains related to them is a topic worth investigating further. While this uncertainty would apply to all of the investigated scenarios, one could argue that the data sets derived from weather forecasts could be more sensitive to these, due to their generally lower signal-to-noise ratio compared to the data sets relying on on-site sensors.

Furthermore, despite the seemingly large differences in comfort violations resulting from the different scenarios, detailed inspection of the results indicated that the bulk of the comfort violations were of small amplitude; 74% of the observed degree-hours were caused by violations of less than half a degree, which are considered likely to go unnoticed by occupants. The comfort violations surpassing the 0.5 °C threshold typically occurred in hours with high solar radiation. This is likely due to the adoption of the global solar radiation as the measure of solar heat gains which, due to the East/West oriented facades of the building, overestimates the solar heat gains during mid-day when a high amount of solar radiation is on the windowless South-oriented part of the envelope.

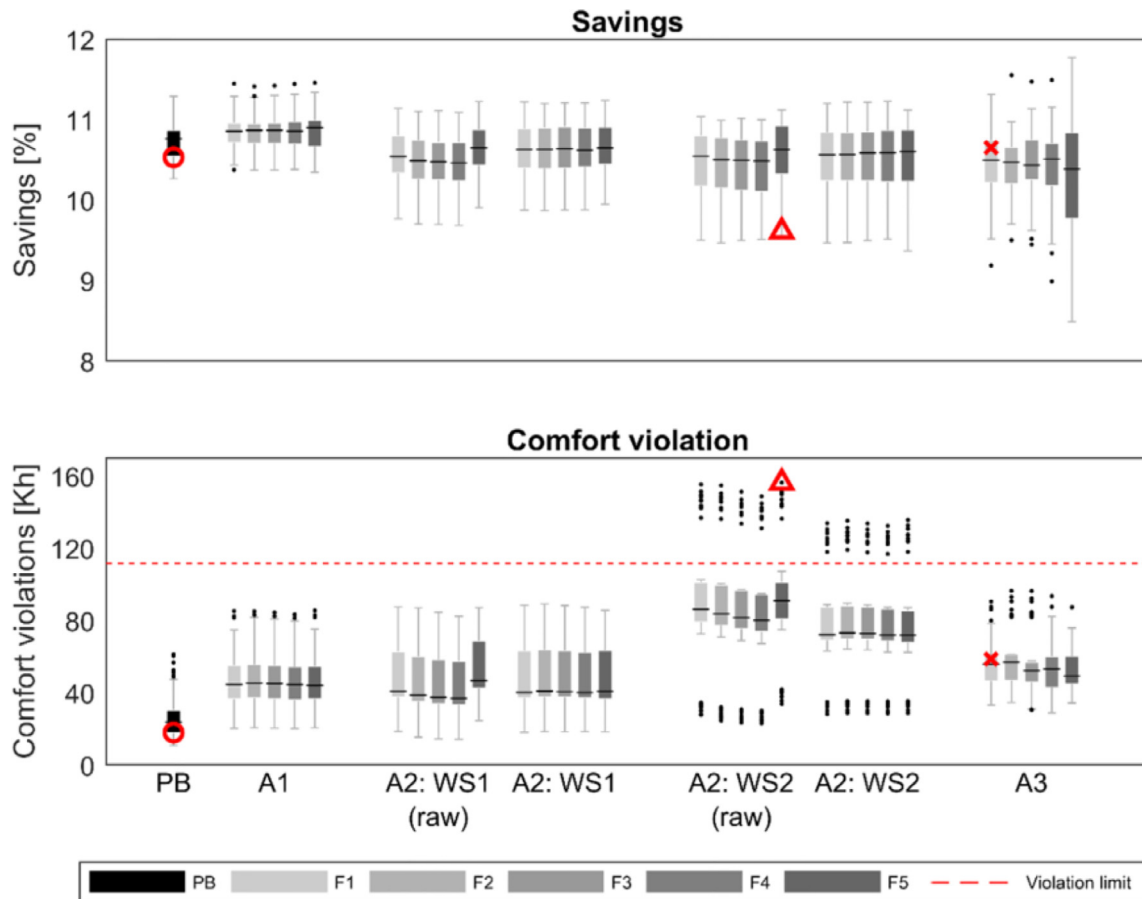


Fig. 10. Energy savings and comfort violations from the MPC simulations of the different scenarios (see Table 1) using weather forecasts from different locations (see Fig. 1). Red symbols refer to specific simulations shown on Fig. 9. (For interpretation of the references to color in this figure legend, the reader is referred to the web version of this article.)

However, this issue can to a wide extent be addressed by implementing a P(ID)-control to maintain the lower temperature set points as previously proposed in Pedersen et al [4].

Finally, we acknowledge that the results from the A2 scenarios involving public weather stations are case specific. These scenarios were included merely to illustrate how the perhaps most obvious alternative to on-site measurements may affect performance. However, the ability to identify building models using on-site measurements as in scenario A1 does not depend on the location. Similarly, it is reasonable to assume that the accuracy of the HIRLAM (or similar) meteorological forecast model used in scenario A3 does not vary significantly with location.

We therefore consider it likely that the results from the A1 and A3 scenarios can be reproduced in other locations – at least in locations with temperate climate like the Danish.

5. Conclusion

A practical barrier for deploying MPC of space heating in residential buildings is the cost of obtaining on-site or public weather measurements needed for identifying the building models in the MPC scheme. In this paper, we have therefore presented an analysis on whether this cost can be eliminated by using a weather forecast service as an alternative to weather measurements.

The results indicated that identifying models using on-site measurements led to the best MPC performance. In comparison, the use of public weather stations led to a generally lower performance – the degree of the impact depending on the particular weather station investigated. The results from the proposed ap-

proach relying on access to a weather forecast service only led to a minor impact on the MPC performance; the average savings decreased by less than 0.5% points while the daily average comfort violations increased with less than 0.1 Kh (degree hours) compared to the use of on-site measurements. The simulation results thereby suggest that an MPC setup for space heating of residential buildings relying solely on a weather forecast service and two internal sensors (zone temperature and heating power) may constitute a cost-efficient alternative to a setup relying on on-site or near-by weather measurements. However, more case studies are needed to support the key conclusion of this paper. Furthermore, future studies should investigate the viability of the method when applied in real buildings under the influence of stochastic occupancy and other uncertainties.

Acknowledgments

The authors gratefully acknowledge the support of this work from the project “READY.dk” financed by the Danish energy research and development program ForskEl and the project ‘Resource Efficient Cities Implementing Advanced Smart City Solutions’ (READY) financed by the 7th EU Framework Program (FP7-Energy project reference: 609127). Furthermore, the authors would like to thank the Danish Meteorological Institute for providing the used forecasts, as well as the district heating supply company AalborgVarme Aarhus for providing the measurements from the two commercial weather stations used in the analysis.

References

- [1] M. Killian, M. Kozek, Ten questions concerning model predictive control for energy efficient buildings, *Build. Environ.* 105 (2016) 403–412.
- [2] F. Oldewurtel, A. Parisio, C.N. Jones, D. Gyalistras, M. Gwerder, V. Stauch, B. Lehmann, M. Morari, Use of model predictive control and weather forecasts for energy efficient building climate control, *Energy Build.* 45 (2012) 15–27, doi:10.1016/j.enbuild.2011.09.022.
- [3] R. Halvgaard, N.K. Poulsen, H. Madsen, J.B. Jørgensen, Economic model predictive control for building climate control in a smart grid, *IEEE PES Innovative Smart Grid Technologies*, 2012 Washington, DC, doi:10.1109/ISGT.2012.6175631.
- [4] T.H. Pedersen, R.E. Hedegaard, S. Petersen, Space heating demand response potential of retrofitted residential apartment blocks, *Energy Build.* 141 (2017) 158–166.
- [5] M. Ali, A. Alahäivälä, F. Malik, M. Humayun, A. Safdarian, M. Lehtonen, A market-oriented hierarchical framework for residential demand response, *Electr. Power Energy Syst.* 69 (2015) 257–263, doi:10.1016/j.ijepes.2015.01.020.
- [6] J. Ma, J. Qin, T. Salsbury, P. Xu, Demand reduction in building energy systems based on economic model predictive control, *Chem. Eng. Sci.* 67 (2012) 92–100, doi:10.1016/j.ces.2011.07.052.
- [7] F. Oldewurtel, A. Ulbig, A. Parisio, A. G., M. M., Reducing peak electricity demand in building climate control using real-time pricing and model predictive control, in: 49th IEEE Conference on Decision and Control, Atlanta, 2010, pp. 1927–1932, doi:10.1109/CDC.2010.5717458.
- [8] S. Privara, J. Cigler, Z. Váňa, F. Oldewurtel, C. Sagerschnig, E. Žáčková, Building modeling as a crucial part for building predictive control, *Energy Build.* 56 (2013) 8–22, doi:10.1016/j.enbuild.2012.10.024.
- [9] U. S. Department of Energy, EnergyPlus.net, 2016 [Online]. Available: <https://energyplus.net/> [Accessed 29-01-2016].
- [10] The MathWorks, inc., MATLAB 2016a (9.0.0.341360), 2016.
- [11] Lawrence Berkeley National Laboratory, Buildings Control Virtual Test Bed - BCVTB (1.4.0) [Online].
- [12] Danish Meteorological Institute, HIRLAM: DMI DMI, [Online]. Available: <https://www.dmi.dk/laer-om/temaer/atmosfaeren/hirlam> (Accessed 12-07-2017).
- [13] R. Libonati, I. Trigo, C.C. DaCamara, Correction of 2 m-temperature forecasts using Kalman filtering technique, *Atmos. Res.* 87 (2008) 183–197.
- [14] O.A. Alduchov, R.E. Eskridge, Improved Magnus Form Approximation of Saturation Vapor Pressure, 1997 United States, doi:10.2172/548871.
- [15] A.S. Kalogirou, *Solar Energy Engineering*, Academic Press, Cambridge, 2013.
- [16] R.E. Hedegaard, S. Petersen, Evaluation of grey-box model parameter estimates intended for thermal characterization of buildings, *Energy Procedia* 132 (2017) 982–987.
- [17] The MathWorks, inc., System identification toolbox 9.4, [Online]. Available: <https://se.mathworks.com/help/ident/ref/greyest.html> (Accessed 24-01-2018).
- [18] G. Reynders, J. Diriken, D. Saelens, Quality of grey-box models and identified parameters as function of the accuracy of input and observation signals, *Energy Build.* 82 (2014) 263–274.
- [19] T.H. Pedersen, R.E. Hedegaard, M.D. Knudsen, S. Petersen, Comparison of centralized and decentralized model predictive control in a building retrofit scenario, *Energy Procedia* 122 (2017) 979–984.
- [20] European Committee for Standardization. (2007). EN 15251: Indoor environmental Input Parameters For Design and Assessment of Energy Performance of Buildings Addressing Indoor Air quality, Thermal environment, Lighting and Acoustics Brussels, European Standard.
- [21] ASHRAE, Standard 55-2010: Thermal Environmental Conditions for Human Occupancy, ASHRAE, Atlanta, 2010.
- [22] Energinet.dk, The wholesale market: download of market data, [Online]. <http://www.energinet.dk/EN/El/Engrosmarked/Udtraek-af-markedsdata/Sider/default.aspx> [Accessed 23-04-2016].
- [23] M. Homleid, Diurnal corrections of short-term surface temperature forecasts using the Kalman filter, *Weather Forecasting* 10 (1995) 689–707 nr. doi:10.1175/1520-0434(1995)010<0689:DCOSTS>2.0.CO;2.
- [24] L. Delle Monache, J. Wilczak, S. McKeen, G. Grell, M. Pagowski, S. Peckham, R. Stull, J. McHenry, J. McQueen, A Kalman-filter bias correction method applied to deterministic, ensemble averaged and probabilistic forecasts of surface ozone, *Tellus B* 60 (2) (2008) 238–249, doi:10.1111/j.1600-0889.2007.00332.x.
- [25] D. Gyalistras, M. Gwerder, Use of weather and occupancy forecasts for optimal building climate control (OptiControl): two years progress report, Terrestrial Systems Ecology, ETH Zurich & Building Technologies Division, Siemens Switzerland Ltd., Zürich, 2010.

5.2 Epilogue

This study investigated whether the task of obtaining control-oriented models of residential buildings could be simplified by substituting weather measurements with forecasts from a meteorological weather service. In the study, excitation was imposed on the building through a conventional night-setback scheme. Identification of models suited for MPC was achieved, despite the lower frequency content associated with this input signal. In this context, a significant assumption made in the analysis was the neglect of stochastic occupancy and the effects that it can have not only on MPC performance, but also in particular on the input-output data used for identifying the control-model. While this simplification could potentially affect the robustness of the conclusions, the study of Reynders et al. [54] found that the impact of occupants could be reasonably accounted for by using the domestic electricity consumption as an indication of the internal heat gains. The same study also suggested that the accuracy of model predictions could be improved by projecting the solar radiation onto vertical surfaces facing each cardinal direction, as opposed to the approach of using the horizontal global radiation that was applied in the present study. Despite the potential performance gain, oriented solar radiation inputs were not adopted since they would require the introduction of either additional model parameters (effective window areas facing each direction) or, alternatively, an assumed distribution of windows on each building façade.

The results indicated that the use of forecasts only resulted in a minor impact on the performance of the MPC algorithms. If similar performance can be achieved in actual buildings as well as for locations other than the one featured in the study, the analysis suggests this implementation method to be an effective means of reducing the complexity of the technical infrastructure needed to implement MPC in residential buildings and, by extension, the associated costs. Conducting proof-of-concept experiments in actual buildings is considered a relevant future research endeavour.

This chapter concludes Part I of this thesis. In Part II, an outline of the historical developments that have led to the current peak of interest in demand response is presented along with chapters presenting the research related to the research objectives of Part II.

PART II
DEMAND RESPONSE IN
RESIDENTIAL SPACE HEATING

6 DEMAND RESPONSE – THEN AND NOW

In recent years, the concept of balancing supply and demand by controlling the demand for electricity has received a great deal of attention from researchers. While this may seem like a break away from the load-driven structure of the electricity grid we are mostly familiar with today, the practice of interfering with *when* and *how* consumers consume electricity is not by any means new. In a historic review, Kidd [58] stated that the first known attempts to introduce time-varying price tariffs date back to 1897, and were motivated by the large daily fluctuation in demand caused by street lighting in the evenings. In the period following the Second World War, several utility companies retained the right to switch off water heaters during daily recurring peaks, which at this time were caused by midday cooking. The energy crisis of 1973 sparked new development in the field of *load management* throughout the 1970s. In spite of these developments, the field was still in its infancy, with a lack of common terminology [59]. In the 1980s, a series of articles by Clark Gellings et al. on the topic attempted to remedy this by formalizing the concept of demand side management (DSM) [60–62]. In 1985, Gellings provided the following definition of DSM [61]:

‘DSM is the planning, implementation, and monitoring of those utility activities designed to influence customer use of electricity in ways that will produce desired changes in the utility’s load shape, i.e., changes in the time pattern and magnitude of a utility’s load.’ – Clark W. Gellings

This definition clearly suggests that *demand side management* spans demand-side initiatives aimed at both energy conservation (e.g. energy retrofits) and load management initiatives that alter the temporal distribution of demand. In recent years, however, the terminology surrounding DSM has again become subject to confusion with the introduction of the term *demand response* (DR). Among the earliest identified occurrences of the *demand response*-term in the context of DSM is the conference article written by Fereidoon Sioshansi titled *‘Demand response: the sequel*

to DSM?’ [63], which was later expanded in [64]. In these works, the authors argue that the load management techniques of DSM such as real-time pricing (RTP) and DR are two different (but complementary) initiatives, and promote the following distinction between them: RTP programmes advise customers on how to adjust their consumption based on variable electricity prices, thereby incentivizing behaviour that has a low impact on the grid. DR programmes, on the other hand, deal with immediate capacity issues and address these by encouraging flexible consumers to reduce their load when networks are congested.

Regardless of exact definitions, the close resemblance between the concepts of DR and DSM has led many researchers to use the two terms interchangeably. Recently, several larger entities have also adopted DR in their active terminology. This is the case in the federal ruling in Order No. 745 of the U.S. Federal Energy Regulatory Commission (FERC) – in which the FERC dictates that DR resources capable of reducing consumption should be compensated with the same marginal prices in the electricity wholesale markets as if they met that demand by generating electricity [65]. Similarly, the International Energy Agency used DR to cover both RTP schemes and other price-based schemes aimed at altering the demand of consumers [66]. The growing consensus seems to be that DSM can refer to both permanent measures (e.g. promoting energy efficiency) and temporary measures (load shifting and curtailment), whereas DR can only refer to the latter; I will not engage in further discussion of terminology here, but simply adopt this definition. Furthermore, the term *DR schemes* (or *DR programmes*) will refer to the agreement between actors on the demand and supply side, which may include details related to incentive mechanisms as well as other consumer or grid-related constraints relevant to the given DR initiative. Finally, a *DR event* refers to a given period during which normal operation has seized and DR is in effect. In this context, DR may refer to a deviation from the business-as-usual demand profile that may be both positive and negative.

The literature on DR (or DSM) shows that consumers, although motives may have shifted along the way, have been brought into play in the task of balancing supply and demand at several moments throughout history. The recent large-scale expansion of energy production from intermittent renewable sources constitutes a new challenge in this regard, which has prompted a new wave of research activity within the area of DR. The significant amount of consumption that takes place in buildings has naturally resulted in them being considered suitable candidates for DR [3, 18–19]. However, just as DR is not a new concept, neither is the idea of utilizing the thermal inertia of buildings for DR purposes. Already in 1981, Gellings [60] listed several

manufacturers of systems that were aimed at conducting DR by utilizing underfloor heating systems as structural thermal energy storage. However, the author states that the control methods used at the time were unable to ensure acceptable thermal conditions in the building and thus resulted in overheating. These issues dampened enthusiasm for the concept and hindered its use in practice. Recent developments in advanced control schemes, wireless technology and smart metering have reignited research on the utilization of structural thermal energy storage. In their review, Shaikh et al. [23] found several control methods that have been applied in research on so-called *smart buildings*. The list included dynamic programming, fuzzy logic, artificial neural networks and model predictive control. Of these methods, model predictive control (MPC) was found to be the most frequently used by researchers.

MODEL PREDICTIVE CONTROL

MPC schemes that control space heating in buildings rely on a dynamic model of the building to predict the influence of its own control actions as well as the effects of external phenomena such as weather conditions, and use these predictions to identify the optimal sequence of control actions. In addition to the predictive nature of these control schemes, other often-praised advantages of MPC schemes are their ability to handle multiple objectives; incorporate explicit constraints on the system state or control actions; and account for interactions between different sub-systems with possibly conflicting objectives [67]. These advantages and consideration of the future impacts of current control actions make MPC highly suitable for addressing the comfort issues that, according to Gellings, had previously hindered attempts to utilize structural thermal energy storage for DR purposes. Although MPC was developing as a control method around the same time that Gellings noted comfort-related issues in his 1981 article (see e.g. [68–69]), the control method would for many years primarily be used in refinery and chemical process control applications [70]. Only in approximately the last two decades, have researchers have started to consider MPC as a viable approach to building control [25]. Early research related to MPC in buildings includes that of Florita and Henze [71], Oldewurtel et al. [72], and Dong et al. [73].

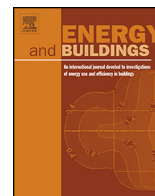
Recent years have seen a steep increase in the number of studies on MPC and its potential for enabling DR in buildings [74]. Several authors have conducted extensive reviews of MPC and its uses in buildings; see e.g. the recent reviews of Clauß et al. [75] and Benndorf et al. [67]. The authors of the latter especially provide an extensive overview of current literature, and also dedicate a significant portion of their review to describing the various aspects of MPC, including

modelling approaches; optimization approaches; introduction of feedback (state estimation); handling of uncertainties; and choice of optimization objectives. Therefore, no review of MPC theory or the current body of research on MPC is given here.

The following sections present the research contributions of this project that relate to DR in residential buildings. Each chapter presents one of the primary research publications, which may be concerned with one or several of the objectives of this second part of the thesis. Relevant secondary research contributions are referenced and discussed where appropriate.

7 IMPACT OF BUILDING CHARACTERISTICS

The potential of utilizing the inherent thermal mass of buildings for short-term thermal energy storage depends on several factors. The fundamental analysis of Reynders [33] indicated that increasing the energy efficiency of a building (e.g. through retrofitting) increases the efficiency at which thermal energy may be stored in the structural mass of the building and, by extension, the efficiency at which demand may be shifted in time. However, the analysis also indicated that storage capacity, i.e. the amount of energy that can be stored in the thermal mass during a DR event, decreases as the energy efficiency of a building is improved. A factor that may affect DR enabled through MPC schemes is the heat exchange between adjacent thermal zones (e.g. adjacent apartments), which has been shown to potentially deteriorate MPC performance if not incorporated in the control scheme [76]. Finally, in addition to aspects related to the specific building and the MPC implementation method, the potential of DR is also inherently dependent on the economic incentive offered to consumers for participating in DR events. Several studies have used hourly tax-free prices from the day-ahead wholesale electricity market as the main incentive for consumers to engage in DR, see e.g. [34–35, 77]. However, the study presented in (S3) indicated that time-invariant tax components of the electricity price paid by consumers is inhibitive of price-based DR [78]. The following section presents a paper on how these aspects influence the potential of conducting DR by using MPC to exploit the structural thermal mass of a typical Danish apartment building. The results are evaluated for both an existing and several retrofitted versions of the building in order to investigate how the relationships between building characteristics and storage capability identified by Reynders [33] manifest themselves in the control actions of both centralized and decentralized MPC schemes. The tax components of the Danish electricity price were included in the analysis, but made time varying by redistributing them according to the methodology described in [78]. The analysis thereby aims to provide insights on thesis objectives **2.1**, **2.2** and **2.3**.



Space heating demand response potential of retrofitted residential apartment blocks



Theis Heidmann Pedersen*, Rasmus Elbæk Hedegaard, Steffen Petersen

Department of Engineering, Inge Lehmanns Gade 10, Aarhus University, DK-8000 Aarhus C, Denmark

ARTICLE INFO

Article history:

Received 23 September 2016

Received in revised form

21 December 2016

Accepted 13 February 2017

Available online 17 February 2017

Keywords:

Economic model predictive control

Demand response

Energy flexibility

Residential space heating

Structural thermal storage

ABSTRACT

In future and smarter energy systems, time varying energy prices enable indirect demand response (DR) to assist the electricity supply system to meet demand. This simulation-based study investigates how economic model predictive control (E-MPC) schemes for space heating operation can utilize the thermal mass in an existing multi-story apartment block and eight retrofit scenarios to provide DR. The performance of the E-MPC scheme was evaluated in terms of its ability to enable end-user cost savings, reduce CO₂ emissions and to perform load shift of the heating demand compared to a conventional PI controller. Two E-MPC approaches were considered: centralized E-MPC where inter-zonal effects were considered and decentralized E-MPC that neglected heat transfer between adjacent apartments. The E-MPC schemes led to increasing cost savings (up to approx. 6%) and reduced CO₂ emissions (up to approx. 3%) as a function of increasing energy efficiency of the retrofit scenarios. The absolute amount of shifted power from peak load periods was rather consistent (approx. 2 kWh/m² heated net area) across all retrofit scenarios compared to the existing building. The centralized E-MPC scheme led to marginally better results than the decentralized E-MPC. The added complexity involved in establishing a centralized E-MPC compared to a decentralized E-MPC may therefore not be worth the effort.

© 2017 Elsevier B.V. All rights reserved.

1. Introduction

Instantaneous balance between supply and demand is a mandatory characteristic of the electricity supply system. Today, this balance is ensured almost exclusively by adjusting supply to meet demand. However, sheer supply-side management (SSM) is inefficient in systems with a high penetration of intermittent renewable energy sources (RES) such as wind turbines and photovoltaics [1]. Demand-side management (DSM) can to some extent assist supply-side management in such systems. There are different categories of DSM [2]. Traditionally, the most favored aspect of DSM has been energy efficiency [3,4] but recently several studies have explored the potential of demand response (DR), where consumers adjust their demand to meet supply [5–9]. It has mainly been applied by large scale industrial and commercial customers [10] but DR programs for space heating for residential customers could also be considered as they represents a large share of the total consumption: Private households accounted for approx. 25% of the total energy consumption in the European Union (EU) in 2011 [11] of

which approx. 67% was used for space heating in the Northern and Western regions of the EU [12].

Several studies have demonstrated DR potentials in residential space heating operation. A simulation-based study by Acvi et al. [13] obtained a 13% cost reduction and reduced the energy consumption in peak-hours by 23.6% compared to a baseline controller by applying real time prices (RTP) together with economic model predictive control (E-MPC) of an AC unit in a single residence. Halvgaard et al. [14] investigated the performance of a residential-scale heat pump operated by an E-MPC scheme using RTP. The control scheme achieved 25% cost savings using hard comfort constraints and 35% using softened constraints. Vrettos et al. [15] used day-ahead prices in an E-MPC scheme to investigate the DR potential of a residential building equipped with several installations for efficient DR (heat pump, slab cooling, electrical water heater, PV and battery) and achieved an energy consumption reduction of 20% and cost savings of 28% compared to a rule-based controller (RBC). Knudsen and Petersen [16] applied RTP and corresponding CO₂ intensity signals to an E-MPC scheme for space heating operation in a residential apartment and demonstrated a potential for cost savings together with CO₂ emission reductions as well as shifting consumption from periods of peak load to low load periods.

However, to the knowledge of the authors, there have been only a few studies on how the thermal characteristics of existing resi-

* Corresponding author.

E-mail address: thp@eng.au.dk (T.H. Pedersen).

Table 1
Construction characteristics of the existing building.

Construction type	Material	Thickness	Thermal Properties	
Interior Wall	Concrete	0.120 m	$\lambda = 1.10 \text{ W}/(\text{m K})$	$c = 920 \text{ J}/(\text{kg K})$
	Wood	0.020 m	$\lambda = 0.15 \text{ W}/(\text{m K})$	$c = 1630 \text{ J}/(\text{kg K})$
Floor/Ceiling	Insulation	0.050 m	$\lambda = 0.04 \text{ W}/(\text{m K})$	$c = 1210 \text{ J}/(\text{kg K})$
	Air space	0.050 m	$R = 0.18 \text{ (m}^2 \text{ K)}/\text{W}$	
	Hollow concrete slab	0.180 m	$\lambda = 1.29 \text{ W}/(\text{m K})$	$c = 270 \text{ J}/(\text{kg K})$
	Concrete	0.070 m	$\lambda = 1.10 \text{ W}/(\text{m K})$	$c = 920 \text{ J}/(\text{kg K})$
Exterior Wall – Facades	Insulation	0.060 m	$\lambda = 0.04 \text{ W}/(\text{m K})$	$c = 1210 \text{ J}/(\text{kg K})$
	Concrete	0.080 m	$\lambda = 1.10 \text{ W}/(\text{m K})$	$c = 920 \text{ J}/(\text{kg K})$
	Concrete	0.095 m	$\lambda = 1.10 \text{ W}/(\text{m K})$	$c = 920 \text{ J}/(\text{kg K})$
Exterior Wall – Gables	Insulation	0.060 m	$\lambda = 0.04 \text{ W}/(\text{m K})$	$c = 1210 \text{ J}/(\text{kg K})$
	Air space	0.015 m	$R = 0.15 \text{ (m}^2 \text{ K)}/\text{W}$	
	Concrete	0.150 m	$\lambda = 1.10 \text{ W}/(\text{m K})$	$c = 920 \text{ J}/(\text{kg K})$
	Air space	0.015 m	$R = 0.15 \text{ (m}^2 \text{ K)}/\text{W}$	
	Insulation	0.060 m	$\lambda = 0.04 \text{ W}/(\text{m K})$	$c = 1210 \text{ J}/(\text{kg K})$
	Concrete	0.090 m	$\lambda = 1.10 \text{ W}/(\text{m K})$	$c = 920 \text{ J}/(\text{kg K})$
	Concrete	0.090 m	$\lambda = 1.10 \text{ W}/(\text{m K})$	$c = 920 \text{ J}/(\text{kg K})$
Existing window	Double glazing (4-12Air-4)	0.020 m	$U_{\text{glazing}} = 2.84 \text{ W}/(\text{m}^2 \text{ K})$	$g_{\text{glazing}} = 0.773$
	Wood frame		$U_{\text{frame}} = 1.700 \text{ W}/(\text{m}^2 \text{ K})$	

Table 2
Facade retrofit measures.

Construction name	Material	Thickness	Thermal Properties	
Facade 1	External insulation	0.125 m	$\lambda = 0.036 \text{ W}/(\text{m K})$	$c = 920 \text{ J}/(\text{kg K})$
Facade 2	External insulation	0.205 m	$\lambda = 0.036 \text{ W}/(\text{m K})$	$c = 920 \text{ J}/(\text{kg K})$
2-layer window	Low-E glazing (4-14Ar-LowE4)	0.022 m	$U_{\text{glazing}} = 1.220 \text{ W}/(\text{m}^2 \text{ K})$	$g_{\text{glazing}} = 0.671$
	Wood/Alu frame		$U_{\text{frame}} = 1.700 \text{ W}/(\text{m}^2 \text{ K})$	
3-layer window	Low-E glazing (4LowE-14Ar-4-14Ar-LowE4)	0.040 m	$U_{\text{glazing}} = 0.688 \text{ W}/(\text{m}^2 \text{ K})$	$g_{\text{glazing}} = 0.547$
	Wood/Alu frame		$U_{\text{frame}} = 1.700 \text{ W}/(\text{m}^2 \text{ K})$	

dential buildings affect DR potentials of space heating operation. Reynders et al. [17] applied an RBC scheme to investigate the relation between energy efficiency of the building envelope and the potential for exploiting the structural thermal storage for DR in dwellings. Simulation results for six test cases showed that up to 40% of the stored energy was lost due to poor thermal characteristics. A subsequent parametric study of the building envelope thermal characteristics suggested that increased insulation level and air tightness were the two most important factors to increase the DR efficiency [18]. Upgrading the thermal performance of building envelopes of existing residential buildings in an energy system with a high penetration of renewable energy production therefore seems to be critical if space heating is to be used for DR.

The aim of the work reported in this paper is to contribute with further knowledge regarding the importance of the thermal characteristics of existing residential building envelopes on the latent DR potentials in residential space heating. The paper reports on a simulation-based study where centralized and decentralized E-MPC were used to operate the space heating in eight retrofit scenarios of an existing residential multi-story apartment block. The E-MPC scheme was evaluated in terms of its ability to reduce end-user cost, CO₂ emission and the resulting load shift of heating demand.

2. Method

A section of an existing apartment block was modelled in EnergyPlus (EP) [19] and represents as such an actual building to be controlled by E-MPC. The E-MPC scheme was implemented in MATLAB [20] and used to operate the space heating (electrical baseload) of the EP model through co-simulation using the Building Controls Virtual Test Bed (BCVTB) [21,22]. The following sections provide further information on the modelling of the test case in EP, the building model used in the E-MPC, the E-MPC scheme and the performance evaluation metrics used for performance evaluation of the E-MPC scheme.

2.1. EnergyPlus model

The third floor of an existing four-story apartment block was used as test case and thus modelled in EP. The EP files are provided in ref. [23]. The block was built in 1978 and has only undergone minor refurbishments since then. The geometry is depicted in Fig. 1 and consists of five stairwells (S) and ten apartments: one 1-room apartment (9), four 3-room apartments (1, 3, 5 and 7) and five 4-room apartments (2, 4, 6, 8 and 10) with east-west oriented facades where the west oriented facades have unheated balconies (blue boxes in Fig. 1). The stairwells and apartments were modelled as individual thermal zones with adiabatic horizontal surfaces (floor and roof). The stairwells were kept at a minimum temperature of 15 °C while the apartments had individual heating with different set points as explained in Section 2.4.

The thermal characteristics of the existing building envelope used in the EP model are specified in Table 1. The windows were modelled in WINDOW [24] and imported into the EP model. The infiltration air change rate was modelled as a constant rate of 0.5 h⁻¹. Internal loads from people and equipment were neglected to make the results easier to interpret. The Conduction Finite Difference algorithm in EP was used to calculate the construction heat balances with a 60 s time step. The standard EP weather data file for Copenhagen, Denmark was used in all simulations [25]. The simulation period was November 1, 2015 to February 28, 2016, which constitutes the coldest period of the heating season in Denmark.

To investigate the influence of the energy efficiency of the building envelope, a range of typically used retrofit solutions for existing Danish apartment blocks (Table 2) were combined into eight retrofit scenarios (Table 3) with gradually increasing energy efficiency. All scenarios were assumed to increase the air tightness due to the increased focus on the importance of building air tightness compared to when the existing building was constructed; hence, the infiltration rate was reduced to either 0.18 h⁻¹ or 0.1 h⁻¹ in an attempt to investigate the effect of different retrofit ambitions. Mechanical ventilation with heat recovery efficiency of 80% was assumed in all retrofit scenarios to ensure a constant air change of

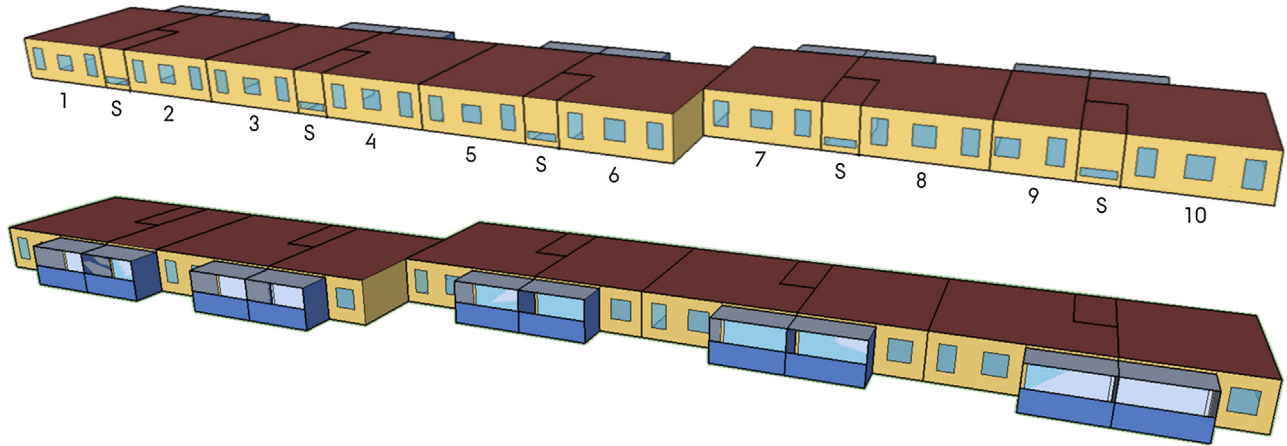


Fig. 1. Test case geometry as modelled in EnergyPlus with applied apartment numbering.

Table 3
Retrofit scenarios.

	External insulation	Window	Infiltration rate
Existing	–	existing	0.50 h ⁻¹
Retrofit1	0.125 m	2-layer	0.18 h ⁻¹
Retrofit2	0.125 m	2-layer	0.10 h ⁻¹
Retrofit3	0.205 m	2-layer	0.18 h ⁻¹
Retrofit4	0.205 m	2-layer	0.10 h ⁻¹
Retrofit5	0.125 m	3-layer	0.18 h ⁻¹
Retrofit6	0.125 m	3-layer	0.10 h ⁻¹
Retrofit7	0.205 m	3-layer	0.18 h ⁻¹
Retrofit8	0.205 m	3-layer	0.10 h ⁻¹

Table 4
Average model fit-percentage compared to validation data.

	Multi-zone	Single-zone
Existing	84%	91%
Retrofit1	86%	88%
Retrofit2	84%	87%
Retrofit3	87%	88%
Retrofit4	85%	88%
Retrofit5	87%	85%
Retrofit6	86%	84%
Retrofit7	88%	86%
Retrofit8	87%	86%

0.5 h⁻¹ in all apartments. The retrofit measures facade 1 and facade 2 in Table 2 would, in practice, also consist of an external cladding and other materials but the thermal characteristics of these were neglected in the model.

2.2. Control model

A model describing the thermal dynamics of the building is required when applying MPC schemes. In this study, the model is defined as a discrete-time linear time-invariant system specified on state-space form (Eq. (1a)) with state matrix \mathbf{A} , system states x_k , input matrix \mathbf{B} , control inputs u_k , disturbance matrix \mathbf{E} , disturbances d_k and controlled system states y_k (Eq. (1b)) with output matrix \mathbf{C} .

$$x_{k+1} = \mathbf{A}x_k + \mathbf{B}u_k + \mathbf{E}d_k \quad (1a)$$

$$y_k = \mathbf{C}x_k \quad (1b)$$

There are several modelling techniques for representing the building dynamics [26] commonly categorized as white box (e.g. [19]), grey box (e.g. [27,28]) or black box model approaches (e.g. [29,30]). In this study, a grey box model approach was chosen as it provides the additional possibility of identifying the actual physical parameters of the building, e.g. the total heat loss coefficient, which could be beneficial to document the effects of retrofits in practice. Furthermore, grey box models are characterized by having relatively low requirements in terms of the amount of data needed to obtain them compared to the alternatives.

The model structure of the apartments was defined as a multi-zone model as illustrated in Fig. 2 for apartment j with adjacent apartments i , where T_{ext} is the external temperature [°C], Q_{sun} is the solar heat gains [W], Q_{heat} is the thermal energy from the space heating system [W], T is the temperature [°C], C is the thermal capacity [J/K], H is the heat transfer coefficients [W/K] and subscripts m , e and a represent the construction mass, ambient air and

room air, respectively. The multi-zone model can be reduced to a set of single-zone models by setting $H_{interaction} = 0$ throughout the model, i.e. neglecting the inter-zonal effects.

An inherent part of grey box modelling is to make data-based estimations of the parameters describing the thermal dynamic characteristics of the building (C and H in Fig. 2). The parameters were estimated for the multi-zone and the set of single-zone models, respectively, based on output data from a simulated experiment with a duration of 14 days (01.01.2016–14.01.2016). During the experiment the output of the heaters were controlled to follow a so-called Pseudo Random Binary Signals (PRBS) designed to excite systems with multiple time constants [31,32]. Ten different PRBS signals were used in the ten apartments. The output from the first seven days of data was used for parameter estimation using the MATLAB system identification toolbox [33,34] by minimizing the multiple-step ahead prediction error, while the output from the remaining seven days was used for model validation. The average model fits (NRMSE) [35] across all zones on the validation data for the multi-zone and single-zone model, respectively, are shown in Table 4. The fits of the multi-zone and single-zone model are within the same range. Differences in model fits are due to the different parameter estimations as shown in Fig. 3.

The estimated room air capacities for the two modelling approaches was similar, whereas the construction mass capacities differ slightly, presumably because the single-zone models lump the effects of inter-zonal heat exchange into other parameters. The complexity of one comprehensive multi-zone model also complicates the system identification, which is seen by the greater parameter estimation uncertainties.

When the multi-zone model is used in E-MPC as one comprehensive building model, the optimal control inputs for all apartments are calculated simultaneously for each discrete time step. This is called *centralized E-MPC* [36]. Using the set of single-zone models for E-MPC, i.e. each optimal control input is

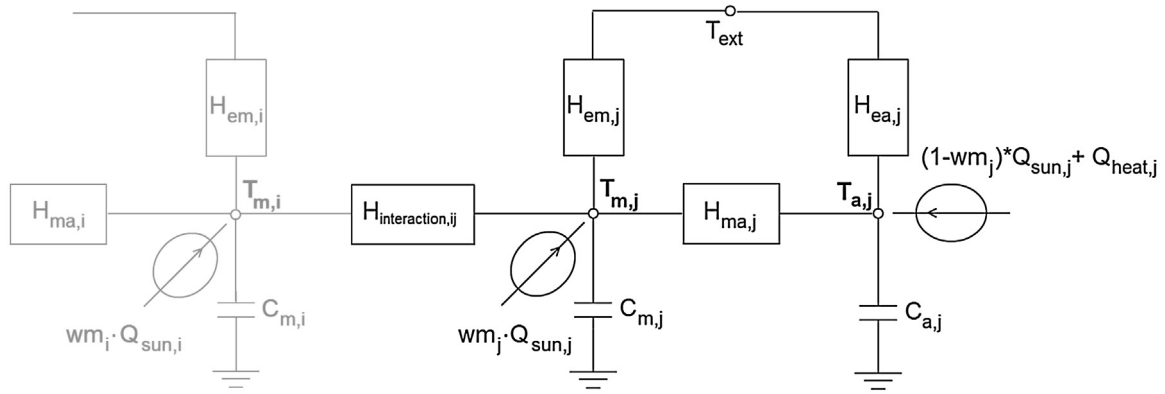


Fig. 2. Illustration of the model structure for apartment j and adjacent apartments i.

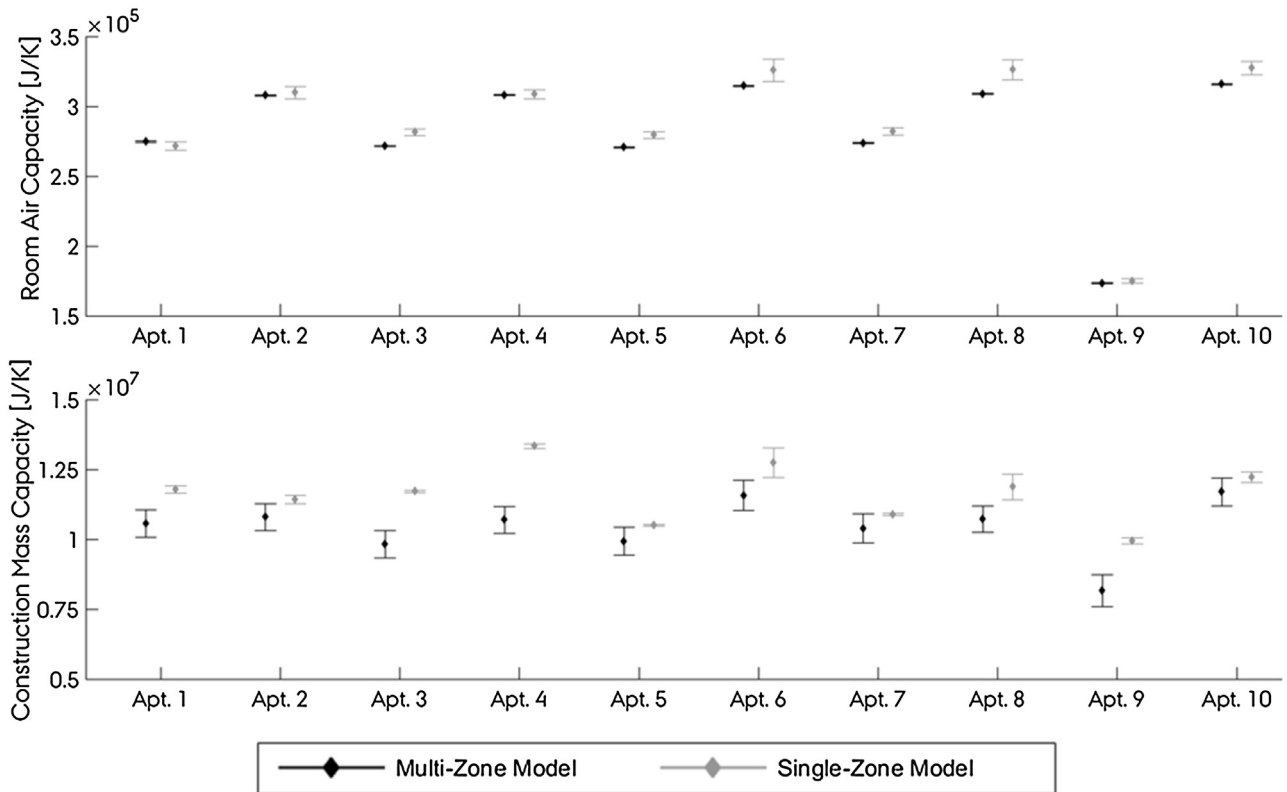


Fig. 3. Parameter estimations and standard deviation of the thermal capacity of the room air (top) and construction mass (bottom).

determined for each zone individually, is called *decentralized E-MPC* [36]. Thus, in theory, decentralized E-MPC will return a sub-optimal control strategy compared to the centralized E-MPC due to the neglect of inter-zonal effects. However, the decentralized control approach may be more practical since it does not require mapping of zone adjacency or exchange of information between controlled zones. This paper therefore investigates the performance differences between a decentralized and centralized control approach.

2.3. Economic model predictive control

The objective of the E-MPC scheme formulated in Eqs. (2a)–(2g) is to minimise the total operational cost for a finite prediction horizon N . At each discrete time step k , measurements of the room air temperatures are taken and the optimization problem is solved yielding a sequence of optimal space heating control input u^* [W]. The first element of u^* is then applied to the space heating system

in the EP building model. At the next time-step $k + 1$ the optimization problem is solved again with a prediction horizon shifted one time-step ahead in time and with updated room air temperature measurements. This receding horizon introduces feedback in the control scheme [37]. The optimal sequence of control inputs u^* is constrained by the maximum heating design power P_{max} (Eq. (2d)) and the value and rate of change of the room air temperatures y (Eqs. (2e) and (2f), respectively). All of the inequality constraints (Eqs. (2d)–(2f)) were enforced as equality constraints by introducing slack variables, which ensured that a feasible solution was always available. Furthermore, a low-level proportional controller is introduced in the EP model that ensures thermal comfort since model mismatch in the E-MPC scheme could lead to thermal comfort violations. The prediction horizon N and the discrete time step k were set to 3 days and 1 hour, respectively. To simplify the interpretation of the results, perfect predictions of the input weight c (Eq. (3)), in this case the electricity price and weather forecasts,

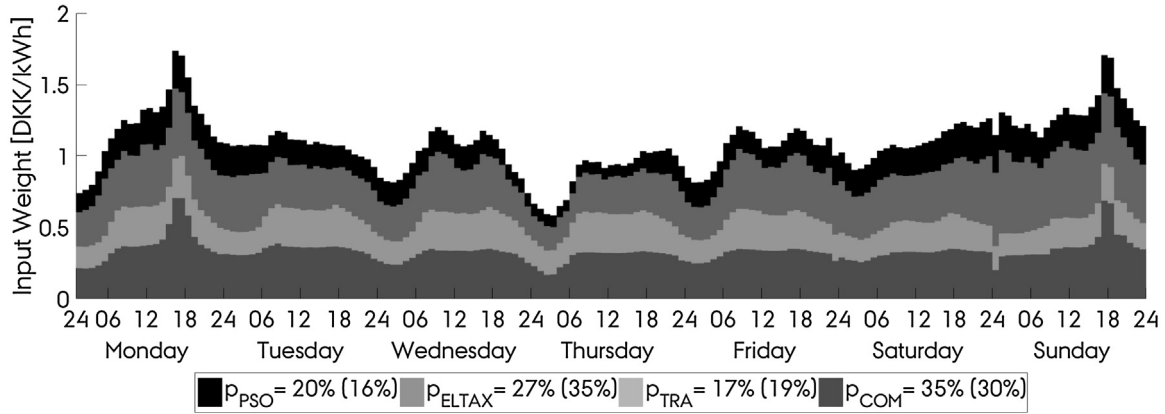


Fig. 4. Input weight for the period of December 7–14, 2015.

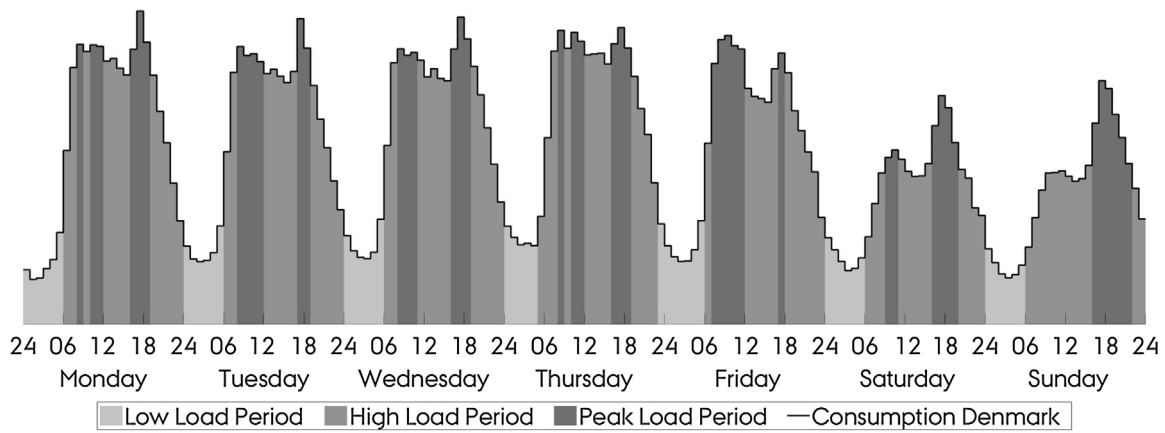


Fig. 5. Partition of the daily consumption into periods of low, high and peak load for December 7–14 2015 [6](Nord Pool).

are assumed. Hence, the optimization problem forms a deterministic linear program (LP). The LP can be solved efficiently using the MOSEK solver [38].

$$\underset{u}{\text{minimize}} \sum_{k=1}^N c_k^T \cdot u_k \quad (2a)$$

$$\text{subject to } x_{k+1} = Ax_k + Bu_k + Ed_k \quad (2b)$$

$$y_k = Cx_k \quad (2c)$$

$$0 \leq u_k \leq P_{max} \quad (2d)$$

$$T_{min,k} \leq y_k \leq T_{max,k} \quad (2e)$$

$$\Delta T_{min,k} \leq \frac{\Delta y_k}{\Delta t} \leq \Delta T_{max,k} \quad (2f)$$

$$x_0 = x(0) \quad (2g)$$

2.4. Constraints and input weight

In this study, the control input and state constraints (Eqs. (2d)–(2f)) are time-invariant but differ for each apartment as specified in Table 5.

The input weight vector c in Eq. (2a) is a signal designed to transform a multi-objective optimization problem into a single-

Table 5
Specification of input and state constraints.

Zone	P_{max}	T_{min}	T_{max}	ΔT_{min}	ΔT_{max}
Apartment 1	50 W/m ²	20 °C	24 °C	-2.1 °C/h	2.1 °C/h
Apartment 2	50 W/m ²	22 °C	26 °C	-2.1 °C/h	2.1 °C/h
Apartment 3	50 W/m ²	20 °C	24 °C	-2.1 °C/h	2.1 °C/h
Apartment 4	50 W/m ²	22 °C	26 °C	-2.1 °C/h	2.1 °C/h
Apartment 5	50 W/m ²	20 °C	24 °C	-2.1 °C/h	2.1 °C/h
Apartment 6	50 W/m ²	22 °C	26 °C	-2.1 °C/h	2.1 °C/h
Apartment 7	50 W/m ²	20 °C	24 °C	-2.1 °C/h	2.1 °C/h
Apartment 8	50 W/m ²	22 °C	26 °C	-2.1 °C/h	2.1 °C/h
Apartment 9	50 W/m ²	20 °C	24 °C	-2.1 °C/h	2.1 °C/h
Apartment 10	50 W/m ²	22 °C	26 °C	-2.1 °C/h	2.1 °C/h

objective optimization problem [16], which is summarised in Eq. (3).

$$c[k] = \underbrace{\overline{spot}[k]}_{P_{COM}} \cdot c_{COM} + \underbrace{\overline{load}[k]}_{P_{TRA}} \cdot c_{TRA} + \underbrace{\overline{CO_2}[k]}_{P_{EL_TAX}} \cdot c_{EL_TAX} + \underbrace{f_{PSO}[k]}_{P_{PSO}} \cdot c_{PSO} \quad (3)$$

where k is a discrete hourly time step, $spot$ is the hourly electricity spot price, \overline{spot} is the mean electricity spot price, c_{COM} is the yearly average commercial tariff on electricity, $load$ is the hourly grid load, \overline{load} is the mean grid load, c_{TRA} is the yearly average cost of electricity transportation through the transmission and distribution grid, $\overline{CO_2}$ is the mean intensity and c_{EL_TAX} is the yearly average taxes and levies. c_{PSO} is the yearly average cost of a Danish public service obligation (PSO) levy put on electricity use

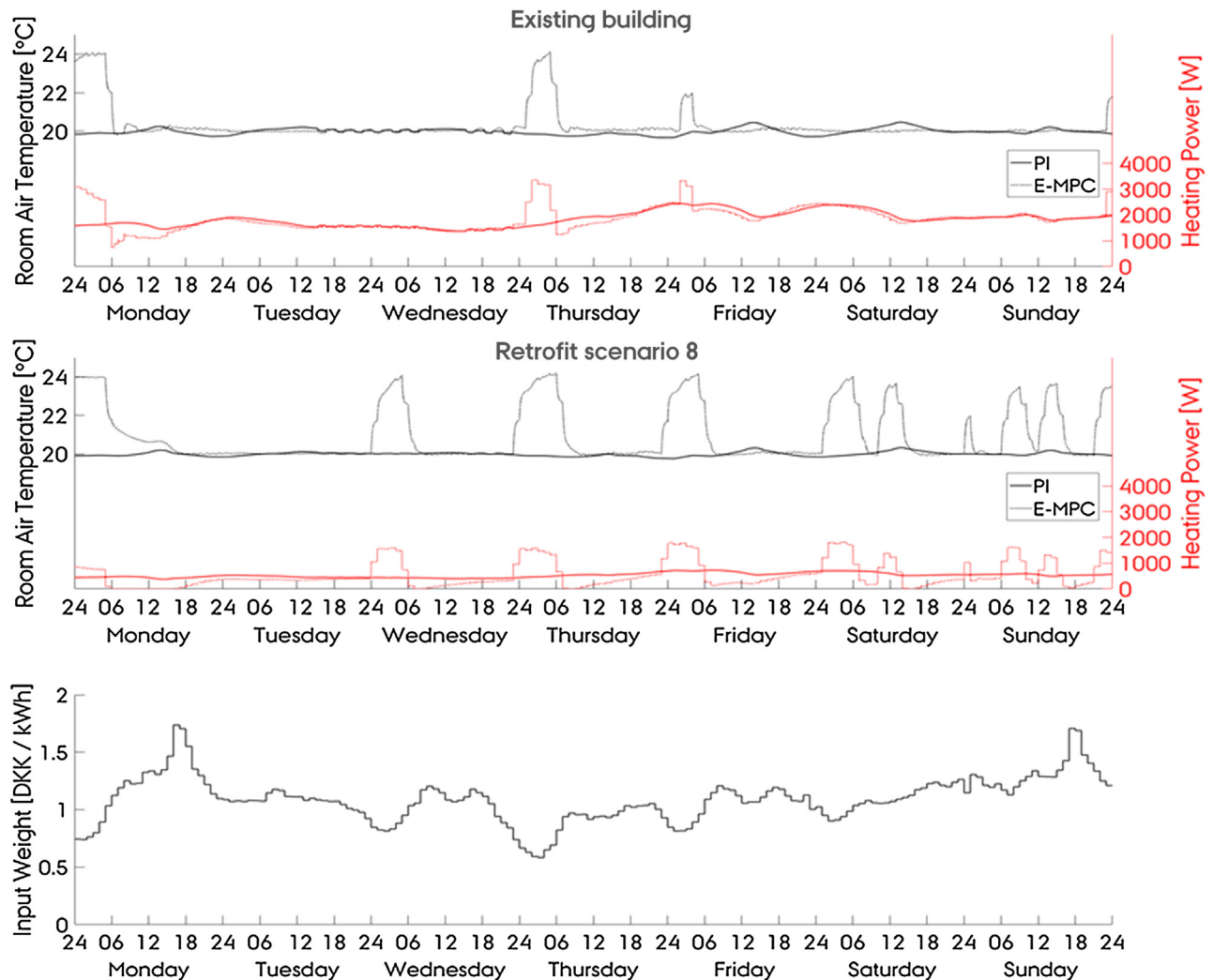


Fig. 6. Simulation results for apartment 7 for the existing building (top) and retrofit scenario 8 (middle) using a PI controller and E-MPC scheme, respectively, during the period December 7–14, 2015. The bottom chart shows the energy price (input weight c) during the same period.

where f_{PSO} is the PSO scaling factor. Approximately half of the PSO levy covers subsidies for wind turbines as supplement to the market price. The proposed f_{PSO} scaling factor is constructed in such a way that it is low in periods with low spot prices and high wind power production.

The data used in this study for Eq. (3) are electricity spot prices, grid load, CO₂ intensity signals and wind production from Nord Pool market data for Western Denmark during the simulation period [39] and Danish average component tariffs for 2015 [40]. Fig. 4 depicts an example of the input weight c as defined in Eq. (3) for the period December 7–14, 2015. The component share of the total tariff is specified in the legend where the percentage in brackets indicates the 2015 yearly shares.

2.5. E-MPC performance evaluation

Determining the true value of residential DR programs for the electricity supply system is a challenge of great concern [9]. The economic DR incentive may be limited on a household scale while significant on a societal level [6]. In this study, the performance of the E-MPC for residential space heating will be evaluated relative to a traditional PI controller in terms of achieved reductions of costs and CO₂ emissions as suggested by Knudsen and Petersen [16]. This form of evaluation will provide some insights into the

value of the proposed E-MPC, but it will not provide evaluation of other potential benefits such as the amount, time and duration of shifted energy which may affect production patterns and societal energy infrastructure investments. Several performance evaluation measures have been proposed to quantify the amount of shifted energy using active demand response [41,18]. However, quantifying the time to which the load is shifted is an equally relevant aspect of DR. A simple approach is to consider static periods of low, high and peak load; hence, evaluate the amount of energy shifted from peak periods to periods of low or high load [16]. In this study, the shifted energy of the E-MPC relative to the PI controller is evaluated with respect to a dynamic metric where each time step of the simulation period is categorized as either a period of low, high or peak load based on historical grid load data as illustrated in Fig. 5. For each day, the hours with grid load below the 25% quantile and above the 75% quantile were defined as low and peak load periods, respectively. The remaining hours were characterized as high load periods.

3. Results

To illustrate the mechanisms of the E-MPC scheme, Fig. 6 (top and middle) depicts the temperature conditions and heating consumption for apartment 7 in one week using the PI controller and

the centralized E-MPC, respectively. Fig. 6 (top) shows results from simulations of the existing building and Fig. 6 (middle) shows results from the most extensive energy retrofit scenario 8 (see Table 3 for details). In both cases, the PI controller maintained a room air temperature near the specified minimum comfort set point of 20 °C at all times, resulting in a smooth and fairly constant heating pattern. The E-MPC scheme, however, increased the room air temperature at times with low energy cost (Fig. 6 bottom) and thereby exploited the thermal mass of the constructions, which then reduced the need for space heating in the following periods characterized by higher energy cost.

Immediate comparison of the control actions in the two buildings indicates that improved energy efficiency of the building envelope increased the frequency at which load shifting was profitable.

3.1. Economic and environmental assessment

The cost and CO₂ emissions over the simulation period were accumulated for each combination of the nine buildings (the existing and the eight retrofit scenarios) and the three control schemes (PI, centralized E-MPC and decentralized E-MPC). Fig. 7 depicts the achieved cost and emission reductions for the centralized and decentralized E-MPC scenarios relative to the PI controller for all simulations. Both E-MPC schemes of the existing building led to minor cost savings while increasing CO₂ emissions slightly. In all retrofit scenarios both E-MPC schemes reduced the cost and CO₂ emissions compared to the PI controller. However, the centralized E-MPC had a marginally better performance than the decentralized E-MPC in all scenarios.

3.2. Load shifting potential

The absolute and relative ability of the E-MPC scheme to shift space heating consumption to low load periods as defined in Section 2.4 is exemplified by the performance of the centralized E-MPC in Fig. 8. Applying E-MPC on the existing building (R0) shifted

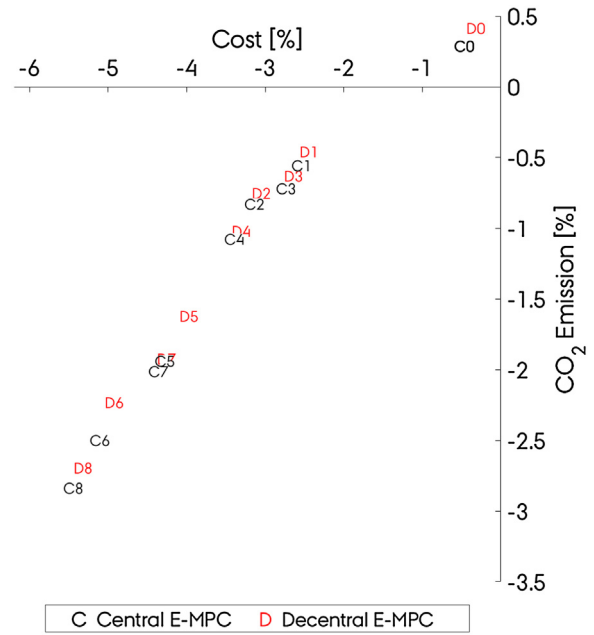


Fig. 7. Achieved cost and emission reductions for the centralized and decentralized E-MPC schemes relative to the PI controller for all simulations. The existing building is referred to with index 0 and the remaining numbers refer to the retrofit scenarios.

approx. 7% of the energy use away from peak load periods. For the retrofit scenarios, the shifted load was in the range of 30–47%.

4. Discussion

A tendency of decreasing cost and CO₂ emission as a function of the increasing energy efficiency can be observed in Fig. 7, which is a consequence of an increasing number of load shift events (as illustrated in Fig. 6). Fig. 7 suggests that reducing the infiltration

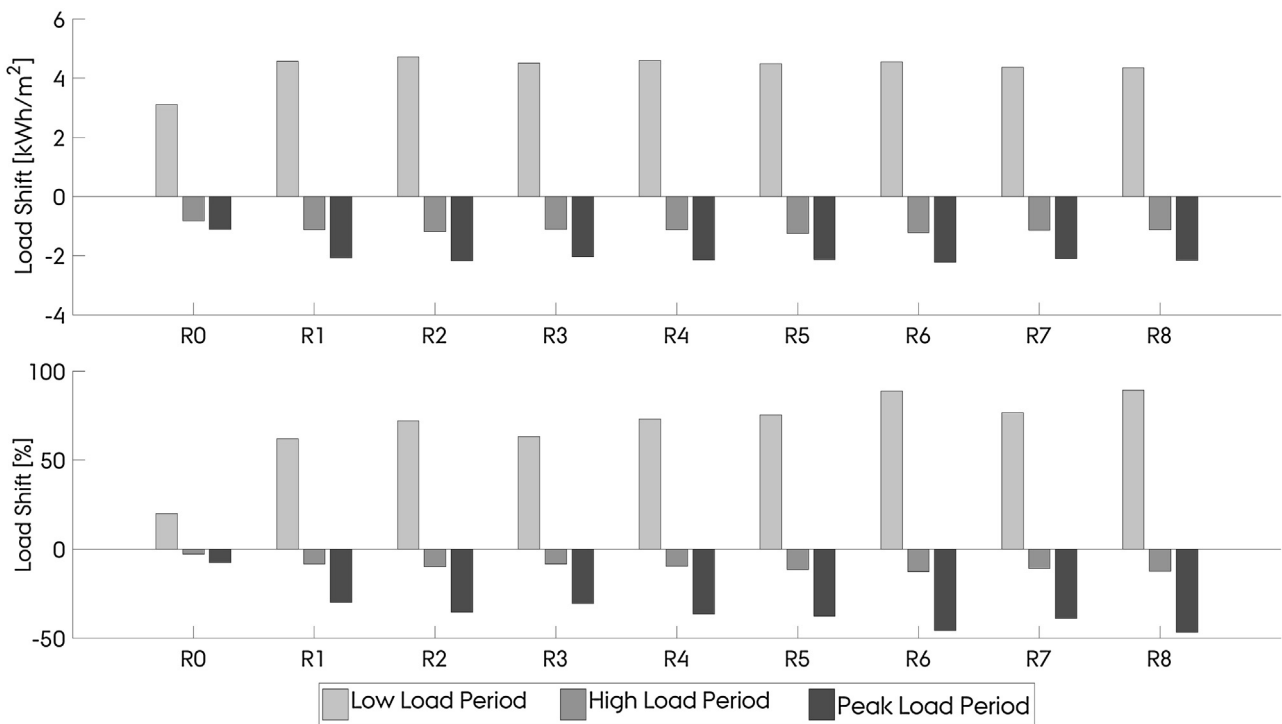


Fig. 8. Accumulated load shift of centralized E-MPC for all retrofit scenarios compared to the baseline PI control. Top: Absolute load shift. Bottom: Relative load shift.

air change rate was an important measure in terms of both cost and CO₂ emission reduction. The clustering of data with respect to the two types of window glazing indicates that reducing heat loss through windows influenced the potential. The added external insulation was most efficient in the buildings with 3-layer glazing since the heat loss through the envelope was a more dominating factor in these scenarios compared to the 2-layer glazing scenarios. While it is difficult to make a general valid ranking of the specific measures such as increasing the air tightness or lowering the transmission losses, the results show that reductions in the overall heat loss have a significant effect on cost savings, CO₂ emissions and load shifting in a building heated by a convective radiator system.

Fig. 8 shows that the relative load shift potential of the scenarios increased with increasing energy efficiency. This was primarily due to the corresponding reduction of the baseline space heating consumption: The absolute load shifting potential is seen to be rather constant across all retrofit scenarios.

The simulation results indicate that the centralized E-MPC scheme resulted in marginally better results than the decentralized E-MPC. Though not investigated, it is likely that inter-zonal effects would be less pronounced with insulated interior walls instead of the 0.12 m massive concrete walls used in this study. The difference in performance compared to the increased complexity of centralized E-MPC and the challenge of obtaining suitable multi-zone model suggests that decentralized E-MPC is sufficient for many practical applications.

5. Conclusion

This paper reports on a simulation-based study of the theoretical potential for utilizing the thermal mass in an existing and eight retrofit scenarios of a multi-story apartment block for demand response enabled by E-MPC of the space heating system. The control objective was to minimize the cost of space heating for the end-user, and performance was evaluated by comparison to a conventional controller. The E-MPC was also evaluated in terms of its ability to reduce CO₂ emissions and to perform load shift of the heating demand. Two E-MPC approaches were considered: centralized E-MPC where inter-zonal effects were considered and decentralized E-MPC that neglected heat transfer between adjacent apartments.

The E-MPC schemes yielded increased cost savings (up to approx. 6%) and reduced CO₂ emissions (up to approx. 3%) as a function of increasing energy efficiency of the retrofit scenarios. The centralized E-MPC only performed marginally better than the decentralized E-MPC, suggesting that using the more practical decentralized approach, which does not need configuration of zone adjacency or exchange of information between controlled zones, is sufficient in many situations.

The simulation results also suggest that the E-MPC schemes shifted consumption more frequently in the retrofit scenarios compared to the existing building. However, the absolute amount of shifted energy across the retrofit scenarios compared to the existing building was rather consistent. The relative amount of energy shifted from peak periods increased slightly with increasing energy efficiency due to the decreased baseline energy use in each retrofit scenario.

This study used perfect predictions of disturbances (weather and occupancy) to identify the theoretical potential of the E-MPC scheme. Future studies should include investigations on how this potential will be affected by uncertainties in weather forecasts and occupancy. Furthermore, experimental verification of the demonstrated potentials is recommended.

Acknowledgements

The authors gratefully acknowledge the support of this work from the project “READY.dk” financed by the Danish energy research and development program ForskEL (grant number: 12305) and the project ‘Resource Efficient Cities Implementing Advanced Smart City Solutions’ (READY) financed by the 7th EU Framework Programme (FP7-Energy project reference: 609127). Furthermore, the authors express gratitude to the participants and the work done in the IEA-EBC Annex 67 on Energy Flexible Buildings.

References

- [1] M.H. Albadi, E.F. El-Saadany, A summeray of demand response in electricity markets, *Electr. Power Syst. Res.* 78 (2008) 1989–1996, <http://dx.doi.org/10.1016/j.epsr.2008.04.002>.
- [2] North American Electric Reliability Corporation, Demand Response Availability Report, 2011 (03 2013). [Online]. Available: <http://www.nerc.com/docs/pc/dadswg/2011%20DADS%20Report.pdf>. [Senest hentet eller vist den 23 08 2016].
- [3] T. Ashrafiyan, A.Z. Yilmaz, S.P. Corgnati, N. Moazzen, Methodology to define cost-optimal level of architectural measures for energy efficient retrofits of existing detached residential buildings in Turkey, *Energy Build.* 120 (2016) 58–77, <http://dx.doi.org/10.1016/j.enbuild.2016.03.074>.
- [4] D. Palensky, D. Dietrich, Demand side management: demand response, intelligent energy systems, and smart loads, *IEEE Transactions on Industrial Informatics* 7 (3) (2011), <http://dx.doi.org/10.1109/tii.2011.2158841>.
- [5] R. D’Hulst, W. Labeeuw, B. Beusen, S. Claessens, G. Deconinck, K. Vanthournout, Demand response flexibility and flexibility potential of residential smart appliances: experiences from large pilot test in Belgium, *Appl. Energ.* 155 (2015) 79–90, <http://dx.doi.org/10.1016/j.apenergy.2015.05.101>.
- [6] N. O’Connell, P. Pinson, H. Madsen, M. O’Malley, Benefits and challenges of electrical demand response: a critical review, *Renew. Sustain. Energy Rev.* 39 (2014) 686–699, <http://dx.doi.org/10.1016/j.rser.2014.07.098>.
- [7] K.O. Aduda, T. Labeodan, W. Zeiler, G. Boxem, Y. Zhao, Demand side flexibility: potentials and building performance implications, *Sustain. Cities Soc.* 22 (2016) 146–163, <http://dx.doi.org/10.1016/j.apenergy.2015.05.101>.
- [8] B.P. Esther, K.S. Kumar, A survey on residential Demand Side Management architecture, approaches, optimization models and methods, *Renew. Sustain. Energy Rev.* 59 (2016) 342–351, <http://dx.doi.org/10.1016/j.rser.2015.12.282>.
- [9] S. Nolan, M. O’Malley, Challenges and Barriers to demand response deployment and evaluation, *Appl. Energ.* 152 (2015) 1–10, <http://dx.doi.org/10.1016/j.apenergy.2015.04.083>.
- [10] M. Gweder, D. Gyalistras, C. Sagerschnig, R.S. Smith, D. Sturznegger, Final Report: Use of Weather And Occupancy Forecasts For Optimal Building Climate Control –Part II: Demonstration (OptiControl-II), 2013, Zürich, Switzerland.
- [11] European Commission, Eurostat, 2017 (Online. Available: <http://ec.europa.eu/eurostat>. [Senest hentet eller vist den 30 03 2016]).
- [12] Buildings Performance Institute Europe (BPIE), Europe’s Buildings Under the Microscope ? A Country-by-country Review of the Energy Performance of Buildings, BPIE, 2011.
- [13] M. Avci, M. Erkoç, A. Rahmani, S. Asfour, Model predictive HVAC load control in buildings using real-time electricity pricing, *Energy Build.* 60 (2013) 199–209, <http://dx.doi.org/10.1016/j.enbuild.2013.01.008>.
- [14] R. Halvgaard, N.K. Poulsen, H. Madsen, J.B. Jørgensen, Economic Model predictive Control for Building Climate Control in a Smart Grid, in: IEEE PES Innovative Smart Grid Technologies (ISGT), Washington, D.C., United States, 2012, pp. 1–6, <http://dx.doi.org/10.1109/ISGT.2012.6175631>.
- [15] E. Vrettos, K. Lai, F. Oldewurtel, G. Andersson, Predictive Control of Buildings for Demand Response with dynamic day-ahead and real-time prices, in: Control Conference (ECC), Zürich, 2013.
- [16] M.D. Knudsen, S. Petersen, Demand response potential of model predictive control of space heating based on price and carbon dioxide intensity signals, *Energy Build.* 125 (2016) 196–204, <http://dx.doi.org/10.1016/j.enbuild.2016.04.053>.
- [17] G. Reynders, T. Nuytten, D. Saelens, Potential of structural thermal mass for demand-side management in dwellings, *Build. Environ.* 64 (2013) 187–199, <http://dx.doi.org/10.1016/j.buildenv.2013.03.010>.
- [18] G. Reynders, Quantifying the Impact of Building Design on the Potential of Structural Storage for Active Demand Response in Residential Buildings, PhD Dissertation, 2015, KU Leuven.
- [19] U.S. Department of Energy, EnergyPlus 8.1.0, [Online].
- [20] The MathWorks, inc., MATLAB 2015 (8.6.0.267246), [Online].
- [21] Lawrence Berkeley National Laboratory, Buildings Control Virtual Test Bed – BCVTB (1.4.0), [Online].
- [22] M. Wetter, Co-simulation of building energy and control systems with the building controls virtual test bed, *J. Build. Perform. Simul.* 3 (4) (2010) 1–19, <http://dx.doi.org/10.1080/19401493.2010.518631>.
- [23] Pedersen, Theis Heidmann, Hedegaard, Rasmus Elbæk, Petersen, Steffen (2017) “IDF EnergyPlus files of an existing Danish apartment block and eight

- retrofit scenarios", Mendeley Data, v2 <http://dx.doi.org/10.17632/6dhk66w5gj.2>.
- [24] Berkeley Lab WINDOW v7.4.8.0. (2016). [Online]. Available: <https://windows.lbl.gov/software/window/7/index.7.4.8.html>.
- [25] U.S. Department of Energy, EnergyPlus Weather Data: Copenhagen 061800 (IWEC), [Online]. Available: https://energyplus.net/weather-region/europe-wmo_region.6/DNK%20%20. [Senest hentet eller vist den 06 04 2016].
- [26] S. Prívará, J. Cigler, Z. Vána, F. Oldewurtel, C. Sagerschnig, E. Žáčková, Building modeling as a crucial part for building predictive control, *Energy Build.* 56 (2013) 8–22, <http://dx.doi.org/10.1016/j.enbuild.2012.10.024>.
- [27] P. Bacher, H. Madsen, Identifying suitable models for the heat dynamics of buildings, *Energy Build.* 43 (2011) 1511–1522, <http://dx.doi.org/10.1016/j.enbuild.2011.02.005>.
- [28] S. Goyal, C. Liao, P. Barooah, Identification of multi-zone building thermal interaction model from data, in: 50th IEEE Conference on Decision and Control, Orlando, FL, USA, 2011, <http://dx.doi.org/10.1109/CDC.2011.6161387>.
- [29] S. Prívará, Z. Vána, D. Gyalistras, J. Cigler, C. Sagerschnig, M. Morari, L. Ferkl, Modeling and identification of a large multi-zone office building, in: IEEE International Conference on Control Applications (CCA), Denver, CO, USA, 2011, <http://dx.doi.org/10.1109/CCA.2011.6044402>.
- [30] J. Cigler, S. Prívará, Subspace identification and model predictive control for buildings, in: 11th International Conference Control, Automation, Robotics and Vision, Singapore, 2011, p. 1, <http://dx.doi.org/10.1109/ICARCV.2010.5707821>.
- [31] S.V. Gaikwad, D.E. Rivera, *Control-Relevant Input Signal Design for Multivariable System Identification: Application to High-Purity Distillation*, 1996, San Francisco.
- [32] R.E. Hedegaard, T.H. Pedersen, M.D.S. Knudsen Petersen, Identifying a comfortable excitation signal for generating building models for model predictive control: a simulation study, in: CLIMA 2016 ? Proceedings of the 12th REHVA World Congress: Volume 10, Aalborg, 2016.
- [33] The MathWorks, inc., *System Identification Toolbox 9.3*, [Online].
- [34] L. Ljung, *System Identification. Theory for the User*, Prentice Hall PTR, New Jersey, 1999.
- [35] A.K. Tangirala, *Principles of System Identification. Theory and Practice*, CRC Press, Taylor & Francis Group, 2015.
- [36] P.-D. Moroşan, R. Bourdais, D. Dumur, J. Buisson, Building temperature regulation using a distributed model predictive control, *Energy Build.* 42 (2010) 1445–1452, <http://dx.doi.org/10.1016/j.enbuild.2010.03.014>.
- [37] F. Oldewurtel, A. Parisio, C.N. Jones, D. Gyalistras, M. Gweder, V. Stauch, B. Lehmann, M. Morari, Use of model predictive control and weather forecasts for energy efficient building climate control, *energy and buildings*, *Energy Build.* 45 (2012) 15–27.
- [38] MOSEK ApS, *The MOSEK optimization toolbox for MATLAB manual*. Version 7.1 (Revision 49), (2015). [Online]. Available: <http://docs.mosek.com/7.1/toolbox/index.html>.
- [39] Nord Pool, [Online]. Available: <http://www.nordpoolspot.com/>. [Senest hentet eller vist den 02 04 2016].
- [40] Association of Danish Energy Companies, *Elforsyningsens tariffer & elpriser pr. 1. januar 2015*, Dansk Energi, (2015).
- [41] F. Oldewurtel, D. Sturznegger, G. Andersson, M. Morari, R.S. Smith, Towards a standardized building assessment for demand response, in: 52nd IEEE Conference on Decision and Control, Florence, Italy, 2013, <http://dx.doi.org/10.1109/CDC.2013.6761012>.

7.2 Epilogue

The analysis of the previous section used MPC to engage a residential building in price-driven DR by altering its energy consumption for space heating. In this analysis, the impact that the energy efficiency of the building had on the potential for conducting DR was investigated. In this regard, the results of the study were found to agree with the findings of Reynders [33]: an increase in the energy efficiency of the building led to 1) higher storage efficiency, thus resulting in the MPC scheme engaging in DR events more frequently; and 2) a lower storage capacity, and thus less energy shifted per DR event. The results of the study indicated that the absolute amount of energy consumption shifted to periods of low grid load remained approximately constant across the retrofitted buildings (buildings R1-R8), while the poor energy efficiency of the existing building led to less energy being shifted.

The similar results achieved for the retrofitted buildings may be explained by the two contradictory effects that increased energy efficiency has on the amount of load shifting occurring (increased efficiency, decreased capacity). This would also suggest that an optimal degree of building energy efficiency (in terms of DR) may exist, since the DR potential of buildings at either end of the energy efficiency scale would suffer from either a low storage efficiency or capacity, respectively. To investigate this further, the analysis was repeated for a building built after the *passive house* standard (assumed: 400 mm wall insulation, 0.08 1/h infiltration rate). Figure 11 presents the results of the paper extended with the *passive house* (PH) simulation. The building labelling approach originally used in the paper was based on the implemented retrofit measures – and not their impact on the energy efficiency of the building. To improve the clarity of the figure, the buildings were reordered according to their total heat loss coefficients, which are now also depicted in the figure.

Similar to the findings in the paper, Figure 11 indicates a consistent relationship between the energy efficiency of a building and the *relative* amount of energy shifted in that building. In contrast, close inspection of the *absolute* amount of load shifting reveals that the *passive house* building shifted the second-least amount of energy – in this aspect only performing better than the existing building. The similar results of the retrofitted buildings (R1-R8) suggest that the exact retrofit-level only had a minor impact on the overall energy quantities shifted. However, the lower storage capacities of the more retrofitted buildings imply that, although they may shift similar amounts on the aggregated level, their impact on individual DR events is limited compared to that

of existing buildings. Because of this, the potential for highly energy efficient buildings depends on the nature of the challenges faced by the grid and the associated price volatility. Finally, fundamental research has indicated that storage capacity also depends on the heating system of the building [79]. Therefore, expanding the analysis to include underfloor heating, which is the predominant heating system in new buildings, could be an interesting topic of future research.

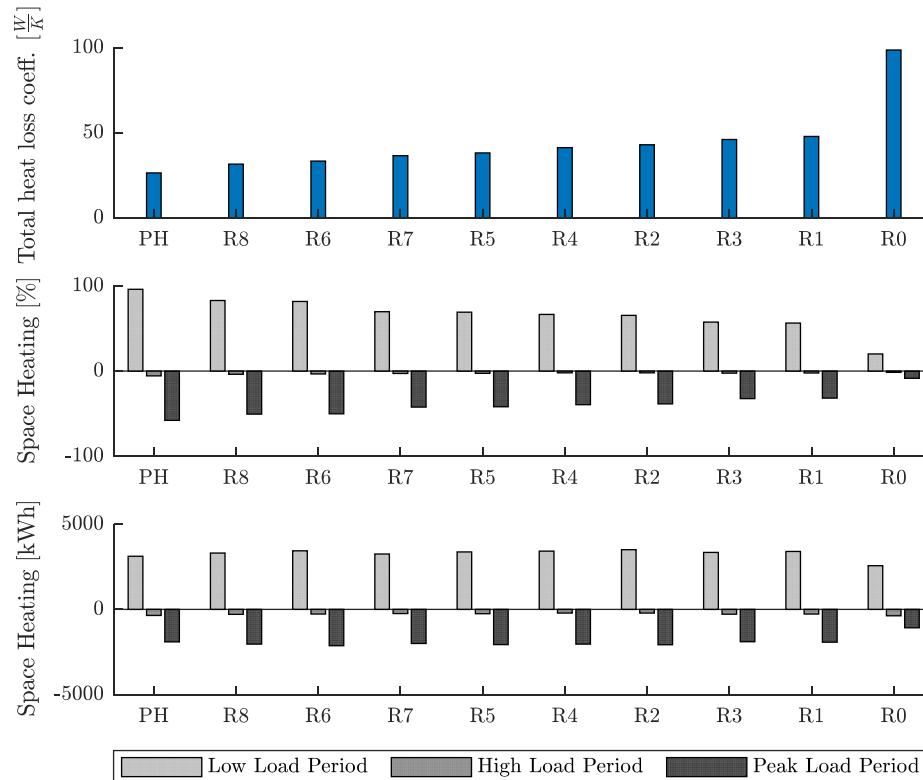


Figure 11 Impact of energy efficiency on the energy quantities shifted to periods of low grid load. Top) Total heat loss coefficient of each building, middle/bottom) the amount of space heating consumption that was shifted to/from each period.

The analysis also indicated a modest, but consistent, difference between the performance of centralized and decentralized MPC schemes. Clearly, the significance of the heat transfer between adjacent thermal zones affects the performance impact of neglecting such interactions. Therefore, in a more recent paper (S5) [80], the centralized and decentralized MPC implementation methods were also evaluated for a building in which the internal walls contained a layer of thermal insulation (due to noise concerns). In this case, the results showed that the benefits of a centralized MPC approach were reduced to a point where it is unlikely that the added efforts associated with this approach can be justified. In both studies, each apartment was modelled as a single zone in both EnergyPlus and in the MPC schemes. In practice, the layout of a building may necessitate

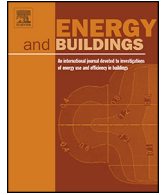
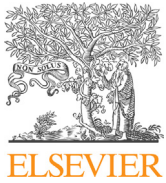
the use of multi-zone models. The added complexity of such a case, both in terms of model identification and control optimization, would further suggest neglecting the less significant coupling between adjacent apartments.

Finally, the analysis applied a price signal that was derived through the method described in [78]. The price signal, which incorporated both societal and grid-related objectives, proved capable of incentivizing DR that reduced consumption in periods characterized by either high grid loads or by CO₂-intense electricity production. On the other hand, the method was incapable of generating significant economic incentives for consumers, as these ranged from approximately 0-6%. It seems questionable whether economic savings in this range will be sufficient incentive for consumers to engage in DR. The analysis presented in the following chapter therefore investigates alternative means of generating economic incentives for consumers while contributing towards grid balancing.

8 MULTI-MARKET APPROACH

One of the barriers for the utilization of electrical demand response is a lack of market structures to support such activities [28]. Vrettos et al. [77] evaluated the use of time-varying prices of both the day-ahead electricity wholesale market and real-time balancing market as incentive mechanisms for enabling DR. The authors argued that day-ahead prices could be suitable for shifting demand to hours of high renewable energy production, while the real-time balancing market prices could be used to balance the grid in real-time. A disadvantage of real-time DR, however, is the lack of ability to prepare the thermal state of the building for a demand response event. Furthermore, since higher requirements are associated with bids on the balancing power market (e.g. minimum capacity), not all of the available flexibility may be readily offered on this market in practice [12]. An alternative to the real-time market is the *intraday market*, which allows electricity market actors to trade in the period between the clearing of the day-ahead market and the opening of the balancing market. Trading on this market thereby allows market actors to correct the energy volumes they originally contracted on the day-ahead market. This is especially desirable for actors who are exposed to high uncertainties in their daily operation – e.g. electricity producers with a large portfolio of production from intermittent renewable energy sources. Scharff et al. [12] argue that the need to account for uncertainties in production could result in the intraday market playing a vital role in integrating increasing levels of intermittent renewable energy production, and therefore expect the intraday market trading volumes to increase as more production from intermittent renewable energy sources is integrated in the energy system.

The intraday market could provide flexible consumers with economic incentives since market actors who face imbalanced operation may be willing to offer favourable prices to acquire the contracted consumption of others in order to reduce their own imbalance. The following section presents an analysis of the potential associated with using the intraday market as a DR incentive mechanism. To ensure that the prices of the two different markets are aligned and to reduce the impact of nation-specific tax structures, all tax components of the prices were neglected in the analysis. As the analysis is carried out for an existing and retrofitted building, the analysis contributes towards thesis objectives **2.1** and **2.3**.



Multi-market demand response using economic model predictive control of space heating in residential buildings



Rasmus Elbæk Hedegaard*, Theis Heidmann Pedersen, Steffen Petersen

Department of Engineering, Inge Lehmanns Gade 10, Aarhus University, DK-8000 Aarhus C, Denmark

ARTICLE INFO

Article history:

Available online 20 June 2017

Keywords:

Residential demand response
Economic model predictive control
Intraday market trading
Energy flexibility

ABSTRACT

Several studies have evaluated the potential for residential buildings participating in demand response programs based on the day-ahead electricity market prices. However, little is known about the benefits of residential buildings providing demand response by engaging in trading on the intraday market. This paper presents a simulation-based study of the performance of an economic model predictive control scheme used to enable demand response through parallel utilization of day-ahead market prices and intraday market trading. The performance of the control scheme was evaluated by simulating ten apartments in a residential building located in Denmark through a heating season (four months) using historical market data. The results showed that the addition of intraday trading to the more conventional day-ahead market price-based control problem increased the total cost savings from 2.9% to 5.6% in the existing buildings, and 13%–19% in retrofitted buildings with higher energy-efficiency. In the existing building the proposed control scheme traded on average 12.7 kWh/m² on the intraday market throughout the simulation corresponding to 21% of the reference consumption. For a retrofitted building the traded volume was 9.6 kWh/m² which corresponds to 52% of the reference consumption. These results suggest that the benefits of considering intraday market trading as a demand response incentive mechanism apply to a wide range of buildings.

© 2017 Elsevier B.V. All rights reserved.

1. Introduction

As the penetration of intermittent renewable energy sources (RES) such as wind power increases, so will the uncertainty associated with electricity production prognoses because of the inherent uncertainties of weather forecasts. This uncertainty complicates the task of maintaining an instantaneous balance between electricity supply and demand [1,2]. A commonly suggested way of addressing the issue of grid balancing under more volatile electricity production is the implementation of smart grids [3–6]. A characteristic of smart grids is effective utilization of Demand Response (DR) programs, where consumers are encouraged to adjust their demand to meet supply and thereby increase the overall efficiency of the energy system. Energy use in residential buildings constitutes a significant potential for DR as it accounts for 25% of the total energy consumption in the EU of which 67% is used for space heating in the North and West regions of EU [7]. This flexible consumption can be activated through different types of DR programs.

1.1. Demand response programs

DR programs are often divided into *direct* and *indirect* control programs [4,8,9]. In direct control programs, the consumer entrusts the energy planners and operators (PO) with direct control of their electrical loads; the PO can change consumption pattern directly. In indirect control programs, the consumer has full control of the electrical loads and the PO can only provide incentives for consumers to change their consumption pattern. One incentive from PO to consumers is to provide time-varying energy prices, which motivates consumers to reduce consumption in high price periods, e.g. by shifting consumption to periods with lower prices. This approach is referred to as *indirect price-based* DR programs. Previous studies have demonstrated that residential building owners may benefit from this type of DR programs. Halvgaard et al. [10] operated a residential-scale heat pump using Economic Model Predictive Control (E-MPC) with day-ahead prices and achieved 25–35% cost savings compared to traditional set point control dependent on comfort constraints. Avci et al. [11] used E-MPC to achieve a 13% cost reduction compared to a two-position thermostatic control of a residential heat pump, and Oldewurtel et al. [12] used MPC with a multi-objective cost-function to reduce consumption peaks by up to 39% and costs by 31.2%. Knudsen and Petersen [13] demonstrated that using E-MPC for space heating can enable cost savings, CO₂

* Corresponding author.

E-mail address: reh@eng.au.dk (R.E. Hedegaard).

Nomenclature

Abbreviations

DR	Demand response
E-MPC	Economic model predictive control
RES	Renewable energy sources
PO	(Energy) Planners and operators
SSM	Supply-side management
TSO	Transmission system operator
BRP	Balance responsible party
MILP	Mixed integer linear problem
ITH	Intraday trading horizon
ID	Intraday (market)
DA	Day-ahead (market)

Symbols

x	State vector of the resistance-capacitance building model
p_{da}	Vector containing forecasted day-ahead market prices
u_{da}^*	Optimal sequence of control actions with respect to day-ahead prices
p_{id}	Vector containing prices from intraday market trades
u_{id}^*	Optimal sequence of control actions after intraday optimization
J	Cost of implementing the entire optimal control strategy

emission reductions, and shift consumption from periods of peak load to low load periods. The large spread in savings found in the above-mentioned studies may be caused by several factors including the magnitude of price fluctuations, how the reference case is defined as well as the inclusion of taxes. For example, Knudsen et al. [14] demonstrated that the economic incentive of performing DR using E-MPC of residential space heating strongly depends on the taxation mechanism of energy: a case study led to end-user energy cost savings between 2% and 9% depending on the taxation. Furthermore, Pedersen et al. [15] demonstrated that the cost savings of indirect price-based DR programs using E-MPC depends on the energy-efficiency of the building envelope and consequently the storage efficiency, which relates the amount of energy lost during the storage process to the amount of energy actually stored.

All of the mentioned studies use forecasts of energy prices and weather with durations upwards of days to prepare the building for DR by utilizing the inherent thermal inertia of the building as an energy storage. However, previous studies have demonstrated that buildings can also help solve grid balancing issues that arise on a shorter time scale. Oldewurtel et al. [16] used MPC with critical peak pricing to quantify the flexible consumption immediately available in buildings that have not been prepared to deliver flexibility, by introducing two performance metrics: Power Shifting Potential and Power Shifting Efficiency. De Coninck et al. [17] used MPC to derive cost curves describing the costs associated with deviation from optimal control strategies to activate flexibility. Both studies conclude that the availability and associated cost of flexibility in building space heating depend on several dynamic factors such as the current thermal state of the building and weather conditions, but they do not attempt to investigate whether the cost of the flexibility is aligned and compatible with the current electricity markets or incentive mechanisms. The following section describes the structure of wholesale electricity markets and clarifies why these may be suitable for activating the DR potential in residential space heating.

1.2. Electricity markets as DR platforms

This study evaluates an indirect price-based DR program utilizing two European-based wholesale electricity markets: the day-ahead market Elspot and the intraday market Elbas. Both markets are a part of the cross-border electricity market Nord Pool. Each participating country is divided into individual bidding areas that reflect geographical and grid characteristics. For example, Denmark consists of two bidding areas of which the Western Denmark region (DK1) is characterized by a high penetration of wind power production [18]. In 2015 the accumulated annual wind power production constituted approximately 55% of the total annual consumption of the DK1 region [19].

In DK1, the majority of electricity is traded on the day-ahead market Elspot, where electricity trades confirmed upon market closure is to be delivered the following day. The market closes each day at 12:00 CET and shortly thereafter the hourly day-ahead prices (p_{da}) for the following day are available to the public. The hourly price is settled through the pay-as-clear principle in which, for each hour, the price that balances supply and demand applies to all electricity traded across different market regions. However, in periods where transmission lines between bidding areas are congested (bottlenecks), a market split occurs resulting in different prices on each side of the congestion. The physical limitations of transmission lines thus lead to increased price fluctuations in regions with high shares of intermittent RES such as DK1. Fig. 1 shows how high wind power production within the region has a tendency to reduce the DK1 day-ahead clearing prices in 2015. Furthermore, the production from wind exceeded the regional consumption in 1442 h while negative prices were observed in 65 h. It is these day-ahead prices that have served as the sole price signal in many E-MPC or rule-based studies on DR for space heating in buildings [10,12,13,20–23].

The significance of wind power production in the region for the day-ahead market principle means that the trades depend strongly on the accuracy of production (and consumption) prognoses. The market therefore needs a way of correcting the already traded quantities on the day-ahead market to be consistent with updated production prognoses. Such corrections can be made through trading on the intraday electricity market (Elbas) which remains open from the day-ahead market closure up until one hour before the electricity is to be delivered. Despite the fact that trades can be made up to 33 h before delivery, over 50% of all intraday trades are made within the last three hours before intraday market closure as the accuracy of prognoses increase [18]. The total volumes traded on the Elbas market are currently small, constituting only approximately 3% of the annually sold and bought electricity on Elspot in 2015 [19]. However, Scharff et al. [18] identified high shares of intermittent production from RES to be a contributing factor towards increased intraday trading.

In conventional power systems grid balancing is achieved through supply-side management (SSM), where the transmission system operator (TSO) hires power plants that are able to adjust their power output to address any imbalanced operation from market actors. In all trades on the day-ahead electricity market, one of the actors involved with the trade assumes the role of the Balance Responsible Party (BRP). The BRP is committed to cover any expenses of the TSO to counteract any imbalance associated with the trade. The balancing power price is thus directly linked to the expenses associated with balancing carried out by the TSO. As the share of fluctuating renewable production increases, the task of balancing the grid becomes increasingly complicated which, consequently, increases the expenses resulting from imbalanced operation. As the balancing expenses increase, BRPs are expected to be more involved in intraday trading to ensure a balanced operation.

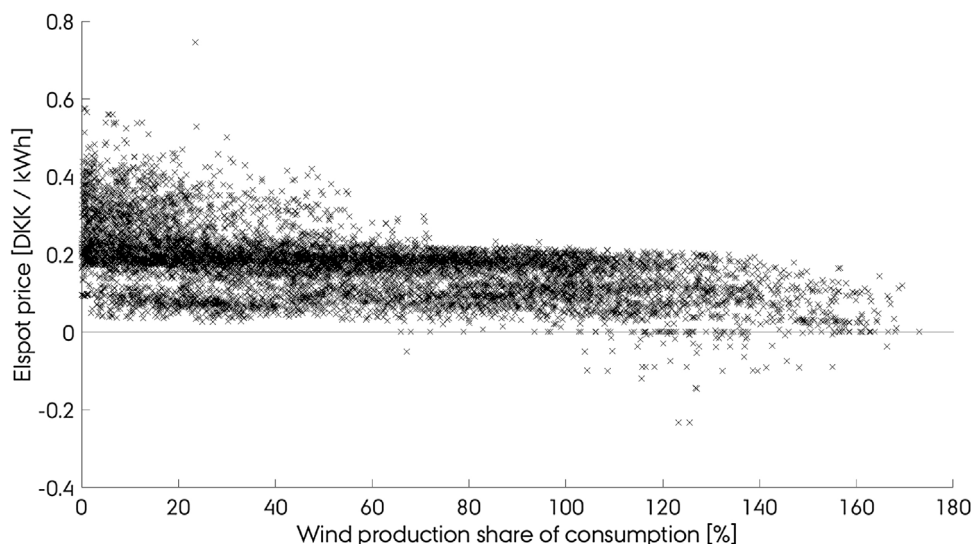


Fig. 1. The effect of wind power production on day-ahead electricity prices in the DK1 area. Source: Nord Pool, 2015 data.

The intraday electricity market prices (p_{id}) are settled according to the pay-as-bid principle, which means that individual trade prices are determined when market participants accept available offers. Therefore, prices may vary within any given hour [18]. Fig. 2 shows the marginal price of the day-ahead market and the interval for each hour in which trades settled on the intraday market over a three-day period in December 2015. The average intraday price and the day-ahead price are strongly correlated with a Pearson correlation factor of 0.91. However, as shown in Fig. 2, significant deviations between intraday and day-ahead prices occurred in several hours of the depicted period.

While the day-ahead price is a product of supply and demand, the intraday price is an indication of imbalances expected by the BRPs themselves. BRPs with flexible buildings in their own consumer portfolio may utilize this flexible demand to lower or avoid entirely the need for intraday trading. Similarly, other actors may use flexible consumption as a virtual power plant, offering energy on the intraday market.

1.3. Aim of this paper

Residential building owners or aggregators may increase their economic incentive to deliver DR to the electricity grid when mul-

multiple electricity markets are considered. A study by Ali et al. [24] demonstrated that the charging pattern of domestic hot water tanks can be planned taking both day-ahead market prices and (artificial) instantaneous balancing events into consideration. It therefore seems reasonable to assume that space heating can be planned in a similar manner. However, to the knowledge of the authors, there have been no reported studies on whether space heating of residential buildings can participate in multiple DR programs using day-ahead and intraday prices simultaneously. This study therefore investigates whether space heating can be operated to respond to both day-ahead and intraday market-driven DR programs in parallel without compromising thermal comfort.

2. Method

The following sections introduce the proposed control scheme capable of utilizing market conditions on the day-ahead and intraday market in parallel. First, Section 2.1 presents economic model predictive control in its more conventional configuration where only day-ahead prices are used to optimize operation of the building. Then, Section 2.2 expands upon the control scheme by introducing the expanded multi-market algorithm. Finally, Section

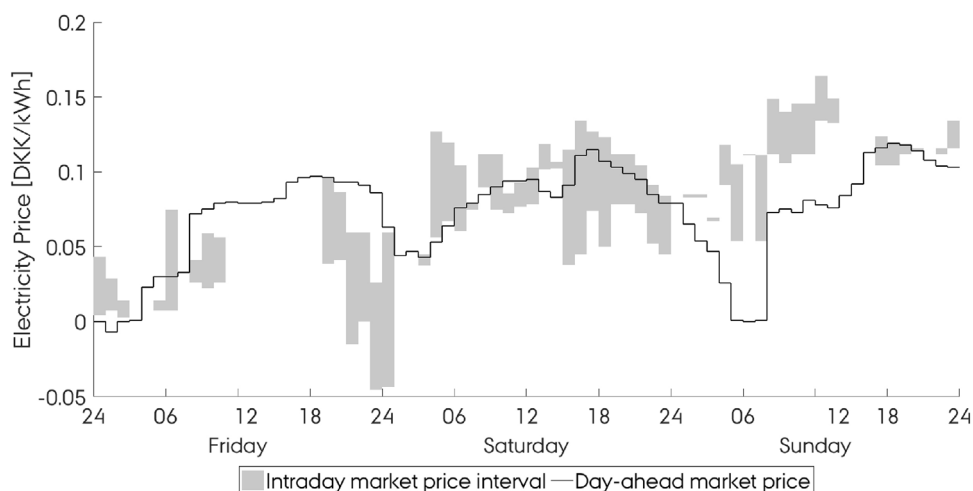


Fig. 2. Day-ahead clearing price and intraday market price-intervals (week 8, 2016).

2.3 presents the assumptions made for a case study used to illustrate the performance of the proposed control method.

2.1. Economic model predictive control

Economic model predictive control solves an optimization problem to determine the optimal sequence of control actions, u , for the space heating system by minimising the total operational cost for a finite prediction horizon N :

$$\underset{u}{\text{minimize}} \quad \sum_{k=1}^N C_k^T \cdot u_k \quad (2a)$$

$$\text{subject to } x_k = \mathbf{A}x_{k-1} + \mathbf{B}u_{k-1} + \mathbf{E}d_{k-1} \quad (2b)$$

$$y_k = \mathbf{C}x_k \quad (2c)$$

$$0 \leq u_k \leq P_{\max} \quad (2d)$$

$$T_{\min,k} \leq y_k \leq T_{\max,k} \quad (2e)$$

$$\Delta T_{\min,k} \leq \frac{\Delta y_k}{\Delta t} \leq \Delta T_{\max,k} \quad (2f)$$

$$x_0 = x(0) \quad (2g)$$

where c_k is the time varying price associated with control action, u_k . The thermodynamics behaviour of the building to be controlled is described by Eqs. (2b) and (2c), and the control actions are constrained by the maximum design power of the space heating system by Eq. (2d). The controlled variable is the room air temperature, y_k , whose value and rate of change are constrained by Eqs. (2e) and (2f), respectively. Measurements are used to define the current state of the building in Eq. (2g), where the unobservable states are estimated using a Kalman Filter.

The model of the building thermodynamics used in this study was a grey-box model formulated in state space form. Grey-box models are categorised by having a predefined structure of physically meaningful parameters such as heat loss coefficients and thermal capacities. These parameters are estimated from measurement data through methods from the field of System Identification. The model used in this study is a simple two-state model, where the two states represent the lumped thermal capacity of the zone air and the construction components, respectively. Forecasts of ambient temperature, solar heat gains and space heating are treated as inputs from which the model produces a prediction of the zone air

temperature as output. A detailed description of the model structure used in this study is provided in Ref. [15].

At each discrete time step k , the states of the building model are updated and the optimization problem is solved using the MOSEK solver [25] resulting in a sequence of optimal space heating control inputs u^* . The output of the control scheme is thus the control strategy that, over a predefined prediction horizon N , satisfies the imposed constraints at the lowest operational cost. Only the first control action of each control sequence is implemented in the building after which a new sequence is computed at the start of the following time step – a control principle referred to as *receding horizon control* [26]. This approach allows for the control scheme to update weather and price forecasts continuously while enabling the use of building measurements to introduce feedback in the control loop.

2.2. Scenario-based optimization

The control scheme in Section 2.1 was expanded to enable the use of intraday price intervals in the optimization. A challenge in relation to this is to prevent the control scheme from purchasing and selling electricity within the same hour. One way of preventing such behaviour is to implement logic in the optimization problem that restricts the algorithm to be either in *selling-mode* or *buying-mode*. The resulting optimization problem would be a mixed integer linear problem (MILP) – an approach that was used in Bianchini et al. [27] to obtain on/off control of heaters. However, as the authors point out, MILPs are significantly more complex to solve than linear or quadratic programs, which limits the computationally tractable size of the problem. To avoid restricting the size of the optimization problem we chose a scenario-based approach instead, where optimization problems with different cost vectors corresponding to each relevant scenario were solved individually and then compared.

The decision making process including both the day-ahead and intraday market can be condensed to the principle described in Table 1. First, the optimal control strategy, u^* , is computed in each hour by solving the optimization problem defined in Eqs. (2a)–(2g) which only consider the day-ahead prices over a three day prediction horizon. While prices may not be available three days ahead, studies have shown E-MPC to be robust to simply repeating the price fluctuations from the first day [13]. This study assumes perfect price predictions for simplicity. Secondly, a shorter intraday trading horizon (ITH) is introduced – in this study ITHs of one and

Table 1
Breakdown of the new control algorithm.

Control Algorithm
<pre> for each timestep $k = 1, 2, \dots$ do for each zone $i = 1:10$ do measure zone states $x_{0,i}$ obtain weather and price forecasts solve Eq. (2) using day-ahead prices, p_{da}, to obtain control strategy u_{da}^* if intraday trading within ITH then for scenario $j = 1, 2, \dots$ do solve Eq. (2) using intraday market prices, $p_{id,j}$, within ITH to obtain control strategy, $u_{id,j}^*$ end find minimal objective value J_j^* implement first control action of $u_{id,j}^*$ else implement first control action of u_{da}^* end end end end </pre>

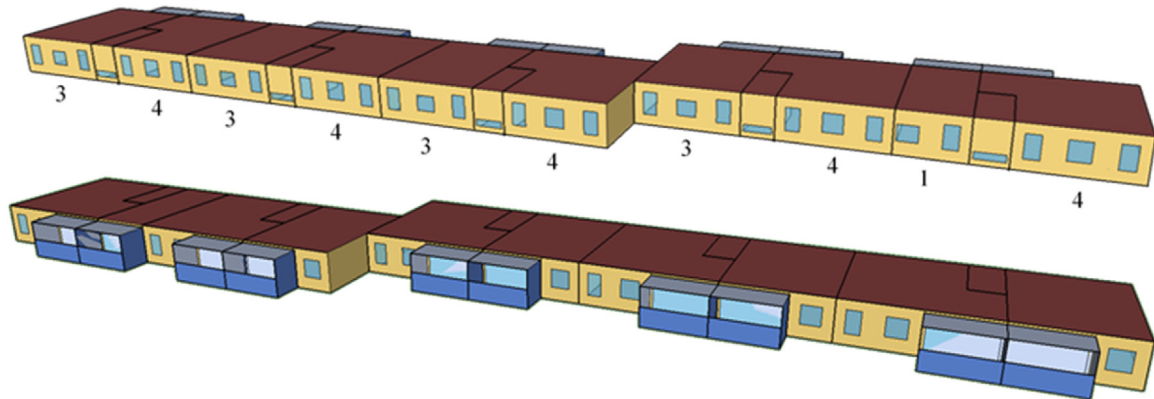


Fig. 3. Façades of case building with numbers indicating the apartments' number of rooms.

three hours were evaluated. Within the span of the ITH the algorithm evaluates currently available offers on the intraday market. If no offers are available, the intraday trading stage of the algorithm is not activated and the building is operated solely based on optimization using day-ahead prices. If trading offers are available inside the ITH, the algorithm treats the consumption procured on the day-ahead market as a trade commodity in the following intraday scenario optimization problems. These optimization problems evaluate all possible combinations of purchasing additional consumption or selling already procured consumption in each hour within the ITH. The controller then implements the intraday trading strategy that yields the highest profit, which may be to either store energy, sell part of the procured electricity back or stick to the original day-ahead optimized control sequence. In either case, the same comfort-related constraints used in the day-ahead optimization problem apply to all intraday scenarios, meaning that the algorithm will only sell energy in the extent that the thermal indoor climate remain within predefined comfort boundaries. To ensure compliance with the intraday market structure where the market closes one hour before delivery, each control strategy is computed one hour before implementation; hence, the strategy computed at time $t = 8:00$ is implemented in the building from $t = 9:00$ to $10:00$.

An ITH of one hour results in three optimization problems to be solved: the initial *day-ahead problem*, a *sell-scenario* and a *buy-scenario*. Expanding the ITH by one hour introduces, in addition to the three previous scenarios, the two scenarios where electricity is bought in the first hour and sold in the second hour, and vice-versa. The number of scenarios and thereby optimization problems $n_{scenario} = 1 + 2^{ITH}$ to be solved in each time step increases exponentially with the ITH and is consequently

However, as mentioned in Section 1.2, approximately half of all trades are made within the last three hours before intraday market closure. Therefore, in order to limit the number of scenarios to evaluate, a maximum ITH of three hours was chosen in this study.

2.3. Case study

This section presents the simulation-based case study used for demonstrating the performance of the proposed control scheme. The building to be controlled is a four-story apartment block built in 1978 and located in Aarhus, Denmark. An EnergyPlus [28] model of the building serves as a representation of the actual building. The apartment block has east-west oriented window configurations and west-oriented open balconies, see Fig. 3. To simplify the modelling and simulation process, only the third floor was investigated which is comprised of ten differently sized apartments. All apartments were modelled as individual thermal zones with all

horizontal zone boundaries (ceiling, floor) assumed adiabatic. All thermal zones were modelled with electrical baseboard heating systems operated by the E-MPC control algorithm implemented in MATLAB [29]. The maximum allowed temperature increase of Eq. (2e) was chosen as four degrees above the set point in all apartments. Furthermore, the maximum rate of change in Eq. (2f) was specified as 2.1° per hour in accordance with ASHRAE's recommendations [30]. The link between MATLAB and EnergyPlus was facilitated with the Building Controls Virtual Test Bed (BCVTB) [31].

The simulation period was chosen as November 1 to February 28 corresponding to the main heating season in Denmark using the standard EnergyPlus weather data file of Copenhagen, Denmark [32]. Historical market data of electricity production, trading and prices (2015/16) from the day-ahead and intraday markets were used in the simulation as forecasts for operational planning of the building. The data was acquired through the Danish TSO, Energinet.dk [22] and Nord Pool [33,34]. Taxation of electricity was omitted in this study for the sake of simplicity in interpretation of results. Consequently, results presented in absolute values cannot be directly compared to the actual price paid by building owners. The case study does not investigate how weather and price forecast uncertainties affect the performance of the proposed control scheme.

Detailed information on the intraday trading was not available. The only data publicly available was the minimum, average and maximum prices of settled intraday trades for each hour. Because of this, optimal trading conditions were assumed, meaning that the algorithm achieves the lowest intraday price observed while energy is being purchased and highest when energy is sold back to the market. Another piece of information that was unavailable was the period during which a trade offer was available on the intraday market. Because of this, all trades settled during the ITH were assumed to be available at the beginning of the ITH. To reduce the significance of this assumption the ITH was limited to a maximum of three hours in this study. Finally, day-ahead prices were assumed outside the ITH interval.

Previous studies have indicated that the energy efficiency of the building envelope is an important factor in relation to DR quantity and duration [15,35]. The performance of the proposed control scheme was therefore also tested on two retrofitted versions of the existing building to investigate how increased energy-efficiency affected the potential for residential multi-market DR. Both retrofits involve more energy-efficient windows, additional external facade insulation, reduced infiltration rate, and a mechanical constant air volume ventilation rate of 0.5 h^{-1} with 80% heat recovery efficiency as listed in Table 2. The table also lists the reference consumption for space heating over the four months sim-

Table 2
Specification of retrofit scenarios and reference consumption in the simulated period.

	Additional façade insulation	Infiltration rate	Window configuration	Reference consumption
Existing	–	0.50 [h ⁻¹]	existing	59.9 kWh/m ²
Retrofit1	0.125 m	0.18 [h ⁻¹]	2-layer glazing	28.1 kWh/m ²
Retrofit2	0.205 m	0.10 [h ⁻¹]	3-layer glazing	18.6 kWh/m ²

ulated for each respective building controlled with a PI-controller with constant set point. A more detailed description of the building model and the retrofit scenarios can be found in ref. [15].

3. Results

The following sections present the results from the simulations of the case building. The mechanism of the proposed control scheme is illustrated and evaluated on its impact on energy consumption, overall cost savings, utilization of the intraday market, and the fraction of trades that contributed towards grid balance.

3.1. The mechanism

The air temperature and heating rate in a three-room apartment using a conventional PI-control scheme with a constant set point, E-MPC using only day-ahead prices, and the proposed multi-market control scheme are shown in Fig. 4 to illustrate the mechanism of the controller. The intraday action (Fig. 4 bottom) shows how the control scheme interacted with the intraday market in each time step. As a guide to the remaining figures of this article, it should be noted that any control scheme that involve intraday trading (marked ITH) also includes day-ahead trading.

It is not possible to compare results from the two E-MPC-based control schedules directly because they are outcomes of separate simulations where the state of the building may deviate significantly at any given time. However, on multiple occasions the effects of intraday trading are easily distinguishable. For example on Friday where the intraday trading resulted in additional temperature boosting before noon and again in the evening compared to the E-MPC based on only day-ahead prices. On Sunday the opposite happened, where extended periods of temperature boosting were cancelled since selling the procured energy was more profitable.

3.2. Energy consumption and cost savings

The extension of the E-MPC scheme to include intraday trading enables the building to participate in grid balancing while also increasing the potential for cost savings. Fig. 5 shows the performance of three E-MPC schemes when implemented in the case building and the two retrofit scenarios. For transparency, results are presented both in absolute and relative terms compared to a PI-controlled baseline of each building case (origo).

The results from the E-MPC based on day-ahead prices indicated that the retrofitted buildings (R1 and R2) only achieved moderately higher absolute cost savings compared to the existing building (R0). The reason is that, although the E-MPC scheme in the retrofitted buildings tended to load shift more often, the magnitude of load shifts in the existing building is larger due to the higher reference consumption, as also seen in [15]. The introduction of intraday trading reduces the difference in absolute cost savings achieved in the three buildings. This can be explained by relatively low fluctuations in the day-ahead prices that were only sufficient to make utilization of flexibility profitable in the retrofitted buildings, but not in the existing building where a higher loss is associated with the storage process. Since the prices on the two markets, as mentioned in Section 1.2, are strongly correlated, this often resulted in the energy-efficient buildings having already utilized all the available flexibility before trading on the intraday market, whereas this was not the case with the existing building. Ali et al. [24] addressed this issue by reserving part of the flexibility by using more restrictive comfort constraints in the initial day-ahead optimization than the following intraday optimization problems. However, the authors argued that reserving flexibility may just as well influence the economic potential negatively as positively since the benefits and viability of reserving flexibility depend strongly on the frequency of DR-events, the size of the economic incentives offered, and the risk-willingness of the consumer.

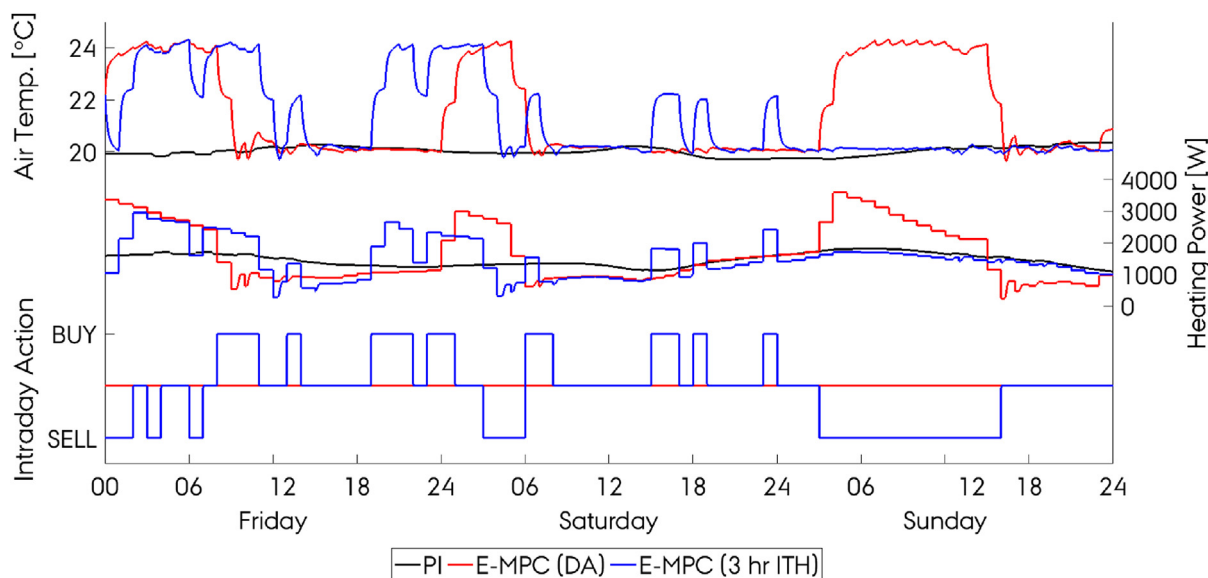


Fig. 4. Example period of both upward and downward regulation in the Retrofit2 building.

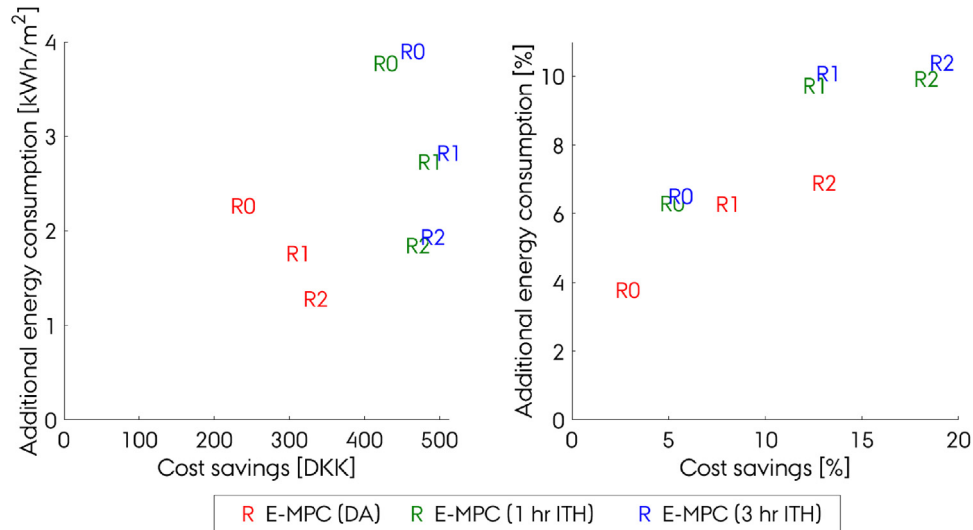


Fig. 5. Economic performance of the algorithm and effect on consumption aggregated for all apartments. Left (a) absolute differences from reference, right (b) relative to the reference.

Fig. 5b, which shows the cost savings in relative terms, indicates a significant difference in the achieved cost savings between the three buildings, suggesting that a higher fraction of the consumption can be made flexible in retrofitted buildings. Furthermore, the effect of enabling the control scheme to trade on the intraday market is seen to positively influence the potential in all cases significantly. The increase in consumed energy seen in Fig. 5 happens since heat is stored by increasing the air temperature. This increase in temperature naturally results in a higher heat loss to the surroundings, and thereby a higher overall consumption. The control algorithm determined when market conditions were sufficiently profitable to make up for the heat lost in the storage process. Finally, Fig. 5 suggest that the economic potential gained by increasing the ITH from one to three hours is marginal.

3.3. Interaction with the intraday market

This section presents how the proposed control scheme interacts with the two electricity markets. The electricity volumes traded by the E-MPC using day-ahead only and the proposed multimarket E-MPC are displayed in Fig. 6.

The results indicate that extending the ITH leads to a moderate increase in intraday trading activity. The reason is that this allows the control scheme to use more elaborate trading patterns including scenarios where electricity was bought in one hour in order to sell procured electricity in the next hour. Furthermore, the share of electricity procured through intraday trading increased for the retrofitted scenarios. This suggests that energy-efficient buildings, retrofitted or new, could on an aggregated level be considered assets in terms of short-notice residential DR.

As described in Section 1.2, BRPs with imbalanced operation are motivated to engage in intraday trading to avoid paying balancing prices. This suggests a certain correlation between the intraday trading and the expected grid balance. The philosophy behind the proposed control scheme is that, by contributing to the balance of individual market actors, the resulting DR will on average have contributed more to overall grid balance than imbalance. However, since balancing out a single BRP does not necessarily equate to increased grid balance, it is necessary to evaluate whether the performed DR actually contributed to balancing the grid.

This was done by labelling all intraday trades carried out by the control scheme based on whether it contributed to balancing

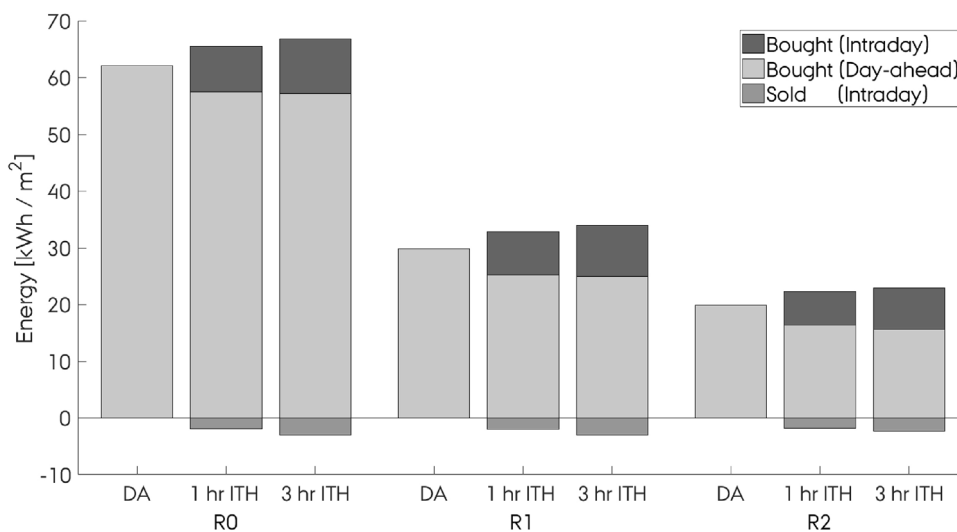


Fig. 6. Electricity traded on the day-ahead and intraday markets (mean of all zones).

Table 3
Percentage of time the DR contributed to balance and imbalance, respectively.

Grid state	Building Control action	R0		R1		R2	
		1 h ITH	3 h ITH	1 h ITH	3 h ITH	1 h ITH	3 h ITH
Downregulation (48% of time)	Correct	33.1%	39.8%	36.9%	42.7%	35.0%	41.4%
	Incorrect	2.5%	8.1%	3.9%	8.8%	4.4%	7.7%
	No action	64.4%	52.1%	59.2%	48.5%	60.6%	50.9%
Upregulation (28% of time)	Correct	9.6%	17.8%	11.8%	18.6%	14.6%	17.4%
	Incorrect	17.4%	24.6%	17.4%	23.9%	15.6%	21.7%
	No action	72.9%	57.6%	70.9%	57.6%	69.8%	60.9%

the grid or introduced further imbalance. The terminology used in the following takes offset in the grid point of view. This means that buildings can provide *upward regulation* to the grid by lowering the consumption and, conversely, *downward regulation* by increasing consumption. According to Table 3, the grid was in need of downregulation 48% of the time and upregulation 28% of the time during the simulation period [19].

Furthermore, Table 3 indicates how the algorithm operated during these hours by dividing control actions into ‘correct’ ones that aided the grid and ‘incorrect’ ones that would have negatively impacted grid balance. As such, the following is an evaluation of both the proposed control scheme and the historical market conditions in relation to the needs of the electricity grid. Periods where the grid was not in need of balancing power was left out of this analysis.

It is seen that the control scheme, in a relatively large fraction of the time where the grid was in need of regulation, did not engage in intraday trading, but merely implemented the control action optimized with respect to day-ahead prices. Depending on the specific simulation, this tendency was observed between 48% and 73% of the time, which can be caused by e.g. poor price conditions or a lack of available flexibility.

The results in Table 3 also indicate that the algorithm performed well during times where the grid was in need of downregulation during which the actions carried out by the controller mostly favoured the grid. During these periods, the controller increased the consumption of the building to store energy between 33% and 43% of the time. On the other hand, it is seen that the control scheme was less efficient at providing services to a grid in need of upregulation. In these periods, more incorrect actions than correct were carried out. Inspecting the historical data revealed that the intraday prices often did not reflect the state of the grid correctly. When the grid needed downregulation, the prices indicated the opposite 22% of the time while in the upregulation scenario this was the case 47% of the time.

4. Discussion

The case results presented in Section 3.2 indicate that the majority of the economic benefits of including intraday trading can be achieved with a one-hour ITH, and thereby – compared to three-hour ITH – reduce the complexity of the planning phase. This implies that simple *one-way* trading patterns (i.e. buy-only or sell-only strategies) were sufficient. However, in real-world application, the ability to consider multiple offers at the same time may allow for easier integration with the market, where offers may be placed at any time throughout the trading window corresponding to the relevant hour. Longer trading horizons allowing utilization of offers entering the intraday market early may therefore be more practical, also bearing in mind that the computational time of the three-hour ITH control problem including both the day-ahead and all eight intraday scenarios for all ten zones was approximately 1.2 s. Rule-based logic could potentially speed this up further by ruling out

scenarios that are unlikely to produce optimal solutions based on price characteristics.

The economic optimization in the E-MPC control scheme will often result in the control scheme tracking the lower temperature set point to minimise the energy consumption – only raising the temperature when prices encourage it. During periods of set point tracking the building has, due to the zero-tolerance for comfort violations, no negative flexibility to offer to the intraday market. Consequently, the controller was only able to sell electricity when temperature boosting had occurred as a result of the day-ahead optimization. This relationship can be found in Fig. 4 where it is clear that electricity was only sold in periods where the day-ahead algorithm was performing temperature boosting. This limitation, in combination with misleading prices, is seen to impact the results of Section 3.3, where the control scheme is less efficient at reducing consumption (i.e. providing upward regulation) than increasing consumption (downward regulation). Enabling buildings to provide upward regulation could be done by allowing temperature violations based on either the profitability of prices or simply a certain fraction of time could to some extent address this limitation.

5. Conclusion

This simulation-based study indicates that consumers may increase their economic incentive to invest in economic predictive control of residential space heating by engaging in trades on the intraday electricity market in parallel with the day-ahead electricity market. Especially buildings that do not provide sufficient storage-efficiency to frequently exploit day-ahead price fluctuations through load shifting benefited from the multi-market approach; here, cost savings were approx. doubled compared to the single-market approach. The results also indicated that increasing the energy efficiency of the building, despite the reduction in overall consumption, only had a small negative impact on the quantities of energy traded on the intraday market. This suggests that also new or recently retrofitted buildings may benefit from participating in intraday market-driven demand response.

Finally, future work should investigate how an alternative formulation of comfort constraints that allows temporary set point violations increases the potential for buildings to provide services to electricity grids in need of upward regulation.

Acknowledgements

The research was conducted as part of the ‘Resource Efficient Cities Implementing Advanced Smart City Solutions’ (READY) financed by the 7th EU Framework Programme (FP7-Energy project reference: 609127) and the project “READY.dk” financed by the Danish Energy Research and Development program ForskEl. Furthermore, the authors express gratitude to the participants and the work done in the IEA-EBC Annex 67 on Energy Flexible Buildings.

References

- [1] C. Weber, Adequate intraday market design to enable the integration of wind energy into the European power systems, *Energy Policy* 38 (2010) 3155–3163, <http://dx.doi.org/10.1016/j.enpol.2009.07.040>.
- [2] J. Kiviluoma, M. O'Malley, A. Tuohy, P. Meibom, M. Milligan, B. Lange, H. Holttinen, M. Gibescu, Impact of wind power on the unit commitment, operating reserves, and market design, in: IEEE Power and Energy Society General Meeting, San Diego, CA, 2011, <http://dx.doi.org/10.1109/PES.2011.6039621>.
- [3] R. D'Hulst, W. Labeeuw, B. Beusen, S. Claessens, G. Deconinck, K. Vanthournout, Demand response flexibility and flexibility potential of residential smart appliances: experiences from large pilot test in Belgium, *Appl. Energy* 155 (2015) 79–90, <http://dx.doi.org/10.1016/j.apenergy.2015.05.101>.
- [4] P. O'Connell, H. Madsen, M. O'Malley, Benefits and challenges of electrical demand response: a critical review, *Renew. Sustain. Energy Rev.* 39 (2014) 686–699, <http://dx.doi.org/10.1016/j.rser.2014.07.098>.
- [5] S. Nolan, M. O'Malley, Challenges and Barriers to demand response deployment and evaluation, *Appl. Energy* 152 (2015), <http://dx.doi.org/10.1016/j.apenergy.2015.04.083>.
- [6] B.P. Esther, K.S. Kumar, A survey on residential Demand Side Management architecture, approaches, Optimization models and methods, *Renew. Sustain. Energy Rev.* 59 (2016) 342–351, <http://dx.doi.org/10.1016/j.rser.2015.12.282>.
- [7] Buildings Performance Institute Europe (BPIE), *Europe's Buildings Under the Microscope – A Country-by-country Review of the Energy Performance of Buildings*, BPIE, 2011.
- [8] M.H. Albadi, E.F. El-Saadany, A summary of demand response in electricity markets, *Electron. Power Syst. Res.* 78 (11) (2008) 1989–1996, <http://dx.doi.org/10.1016/j.ejepsr.2008.04.002>.
- [9] P. Siano, Demand response and smart grids – a survey, *Renew. Sustain. Energy Rev.* 30 (2014) 461–478, <http://dx.doi.org/10.1016/j.rser.2013.10.022>.
- [10] R. Halvgaard, N.K. Poulsen, H. Madsen, J.B. Jørgensen, Economic Model Predictive Control for Building Climate Control in a Smart Grid, IEEE PES Innovative Smart Grid Technologies, Washington, DC, 2012, <http://dx.doi.org/10.1109/ISGT.2012.6175631>.
- [11] M. Avci, M. Erkoça, A. Rahmanib, S. Asfoura, Model predictive HVAC load control in buildings using real-time electricity pricing, *Energy Build.* 60 (2013) 199–209, <http://dx.doi.org/10.1016/j.enbuild.2013.01.008>.
- [12] F. Oldewurtel, A. Ulbig, A. Parisio, G. Anderson, M. Morari, Reducing peak electricity demand in building climate control using real-time pricing and model predictive control, in: 49th IEEE Conference on Decision and Control 2010, Atlanta, GA, 2012, <http://dx.doi.org/10.1109/CDC.2010.5717458>.
- [13] M.D. Knudsen, S. Petersen, Demand response potential of model predictive control of space heating based on price and carbon dioxide intensity signals, *Energy Build.* 125 (2016) 196–204, <http://dx.doi.org/10.1016/j.enbuild.2016.04.053>.
- [14] M.D. Knudsen, S. Petersen, Demand response potential of model predictive control of space heating based on price and CO2 intensity signals, *Energy Build.* 125 (2016) 196–204 <https://doi.org/10.1016/j.enbuild.2016.04.053>.
- [15] T.H. Pedersen, R.E. Hedegaard, S. Petersen, Space heating demand response potential of retrofitted residential apartment blocks, *Energy Build.* 141 (2017) 158–166 <https://doi.org/10.1016/j.enbuild.2017.02.035>.
- [16] F. Oldewurtel, D. Sturznegger, G. Andersson, M. Morari, R.S. Smith, Towards a standardized building assessment for demand response, in: 52nd IEEE Conference on Decision and Control, Florence, Italy, 2013, <http://dx.doi.org/10.1109/CDC.2013.6761012>.
- [17] R. De Coninck, L. Helsen, Quantification of flexibility in buildings by cost curves – methodology and application, *Appl. Energy* 162 (2016) 653–665, <http://dx.doi.org/10.1016/j.apenergy.2015.10.114>.
- [18] R. Scharff, M. Amelin, Trading behaviour on the continuous intraday market ELBAS, *Energy Policy* 88 (2016) 544–557, <http://dx.doi.org/10.1016/j.enpol.2015.10.045>.
- [19] Energinet.dk, The Wholesale Market: Download of Market Data (Accessed 23 04 2016) Available: <http://www.energinet.dk/EN/El/Engrosmarked/Udtraek-af-markedsdata/Sider/default.aspx>.
- [20] D.I. Mendoza-Serrano, D.J. Chmielewski, Smart grid coordination in building HVAC systems: EMPC and the impact of forecasting, *J. Process Control* 24 (2014) 1301–1310 <https://doi.org/10.1016/j.jprocont.2014.06.005>.
- [21] E. Vrettos, K. Lai, F. Oldewurtel, G. Andersson, Predictive Control of Buildings for Demand Response with Dynamic Day-ahead and Real-time Prices, in 2013, European Control Conference Zürich, 2013.
- [22] L. Schibuola, M. Scarpa, C. Tambani, Demand response management by means of heat pumps controlled via real time pricing, *Energy Build.* 90 (2015) 15–28 <https://doi.org/10.1016/j.enbuild.2014.12.047>.
- [23] A. Staino, H. Nagpal, B. Basu, Cooperative optimization of building energy systems in an economic model predictive control framework, *Energy Build.* 128 (2016) 713–722 <https://doi.org/10.1016/j.enbuild.2016.07.009>.
- [24] M. Ali, A. Alahäivälä, F. Malik, M. Humayun, A. Saffarian, M. Lehtonen, A market-oriented hierarchical framework for residential demand response, *Electr. Power Energy Syst.* 69 (2015) 257–263, <http://dx.doi.org/10.1016/j.ijepes.2015.01.020>.
- [25] MOSEK ApS, The MOSEK Optimization Toolbox for MATLAB Manual. Version 7.1 (Revision 49), 2015, Available: <http://docs.mosek.com/7.1/toolbox/index.html>.
- [26] M. Gwerder, D. Gyalistras, C. Sagerschnig, R. Smith, D. Sturznegger, Final Report: Use of Weather And Occupancy Forecasts for Optimal Building Climate Control – Part II: Demonstration (OptiControl-II), 2013.
- [27] G. Bianchini, M. Casini, A. Vicino, D. Zarrilli, Demand-response in building heating systems: a model predictive control approach, *Appl. Energy* 168 (2016) 159–170, <http://dx.doi.org/10.1016/j.apenergy.2016.01.088>.
- [28] U.S. Department of Energy, EnergyPlus 8.1.0, [Online].
- [29] The MathWorks, inc., MATLAB 2015 (8.6.0.267246).
- [30] ASHRAE, Standard 55-2010: Thermal Environmental Conditions for Human Occupancy, ASHRAE, Atlanta, 2010.
- [31] M. Wetter, Co-simulation of building energy and control systems with the Building Controls Virtual Test Bed, *J. Build. Perform. Simul.* 3 (4) (2010) 1–19, <http://dx.doi.org/10.1080/19401493.2010.518631>.
- [32] U.S. Department of Energy, EnergyPlus Weather Data: Copenhagen 061800 (IWEC) (Accessed 06 04 2016) Available: https://energyplus.net/weather-region/europe_wmo_region_6/DNK%20%20.
- [33] Nord Pool, Elspot market data, [Online]. Available: <http://www.nordpoolspot.com/Market-data1/Elspot/> (Accessed 29 04 2016).
- [34] Nord Pool, Elbas market data, [Online]. Available: <https://www.nordpoolspot.com/Market-data1/Elbas/> (Accessed 29 04 2016).
- [35] G. Reynders, Quantifying the Impact of Building Design on the Potential of Structural Storage for Active Demand Response in Residential Buildings. PhD Dissertation, KU Leuven – Faculty of Engineering Science, 2015.

8.2 Epilogue

The purpose of this paper was to shed light on the potential of offering the flexible consumption of buildings on the day-ahead and intraday electricity markets in parallel, and to investigate how such an approach could benefit consumers as well as the grid. The results indicate that significant economic benefits were achieved when going from the single-market approach to the multi-market approach. The benefits of intraday trading were especially high in buildings that had not undergone retrofitting, which, due to their generally lower storage efficiency (see previous chapter), often was not sufficiently incentivized by the day-ahead market prices alone to engage in DR. In these buildings, the economic incentives approximately doubled, while the retrofitted building saw a slightly lower economic gain. However, the neglect of taxes mean that these results do not reflect the regulatory and market conditions, but should instead be interpreted as a preliminary investigation of the potential role of the intraday electricity market in a DR setting.

Another finding was that the intraday market prices did not always reflect the actual needs of the grid. Therefore, relying on the *maximization of profits*-approach to guide how flexible demand is offered on the intraday market sometimes resulted in the actions of the control unit contributing towards the overall grid imbalance. This issue was also documented by Scharff et al. [12] in their analysis of the trading behaviour on the Nordic intraday market, Elbas. In theory, the principles of balancing power settlement should prevent such issues, since balance responsible parties are only incentivized to reduce their own imbalances if they expect them to contribute to an overall grid imbalance. If the imbalance an actor imposes on the grid is opposite in direction to an overall grid imbalance (and thereby has a mitigating effect), the imbalance settlement takes place using the day-ahead price of that hour. As such, the imbalance poses no further risk to an actor in this position, and therefore does not incentivize the actor to engage in trading³. Scharff et al. argue that the most likely cause of such irrational trading activity still occurring on the intraday market is that the market participants lack information about the current grid conditions, and are therefore

³ Clarification: An actor in this position may still benefit from trading on the intraday market – but only if other market actors who are more exposed to imbalance costs allow the actor to eliminate his own imbalance at prices more favourable than the day-ahead prices. However, this scenario is irrelevant for our purposes, since flexible consumers would not be inclined to sell their contracted energy acquired at day-ahead prices for lower prices – and vice-versa in the opposite scenario.

unsure of their exposure to imbalance expenses. The authors describe how the latest information on the state of the grid that is available to market actors at the time of intraday market gate closure is four hours old. As such, although both the intended purpose and structure of the intraday market makes it seem suited for utilization of consumer flexibility through DR, current market conditions make it difficult to ensure that such endeavours also result in *grid-friendly* DR.

Finally, as described in the discussion section of the paper, the comfort constraints of the implemented MPC scheme rendered it unable to reduce consumption levels and provide negative DR (*upward regulation* in grid-terms). To address this issue, we proposed altering the comfort constraints of the MPC scheme such that they allow a certain extent of comfort violations. In a more recent article (S6), we proposed both single and multi-objective control problems designed with this in mind [81]. The analysis showed that the proposed single-objective control problem, which was both computationally more efficient and considered to be more intuitive to occupants specifying their comfort preferences, was almost on par with the performance of the multi-objective control problem. This paper did not apply the proposed way of handling comfort constraints in the intraday market context of the present paper – but this could constitute a topic for future research.

9 URBAN-SCALE ANALYSIS

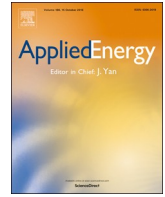
Several studies, including those presented in the two previous chapters, have indicated a potential for conducting DR through studies of individual buildings, see e.g. [32–33, 79, 82–83]. However, as argued by O’Connell et al. [28], it is not a given that the findings resulting from such analyses of individual buildings may be readily extrapolated to scenarios of large-scale utilization of DR. In this context, load-shifting activities that seem desirable on a small scale may prove to be problematic when conducted on a larger scale. Therefore, upscaling the analysis on DR to larger groups of buildings is an important step towards assessing its actual potential.

The field of *urban building energy modelling* (UBEM) is concerned with modelling the energy consumption of buildings on the large scale, and applies both top-down or bottom-up approaches do to so [84]. Top-down approaches typically neglect the physical phenomena that drive energy consumption, and instead resort to statistical models using e.g. socioeconomic explanatory variables. The lack of a physics-based representation of buildings makes these methods unfit for analysis of topics such as DR, in which these phenomena play a central role. As the name suggests, bottom-up methods approach the modelling task of describing the aggregated consumption by representing each of the energy consuming processes that contribute to it. As stated by Reinhart and Davila [84], the task of obtaining the required information needed for detailed modelling of individual buildings makes this approach infeasible for large-scale applications. Several studies, including (S1), have therefore used archetype approaches in their efforts to represent buildings on the large scale [85–88]. These approaches represent the building stock by segmenting it into archetypes defined by characteristics such as construction year or use type, and then applying a set of assumptions that are considered applicable for that archetype. An example of a frequently used segmentation is the one defined in the TABULA project [89].

A potential disadvantage of this approach is its inability to represent the diversity of real groups of buildings. As indicated both by Reynders [33] and the analysis presented previously in this thesis, the thermodynamic characteristics of a building have a significant effect on the efficiency at which the building may be used to conduct DR. Therefore, models that accurately represent

this diversity are an essential prerequisite for obtaining a realistic response from a group of buildings in a DR context. This is especially true in the case of indirect DR schemes, where the decision of engaging in DR lies entirely with the consumers themselves. In this case, the characteristics of the individual building not only affect *how* the building engages in DR, but also *whether* it does.

In recent years, several Danish municipalities have begun a large-scale rollout of smart-meters that report the district heating consumption of buildings in an hourly temporal resolution. While bottom-up modelling of entire cities is still considered infeasible in practice (but only due to the computational efforts involved), the enormous amount of data that results from these smart-meters constitutes new and exciting opportunities for bottom-up modelling of *individual* buildings on the neighbourhood or district level. Combining grey-box modelling techniques with consumption data could allow bottom-up UBEM models to achieve novel levels of accuracy. This approach allows us to emphasize the identification of the phenomena that govern the energy consumption of buildings – including both important aspects of occupant behaviour and building characteristics. The result is a diverse pool of building models, each parameterized with the parameters that best describe the energy consumption of that building. Such an approach is not only likely to improve the predictive performance of the UBEM model in general, but it could also constitute a suitable framework for conducting analyses of large-scale DR. Therefore, the following section presents a paper in which a methodology for establishing urban building energy models through grey-box modelling techniques is proposed. The work presented in the paper thereby contributes to thesis objective **2.4**.



Bottom-up modelling methodology for urban-scale analysis of residential space heating demand response



Rasmus Elbæk Hedegaard^{a,*}, Martin Heine Kristensen^{a,b}, Theis Heidmann Pedersen^a, Adam Brun^b, Steffen Petersen^a

^a Department of Engineering, Aarhus University, Inge Lehmanns Gade 10, 8000 Aarhus C, Denmark

^b AffaldVarme Aarhus (Department of Waste and District Heating), Aarhus Municipality, Bautavej 1, 8210 Aarhus, Denmark

HIGHLIGHTS

- Calibration of models using smart-meter data and basic building characteristics.
- Separation of district heating into space heating and domestic hot water components.
- Use of priors in Bayesian calibration framework to address data-related uncertainty.
- Performance showcased in case study modelling 159 residential single-family houses.
- Models used to investigate demand response schemes aimed at peak reduction.

ARTICLE INFO

Keywords:

Bayesian calibration
Urban scale bottom-up modelling
Demand response
Space heating
Domestic hot water
Smart-meter data

ABSTRACT

Several studies have indicated a potential to exploit the thermal inertia of individual residential buildings for demand response purposes using model predictive control and time-varying prices. However, studies that investigate the response obtained from applying these techniques to larger groups of buildings, and how this response affects the aggregated load profile, are needed. To enable such analysis, this paper presents a modelling methodology that enables bottom-up modelling of large groups of residential buildings using data from public building registers, weather measurements, and hourly smart-meter consumption data. The methodology is based on describing district heating consumption using a modified version of the building energy model described in ISO 13790 in combination with a model of the domestic hot water consumption, both of which are calibrated in a Bayesian statistical framework. To evaluate the performance of the methodology, it was used to establish models of 159 single-family houses within a residential neighbourhood located in the city of Aarhus, Denmark. The obtained bottom-up model of the neighbourhood was capable of predicting the aggregated district heating consumption in a previously unseen validation period with high accuracy: CVRMSE of 5.58% and NMBE of -1.39% . The model was then used to investigate the effectiveness of a simple price-based DR scheme with the objective of reducing fluctuations in district heating consumption caused by domestic hot water consumption peaks. The outcome of this investigation illustrates the usefulness of the modelling methodology for urban-scale analysis on demand response.

1. Introduction

The increasing availability of various high-resolution monitoring data from energy systems in operation leads to new opportunities for maintaining the balance between supply and demand while increasing the efficiency of energy systems as a whole. One of these opportunities is improved demand side management initiatives, i.e. attempts to adapt demand to supply. The conventional notion of demand side

management covers both initiatives that seek to reduce the overall demand as well as initiatives that seek to optimize the temporal distribution of demand. The latter is often referred to as demand response (DR); an approach which is increasingly being considered a viable tool for supporting the transition to an energy system based on renewable energy sources [1,2], in which an inherent challenge is to maintain an instantaneous match between demand and fluctuating energy production. Here, the availability of high-resolution monitoring data is an

* Corresponding author.

E-mail address: reh@eng.au.dk (R.E. Hedegaard).

<https://doi.org/10.1016/j.apenergy.2019.03.063>

Received 7 November 2018; Received in revised form 21 February 2019; Accepted 7 March 2019
0306-2619/ © 2019 Elsevier Ltd. All rights reserved.

Nomenclature

Abbreviations

DR	demand response
DH	district heating
UBEM	urban building energy modelling
MPC	model predictive control
DHW	domestic hot water
MAP	maximum a posteriori
RC	resistance capacitance (model)

Symbols and variables

Φ_{DH}	consumption rate: Vector of district heating measurements
Φ_{sim}	consumption rate: Simulated energy consuming process
Φ_b	consumption rate: Space heating component
Φ_{DHW}	consumption rate: Domestic hot water component
ϵ	stochastic component (assumed normally distributed and i.i.d.)
σ	standard deviation of normal distribution
\mathbf{X}	vector containing values for fixed parameters (see Appendix A)
θ_b	vector of calibrated building-specific parameters
θ_{DHW}	vector of calibrated DHW-specific parameters
\mathbf{W}	matrix containing relevant weather measurements
t	time (in hours) in simulation
n_t	duration of simulation (in hours)
d	categorical value describing the type of day (weekday/weekend day)
C_i	thermal capacity of interior
C_m	thermal capacity of thermal mass (heavy building elements)
T_i	temperature of interior
T_s	surface temperature
T_m	temperature of thermal mass
$T_{exterior}$	outdoor air temperature
T_{supply}	temperature of ventilation supply air
Φ_{ia}	internal gains affecting room air (interior node)
Φ_{st}	internal gains affecting internal surfaces
Φ_m	internal gains affecting thermal mass
A_m	effective surface area of thermal mass
H_v	ventilation and infiltration heat transfer coefficient (HTF)
H_w	HTF for transmission loss through windows (massless)
H_{em}	HTF for transmission loss through opaque building envelope elements
H_{is}	HTF between interior and internal surfaces
H_{ms}	HTF between thermal mass and internal surfaces
b	venting factor for scaling design air change rate
MAPE	mean absolute percentage error
MCMC	Markov Chain Monte Carlo

PSRF	post scale reduction factor
NMBE	normalized mean biased error
CVRMSE	coefficient of variance of the root mean squared error
PMV	predicted mean vote
Φ_{occ}	rate of heat gains from occupant metabolism
Φ_{app}	rate of heat gains from appliances
E_{app}	energy quantity: Annual electricity consumption for appliances
$A_{footprint}$	building footprint area obtain from Building and Dwelling Register (see Section 2.2)
E_{DHW}	energy quantity: Annual DHW consumption of a household
$c_{p,water}$	specific thermal heat under constant pressure of water
ρ_{water}	density of water
V_{occ}	annual consumption of hot water [m^3]
T_{DHW}	assumed temperature of tapping water
T_{mains}	assumed temperature of mains water
θ_{occ}	number of occupants of the household (calibrated)
Σ_B	covariance matrix of Metropolis proposal distribution of building-specific parameters
Σ_{DHW}	covariance matrix of Metropolis proposal distribution of DHW parameters
α	vector of shape parameters for specification of prior Gamma distributions
β	vector of scale parameters for specification of prior Gamma distributions
\mathbf{c}	optimization problem: Vector of energy costs
\mathbf{u}	optimization problem: Vector of control inputs (heating power)
\mathbf{d}	optimization problem: Vector of disturbances (weather conditions, internal gains)
\mathbf{x}	optimization problem: States of the state space models
$\mathbf{A}, \mathbf{B}, \mathbf{C}$ and \mathbf{E}	matrices of state space representation of the building energy model (see Appendix B)
P_{max}	optimization problem: Maximum available heating power
T_{min}, T_{max}	optimization problem: Boundaries of allowed temperature interval during DR events
Φ_{DR}	vector of combined consumption rate of case-buildings in the DR scenario
Φ_{ref}	vector of combined consumption rate of case-buildings in the reference scenario
$\Delta\Phi_{charge}$	vector containing the rates at which each case-building stores energy before peak
$\Delta\Phi_{discharge}$	vector containing the reduction in consumption of each building during peak
$\mathbf{h}_{charging}$	vector of hours in which charging is allowed in Eq. (12a)
\mathbf{h}_{peak}	vector of hours in which discharging is allowed in Eq. (12b)
$\Phi_{max,event}$	maximum consumption during DR event
η_{DR}	demand response efficiency as defined by Eq. (13)

important prerequisite for enabling DR in practice.

The energy use in residential buildings constitutes a significant potential for DR as they account for 25% of the total energy consumption in the EU, whereof 67% is used for space heating in the North and West regions of EU [3,4]. Several simulation-based studies have demonstrated that DR schemes for residential space heating may be used to achieve societal objectives such as reductions of peak demand [5,6], but also cost savings for consumers through strategic consumption [7–9]. These studies exploit the thermal inertia of the buildings to shift the energy consumption used for space heating in time, thereby achieving economic or societal benefits while ensuring acceptable thermal conditions inside the buildings. While most of these studies

focus on the DR potential with respect to the electrical grid, the same type of DR initiatives could in principle also be used for generating benefits for other parts of the energy system such as district heating (DH) networks, e.g. as it was done for production of domestic hot water (DHW) by Knudsen and Petersen [10]. Furthermore, previous studies have primarily focused on investigating the DR potential of individual buildings or apartments, see e.g. [5–9,11–14]. O'Connell et al. [15] argue that, while such studies provide great insights on the DR for the specific scenarios considered, such isolated cases may not describe the behaviour of DR on the larger scale. To develop the current body of research on the potential for DR in space heating of residential buildings, it therefore seems reasonable to investigate the DR potential of

buildings on an aggregated level using techniques inspired by the emerging field of urban building energy modelling (UBEM) [16]. Research within this field has modelled the aggregated consumption of groups of buildings through a variety of methods and tools including neural networks [17–18], reduced order models [19] and high-fidelity building simulation tools [20,21]. Among the topics investigated within the field are the performance-gap between theoretical and actual energy consumption [22] and the potential for energy retrofitting on city-scale [23]. Currently, studies on how the aggregated DR from several individual buildings affects operational challenges in urban district heating systems are rare; the only identified studies are those of Dominkovic et al. [24] and Cai et al. [25]. Dominkovic et al. used archetype building models calibrated with data from 54 households to extract performance characteristics of typical DR events. Here, the term DR event refers to a period of time during which the normal operation of the building is modified through demand response. This condensed representation of the building stock and the use of predefined set of example DR events allowed the authors to evaluate the potential for utilizing the thermal mass of buildings for generating flexible consumption in an energy system level optimization. The authors demonstrated that the flexible demand generated by buildings in their case accounted for 5.5–7.7% of the total demand. Cai et al. used first order models to represent the space heating requirements and hot water tanks of 20 residential apartment buildings as well as a commercial consumer. These models were used in optimization to reduce the operational costs of the supply side through utilization of flexible consumption, while ensuring consumer comfort. The optimization resulted in achieved savings of up to 11% when compared to a baseline.

While these studies indicate a potential for utilization of passive thermal storage, both studies used simplified representations of buildings in their analysis, either through the use of archetype models which neglect diversity, or by relying on first order models that are a relatively crude representation of the thermodynamic phenomena that are exploited when using the thermal mass of buildings for storage purposes. In this paper, we propose a different take on the evaluation of residential DR utilizing passive thermal storage, which rely on statistical calibration of physics-based models of individual single-family houses. We introduce a physics-based second order model describing the thermal dynamics of the buildings, and validate its ability to describe dynamic conditions in buildings through experiment data. We couple this model to a proposed model of the DHW consumption. Together, these two models can be used to predict the combined district heating consumption in buildings (space heating and DHW), thereby allowing us to use hourly district heating consumption data from smart meters to calibrate the two models in parallel. The calibration relies on the repetitive and weather-independent nature of DHW consumption to separate it from the space heating consumption. We demonstrate the performance of the proposed modelling method by calibrating a bottom-up model of a neighbourhood that consist of individual building models each with their own thermal characteristics and domestic hot water draw profiles. The modelling method is evaluated both on the scale of individual buildings and on the neighbourhood-scale. Finally, we demonstrate the application of the models by using them to evaluate the performance of a simple price-based DR scheme aimed at achieving peak load reductions in urban district heating systems. Although several interesting results are presented in this analysis, the main objective of this paper is to present the developed modelling method with a level of detail that allows other researchers to apply and possibly further develop it in their analysis. Therefore, the application of the models for DR analysis should be seen as a demonstration of the usefulness of the models rather than an in-depth analysis on DR schemes.

The paper is structured as follows: Section 2 describes the proposed methodology in terms of the established statistical framework, the physics-based building energy model and the model of DHW consumption. In Section 3, we apply the methodology in a case study where we model the consumption of 159 detached single-family houses. The

obtained UBEM model is validated both on the scale of the individual building and on the aggregated level before it is applied in a case study on the residential DR potential using model predictive control (MPC). Finally, we draw our final conclusions and outline future work in Section 4.

2. Method

The current field of UBEM consists of a variety of methods for modelling of the energy use of groups of buildings. In general, UBEM models can be categorized as either top-down or bottom-up models. Top-down models tend to rely on socio-economic factors such as energy prices, population size and weather conditions for modelling energy use [26]. The use of aggregated data for obtaining top-down models leads to little emphasis on ensuring accurate representation of the energy-consuming processes themselves, thus rendering them ill-suited for evaluating the DR potential of utilizing building thermal mass as passive thermal storage. Bottom-up models, on the other hand, does not suffer from this issue, since they model the physical processes and phenomena of the energy-consuming processes themselves before aggregating the results [27,28]. These models may be rooted in either statistical methods, physical principles or a combination thereof. Statistical methods include regression analysis, support vector machines and artificial neural networks, whereas physics-based models rely on the first principles to model the energy consuming process [26]. These two modelling paradigms differ significantly in the prerequisites needed to obtain the model. Statistical methods rely on measurement data describing input-output relationships of the process, whereas physics-based methods rely on knowledge about the process itself. While both modelling approaches have advantages and disadvantages, it is the combination of them that truly makes them useful in practical applications. Combining the two paradigms typically involves setting up an initial model based on thermodynamic principles and any available information regarding the buildings, and then calibrating or identifying the parameters of said model using measured input-output data. This significantly improves the accuracy of the resulting models compared to those derived from the purely physics-based approach, while at the same time lowering the requirements for both the quality and quantity of the data needed in the statistical approach [29,30]. Examples of studies combining the physics-based and data driven modelling approaches to model individual buildings are plentiful – studies that have modelled buildings on the larger scale include Kristensen et al. [31], who calibrated a UBEM for prediction of the annual energy use in Danish detached single-family-houses, and Giannou et al. [32], who used ordinary-least-squares linear regression and the degree-day method to derive estimates of the indoor set point temperature and overall heat losses of over 15,000 residential buildings from similar smart-meter data. More recently, Kristensen et al. [33] used smart-meter data in a 3-hourly resolution and a hierarchical modelling approach to construct archetype models capable of predicting the aggregated consumption of out-of-sample groups of buildings.

Taking experiences from previous UBEM studies in literature into account, it seems reasonable to use a bottom-up modelling approach that calibrates physics-based models with measured data to explore the DR potential of flexible space heating consumption through exploitation of the thermal inertia that is inherent to buildings. We therefore propose a modelling methodology which relies on Bayesian calibration methods to derive physics-based models of individual houses. The proposed methodology is unfolded in the following sections. First, the Bayesian statistical framework used for the inference of model parameters is described. Then details on the building modelling including the physics-based model structure as well as assumptions used for modelling building geometries, venting and internal loads are provided. Finally, a novel method for separating measurements of the total district heating consumption into its space heating and domestic hot water components is proposed.

2.1. Statistical framework

The statistical calibration of the physics-based models is based on the Bayesian paradigm, which enables incorporation of a-priori information in an otherwise measurement data-driven model calibration – not in the form of best-guesses, but as arbitrary probability distributions reflecting the uncertainty of the information. This coupling of measurement data and prior knowledge is particularly useful in applications where the data alone may not be sufficiently informative to identify the value of a given model parameter. In the context of buildings, priors may therefore be used to guide the inference of parameters which are only vaguely described by the data towards regions of high prior probability. Another benefit of the Bayesian modelling approach is that the resulting models contain full approximations of the parameter posterior distributions, thus allowing all the uncertainty indicated by the inference to be included in future analysis. These posteriors may be reduced to point estimates such as the maximum a posteriori (MAP) estimate to be used in applications where the full Bayesian model description including the uncertainties are of less relevance.

A key assumption made in the Bayesian inference of the proposed method was that measurements of district heating consumption Φ_{DH} in a residential building can be modelled as the sum of an energy-consuming process, Φ_{sim} , and a stochastic component, ϵ_t . Furthermore, the output of the energy-consuming process was assumed to consist of two components: energy used for space heating (Φ_h) and for preparation of domestic hot water (Φ_{DHW}). Time is denoted by t throughout Eq. (1a)–(1e). In Eq. (1e), hr refers to the hour number within a day while d is a categorical variable denoting the current type of day (“workday” or “weekend day”). n_t denotes the length of a simulation. The relationship between a time series of district heating measurements $\Phi_{DH,t}$ for $t = [1, 2, \dots, n_t]$ and the vector containing the output of the model, $\Phi_{sim,t}$ are described by Eqs. (1a)–(1c). As indicated by the index, $\Phi_{sim,t}$ is the simulated prediction, thus implying that the calibration applies the infinite-step-ahead error criterion.

$$\Phi_{DH,t} = \Phi_{sim,t} + \epsilon_t \quad (1a)$$

$$\Phi_{sim,t} = \Phi_{h,t} + \Phi_{DHW,t} \quad (1b)$$

$$\epsilon_t \sim N(0, \sigma^2) \quad (1c)$$

$$\Phi_{h,t} = F(\mathbf{X}, \theta_B, \mathbf{W}, t) \quad (1d)$$

$$\Phi_{DHW,t} = F(\theta_{occ}, \theta_{DHW}, d, hr) \quad (1e)$$

The input arguments used in the individual models for space heating and domestic hot water preparation are listed in Eqs. (1d) and (1e). Here, θ_B and θ_{DHW} are vectors containing the calibrated parameters of the building model and DHW model, respectively, while \mathbf{X} is a vector containing the fixed parameters of the thermal model not subject to calibration, see Appendix A of this paper. The matrix \mathbf{W} of height n_t contains columns with measurements of relevant weather conditions. Finally, the scalar $\theta_{occ} \in \theta_B$ denotes the inferred number of occupants of the building.

The stochastic component ϵ_t in Eq. (1a) governs any unpredictable variation caused by potentially noisy measurements of both weather and district heating consumption, process noise (occupancy) as well as the inevitable mismatch between the chosen model-structure and the true energy-consuming process. An assumption in the inference is that the residuals of the model output on the measurement data, ϵ_t , are independent realizations of a normally distributed random variable with zero-mean and homoscedastic variance σ^2 . These assumptions are unlikely to hold in all cases due to the many complex phenomena that affect the district heating consumption in a building. For buildings where these assumptions are subject to a significant violation, the resulting models may fail to provide accurate estimates of the confidence intervals associated with predictions [34]. While we do not necessarily

require this functionality of the models for our purposes, we acknowledge this as an aspect of the modelling approach which could be improved in future work – e.g. by moving from deterministic to stochastic models. The likelihood of the data conditional on all the calibrated model parameters (θ_B , θ_{DHW} and σ) is then:

$$p(\Phi_{DH}|\theta_B, \theta_{DHW}, \sigma) = \frac{1}{\sqrt{2\pi\sigma^2}} e^{-\frac{1}{2\sigma^2} \sum_{t=1}^{n_t} \epsilon_t^2} \quad (1f)$$

Assuming that the model accurately describes the measured phenomenon, Bayes’ theorem states that the joint posterior probability of the parameters conditional on the measurement data, $p(\theta_B, \theta_{DHW}, \sigma|\Phi_{DH})$, is proportional to the RHS of Eq. (1g), where $p(\Phi_{DH}|\theta_B, \theta_{DHW}, \sigma)$ is the likelihood of the data while $p(\theta_B)$, $p(\theta_{DHW})$ and $p(\sigma)$ denote the probability of the building model parameters under their respective priors.

$$p(\theta_B, \theta_{DHW}, \sigma|\Phi_{DH}) \propto p(\Phi_{DH}|\theta_B, \theta_{DHW}, \sigma) \cdot p(\theta_B) \cdot p(\theta_{DHW}) \cdot p(\sigma) \quad (1g)$$

The objective of the Bayesian inference was to identify the values for each of the calibrated parameters of the building energy model and DHW model that yield the highest joint posterior probability. There are several algorithms that are capable of achieving this through by iterative sampling from Eq. (1g) which is proportional to the joint posterior probability. Our approach relies on the Metropolis algorithm [35] to do so – further details are given in Section 3.1. The following section provides details on the physics-based model structure chosen to describe the energy-consuming process (Φ_{sim}) of Eq. (1a).

2.2. Physics-based model structure

The functional traits required for a model to be suitable for bottom-up modelling of the energy consumption of buildings on the urban scale using the Bayesian calibration approach are 1) a relatively low number of input parameters as only scarce information about the modelled buildings is available, 2) a low computational cost of simulation due to the iterative process of calibrating models for a large group of buildings and 3) physically interpretable parameters for which prior specification is possible. An implication of the first two traits is that high-fidelity models such as EnergyPlus, TRNSYS or IDA-ICE were dismissed in favour of simpler reduced order resistance-capacitance (RC) models. In addition to the computational efficiency, another benefit of RC models is that they are suitable for implementing optimization-based control schemes such as MPC [36] – the control method most frequently used in studies on smart buildings [37]. Finally, the last trait not only rules out black-box models that does not have physically interpretable parameters, but also many physics-based grey-box models which have lumped parameters that are difficult to specify priors for. This led us to adopt the model described in the “simple hourly method” presented in ISO 13790 [38] as the model structure used in this methodology. The model is based on the principles of thermodynamics and consists of five thermal resistances as well as a single thermal capacity (in short: 5R1C). The model is a first order model as it only contains a single thermal capacity. The state of the model describes the temperature of the thermal mass (C_m), while both the air (T_i) and mean surface (T_s) temperatures are represented as mass-less temperature nodes without inertia. Several reports have documented detailed tests on the ability of the model to describe the energy consumption of buildings accurately under typical operating conditions by comparing the RC model to more complex building energy modelling tools such as the EnergyPlus or TRNSYS [39,40].

The modelling framework specified in ISO 13790 requires geometric information about the building as well as information about the thermal dynamic properties of its components to set up a model. Since detailed information about geometry is typically unavailable, a simplified geometric model was used instead. This model relies on basic geometry-related information that is often available in public building registers – in our case in the Danish Buildings and Dwellings Register [41]. From

this database we extracted the footprint area, number of stories and the areas of any conditioned attic and/or basement. Fig. 1 depicts the geometric model that was used to translate this basic geometrical information into building envelope surface areas. The geometric model assumes a certain length-to-width ratio and room height in this translation – a method previously applied in [31,33]. Furthermore, the geometric model assumed each facade of a building to be facing one of the four cardinal directions. Appendix A lists the assumed values of parameters both in the geometric model and the ISO 13790 model. In addition to the assumed relationships related to the overall geometry of the buildings, a simplified representation of the window-distribution was assumed. This assumption was introduced to reduce the number of parameters governing the solar heat gains of the model. The assumed distribution was equal to the distribution used in the Danish window energy balance calculation methodology (E_{ref} [42]) North = 26%, West = 16.5%, East = 16.5% and South = 41%.

The first order model described in ISO 13790 is intended for simulating the heating and/or cooling consumption in buildings under relatively stationary operating conditions with constant heating or cooling set points. The limited fluctuations in air temperature under set point tracking mean that the thermal capacity of the indoor air and furniture can be neglected without significantly impacting the ability of the model to describe the heating demand of the building. However, the results of a study by Reynders et al. [29] suggested first order models to be unable to describe the thermal conditions in buildings under dynamic operating conditions (e.g. changing set points). This is problematic given our intent of using the model for evaluating demand response based on exploiting the thermal characteristics of the building, since the majority of Danish residential buildings are heated with hydronic radiator-based systems. In buildings equipped with these primarily convection-driven heating systems, energy is stored in the heavy building elements by increasing the room temperature to initiate a flow of energy from the interior environment to the heavy thermal mass. Therefore, a stationary indoor air temperature cannot be maintained during DR activities. This issue with first order models has led several researchers to suggest using models of higher orders to represent the thermal dynamics of buildings: Reynders et al. [29] suggested using high-quality data including heat flux measurements from the building envelope to calibrate fourth and fifth order models, but argued that models of lower orders could suffice for predictive control applications. Hedegaard and Petersen [43] compared second and third order models on the physical meaningfulness of their parameters and concluded a second order model to perform well. Harb et al. [44] tested RC-models of orders one to three and concluded that the second order model provided the best compromise between good predictive capabilities and

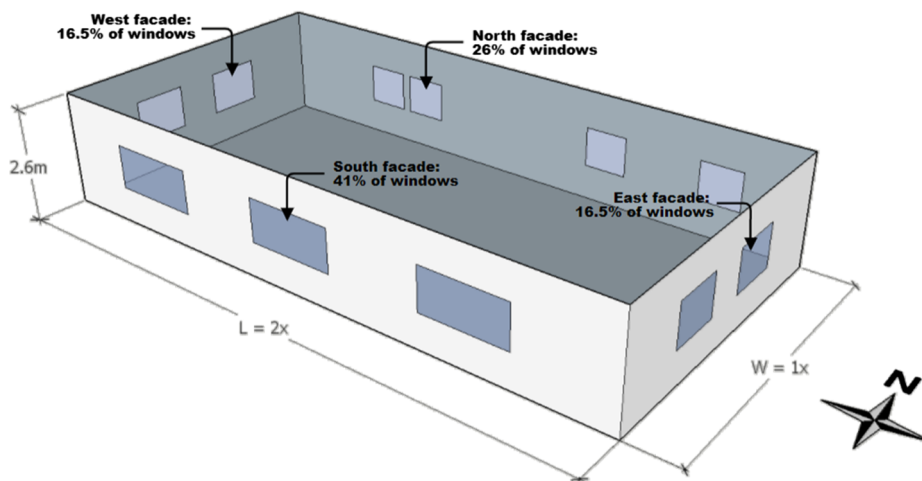


Fig. 1. Geometric model used for approximating the areas of the building envelope from the building's floor area. The model assumes a length/width ratio of 0.5, a room height of 2.6 m, and distribution of windows as depicted.

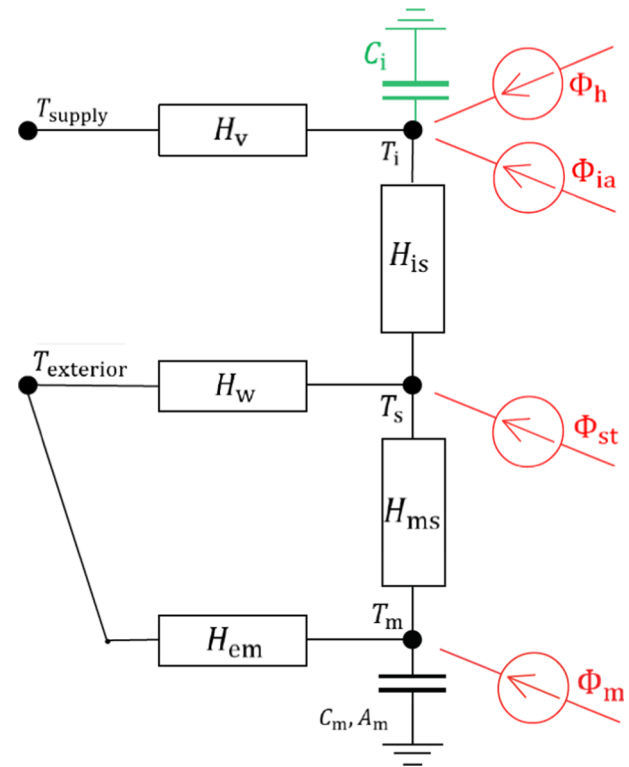


Fig. 2. Modified RC-network of the model used in ISO 13790's hourly method for calculating heat consumption. Green: modification, red: thermal loads.

interpretability of model parameters. Finally, Vivian et al. [38] concluded a second order model to be preferable to the first order model of ISO 13790.

As the ISO 13790 model is well-suited in terms of all other traits that are desirable for the intended purpose of the modelling methodology, we opted for a modification of the original model structure instead of replacing it with a different structure. The modification was to model the thermal inertia of the interior (room air, furniture, etc.) by turning the previously mass-less air temperature node into a temperature state with an associated thermal capacity (C_i), thereby expanding the previously first order model to a second order model. In order to keep the model simple and true to the framework described in the 13790 standard, we did not introduce further modifications. A resistance-capacitance network of the proposed 5R2C-model including the modification

(in green) is shown in Fig. 2. Since the air change in the residential buildings are assumed maintained through natural ventilation, the ventilation supply temperature indicated on the figure (T_{supply}) is assumed to be equal to the exterior air temperature (T_{exterior}).

To evaluate whether the proposed modification sufficiently improved the ability of the model to describe the temperature conditions in buildings under dynamic operating conditions, we compared the original 5R1C model structure to the modified 5R2C model structure using two datasets captured in real buildings that both featured dynamic thermal excitation: an *Experimental dataset* generated in a laboratory room at the Aarhus University campus and a *Field dataset* generated in a newly built and unoccupied terraced house. The experimental dataset consisted of three days of hourly measurements during which a pseudo-random binary sequence was used to control the valve opening in a hydronic heating system and impose temperature fluctuations on the test room. The field dataset consisted of a seven days of hourly measurements during which electrical heaters were used to excite the building by modulating the temperature set points. Both datasets included measurements of the internal air temperature (T_i), heating power (Φ_h) and weather conditions (solar irradiance and air temperature).

The five parameters present in both the original 5R1C-model and the modified 5R2C-model that were selected to be calibrated in the urban-scale application of the models (see Section 3.1.1) were calibrated using each of the two datasets. The added thermal capacity of the interior was calibrated for the modified model structure. Fig. 3 shows the model output of both model structures after calibration. The mean absolute percentage error (MAPE) calculated for each model is provided in the legend.

The comparison of the two model structures depicted in Fig. 3 indicates that the modification significantly improves the ability of the model to represent the thermal conditions in buildings under dynamic operating conditions. The calibration was carried out without the use of priors to remove any impact of our a-priori beliefs on the result of the model evaluation. The simulated time-series of Fig. 3 thereby correspond to the predictions of models that were parameterized with maximum likelihood parameter estimates. The main benefit of the modification was that it allowed us to remove the feedthrough component of the original ISO 13790 model. In modelling, feedthrough is

when inputs (in this case heating power Φ_h and solar gains in Φ_{ia}) act directly on the output of the model, as opposed to acting indirectly on the output by affecting the states of the model. Removing the feedthrough and adding thermal inertia to the interior (C_i) eliminates unrealistic changes in the temperature output of the model caused by e.g. a sudden change in heating output due to a change in the heating set point – an effect that is clearly seen in Fig. 3. This tendency of large fluctuations was also found by Bruno et al. [45], who compared the ISO 13790 5R1C model to the more complex TRNSYS Type56 building model. The full state-space representation of the modified model structure is provided in Appendix B of this paper.

Despite the indicated benefits of calibrating the thermal capacity of the interior, it is considered infeasible to estimate this model parameter during the modelling of urban areas, as the available data does not include measurements of the indoor air temperature. Therefore, we chose to fix the value of the thermal capacity. By default, EnergyPlus models the thermal capacity of the interior as that of the air volume inside the building alone [46]. We do not consider this realistic in the context of low-order resistance-capacitance models used in simulations of hourly temporal resolution. Instead, we find it likely that contributions from the interior (e.g. furniture), the heat delivery system itself, and even the inner-most layers of construction elements are all lumped into the interior thermal capacity (C_i). Therefore, it seemed reasonable to fix the value based on the results from the calibration the unfurnished terraced house (“Field data” in Fig. 3). The obtained empirical posterior distribution of the interior thermal capacity resembled a Normal distribution with a mean of $56.6 \frac{\text{kJ}}{\text{m}^2\text{K}}$, std. dev. of $2.46 \frac{\text{kJ}}{\text{m}^2\text{K}}$, and a minimum-maximum from approximately 45 to $65 \frac{\text{kJ}}{\text{m}^2\text{K}}$. In the context of exploiting the dynamic behaviour of buildings for realizing flexible consumption, choosing a lower estimate of the available thermal capacity would be on the safe side. Therefore, we chose the minimum value from the obtained posterior, i.e. $C_i = 45 \frac{\text{kJ}}{\text{m}^2\text{K}}$. This value is considered to be conservative, especially when considering that the terraced house was unfurnished. Appendix C provides details as well as the estimated posteriors of the parameters obtained in this calibration.

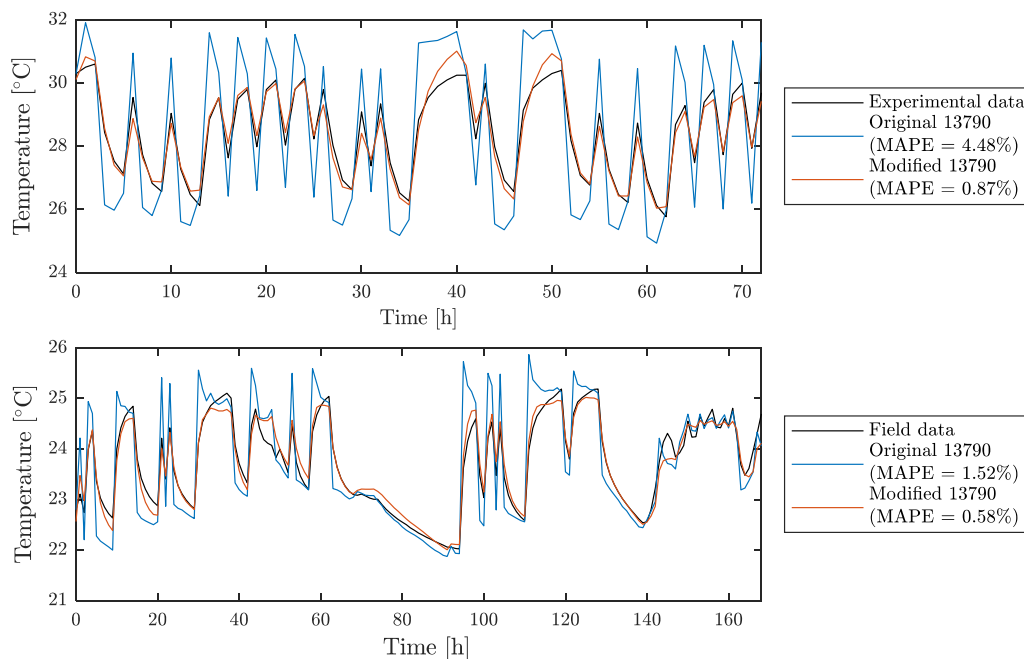


Fig. 3. Impact of the modification of the ISO 13790 model. The upper and lower graphs show simulation performance of the models when calibrated with experimental data and field data, respectively. The depicted models are parameterized with the maximum likelihood-estimates of the calibrated parameters.

2.3. Occupancy

In addition to the thermal properties and insulation level of the building that are described by the physics-based RC model, the heat balance of the building is also affected by the actions of occupants. One of the ways that occupants influence the heat balance of buildings is through venting. The vast majority of existing Danish detached single-family houses are naturally ventilated. The air change in each building was therefore modelled as an intentional component (venting) and infiltration, respectively. Since occupants are expected to vent less in colder periods, a model for the intentional venting reflecting this relationship was introduced. The model for venting was based on Rijal et al. [47] who proposed the use of a logistic model for describing the nonlinear relationship between the external temperature and the fraction of open windows in office buildings based on field surveys. In our study, we adapted the coefficients of this model so that it describes the effective amount of natural ventilation as a fraction of a design flow-rate. Fig. 4 depicts the relation between the external air temperature and the venting factor b used to scale a base venting rate fixed at $0.4 \frac{l}{s \cdot m^2}$ used in the model. Here, the whole design air change rate is in effect at external temperatures (T_{ext}) equal to the internal temperature (20°C), while all venting ceased at external temperatures of -20°C .

Occupant behaviour may also contribute positively to the heat balance of the building through the internal heat gains generated by the metabolism of the occupants themselves (Φ_{occ}) as well as their use of appliances (Φ_{app}). Each occupant was assumed to each generate 80 W of sensible heat and occupy the dwelling two-thirds of the time, see Eq. (2). The internal heat gains from appliances were modelled as the electricity consumption of a typical Danish household - an assumption considered appropriate in Danish dwellings where cooking is predominantly done using electricity. Gram-Hanssen [48] derived the empirical regression in Eq. (3) for the annual electricity consumption in detached single-family houses (E_{app}) based on data from 8500 dwellings. The regression relies on the area of the building and the number of occupants as predictors for the annual consumption in kWh. Since no information was available on the specific use-times of each dwelling, we assumed flat profiles for both internal heat gains - i.e. Eqs. (2) and (4).

$$\Phi_{occ} = \frac{2}{3} \cdot 80 \quad (2)$$

$$E_{app} = 530 + 12 \cdot A_{\text{footprint}} + 690 \cdot \theta_{occ} \quad (3)$$

$$\Phi_{app} = \frac{E_{app} \cdot 1000}{8760} \quad (4)$$

2.4. Domestic hot water

The smart meters that reported the measurements of district heating consumption featured in this study are primarily intended for billing purposes. As such, they are not designed in a way that allows them to separate the consumption related with space heating and preparation of DHW. It is therefore necessary to introduce a model of the daily DHW consumption profiles in order to 1) improve the predictive performance of the model, 2) avoid neglecting variation in the DHW component of the district heating measurements which could potentially affect the estimates of the remaining building-specific parameters, and 3) to distinguish between inflexible and flexible demand. While hot water tanks can be charged in a flexible manner as demonstrated in [10], the DHW production in the majority of the residential buildings featured in this study is handled with a flow heat exchanger, thus rendering the DHW consumption inflexible.

Previous studies have proposed various methods for separating district heating consumption into the two components dedicated towards DHW preparation and space heating. Bacher et al. [49] separated

DHW and space heating by using a kernel smoother to identify peaks in measurements of 10 min temporal resolution. However, this method would not work using the hourly smart-meter data available for this study, since the peaks caused by DHW consumption due to the hourly time-resolution of the data are essentially averaged out to an extent where distinguishing between space heating and DHW consumption in this way is infeasible. Burzynski et al. [50] interpreted district heating consumption measured outside the heating season (during summer months) as domestic hot water consumption alone and assumed this consumption pattern to apply throughout the year. While this approach in principle would work despite the low temporal resolution of the smart meter measurements, using data collected during the summer months makes the process of inferring DHW consumption prone to any errors caused by differences in consumption levels between the warmer summer period and the rest of the year - e.g. due to holidays or an increased frequency of showering due to the generally warmer weather.

Because of the above-mentioned limitations of the existing methods, we chose to model the DHW consumption for each building directly and infer it in parallel with the inference of the building-specific parameters. Assuming significant differences in use patterns between weekdays and weekends, two distinct DHW daily profiles of 24 hourly values were inferred for each building; one profile for weekdays and one profile for weekend days, respectively. The model relies on two elements to describe the DHW consumption of a given house on a given day: a normalized shape-profile ($\theta_{DHW,d}$) and a scaling factor (E_{DHW}) denoting the average daily district heating consumption for preparation of domestic hot water. An underlying assumption was that the average annual DHW consumption per occupant (V_{occ}) amounted to 15 m^3 hot water [51], which was assumed evenly distributed across all days of the year. The daily energy consumption for preparation of DHW (E_{DHW}) is given in kWh by Eq. (5).

$$E_{DHW} = \frac{c_{p,\text{water}} \rho_{\text{water}} V_{occ} \theta_{occ} (T_{DHW} - T_{\text{mains}})}{365} \quad (5)$$

where θ_{occ} denotes the inferred number of occupants in the building, while $c_{p,\text{water}}$ and ρ_{water} denote the thermal capacity and density of water at 30°C , respectively. Finally, a mains water temperature (T_{mains}) of 10°C and a DHW draw-temperature (T_{DHW}) of 55°C were assumed. The daily consumption, E_{DHW} , was distributed onto each hour within a day by the inferred DHW profile ($\theta_{DHW,d}$) associated with that type of day in accordance with Eq. (6):

$$\Phi_{DHW,t} = E_{DHW} \theta_{DHW,d,hr} \quad (6)$$

where $\theta_{DHW,d,hr}$ describes the share of E_{DHW} within a particular hour (hr) on either a working day or weekend day (d). There are two main factors contributing to the inferred shape of the DHW profiles ($\theta_{DHW,d}$), namely the prior information introduced by us (see Section 3.1.2), and the repeated and weather-independent daily patterns observed in the measurement data. This use of repeated patterns may result in other

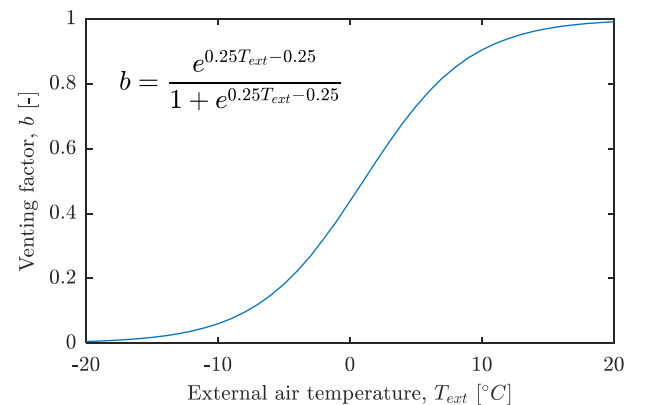


Fig. 4. Model for external temperature-dependent manual venting.

phenomena than DHW consumption being absorbed by the DHW model. Examples of these are routine venting (e.g. each morning) or heating set points which are scheduled through home automation systems. The latter violates one of the core assumptions of the statistical calibration framework (a constant temperature set point), and buildings whose consumption data is characterized by strongly repetitive consumption patterns should either be excluded from the analysis or calibrated under other assumptions. Phenomena such as routine venting, which may be more difficult to identify due to their relatively limited impact, are absorbed by the DHW model in its current implementation. However, this is not considered a critical issue since one of the main purposes of the DHW model is to distinguish potentially flexible and inflexible demand. Since increased space heating consumption due to venting is not considered flexible, it is a desired behaviour of the calibration to assign this consumption to the DHW model.

3. Case study

The urban residential neighbourhood selected for the case-study is depicted in Fig. 5. The neighbourhood consists of 206 detached single-family houses in Aarhus, Denmark, all located in a hydraulically well-defined area in the city district heating network: all consumers are supplied from the same point in the distribution grid located in the lower left corner of the figure.

Each building is equipped with a smart meter that reports the

district heating consumption in a truncated hourly kWh-resolution, i.e. in an unrounded state and without decimal points. However, a total of 47 out of the 203 dwellings in the neighbourhood (marked in red in Fig. 5) were excluded from the case study due to one of the following three data-related issues: 1) some/all consumption data was missing (12 buildings), 2) data indicated night setback heating control (16 buildings), and finally 3) odd heating patterns perhaps caused by the presence of secondary heating systems (e.g. wood-fired stoves) or frequent occupant intervention of temperature set points (19 buildings). Fig. 6 depicts the aggregated consumption of the remaining 159 houses for the months of January and February 2017, along with the weather conditions for the same period. It is evident that the heating profile is characterized by relatively fast daily fluctuations as well as slower fluctuations exhibiting a large dependency on especially the external air temperature.

In the following sections we apply the proposed modelling methodology to obtain a UBEM model of the urban residential neighbourhood. Section 3.1 presents the choices made in relation to setting up the calibration algorithm, the selection of calibration parameters, and specification of their respective priors. Section 3.2 presents an evaluation of the obtained UBEM model first on the individual building level and then on the urban area level.

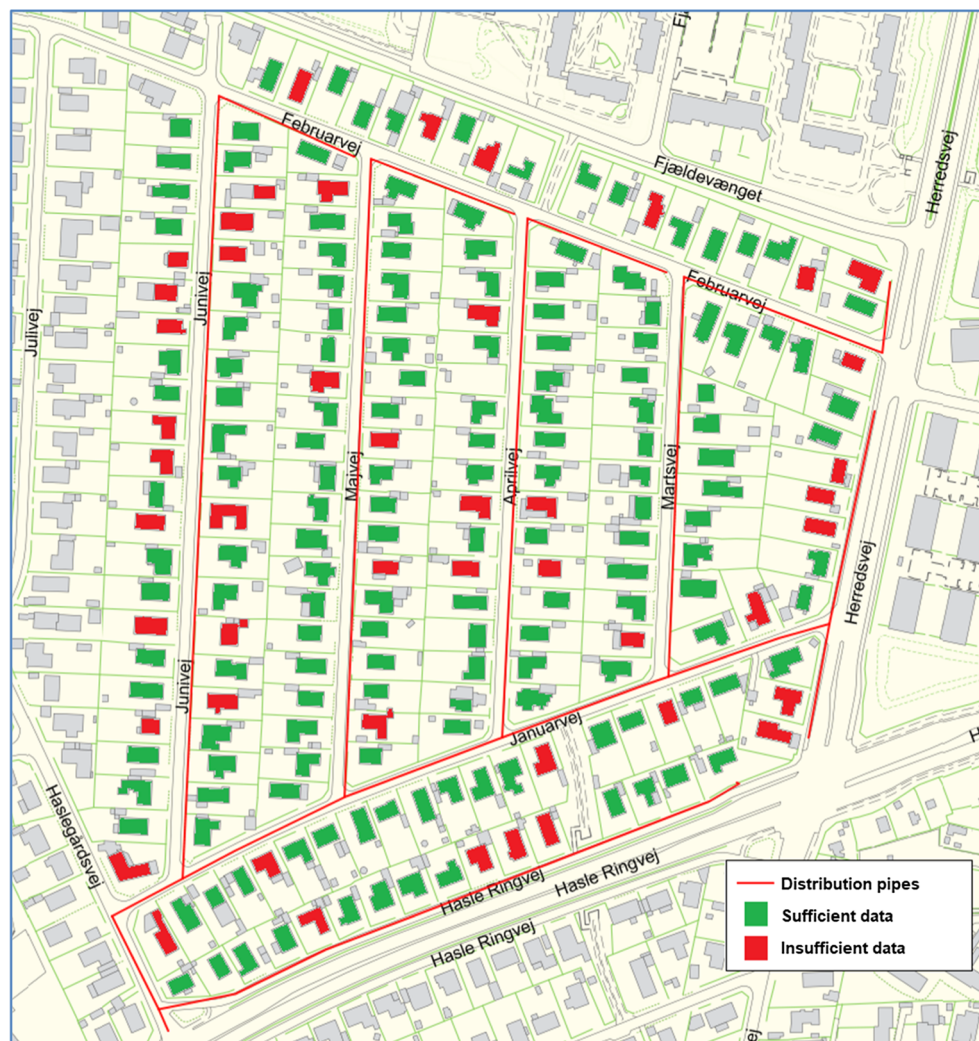


Fig. 5. The urban neighbourhood used as case-study. All buildings within the neighbourhood are supplied with district heating from the same point in the grid.

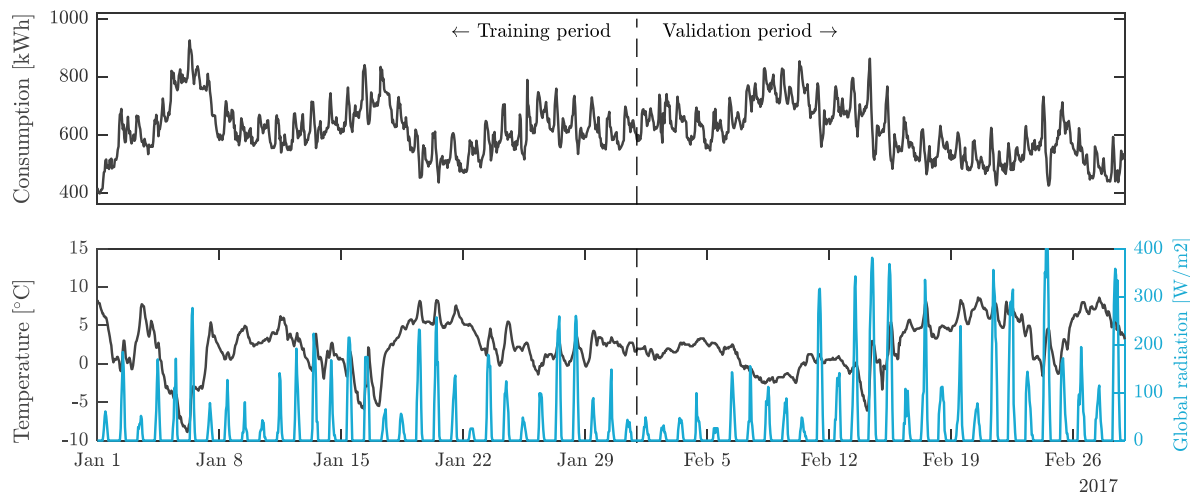


Fig. 6. Aggregated DH-consumption of urban district (only the 159 buildings marked in green in Fig. 5) and weather data for the training period (January 2017) and the validation period (February 2017).

3.1. Inference

An approximation of the joint posterior probability distribution for all model parameters given the data can be obtained using one of several Markov Chain Monte Carlo (MCMC) based methods. These methods are characterized by their ability to sample from particularly high-dimensional parameter spaces. The methodology presented in this paper relies on an implementation based on the Metropolis algorithm [35], which from a randomly selected starting point in the parameter space walks randomly through (i.e. samples from) a multi-dimensional Markov chain – a stochastic process satisfying the Markov property – to approximate the joint posterior distribution. When converged, the Metropolis algorithm produces an unbiased mapping of the posterior probability density distribution. The part of the algorithm which allows it to focus on the regions of the parameter space of high probability, and eventually converge to a stationary estimate the posterior density function, is the fact that not all steps of the random walk are successful. Whether a step is rejected or accepted is determined by the ratio between the joint posterior probability of the current draw and the newly proposed draw. The computation of probabilities are carried out in the log-domain to ensure numerical stability. Each proposed step of the random walk in the parameter space is done by drawing from a so-called proposal distribution. For this, the Metropolis algorithm applies a marginal normal distribution (or a multivariate normal distribution) centred at the algorithm's current position in the parameter space. It is essential to tune the parameters of the proposal distribution (i.e. the variance for one-dimensional sampling, and the covariance matrix for multi-dimensional sampling) if fast convergence and efficient sampling from the posterior is desired [52].

The building model parameters (θ_B in Eq. (1d)) and the DHW model parameters (θ_{DHW} in Eq. (1e)) were kept separate in the implementation of the Metropolis algorithm, and therefore each had their own proposal distributions. Due to differences in how the building-specific parameters and the DHW-related parameters acted upon the model, the tuning of the two proposal distributions were carried out in slightly different ways. The building model parameters were all proposed from a multivariate normal distribution with zero-mean and covariance matrix Σ_B . The tuning of this proposal distribution included a full covariance adaptation including the correlation between parameters [52]. Since the parameters of the building models may be significantly correlated, the tuning of the parameter-correlation entries of Σ_B ensured a much more efficient sampling and quicker convergence than using a proposal distribution which neglects parameter correlation. In spite of this, tuning of the covariance matrix of the DHW model's proposal distribution (Σ_{DHW}) did not involve tuning of the off-diagonal elements

of the matrix. The reason for neglecting the correlation was that the DHW model describes a normalized consumption profile, which after each proposed change required a post-processing of the proposal in the form of a renormalization of the entire profile. This post-processing reduced the effectiveness of the covariance tuning that was used for the building model parameters.

After a number of iterations, the algorithm converges to a stationary state in the high-probability region of the parameter space. Until this happens the algorithm is considered cold, and all samples are discarded since they may still be influenced by the random point in the parameter space where the algorithm was initialized. The algorithm is considered warm once the marginal Markov chains of all parameters have converged – after which further sampling contributes to the approximation of the posterior distributions. The potential scale reduction factor (PSRF) was used to indicate convergence (see Section 3.2.1) [53]. For each building, three separate instances of the algorithm were run for 10,000 iterations – out of which the first 8000 iterations were discarded. The three remaining batches of 2000 samples were joined and used to form an empirically based posterior distribution. For further details on the Metropolis algorithm we refer to the original work by Metropolis et al. [35]. The following sections present the chosen calibration parameters and their associated prior distributions.

3.1.1. Calibration parameters

Using physics-based building energy models (BEM) to represent the performance of an existing building requires calibration of a range of user-defined input parameters. Standard practice is to assign fixed values to all of the model parameters that are either known with reasonable certainty or do not have a significant effect on the output of the model. Limiting the number of calibrated parameters reduces issues related to the identifiability of these parameters – especially in cases where the available data is of limited quantity or quality. Table 1 lists the five building-related parameters (θ_B) that were chosen for calibration in this study, while the rest were fixed at values considered suitable for the type of buildings featured in this case study (see Appendix A for details). The selection of these specific five parameters was based on a compromise between the sensitivity of the model output to the specific parameter (and thus the identifiability of the parameter), and the relevance of the parameter in light of the intended application of the model.

The first three parameters in Table 1 are related to how weather conditions (external temperature and solar radiance) affect the heat balance of the building. The occupant density (used to derive θ_{occ}) determines the impact of occupants by scaling both the internal heat gains and the DHW consumption. Finally, the effect of the thermal mass in

Table 1
Model parameters selected for Bayesian inference (θ_B).

Abbreviation	Description	Unit
1 WFR	Window-to-floor ratio	[-]
2 q_{inf}	Infiltration rate (at 50 Pa)	$\left[\frac{1}{s \cdot m^2}\right]$
3 $U_{envelope}$	U-value for roof and façade walls (assumed equal)	$\left[\frac{W}{K}\right]$
4 Occ	Occupant density	$\left[\frac{m^2}{occupant}\right]$
5 C_m	Thermal capacity of construction elements	$\left[\frac{kJ}{m^2 \cdot K}\right]$

the ISO 13790 standard models is governed by two parameters; the effective thermal capacity (C_m) and the effective mass area (A_m). ISO 13790 proposes five classes of thermal mass in buildings ranging from very light to very heavy – each class with its respective values for the thermal capacity and effective mass area. To avoid calibrating both of these parameters, we chose to couple them by a simple piecewise linear relationship for the effective mass area as a function of the thermal mass as depicted in Fig. 7, and only calibrate the thermal capacity (C_m).

3.1.2. Specification of priors

A prior was specified for each of the BEM parameters of Table 1. The marginal prior for the WFR was specified as a beta-distribution according to Eq. (7), while the priors for the remaining BEM and DHW model parameters were specified as gamma-distributions according to Eq. (8). The reason for using a beta-distribution for the WFR is that this particular parameter is a ratio and therefore only is defined in the range 0 to 1.

$$WFR \sim \text{Beta}(5, 25) \quad (7)$$

$$[q_{inf}, U_{envelope}, Occ, C_m, \theta_{DHW}] \sim \text{Gamma}(\alpha, \beta) \quad (8)$$

In Eq. (8), the vectors α and β contain the shape and scale parameters that describe the prior for each of the remaining parameters of the model. The specific values for each parameter prior distribution are listed in Appendix A while Fig. 8 depicts the distributions for the BEM parameters and Fig. 9 depicts the prior profile used for the DHW parameters.

The prior describing the insulation level of a given building to be modelled (envelope U-value) was determined by the construction year according to the Danish archetypes identified in the TABULA-project [54]. The priors for the other parameters were assumed identical across all buildings regardless of the construction year. The prior for the infiltration rate was based on air tightness measurements of multiple dwellings [55]. It is likely that some of the case buildings to be modelled have undergone minor refurbishments since they were built, but we have no reliable information on this. To account for this uncertainty, we specified fairly broad prior distributions for both the envelope U-values and the airtightness of the buildings. The prior for the occupant density was based on statistical estimates [56], while the prior on the thermal capacity was specified to reflect the construction classes of ISO 13790 [38].

The shape of the priors for the two DHW profiles (θ_{DHW}) was based on the average measured DHW consumption for a sample of 107 British dwellings [57]. The prior for each hour was specified as a gamma-distribution parameterized in a way such that the mean value of the distribution coincided with the (normalized) profile from [57]. Since the hourly priors are specified for the normalized profiles, they describe the probability of a given share of the daily consumption falling inside each given hour. Since the report on the DHW consumption in the British dwellings does not provide separate results for weekends and weekdays, the same prior specification was used for both profiles. Fig. 9 shows a contour of the prior distributions for each hour of the day, where the intensity of the contour indicates the probability, while the x-

and y-coordinates indicate the hour number and share of daily consumption, respectively. Here, it should be noted that, despite the continuous appearance of the contours visualizing the distributions, the contour at a given x-coordinate (hour) describes the marginal distribution of that specific hour. The distribution related to a given hour of the day, say $x = 19$ (depicted), is totally separate from the marginal distribution specified for the 18th hour of the day ($x = 18$).

Finally, the last parameter of the statistical framework outlined in Section 2.1 is the prior distribution of the standard deviation σ describing the residual errors (ϵ) of Eq. (1a). Here, the prior distribution was chosen as the half-Cauchy distribution with mode 0 and a scale value of 0.25, thus producing a distribution that favours small values of σ .

3.2. Model performance

While the intended application of the obtained UBEM model is analysis on an aggregated level, the phenomena that enables utilization of flexible consumption require the individual BEM to describe the involved energy consuming processes with sufficient accuracy. Therefore, an evaluation of the performance of individual BEMs is a necessary part of interpreting the validity of the bottom-up UBEM model. Section 3.2.1 evaluates the UBEM model on the scale of the individual BEM before the aggregated scale is evaluated in Section 3.2.2.

3.2.1. Individual building performance

The output of the MCMC-based parameter inference are approximations of the posterior distributions for the calibration parameters. The validity of these posterior distributions rely heavily on the convergence of the MCMC algorithm to a stationary state within the solution space of high probability. A method for quantifying the convergence of MCMC algorithms is to run the algorithm multiple times and use the part of each chain which is assumed to have converged to compute the Potential Scale Reduction Factor (PSRF) [53]. The PSRF estimates the reduction of the scale (uncertainty) of the posterior distribution achievable if the number of MCMC draws were increased to infinity. As such, PSRF values near 1.0 indicate that the algorithm has converged to a stationary distribution. PSRF values below 1.2 can generally be interpreted as an approximate convergence [58]. The PSRF was calculated for all of the obtained marginal distributions for the parameters of each individual BEM. The model parameter posterior estimates achieved PSRF values below 1.1 (highly converged) for all but two BEMs that achieved values below 1.2 (approximate convergence). Convergence alone, however, does not imply that the resulting models have good predictive performance. The predictive performance was therefore evaluated using the normalized mean bias error (NMBE) and the coefficient of variation of the root mean square error (CVRMSE) as proposed by ASHRAE guideline 14 [59]. The NMBE is derived

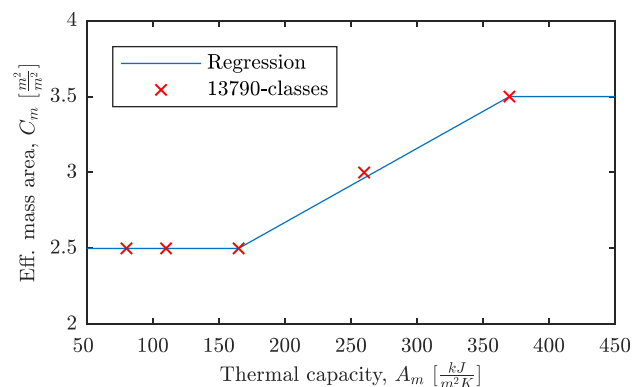


Fig. 7. Regression used to couple the thermal capacity (C_m) and the effective mass area (A_m) of ISO 13790.

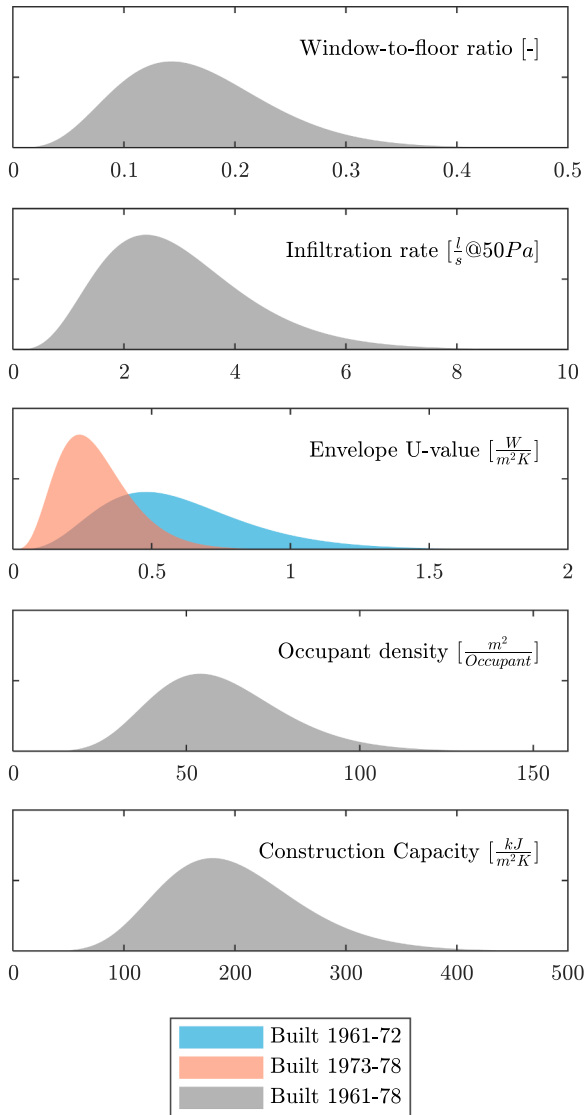


Fig. 8. Prior-specification of building-specific parameters (θ_B). The prior of the WFR (top graph) is specified as a Beta distribution, while all other priors were specified as Gamma distributions.

according to Eq. (9), and indicates whether the model is accurate on average by describing the bias of the model output as a percentage of the mean value of the measurements. The CVRMSE is defined by Eq. (10), and gives the sample standard deviation of the prediction errors, also normalized by the mean of the dataset.

$$NMBE = \frac{\sum (y_i - \hat{y}_i)}{(n - 1)\bar{y}} \tag{9}$$

$$CVRMSE = \frac{100}{\bar{y}} \cdot \sqrt{\frac{\sum (y_i - \hat{y}_i)^2}{n - 1}} \tag{10}$$

The CVRMSE can (contrary to the NMBE) be interpreted as the ability of the model to correctly predict variation in the data, and assumes only positive values, whereas the NMBE may be both negative and positive. Both metrics indicate higher performance as the value of the metric approaches zero. For calibration data of hourly resolution, the maximum values recommended by ASHRAE [59] are $\pm 10\%$ for the NMBE metric and 30% for the CVRMSE metric. The two metrics were computed by comparing the output of a model parameterized with the MAP parameter estimates to measurements from the training and validation periods indicated in Fig. 6. Fig. 10 presents the performance of the remaining 159 models to measurements from the training and validation periods indicated in Fig. 6. The performance of the five buildings highlighted in red and denoted with letters A–D are further investigated and depicted in Fig. 11.

The vast majority of building models achieve an NMBE within the limits suggested by ASHRAE: All models pass on the training period while only five models (3%) were not able to pass on the validation data set. It is noted that a significant number of models actually had higher CVRMSE values than the recommended 30%: 31 models (19%) when evaluating on the training period and 43 models (27%) for the validation period. However, inspection of measurement time series and model predictions revealed that the metrics alone were not suited for deciding whether or not a given model should be discarded. In some cases, high CVRMSE values were caused by extreme consumption peaks that were relatively far-in-between, and thus not represented well by the inferred DHW profiles that describe the average daily DHW-consumption. In other cases it would seem that the building had been vacant for extended periods of time, which were characterized by a lack of DHW consumption and sometimes also a reduced consumption for space heating (lowered temperature set points). Finally, the truncated nature of the smart-meter data used for the comparison is also a cause of discrepancies between measurements and model output.

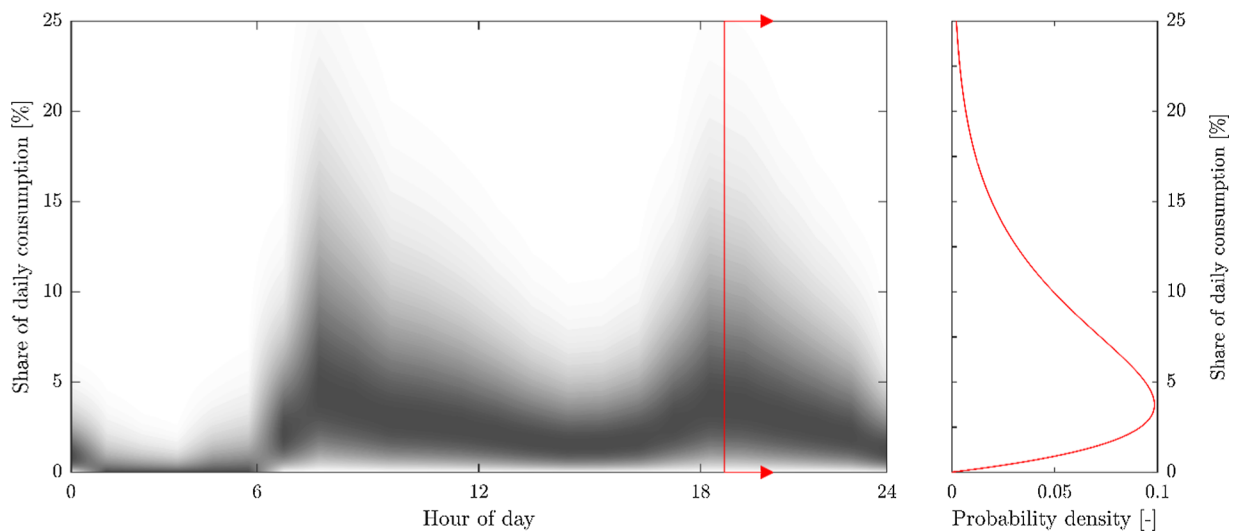


Fig. 9. Contours of marginal prior distributions for both DHW profiles (workdays/weekends). The contour at each x-coordinate depicts the marginal distribution for that specific hour of the day – see highlighted hour.

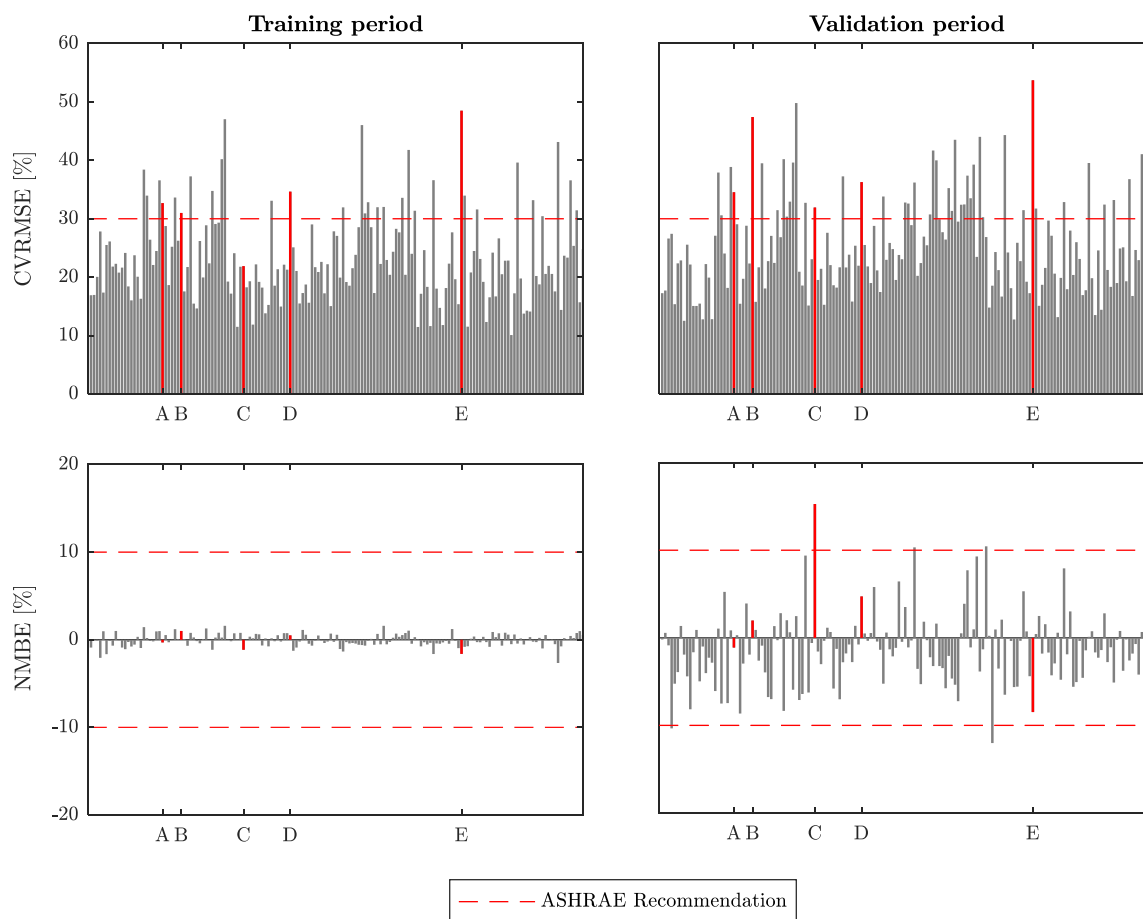


Fig. 10. Performance metrics CVRMSE and NMBE for each building model parameterized with the MAP parameter estimates. Time series of the five highlighted buildings (A–E) are presented in Fig. 11.

To illustrate examples of these issues, Fig. 11 depicts time series of the five buildings (A–E) that are highlighted in red in Fig. 10. These buildings serve as examples of the conditions that in many cases contributed to a violation of one or both of the recommendations of ASHRAE in relation to the CVRMSE and NMBE metrics. The figure depicts time-series of the district heating consumption and the simulated output of the calibrated models associated with each building. The simulation of the models during the calibration assumed a constant heating temperature set point of 20 °C. While both the calibration and the calculation of the two metrics were carried out using hourly values, we present the time series in a 3-hourly resolution for readability. Periods where the consumption deviated from the expected level have been highlighted and, even though it is impossible to identify the exact causes by analysing the existing data, labelled with plausible explanations of the observed deviation. The assumptions related to occupancy and set points in the simulations of the models were not adjusted to match the conditions that are suspected to have applied in the buildings.

In addition to the various phenomena indicated in Fig. 11, a recurring cause of mismatch between the predicted and measured consumption was peaks that are likely related to DHW consumption. Only a small number of the buildings (e.g. B in Fig. 11) did not feature such peaks – a likely explanation being that they are fitted with domestic hot water tanks that distribute DHW consumption over longer time periods. Even though separate weekday and weekend DHW profiles were inferred for each dwelling, the DHW model assumes these profiles to apply equally to all of the days for which they were defined (i.e. weekdays or weekend days). Therefore, in cases where large peaks (presumably showering) are spaced randomly with one or multiple days in-between, the inferred DHW profile tend to indicate peaks of average

size on all days.

While the challenges related to DHW consumption contribute significantly to the value of CVRMSE, we do not consider them critical to the validity of the models in an urban-scale context, where the stochastic behaviour of occupants from many different buildings to a large extent is averaged out. Similarly, due to the relative rarity of the phenomena depicted in Fig. 11, we expect the impact of these phenomena on the parameter estimates to be insignificant. Therefore, although many building models did fulfil the ASHRAE recommendation, the suggested limits proved perhaps too strict to act as a hard requirement for this application, where the measurements were both truncated and heavily influenced by effects of stochastic occupancy. The inferred DHW profiles for all 159 buildings are shown in Fig. 12. Both normalized and absolute profiles are presented as the former is useful for comparing the distribution of DHW consumption between buildings with varying overall consumption, while the absolute profiles describe the actual impact on the grid.

Not surprisingly, comparison of the mean profiles indicate that the largest difference between weekdays and weekends is the pickup in consumption in the morning hours: On weekdays, the consumption has a steep incline starting at 06:00 before it peaks in the hour 07:00–08:00. Weekend days are characterized by a smoother pickup in consumption and a peak which happens two hours later than the weekday peak in the hour 09:00–10:00. Although there currently is no way of evaluating the validity of the inferred DHW-profiles, the profiles are considered plausible since the differences between weekend and weekday profiles that are observed despite the use of identical prior information, match both our own expectations and agree with previous research findings [60].

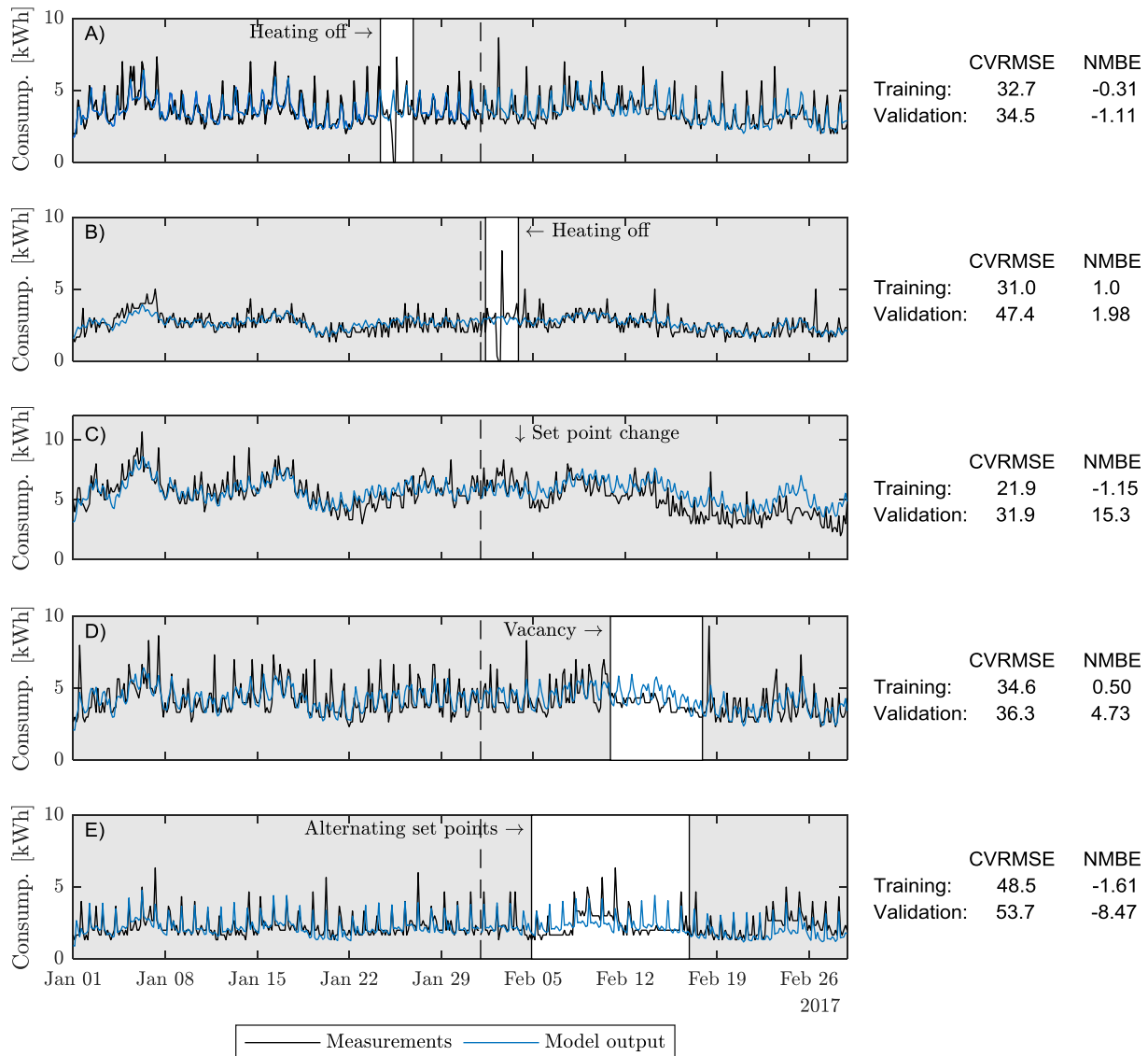


Fig. 11. Evaluation of individual building models that performed poorly in terms of CVRMSE/NMBE through comparison of time series. The dashed line separates the training and validation period. Time series of 3-hourly averages were used for readability. The NMBE and CVRMSE metrics are indicated next to the time series.

3.2.2. Urban scale performance

The performance of the UBEM of the 159 case-buildings is depicted in Fig. 13, where the predicted consumption is compared to measurements. The aggregation of data from the entire pool of buildings improves the readability, thus allowing us to show these results in hourly resolution. The upper part of the figure depicts the period used to calibrate the models, while the lower part depicts the performance on previously unseen validation data.

Visual inspection of the time series suggest an overall good performance of the model in both periods which is supported by the CVRMSE and NMBE metrics. Furthermore, it is clear that the UBEM is able to accurately describe the majority of the daily peaks in consumption, thus indicating not only that the aggregation of multiple buildings have indeed lowered the issues related to DHW consumption peaks that were seen on the scale of individual buildings in the previous section, but also that the proposed modelling method is capable of separating weather-dependent and -independent district heating consumption successfully. A drop followed by a pick-up in consumption in the hours afterwards is seen on January 25. This coincides with the highlighted drop in the consumption of “dwelling A” in Fig. 11, and may therefore suggest that multiple buildings were taken off the grid temporarily

possibly due to pipe maintenance.

While top-down UBEMs may achieve similar performance when calibrated with the aggregated data directly, the advantage of the bottom-up approach is that the diversity of the buildings producing the aggregated consumption profile is preserved. It is this characteristic of the bottom-up UBEM that allows it to be used as a basis for more detailed analysis such as investigating the combined response of the building stock to proposed DR initiatives. The following section provides demonstrates how the UBEM may be applied in analysis of DR schemes and incentives on the urban level.

4. Urban-scale demand response

As indicated by previous studies, the thermal inertia inherent to buildings can be exploited to allow the consumption dedicated towards space heating to be shifted in time without significantly impacting the indoor thermal climate in the buildings [5–9,11–14]. In this case study we evaluate the performance of a DR scheme aimed at utilizing this phenomenon to achieve peak reductions in the district heating consumption profile of an urban neighbourhood. Strategic peak reductions benefit utility companies by allowing them to optimize the daily

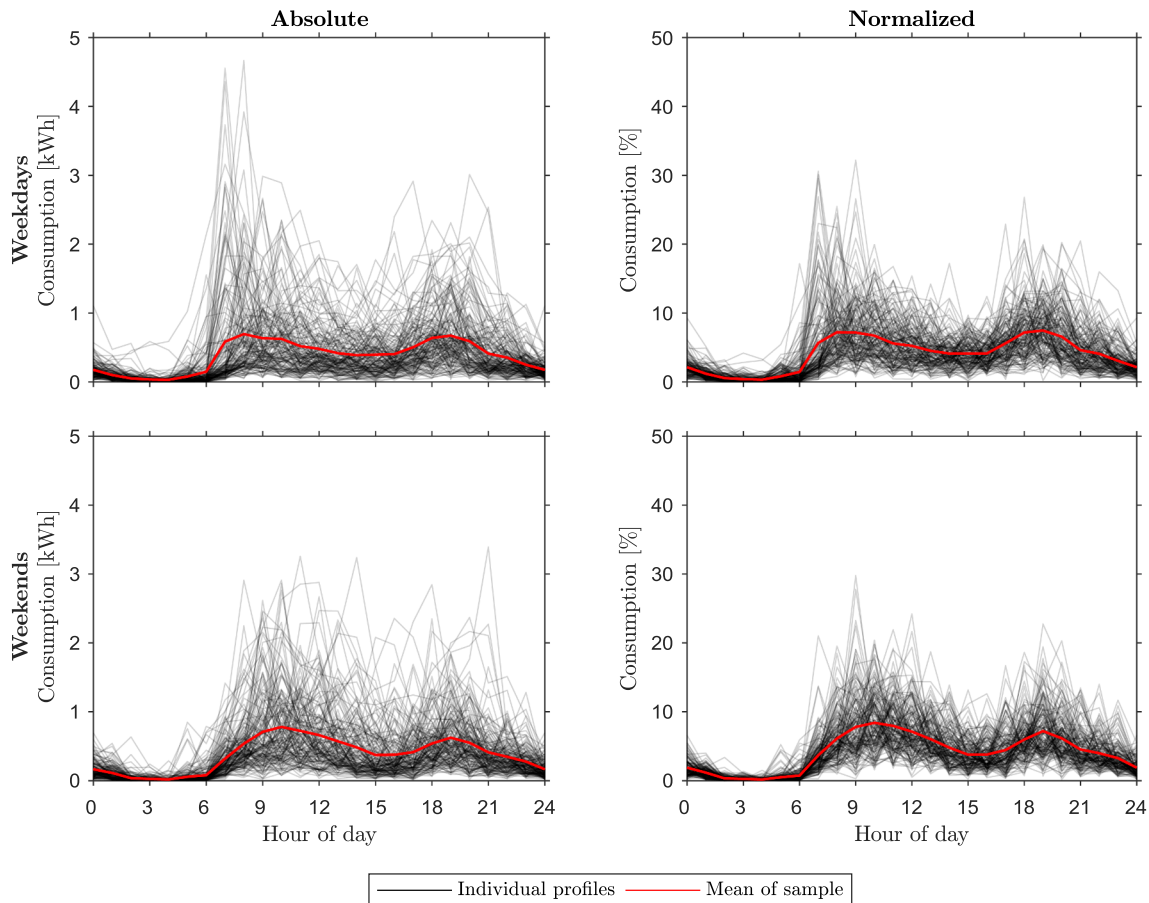


Fig. 12. Inferred DHW profiles in absolute and normalized terms along with the average profile of the entire sample. First row presents weekday profiles while the second row presents the profiles of weekend days. In the normalized profiles, each entry represent the share of daily consumption associated with that hour.

operation, e.g. by avoiding having to fire up cold boiler plants during peak hours. An even larger potential may be associated with the ability to address congestion issues in distribution networks and reduce the need for maintaining standby generation capacity for critical peak events. A way to incentivize building owners to engage in DR is through time-varying prices, e.g. by offering cheaper prices at off-peak times than during peak times. This approach to demand response is generally referred to as *indirect price-based DR* [61] due to the fact that the decision of whether to engage in DR lies entirely with the consumers themselves while the incentive (i.e. the time-varying prices) is determined by the utility company. Fig. 14 presents the principle of how a building can participate in a price-based DR scheme; (A) and (B) depict the fluctuating demand targeted by the DR scheme and the resulting price increase during a peak period, respectively, while (C) and (D) depict the actions made by a building energy management system in order to minimize the economic expenses of the building owner. Here, the thermal mass of the building is charged by raising the room temperature prior to the peak, thus allowing the building to become autonomous for either the whole or a part of the duration of the peak. This control strategy thereby allows the energy flexible building to negate some of the costs associated with the higher peak time prices.

Model predictive control (MPC) is a control method that is capable of implementing price-based DR schemes in the operation of space heating in buildings. MPC schemes use a model of the building to identify the course of actions that yields the best result in terms of a predefined objective function [12]. This objective function may reflect a wish to minimize the economic expenses of the building owner, maximize utilization of renewable energy, or minimize any negative impact of the building on the electricity grid or district heating network. In practice, MPC schemes do this by solving a control

optimization problem that through the building model incorporates the thermal dynamics of the building as well as the influence of both internal and external factors such as internal heat gains and weather conditions. These control problems may include a variety of constraints relevant to the operation of the building and the perceived comfort of occupants. Similarly, the control problem can be configured to reflect characteristics of a DR scheme including time-varying prices and other relevant constraints. The building models used to implement MPC schemes are similar to those resulting from the calibration approach described in this paper. Therefore, the obtained building models can be directly applied in an investigation of how buildings controlled by MPC schemes would respond to various incentives offered in DR schemes. In the following sections we formulate an MPC problem that reflects a price-driven DR scenario and evaluate its performance in terms of peak reductions.

4.1. Setting up the MPC problem

This case study investigates the relatively simple DR scheme depicted in Fig. 14, in which increased prices during hours of peak load are used to incentivize consumers to shift their consumption out of these periods. The consumers are assumed to operate their buildings in a way that minimizes their economic expenses for space heating while maintaining an indoor temperature within a predefined range of acceptable temperatures. Previous studies have investigated more elaborate representations of the comfort preferences of consumers. Cigler et al. [62] proposed using the *predicted mean vote* or PMV index of thermal comfort developed by Fanger [63] to incorporate comfort considerations in MPC schemes. The authors found that the use of the more comprehensive comfort measure of the PMV index allowed them

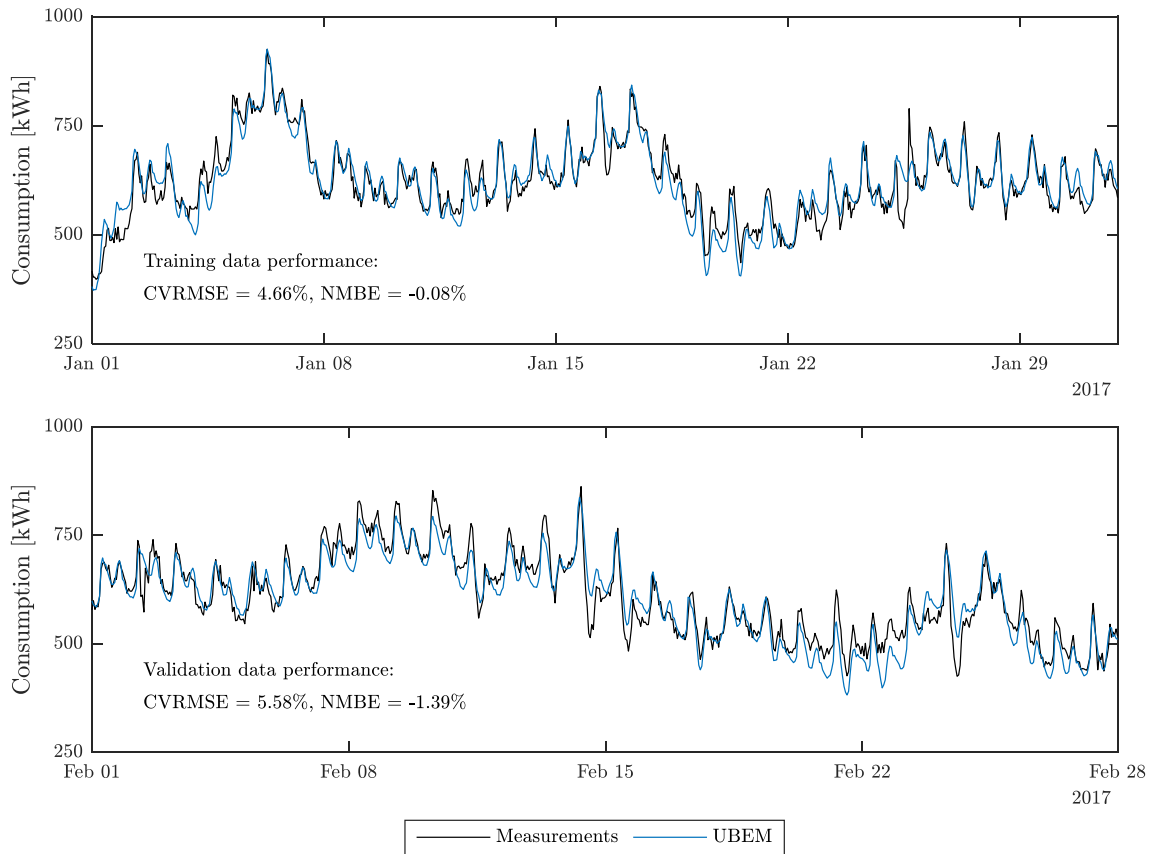


Fig. 13. Performance evaluation of the aggregated UBEModel (159 buildings) on the dataset used for training (top) and on a previously unseen validation dataset (bottom). Both datasets are in hourly temporal resolution. CVRMSE and NMBE metrics for each period are indicated on each graph.

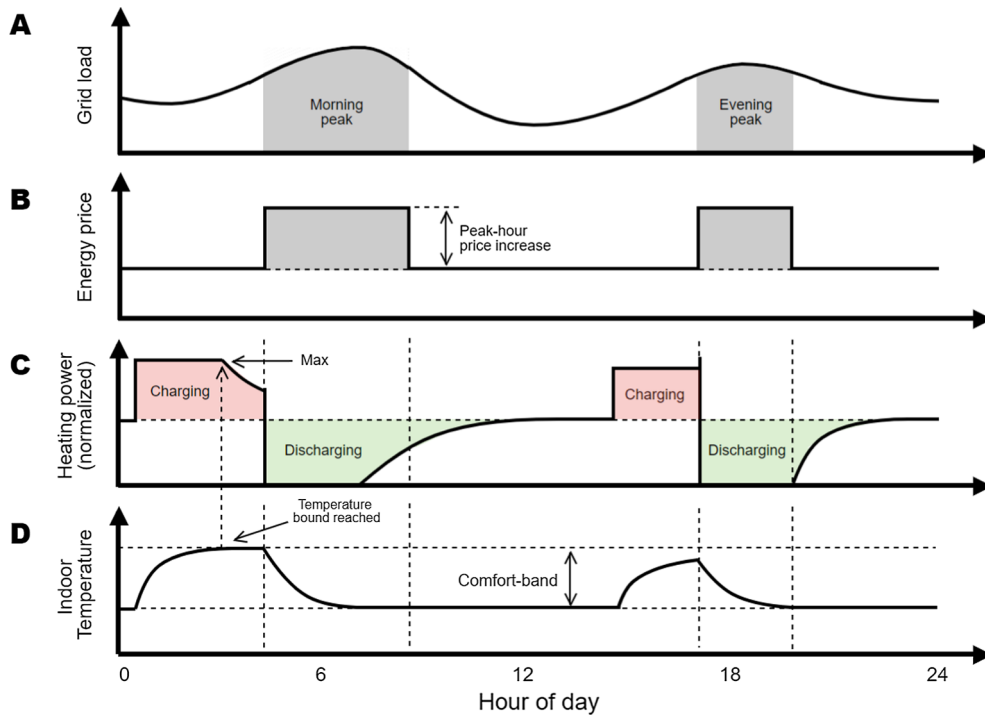


Fig. 14. Principle of the price-based demand response scheme evaluated in this study.

to be less conservative in their consideration of thermal comfort during MPC operation. However, the authors also point to two issues associated with the method: (1) incorporating the PMV equations directly would result in a non-linear optimization problem which is difficult or sometimes infeasible to solve, and (2) the PMV model requires several inputs that are typically not available in practice (e.g. clothing and activity levels). Pedersen et al. [64] investigated both single and multi-objective MPC formulations designed to maintain a specified set point temperature while allowing occasional temperature deviations for DR purposes. The proposed multi-objective scheme is based on identifying the Pareto-optimal weighing between the two objectives of maintaining a comfortable indoor climate and achieving economic savings, while the single-objective scheme is a computationally less demanding approach that achieves a similar control behaviour through the use of constraints and slack variables. Compared to how comfort preferences are handled in the scheme depicted in Fig. 14, an advantage of these schemes is that they do not track the lower bound of the allowable temperature interval during typical operation, and may therefore conduct DR through both positive and negative deviation of the reference temperature set point. On the other hand, the DR scheme depicted in Fig. 14, which tracks the lowest indoor temperature that is considered comfortable to the occupants, produces a conservative baseline scenario which under a constant energy price minimizes both energy consumption and the associated costs. These examples illustrate that there are several ways of handling thermal comfort – each with their own merits. The temperature-interval approach to incorporating the comfort preferences of consumers depicted in Fig. 14 was adopted in this case study in order to extend previously conducted research [7–9] into a setting involving larger groups of buildings. The resulting MPC scheme is defined by Eqs. (11a)–(11e).

$$\text{minimize } \sum_{t=1}^{n_t} c_t \cdot u_t \tag{11a}$$

$$\text{subject to } \mathbf{x}_{t+1} = \mathbf{A}_t \mathbf{x}_t + \mathbf{B} u_t + \mathbf{E}_t \mathbf{d}_t \tag{11b}$$

$$T_{i,t} = \mathbf{C} \mathbf{x}_t \tag{11c}$$

$$0 \leq u_t \leq P_{\max} \tag{11d}$$

$$T_{\min} \leq T_{i,t} \leq T_{\max} \tag{11e}$$

where Eq. (11a) specifies the objective function of minimizing the product of a vector of time-varying energy costs (c) and a vector of the energy consumption for each hour (u). The latter is the decision variable of the control problem – i.e. the variable that may be manipulated by the control scheme. Since DHW consumption is considered inflexible it is not necessary to include it in the optimization problem, and u_t thereby corresponds to the consumption aimed towards space heating only. Eqs. (11b) and (11c) are the constraints of the optimization problem solved by the control unit. Here, (11b) describes the dynamic behaviour of the building through the building model and (11c) relates the internal states of the building model (x_t), to the indoor temperature output of the model ($T_{i,t}$). The remaining equations are used to specify constraints relevant for the operation of the building; (11d) describes the maximum heating rate the heating system can deliver and (11e) limits the indoor temperature to be within some user-specified threshold.

For the sake of a clear interpretation of results, the range of acceptable indoor temperature for the MPC was chosen to be between $T_{\min} = 20 \text{ }^\circ\text{C}$ and $T_{\max} = 24 \text{ }^\circ\text{C}$ in all buildings even though the comfort preferences in individual buildings would differ in practice. The maximum power output achievable for each building P_{\max} was assumed to follow the Danish design conditions, where the heating system should be able to maintain an indoor temperature of $T_i = 20 \text{ }^\circ\text{C}$ at outdoor

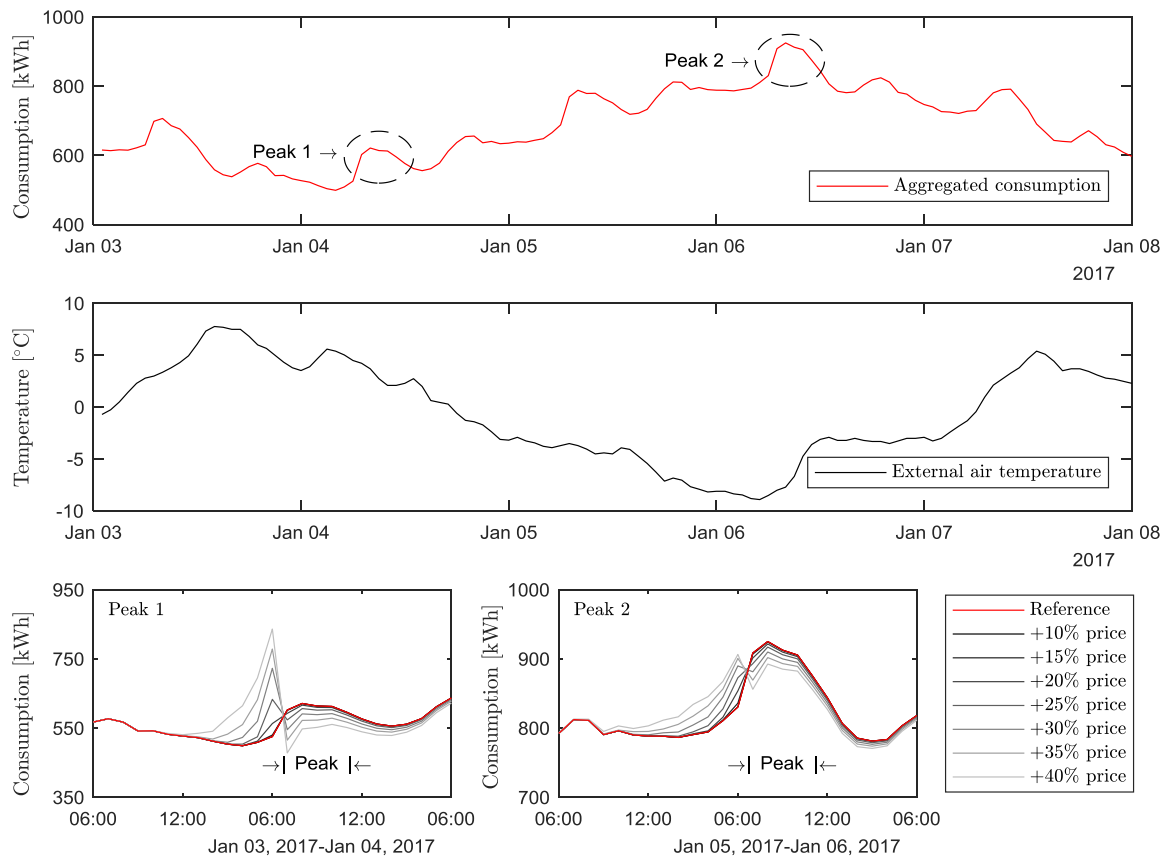


Fig. 15. Top: Aggregated heating consumption from the UBEM. Middle: External air temperature for the period. Bottom: The response of the UBEM obtained by solving the optimization problem of Eqs. (11a)–(11e) with different peak prices during the four hours of the peak period.

temperatures of $T_{\text{exterior}} = -12\text{ }^{\circ}\text{C}$. This design load was approximated by comparing the indoor-outdoor temperature difference (ΔT) of the coldest hour of the measurement data and then scaling the corresponding (inferred) space heating consumption (disregarding DHW component) for that hour to match the $\Delta T = 32\text{ }^{\circ}\text{C}$ temperature difference used for determining the needed size of the heating system in Danish residential buildings. Here, we disregard the discrepancy between the dynamic data used for this extrapolation and the stationary conditions assumed in design calculations. This approach suggests that buildings which have undergone retrofits also have downgraded the capacity of the installed heating system which is considered very unlikely. Both of these factors contribute to a conservative estimate of the maximum power output P_{max} available in each building.

4.2. Price-driven demand response

A reference scenario was defined in which the buildings were operated in the most energy efficient way, meaning that the indoor temperature was maintained at T_{min} throughout the simulations to minimize heat loss. Since the conditions in the reference scenario are the same as those assumed in the calibration of the models, the consumption indicated by the models in the reference scenario is equal to the consumption predicted by the UBEM in Fig. 13. When the heating systems in the buildings engage in DR, the models are no longer used under the same conditions as they were calibrated under. Here, our confidence in the meaningfulness of the model simulations of DR events are based on (1) the fact that we use a physics-based model structure and incorporate prior knowledge [65], and (2) the validation of the ability of the model structure to describe the temperature in buildings under dynamic

conditions. Fig. 15 (top) depicts the aggregated district heating consumption (space heating and DHW) indicated by the 159 building models in a reference scenario for the period 3–8 January with external air temperatures as depicted in Fig. 15 (middle). The marked consumption peaks (peak 1 and peak 2) occurring on January 4 and January 6, respectively, were chosen as targets for a DR scheme seeking to lower the daily fluctuation. For simplicity, the two DR events were spaced 48 h apart from one another to avoid “spill over” from one DR event to the next. Similar to Fig. 14B, the consumers were incentivized to engage in DR through increased prices during the peak periods, which were chosen as the four consecutive hours with the highest demand during each of the two days. The lower part of Fig. 15 depicts the response of the case buildings when subjected to seven different peak period prices.

Fig. 15 (bottom) indicates critical issues associated with the charging and discharging as a result of the DR scheme. During “Peak 1”, where external temperatures between $2\text{ }^{\circ}\text{C}$ and $5\text{ }^{\circ}\text{C}$ meant that over 50% of the heating system capacity in each building was available for charging, the amount of load shifting increased quickly as the incentive (i.e. the energy price during the peak) increased. Since the efficiency associated with load shifting decreases as the length of the load shift increases, the majority of the load shifting occurred in the hour just before the peak of the reference scenario. While the same behaviour would be expected from “Peak 2”, the effect in this DR event was less evident due to colder external temperatures ranging from $-8\text{ }^{\circ}\text{C}$ to $-4\text{ }^{\circ}\text{C}$ (the coldest day of the dataset used for model calibration and validation), which meant that less than 10% of the heating system capacity was available for charging. While a high efficiency is desirable, the simulations indicate that concentrated charging as a consequence of

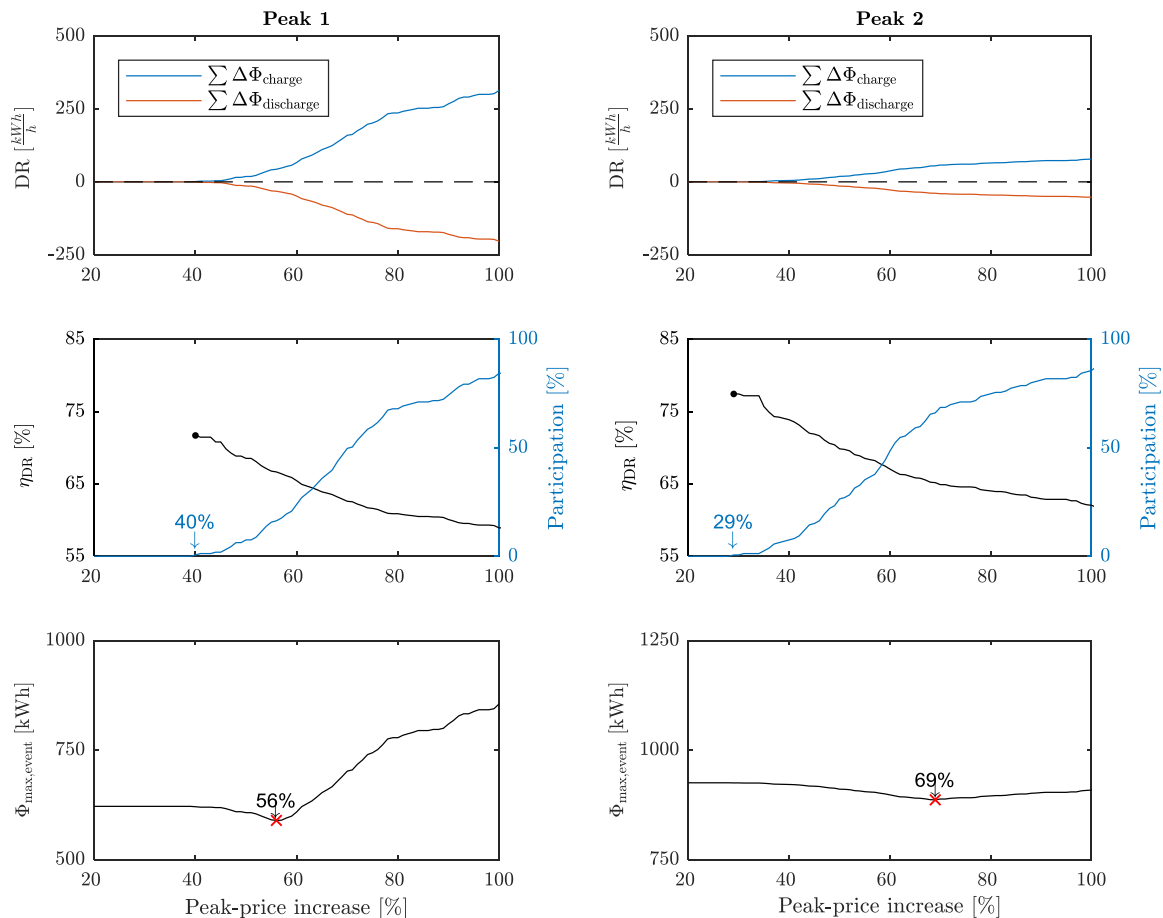


Fig. 16. Metrics describing the aggregated response of the buildings of the urban neighbourhood as a function of the increase in peak energy price. Top: pre-peak increase and on-peak reduction in consumption. Middle: load shifting efficiency and participation rate. Bottom: maximum consumption during event.

the DR scheme can lead to the formation of new peaks in the hours prior to the original peak of the reference scenario. These peaks tend to grow as the DR incentive is increased and it then becomes economically viable for more buildings to engage in load shifting. Another issue indicated by the figure is that the majority of the stored thermal energy is discharged at an early stage of the reference case peak period, thus resulting in a significantly lower reduction in the last hours of the peak period. This is problematic since the size of the peak seen over the four hour period is then hardly reduced. Finally, the relatively fast charging and discharging of the thermal mass would result in a fast rise and drop in indoor air temperature which may be uncomfortable to the occupants of the buildings.

4.3. Addressing the formation of new peaks

The observed issues associated with the proposed DR scheme suggests that modifications are necessary to achieve a more suitable response from the case buildings if the objective is to reduce peaks in the overall DH system. Our first proposal was to see if a constraint on the rate-of-change of the indoor temperature could address the observed issues. While this approach clearly solves the potential issue of discomfort associated with temperature transients, it did not solve the issue of new peaks being formed. The MPC optimization problem was therefore expanded with the constraints shown in Eqs. (12a) and (12b). These constraints are directly aimed at preventing the creation of new peaks by introducing the concept of a charging period. The first constraint requires the buildings to distribute the charging of the thermal mass across several hours, while the second constraint ensures an evenly distributed discharging throughout the peak period.

$$\Phi_{DR,t} = \Phi_{ref,t} + \Delta\Phi_{charge} \quad \forall t \in \mathbf{h}_{charging} \quad (12a)$$

$$\Phi_{DR,t} = \Phi_{ref,t} + \Delta\Phi_{discharge} \quad \forall t \in \mathbf{h}_{peak} \quad (12b)$$

where $\Phi_{DR,t}$ denotes the consumption during the hour t resulting from DR activities while $\Phi_{ref,t}$ refers to the consumption in the reference scenario without DR. The scalars $\Delta\Phi_{charge}$ and $\Delta\Phi_{discharge}$ denote the pre-

peak increase and on-peak decrease in consumption; for instance, a value of $\Delta\Phi_{charge} = 100$ indicates that a given building consumes an extra 100 W intended for storing energy in the thermal mass throughout the designated charging period. Finally, $\mathbf{h}_{charging}$ and \mathbf{h}_{peak} are sets denoting the hours where consumers may charge their buildings and the hours constituting the peak period with increased prices.

As indicated by the simulation results of Fig. 15, it is essential to identify the incentive that yields the most suitable response from the group of buildings. We introduce $\Phi_{max,event}$ as the maximum consumption resulting from a given incentive during the entire DR event – i.e. both the charging and discharging period. Since this metric also takes the formation of new peaks into account, minimizing it may be seen as the objective in the task of determining the incentive (peak-price increase) for each DR event that yields the optimal response in terms of the achieved peak reduction. In addition to the ability of the DR scheme to reduce the daily fluctuations in demand, it is also relevant to evaluate the costs in terms of the energy losses associated with redistributing demand. Eq. (13) formalizes the load shifting efficiency used in this study, η_{DR} , which was inspired by the formulation in [6] but modified slightly to make it consistent with the economic incentive that can be generated through load shifting. The index label “peak” refers to hours inside the peak period, while the label “offpeak” refer to hours on both sides of the peak. As such, $\Phi_{DR,offpeak}$ in Eq. (13) includes both the period prior to the peak with increased consumption (charging), and the period following the peak with reduced consumption due to leftover thermal energy still being discharged. The load shifting efficiency describes the share of stored thermal energy that is recovered and used to lower the consumption – both during and after the peak.

$$\eta_{DR} = \frac{-\sum \Phi_{ref,peak} - \Phi_{DR,peak}}{\sum \Phi_{ref,peak} - \Phi_{DR,offpeak}} \cdot 100 \quad (13)$$

Fig. 16 describes the response of the case buildings as a function of the price-increase imposed on them during the two peaks for new simulations featuring the constraints in Eqs. (12a) and (12b). The response is presented in terms of the two $\Delta\Phi$ variables of Eqs. (12a) and

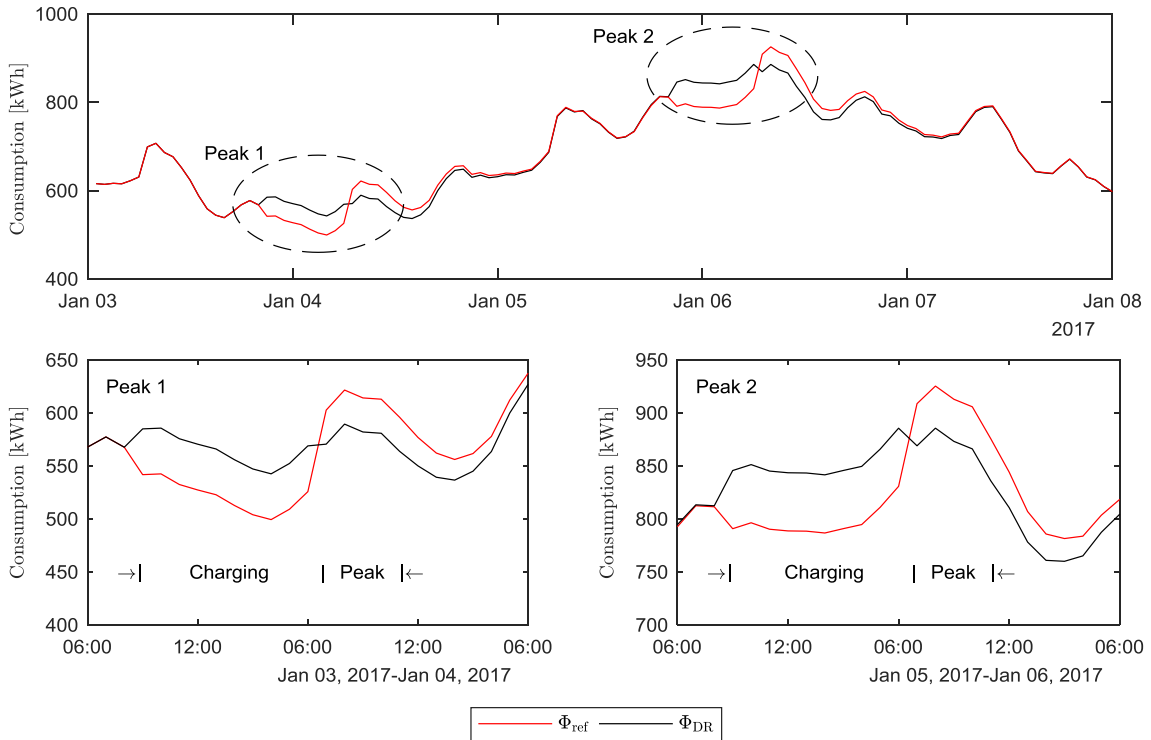


Fig. 17. The response of the case buildings obtained by solving the optimization problem of Eqs. (11a)–(11e) including the constraints of Eqs. (12a) and (12b), and imposing the optimal increase in price indicated in Fig. 16 during peak periods.

(12b) aggregated across all buildings (top), load shifting efficiency (η_{DR}) and the participation rate (middle), and maximum consumption of the event ($\Phi_{\max, \text{event}}$) along with red crosses marking the price that yielded the lowest maximum consumption (bottom). Prices to the left of this optimum are too low to incentivize the optimal amount of load shifting, while prices to the right of the optimum over-incentivize DR and thereby result in new peaks being formed.

It is clear from the results depicted in Fig. 16 that there is a significant difference in how the case buildings responded during each of the two DR events. The main driver behind these differences was the significantly colder weather conditions in the period surrounding the second DR event. The aggregated amount of DR possible during Peak 1 was significant as indicated by $\Delta\Phi_{\text{charge}}$ and $\Delta\Phi_{\text{discharge}}$, respectively. During the second peak, the response of the case buildings was limited by a lack of reserve heating capacity. Surprisingly, the simulation results revealed that the buildings required a lower incentive to engage in DR during the second peak, as seen by the fact that the incentive required for the first building to engage in DR was 40% and 29% for Peak 1 and 2, respectively. Similarly, the results indicate a higher initial load shifting efficiency for the second peak. The cause of the increased efficiency during the period with colder weather was found to be tied to the venting model described in Section 2.3, which assumes increased natural ventilation in periods of milder weather. The higher air change rates associated with increased natural ventilation results in increased heat losses during the charging period, where indoor temperature levels are elevated to enable heat to flow into the thermal mass of the building. Finally, the $\Phi_{\max, \text{event}}$ metric indicates that there is a serious risk of generating new peaks during the first DR event if the imposed peak prices are too high, whereas the lack of reserve capacity during the second DR event reduces this risk. Imposing the optimal peak price for each respective DR event (marked with red crosses in Fig. 16) produces the aggregated demand profile depicted in Fig. 17.

Fig. 17 shows that the case buildings were able to reduce peak consumption levels by engaging in DR: a reduction of 5.2% and 4.3% was achieved for Peak 1 and 2, respectively. The peak prices needed to incentivize the optimal response from the case buildings were relatively high; 56% and 69%, respectively. These high prices were necessitated by the relatively low efficiency (η_{DR}) at which peak load was shifted; 66.7% and 65.2%, respectively. These percentages imply that approximately a third of the energy dedicated towards load shifting was lost in the process, which suggests that the charging period concept should be further investigated and optimized in future studies. The additional costs for the consumers associated with each DR event was derived by considering the consumption between the beginning of each charging period and until only an insignificant amount of thermal charge was left in the buildings – here assumed to be 24 h after the end of each peak. Compared to the reference scenario and assuming that all buildings were exposed to the elevated peak prices, the two DR events resulted in average cost increases of 6.7% and 9.5%, respectively. This added cost was unevenly distributed between the buildings since only some buildings mitigated a part of the added costs by engaging in DR and shifting their consumption from peak to off-peak hours. Clearly, the economic benefits of the peak reductions should be large enough to enable the utility company to compensate consumers and provide them with on-average cheaper district-heating.

4.4. Suggestions for future work

Future work should focus on evaluating the effectiveness of DR schemes to generate direct benefits and savings for utility companies, as this would also allow for a more detailed analysis of the economic aspects of designing DR schemes. A relevant scenario related to district heating systems is the design phase where utilization of DR could affect the sizing of network components and pipes, where e.g. a reduction in pipe sizes could generate significant savings in both materials and reduced heat losses during the operation of the network. Another topic

related to the operational phase of district heating networks is the possibility of using DR to address congestion issues in the distribution grid.

The case study presented in this paper indicated that DR schemes must be designed such that the formation of new peaks is prevented. We therefore investigated a DR scheme with a set of constraints designed to prevent this. Such constraints are not normally a part of *indirect* DR schemes – thereby to some extent making the investigated DR scheme a hybrid between the indirect and direct approaches to implementing DR. These constraints accommodated the conflict of interest described by O'Connell et al. [15], which in this context refers to the fact that the most efficient (and thereby cheapest) way that buildings can shift their consumption out of high-price periods does not align well with a supply-side objective of achieving peak reductions. Comparison of Figs. 15 and 17 shows that the buildings prior to the introduction of these constraints required a much lower incentive to engage in DR. Although the constraints lowered the issue with new peaks being formed, this comparison indicates they also significantly impacted the efficiency at which the buildings were capable of shifting demand. This relationship agrees with the analysis of Reynders [66], who found that increasing the duration of a DR event significantly reduces the storage efficiency. This raises the question of whether other approaches to DR would be capable of achieving similar or better results at a higher efficiency. One such approach could be replace the two-level pricing scheme evaluated in this paper with fully time-varying prices (hourly prices) that are designed to incentivize the exact response wanted by the utility company. Corradi et al. [67] investigated models for predicting the response of consumers to time-varying prices in a power-systems context. The authors concluded that the assumption of a linear relationship between price and consumption in the presented models is an aspect of these models that should be improved in order to allow them to describe saturations in the response of the consumers. The differences between the observed DR of Peak 1 and 2 of the present case study suggests that such capabilities would indeed be necessary, as demonstrated by the lower response during Peak 2 due to the lack of available heating capacity. For similar reasons, such a model would also need to incorporate the influence of weather conditions on the price responsiveness of consumers. An alternative to establishing a model for the relationship between incentive and response is to rely on bi-level optimization algorithms as proposed in the study by Hobbs and Nelson [68], in which an optimization problem representing consumer behaviour is nested in an upper-level optimization problem representing the utility company. The objective of the upper-level optimization problem is to identify the price signal that results in the desired consumer response.

Finally, a fundamentally different approach that could be used ensure a suitable response from consumers is *direct incentive-based DR schemes*. A advantage of this type of DR scheme is that the behaviour of the participating consumers is not tied to variation in a broadcasted price signal, but may instead be determined through centralized optimization and coordination of participants. Such coordination can ensure that the optimal response in terms of supply side objectives and energy efficiency is achieved. In this case, the incentive would not be provided through time-varying prices, but e.g. directly through pre-determined energy bill discounts.

5. Conclusion

In this paper we described a methodology for bottom-up modelling of the district heating consumption of buildings in urban neighbourhoods. The objective of the method was to enable investigations of the aggregated demand response (DR) potential associated with residential space heating consumption. The methodology uses Bayesian calibration to identify both domestic hot water draw profiles and the parameters of a second order RC model describing the thermal dynamic characteristics of each individual building. The methodology was applied in a

case study featuring an urban area in the city of Aarhus, Denmark, consisting of 159 single-family houses. The aggregated profile of hourly consumption for the neighbourhood simulated for an unseen one-month validation period indicated a high accuracy: A CVMSE of 5.58% and an NMBE of -1.39% was achieved. The calibrated urban building energy model was then used to investigate the efficiency at which model predictive control (MPC) of space heating for larger groups of buildings may be used in DR initiatives to benefit district heating production and distribution. In this case study, the objective was to lower the daily morning peaks in the demand profile caused by domestic hot water consumption. An indirect price-based DR scheme which involved elevated energy prices during peak hours were used to incentivize the buildings to participate in DR events. MPC was used to enable individual buildings to engage in DR by exploiting the inherent thermal mass in the buildings while maintaining the indoor temperature at comfortable levels. The DR scheme was found to be unfit for the peak reduction application since it resulted in the formation of new and larger peaks prior to the original peak. To prevent this, additional constraints which ensured a more evenly distributed response from the participating buildings were incorporated in the DR scheme. This modified DR scheme allowed the buildings to reduce two investigated peaks by 5.2% and 4.3%, respectively. However, the introduction of these constraints also reduced the efficiency at which the buildings were able to shift consumption out of peak periods. This suggests that future research exploring and comparing various DR schemes on their effectiveness and efficiency at addressing various supply-side objectives is needed. The modelling methodology presented in this paper is considered well-suited for such analysis.

Appendix A. Parameters values and priors

Table 2 lists the parameters used to parameterize the 5R2C reduced-order model used to describe the energy consumption of residential buildings in this study. Each parameter was either attributed a fixed value or given a prior distribution describing our a-priori beliefs related to the likelihood of the parameter value.

The prior for the DHW model parameters were specified as Gamma distributions. The same prior was specified for the “workday” and the “weekend” profiles, respectively. The priors describe the probability distribution of DHW consumption in a given hour as a share of the daily consumption in percent.

Table 2

Fixed parameter values and priors of the building energy model. * indicates value defined by ISO 13790:2008.

	Model parameter	Selected value	Prior (where applicable)
Geometry			
1	Length-width ratio, LWR [-]	0.50	
2	Room height [m]	2.60	
3	Window-to-floor ratio, WFR [-]	Calibrated	1961–78: <i>Beta</i> (5, 25)
4	Window frame fraction [-]	0.25	
5	Shading factor (overhang, surroundings)	0.5	
6	Internal surface-to-floor ratio	4.5*	
Transmission & capacity			
7	Temp. adjustment factor (ground) [-]	0.70	
8	U-value (floors) [W/(m ² K)]	0.5	
9	U-value (basement-walls) [W/(m ² K)]	0.6	
10	U-value (walls/roof) [W/(m ² K)]	Calibrated	1961–72: <i>Gamma</i> (5, $\frac{0.6}{5}$) 1973–78: <i>Gamma</i> (5, $\frac{0.3}{5}$)
11	U-value (windows) [W/(m ² K)]	1.6	
12	g-value (windows) [-]	0.60	
13	Thermal capacity of interior [kJ/(m ² K)]	Assumed from experimental calibration: $45 \frac{\text{kJ}}{\text{m}^2\text{K}}$	
14	Thermal capacity of heavy mass [kJ/(m ² K)]	Calibrated	1961–78: <i>Gamma</i> (10, 20)
15	Effective mass area [m ² /m ²]	Regression, $f(C_m)$	
16	Heat transfer coef. (mass-surf.) [W/(m ² K)]	$9 \cdot 10^{-7}$	
17	Heat transfer coef. (surf.-air) [W/(m ² K)]	3.45^{-7}	
Ventilation			
18	Infiltration airflow @ 50 Pa [l/s/m ²]	Calibrated	1961–78: <i>Gamma</i> (5, $\frac{3}{5}$)
19	Design airflow (nat. ventilation) [l/s/m ²]	0.4	
Occupancy			
20	Occupant density [m ² /pers.]	Calibrated	1961–78: <i>Gamma</i> (10, 6)

(continued on next page)

Table 2 (continued)

	Model parameter	Selected value	Prior (where applicable)
21	Occupant heat load [W/pers.]	80	
22	Room heating set point [°C]	20	
23	Appliances heat load [W/m ²]	Regression, $f(A_f, nOcc)$	
Domestic hot water			
24	DHW flow temperature [°C]	55.0	
25	Mains temperature [°C]	10.0	
26	Hot water consumption [m ³ /pers./year]	15	
Material properties			
27	Specific heat capacity of air, $c_{p,air}$ [J/kg/K]	1005	
28	Density of air, ρ_{air} [kg/m ³]	1.205	

Table 3

Prior specification for DHW profiles. Based on data from 107 British residential buildings [57].

hour, i	1	2	3	4	5	6	7	8	9	10	11	12	13	14	15	16	17	18	19	20	21	22	23	24
α	2	1	1	1	1	1	2	2	2	2	2	2	2	2	2	2	2	2	2	2	2	2	2	2
$\mu = \alpha\beta$	1.8	1.1	0.8	0.7	1.4	1.7	4.4	8.9	7.5	6.0	5.6	5.0	4.3	3.5	3.0	3.1	3.6	5.3	7.6	7.1	6.0	6.0	4.1	2.5

Table 3 lists the shape parameter and the mean associated with each hour, which may be expressed as $\mu = \alpha\beta$. The values correspond to the contours of Fig. 9.

Appendix B. State space model representation

This appendix presents the continuous-time state space representation of the modified ISO 13790 building model. The standard notation for representing state space models is given in Eqs. (15a) and (15b).

$$\mathbf{x}_{k+1} = \mathbf{A}\mathbf{x}_k + \mathbf{B}^*\mathbf{u}_k^* \quad (15a)$$

$$y_k = \mathbf{C}\mathbf{x}_k + \mathbf{D}\mathbf{u}_k^* \quad (15b)$$

This representation is slightly different from the representation used when including the models in the MPC optimization problem of Eqs. (11a)–(11e), since the formulation of the control problem requires that controllable input variables are separated from the uncontrollable input variables (the disturbances). To make this difference clear, the input matrix \mathbf{B}^* and the input vector \mathbf{u}_k^* are marked with a star in this standard representation. In optimization problem of Eqs. (11a)–(11e), the matrices \mathbf{B} and \mathbf{E} of Eq. (11b) are obtained by separating out the columns of the \mathbf{B}^* matrix that describe the impact of disturbances and forming the disturbance matrix, \mathbf{E} . The remaining column of \mathbf{B}^* that describes the effect of the control variable (heating power, Φ_h) on the model is then \mathbf{B} of Eq. (11b). Similarly, \mathbf{u}^* is split into the control variables, \mathbf{u} , and the disturbances, \mathbf{d} .

The states (\mathbf{x}) and inputs (\mathbf{u}^*) are column vectors, and are organized as follows:

$$\mathbf{x} = [T_i, T_m]^T \quad (15c)$$

$$\mathbf{u}^* = [T_{ext}, \Phi_{solar}, \Phi_{int}, \Phi_h]^T \quad (15d)$$

Here, T_{ext} is the external air temperature, Φ_{solar} is the solar heat gains per window area (in m^2), Φ_{int} denote the internal loads and Φ_h is the heating output of the building's heating system. The geometric model applied in this study assumed a fixed distribution of windows facing each cardinal direction (see Section 2.2). Therefore, Φ_{solar} is pre-processed in the following way:

$$\Phi_{solar} = \sum_{dir=[N,S,E,W]} \Phi_{solar,dir} \cdot g_{glass} \cdot (1 - F_{frame}) \cdot F_{shading} \quad (15e)$$

where $\Phi_{solar,dir}$ is the incoming solar radiation in W/m^2 on a vertical surface facing the cardinal direction dir and with the solar heat gains coefficient of the glass $g_{glass} = 0.6$, the frame factor $F_{frame} = 0.25$ and the external shading factor $F_{shading} = 0.5$. The latter accounts for window overhangs and other shadowing objects such as surrounding trees and buildings.

The system matrices describing the continuous-time properties of the system are given by the following. The matrices \mathbf{A}_c and \mathbf{B}_c^* rely on the time step (k) indirectly, as the variable H_{ve} depend on the time-varying external temperature $T_{ext,k}$. The starred notation of \mathbf{B}^* is used here to distinguish it from the \mathbf{B} matrix of Eq. (11b).

$$\mathbf{A}_c(k) = \begin{bmatrix} \left(-H_{ve}(T_{ext,k}) + H_{is} \left(\frac{H_{is}}{H_w + H_{is} + H_{ms}} - 1 \right) \right) \cdot \frac{1}{C_i} & \frac{H_{ms}H_{is}}{(H_w + H_{is} + H_{ms})C_i} \\ \frac{H_{ms}H_{is}}{(H_w + H_{is} + H_{ms})C_m} & \left(H_{ms} \left(\frac{H_{ms}}{H_w + H_{is} + H_{ms}} - 1 \right) - H_{em} \right) \cdot \frac{1}{C_m} \end{bmatrix} \quad (15f)$$

$$\mathbf{B}_c^*(k) = \begin{bmatrix} \left(H_{ve}(T_{ext,k}) + \frac{H_{is} \cdot H_w}{H_w + H_{is} + H_{ms}} \right) \cdot \frac{1}{C_i} & \left(\frac{H_{is} \left(1 - \frac{A_m}{A_t} - \frac{H_w}{h_{ms} \cdot A_t} \right)}{(H_w + H_{is} + H_{ms})} \right) \cdot \frac{A_w}{C_i} & \left(\frac{H_{is} \left(0.5 - \frac{0.5 \cdot A_m}{A_t} - \frac{0.5 \cdot H_w}{h_{ms} \cdot A_t} \right)}{H_w + H_{is} + H_{ms}} + 0.5 \right) \cdot \frac{1}{C_i} & \frac{1}{C_i} \\ \left(\frac{H_{ms} \cdot H_w}{H_w + H_{is} + H_{ms}} + H_{em} \right) \cdot \frac{1}{C_m} & \left(\frac{H_{ms} \left(1 - \frac{A_m}{A_t} - \frac{H_w}{h_{ms} \cdot A_t} \right)}{H_w + H_{is} + H_{ms}} + \frac{A_m}{A_t} \right) \cdot \frac{A_w}{C_m} & \left(\frac{H_{ms} \left(0.5 - \frac{0.5 \cdot A_m}{A_t} - \frac{0.5 \cdot H_w}{h_{ms} \cdot A_t} \right)}{H_w + H_{is} + H_{ms}} + \frac{0.5 \cdot A_m}{A_t} \right) \cdot \frac{1}{C_m} & 0 \end{bmatrix} \quad (15g)$$

$$\mathbf{C} = [1 \ 0] \quad (15h)$$

$$\mathbf{D} = [0 \ 0 \ 0 \ 0] \quad (15i)$$

The time-varying parameter, H_{ve} depends on the external temperature, T_a in the following way:

$$H_{ve}(T_{ext}) = c_{p,air} \cdot \rho_{air} \cdot \frac{(q_{infiltration} + q_{venting}(T_{ext}))}{1000} \cdot A_{floor} \quad (15j)$$

where $q_{infiltration}$ is a function of the calibrated infiltration rate at a pressure difference of 50 Pa (q_{inf}), and the air change associated with venting ($q_{venting}$) is a function of the external temperature. The two air change rates are obtained in $\left[\frac{l}{s \cdot m^2} \right]$ by the following expressions:

$$q_{infiltration} = (0.04 + 0.06 \cdot q_{inf}) \quad (15k)$$

$$q_{venting}(T_a) = b(T_a) \cdot q_{designflow} \quad (15l)$$

The equation for $q_{infiltration}$ is specified in the Danish building energy performance calculation method [69]. In this study, the design air change rate ($q_{designflow}$) was fixed at $0.4 \frac{l}{s \cdot m^2}$ and the scaling factor for venting, b , was defined as:

$$b(T_{ext}) = \frac{e^{0.25T_{ext}-0.25}}{1 + e^{0.25T_{ext}-0.25}} \quad (15m)$$

Finally, the thermal capacity of the interior was defined as

$$C_i = A_{floor} \cdot (\rho_{air} c_{p,air} H_{floor} + C_{furniture}) \quad (15n)$$

where H_{floor} is an assumed room height of 2.6 m and $C_{furniture}$ is the contribution from furniture and the innermost layers of construction elements. The value of $C_{furniture}$ was for this paper fixed at $45,000 \frac{J}{m^2 \cdot K}$ through field trials (see Section 2.2 and Appendix C). Equations for the remaining parameters used to establish the state space model are given in [38].

B.1. Discretization

The time-varying parameter necessitates repeated discretization of the matrices for each time step. The simple and computationally efficient Euler discretization scheme was therefore adopted:

$$\mathbf{A} = \mathbf{I} + \mathbf{A}_c \cdot TS \quad (15o)$$

$$\mathbf{B}^* = \mathbf{B}_c^* \cdot TS \quad (15p)$$

where \mathbf{I} is the identity matrix (here, 2-by-2) and TS is the simulation time step (3600 s).

Appendix C. Model validation

Fig. 18 shows the obtained estimates of model parameter posterior distributions, which were approximated using non-informative priors to remove any influence of our own beliefs related to the likelihood of parameter-values.

The estimates of the thermal capacity of the heavy building components is seen to be higher than the values attributed to any of the building classes of the 13790 standard. Whether this difference can be attributed to the increased excitation of the buildings thermal mass during the dynamic measurement experiments was not investigated further.

The broad posteriors of the infiltration rate and envelope U-value indicate that distinguishing between these two heat loss phenomena using the measurements of this dataset alone is difficult, thus agreeing with the conclusions drawn in [43]. A strong correlation was found between the two heat loss parameters (-0.99), thus indicating that whenever a high estimate the heat loss through transmission (Envelope U-value) appeared in the posterior, this added heat loss was compensated for through a lower infiltration heat loss (Infiltration rate) and vice versa. This effect is clear if we add the heat losses of each of the two components together, thus obtaining a much more confined estimate of the posterior distribution for the overall heat loss, as depicted on the lower-right histogram of Fig. 18.

Typically, such a strong correlation between two parameters would suggest that changes should be made – either to the set of calibrated parameters or to the model structure itself. Such a change could be to infer the combined heat loss coefficient instead of its components which, as indicated by Fig. 18, is much easier to identify. While this would remove the issue with strongly correlated parameters, it would introduce a need for assumptions regarding the distribution of the total heat loss – this without ensuring a better performance of the resulting model. Because of this, and because the objective of this work is not necessarily to obtain the “true” parameter estimates, we opted to keep the initially proposed structure and set of calibration parameters.

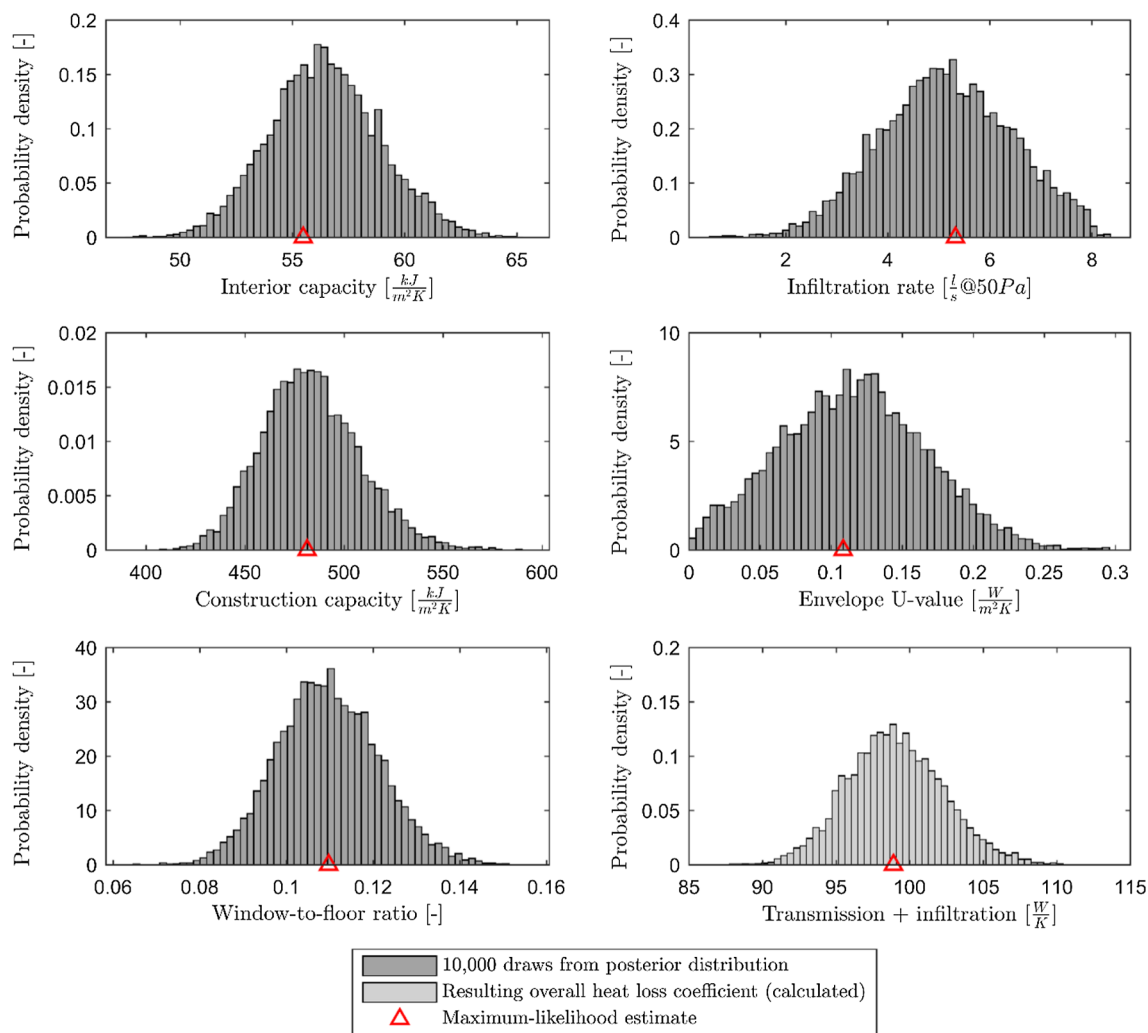


Fig. 18. Estimates of model parameter posterior distributions for the modified model structure. The estimates were obtained from the calibration using measurement data from a terraced house. Red markers indicate the ML-estimate of model parameters of the modified model used for the model-comparison of Fig. 3 (lower graph).

References

- [1] The Danish Energy Agency, "Energiscenarier for mod 2020, 2035 og 2050 (in Danish)," The Danish Energy Agency, Copenhagen, 2014.
- [2] Torriti J, Hassan MG, Leach M. Demand response experience in Europe: policies, programmes and implementation. *Energy* 2010;35(4):1575–83.
- [3] Buildings Performance Institute Europe (BPIE), "Europe's Buildings under the Microscope – A country-by-country review of the energy performance of buildings," BPIE; 2011.
- [4] Commission of European Union, "Energy consumption in households," 03 2018. [Online]. Available: https://ec.europa.eu/eurostat/statistics-explained/index.php/Energy_consumption_in_households. [accessed 17.09.2018].
- [5] Oldewurtel F, Ulbig A, Parisio A, Andersson G, Morari M. Reducing peak electricity demand in building climate control using real-time pricing and model predictive control. In: 49th IEEE Conference on Decision and Control (CDC), Atlanta; 2009.
- [6] Le Dréau J, Heiselberg P. Energy flexibility of residential buildings using short term heat storage in the thermal mass. *Energy* 2016;111:991–1002.
- [7] Hedegaard RE, Pedersen TH, Petersen S. Multi-market demand response using economic model predictive control of space heating in residential buildings. *Energy Build* 2017;150:253–61.
- [8] Pedersen TH, Hedegaard RE, Petersen S. Space heating demand response potential of retrofitted residential apartment blocks. *Energy Build* 2017;141:158–66.
- [9] Halvgaard R, Poulsen NK, Madsen H, Jørgensen JB. Economic model predictive control for building climate control in a smart grid. In: 2012 IEEE PES Innovative Smart Grid Technologies (ISGT), Washington, DC; 2012.
- [10] Knudsen MD, Petersen S. Model predictive control for demand response of domestic hot water preparation in ultra-low temperature district heating systems. *Energy Build* 2017;146:55–64.
- [11] Avci M, Erkoca M, Rahmanib A, Asfoura S. Model predictive HVAC load control in buildings using real-time electricity pricing. *Energy Build* 2013;60:199–209. <https://doi.org/10.1016/j.enbuild.2013.01.008>.
- [12] Oldewurtel F, Parisio A, Jones CN, Gyalistras D, Gwerder M, Stauch V, et al. Use of model predictive control and weather forecasts for energy efficient building climate control. *Energy Build* 2012;45:15–27.
- [13] Knudsen MD, Petersen S. Demand response potential of model predictive control of space heating based on price and carbon dioxide intensity signals. *Energy Build* 2016;125:196–204. <https://doi.org/10.1016/j.enbuild.2016.04.053>.
- [14] Vogler-Finck PJC, Wisniewski R, Popovski P. Reducing the carbon footprint of house heating through model predictive control – a simulation study in Danish conditions. *Sustain Cities Soc* 2018;42:558–73.
- [15] O'Connell N, Pinson P, Madsen H, O'Malley M. Benefits and challenges of electrical demand response: a critical review. *Renew Sustain Energy Rev* 2014;39:686–99.
- [16] Reinhart CF, Davila CC. Urban building energy modeling – a review of a nascent field. *Build Environ* 2016;97:196–202.
- [17] Aydinalp-Koksal M, Ugursal VI. Comparison of neural network, conditional demand analysis, and engineering approaches for modeling end-use energy consumption in the residential sector. *Appl Energy* 2008;85(4):271–96.
- [18] Nagpal S, Mueller C, Aijazi A, Reinhart CF. A methodology for auto-calibrating urban building energy models using surrogate modeling techniques. *J Build Perform Simul* 2018.
- [19] Buffat R, Froemelt A, Heeren N, Raubal M, Hellweg S. Big data GIS analysis for novel approaches in building stock modelling. *Appl Energy* 2017;208:277–90.
- [20] Lim H, John Z. Influences of energy data on Bayesian calibration of building energy model. *Appl Energy* 2018;231:686–98.
- [21] Nageler P, Zahrer G, Heimrath R, Mach T, Mauthner F, Leusbrock I, et al. Novel validated method for GIS based automated dynamic urban building energy simulations. *Energy* 2017;139:142–54.
- [22] Balaras CA, Dascalaki EG, Drousta KG, Kontoyiannidis S. Empirical assessment of calculated and actual heating energy use in Hellenic residential buildings. *Appl Energy* 2016;164:115–32.
- [23] Mastrucci A, Baume O, Stazi F, Leopold U. Estimating energy savings for the residential building stock of an entire city: a GIS-based statistical downscaling approach applied to Rotterdam. *Energy Build* 2014;75:358–67.

- [24] Dominkovic DF, Giannou P, Münster M, Heller A, Rode C. Utilizing thermal building mass for storage in district heating systems: combined building level simulations and system level optimization. *Energy* 2018;153:949–66.
- [25] Cai H, Ziras C, You S, Li R, Honoré K, Bindner HW. Demand side management in urban district heating networks. *Appl Energy* 2018;230:506–18.
- [26] Li W, Zhou Y, Cetin K, Eom J, Wang Y, Chen G, et al. Modeling urban building energy use: a review of modeling approaches and procedures. *Energy* 2017;141:2445–57.
- [27] Swan LG, Ugursal VI. Modeling of end-use energy consumption in the residential sector: a review of modeling techniques. *Renew Sustain Energy Rev* 2009;13(8):1819–35.
- [28] Kavgić M, Mavrogianni A, Mumovic D, Summerfield A, Stevanovic Z, Djurovic-Petrovic M. A review of bottom-up building stock models for energy consumption in the residential sector. *Build Environ* 2010;45(7):1683–97.
- [29] Reynders G, Diriken J, Saelens D. Quality of grey-box models and identified parameters as function of the accuracy of input and observations signals. *Energy Build* 2014;82:263–74.
- [30] De Coninck R, Magnusson F, Åkesson J, Helsen L. Grey-box building models for model order reduction and control. Proceedings of the 10th international Modelica conference Linköping. 2014.
- [31] Kristensen M, Choudhary R, Høst Pedersen R, Petersen S. Bayesian calibration of residential building clusters using a single geometric building representation. In: *Building Simulation*, San Francisco, CA; 2017.
- [32] Giannou P, Reinhart C, Hsu D, Heller A, Rode C. Estimation of temperature set-points and heat transfer coefficients among residential buildings in Denmark based on smart meter data. *Build Environ* 2018;139:125–33.
- [33] Kristensen M, Hedegaard RE, Petersen S. Hierarchical calibration of archetypes for urban building energy modeling. *Energy Build* 2018;175:219–34.
- [34] Gelman A, Hill J. *Data analysis using regression and multilevel/hierarchical models*. New York: Cambridge University Press; 2007.
- [35] Metropolis N, Rosenbluth AW, Rosenbluth MN, Teller AH, Teller E. Equation of state calculations by fast computing machines. *J Chem Phys* 1953;21(6):1087–92.
- [36] Prívvara S, Cigler J, Váňa Z, Oldewurtel F, Sagerschnig C, Žáčková E. Building modeling as a crucial part for building predictive control. *Energy Build* 2013;56:8–22.
- [37] Shaikh PH, Nor NBM, Nallagownden P, Elamvazuthi I, Ibrahim T. A review on optimized control systems for building energy and comfort management of smart sustainable buildings. *Renew Sustain Energy Rev* 2014;34:409–29.
- [38] European Committee for Standardization, “EN/ISO 13790:2008 - Energy performance of buildings - Calculation of energy use for space heating and cooling.” Brussels: European Committee for Standardization; 2008.
- [39] Zangheri P, Armani R, Pietrobbon M, Pagliano L, Boneta MF, Müller A. Heating and cooling energy demand and loads for building types in different countries of the EU. *ENTRANZE*; 2014.
- [40] Vivian J, Zarrella A, Emmi G, De Carli M. An evaluation of the suitability of lumped-capacitance models in calculating energy needs and thermal behaviour of buildings. *Energy Build* 2017;150:447–65.
- [41] SKAT; KL; Kombit, “Bygnings- og boligregistret (in Danish only),” [Online]. Available: <https://bbr.dk> [accessed 29.04.2018].
- [42] Danish Transport, Construction and Housing Authority, “Eref: Danish building regulations 2018 (BR18),” 01.01.2018. [Online]. Available: http://byggningsreglementet.dk/Tekniske-bestemmelser/11/BRV/Energiforbrug/Kap-1_6#f74d9134-db45-4deb-b6b2-dc5ae1fe9ffc [accessed 20.02.2018].
- [43] Hedegaard, Rasmus Elbæk, Petersen, Steffen. Evaluation of grey-box model parameter estimates intended for thermal characterization of buildings. In: 11th Nordic symposium on building physics, Trondheim; 2017.
- [44] Harb H, Boyanov N, Hernandez L, Streblov R, Müller D. Development and validation of grey-box models for forecasting the thermal response of occupied buildings. *Energy Build* 2016;117:199–207.
- [45] Bruno R, Pizzuti G, Arcuri N. The prediction of thermal loads in buildings by means of the EN ISO 13790 dynamic model: a comparison with TRNSYS. *Energy Proc* 2016;101:192–9.
- [46] U.S. Department of Energy. *EnergyPlus version 8.8.0 Documentation: Engineering Reference*. Washington, D.C.: U.S. Department of Energy; 2017.
- [47] Rijal HB, Tuohy P, Humphreys MA, Nicol JF, Samuel A, Clarke J. Using results from field surveys to predict the effect of open windows on thermal comfort and energy use in buildings. *Energy Build* 2007;39(7):823–36.
- [48] Gram-Hanssen K. SBI2005:12 - Husholdnings elforbrug - hvem bruger hvor meget, til hvad og hvorfor? Hørsholm: SBI forlag; 2005.
- [49] Bacher P, de Saint-Aubain PA, Christiansen LE, Madsen H. Non-parametric method for separating domestic hot water heatingspikes and space heating. *Energy Build* 2016;130:107–12.
- [50] Burzynski R, Crane M, Yao R, Becerra VM. Space heating and hot water demand analysis of dwellings connected to district heating scheme in UK. *J Central South Univ* 2012;19(6):1629–38.
- [51] Statens byggeforskningsinstitut. SBI 2009:10 - Varmt brugsvand. Hørsholm: Statens byggeforskningsinstitut; 2009.
- [52] Vihola M. Robust adaptive Metropolis algorithm with coerced acceptance rate. *Stat. Comput.* 2012;22(5):997–1008.
- [53] Gelman A, Carlin JB, Stern HS, Dunson DB, Vehtari A, Rubin DB. *Bayesian data analysis*. Boca Raton: CRC Press; 2014.
- [54] Cyx W, Renders N, Holm MV, Verbeke S. IEE TABULA - typology approach for building stock energy; 2011.
- [55] Statens Byggeforskningsinstitut. SBI 2015:25 - Tæthed i eksisterende bygninger [in Danish]. København: Statens Byggeforskningsinstitut, Aalborg Universitet; 2015.
- [56] Statistics Denmark. Nyt fra Danmarks Statistik: På øerne er der god plads (in Danish). [4.04.2016] [Online]. Available: <https://www.dst.dk/da/Statistik/nyt/NytHtml?cid=21543> [accessed 13.03.2018].
- [57] Department for Environment Food and Rural Affairs. *Measurement of Domestic Hot Water Consumption in Dwellings*; 2008.
- [58] Brooks SP, Gelman A. General methods for monitoring convergence of iterative simulations. *J Comput Graph Stat* 1997;7:434–55.
- [59] ASHRAE Standards Committee 2001-2002. *ASHRAE Guideline 14: Measurement of Energy and Demand Savings*. ASHRAE, Atlanta; 2002.
- [60] Dahl M, Brun A, Kirsebom OS, Andresen GB. Improving short-term heat load forecasts with calendar and holiday data. *Energies* 2018;11(7):1678.
- [61] Haider TH, See OH, Elmenreich W. A review of residential demand response of smart grid. *Renew Sustain Energy Rev* 2016;59:166–78.
- [62] Cigler J, Prívvara S, Váňa Z, Žáčková E, Ferkl L. Optimization of predicted mean vote index within model predictive control framework: computationally tractable solution. *Energy Build* 2012;52:39–49.
- [63] Fanger Povl O. *Thermal comfort. Analysis and applications in environmental engineering*. Copenhagen, Denmark: Danish Technical Press; 1970.
- [64] Pedersen TH, Knudsen MD, Hedegaard RE, Petersen S. Handling thermal comfort in economic model predictive control schemes for demand response. *Energy Proc* 2017;122:985–90.
- [65] Tangirala AK. *Principles of system identification – theory and practice*, Boca Raton, Florida: CRC Press; 2015.
- [66] Reynders G. Quantifying the impact of building design on the potential of structural thermal storage for active demand response in residential buildings. PhD Thesis. KU Leuven; 2015.
- [67] Corradi O, Ochsenfeld H, Madsen H, Pinson P. Controlling electricity consumption by forecasting its response to varying prices. *IEEE Trans Power Syst* 2013;28(1):421–9.
- [68] Hobbs BF, Nelson SK. A nonlinear bilevel model for analysis of electric utility demand-side planning issues. *Ann Oper Res* 1992;34(1–4):255–74.
- [69] Statens byggeforskningsinstitut. SBI-Anvisning 213: Bygningers Energibehov (3. udgave). Hørsholm: Statens Byggeforskningsinstitut, Aalborg Universitet; 2014.

9.2 Epilogue

The purpose of the work presented in this chapter was to first develop and present a methodology that enables bottom-up modelling of buildings on the urban scale, and to then apply and evaluate the methodology in a case study of large-scale DR. Therefore, this epilogue first discusses the presented modelling methodology and important assumptions that were necessary to introduce, before discussing the findings of the preliminary work presented in the case study.

MODELLING METHODOLOGY

The development of the methodology was guided by a requirement for the modelling approach to rely only on data that is, or is becoming, highly available (to researchers). An immediate implication of this requirement was that the modelling approach had to be independent of measurements of the indoor temperature in the modelled buildings. The parameters of each building model were therefore inferred under the assumption of a constant heating set point. As argued by Killian and Kozek [24], the emerging market of smart home automation systems may in the future extend the data available for modelling to include measurements of indoor temperature conditions at a central or even multiple points throughout the building. Therefore, not only is it interesting to investigate how the lack of temperature measurements affects the estimates of the building characteristics in the current implementation of the method, but also how the predictive performance may be improved if these measurements become available.

Several challenges were associated with the smart-meter consumption data itself. First, the hourly consumption was reported by the smart meters in truncated kilowatt-hours. With the data showing that many of the featured buildings consumed 3 to 6 kW (kWh per hour) during the coldest periods of the year, this truncation errors may be significant. Clearly, this issue increases as the consumption decrease in the warmer periods of the year. Another uncertainty is that related to the stochastic behaviour of the occupants, which could have a significant impact on the thermal state of the building, e.g. due to venting or use of appliances. This challenge was further increased by the fact that the district heating measurements also contained the consumption related to the preparation of domestic hot water, which thereby constituted an occupancy-related source of uncertainty that entered the consumption data directly. A final issue was that the data was measured during operating conditions that can only be assumed to involve conventional set point tracking control, and was therefore characterized by low levels of excitation primarily driven by solar heat gains.

The latter of these challenges meant that the data in many cases did not provide sufficient information to distinguish between candidate models (i.e. models with different parameters). The estimates of the thermal capacity were particularly prone to this issue due to the lack of excitation. This led to Bayesian calibration being adopted as the parameter identification method, as it offers a powerful framework for incorporating prior knowledge that can guide the parameter search towards regions of the parameter space that are characterized by high prior probability. As such, in the cases where the data in itself did not contain sufficient information to identify a given parameter, the prior distribution associated with that parameter became the dominant component of the posterior distribution. Clearly, the use of priors does not ensure that the obtained parameter estimates agree with the characteristics of the actual building. However, they allow us to obtain models that on one hand have good predictive performance during the typical operating conditions described by the calibration data, and on the other hand have realistic dynamic behaviour that – in the absence of data suited for dynamic modelling – is rooted in prior knowledge and a physics-based model structure. Although this study only made use of the parameter estimates associated with the *maximum a posteriori* probability (the MAP estimates), the posterior obtained from the Metropolis algorithm [90] also describe the uncertainty associated with each parameter estimate. This information is therefore readily available and may be used to conduct sensitivity analyses in studies where this is deemed necessary.

Finally, the methodology did not involve the model structures evaluated in Part I of this thesis (P6). The primary reason for this was that specification of priors for the parameters of those model structures would require setting up equations defining each parameter in terms of building-specific characteristics. Since the method described in ISO 13790 [93] essentially already contained such equations, it was considered more natural to rely on this calculation method and introduce the necessary modifications to the model structure that would allow it to be used under more dynamic conditions. The modified 13790 model structure that was used in the study contains an algebraic surface temperature node, and is generally constrained in its structure by the equations describing heat transfer between nodes these nodes. In spite of this, its ability to describe the thermal conditions in buildings is considered similar to that of e.g. the 3R2C model, which was the preferred model structure in the analysis of (P6).

CASE STUDY: LARGE-SCALE DEMAND RESPONSE

The case study demonstrated that the modelling methodology can be used to obtain bottom-up models of the buildings in urban areas that are capable of predicting their district heating consumption with high levels of accuracy. Furthermore, the resulting reduced-order models may be readily implemented in MPC schemes, thereby making them ideal for analysis related to space heating demand response in residential buildings. In the case study, the obtained building models were used to evaluate two DR schemes in terms of their effectiveness in achieving peak-load reductions. To enable clear interpretation of the results, both of these DR schemes used simple time-of-use prices to incentivize load shifting. The analysis revealed that the first DR scheme, which did not impose constraints on the nature of the response from the buildings, resulted in the formation of new peaks. The second DR scheme featured utility-related constraints to ensure a more evenly distributed response from the buildings. These constraints prevented the formation of new peaks and enabled peak-load reductions, but also lowered the overall efficiency of conducted load shifting.

The case study indicated that some of the metrics that were used to evaluate DR in the previous chapters of this thesis do not necessarily tell the whole story. An example of this is the analysis of (P1), which evaluated the shifted energy quantities from high- or peak-load periods to low-load periods, but did not discuss how such control behaviour could affect the aggregated load profile. The scenario featured in the case study thereby demonstrates the need to further consider the effects of proposed DR schemes when they are applied to larger groups of buildings.

10 CONCLUSIONS

10.1 Main findings

In this thesis, I set out to address some of the challenges that are widely considered inhibitive of the viability of implementing MPC schemes in the residential building sector. To this end, a set of research objectives were defined. The work of addressing these research objectives was documented in a series of published research papers – some of which make up the main body of present thesis. The following paragraphs provide the main findings of these studies, organized by the research objectives of section 1.2.

PART I

The first part of this thesis was concerned with aspects of building energy modelling. In this broad setting, my analysis was aimed at aspects that were considered particularly relevant for implementation of model predictive control (MPC) schemes for space heating in residential buildings. Therefore, the conducted research efforts were aimed at the following three objectives:

OBJ. 1.1: EXPERIMENT DESIGN AND COMFORT (P5)

The analysis in (P5) indicated that sufficiently informative data for identifying models for MPC implementation could be obtained through experiments that do not impose significant thermal discomfort on occupants. This result was further supported by a separate analysis in (S7), which suggested that data collected during operation of an (un-calibrated) MPC scheme may be an appropriate substitute for the otherwise typically used PRBS signals. Finally, simulations of MPC with relatively poor performing models indicated the control scheme to be relatively robust.

OBJ. 1.2: MODEL STRUCTURE SELECTION (P6)

The analysis in (P6) indicated that the four low-order (second and third order) models that were evaluated are capable of describing the dynamic conditions in buildings with an accuracy considered sufficient for MPC applications. Of these model structures, two were also found capable of producing consistent and relatively accurate estimates of the thermal capacities and overall heat loss coefficient of buildings (compared to ‘white-box’ estimates). On the other hand, the results indicated that the models could not be used to estimate the transmission and infiltration

components that together constitute the total heat loss. A second-order (3R2C) model structure was concluded to be the best trade-off between simplicity and performance.

OBJ. 1.3: PRACTICAL WEATHER DATA ACQUISITION (P3)

A method for constructing weather data time-series from meteorological forecasts was proposed to eliminate the need for *actual* weather measurements in the identification of building models for MPC implementation. Compared to implementation methods that require measurements, the results indicated that the performance impact (on economic savings and comfort) of the proposed method was insignificant. Therefore, the main conclusion of the paper was that the method is a promising alternative to the more expensive and less practical method of using actual measurements.

PART II

The second part of this thesis addressed the four research objectives related to the potential of enabling demand response through space heating of residential buildings:

OBJ. 2.1: THE IMPACT OF BUILDING ENERGY EFFICIENCY (P1, P2)

The results of two studies (P1, P2) featuring buildings with different levels of energy efficiency were found to agree with the findings of previous studies: an increase in energy efficiency improves the storage efficiency while decreasing the storage capacity. During MPC operation, these two contradicting effects led to the absolute energy quantities shifted from high- or peak-load periods to low-load periods remaining approximately constant across most of the retrofitted buildings. However, for the most energy-efficient buildings, the shifted energy quantities were achieved through a high frequency of relatively low-impact load shifts. Therefore, the potential associated with a building with a given energy efficiency is likely to depend on the type of issues that are to be addressed by the demand response initiative – and how often they occur.

OBJ. 2.2: CENTRALIZED VS. DECENTRALIZED MPC (P1, S5)

MPC schemes may be implemented in a centralized or decentralized manner, where only the former incorporates interaction between adjacent apartments or thermal zones. The decentralized approach neglects these inter-zonal effects, and is in theory therefore sub-optimal. However, the results of two studies (P1, S5) indicated that the benefits of the more complex centralized MPC scheme were modest at best. The results thereby suggest that the centralized approach is unlikely to be worthwhile in practice. An exception, however, is in control of buildings with a high thermal coupling between zones, e.g. where a single dwelling due to an uneven temperature distribution is modelled as multiple thermal zones.

OBJ. 2.3: MARKET STRUCTURES AND DEMAND RESPONSE MECHANISMS (S3, P1, P2, P4)

Several incentive mechanisms have been applied in the papers of this thesis that relates to demand response; these include day-ahead market prices (P2, P3, P5, S2, S4, S5, S6), intraday market prices (P2), time-of-use prices (P4), and multi-objective signals (P1, S3). Although it is difficult to compare the results from these studies directly, several observations were made (numbered for clarity). **1)** Constant tax components reduce the DR potential (dramatically in the case of the current Danish taxes), as they essentially reduce the volatility of the prices (S3). **2a)** In the analysis of (P2), excluding taxes and relying on pure day-ahead prices resulted in cost savings ranging from approximately 3-13% (P2). **2b)** Expanding these efforts to include intraday market prices doubled the economic savings achieved in some cases (P2). **2c)** However, as previously concluded, these results would be affected by potential taxes. **3a)** In relation to the ability of incentive mechanisms to generate societal benefits, the analysis of (P2) indicated that the current trading behaviour on the intraday-market rendered the method of engaging in intraday trading undesirable from a power-balancing point of view. **3b)** On the other hand, the analysis presented in (P1, S3) indicated that multi-objective signals could be used to incentivize the utilization of renewable energy production, lower the energy demand at peak times, and reduce CO₂-emissions.

OBJ. 2.4: LARGE-SCALE DEMAND RESPONSE (P4)

The modelling methodology presented in (P4) was developed to provide a framework for conducting studies on large-scale demand response. The methodology was evaluated on a case study involving 159 single-family houses. The results indicated that the models obtained from applying the methodology were capable of predicting the aggregated energy consumption of the neighbourhood with high accuracy. A part of this performance was gained due to the inference of average domestic hot water draw profiles for each building, which also allowed the models to reproduce the peaks that may be targeted by demand response schemes accurately. The models were used to investigate a DR scheme using time-of-use prices to incentivize peak load reductions in a district heating network. The analysis revealed that measures had to be taken to ensure a sensible response from the case buildings that lowered the original peak without leading to the formation of new peaks. This issue exemplifies a challenging aspect of demand response that would have not have been indicated by studies focusing on demand response on the scale of individual buildings.

10.2 Future work

The following is a brief outline of the research directions that are considered relevant given my understanding of the current state-of-the-art related to demand response initiatives involving the thermostatic load of space heating in residential buildings.

THEORETICAL STUDIES

Despite the large research efforts taking place within the fields of dynamic building modelling and demand response, several relevant topics for future theoretical research efforts remain.

BUILDING MODELLING

The work related to the selection of grey-box model structures revealed discrepancies between the observed results and conclusions of previous studies on the same topic. Therefore, identifying a set of grey-box model structures that prove consistent in their ability to describe the thermodynamic behaviour of buildings and estimate their physical characteristics is considered an important future research endeavour. Furthermore, two practical approaches for generating input-output data for parameter identification were featured in studies: MPC data (S7) and night-setback data (P3). Further research is needed to investigate whether simpler experiments such as these are also successful when the data is influenced by occupancy-related disturbances that are more realistic.

DEMAND RESPONSE

Many studies have investigated price-based demand response schemes – likely due to the intuitive nature of the concept and the fact that price signals are readily available from various markets. However, studies comparing the achievable performance of the price-based (indirect) and incentive-based (direct) approaches to DR schemes are needed, as the less restrictive nature of the latter could allow DR to be conducted more efficiently. Such analyses could be facilitated using the modelling methodology developed in (P4). Another important topic for future research is the potential influence that large-scale DR implementation can have on the infrastructure-determining scenarios in both electricity and district heating networks. The costs associated with standby boilers or power plants may be a low-hanging fruit in this regard.

EXPERIMENTAL STUDIES

A common feature of the majority of analyses presented in this thesis is the use of EnergyPlus simulations as analogues for actual buildings. Therefore, it is relevant to evaluate the validity of the applied assumptions and to what extent they may have influenced the drawn conclusions. While each of the papers of the thesis themselves outline relevant topics for future research, the following two assumptions was applied to several of the presented studies, and are therefore considered to be of high priority.

FULLY-MIXED TEMPERATURE DISTRIBUTION

This assumption is applied in the vast majority of simulation-based studies, likely due to the difficulties associated with simulating the airflow between rooms realistically including the opening and closing of doors. I consider it likely that a single-zone representation may be sufficient in some buildings, while others may require multi-zone models due to e.g. differences in the heat loads or exposure to weather conditions between different parts of the building. The latter would undoubtedly constitute new challenges to both model identification and MPC control.

OCCUPANCY

In the context of the topics of this thesis, two different but equally important areas of future research are related to occupants.

First, occupants constitute a significant source of uncertainty. Similar to the fully-mixed assumption, this uncertainty may affect both the model identification and the performance of the MPC schemes. Two of the analyses of this thesis applied simple occupancy-models for imposing coloured noise on the data used to obtain models (P5, S7). A natural next step would be to replicate such analyses in actual buildings with real occupants.

The second occupancy-related topic for future research is the validity of the assumptions about thermal comfort that that may affect analyses related to both experiment design (system identification) and to the specification of the constraints that are typically incorporated in MPC schemes. Especially in the case of the latter, these assumptions may significantly affect the indicated DR potentials – both positively and negatively.

TERMINOLOGY, QUANTIFICATION METHODS AND OBJECTIVES

Although demand response in buildings has developed significantly throughout the last decade, there are signs that the research field has not yet matured. Further development of a common terminology, quantification methods and common test scenarios is needed. The latter especially refers to the set of assumptions that are often necessary to introduce in studies featuring DR and MPC, including those related to the characteristics of the building, stochastic occupancy, reference control method (baseline), and finally the mechanism that incentivizes DR. Many of these concerns are currently being addressed in the work conducted in *IEA EBC Annex 67* on Energy Flexible Buildings.

Furthermore, a higher involvement from supply-side actors is needed to enable researchers to focus on the use-cases where DR in buildings is most likely to benefit the energy system – both currently and in the future. A similar argument can be made for regulators, as their participation in discussions on demand response could bring clarity to current regulatory concerns that may inhibit the utilization of DR in practice.

11 REFERENCES

- [1] Buildings Performance Institute Europe (BPIE), “Europe's Buildings under the Microscope - A country-by-country review of the energy performance of buildings,” BPIE, (2011).
- [2] Eurostat, “Eurostat: Final energy consumption in households,” Eurostat, 30 11 2016. [Online]. Available: http://ec.europa.eu/eurostat/tgm/table.do?tab=table&init=1&language=en&pcode=t2020_rk200&plugin=1. [Accessed 01 12 2016].
- [3] D. Olsthoorn, F. Haghighat, A. Moreau and G. Lacroix, “Abilities and limitations of thermal mass activation for thermal comfort, peak shifting and shaving: A review,” *Building and Environment*, vol. 118, pp. 113-127, 2017.
- [4] European Parliament, “Directive 2002/91/EC of the European Parliament and of the Council of 16 December 2002 on the energy performance of buildings,” *Official Journal of the European Union*, pp. 65-71, 2002.
- [5] European Parliament, “Directive 2010/31/EU of the European Parliament and of the Council of 19 May 2010 on the energy performance of buildings (recast),” *Official Journal of the European Union*, pp. 13-35, 2010.
- [6] Ministry of Transport, Building and Housing, “Bygningsklasse 2020 (Building class 2020),” 1 7 2010. [Online]. Available: http://historisk.bygningsreglementet.dk/br10_01_id1610/0/42. [Accessed 15 10 2018].
- [7] Ministry of Transport, Building and Housing, “Regeringen reviderer energikrav til nye bygninger i 2020,” 8 11 2017. [Online]. Available: <https://www.trm.dk/da/nyheder/2017/regeringen-reviderer-energi-til-nye-bygninger-i-2020>. [Accessed 15 10 2018].
- [8] Ministry of Transport, Building and Housing, “Lavenergiklasse (Low-energy building class),” 1 7 2018. [Online]. Available: <http://bygningsreglementet.dk/Ovrige-bestemmelser/25/Krav>. [Accessed 15 10 2018].
- [9] European Commission, “Eurostat database,” European Commission, [Online]. Available: <https://ec.europa.eu/eurostat/data/database>. [Accessed 12 09 2018].
- [10] Eurostat, “Statistics explained: Electricity production, consumption and market overview,” 10 11 2018. [Online]. Available: https://ec.europa.eu/eurostat/statistics-explained/index.php?title=Electricity_production,_consumption_and_market_overview.
- [11] Energinet.dk, “energidataservice.dk,” [Online]. Available: <https://www.energidataservice.dk/dataset>. [Accessed 10 09 2018].
- [12] R. Scharff and M. Amelin, “Trading behaviour on the continuous intraday market ELBAS,” *Energy Policy* 88 (2016), p. 544–557, DOI: 10.1016/j.enpol.2015.10.045.
- [13] A. Orioli and A. Di Gangi, “Load mismatch of grid-connected photovoltaic systems: Review of the effects and analysis in an urban context,” *Renewable and Sustainable Energy Reviews*, vol. 2013, pp. 13-28, 2013.
- [14] G. Reynders, T. Nuytten and D. Saelens, “Potential of structural thermal mass for demand-side management in dwellings,” *Building and Environment*, vol. 64, pp. 187-199, 2013.
- [15] R. Baetens, R. De Coninck, J. Van Roy, B. Verbruggen, J. Driesen, L. Helsen and D. Saelens, “Assessing electrical bottlenecks at feeder level for residential net zero-energy buildings by integrated system simulation,” *Applied Energy*, vol. 96, pp. 74-83, 2012.
- [16] European Commission, “European Technology Platform SmartGrids - Vision and Strategy for Europe's Electricity Networks in the Future,” Office for Official Publications of the European Communities, Luxembourg, 2006.
- [17] H. Lund, A. N. Andersen, P. A. Østergaard, B. V. Mathiesen and D. Connolly, “From electricity smart grids to smart energy systems - A market operation based approach and understanding,” *Energy* 42, pp. 96-102, 2012.
- [18] K. Shan, S. Wang, C. Yan and F. Xiao, “Building demand response and control methods for smart grids: A review,” *Science and Technology for the Built Environment*, vol. 22, no. 6, pp. 692-704, 2016.

- [19] X. Li and J. Wen, "Review of building energy modeling for control and operation," *Renewable and Sustainable Energy Reviews*, vol. 37, pp. 517-537, 2014.
- [20] European Parliament, "Directive 2018/844 of the European parliament and of the council of May 30 2018," *Official Journal of the European Union*, pp. 75-91, 2018.
- [21] T. H. Haider, O. H. See and W. Elmenreich, "A review of residential demand response of smart grid," *Renewable and Sustainable Energy Reviews*, vol. 59, pp. 166-178, 2016.
- [22] M. D. Knudsen and S. Petersen, "Model predictive control for demand response of domestic hot water preparation in ultra-low temperature district heating systems," *Energy and Buildings*, vol. 146, pp. 55-64, 2017.
- [23] P. H. Shaikh, N. B. M. Nor, P. Nallagownden, I. Elamvazuthi and T. Ibrahim, "A review on optimized control systems for building energy and comfort management of smart sustainable buildings," *Renewable and Sustainable Energy Reviews*, vol. 34, pp. 409-429, 2014.
- [24] M. Killian and M. Kozek, "Ten questions concerning model predictive control for energy efficient buildings," *Building and Environment*, vol. 105, pp. 403-412, 2016.
- [25] S. Prívará, J. Cigler, Z. Váňa, F. Oldewurtel, C. Sagerschnig and E. Žáčková, "Building modeling as a crucial part for building predictive control," *Energy and Buildings*, vol. 56, pp. 8-22, 2013.
- [26] E. Cutter, C. Woo, F. Kahrl and A. Taylor, "Maximizing the Value of Responsive Load," *The Electricity Journal*, vol. 25, no. 7, pp. 6-16, 2012.
- [27] O. Ma, N. Alkadi, P. Cappers, P. Denholm, J. Dudley, S. Goli, M. Hummon, S. Kiliccote, J. MacDonald, N. Matson, D. Olsen, C. Rose, M. D. Sohn, M. Starke, B. Kirby and M. O'Malley, "Demand Response for Ancillary Services," *IEEE TRANSACTIONS ON SMART GRID*, vol. 4, no. 4, pp. 1988-1995, 2013.
- [28] N. O'Connell, P. Pinson, H. Madsen and M. O'Malley, "Benefits and challenges of electrical demand response: A critical review," *Renewable and Sustainable Energy Reviews*, vol. 39, pp. 686-699, 2014.
- [29] Commission of European Union, "Energy consumption in households," 03 2018. [Online]. Available: https://ec.europa.eu/eurostat/statistics-explained/index.php/Energy_consumption_in_households. [Accessed 17 09 2018].
- [30] J. Široký, F. Oldewurtel, J. Cigler and S. Prívará, "Experimental analysis of model predictive control for an energy efficient building heating system," *Applied Energy*, vol. 88, pp. 3079-3087, 2011.
- [31] J. Ma, J. Qin, T. Salsbury and P. Xu, "Demand reduction in building energy systems based on economic model predictive control," *Chemical Engineering Science*, vol. 67, no. 1, pp. 92-100, 2012.
- [32] F. Oldewurtel, A. Ulbig, A. Parisio, G. Andersson and M. Morari, "Reducing peak electricity demand in building climate control using real-time pricing and model predictive control," in *49th IEEE Conference on Decision and Control (CDC)*, Atlanta, 2009.
- [33] G. Reynders, "Quantifying the impact of building design on the potential of structural thermal storage for active demand response in residential buildings," PhD Thesis, KU Leuven, 2015.
- [34] R. Halvgaard, N. K. Poulsen, H. Madsen and J. B. Jørgensen, "Economic Model Predictive Control for building climate control in a Smart Grid," in *2012 IEEE PES Innovative Smart Grid Technologies (ISGT)*, Washington, DC, 2012.
- [35] M. D. Knudsen and S. Petersen, "Demand Response Potential of Model Predictive Control of Space Heating based on Price and Carbon Dioxide Intensity Signals," *Energy and Buildings* 125 (2016), pp. 196-204, DOI: 10.1016/j.enbuild.2016.04.053.
- [36] A. K. Tangirala, Principles of System Identification - Theory and practice, Boca Raton, Florida : CRC Press, 2015.
- [37] L. Ljung, "Prediction Error Estimation Methods," Dept. of Electrical Engineering, Linköping University, Linköping, 2001.
- [38] O. Mohamed, D. Younis, H. Abdelwahab, A. Anizei and B. T. Elobidy, "Comparative Study Between Subspace Method and Prediction Error Method for Identification of Gas Turbine Power Plant," in *Proceedings of the 6th International Congress on Ultra Modern Telecommunications and Control Systems and Workshops*, St. Petersburg, Russia, 2014.
- [39] U. Forssell, "Closed-loop Identification: Methods, Theory and Applications," Department of Electrical Engineering, Linköping University, Linköping, 1999.
- [40] J. Zhao, Y. Zhu and R. Patwardhan, "Some Notes on MPC relevant Identification," in *Proceedings of the 2014 American Control Conference (ACC)*, Portland, Oregon, 2014.

- [41] D. S. Shook, C. Mohtadi and S. L. Shah, "A Control-Relevant Identification Strategy for GPC," *IEEE Transactions on Automatic Control*, vol. 37, no. 7, pp. 975-980, 1992.
- [42] J. B. Jørgensen and S. B. Jørgensen, "MPC-Relevant Prediction-Error Identification," in *Proceedings of the 2007 American Control Conference*, New York City, 2007.
- [43] U.S. Department of Energy, "EnergyPlus version 8.8.0 Documentation: Engineering Reference," U.S. Department of Energy, Washington, D.C., 2017.
- [44] M. Wetter, "Co-simulation of building energy and control systems with the Building Controls Virtual Test Bed," *Journal of Building Performance Simulation (2010)*, vol. 3, no. 4, pp. 1-19, DOI: 10.1080/19401493.2010.518631.
- [45] The MathWorks, Inc., *MATLAB 2017b (9.3.0.713579)*, 2017.
- [46] D. E. Rivera, S. V. Gaikwad and X. Chen, "CONTROL-ID: A Demonstration Prototype for Control-Relevant Identification," in *Proceedings of the American Control Conference*, Baltimore, Maryland, 1994.
- [47] S. V. Gaikwad and D. E. Rivera, "Control-Relevant Input Signal Design for Multivariable System Identification: Application to High-Purity Distillation," San Francisco, 1996.
- [48] L. Ljung, "System Identification - Theory for the User," Prentice Hall, New Jersey, 1998.
- [49] R. E. Kalman, "A New Approach to Linear Filtering and Prediction Problems," *Journal of Basic Engineering*, vol. 82, no. 1, pp. 35-45, 1960.
- [50] G. Reynders, J. Diriken and D. Saelens, "Quality of grey-box models and identified parameters as function of the accuracy of input and observations signals," *Energy and Buildings*, vol. 82, pp. 263-274, 2014.
- [51] H. Harb, N. Boyanov, L. Hernandez, R. Streblow and D. Müller, "Development and validation of grey-box models for forecasting the thermal response of occupied buildings," *Energy and Buildings*, vol. 117, pp. 199-207, 2016.
- [52] P. Bacher and H. Madsen, "Identifying suitable models for the heat dynamics of buildings," *Energy and Buildings*, vol. 43, no. 7, pp. 1511-1522, 2011.
- [53] G. Bellu, M. P. Saccomani, S. Audoly and L. D'Angio, "DAISY: A new software tool to test global identifiability of biological and physiological systems," *Computer Methods and Programs in Biomedicine*, vol. 88, pp. 52-61, 2007.
- [54] G. Reynders, J. Diriken and D. Saelens, "Quality of grey-box models and identified parameters as function of the accuracy of input and observation signals," *Energy and Buildings*, vol. 82, pp. 263-274, 2014.
- [55] J. Řehoř and V. Havlena, "Grey-box model identification – control relevant approach," *IFAC Proceedings Volumes*, vol. 43, no. 10, pp. 117-122, 2010.
- [56] J. Řehoř and V. Havlena, "A Practical Approach to Grey-box Model Identification," in *Proceedings of the 18th World Congress*, Milano, 2011.
- [57] D. Gyalistras and M. Gwerder, "Use of Weather And Occupancy Forecasts For Optimal Building Climate Control (OptiControl): Two years progress report," Terrestrial Systems Ecology, ETH Zurich & Building Technologies Division, Siemens Switzerland Ltd., Zürich, 2010.
- [58] W. Kidd, "Development, Design and Use of Ripple Control," *Proceedings of the IEE*, vol. 122, no. 10, pp. 993-1008, 1975.
- [59] L. Isaksen, F. S. Ma, N. W. Simons and C. W. Gellings, "Bibliography on Load Management," *IEEE Transactions on Power Apparatus and Systems*, Vols. PAS-100, no. 5, pp. 2597-2601, 1981.
- [60] C. W. Gellings, "Demand-side load management: The rising cost of peak-demand power means that utilities must encourage customers to manage power usage," *IEEE Spectrum*, vol. 18, no. 12, pp. 49-52, 1981.
- [61] C. W. Gellings, "The Concept of Demand-Side Management for Electric Utilities," *Proceedings of the IEEE*, vol. 10, pp. 1468-1470, 1985.
- [62] C. W. Gellings, W. Barron, F. M. Betley, W. A. England, L. L. Preiss and D. E. Jones, "Integrating Demand-Side Management into Utility Planning," *IEEE Transactions on Power Systems*, vol. 1, no. 3, pp. 81-87, 1986.
- [63] F. Sioshansi, "Demand response: the sequel to DSM?," in *ECEEE Summer Study proceedings*, Mandelieu, France, 2001.
- [64] F. Sioshansi and A. Vojdani, "What Could Possibly Be Better Than Real-Time Pricing? Demand Response," *The Electricity Journal*, vol. 14, no. 5, pp. 39-50, 2001.
- [65] Federal energy regulatory commission, "Order No. 745: Demand Response Compensation in Organized Wholesale Energy Markets," Federal energy regulatory commission, Washington, 2011.

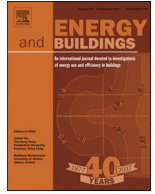
- [66] International Energy Agency, “Re-powering markets,” International Energy Agency, Paris, 2016.
- [67] G. A. Benndorf, D. Wyrstcil and N. Réhault, “Energy performance optimization in buildings: A review on semantic interoperability, fault detection, and predictive control,” *Applied Physics Reviews*, vol. 5, no. 4, 2018.
- [68] J. Richalet, A. Rault, J. Testud and J. Papon, “Model predictive heuristic control: Applications to industrial processes,” *Automatica*, vol. 14, no. 5, pp. 413-428, 1978.
- [69] C. R. Cutler and B. L. Ramaker, “Dynamic matrix control - A computer control algorithm,” in *AICHE National Meeting*, Houston, 1979.
- [70] J. Qin and T. Badgwell, “A survey of industrial model predictive control technology,” *Control Engineering Practice*, vol. 11, pp. 733-764, 2003.
- [71] A. R. Florita and G. P. Henze, “Comparison of Short-Term Weather Forecasting Models for Model Predictive Control,” *HVAC&R Research*, vol. 15, no. 5, pp. 835-853, 2009.
- [72] F. Oldewurtel, A. Parisio, C. N. Jones, M. Morari, D. Gyalistras, M. Gwerder, V. Stauch, B. Lehmann and K. Wirth, “Energy Efficient Building Climate Control using Stochastic Model Predictive Control and Weather Predictions,” in *Proceedings of the 2010 American Control Conference*, Baltimore, USA, 2010.
- [73] B. Dong, K. P. Lam and C. P. Neuman, “Integrated building control based on occupant behavior pattern detection and local weather forecasting,” in *12th Conference of International Building Performance Simulation Association*, Sydney, 2011.
- [74] G. P. Henze, “Model predictive control for buildings: a quantum leap?,” *Journal of Building Performance Simulation*, vol. 6, no. 3, pp. 157-158, 2013.
- [75] J. Clauß, C. Finck, P. Vogler-Finck and P. Beagon, “Control strategies for building energy systems to unlock demand side flexibility – A review,” in *Proceedings of the 15th IBPSA Conference*, San Francisco, CA, 2017.
- [76] P.-D. Moroşan, R. Bourdais, D. Dumur and J. Buisson, “Building temperature regulation using a distributed model predictive control,” *Energy and Buildings*, vol. 42, no. 9, pp. 1445-1452, 2010.
- [77] E. Vrettos, K. Lai, F. Oldewurtel and G. Andersson, “Predictive Control of Buildings for Demand Response with Dynamic Day-ahead and Real-time Prices,” in *2013 European Control Conference (ECC)*, Zurich, 2013.
- [78] M. D. Knudsen, R. E. Hedegaard, T. H. Pedersen and S. Petersen, “Model Predictive Control of Space Heating and the Impact of Taxes on Demand Response: A Simulation Study,” in *CLIMA 2016 - proceedings of the 12th REHVA World Congress: Volume 10*, Aalborg, 2016.
- [79] J. Le Dréau and P. Heiselberg, “Energy flexibility of residential buildings using short term heat storage in the thermal mass,” *Energy*, vol. 111, pp. 991-1002, 2016.
- [80] T. H. Pedersen, R. E. Hedegaard, M. D. Knudsen and S. Petersen, “Comparison of centralized and decentralized model predictive control in a building retrofit scenario,” in *CISBAT 2017 International Conference – Future Buildings & Districts – Energy Efficiency from Nano to Urban Scale, CISBAT 2017 6-8 September 2017*, , Lausanne, Switzerland, 2017.
- [81] T. H. Pedersen, M. D. Knudsen, R. E. Hedegaard and S. Petersen, “Handling thermal comfort in economic model predictive control schemes for demand response,” *Energy Procedia*, vol. 122, pp. 985-990, 2017.
- [82] G. Bianchini, M. Casini, A. Vicino and D. Zarrilli, “Demand-response in building heating systems: A Model Predictive Control approach,” *Applied Energy*, vol. 168, pp. 159-170, 2016.
- [83] T. H. Pedersen and S. Petersen, “Investigating the performance of scenario-based model predictive control of space heating in residential buildings,” *Journal of Building Performance Simulation*, vol. 11, no. 4, pp. 485-498, 2018.
- [84] C. F. Reinhart and C. C. Davila, “Urban building energy modeling – A review of a nascent field,” *Building and Environment*, vol. 97, pp. 196-202, 2016.
- [85] É. Mata, A. S. Kalagasidis and F. Johnsson, “Building-stock aggregation through archetype buildings: France, Germany, Spain and the UK,” *Building and Environment*, vol. 81, pp. 270-282, 2014.
- [86] C. Cerezo, J. Sokol, C. Reinhart and A. Al-Mumin, “Three methods for characterizing building archetypes in urban energy simulation. A case study in Kuwait City,” in *Proceedings of BS2015: 14th Conference of International Building Performance Simulation Association*, Hyderabad, India, 2015.
- [87] G. Dall’O’, A. Galante and M. Torri, “A methodology for the energy performance classification of residential building stock on an urban scale,” *Energy and Buildings*, vol. 48, pp. 211-219, 2012.
- [88] M. Kristensen, R. E. Hedegaard and S. Petersen, “Hierarchical calibration of archetypes for urban building energy modeling,” *Energy and Buildings*, vol. 175, pp. 219-234, 2018.

- [89] W. Cyx, N. Renders, M. V. Holm and S. Verbeke, "IEE TABULA - Typology Approach for Building Stock Energy," 2011.
- [90] N. Metropolis, A. W. Rosenbluth, M. N. Rosenbluth, A. H. Teller and E. Teller, "Equation of State Calculations by Fast Computing Machines," *The Journal of Chemical Physics*, vol. 21, no. 6, pp. 1087-1092, 1953.
- [91] G. Reynders, "Quantifying the impact of building design on the potential of structural storage for active demand response in residential buildings," PhD Dissertation, KU Leuven, 2015.
- [92] Buildings Performance Institute Europe, "Financing energy efficiency in European Buildings: How to boost large-scale retrofit?," Buildings Performance Institute Europe, Brussels, 2010.
- [93] European Committee for Standardization, "EN/ISO 13790:2008 - Energy performance of buildings - Calculation of energy use for space heating and cooling," European Committee for Standardization, Brussels, 2008.

12 APPENDICES

APPENDIX 1 PAPER: HIERARCHICAL CALIBRATION OF ARCHETYPES FOR URBAN BUILDING ENERGY MODELING (S1).....	150
APPENDIX 2 PAPER: THE EFFECT OF INCLUDING HYDRONIC RADIATOR DYNAMICS IN MODEL PREDICTIVE CONTROL OF SPACE HEATING (S2).....	167
APPENDIX 3 PAPER: MODEL PREDICTIVE CONTROL OF SPACE HEATING AND THE IMPACT OF TAXES ON DEMAND RESPONSE: A SIMULATION STUDY (S3).....	181
APPENDIX 4 PAPER: HANDLING STOCHASTIC OCCUPANCY IN AN ECONOMIC MODEL PREDICTIVE CONTROL FRAMEWORK FOR HEATING SYSTEM OPERATION IN DWELLINGS (S4)	193
APPENDIX 5 PAPER: COMPARISON OF CENTRALIZED AND DECENTRALIZED MODEL PREDICTIVE CONTROL IN A BUILDING RETROFIT SCENARIO (S5)	205
APPENDIX 6 PAPER: HANDLING THERMAL COMFORT IN ECONOMIC MODEL PREDICTIVE CONTROL SCHEMES FOR DEMAND RESPONSE (S6).....	212
APPENDIX 7 PAPER: SYSTEM IDENTIFICATION OF THERMAL BUILDING MODELS FOR DEMAND RESPONSE – A PRACTICAL APPROACH (S7).....	219
APPENDIX 8 PAPER: URBAN-SCALE DYNAMIC BUILDING ENERGY MODELING AND PREDICTION USING HIERARCHICAL ARCHETYPES: A CASE STUDY OF TWO DANISH TOWNS (S8)	226

APPENDIX 1 PAPER: HIERARCHICAL CALIBRATION OF
ARCHETYPES FOR URBAN BUILDING ENERGY MODELING
(S1)



Hierarchical calibration of archetypes for urban building energy modeling

Martin Heine Kristensen*, Rasmus Elbæk Hedegaard, Steffen Petersen

Department of Engineering, Aarhus University, 8000 Aarhus, Denmark

ARTICLE INFO

Article history:

Received 23 April 2018

Revised 3 July 2018

Accepted 6 July 2018

Available online 17 July 2018

Keywords:

Archetypes

Building energy use

Hierarchical modeling

Multilevel modeling

Bayesian calibration

Prediction

Archetype homogeneity

Smart meter

ABSTRACT

The application of building archetypes is a widespread approach used in urban building energy modeling. Working with archetypes has a range of benefits, but it is important that modelers avoid using oversimplified approaches when establishing the archetype as they lead to loss of uncertainty and, consequently, to models with inferior predictive capabilities. In this paper, we propose a multilevel take on the challenge of establishing archetypes. A simultaneous modeling and calibration framework is formulated using Bayesian inference techniques – a technique that allows for the propagation of uncertainty throughout the calibration process. By means of hierarchical modeling, information from training buildings is partially pooled together to form an optimal solution between separate building energy models and a completely pooled model. This enables the inference of uncertain archetype parameters that are less prone to building outliers than what is achieved using ordinary aggregation of individual building estimates. The proposed framework incorporates dynamic building energy modeling of arbitrary temporal resolution where uncertain parameters are fitted for individual building models and the archetype model simultaneously. The application of the framework is demonstrated using case-study data from the Danish residential building stock, containing 3-hourly measurements of energy use for 50 training buildings. The model is tested for the prediction of 100 out-of-sample test buildings' aggregated energy use time series on a holdout validation period. With a prediction error of only $NMBE = 2.9\%$ and $CVRMSE = 7.8\%$, the archetype framework promises well for urban modeling applications.

© 2018 Elsevier B.V. All rights reserved.

1. Introduction

City governments, utility companies, and other energy policy stakeholders work on the urban scale of neighborhoods, cities, or even entire building stocks when planning and predicting the effect of various energy efficiency and production strategies. They are in need of tools and platforms that enable the analysis of aggregated effects rather than individual building-level effects.

Urban building energy modeling (UBEM) is a growing research field that seeks to facilitate such analyses by combining the effects of individual buildings into an aggregated urban model. The modeling approach of UBEM is either to model buildings independently and then aggregate their simulated energy use, or to model buildings collectively in an all-inclusive urban model with context-specific boundary conditions and interactive effects. Regardless of the modeling approach, the overall challenge of UBEM is to collect and assign all the necessary data inputs for establishing sufficiently detailed building energy models of all buildings in the

urban area without introducing too many assumptions and simplifications [1]. Because of this, the establishment of an accurate all-inclusive physics-based UBEM persists to be an extremely difficult task. However, one can make use of different techniques for reasonable tradeoffs between feasibility and accuracy to overcome this; of these techniques, the application of archetype models seems to offer an attractive solution.

1.1. Archetype modeling

The archetype approach seeks to reduce the number of buildings in a given building stock or urban area to a much smaller subset of homogeneous archetypes that represent groups of typologically identical buildings where information that would allow further differentiation is typically not available. This approach inevitably obscures the natural variability of occupant behavior and construction elements, but in turn reduces requirements for data acquisition and computational load.

The definition and use of building archetypes for urban-scale modeling have undergone a lot of work in recent years. In general, the literature describes the process of defining archetypes as consisting of three steps before simulation: (1) classification of build-

* Corresponding author.

E-mail address: mhk@eng.au.dk (M.H. Kristensen).

Nomenclature

Variables and parameters

A_m	effective area of thermal mass [m^2/m^2]
b_{ground}	temperature adjustment factor for building elements facing the ground [-]
C_m	capacity of thermal mass [$\text{kJ}/(\text{m}^2\text{K})$]
h_{room}	room height [m]
H	heat loss coefficient (subscripts are used to define the element) [W/K]
f_{frame}	window frame fraction [-]
LWR	length-width ratio of building geometry [-]
n_b	number of buildings
n_s	number of simulations from the building energy model
n_t	number of simulation time steps
n_θ	number of calibration parameters
p	number of levels for Morris sensitivity analysis
$q_{\text{inf}@50Pa}$	infiltration airflow at 50 Pa pressure difference [$1/(\text{s m}^2)$]
q_{vent}	ventilation airflow [$1/(\text{s m}^2)$]
r	number of trajectories for Morris sensitivity analysis
\hat{R}	potential scale reduction factor (abbrev.: PSRF) [-]
$SHGC$	solar heat gain coefficient [-]
T	temperature (index defines which temperature) [$^\circ\text{C}$]
U	heat transfer coefficient (index defines which element) [$\text{W}/(\text{m}^2\text{K})$]
V_{occ}	hot water consumption of occupants [$\text{m}^3/(\text{pers. year})$]
W	matrix of weather parameter inputs for building energy model (subscripts are used)
WFR	window-floor-ratio of building geometry [-]
X	matrix of fixed parameter inputs for building energy model (subscripts are used)
y	vector of measured time series energy use (subscripts are used) [kW]
y*	vector of simulated time series energy use (subscripts are used) [kW]
γ	archetype-level scale parameter in half-Cauchy distribution
ε	building-level error between measured and simulated energy use ($y-y^*$) [kW]
θ	vector of building-level calibration parameters (subscripts are used)
κ_0	a-priori number of “observations” of archetype-level means μ on the Σ scale
Λ_0	a-priori scale-matrix of the archetype-level covariance matrix Σ
μ	vector of means of the building-level parameters θ
μ_0	a-priori vector of mean values for archetype-level means μ
ν_0	a-priori degrees of freedom of the archetype-level covariance matrix Σ
Σ	covariance matrix of the building-level parameters θ
σ	standard deviation of building-level error ε [kW]
τ	vector of standard deviations of the building-level parameters θ
Φ_{app}	appliances, equipment and lighting heat load [W]
Φ_{DH}	district heating energy use ($\Phi_{\text{DHW}} + \Phi_{\text{SH}}$) [W]
Φ_{DHW}	energy use for domestic hot water [W]
Φ_{occ}	occupant heat load [W]
Φ_{SH}	energy use for space heating [W]

Φ_{sol}	solar radiation [W]
ω_0	a-priori upper boundary on archetype-level scale-parameter γ

Indices and subscripts

b	indexing buildings $b = 1, 2, \dots, n_b$
i	indexing parameters for Morris sensitivity analysis
s	indexing simulations $s = 1, 2, \dots, n_s$
t	indexing time steps $t = 1, 2, \dots, n_t$
out-of-sample	quantity based on out-of-sample buildings
post	posterior quantity
pred	predictive quantity
train	quantity based on training data period
valid	quantity based on validation data period
within-sample	quantity based on within-sample buildings

Abbreviations

BEM	building energy model (or “modeling”)
BDR	building and dwelling register (Danish building and property database)
CVRMSE	coefficient of variation of the root mean squared error
DHW	domestic hot water
EPC	energy performance certificate
GIS	geographic information system
GPR	Gaussian process regression
MAP	maximum a-posteriori probability
MCMC	Markov chain Monte Carlo
ML	maximum likelihood
NMBE	normalized mean bias error
PDF	probability density function
PSRF	potential scale reduction factor (symbol: \hat{R})
UBEM	urban building energy model (or “modeling”)

ings into archetypes, (2) characterization of archetype parameters, and (3) calibration and validation of uncertain archetype parameters [2–6]. In many studies, the application of classifiers such as *usage type*, *construction year*, and *geometry* (e.g. surface-volume ratio) serves as segmentation parameters for clustering buildings into archetypes [2,7–9]. These simple segmentation parameters are often readily available from public databases such as geographic information systems (GIS) and tax and property registers. Parameter characterization, on the other hand, is often more difficult. Modelers can compile parameter data from a mixture of different information sources in an effort to draw a holistic picture of the archetype; however, the availability of data is very specific to the city, region or country in question. Moreover, as data access is often limited due to legal constraints and privacy considerations, data acquisition easily becomes a delicate compromise. A particularly difficult task is the description of occupant-related parameters that influence many aspects of building operation and thereby energy use. One can thus seldom expect to have data that is elaborate enough to obtain a purely deterministic description of the archetype parameters. Instead, modelers often have to resort to ‘guessing’, either by means of educated guesses, some kind of analysis of historical data, or through a stochastic treatment of uncertain data. For that reason, it is necessary to apply calibration to uncertain archetype parameters [4]. The literature holds a growing body of work on calibration methodologies for building energy models [10,11] of which the probabilistic calibration approaches, e.g. approaches based on Bayesian inference, have become increasingly popular in recent years [3,4,6,12–20]. As the whole concept of archetypes rests on a stochastic treatment of building data, it would then only seem natural to expand the probabilistic calibra-

tion methodologies to the scale of archetypes and building stocks. Nonetheless, there are only few attempts to do so [3,4,6,12,13].

1.2. Bayesian calibration of archetypes

In one of the earliest attempts at probabilistic calibration of archetypes by Booth et al. [12], a Bayesian framework was proposed for the calibration of a bottom-up physics-based archetype based on earlier work by Kennedy and O'Hagan [21]. They applied Gaussian process regression (GPR) for fitting four uncertain parameters of a quasi-steady-state building energy model (BEM) – the archetype model – to the daily building-averaged energy consumption data from 35 similar buildings, matching the archetype classification, over 61 winter days. Booth et al. [12] list several sources of uncertainty related to building stock modeling, which can be summarized to the following four types:

- *Parameter uncertainty*: Building-level variability due to insufficient knowledge about BEM input parameters. This also includes variability due to human behavior in terms of occupancy, operation of appliances, heating and cooling set point preferences, etc.
- *Structural uncertainty*: Variability due to the inadequacy of the BEM in describing the true energy consumption process of the building. This is also known as model bias or model discrepancy.
- *Archetype heterogeneity*: Archetype-level variability due to differences in building characteristics across the sampled buildings.
- *Numerical uncertainty*: Algorithmic variability due to numerical approximations, too small sample sizes, insufficient convergence of calibration, etc.

Booth et al. [12] explicitly addressed and incorporated *parameter uncertainty* by using the GPR technique to fit uncertain parameter distributions from a-priori uncertainty specifications, and to some degree *structural* and *numerical uncertainty* by including a statistical bias-correcting term. However, by fitting the calibration regression line to averaged building data, they did not account for *archetype heterogeneity*.

Kristensen et al. [22] also used the GPR technique, but on the annual heating energy use from a cluster of 450 similar residential buildings to estimate seven shared archetype parameters of a dynamic BEM. They fitted the calibration regression line to the non-averaged, building-specific training data, whereby they acknowledged the uncertainty due to differences in the sampled archetype buildings, i.e. *archetype heterogeneity*. This introduction of a disaggregated building-level likelihood assessment was important as archetype-aggregated data tends to average out much of the variability of the building stock, resulting in less informed posterior estimates.

In studies by Cerezo et al. [3,4,6], a new semi-Bayesian approach was proposed relying on an iterative error-analysis between dynamic BEM simulations and annually or monthly aggregated data, respectively. They used an upper limit for the simulated errors as a binary likelihood function to filter building-specific distributions for the calibration parameters for each building independently. The inferred building-specific parameter estimates were subsequently merged together into joint archetype-estimates to be used for prediction. By evaluating the likelihood of each building independently before combining the data, they implicitly accounted for archetype heterogeneity.

In agreement with the abovementioned sources of uncertainty, previous studies on the calibration efficacy of individual buildings have shown that the Bayesian framework is affected by the level of uncertainty in fixed and uncalibrated model parameters [23], the amount of training data [17], and the level of temporal aggregation

of calibration data [23,24]. Even though these findings apply to the calibration of individual buildings, they presumably also hold for the calibration of archetypes; however, this remains unaccounted for. A natural next step would thus be to investigate the effect of applying calibration data of high temporal resolution, e.g. hourly measurements of energy use. The application of high-resolution data, in combination with a detailed dynamic BEM, will most likely allow for a better estimation of dynamical parameters [23]. However, a binary likelihood function as proposed by Cerezo et al. [3,4,6] could prove to be too simple to fully exploit the information embedded in high-resolution data; for this end, a fully Bayesian continuous likelihood, e.g. Gaussian-distributed errors, would probably serve as a better 'filter'. Furthermore, a specific feature of estimating archetype parameters is the potential correlation between calibrated parameters. To our knowledge, this correlation has not previously been addressed in the literature of BEM calibration despite its importance for making accurate out-of-sample predictions of new buildings subscribing to the same archetype.

1.3. Contributions of this paper

In this paper, we present a new probabilistic archetype modeling and calibration framework where we use data from a number of observed training buildings to calibrate uncertain archetype parameters in a hierarchical setting. This feature allows the archetype calibration to draw strength from all training building datasets simultaneously, hereby exploring the true diversity of the archetype. In addition to the propagation of uncertainty throughout the calibration process due to the abovementioned sources of uncertainty, the proposed framework introduces the inclusion of four key features:

1. Dynamic physics-based building energy modeling;
2. Time series data and model outputs of arbitrary temporal resolution, e.g. hourly resolution;
3. Hierarchical/multilevel likelihood assessment of parameter proposals (both on building level and archetype level);
4. Calibration of both building-level and archetype-level parameters including their correlation.

We have organized the paper with an initial presentation of the proposed hierarchical framework in Section 2. All assumptions and necessary statistical definitions are laid out openly allowing readers to implement the model using their own data, if wanted. In Section 3, we demonstrate the application of the framework using an archetype case study from the Danish residential building stock. It is demonstrated how to draw inference about archetype parameters even though parameter values of the individual training buildings are not themselves observed, and how to perform out-of-sample predictions of unseen buildings matching the archetype definition. In Section 4, we provide a discussion on the applicability, limitations and possible future work for further optimization of the framework before we draw conclusions in Section 5.

2. Proposed archetype framework

We propose a hierarchical archetype modeling and calibration framework using a statistical formulation to describe the correlation between buildings that share the same archetype classification, as depicted in Fig. 1. At the archetype level, it is assumed that the buildings in the archetype exhibit exchangeable properties, meaning they can be seen as a sequence of exchangeable random variables sharing an underlying distribution function – i.e. a shared archetype description. Uncertain parameters at both building level and archetype level are then calibrated using measured energy use time series from training buildings at the building level

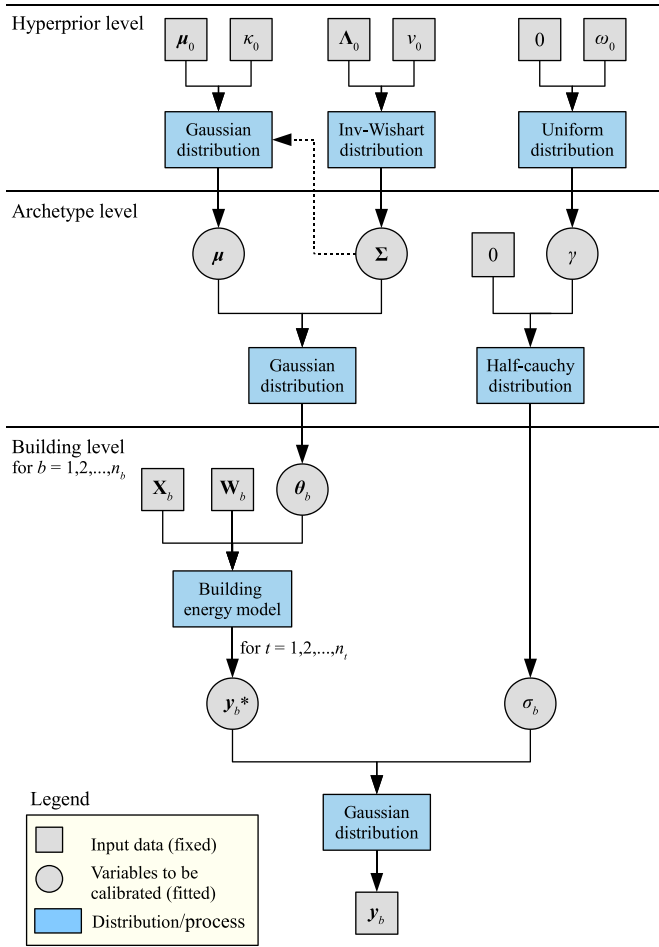


Fig. 1. Statistical representation of hierarchical framework.

in a Bayesian setting. This allows for user-specified prior information about their values to be taken into account at hyperprior level. The following sections describe the procedures of the framework in detail.

2.1. Building-level formulation

First, consider a building for which we observe a time series $\mathbf{y} = [y_1, y_2, \dots, y_{n_t}]^T$ of its energy use. We model the building using a physics-based building energy model (BEM), which we use to create a vector of n_t simulation outputs $\mathbf{y}^* = [y_1^*, y_2^*, \dots, y_{n_t}^*]^T$ matching the vector of observed data \mathbf{y} . The relation between observed and simulated energy use can be described as:

$$\mathbf{y} = \mathbf{y}^* + \boldsymbol{\varepsilon}, \quad (1a)$$

$$\mathbf{y}^* = \mathcal{M}(\mathbf{X}, \mathbf{W}, \boldsymbol{\theta}), \quad (1b)$$

$$\boldsymbol{\varepsilon} \sim \mathcal{N}(\mathbf{0}, \sigma^2 \mathbf{I}), \quad (1c)$$

where $\mathcal{M}(\mathbf{X}, \mathbf{W}, \boldsymbol{\theta})$ denotes the BEM evaluated on a matrix $\mathbf{X} \in \mathbb{R}^{n_t \times n_x}$ of observed and/or fixed building-specific input parameters, a matrix $\mathbf{W} \in \mathbb{R}^{n_t \times n_w}$ of relevant weather measurements, and a vector $\boldsymbol{\theta} = [\theta_1, \theta_2, \dots, \theta_{n_\theta}]^T \in \mathbb{R}^{n_\theta \times 1}$ of unknown parameters that we want to tune. The error-term $\boldsymbol{\varepsilon} = [\varepsilon_1, \varepsilon_2, \dots, \varepsilon_{n_t}]^T \in \mathbb{R}^{n_t \times 1}$ holds any residual variation between observations and simulations that cannot be decomposed as well as observation errors. We assume the errors to be independent and identical (i.i.d.) Gaussian

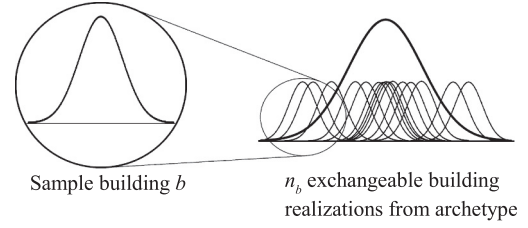


Fig. 2. Conceptual idea of archetype building realizations.

distributed and to exhibit homoscedasticity across time t such that $\text{var}(\varepsilon_t) = \sigma^2 \forall t$.

2.2. Archetype-level formulation

Now, consider $b = 1, 2, \dots, n_b$ buildings as described in Section 2.1, each of which we assume to be i.i.d. realizations from a single archetype building (Fig. 2). Once again, we underline that the process of segmenting building stocks and defining archetypes is not in focus here; we expect the modeler to have gone through this classification process already. For the archetype, we do not presume the sample buildings to be indistinguishable from each other, but whatever difference there is, it is due to random variation around a central archetype building.

For these n_b buildings, we employ a two-stage hierarchical formulation on the relationship between the exchangeable building datasets (Fig. 1). Formally, the first stage of the hierarchy – the building level – reparametrizes the abovementioned data model (1a)–(1c) using b to index individual buildings:

$$\mathbf{y}_b \sim \mathcal{N}(\mathbf{y}_b^*, \sigma_b^2 \mathbf{I}), \quad b = 1, 2, \dots, n_b. \quad (2)$$

We model the observed data \mathbf{y}_b of the b th building as a sample from the corresponding simulated data \mathbf{y}_b^* with i.i.d. random noise across time to account for residual error. The second stage of the hierarchy – the archetype level – defines the link between the n_b sample buildings, i.e. the interconnectivity of the unknown building-level calibration parameters $\boldsymbol{\theta}_b$:

$$\boldsymbol{\theta}_b \sim \mathcal{N}(\boldsymbol{\mu}, \boldsymbol{\Sigma}), \quad b = 1, 2, \dots, n_b. \quad (3)$$

In (3), the vector of n_θ calibration parameters $\boldsymbol{\theta}_b$ of the b th building is taken to be an i.i.d. sample from a multivariate Gaussian distribution with an unknown but shared vector of archetype mean parameters $\boldsymbol{\mu} \in \mathbb{R}^{1 \times n_\theta}$ and unknown covariance matrix $\boldsymbol{\Sigma} \in \mathbb{R}^{n_\theta \times n_\theta}$ describing the variance of the calibration parameters across buildings and their internal correlation. It can be necessary to constrain or augment the calibration parameters $\boldsymbol{\theta}$ to ensure a realistic sampling distribution; for example, U-values, ventilation rates, thermal masses, etc. are all constrained to the positive domain only. By initially log transforming such calibration parameters, physical boundedness is ensured.

Moreover, in the second stage of the hierarchy, we employ an archetype-level formulation for the unknown standard deviation σ_b of the building-specific error vector $\boldsymbol{\varepsilon}_b$ to help pool the individual building estimates towards a common shared estimate. This is particularly useful for buildings with less well-behaved datasets, i.e. for datasets where unusual occupancy patterns, among other things, would otherwise result in larger errors and thereby hinder inference about the calibration parameters. The application of the half-Cauchy⁺ distribution (4) is a weakly informative choice for the distribution of the σ_b s that is centered on zero with a heavy tail towards infinity governed by the scale parameter γ [25]:

$$\sigma_b \sim \text{halfCauchy}^+(0, \gamma), \quad b = 1, 2, \dots, n_b. \quad (4)$$

For individual building datasets obtained using the same data collection methods and under similar general conditions, the employment of a hierarchical pooling of the error standard deviations

σ_b seems reasonable. However, in many cases, the unpredictable and stochastic nature of occupancy may preclude the assumption of exchangeable error-terms across buildings. In such cases, we might abandon the hierarchical pooling (4) in favor of separate building estimates.

2.3. Calibrating archetype parameters

The hierarchical structure describes a combined sampling distribution for the data $\mathbf{y}_{1:n_b}$. However, for the purpose of parameter calibration, we are more interested in viewing the model as a function of the data. The *likelihood* formally sums up all the data as a function of the free, i.e. unknown, parameters of the statistical model and hence describes the plausibility (probability density) of proposed parameter values given the data. The likelihood of the b th building dataset containing $t = 1, 2, \dots, n_t$ data points is a Gaussian probability density function due to the assumption of Gaussian distributed errors (1c):

$$p(\mathbf{y}_b | \boldsymbol{\theta}_b, \sigma_b) = \frac{1}{(2\pi\sigma_b)^{n_t/2}} e^{\left\{ -\frac{1}{2\sigma_b^2} \sum_{t=1}^{n_t} (y_{b,t} - y_{b,t}^*)^2 \right\}}, \quad (5a)$$

The simulated data \mathbf{y}_b^* is obtained through the BEM (1b), which is only a function of $\boldsymbol{\theta}_b$ since we consider the observed input parameters of \mathbf{X} and \mathbf{W} to be fixed. Implementing the full hierarchical structure to fit the entire dataset of $b = 1, 2, \dots, n_b$ buildings, the combined data likelihood, conditional on the hierarchical model, becomes the product of n_b Gaussian likelihoods:

$$p(\mathbf{y}_{1:n_b} | \boldsymbol{\theta}_{1:n_b}, \sigma_{1:n_b}) = \prod_{b=1}^{n_b} \frac{1}{(2\pi\sigma_b)^{n_t/2}} e^{\left\{ -\frac{1}{2\sigma_b^2} \sum_{t=1}^{n_t} (y_{b,t} - y_{b,t}^*)^2 \right\}}. \quad (5b)$$

The likelihood function only describes the dependence of the data on the immediate data-level parameters. However, as we are not specifically interested in these quantities, but more in the archetype-level parameters $\boldsymbol{\mu}$, $\boldsymbol{\Sigma}$, γ that indirectly affect the data through the hierarchical structure, we thus expand the likelihood function by multiplying the immediate data-level likelihood (5b) with the probability density of the building-level parameters ((3)–(4)) to obtain what we could call the joint likelihood function:

$$p(\mathbf{y}_{1:n_b} | \boldsymbol{\mu}, \boldsymbol{\Sigma}, \gamma) = p(\mathbf{y}_{1:n_b} | \boldsymbol{\theta}_{1:n_b}, \sigma_{1:n_b}) p(\boldsymbol{\theta}_{1:n_b} | \boldsymbol{\mu}, \boldsymbol{\Sigma}) p(\sigma_{1:n_b} | \gamma). \quad (6)$$

From the left-hand-side of (6), it is now evident that we do not need to consider the values of individual building-level parameters to draw an inference about the archetype-level parameters as the conditional dependency is accounted for. To infer the values of the unknown archetype-level parameters $\boldsymbol{\mu}$, $\boldsymbol{\Sigma}$, γ , we could apply the method of maximum likelihood (ML) estimation to approximate the *most likely* values (point estimates) given the data. However, as the ML estimate may be seen as a special case of the Bayesian maximum a-posteriori probability (MAP) estimate that allows for a more thorough treatment of uncertainties, we apply the more general Bayesian approach here [26]. In a Bayesian context, the *true*, i.e. calibrated, parameter distributions *after* seeing the data are referred to as posterior distributions following Bayes theorem. The posterior probability density of the parameters in the context of this model is:

$$p(\boldsymbol{\mu}, \boldsymbol{\Sigma}, \gamma | \mathbf{y}_{1:n_b}) \propto p(\mathbf{y}_{1:n_b} | \boldsymbol{\mu}, \boldsymbol{\Sigma}, \gamma) p(\boldsymbol{\mu}, \boldsymbol{\Sigma}, \gamma), \quad (7)$$

where $p(\boldsymbol{\mu}, \boldsymbol{\Sigma}, \gamma | \mathbf{y}_{1:n_b})$ is the joint posterior density of the archetype-level parameters conditional on the data, $p(\mathbf{y}_{1:n_b} | \boldsymbol{\mu}, \boldsymbol{\Sigma}, \gamma)$ is the joint data likelihood conditional on the model and parameters as given in (6), and $p(\boldsymbol{\mu}, \boldsymbol{\Sigma}, \gamma)$ is the

joint prior density of the archetype-level parameters. To fulfill the hierarchical model formulation in a Bayesian context, we thus need to specify prior PDFs that reflect our subjective beliefs about the unknown archetype-level parameters *before* seeing the data – illustrated as the hyperprior level in Fig. 1. Different options of priors are available for the mean $\boldsymbol{\mu}$ and covariance $\boldsymbol{\Sigma}$ of the multivariate normal distribution of the $\boldsymbol{\theta}_b$ s (3); we make the convenient choice of using the conjugated prior – the normal-inverse-Wishart distribution [26] – that ensures the posterior to be multivariate normal as well:

$$\boldsymbol{\Sigma} \sim \text{InvWishart}(\boldsymbol{\Lambda}_0^{-1}, \nu_0), \quad (8a)$$

$$\boldsymbol{\mu} | \boldsymbol{\Sigma} \sim \text{N}(\boldsymbol{\mu}_0, \boldsymbol{\Sigma} / \kappa_0), \quad (8b)$$

$$\gamma \sim \text{U}(0, \omega_0), \quad (8c)$$

where the parameters ν_0 and $\boldsymbol{\Lambda}_0$ represent the degrees of freedom and the scale matrix, respectively, of the inverse-Wishart distribution on $\boldsymbol{\Sigma}$, and the parameters $\boldsymbol{\mu}_0$ and κ_0 represent the prior mean vector and the number of prior observations on the $\boldsymbol{\Sigma}$ scale. Setting $\nu_0 = n_\theta + 1$ and $\boldsymbol{\Lambda}_0 = \mathbf{I}$ (identity matrix) results in a weakly informative prior where each correlation parameter in $\boldsymbol{\Sigma}$ has a marginal uniform prior distribution. Likewise, setting κ_0 to a low number, e.g. 1–10 depending on the number of building datasets n_b being modeled, results in less weight being given to the chosen prior mean values $\boldsymbol{\mu}_0$. For the scale γ of the half-Cauchy distribution (4) that controls the level of pooling of the building-specific error standard deviations σ_b , we apply a uniform prior distribution constrained to the positive domain (8c). Setting ω_0 to a high number relative to the scale of the data ensures a data-driven inference [25].

Employing a straightforward Markov chain Monte Carlo (MCMC) algorithm, e.g. the Metropolis-Hastings algorithm [25], can simulate the joint posterior distribution of the model, and subsequently, the marginal posterior distributions of the individual parameters. We can address the inferred values of calibrated parameters in terms of either the individual MAP estimates, or by using the full posterior probability distribution, effectively retaining all model uncertainty.

Employing an MCMC algorithm to make inferences about the uncertain parameters (inferring their posterior distribution) requires the evaluation of the joint data likelihood (6) and prior distributions (8a)–(8c) thousands of times. Evaluating the likelihood of a given parameter proposal easily becomes computationally inconvenient and even practically impossible for larger datasets, i.e. many buildings and/or many time series data points. This is due to the small probabilities that arise, which often cause numerical instability. The widespread approach of using log-probabilities is therefore strongly encouraged to improve both numerical stability and accuracy (stability is ensured for small probabilities), as well as computational speed (addition in the log-domain is less expensive than multiplication in the arithmetic domain).

2.4. Predictive performance

As is typical in Bayesian data analysis, predictions/forecasts from the hierarchical model are based on the posterior predictive distribution of the parameter of interest, e.g. the predictive distribution of an energy use time series $p_{\text{pred}}(\mathbf{y})$. We hereby aim to report inferences about future predictions of building energy use in such a way that the full uncertainty over \mathbf{y} from all layers of the hierarchical model is accounted for throughout the analysis.

We can easily forecast energy use time series from the existing $b = 1, 2, \dots, n_b$ buildings used to calibrate the archetype by generating random draws from the posterior distributions of the trained

Table 1
Archetype classification applied in demonstration case study.

Segmentation parameter	Value
Usage/Type	Detached single-family house
Construction period	1950–1959
Location	Aarhus, Denmark
Number of stories above ground	1
Basement	No
Attic utilized for living	No
Heating source	District heating (space heating and DHW)
Suppl. heating installations	No

building-specific calibration parameters $p_{\text{post}}(\theta_b)$ and subsequently apply these in the BEM (1b) with existing or forecasted weather conditions to generate $y_b | X_b, W_{\text{new}}, \theta_b$. In general, however, we are more interested in predicting the consumption of other buildings than those used to calibrate the archetype, i.e. we want to predict the performance y_{new} for a new set of building-specific parameters X_{new} . In this case, we have no posterior distribution of the calibration parameters. Instead, we sample the parameters from their predictive distribution, i.e. the archetype posterior distributions of the calibration parameters:

$$p_{\text{pred}}(\theta_{\text{new}}) = N(\mu_{\text{post}}, \Sigma_{\text{post}}). \quad (9)$$

We then apply the BEM (1b) to generate predictions $y_{\text{new}} | \theta_{\text{new}}, W, X_{\text{new}}$ for new buildings using random draws from $p_{\text{pred}}(\theta_{\text{new}})$ in combination with the fixed building-specific parameters X_{new} and existing or forecasted weather conditions as input. Repeating this sampling many times allows us to construct an empirical distribution of the posterior predictive space of time series predictions $p_{\text{pred}}(y_{\text{new}} | \theta_{\text{new}}, W, X_{\text{new}})$ for that specific building and those weather conditions.

3. Demonstration: Danish detached single-family dwellings from the 1950s

In this section, we demonstrate how energy use time series data from a limited number of clustered training buildings can be used for identifying a shared archetype model using the archetype calibration framework described in Section 2. We do not focus on the clustering process itself, i.e. the archetype definition and classification, but rather on quantifying the embedded variability (heterogeneity) in an arbitrary archetype definition selected for the purpose of this case study demonstration, and how this archetype model may be used for prediction. The predictive capabilities of the calibrated archetype are validated against each individual training building on a new holdout validation period (within-sample prediction), and against new unseen test buildings that have not been used for training the archetype (out-of-sample prediction).

3.1. Archetype classification and case data

An archetype was defined covering Danish one-storied detached single-family dwellings constructed in the 1950s (full archetype classification given in Table 1).

3.1.1. Building data

A publicly available database containing building and property characteristics for the Danish building stock – the Building and Dwelling Register (BDR) – was used to identify buildings matching the archetype definition. We filtered the BDR information on the entire residential building stock of Aarhus, Denmark (approx. 80,000 buildings) using the segmentation parameters in Table 1. A pool of 2,775 buildings matching the archetype description was obtained. Of these 2,775 potential archetype buildings, we randomly selected 50 training buildings for the purpose of archetype

calibration, and an additional 100 test buildings for archetype performance testing (out-of-sample validation). Besides the segmentation parameters listed in Table 1, the only additional parameter from the BDR database used for setting up the building energy model was the “heated floor area”.

3.1.2. Time series of building energy use

The local district heating supplier, AffaldVarme Aarhus, supplies most of the city of Aarhus with heat for hydronic space heating and/or on-site domestic hot water (DHW) preparation through its underground distribution system. They began the replacement of their old heat meters with new modern smart meters (Kampstrup Multical® heat meters) in all of its consumer units throughout the city in 2015 and finished in 2017. The accumulated district heating consumption of each building is now digitally read off its smart meter once every hour using a remote reading system and logged by the utility in truncated kWh (an actual consumption of 6,529,999 kWh is reported as 6,529 kWh). No energy is “lost” during the meter reading process though; only the precise temporal fixation of the decimals on individual hourly readings remains unaccounted for. Consequently, minor parts of the energy consumption may be shifted one or two hours forward in time. We were given access to these hourly logged time series readings from the 150 archetype buildings for the purpose of this study. All data was subsequently anonymized.

The reading uncertainty was negligible for the large accumulated meter values, but it was substantial for the hourly differences that were in the order of 0 kWh to 5 kWh (difference between two successive accumulated hourly readings). The reading uncertainty (0 kWh ≤ reading uncertainty < 1 kWh) could potentially amount to as much as 100% of the hourly values in hours with low or no consumption and thus hinder an efficient identification of uncertain building parameters. The effect of reading uncertainty is reduced by reducing the temporal resolution of the data from hourly values into e.g. 2-hourly, 3-hourly, 6-hourly, or 12-hourly values, etc. but at the cost of data resolution, and consequently, the ability to account for model dynamics [24]. We made a compromise and aggregated all hourly values into 3-hourly values (difference between every third accumulated meter reading).

3.1.3. Weather data

A weather file was compiled from hourly measured values of air temperature and global horizontal irradiance from a local weather station in the city of Aarhus located within a 15 km radius from all training buildings.

3.1.4. Training and validation data periods

To identify the thermodynamic behavior and characteristics of a building, one needs response data captured during transient conditions that excite the dynamics of the building sufficiently [27]. Although we selected training and validation periods (Table 2) in which external loads varied substantially (−9 °C < outdoor air temperature < +9 °C), we had no prior knowledge about variations in internal loads, nor the actual heating set points. Therefore, estimates of the dynamic properties remain subject to a high degree of uncertainty.

All building datasets were initially scrutinized for missing energy use data in the training and validation periods. Buildings with missing data in this two-month period were not accepted in the analysis, but instead replaced with a new, randomly sampled building from the city with associated district heating readings in accordance with the archetype classification (Table 1). This was also the case for buildings with erroneous BDR data, i.e. a “negative” or “zero” heated area, and for buildings missing construction year.

Table 2
Size and temporal resolution of data.

	Training buildings (within-sample)	Test buildings (out-of-sample)
Sample size, n_b	50 buildings	100 buildings
Training period	1.1.2017–31.1.2017 ($n_t = 248$ 3-hourly values)	Out-of-sample buildings are not trained
Validation period	1.2.2017–29.2.2017 ($n_t = 248$ 3-hourly values)	1.2.2017–29.2.2017 ($n_t = 224$ 3-hourly values)

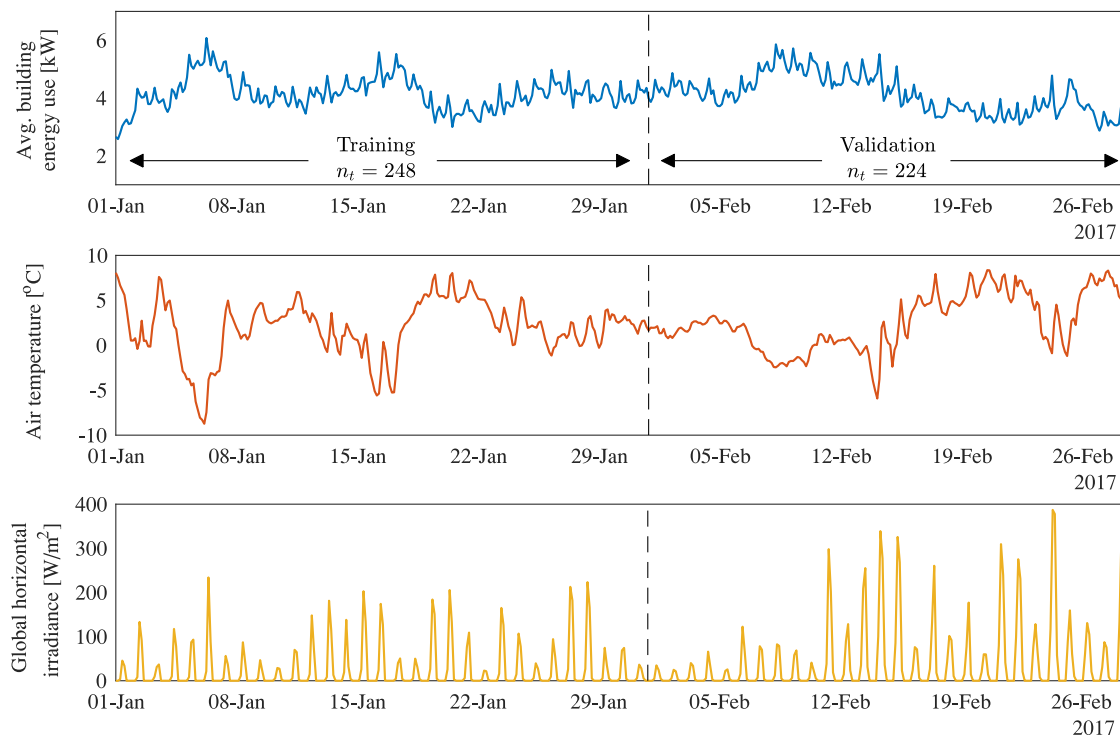


Fig. 3. Measured time series data. Top: Averaged building energy use for all $n_b = 50$ within-sample training buildings. Middle: Outdoor air temperature. Bottom: Global horizontal irradiance. Only data from the training period was used for calibration.

The averaged energy use time series from all $n_b = 50$ training buildings along with corresponding weather data (air temperature and global horizontal irradiance) are shown in Fig. 3 for the training and validation periods.

3.2. Building energy model

The hourly measured district heating energy use (Φ_{DH}) was modeled using two separate models; one for space heating (Φ_{SH}) and one for DHW (Φ_{DHW}), which were subsequently added so that $\Phi_{DH} = \Phi_{SH} + \Phi_{DHW}$. The following sections explain the models for Φ_{SH} and Φ_{DHW} in detail.

3.2.1. Building geometry

The actual and detailed geometric layout of the individual buildings was unknown. We therefore applied a general and scalable geometric representation to be used for all buildings, similar to what was used in Kristensen et al. [22]. The geometric layout consisted of a rectangular box (Fig. 4) with dimensions based on simple rules applied to known information about the floor area (information from BDR), our a-priori beliefs about the length-to-width-ratio (LWR), and the floor height of a typical SFH (Table 3).

The building facades were assumed to face the four cardinal directions. As the total window area was unknown, and because all buildings varied in size, we modeled the total window area as a scalable proportion of the floor area (window-to-floor ratio, WFR). Moreover, we fixed the partitioning of the total window area on the four facades following Danish standard calculation pro-

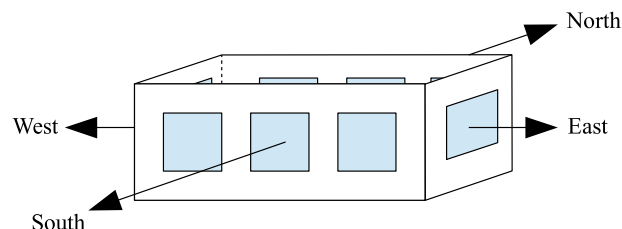


Fig. 4. Geometric model of archetype building.

cedures (North = 26%; South = 41%; East/West = 16.5%) for single-family dwellings [28].

3.2.2. Space heating

Energy use for space heating Φ_{SH} was modeled using a slightly modified version of the hourly dynamic calculation method described in ISO 13790:2008 (Fig. 5). The building was treated as a single thermal zone and the thermal inertia of the building was accounted for by modeling thermal resistances and the effective thermal capacity, as well as the internal and solar heat gains in an equivalent three-node resistance capacitance network (5R1C). The supply air temperature of the ventilation was assumed identical to the external air temperature as the ventilation principle of Danish dwellings from the construction period of the archetype usually is natural ventilation, i.e. infiltration, manual opening of windows, window valves.

Table 3

List of user-specified values for 20 uncertain model input parameters. The top 10 most influential parameters were identified using the Morris sensitivity screening method [29], assuming a uniformly distributed prior data range (max/min).

Uncertain model parameter	Sensitivity analysis			Selected value
	Min. value	Max. value	Result (top 10) *	
<i>Geometry</i>				
Length-width ratio, LWR [-]	0.10	1.00	X	0.50
Room height, h_{room} [m]	2.30	3.00		2.60
Window-floor ratio, WFR [-]	0.10	0.50	X	Calibrated
Window frame fraction, f_{frame} [-]	0.10	0.50		0.25
<i>Transmission</i>				
Temp. adjustment factor (ground), b_{ground} [-]	0.50	1.00		0.70
U -value (floors) [W/(m ² K)]	0.10	0.50	X	0.30
U -value (walls/roof) [W/(m ² K)]	0.10	0.50	X	Calibrated
U -value (windows) [W/(m ² K)]	1.00	5.00	X	1.60
Solar heat gain coef., $SHGC$ [-]	0.50	0.70		0.60
Capacity of thermal mass, C_m [kJ]/(m ² K)]	50	600	X	Calibrated
Effective mass area, A_m [m ² /m ²]	3.00	5.00		2.5–3.5**
Heat conduction (mass) [W/(m ² K)]	8.50	10.00		9.10**
Heat transfer coef. (surf.-air) [W/(m ² K)]	2.00	5.00		3.45**
<i>Ventilation</i>				
Infiltration airflow, $q_{inf@50 Pa}$ [l/s/m ²]	0.10	8.00	X	Calibrated
Design airflow (nat. ventilation), q_{vent} [l/s/m ²]	0.10	2.00	X	0.30
<i>Occupation</i>				
Occupant density, $Occ.Density$ [m ² /pers.]	10	150	X	Calibrated
Room heating set point, $T_{set,H}$ [°C]	18.0	25.0	X	21.5
<i>Domestic hot water</i>				
DHW flow temperature, T_{DHW} [°C]	40.0	60.0		55.0
Mains temperature, T_{mains} [°C]	5.0	15.0		10.0
Hot water consumption, V_{occ} [m ³ /pers./year]	10	20		15

*Top 10 most influential parameters according to the Morris method [29].

**Parameter values are defined in ISO 13790:2008.

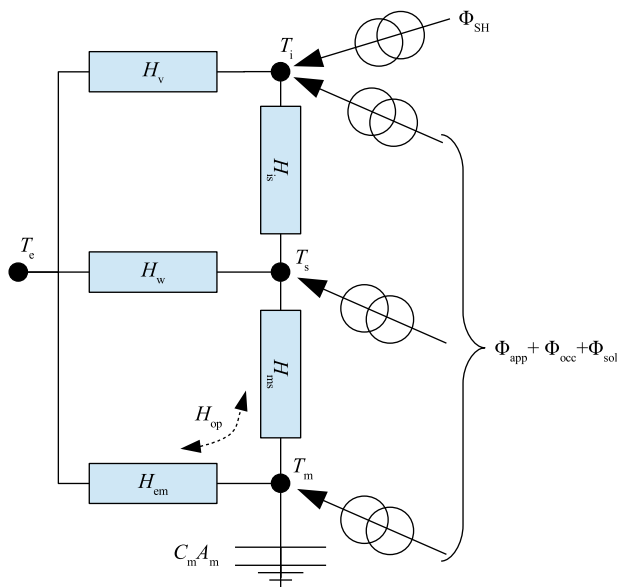


Fig. 5. Space heating model. Modified version of the network presented in ISO 13790:2008. The area of the building elements A is used to transform resistances R into heat transfer coefficients $H = A/R$.

The space heating model (Fig. 5) contains three internal temperature nodes: room air temperature T_i , surface temperature of the thermal mass T_s , and internal temperature of the thermal mass T_m . The nodes are interconnected by three heat transfer coefficients describing the building elements (opaque envelope ele-

ments H_{op} , windows H_w , and ventilation H_v) and two coefficients describing the heat transfer between the indoor air, indoor surfaces, and thermal mass (H_{is} and H_{ms}). Finally, the thermal mass of the building is governed by the capacity C_m . Several of the parameters, e.g. T_s , T_m , and H_{em} , only exist as provisional values in the algorithm of the ISO 13790:2008 calculation method and thus did not need any prescribed value. Other parameters, mainly heat transfer coefficients between building elements, are defined in the standard. User-specified inputs were necessary for the remaining building-specific parameters. As no information was available about U -values, $SHGC$, ventilation airflows, etc., their values were based on the Danish building code in force at the time of construction, historical surveys of the Danish building stock, and our a-priori beliefs (Table 3). Ventilation was assumed a mix of infiltration and opening of windows; no mechanical ventilation was modeled. Based on studies by Rijal et al. [30], the airflow through windows was modeled hourly as a percentage of maximum design airflow using a logistic regression on the outdoor temperature T_e :

$$p_{airflow} = \frac{e^{(0.25T_e - 0.25)}}{1 + e^{(0.25T_e - 0.25)}} \quad (10)$$

The RC network (Fig. 5) is exposed to external boundary conditions in terms of the outdoor air temperature T_e , solar radiation Φ_{sol} , internal heat loads from equipment/lighting Φ_{app} , occupants Φ_{occ} , and space heating Φ_{SH} delivered from the district heating system. Outdoor air temperature T_e and solar irradiation Φ_{sol} were specified using measured weather conditions (Section 0; Fig. 3). The hourly average of Φ_{app} was estimated using a regression model based on statistical data of annual electricity consump-

tion in Danish detached single-family dwellings [31] as follows:

$$\Phi_{app} = \frac{530 \frac{\text{kWh}}{\text{year}} + A_{\text{floor}} 12 \frac{\text{kWh}}{\text{m}^2 \text{year}} + n_{\text{occ}} 690 \frac{\text{kWh}}{\text{pers. year}}}{8760 \frac{\text{h}}{\text{year}}} \quad (11)$$

The heat load from occupants was modeled as the sensible heat load of an average person living in the building (both children and adults):

$$\Phi_{occ} = 80 \frac{\text{W}}{\text{pers.}} n_{\text{occ.}} \quad (12)$$

Schedules for internal loads Φ_{app} and Φ_{occ} were assumed fixed and uniform over time (flat schedules with no variation in internal loads) as no a-priori information was available to reflect the stochastic nature of user-driven phenomena across various buildings.

3.2.3. Domestic hot water

The hourly average energy use for domestic hot water preparation Φ_{DHW} was modeled using a simple linear model proportional to the amount of hot water consumed annually, under the assumption that the rate of consumption was reasonably constant throughout the year:

$$\Phi_{DHW} = \frac{4140 \frac{\text{kJ}}{\text{m}^3 \text{K}} V_{\text{occ}} n_{\text{occ}} (T_{DHW} - T_{\text{mains}})}{8760 \frac{\text{h}}{\text{year}}} \quad (13)$$

The annual hot water consumption $V_{\text{occ.}}$, number of occupants $n_{\text{occ.}}$, flow temperature T_{DHW} and mains supply temperature T_{mains} were unknown and hence based on our a-priori beliefs (Table 3). A flat schedule for DHW energy use Φ_{DHW} was applied as no a-priori information was available to reflect the stochastic nature of user-driven phenomena across various buildings.

3.3. Selecting parameters for calibration

The values of the 20 model input parameters (Table 3) were unknown for each building and thus left for us to specify based on our prior beliefs. Ideally, one ought to calibrate all uncertain parameters. In practice, doing so is infeasible – both due to the high number of parameter dimensions, but also due to the identifiability of the model parameters themselves [32]. We therefore based the selection of calibration parameters on a sensitivity analysis (SA) in which we assigned a uniform distribution to the input space of each parameter to reflect our a-priori knowledge about the archetype (Table 3). Based on recommendations by Kristensen and Petersen [33] who analyzed the performance of three different SA methods using the ISO 13790 energy calculation models, the Morris method [29] was applied to screen the uniformly distributed input space for its global effect on the model output. We applied the annually aggregated energy use from 8,760 hourly calculations as the output measure of interest as we wanted to find parameters that were important for the entire year and not only for the training and validation periods. A total of $r = 500$ trajectories (samples from the input space using the original Morris sampling technique) with $p = 5$ levels (discretization of the input space) was used to obtain a fully converged ranking of the input parameters, resulting in a total of $r(k + 1) = 10,500$ model evaluations. Fewer trajectories, and thus fewer model evaluations, could eventually prove enough for the SA; however, as less than one minute was used to perform the simulations in Matlab on a standard laptop, this was no issue. No correlations between model input parameters were taken into account in the sampling of values. The resulting sensitivity indices are plotted in Fig. 6 for a graphical interpretation.

From the results of the sensitivity screening (Fig. 6), we found that the input parameters primarily affect the output (annually

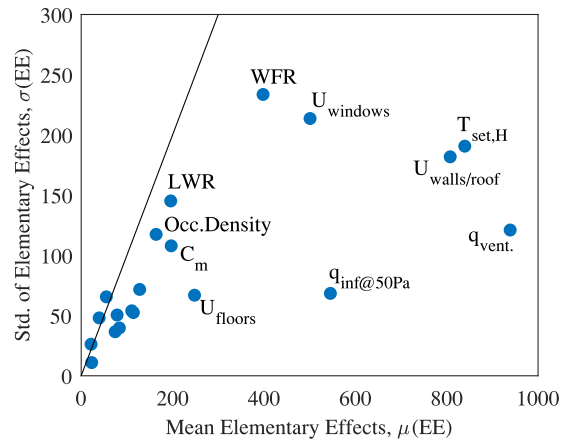


Fig. 6. Graphical presentation of the results of the Morris sensitivity analysis using $r = 500$ trajectories and $p = 5$ levels. The absolute mean elementary effects are plotted against the standard deviation of the elementary effects (20 uncertain model input parameters). The ten most influential parameters are named. The line represents values for which $\sigma(EE) = \mu(EE)$.

Table 4
Prior values selected for archetype-level hyperparameters (hyperpriors).

Hyperparameter	Prior value
μ_0	WFR [-] $U_{\text{walls/roof}}$ [W/(m ² K)] C_m [kJ/(m ² K)] $q_{\text{inf@50 Pa}}$ [l/(m ² s)] $Occ.density$ [m ² /pers.]
κ_0	0.15
Λ_0	0.50
ν_0	300
ω_0	3.50
	50
	1
	5×5 identity matrix, I
	$n_\theta + 1 = 6$
	10

aggregated energy use) through a monotonic linear relationship (indicated by $\sigma(EE)_i$ -values remaining below the dotted line in Fig. 6), which was expected from a model based on the RC model formulation of ISO 13790:2008. Studies on parameter identification using RC-models have shown that it can be difficult to identify and separate linearly related parameters in practice [32,34,35]. Five out of the ten most influential parameters identified were selected for calibration (θ) based on what we found interesting and identifiable in practice: window-floor ratio (WFR), U -value of walls/roof ($U_{\text{walls/roof}}$), internal heat capacity of the thermal mass (C_m), infiltration airflow rate @50 Pa ($q_{\text{inf@50Pa}}$), and occupant density ($Occ.Density$). The remaining 15 parameters were left uncalibrated (fixed) at the selected values (Table 3). These 15 fixed parameters were represented through **X**.

Weakly informative prior distributions were established for the archetype-level parameters μ , Σ , γ using their five hyperparameters μ_0 , κ_0 , Λ_0 , ν_0 , ω_0 for which values are given in Table 4. The resulting prior distributions of μ , Σ , γ are shown in Section 3.4 together with the inferred posterior distributions.

3.4. Calibrated (posterior) parameters

Four chains were run in parallel with randomly dispersed starting points in the parameter space to draw samples from the joint posterior distribution. For each chain, 18,000 MCMC samples were drawn with the first 14,000 samples of the chains being considered cool, meaning that information about the starting point might still prevail; samples from this cold period were thus discarded leaving only the warm part of the chains for analysis.

Convergence in the warm chains was monitored in terms of the potential scale reduction factor (PSRF), a positive rational number

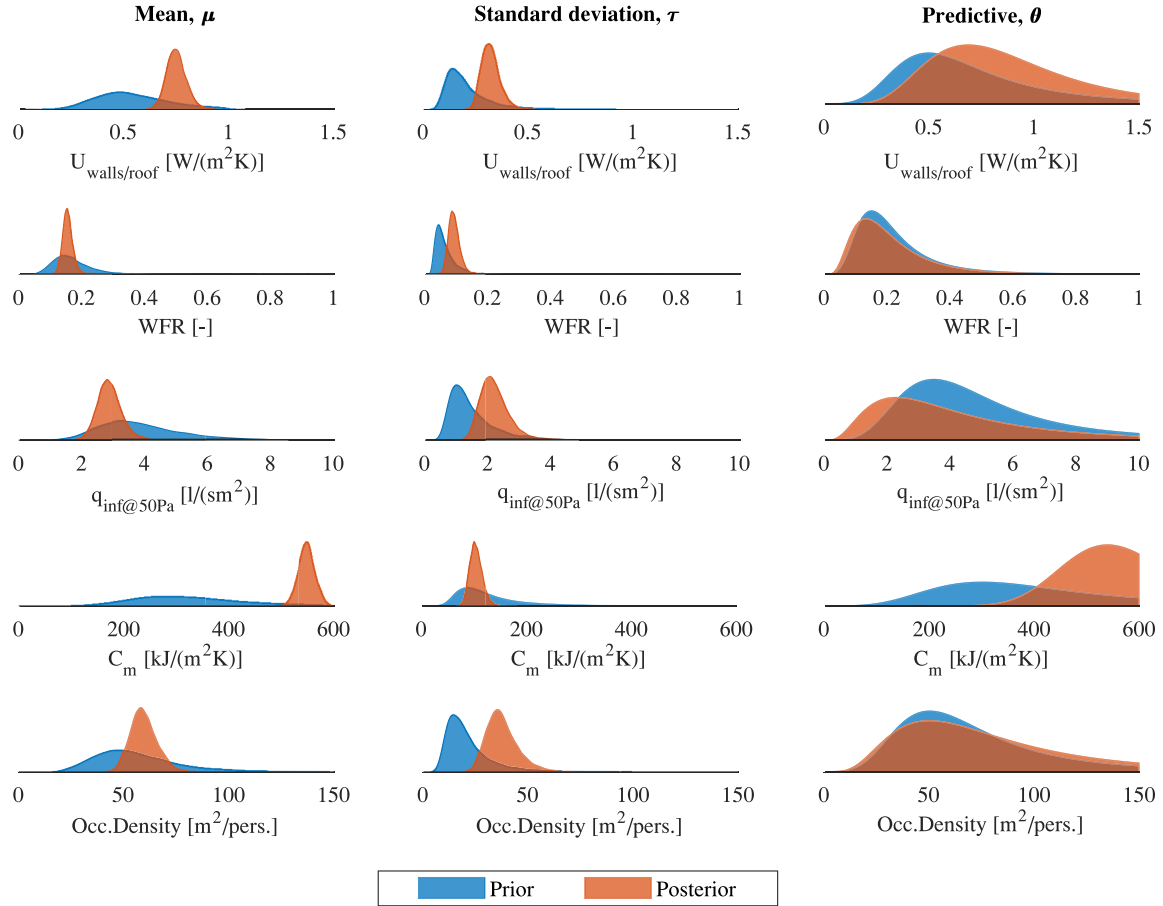


Fig. 7. Marginal prior and posterior distributions of the five archetype-level calibration parameters. The calibration parameter mean values μ are shown in the left-hand column, their decoupled standard deviations τ are shown in the middle column, and their predictive distributions are shown in the right-hand column.

$\hat{R} \in \mathbb{R} | 1 \leq \hat{R} < \infty$ [26]. The PSRF measures how much the scale of the variations in the inferred parameter distributions might have been reduced if the number of draws simulated by the MCMC-algorithm approached infinity, $\lim_{n \rightarrow \infty} (\hat{R} \rightarrow 1)$. By accounting for the within-chain to between-chain variance in the warm chains, the PSRF evaluates both the mixing and stationarity of the chains simultaneously. A stable and converged solution was considered for any given parameter estimation when $\hat{R} < 1.1$.

As it is infeasible to visualize the posterior distributions of the five calibration parameters θ for all 50 training buildings (first level of the hierarchy), we only show the shared archetype-level parameters μ, Σ, γ here (second level of the hierarchy). Furthermore, we have decomposed the covariance matrix Σ into parameter specific variance $\tau^2 = \text{var}(\theta)$ and correlation coefficients $\rho = \text{corr}(\theta)$ for the purpose of visualization. The prior and posterior distributions of the five archetype mean values μ are displayed in Fig. 7 (left-hand column), while their corresponding standard deviations τ are shown in Fig. 7 (middle column). In the right-hand column in Fig. 7, the mean and variances have been applied to draw the predictive distributions $p_{\text{pred}}(\theta_{1:n_\theta}) = N(\mu_{1:n_\theta}, \tau_{1:n_\theta}^2)$ of the five calibration parameters themselves. However, it is important to note that these predictive distributions are marginal and thus do not account for the modeled correlation ρ (Fig. 8) between the parameters, which must be taken into account through the covariance matrix Σ when predicting coherent values of the parameters $p_{\text{pred}}(\theta) = N(\mu, \Sigma)$ for new buildings.

Setting off from broad and weakly informative prior distributions, the data has successfully focused the posteriors of the means $p_{\text{post}}(\mu)$ and to some extent the standard devia-

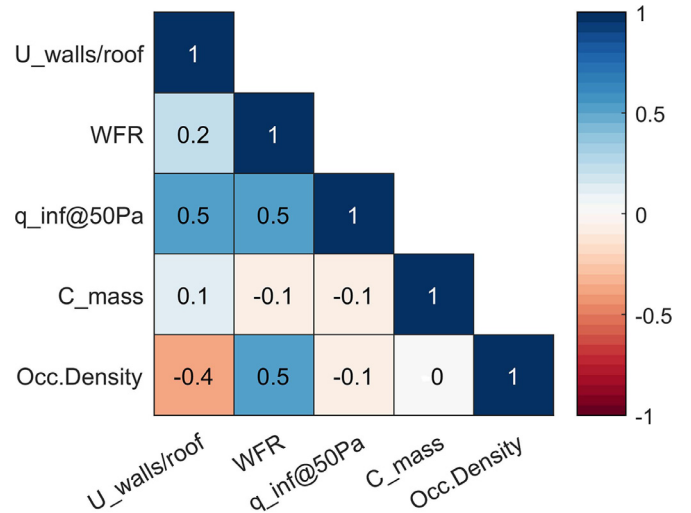


Fig. 8. Expected posterior correlation matrix, $E_{\text{post}}[\text{corr}(\theta)]$, of the five calibration parameters.

tions $p_{\text{post}}(\tau)$. The posteriors of μ_{WFR} , $\mu_{\text{qinf@50Pa}}$ and $\mu_{\text{Occ.Density}}$ are focused near the expected value of their respective priors, whereas for $\mu_{\text{U_walls/roof}}$ and $\mu_{\text{C_mass}}$, the calibration has drawn their posteriors out into the tails towards their maximum values (Table 3). Common for all five posteriors of the standard deviations $p_{\text{post}}(\tau)$ is that the distributions are weakly informative and

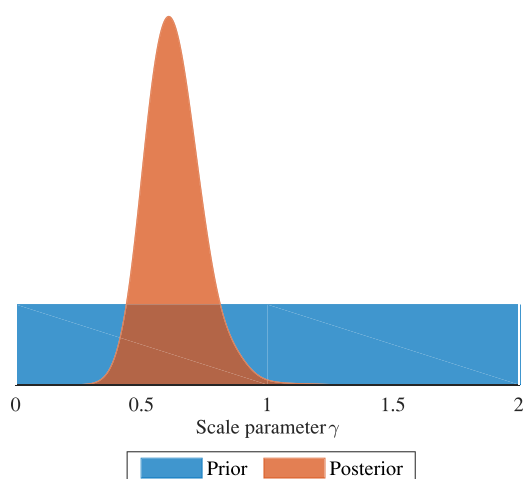


Fig. 9. Prior and posterior distribution of the archetype-level scale parameter γ that controls scale of the error-term standard deviations σ .

located relatively far away from zero. This is especially true for $\tau_{U_{\text{walls/roof}}}$, τ_{WFR} , $\tau_{\text{qinf@50Pa}}$, and $\tau_{\text{Occ.Density}}$ where the amount of uncertainty in the posteriors remains very high and overlaps with the posterior mean values $p_{\text{post}}(\boldsymbol{\mu})$. The posterior uncertainty has only been reduced for one of the standard deviation parameters: the capacity of the thermal mass $\tau_{\text{C}_{\text{mass}}}$. However, even though the uncertainty of the archetype-level parameters $\boldsymbol{\mu}$, $\boldsymbol{\tau}$ may have been reduced, it is the resulting predictive distribution of the building-level parameters $\boldsymbol{\theta}$ that is of most interest. The marginal predictive distributions of the $\boldsymbol{\theta}$ s are shown in the right-hand column in Fig. 7 using the prior and posterior archetype-level parameters, respectively. From the plot of the predictive distributions, the effect of the large standard deviations $\boldsymbol{\tau}$ is immediately evident. For several of the parameters, the priors and posteriors look alike; however, for the capacity of the thermal mass, the high posterior mean value $\mu_{\text{C}_{\text{mass}}}$ has drawn the posterior predictive distribution out to the boundary of 600 kJ/(m²K).

The expected posterior correlation matrix $E_{\text{post}}[\text{corr}(\boldsymbol{\theta})]$ is shown in Fig. 8. No strong correlations are found between the parameters, but all of the parameters are found to correlate moderately with each other (max. correlation strength=0.5), except for the capacity of the thermal mass, which does not exhibit any significant correlation with the other parameters. These correlations are inevitable as the parameters interact through the overall heat balance in every time step; e.g., increasing occupant density [m²/pers.] leads to a smaller heat gain from occupants and therefore brings the heat balance out of equilibrium. This imbalance might be corrected by decreasing the U-value (walls/roof) [W/(m²K)] and thus the heat loss through the envelope (correlation = -0.4). Another possibility could be to increase the WFR and thus the overall window area, whereby more sunlight enters the building. The correlation obviously depends on other factors also, such as overall floor area, U-value (windows), SHGC, window frame fraction, etc.

The posterior distribution for the archetype-level half-Cauchy scale parameter $p_{\text{post}}(\gamma)$ (see Eq. (4)) is displayed in Fig. 9. Since a non-informative prior distribution (uniform) was used, the posterior inference is driven by data alone.

3.5. Performance of calibrated archetype model

The performance and overall quality of the calibrated archetype model were analyzed based on its predictive capabilities on two different hierarchical levels; (1) the within-sample predictive per-

Table 5
ASHRAE Guideline 14-2014 compliance requirements.

Measure	Monthly data	Hourly data
NMBE	< ± 5%	< ± 10%
CVRMSE	< 15%	< 30%

formance for the 50 sampled training buildings, and (2) the out-of-sample predictive performance for another 100 unseen test buildings. Sample details are given in Table 2. The predictive performance was assessed on both the scale of individual buildings and on the aggregated urban scale.

Following definitions by the ASHRAE Guideline 14-2014, we employed two measures to assess the predictive performance of the calibrated building simulations; the normalized mean bias error (NMBE) and the coefficient of variation of the root mean squared error (CVRMSE):

$$\text{NMBE} = \frac{\sum_{t=1}^{n_t} (y_t - y_t^*)}{n_t} \bigg/ \bar{y} \times 100, \quad (14)$$

$$\text{CVRMSE} = \sqrt{\frac{\sum_{t=1}^{n_t} (y_t - y_t^*)^2}{n_t}} \bigg/ \bar{y} \times 100. \quad (15)$$

The ASHRAE Guideline 14-2014 compliance requirements are given in Table 5 for monthly and hourly data, respectively. As we employed 3-hourly data in this study, it seems reasonable to accept levels above the monthly requirements but somewhat below the ones for hourly data.

3.5.1. Within-sample predictive performance

The within-sample predictive performance, i.e. the ability of the model to forecast building energy use time series for the 50 known training buildings, was used to evaluate the immediate quality of fit for the sampled buildings independently and the archetype as a whole. This internal assessment of the inferred building-level parameters $\boldsymbol{\theta}$ was carried out using measured and simulated data from the training period and the holdout validation period (Table 2).

Measured and simulated data is shown in Fig. 10A for training building $b=6$. The figure displays $n_s = 1000$ time series predictions $y_6^* | \mathbf{X}_6, \mathbf{W}_{\text{train/valid}}, \boldsymbol{\theta}_6^{1:1000}$ from the BEM, each simulated using independent draws from the posterior distribution of the building-level parameters $p_{\text{post}}(\boldsymbol{\theta}_6)$, fixed building parameters \mathbf{X}_6 , and the corresponding weather data, either $\mathbf{W}_{\text{train}}$ or $\mathbf{W}_{\text{valid}}$. The fully acceptable performance of the training period generalizes well into the validation period with new weather conditions (Fig. 10A). This suggests that a representative set of parameters was estimated for the building. The performance measures (NMBE and CVRMSE) of building $b=6$ are shown together with the remaining 49 training buildings in Fig. 11 for both the training and validation period.

Values of NMBE and CVRMSE were calculated for all 50 training buildings individually for both the training and validation period (Fig. 11). Some of the buildings do not fulfill the ASHRAE Guideline 14-2014 compliance requirements for monthly data in the training period when using the expected values of NMBE and CVRMSE as points of reference, but most comply with the requirements for hourly data (one building exceeds NMBE = 10% and five buildings exceed CVRMSE = 30% in the training period). We find fairly large variations in especially the NMBE values for many buildings (error bars in Fig. 11 give the 95% confidence interval of individual measures around the mean), but for most buildings, their values reach across NMBE = 0% with 95% confidence, and all buildings have a 95% CI with values from within the NMBE < ± 5% band. One building ($b=15$) stands out as the one with the highest bias by far

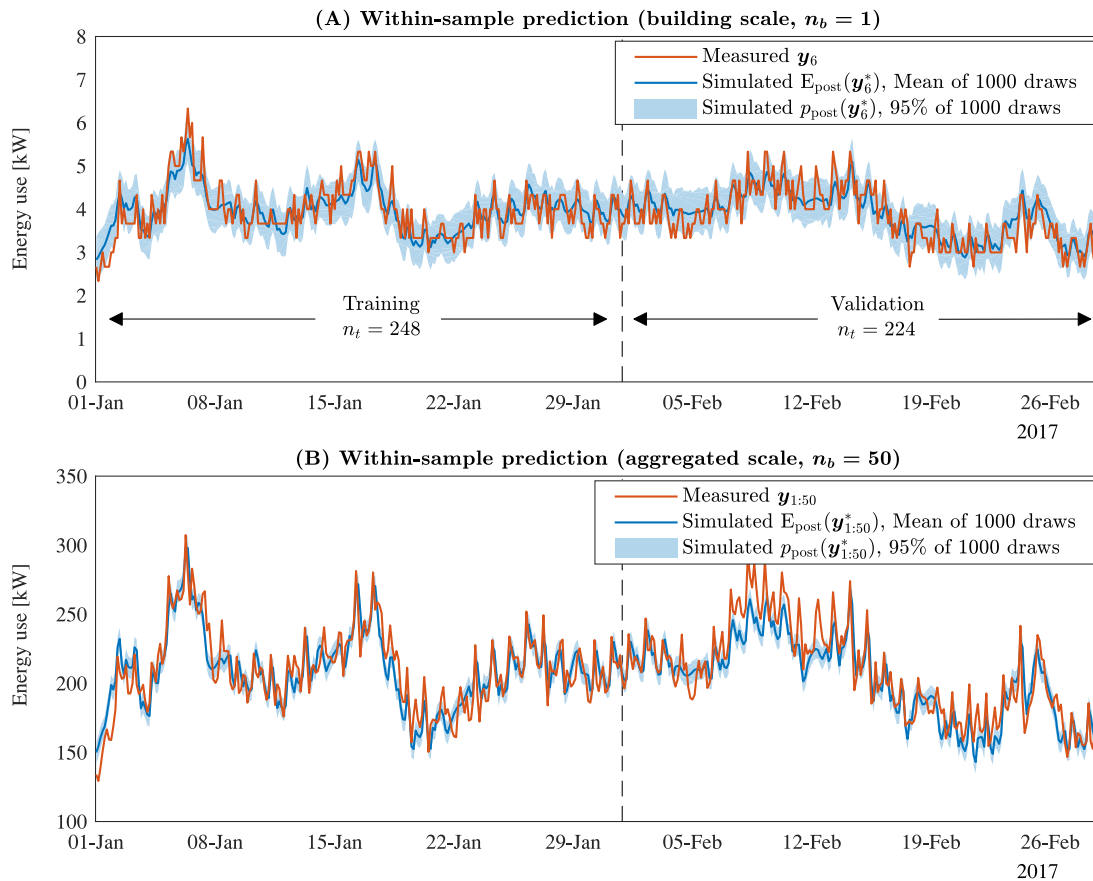


Fig. 10. Predictive performance of within-sample prediction. (A): Energy use predictions of building $b = 6$ against measured data. (B): Aggregated energy use predictions of buildings $b = 1:50$ against aggregated measured data. Simulated data was generated using 1000 draws from the posterior distribution of the calibration parameters $p_{\text{post}}(\theta_b)$, fixed parameters \mathbf{X}_b , and weather conditions for the training period $\mathbf{W}_{\text{train}}$ and validation period $\mathbf{W}_{\text{valid}}$, respectively.

in the training period: $\text{NMBE} = 7.4\% \pm 14.3\%$ (mean \pm 95% CI). Even though the building's bias is higher than that of the other buildings, we chose to not deem it an outlier as there was no reason for doing so, e.g. extraordinary oscillations in the training data, besides the relatively bad fit.

Predictions from the validation period generally perform worse than predictions from the training period as would be expected (the NMBE is often more than three times higher in the validation period for many buildings). This is most likely caused by the unpredictable nature and presence of occupants as their daily movements and presence remain unaccounted for and hence were not modeled explicitly (schedules of occupancy were assumed flat and fixed across time). This simplification create a challenge for the prediction of the validation period (February 2017) as it contains the weeklong Danish winter holiday (public schools are closed) which, in the municipality of Aarhus, took place from 10 February 2017–19 February 2017. From the aggregated time series predictions shown in Fig. 10B, it is clear that much of the bias in the validation period is located within the winter holiday period. As school holidays, bank holidays, etc. are spread across the year, we expect similar predictive performance in the remaining periods of the year. Summary statistics of the mean values of within-sample validation period performance are given in Table 6.

In addition to the building-scale performance, the within-sample predictive performance was also evaluated on the aggregated scale to represent the expected performance in an urban setting (Fig. 10B). Aggregating all 50 within-sample buildings into a single model naturally obscures much of the data variability as an aggregated model pays no regard to the fit of individual

buildings besides their contribution to the summarized consumption pattern. With an $\text{NMBE} = 3.0\% \pm 0.5\%$ (mean \pm 95% CI) and a $\text{CVRMSE} = 7.2\% \pm 0.3\%$ (mean \pm 95% CI) for the validation period, the aggregated performance is good and, as expected, much better than for most of the individual buildings (Table 6).

3.5.2. Out-of-sample predictive performance

The out-of-sample predictive performance, i.e. the ability of the model to forecast time series of energy use from unseen test buildings $\mathbf{X}_{\text{out-of-sample}}$ not used for the calibration of the archetype model, is used to evaluate the external robustness and homogeneity of the archetype calibration. However, no direct posterior estimate exists for the uncertain parameters $\theta_{\text{out-of-sample}}$ of the 100 out-of-sample test buildings to be used for simulation; instead, samples of the parameters are drawn from their posterior predictive distribution (9) that is generated using draws from the posterior distributions of the archetype-level parameters $p_{\text{post}}(\mu, \Sigma)$. As the archetype-level parameters were inferred from the combined information contained by all 50 within-sample training buildings, posterior predictions of $\theta_{\text{out-of-sample}}$ represent a generalized archetype estimate with the inherent variability and heterogeneity of the sampled training buildings.

Aggregated predictions of the 100 out-of-sample test buildings are shown in Fig. 12 against the aggregated measured data for both the training and validation periods. An $\text{NMBE} = 2.9\% \pm 6.2\%$ (mean \pm 95% CI) and a $\text{CVRMSE} = 7.8\% \pm 2.9\%$ (mean \pm 95% CI) are found for the aggregated predictions in the validation period (Table 6).

When comparing the performance of out-of-sample aggregated predictions (Fig. 12) against the performance of within-sample

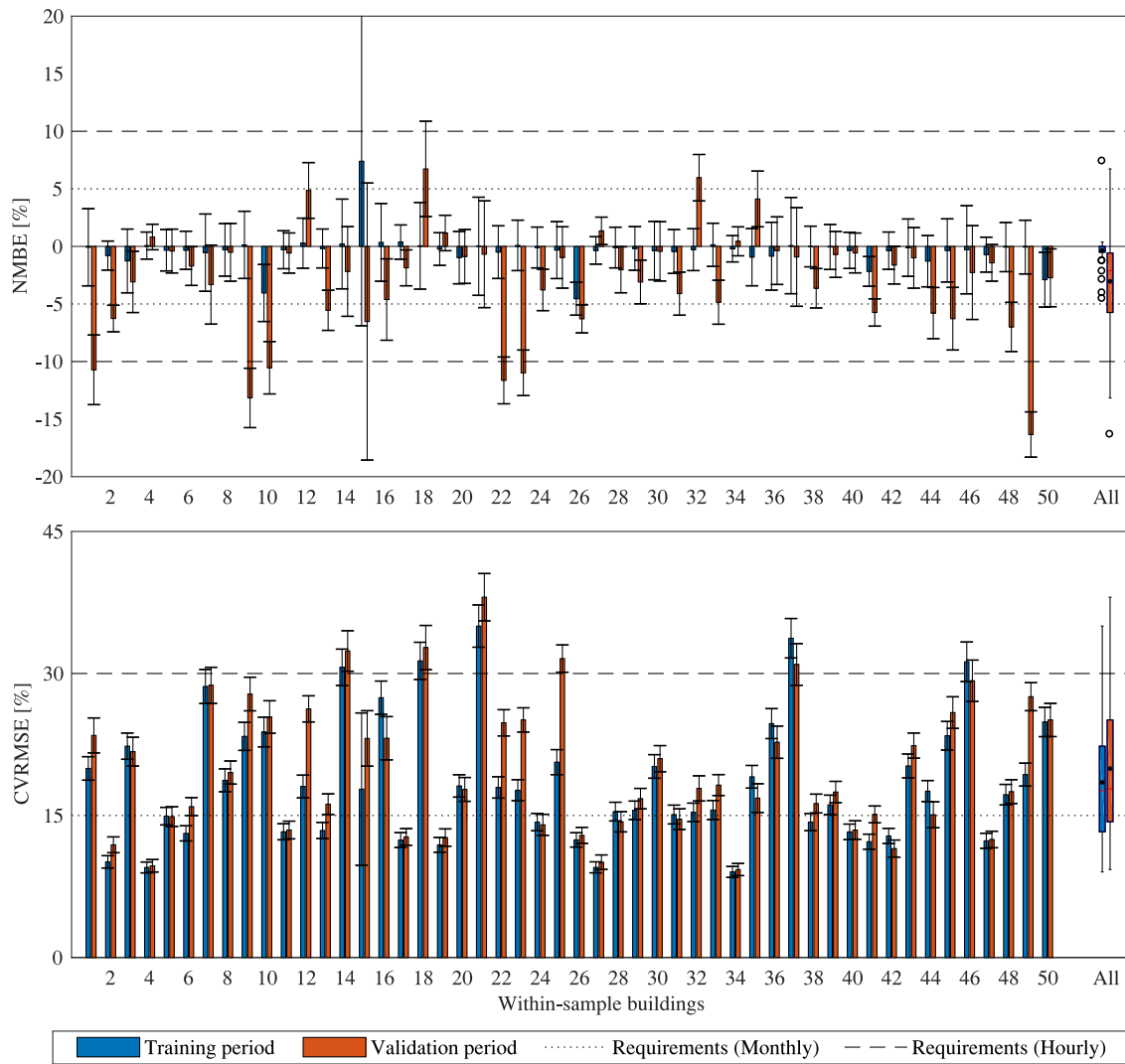


Fig. 11. Normalized mean bias error (NMBE) and coefficient of variation of the root mean squared error (CVRMSE) for the 50 within-sample buildings individually. Measures are calculated using 1000 simulations per building, each using a random draw of the calibrated parameters from their posterior distribution $p_{\text{post}}(\theta_b)$ against measured data y_b . The height of the bars gives the mean value with error bars around covering the 95% CI. The boxplots at x-value “All” comprise the distribution of mean values for all 50 buildings. ASHRAE Guideline 14-2014 compliance requirements are given for both measures.

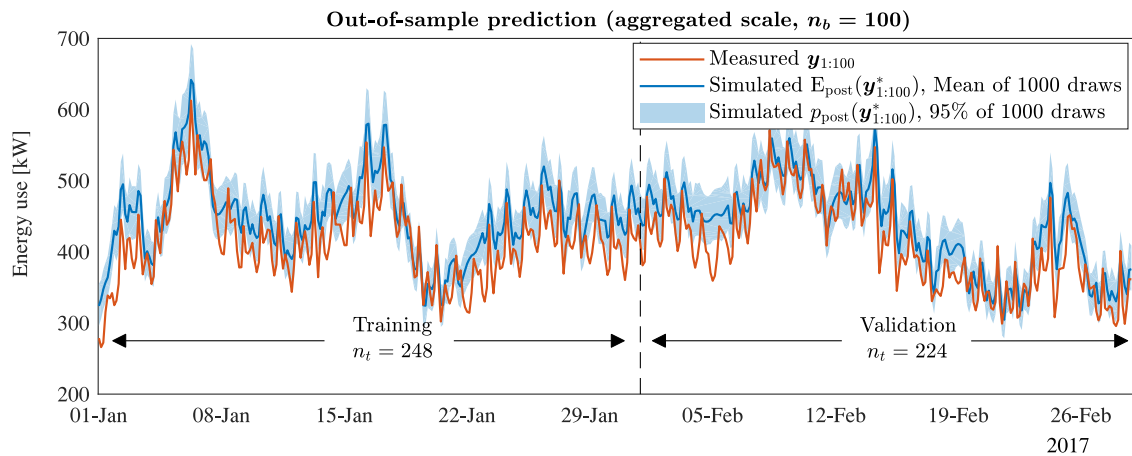


Fig. 12. Aggregated predictive performance of out-of-sample buildings $b = 51:150$ against aggregated measured data. Simulations were generated using draws from the posterior predictive distribution of calibration parameters $p_{\text{post}}(\theta_{\text{out-of-sample}}) = N(\mu, \Sigma)$.

aggregated predictions (Fig. 10B), it is evident that the aggregated out-of-sample predictions suffer from a positive bias compared to the negative bias of the within-sample predictions (2.9% vs. –3.0%). Measures of fit (mean values of NMBE and CVRMSE) for within-sample and out-of-sample predictions are summarized in Table 6 on the disaggregated scale of individual buildings and on the aggregated scale, respectively.

Out-of-sample predictions are, as expected, inferior to within-sample predictions. An insufficient ability to match measured data is seen for most out-of-sample predictions on the scale of individual buildings (95% interval of NMBEs = [–38.7% 112.9%] and CVRMSEs = [28.7% 120.1%]). This mismatch is, however, smeared out on the scale of aggregated predictions where the cancellation effect effectively reduces the differences to an acceptable level (NMBE = 2.9% and CVRMSE = 7.8%) almost identical to that of the within-sample aggregated predictions (NMBE = –3.0% and CVRMSE = 7.2%). Thus, the established archetype model can hardly be used for single-building predictions of high-resolution energy use time series from unseen buildings without considerable uncertainty. However, the results promise good performance for aggregated predictions on an urban level.

4. Discussion

4.1. Why hierarchical modeling?

The proposed archetype framework takes advantage of a hierarchical (multilevel) link between data from individual buildings. It is a generalization of the ordinary Bayesian calibration framework in which the building-specific calibration parameters θ are themselves given an archetype model – in this case the multivariate Gaussian distribution – whose parameters μ , Σ are also estimated from the data. This statistical setup has several appealing features:

- 1 Calibrating uncertain parameters without a hierarchical formulation corresponds to either inferring separate building-specific estimates [3,4,6], or a single pooled archetype estimate [12]. The more general hierarchical model allows for a reasonable compromise between these two extremes.
- 2 It allows for the modeling of the correlation within calibration parameters of the archetype. This is essential for any application that relies on drawing archetype parameter-sets of new unseen buildings.
- 3 Predictions of new unseen buildings draw on a much larger dataset that explores the variability of the archetype and should therefore be more representative.

Fitting separate building-independent estimates of the calibration parameters θ corresponds to assuming that all buildings are unique without sharing any similarities at all. Alternatively, averaging the data and fitting only a single pooled estimate correspond to the opposite case of assuming that all buildings are the same, whereby all differences are ignored. Both cases are unsatisfactory as the reality lies somewhere in between. Applying a hierarchical model allows us to fit in uncertain archetype parameters

μ using the individual building datasets while accounting for archetype heterogeneity among the buildings (represented through the variance in the covariance matrix Σ). Through the process of “shrinking”, the hierarchical model pools the individual building estimates θ towards a common archetype mean μ as a result of the archetype distribution (estimates far away from the archetype mean have very low probability under the normality assumption). Using a non-hierarchical model based on averaging of separately fitted building estimates results in a model more prone to outliers [26].

The explicit modeling of the correlation and variance between calibration parameters at the archetype level, represented through the covariance matrix Σ , allows for informed predictions of unseen buildings under the archetype. This acknowledges not only the heterogeneity of the archetype estimates (variance), but also the potential correlation $\text{corr}(\theta)$ that would otherwise be ignored.

4.2. Within-sample vs. out-of-sample predictions

The lower accuracy of individual out-of-sample building predictions (building-scale) compared to predictions of individual within-sample buildings (Table 6) is most likely a consequence of the uncertainties related to (1) archetype heterogeneity, (2) building sample size n_b , and (3) human behavior and preferences. Within-sample training buildings were all fitted building-specific values of the calibration parameters $p_{\text{post}}(\theta_{\text{within-sample}})$, whereas for out-of-sample buildings, these values were predicted from the posterior predictive distribution $p_{\text{pred}}(\theta_{\text{out-of-sample}}) = N(\mu, \Sigma)$. The posterior archetype estimates $p_{\text{post}}(\mu, \Sigma)$ can be viewed as a compromise between the characteristics of the training buildings, which inevitably will be characterized by some degree of heterogeneity. As such, the archetype model gives us an estimate of the average building, as well as an estimate of the variability that characterizes the archetype. Therefore, evaluating the performance of the archetype model's mean prediction on individual buildings will inevitably indicate a poor performance for some buildings, even if the pool of buildings used for training contained practically identical buildings. The only way of improving out-of-sample prediction performance is to eliminate the heterogeneity of the buildings belonging to the archetype by significantly tightening up the archetype definition. However, as a very tight archetype definition defeats the whole idea of simplifying the building stock into a “few” archetypes, a fairly large degree of error has to be accepted for out-of-sample predictions of single buildings. Finally, even if a very tight and homogeneous archetype definition is applied, human behavior remains a very uncertain factor with a significant effect on building energy use [36–40], which cannot be removed by tightening the archetype definition. Incorporating a stochastic model of occupancy, e.g. using an agent-based [41,42] or a Markov chain-based [43,44] approach, as opposed to the fixed and non-varying flat schedules of the demonstration case could potentially reduce much of the variability in out-of-sample predictions and help reduce archetype heterogeneity to that originating from differences in technical parameters. However, we foresee sev-

Table 6

Summary statistics of expected predictive performance for sampled training buildings (within-sample) and unseen test buildings (out-of-sample). Measures in square brackets cover the [2.5% | 50% (median) | 97.5%] percentiles, i.e. the 95% central interval of the distributions of n_b individual building means. On the aggregated scale, there is only one mean value.

Sample	Period	Buildings in sample, n_b	Predictive performance	
			Building scale	Aggregated scale
Within-sample	Validation	50	[–14.0% –2.1% 6.1%] (NMBE) [9.6% 17.8% 34.1%] (CVRMSE)	–3.0% (NMBE) 7.2% (CVRMSE)
Out-of-sample	Validation	100	[–38.7% 0.6% 112.9%] (NMBE) [28.7% 38.8% 120.1%] (CVRMSE)	2.9% (NMBE) 7.8% (CVRMSE)

eral problems with doing this, e.g. issues of over-parameterization and identifiability, but it remains to be investigated in future work.

The performance of aggregated predictions is not affected by archetype heterogeneity to the same extent as individual building-scale predictions, but is mainly controlled by uncertainty in estimating the mean parameters μ that represent an average archetype realization. The law of large numbers states that the estimated mean of a sample approaches the true mean as the number of samples goes to infinity. Here, obtaining an archetype model can be considered analogous to estimating the mean of a sample, where the archetype model would become more representative of out-of-sample buildings belonging to the archetype as the number of buildings used for training increases. The relatively small difference in aggregated performance between within-sample and out-of-sample buildings (NMBE_{within-sample} = -3.0% vs. NMBE_{out-of-sample} = 2.9%) suggests that the number of buildings n_b needed for estimating the archetype may not be much larger than the sample size used in this case study demonstration.

4.3. Parameter identification

In the demonstration of the framework, we applied a first-order 5R1C building energy model for simulating hourly heating energy use, and subsequently, for calibrating five model parameters. This model was selected for the purpose of demonstration and because of its fast computational speed. However, other model formulations may easily be applied in future applications of the framework, e.g. higher-order RC formulations or high-fidelity BEM tools such as EnergyPlus. In fact, reduced-order models may be too simple for identifying the true estimates of building characteristics [32,34,35]; nevertheless, while the obtained parameter estimates may not compare directly to reality, they give meaningful information about a building's characteristics in the context of the model. Reynders et al. [35] argue that models of at least fourth order (four thermal capacitances) are needed for a reliable identification of building parameters, and that additional boundary conditions are needed in terms of indoor air temperature and heat fluxes through envelope walls. Hedegaard and Petersen [32] addressed similar issues in a simulation-based study of four RC-models with the most complex being a third-order model; however, they infer that a second-order model allows for a fit to data that is fully compatible to that of a more complex third-order model. They further conclude that none of these low-order models are capable of providing a reliable partitioning of the overall heat transfer coefficient into heat transfer by transmission and ventilation, respectively. One should therefore be very cautious about trusting the exact value of calibration parameters θ of individual buildings when using low-order RC models. Whether these issues of parameter interpretation and identifiability persist in applications with high-fidelity BEM tools such as EnergyPlus remains unclear and ought to be studied in future work. However, Heo et al. [23] show, in a case study-based investigation of Bayesian calibration efficacy under different levels of uncertainty in model input data for EnergyPlus models, that the amount of certainty in input data highly affects the posterior estimates of calibration parameters and thus the identifiability of the model. We therefore expect the identifiability of the calibration parameters θ , and the predictive performance of the proposed archetype framework to increase as more concrete and specific data about the training buildings is applied. Such data could originate from detailed surveys and audits in carefully selected training buildings. Another less intrusive option could be to incorporate energy performance certificate (EPC) data if available. Finally, as demonstrated in recent state-of-the-art UBEM studies [5,45], GIS may be employed for establishing more accurate geometric models than those used in this study.

5. Conclusions and outlook

A hierarchical multilevel framework for the calibration of archetype physics-based BEM parameters was proposed. The framework relies on the statistical assumption of exchangeability among archetype buildings, i.e. the buildings represent a homogeneous sample from the archetype. Using Bayesian inference, information available in independent time series datasets is used collectively to pool individual estimates of building parameters towards a common archetype description of the calibration parameters, as well as their variability and correlation. This results in the archetype model being less vulnerable to the presence of outliers in the building stock used to train the archetype model, thus enabling it to make out-of-sample predictions that are more robust than predictions made with models founded on ordinary aggregation of individual building estimates.

The application and performance of the framework were subsequently demonstrated in a case study of Danish residential single-family dwellings from the 1950s. The case demonstrates how the framework can be used to identify a set of shared archetype parameters, and how the inevitable presence of heterogeneity in the buildings used for training is manifested into the variance parameters and the prediction of parameters for new unseen buildings.

The proposed archetype framework is most suited as the central calibration engine for urban-scale building energy modeling where archetype models are used as "puzzle pieces" for modeling urban areas which would otherwise be too complex to model and calibrate using independent building energy models. However, the suitability of the proposed archetype framework for such applications remains to be proven in future work.

Funding

The European Union's Research and Innovation Funding Programme (7th EU Framework Programme) supported this work through the FP7-Energy project "Resource Efficient Cities Implementing Advanced Smart City Solutions" (READY), work package 3 [project reference 609127].

Acknowledgments

The authors would like to thank the district heating company in Aarhus, AffaldVarme Aarhus, for supplying the case data that serves to demonstrate the application of the proposed calibration framework.

Supplementary materials

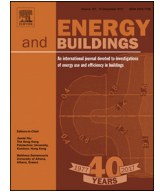
Supplementary material associated with this article can be found, in the online version, at [doi:10.1016/j.enbuild.2018.07.030](https://doi.org/10.1016/j.enbuild.2018.07.030).

References

- [1] C.F. Reinhart, C.C. Davila, Urban building energy modeling – a review of a nascent field, *Build. Environ.* 97 (2016) 196–202, [doi:10.1016/j.buildenv.2015.12.001](https://doi.org/10.1016/j.buildenv.2015.12.001).
- [2] E. Mata, A. Sasic Kalagasidis, F. Johnsson, Building-stock aggregation through archetype buildings: France, Germany, Spain and the UK, *Build. Environ.* 81 (2014) 270–282, [doi:10.1016/j.buildenv.2014.06.013](https://doi.org/10.1016/j.buildenv.2014.06.013).
- [3] C. Cerezo, J. Sokol, C. Reinhart, A. Al-Mumin, Three methods for characterizing building archetypes in urban energy simulation. A case study in Kuwait City, in: *Proceedings of the Fourteenth Conference of International Building Performance Simulation Association Building Simulation, IBPSA, Hyderabad, India, 2015*, pp. 2873–2880. URL: <http://www.ibpsa.org/proceedings/BS2015/p2435.pdf>.
- [4] C. Cerezo, J. Sokol, S. AlKhaled, C. Reinhart, A. Al-Mumin, A. Hajiah, Comparison of four building archetype characterization methods in urban building energy modeling (UBEM): a residential case study in Kuwait City, *Energy Build.* 154 (2017) 321–334, [doi:10.1016/j.enbuild.2017.08.029](https://doi.org/10.1016/j.enbuild.2017.08.029).

- [5] T. Dogan, C. Reinhart, Shoeboxer: an algorithm for abstracted rapid multi-zone urban building energy model generation and simulation, *Energy Build.* 140 (2017) 140–153, doi:10.1016/j.enbuild.2017.01.030.
- [6] J. Sokol, C. Cerezo Davila, C.F. Reinhart, Validation of a Bayesian-based method for defining residential archetypes in urban building energy models, *Energy Build.* 134 (2017) 11–24, doi:10.1016/j.enbuild.2016.10.050.
- [7] G. Dall'O, A. Galante, M. Torri, A methodology for the energy performance classification of residential building stock on an urban scale, *Energy Build.* 48 (2012) 211–219, doi:10.1016/j.enbuild.2012.01.034.
- [8] L. Filogamo, G. Peri, G. Rizzo, A. Giaccone, On the classification of large residential buildings stocks by sample typologies for energy planning purposes, *Appl. Energy* 135 (2014) 825–835, doi:10.1016/j.apenergy.2014.04.002.
- [9] M. Aksoezen, M. Daniel, U. Hassler, N. Kohler, Building age as an indicator for energy consumption, *Energy Build.* 87 (2015) 74–86, doi:10.1016/j.enbuild.2014.10.074.
- [10] D. Coakley, P. Raftery, M. Keane, A review of methods to match building energy simulation models to measured data, *Renew. Sustain. Energy Rev.* 37 (2014) 123–141, doi:10.1016/j.rser.2014.05.007.
- [11] H. Lim, Z.J. Zhai, Review on stochastic modeling methods for building stock energy prediction, *Build. Simul.* 10 (2017) 607–624, doi:10.1007/s12273-017-0383-y.
- [12] A.T. Booth, R. Choudhary, D.J. Spiegelhalter, Handling uncertainty in housing stock models, *Build. Environ.* 48 (2012) 35–47, doi:10.1016/j.buildenv.2011.08.016.
- [13] A.T. Booth, R. Choudhary, D.J. Spiegelhalter, A hierarchical Bayesian framework for calibrating micro-level models with macro-level data, *J. Build. Perform. Simul.* 6 (2013) 293–318, doi:10.1080/19401493.2012.723750.
- [14] Q. Li, G. Augenbroe, J. Brown, Assessment of linear emulators in lightweight Bayesian calibration of dynamic building energy models for parameter estimation and performance prediction, *Energy Build.* 124 (2016) 194–202, doi:10.1016/j.enbuild.2016.04.025.
- [15] Y. Heo, R. Choudhary, G.A. Augenbroe, Calibration of building energy models for retrofit analysis under uncertainty, *Energy Build.* 47 (2012) 550–560, doi:10.1016/j.enbuild.2011.12.029.
- [16] Y. Heo, G. Augenbroe, D. Graziano, R. T. Muehleisen, L. Guzowski, Scalable methodology for large scale building energy improvement: relevance of calibration in model-based retrofit analysis, *Build. Environ.* 87 (2015) 342–350, doi:10.1016/j.buildenv.2014.12.016.
- [17] Y. Kang, M. Krarti, Bayesian-emulator based parameter identification for calibrating energy models for existing buildings, *Build. Simul.* 9 (2016) 411–428, doi:10.1007/s12273-016-0291-6.
- [18] Y.J. Kim, C.S. Park, Stepwise deterministic and stochastic calibration of an energy simulation model for an existing building, *Energy Build.* 133 (2016) 455–468, doi:10.1016/j.enbuild.2016.10.009.
- [19] A. Chong, K.P. Lam, M. Pozzi, J. Yang, Bayesian calibration of building energy models with large datasets, *Energy Build.* 154 (2017) 343–355, doi:10.1016/j.enbuild.2017.08.069.
- [20] W. Tian, R. Choudhary, A probabilistic energy model for non-domestic building sectors applied to analysis of school buildings in greater London, *Energy Build.* 54 (2012) 1–11, doi:10.1016/j.enbuild.2012.06.031.
- [21] M.C. Kennedy, A. O'Hagan, Bayesian calibration of computer models, *J. R. Stat. Soc. Ser. B (Stat. Methodol.)* 63 (3) (2001) 425–464, doi:10.1111/1467-9868.00294.
- [22] M.H. Kristensen, R. Choudhary, R.H. Pedersen, S. Petersen, Bayesian calibration of residential building clusters using a single geometric building representation, in: *Proceedings of the Fifteenth Conference of International Building Performance Simulation Association Building Simulation, IBPSA, San Francisco, August 2017*, pp. 1294–1303. URL: http://www.ibpsa.org/proceedings/BS2017/BS2017_330.pdf.
- [23] Y. Heo, D.J. Graziano, L. Guzowski, R.T. Muehleisen, Evaluation of calibration efficacy under different levels of uncertainty, *J. Build. Perform. Simul.* 8 (3) (2014) 135–144, doi:10.1080/19401493.2014.896947.
- [24] M.H. Kristensen, R. Choudhary, S. Petersen, Bayesian calibration of building energy models: comparison of predictive accuracy using metered utility data of different temporal resolution, *Energy Procedia*. 122 (2017) 277–282, doi:10.1016/j.egypro.2017.07.322.
- [25] A. Gelman, Prior distributions for variance parameters in hierarchical models, *Bayesian Anal.* 1 (3) (2006) 515–534, doi:10.1214/06-ba117a.
- [26] A. Gelman, J.B. Carlin, H.S. Stern, D.B. Dunson, A. Vehtari, D.B. Rubin, *Bayesian Data Analysis*, third ed., Chapman and Hall/CRC, 2013, ISBN 1439840954.
- [27] H. Madsen, P. Bacher, G. Bauwens, A.-H. Deconinck, G. Reynders, S. Roels, E. Himpe, G. Lethe, Thermal Performance Characterization Using Time Series Data – IEA EBC Annex 58 Guidelines, Technical University of Denmark (DTU), Lyngby, Denmark, 2015 'Technical report' URL: http://orbit.dtu.dk/files/127709087/guidelines_IEA58_statisticalModeling_2016_11_28.pdfhttp://orbit.dtu.dk/files/127709087/guidelines_IEA58_statisticalModeling_2016_11_28.pdf.
- [28] K. Duer, S. Svendsen, M.M. Mogensen, J.B. Laustsen, Energy labeling of glazings and windows in Denmark: calculated and measured values, *Solar Energy* 73 (1) (2002) 23–31, doi:10.1016/S0038-092X(02)00031-2.
- [29] M.D. Morris, Factorial sampling plans for preliminary computational experiments, *Technometrics* 33 (2) (1991) 161–174 ISSN 0040-1706, doi:10.1080/00401706.1991.10484804.
- [30] H.B. Rijal, P. Tuohy, M.A. Humphreys, J.F. Nicol, A. Samuel, J. Clarke, Using results from field surveys to predict the effect of open windows on thermal comfort and energy use in buildings, *Energy Build.* 39 (7) (2007) 823–836 ISSN 0378-7788, doi:10.1016/j.enbuild.2007.02.003.
- [31] K. Gram-Hanssen. Husholdningers elforbrug - hvem bruger hvor meget, til hvad og hvorfor? SBI 2005:12. Danish Building Research Institute, 2005. ISBN 87-563-1235-0. URL <https://sbi.dk/Assets/Husholdningers-elforbrug-hvem-bruger-hvor-megget-til-hvad-og-hvorfor/2006-01-12-0481751096.pdf>. Language: Danish.
- [32] R.E. Hedegaard, S. Petersen, Evaluation of grey-box model parameter estimates intended for thermal characterization of buildings, *Energy Procedia*. 132 (2017) 982–987, doi:10.1016/j.egypro.2017.09.692.
- [33] M.H. Kristensen, S. Petersen, Choosing the appropriate sensitivity analysis method for building energy model-based investigations, *Energy Build.* 130 (2016) 166–176, doi:10.1016/j.enbuild.2016.08.038.
- [34] P. Bacher, H. Madsen, Identifying suitable models for the heat dynamics of buildings, *Energy Build.* 43 (7) (2011) 1511–1522 ISSN 0378-7788, doi:10.1016/j.enbuild.2011.02.005.
- [35] G. Reynders, J. Diriken, D. Saelens, Quality of grey-box models and identified parameters as function of the accuracy of input and observation signals, *Energy Build.* 82 (2014) 263–274, doi:10.1016/j.enbuild.2014.07.025.
- [36] W. Abrahamse, L. Steg, How do socio-demographic and psychological factors relate to households' direct and indirect energy use and savings, *J. Econ. Psychol.* 30 (5) (2009) 711–720, doi:10.1016/j.joep.2009.05.006.
- [37] O.G. Santin, L. Itard, H. Visscher, The effect of occupancy and building characteristics on energy use for space and water heating in Dutch residential stock, *Energy Build.* 41 (11) (2009) 1223–1232, doi:10.1016/j.enbuild.2009.07.002.
- [38] G.M. Huebner, I. Hamilton, Z. Chalabi, D. Shipworth, T. Oreszczyn, Explaining domestic energy consumption – the comparative contribution of building factors, socio-demographics, behaviours and attitudes, *Appl. Energy* 159 (2015) 589–600, doi:10.1016/j.apenergy.2015.09.028.
- [39] S. Yang, M. Shipworth, G. Huebner, His, hers or both's? The role of male and female's attitudes in explaining their home energy use behaviours, *Energy Build.* 96 (2015) 140–148, doi:10.1016/j.enbuild.2015.03.009.
- [40] M.H. Kristensen, S. Petersen, Explaining variability in metered energy use for similar buildings using Bayesian inference, *Energy Procedia* 132 (2017) 897–902, doi:10.1016/j.egypro.2017.09.709.
- [41] Y.S. Lee, A. M. Malkawi, Simulating multiple occupant behaviors in buildings: An agent-based modeling approach, *Energy Build.* 69 (2014) 407–416, doi:10.1016/j.enbuild.2013.11.020.
- [42] J. Langevin, J. Wen, P.L. Gurian, Simulating the human-building interaction: development and validation of an agent-based model of office occupant behaviors, *Build. Environ.* 88 (2015) 27–45, doi:10.1016/j.buildenv.2014.11.037.
- [43] D. Aerts, J. Minnen, I. Glorieux, I. Wouters, F. Descamps, A method for the identification and modeling of realistic domestic occupancy sequences for building energy demand simulations and peer comparison, *Build. Environ.* 75 (2014) 67–78, doi:10.1016/j.buildenv.2014.01.021.
- [44] P.D. Andersen, A. Iversen, H. Madsen, C. Rode, Dynamic modeling of presence of occupants using inhomogeneous Markov chains, *Energy Build.* 69 (2014) 213–223, doi:10.1016/j.enbuild.2013.10.001.
- [45] C.C. Davila, C.F. Reinhart, J.L. Bemis, Modeling Boston: a workflow for the efficient generation and maintenance of urban building energy models from existing geospatial datasets, *Energy* 117 (2016) 237–250, doi:10.1016/j.energy.2016.10.057.

**APPENDIX 2 PAPER: THE EFFECT OF INCLUDING HYDRONIC
RADIATOR DYNAMICS IN MODEL PREDICTIVE CONTROL OF
SPACE HEATING (S2)**



The effect of including hydronic radiator dynamics in model predictive control of space heating



Theis Heidmann Pedersen*, Rasmus Elbæk Hedegaard, Kristian Fogh Kristensen, Benjamin Gadgaard, Steffen Petersen

Department of Engineering, Aarhus University, Inge Lehmanns Gade 10, 8000 Aarhus C, Denmark

ARTICLE INFO

Article history:

Received 26 April 2018

Revised 24 September 2018

Accepted 12 November 2018

Available online 17 November 2018

Keywords:

Model predictive control

Demand response

Dynamic radiator model

Space heating

Hydronic heating

ABSTRACT

Existing simulation-based studies on applying model predictive control (MPC) schemes for space heating operation to enable demand response (DR) make use of linear models for the heating system, usually by assuming convective electrical baseboard heaters. However, buildings connected to district heating networks are typically equipped with hydronic heat emitters, such as radiators, that behave nonlinear. This paper therefore investigates the effect of including the nonlinear dynamics of a hydronic heat emitter on the DR potential of MPC for space heating. Furthermore, the performance of a practical two-level control approach suitable for real application, in which a heating setpoint was determined by a linear MPC and communicated to a conventional proportional integral controller, was investigated. The simulation framework for the investigation was based on the application of an experimentally obtained hydronic radiator model applied in different co-simulation setups, featuring a model of a poorly and a highly insulated apartment, respectively. The results indicated that inclusion of the nonlinear thermal effects of hydronic radiators did not significantly affect the DR performance when compared to the results of an MPC scheme controlling convective electrical baseboard heaters. In general, both setups achieved operational cost savings of approx. 5% and 18% in an existing and retrofitted building, respectively, while restricting the amount of thermal comfort violations to a limited extent. This suggests that results obtained in previous studies featuring electrical baseboard heaters also apply to buildings equipped with hydronic heating systems, and that future simulation-based studies and practical implementation of MPC for space heating can continue to rely on the use of far less computationally demanding linear control-models. Furthermore, the results suggest that the two-level control scheme seems like an appropriate control setup suitable for real applications.

© 2018 Elsevier B.V. All rights reserved.

1. Introduction

Demand response (DR) programs where building owners adjust their consumption in response to an external request have been proposed in several studies to overcome challenges related to power imbalances and peak load issues in the electricity grid, e.g. [1,2] to mention a few. However, district heating (DH) networks may also benefit from building owners participating in DR programs as DH networks, in the near future, will be strongly coupled with the electricity grid to increase integration of renewable energy sources [3,4]. Several studies have thus investigated the ability of buildings to provide DR using thermal energy storages, including both active storage (e.g. domestic hot water tanks) [5,6] and passive storage obtained by exploiting their thermal mass [7–13].

Several control approaches can be used to enable DR of which especially the concept of model predictive control (MPC) has re-

ceived significant research attention lately [7,8,11,12]. MPC is an optimization-based control scheme that relies on a simplified control-model of the building thermodynamics to determine an optimal control strategy. Knudsen and Petersen [5] applied an economic MPC (E-MPC) scheme with the objective of minimizing operational costs of domestic hot water preparation in an ultra-low temperature DH system. Considering time varying electricity and district heating prices, the proposed E-MPC scheme simultaneously enabled load-shift from peak periods and operational cost savings of approx. 5%. Avci et al. [11] applied E-MPC together with day-ahead electricity prices to minimize the weighted sum of the operational cost and the temperature deviations from a preferred room air setpoint. Applying the proposed E-MPC scheme to operate an AC unit reduced the energy consumption in peak-hours by 23.6% compared to a conventional two-position control approach. Pedersen, Hedegaard and Petersen [7] applied E-MPC and day-ahead wholesale electricity prices for optimal operation of convective electrical space heaters in ten apartments. Compared to a conventional constant setpoint tracking proportional-integral (PI)

* Corresponding author.

E-mail address: thp@eng.au.dk (T.H. Pedersen).

Nomenclature

Abbreviations

DR	demand response
MPC	model predictive control
E-MPC	economic model predictive control
DH	district heating
N-MPC	nonlinear model predictive control
PRBS	pseudo-random binary signal
PRMS	pseudo-random multi-level signal

Symbols

τ	time step [seconds]
t	temperature [$^{\circ}\text{C}$]
T	temperature [K]
N_s	number of sections[–]
C	heat capacity[J/K]
c_p	specific heat capacity [J/(kg·K)]
ρ	density [kg/m ³]
q	flow rate [m ³ /s]
Q	energy [J]
ϕ	heat power [W]
n	radiator exponent [–]
Δt_{ar}	arithmetic temperature difference [$^{\circ}\text{C}$]
Δt_{lg}	logarithmic temperature difference [$^{\circ}\text{C}$]
β_C	fraction of convective heat emission [–]
β_R	fraction of radiative heat emission [–]
A	state matrix
$\mathbf{x}_{\tau+n \tau}$	state vector predicted for time step $\tau+n$ at time step τ
B	input matrix
u	control actions vector
E	disturbance matrix
d	disturbance vector
KG	Kalman gain
Subscripts	
j	section number
inlet	inlet water temperature
outlet	outlet water temperature
w	water
N	nominal (standard conditions)

controller, the E-MPC scheme achieved load reductions of up to 47% in peak load periods, depending on the energy efficiency and, accordingly, the storage efficiency of the building envelope. However, as suggested by Le Dréau and Heiselberg [9], the type of heat emitter significantly affects the magnitude and duration of DR events. They applied rule-based control to increase and decrease the temperature setpoint for varying durations using two types of heat emitters (i.e. radiators and underfloor heating), and found that the modulation potential differed significantly for the two considered heat emitters.

Existing simulation studies on applying E-MPC schemes to operate the space heating system to enable DR mostly make use of convective electrical baseboard heaters that behave linearly. However, typical heating systems in buildings connected to DH networks consists of hydronic heat emitters, such as radiators, that are characterized by nonlinearities in their heat output, driven by the temperature difference between the radiator and room [14]. Using E-MPC for real applications to operate hydronic heat emitters therefore introduces nonlinearities that, consequently, lead to a less practical and computationally demanding nonlinear MPC (N-MPC) scheme.

To the best of the authors' knowledge, there are no reported studies on whether the nonlinear dynamics of a hydronic heat emitter affect the potential of DR when exploiting the structural thermal mass to shift energy consumption in buildings. This paper therefore reports on a simulation-based study, applying an N-MPC scheme with the objective of minimizing operational cost to investigate the effect of the DR potential. Furthermore, the performance of a two-level MPC scheme suitable for real applications, which allow for a practical coupling between the MPC scheme and existing setpoint-tracking controllers was evaluated.

2. Method

A dynamic radiator model was needed to accurately evaluate the impact of hydronic heating systems; therefore this paper first presents a nonlinear radiator model that adequately represents the thermodynamics of a hydronic radiator (Section 2.1). Subsequently, three MPC scheme setups were formulated: a linear MPC scheme, a two-level MPC scheme, and an N-MPC scheme (Section 2.2). The performance of the three setups was investigated through co-simulations facilitated by the Building Controls Virtual Test Bed [15] of an apartment located in Aarhus, Denmark (see Section 2.3). The apartment was represented by an EnergyPlus (EP) model while the dynamic radiator model and the MPC schemes were implemented in MATLAB.

2.1. Dynamic radiator model

A nonlinear grey-box model of a particular hydronic panel radiator (DeLonghi Radel type 22 [16]) was established. The thermal behavior of the radiator was modeled as a system of nonlinear ordinary differential equations based on the laws of thermodynamics [17], thus the radiator was lumped into N_s equally sized homogeneous horizontal sections in serial connection. The particular radiator dimensions and inlet/outlet locations are illustrated in Fig. 1. Preliminary thermographic investigations confirmed that the assumption of approximately homogeneous horizontal sections of this specific radiator was acceptable (see Fig. 2).

However, it is noted that the modeling was specific to this particular radiator since model parameters, such as heat capacity and nominal power, vary with the size of the radiator while position of the inlet and outlet affects the charging pattern, i.e. the stratification in the radiator.

The energy balance of each section was expressed as an ordinary differential equation (see Eq. (1)), where Q_{stored} denotes the stored heat, and ϕ_{in} and ϕ_{out} denote the power flowing in and out of the radiator, respectively. The ordinary differential equation is specified in detail for the j 'th section of the radiator in Eq. (2) (see Appendix A for the full set of radiator model equations). C_{Rad} is the combined heat capacity of the water and radiator material, q is the flow rate, while $c_{p,w}$ and ρ_w are the specific heat capacity and density of the water, respectively. The nominal power of the radiator determined at standard conditions is denoted ϕ_N , while $\Delta t_{ar,N}$ and n are the arithmetic temperature difference at standard conditions and the radiator exponent, respectively. The water in each radiator sub-section was assumed incompressible and fully mixed, thus the entire water-volume in each section j has temperature t_j (see Fig. 1).

$$\frac{dQ_{\text{stored}}}{d\tau} = \sum \phi_{\text{in}} - \sum \phi_{\text{out}} \quad (1)$$

$$\frac{C_{\text{Rad}}}{N_s} \cdot \frac{dt_j}{d\tau} = c_{p,w} \cdot \rho_w \cdot q \cdot (t_{j-1} - t_j) - \frac{\phi_N}{N_s} \cdot \left(\frac{t_j - t_{\text{room}}}{\Delta t_{ar,N}} \right)^n \quad (2)$$

The model requires the inlet temperature (t_{j-1} for the first section, see Appendix A), the room temperature and the flow rate as

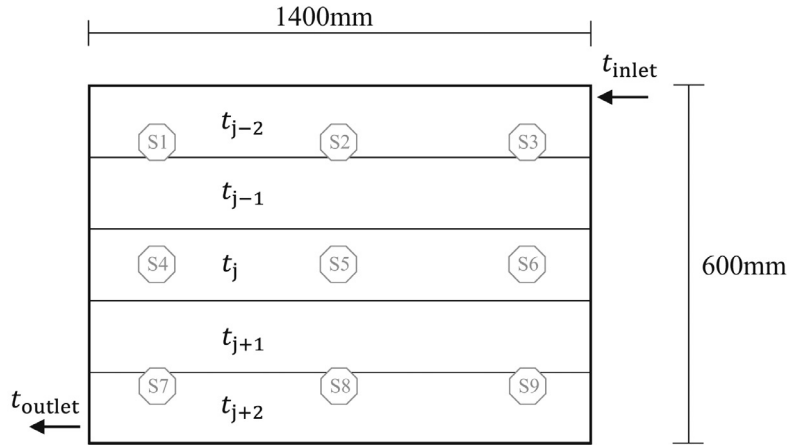


Fig. 1. Principle of the dynamic radiator model exemplified with $N_s = 5$ horizontal sections with different temperatures t . The octagons mark the position of nine thermocouples (type K) used to measure the surface temperature.

inputs. The output of the model is the temperature of the water in the last section, which is assumed to be equal to the outlet water temperature. Modeling the outlet water temperature enables a simple calculation of the heating power to the room, which equals the change in energy of the water (see Eq. (3)).

$$\phi_{Rad} = c_{p,w} \cdot \rho_w \cdot q \cdot (t_{inlet} - t_{outlet}) \quad (3)$$

The heating power is delivered to the room by convective and radiative heat transfer. The fraction of convection and radiation denoted β_C and β_R , respectively, depend on the radiator and room temperature conditions. Knowing $\beta_{R,N}$, i.e. the radiative fraction at standard conditions, enables the calculation of β_R according to Eq. (4) [18]. In this study, $\beta_{R,N}$ was assumed to be 0.3 which is in accordance with other studies [19,20] for a double panel radiator.

$$\beta_R = \beta_{R,N} \cdot \frac{(T_{room} + \Delta t_{lg})^4 - T_{room}^4}{(T_{room} + \Delta t_{lg,N})^4 - T_{room}^4} \cdot \left(\frac{\Delta t_{lg}}{\Delta t_{lg,N}} \right)^n \quad (4)$$

2.1.1. Calibration of radiator model parameters

The model parameters were calibrated based on measurement data from experiments where the radiator was excited by controlling the flow rate according to four experiments as specified in

Table 1. The temperatures of inlet, outlet and room air were, in all experiments, measured at a sampling rate of 15 seconds along with nine surface temperatures (see Fig. 1). Three experiments were conducted using pseudo-random multi-level signals (PRMS) generated by the software Galois [21], and one experiment was conducted using a pseudo-random binary signal (PRBS) generated using the MATLAB function *idinput*. The use of both PRBS and PRMS signals was to test the prevailing notion in literature that a PRBS signal may not provide sufficient perturbation to identify nonlinear models [22]. The duration of the experiments is denoted P , and the number of levels was the number of different flowrates, ranging from a fully closed to a fully open valve position. The switching time, i.e. the shortest amount of time between changing flowrates, was set to 300 seconds for all four experiments.

The radiator model in Eq. (2) contains five unknown parameters. However, the model structure only allows for calibration of two parameters due to issues regarding structural identifiability [17]. To reduce the number of unknown parameters, the parameters describing the properties of water, $c_{p,w}$ and ρ_w , were assumed to be temperature invariant. This assumption seems reasonable as temperature fluctuations between 30 °C–60 °C, only leads to approximately 0.2% and 1.5% variation of $c_{p,w}$ and ρ_w , respectively. For convenience, the material property H_w is introduced according to Eq. (5).

$$H_w = c_{p,w} \cdot \rho_w \quad (5)$$

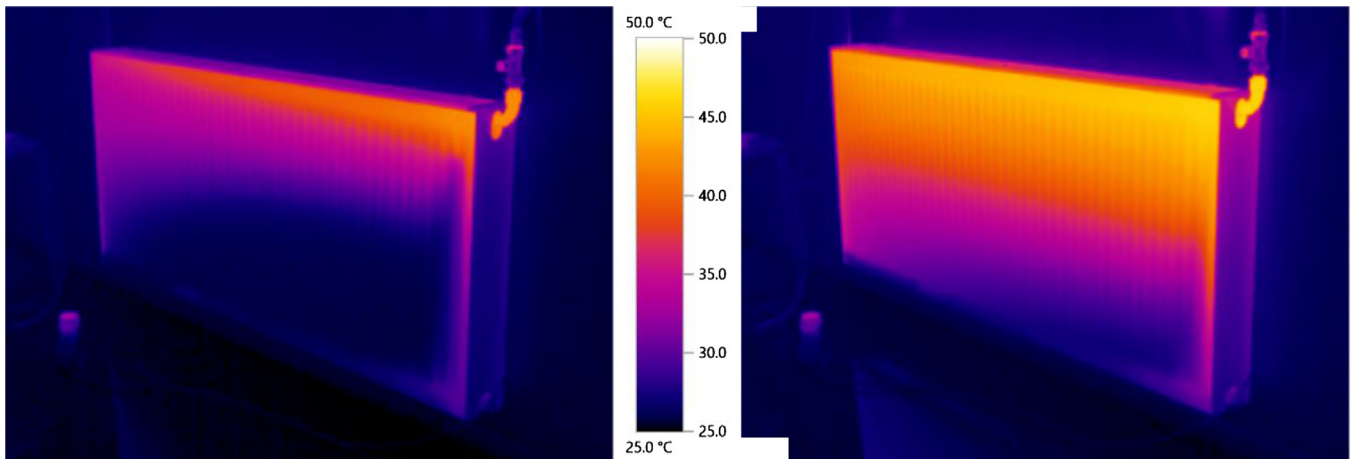


Fig. 2. Thermographic images during heat-up. Left) after 5 minutes. Right) after 8 minutes.

Table 1
Parameters defining the four experiments.

	Experiment 1 Training data	Experiment 2 Training data	Experiment 3 Training data	Experiment 4 Validation data
Excitation signal	PRMS	PRMS	PRBS	PRMS
Number of levels	5	13	2	5
Duration (P)	14 hours	14 hours	14 hours	50 hours

Table 2
Specifications from data sheet.

t_{inlet}	t_{outlet}	t_{room}	Φ_N	$\Delta t_{ar,N}$
75 °C	65 °C	20 °C	2479 W	50.0 °C
70 °C	55 °C	20 °C	2001 W	42.5 °C
55 °C	45 °C	20 °C	1264 W	30.0 °C

Fixing the material properties of the hydronic fluid leaves three unknown parameters: the nominal power at standard conditions, the thermal capacity of the radiator and the radiator exponent. The radiator exponent n was estimated using the standard static least-squares calibration method [23] based on measurements of the nominal power at three standard temperature conditions as stated in Table 2 [16]. The two remaining parameters, i.e. the nominal power and the thermal capacity, were calibrated with the objective to minimize the outlet temperature residuals using the time-series measurements obtained during the experiments. Furthermore, the radiator models were calibrated for $\{N_s \in \mathbb{Z} | 2 \leq N_s \leq 100\}$ to identify the optimal N_s .

The first three experiments were used as separate training data sets for calibrating three versions of the radiator model, and data from the fourth experiment was used to validate the calibrated models. Measurements from experiment 4, i.e. the validation data, are depicted in Fig. 3. It is seen that the room air temperature had an increasing trend during the experiment by a couple of degrees because of the high amount of heat injected into the room. The calibrated models were evaluated in terms of the two standard metrics root mean square error (RMSE) and normalized root mean square error (NRMSE) as defined in Eqs. (6) and (7), respectively. P is the duration of the experiment where the index $\tau s = \{1, 2, \dots, P\}$ denotes the time in 15 seconds increments, z and \hat{z} are timeseries of the measured data and the output of the model, respectively, and $\|\cdot\|$ denotes the Euclidean norm. Considering both metrics in the evaluation ensures reliable evaluation when using three distinct experiments with varying variability to calibrate the models.

$$RMSE = \sqrt{\frac{\sum_{\tau s=1}^P (z_{\tau s} - \hat{z}_{\tau s})^2}{P}} \quad (6)$$

$$NRMSE = \left(1 - \frac{\|z - \hat{z}\|}{\|z - \text{mean}(z)\|}\right) \cdot 100 \quad (7)$$

2.2. Model predictive control

MPC is an optimization based control scheme that, in each discrete time step τ_{MPC} , determines an optimal control sequence for a finite prediction horizon N . The controllable decision variables \mathbf{u} , i.e. space heating control actions, are communicated to the EP representation of the building in a receding horizon approach, where only the first action of the optimal sequence is actually implemented [24]. At the next discrete time step, the optimization problem is solved again with a prediction horizon shifted one time step ahead in time. In this study, a linear objective function was considered for the MPC scheme using a time varying cost signal \mathbf{f} , as

specified in Eq. (8).

$$\text{minimize}_{\mathbf{u}} J = \sum_{\tau=0}^{N-1} f_{\tau} \cdot u_{\tau} \quad (8)$$

The MPC scheme is subject to multiple constraints (Eqs. (9)–(12)). Firstly, the scheme is constrained by a control-model which describes the thermodynamics of the system to be controlled. The dynamics are specified in Eq. (9), and are a function of the system states \mathbf{x}_{τ} , control action u_{τ} and disturbances \mathbf{d}_{τ} (i.e. ambient temperature and transmitted solar irradiance).

$$\mathbf{x}_{\tau+1} = \mathbf{g}(\mathbf{x}_{\tau}, u_{\tau}, \mathbf{d}_{\tau}) \quad (9)$$

At each time step τ_{MPC} , the room air temperature was measured from the EP representation (y^{measured}) and used to correct the states of the control-model using a Kalman filter that updates the observed and unobserved states according to Eq. (10), where KG is the Kalman gain [25].

$$\mathbf{x}_{\tau|\tau} = \mathbf{x}_{\tau|\tau-1} + KG \cdot (y_{\tau}^{\text{measured}} - \mathbf{C} \cdot \mathbf{x}_{\tau|\tau-1}) \quad (10)$$

Addressing thermal comfort when applying MPC schemes can be handled in various ways [26]. One approach is to formulate a multi-objective optimization problem, which simultaneously minimizes operational costs and thermal comfort deviations [11,27]. Another approach is to assume that occupants are comfortable as long as the room air temperature is within a predefined comfort band [7,8]. In this study, the latter approach was chosen, which led to a single objective formulation. The comfort band was defined by the time invariant lower (t_{min}) and upper (t_{max}) comfort bounds, see Eq. (11).

$$t_{min} \leq y_{\tau} \leq t_{max} \quad (11)$$

Furthermore, the space heating control action u_{τ} was restricted by the maximum design heating power according to Eq. (12).

$$0 \leq u_{\tau} \leq u_{max} \quad (12)$$

2.2.1. Investigated MPC setups

In theory, the control-model of the room and heating system dynamics specified in Eq. (9) is a nonlinear function. However, many studies approximate the room thermodynamics as a linear function by neglecting the nonlinear dynamics of hydraulic systems, and assume electrical baseboard heaters in the simulations, thus resulting in a convex linear program, see e.g. [7,8]. To investigate how this approximation affects the control performance, simulations of three MPC setups were carried out:

- Linear MPC controlling an electrical baseboard heater.¹
- Two-level control where a linear MPC determined the optimal heating setpoint to be maintained by a conventional PI-controller² adjusting the water flow to the hydronic radiator model.
- N-MPC scheme, i.e. including the hydronic radiator in the control-model.

The three setups led to distinct co-simulation setups as illustrated in Fig. 4, facilitated by the Building Controls Virtual Test Bed [15].

¹ A constant radiative fraction β_R of 0.3 was assumed.

² The PI controller was tuned using the MATLAB function *pidtune*.

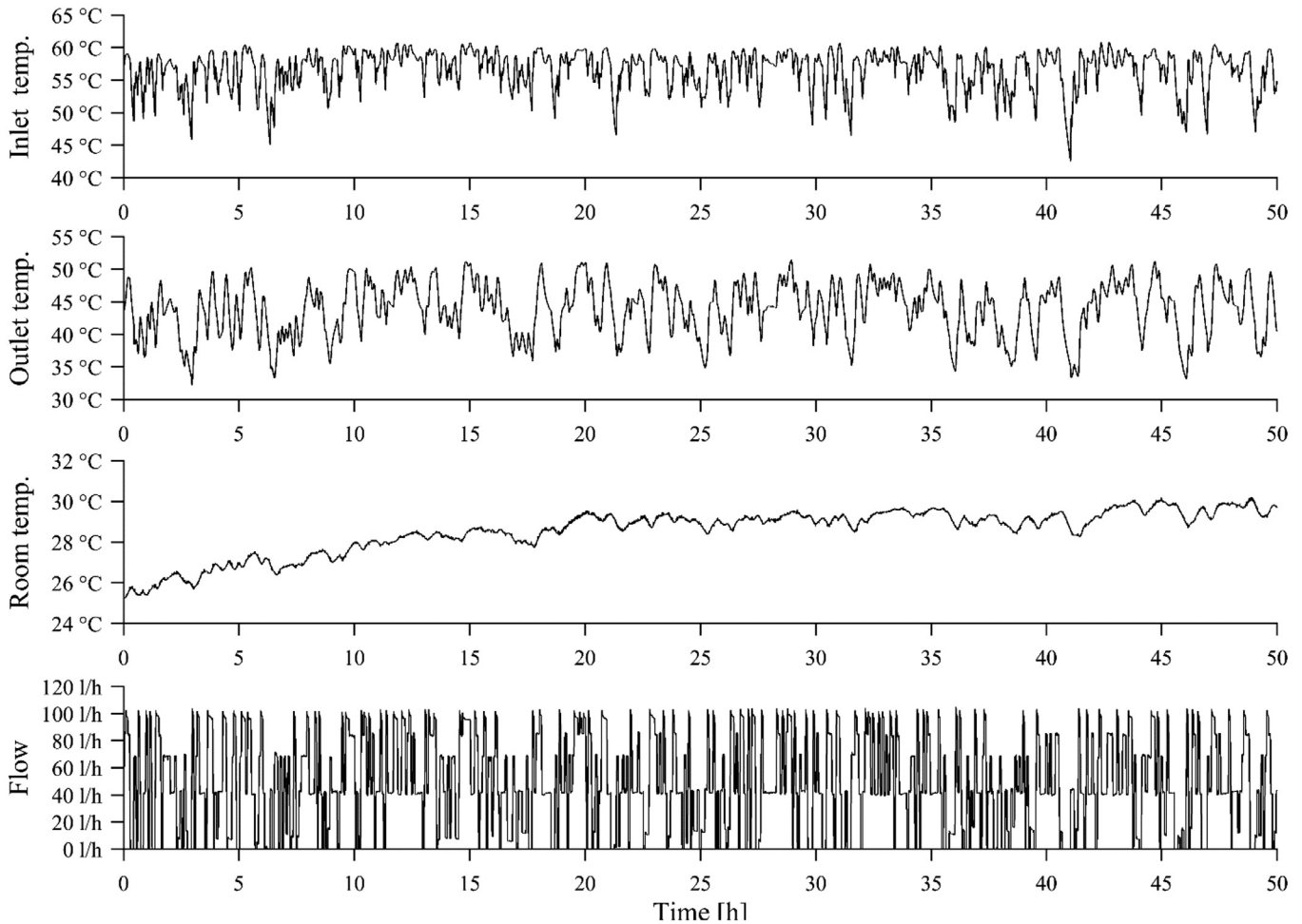


Fig. 3. Data from experiment 4 used for model validation.

Setups *a)* and *b)* relied on a linear two-state grey-box control-model representing the lumped thermal capacity of the zone air and the construction elements. The state space representation of the model is given in Eqs. (13) and (14) with state matrix \mathbf{A} , input matrix \mathbf{B} , disturbance matrix \mathbf{E} and output matrix \mathbf{C} . The control-model was estimated in continuous time and then discretized using the zero-order hold method with a time step of 60 seconds.

$$\mathbf{x}_{\tau+1} = \mathbf{A} \cdot \mathbf{x}_{\tau} + \mathbf{B} \cdot \mathbf{u}_{\tau} + \mathbf{E} \cdot \mathbf{d}_{\tau} \quad (13)$$

$$y_{\tau} = \mathbf{C} \cdot \mathbf{x}_{\tau} \quad (14)$$

The commercial solver *CPLEX* was used to solve the convex linear program and returned the optimal sequence of control actions \mathbf{u} [W], constrained by the maximum installed heating power, i.e. $u_{\max} = \phi_{\max}$ (Eq. (12)). In setup *b)* the predicted temperatures, resulting from applying the optimal sequence \mathbf{u} , were communicated as a setpoint to the low-level PI-controller which then adjusted the flow rate of the hydronic radiator accordingly (hence the name *two-level control*). For setup *c)* the control-model combined the linear room model (Eqs. (13) and (14)) with the model of the hydronic radiators Eq. (2) and Appendix A) leading to a non-linear control-model and a nonconvex optimization formulation.

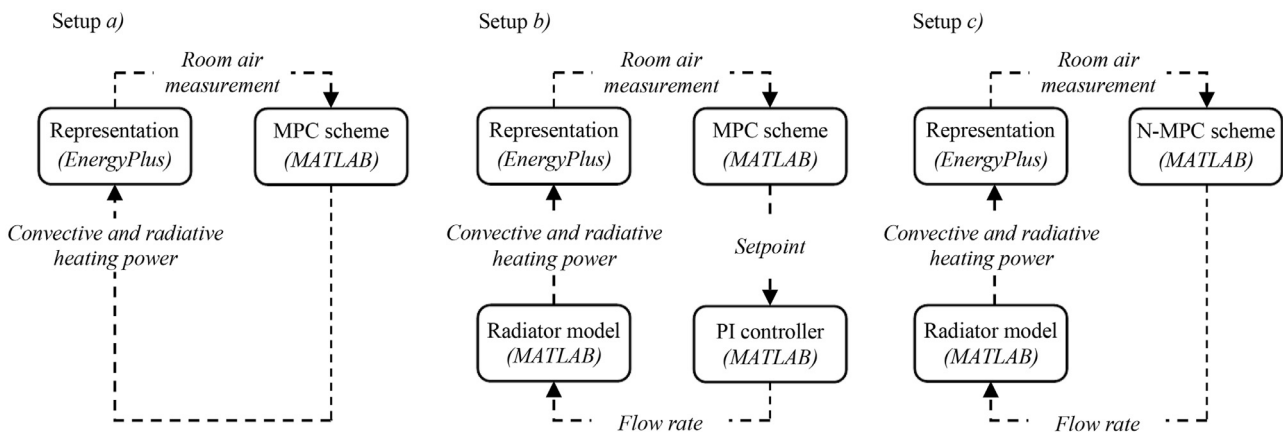


Fig. 4. Co-simulation setups for the three investigated MPC setups.

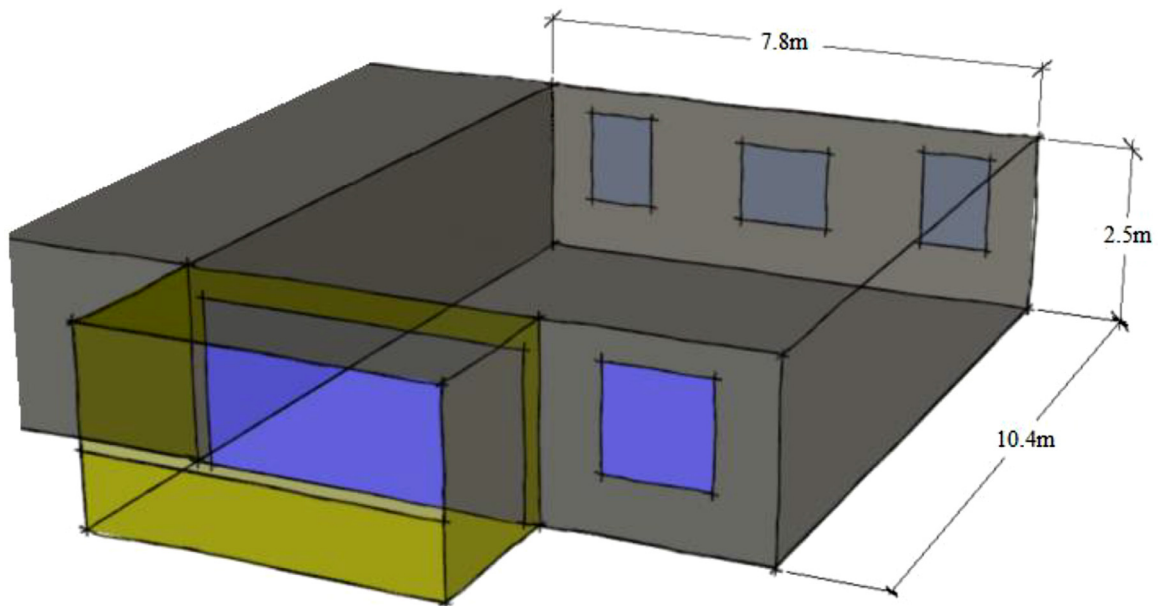


Fig. 5. Test case geometry as modeled in EP.

Instead of linearizing and discretizing the control-model, the MATLAB functions *ode45* and *fmincon* were used to simulate and optimize the model, respectively. The controllable decision variable was the sequence of flow rates \mathbf{q} which was constrained by the maximum flow rate, i.e. $u_{\max} = q_{\max}$ (Eq. (12)). The *ode45* function simulated the system of ordinary differential equations using the fourth and fifth order Runge Kutta to determine an adequate time step size, thus ensuring a reliable simulation. The function *fmincon* contains several optimization algorithms of which the *active set* algorithm was used for the purposes of this study since it has been demonstrated to be able to achieve adequate results in a timely manner [28]. However, we found that the solver algorithm was sensitive towards the initial sequence of control actions. Especially in cases where the initial sequence of flowrates would lead to comfort violations, the algorithm tended to arrive at locally optimal solutions. The optimization problem in this study was therefore solved using two initial guesses, and the resulting solution with the lowest objective value was implemented. The first initial guess was determined by taking the solution obtained when neglecting the hydronic system and translating it into flowrates using Eq. (3). The second initial guess vector was a constant flow rate which was determined so the room air temperature was within the comfort bounds during the entire prediction horizon. After determining the optimal flow rates \mathbf{q} , the resulting radiant and convective emitted heating power were calculated using Eqs. (3) and (4).

2.3. Test case

The three MPC setups were tested on an EP model representing an apartment located in Aarhus, Denmark. The apartment has east-west oriented windows and a west-oriented open balcony illustrated with yellow in Fig. 5. The horizontal zone boundaries (i.e. ceiling and floor) were assumed adiabatic. Insulation was added to the partitioning wall to make it reasonable to neglect heat transfer to the adjacent apartment as suggested in [29], and the temperature in the adjacent apartment was kept constant at 20°C. Previous studies have suggested that the DR potential depends on the energy efficiency of the building envelope [7]. Therefore, the simulations were performed for the existing building and a building with an improved energy efficiency. Further specifications of materials

and constructions are provided in ref. [7] where the building configurations used in this study are denoted *Retrofit0* and *Retrofit8*.

The EP model had a time step of 60 seconds, whereas the MPC scheme determined new control actions every 15 minutes (τ_{MPC} of 900 seconds). On-site weather measurements (see Fig. 6) were used during the one week simulation period from December 12, 2016, to December 18, 2016.

As stated in Eq. (11), the MPC scheme was constrained to maintain a room air temperature within certain comfort bounds. The potential of exploiting the thermal mass as a sensible heat storage depends on the comfort interval, i.e. how large temperature fluctuations occupants will allow. In this study, a rather restrictive comfort interval was chosen with comfort bounds t_{\min} and t_{\max} set to 20°C and 23°C, respectively. The apartment was assumed to be equipped with two radiators which, as described in Section 2.2.1, constrained the linear MPC and N-MPC scheme by the radiator characteristics of $\phi_{\max} = 2025 \text{ W}$ and $q_{\max} = 110 \text{ l/h}$, respectively.

The potential of DR can be evaluated with respect to various objectives [5,7,8]. This study considers price-based demand response, where the objective was to achieve operational cost savings compared to a reference scenario with a control scheme tracking a constant setpoint t_{\min} . Historical day-ahead wholesale electricity prices for the bidding area DK1 were used as cost signal \mathbf{f} (see Eq. (8)) in all control setups. The efficiency factor in the conversion of electricity to thermal energy in setups that include a hydronic heating system, i.e. setups (b) and (c), was assumed to be equal to one. This allowed for a direct performance comparison of the three MPC setups, as well as comparisons with results obtained in previous studies. In practice, however, a heat pump would significantly improve the economic performance of setups (b) and (c). Taxation tariffs are very country specific and were therefore neglected to generalize the interpretation of the results. Consequently, the resulting operational costs cannot be expected to match the actual operational costs paid by consumers. Furthermore, perfect predictions of \mathbf{f} were assumed. A prediction horizon $N = 48$ hours was chosen to ensure that the control scheme utilized the full storage capacity of the thermal mass.

Three key performance indicators were used to evaluate the DR potential. One indicator was the ability of the MPC schemes to achieve operational cost savings relative to a reference controller

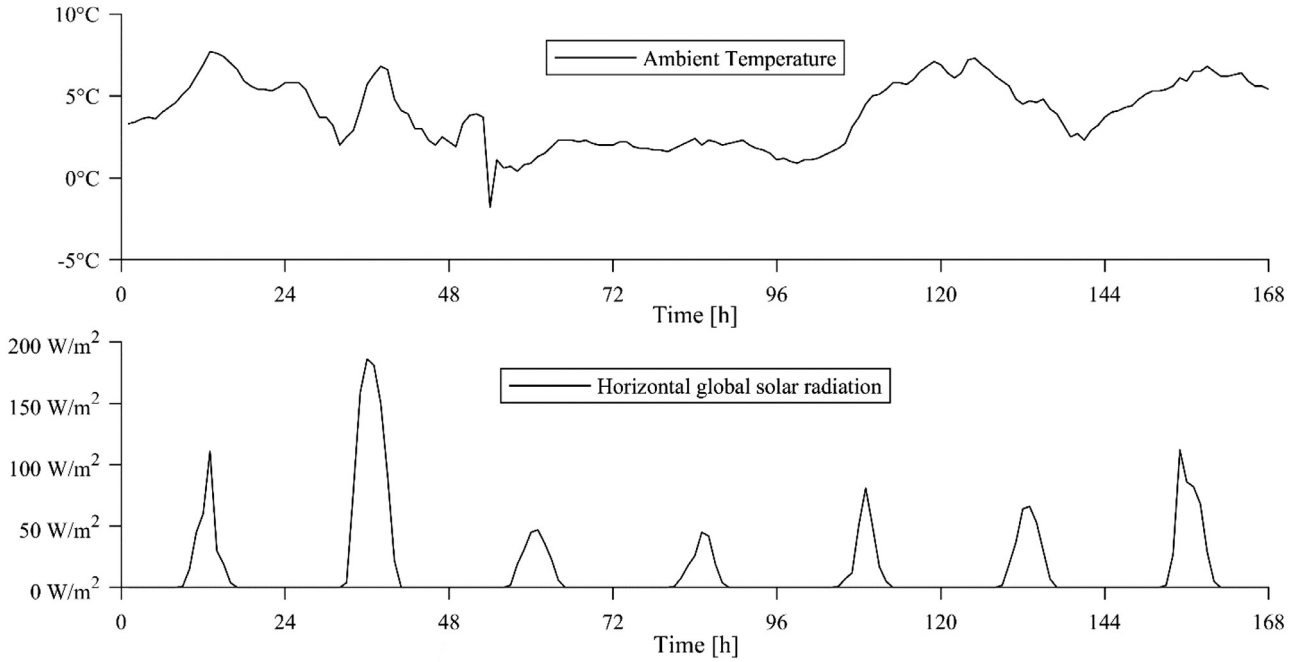


Fig. 6. Weather conditions during the simulation period.

according to Eq. (15), where c_τ denotes the operational cost for time step τ .

$$\overline{\Delta c} = \sum_{\tau=1}^P \frac{c_\tau^{MPC} - c_\tau^{ref}}{c_\tau^{MPC}} \quad (15)$$

The other indicator was the absolute and relative ability of the MPC schemes to shift space heating consumption in each time step compared to a reference controller according to Eqs. (16) and (17), respectively.

$$\Delta\phi_\tau = \phi_\tau - \phi_\tau^{ref} \quad \forall \tau = 1, \dots, P \quad (16)$$

$$\overline{\Delta\phi_\tau} = \frac{\phi_\tau - \phi_\tau^{ref}}{\phi_\tau^{ref}} \quad \forall \tau = 1, \dots, P \quad (17)$$

Furthermore, the shifting efficiency, which is the ratio between decreased and increased heating consumption during charging and discharging periods, was evaluated according to Eq. (18) [9]. The durations of charging and discharging periods is denoted τ^{charge} and $\tau^{discharge}$ and is determined at each load shift event (see Fig. 12).

$$\eta_{shifting} = \frac{-\int_0^{\tau^{discharge}} \Delta\phi_\tau (\Delta\phi_\tau < 0) d\tau}{\int_0^{\tau^{charge}} \Delta\phi_\tau (\Delta\phi_\tau > 0) d\tau} \quad (18)$$

3. Results

3.1. Dynamic radiator model

Three dynamic radiator models were calibrated based on the three separate training datasets (see Table 1) and with an increasing number of horizontal sections. Fig. 7 displays the performance indicators RMSE and NRMSE for the identified models evaluated on the validation data. The results suggest that the models derived using data generated from PRBS excitation signals (experiment 3) were less capable of accurately predicting the outlet temperature of the radiator compared to models derived using data generated from PRMS excitation signals (experiment 1

and 2). This is in agreement with the prevailing notion in literature that PRBS signals are suitable for linear systems, whereas calibration of nonlinear systems benefits from the use of PRMS excitation signals, as they are better at revealing the behavior of dynamic systems [22]. The models calibrated using Experiment 1 and 2 data achieved similar performance. Generally, the performance increases as the number of sections approaches six; hereafter the performance stagnates.

The best performing radiator model was achieved using Experiment 1 as training data and with nine horizontal sections (RMSE = 0.64 °C and NRMSE = 84% on the validation data). This model was therefore chosen for the following investigations of the MPC schemes. The model parameters are stated in Table 3. It can be seen that the calibrated nominal power ϕ_N of 1874 W (using $\Delta t_{ar,N} = 42.5$ °C) is consistent with the declared ϕ_N of 2001 W from the manufacturer (second row of Table 2) with a deviation of approx. 6%.

Fig. 8 shows a comparison of the measured surface temperatures during the experiment used for model validation (Experiment 4) and the simulated states of the horizontal sections in the model using the parameters in Table 3. The measured surface temperatures (see Fig. 1 for their placements) were averaged horizontally and compared with the simulated temperatures of sections two, five and eight. Fig. 8 left column shows the temperature during 12 hours of the experiment, and Fig. 8 right column shows the histogram of residuals during the entire experiment (50 hours). The temperature deviations increased slightly from the bottom section towards the top section, where the RMSE for the four sections was 3.55 °C, 1.77 °C, 0.95 °C and 0.64 °C, respectively. As expected, the residuals of the outlet temperature were the lowest since the model was calibrated with the objective of minimizing the outlet residuals. Another reason for this vertical increment is the model

Table 3

Calibrated and calculated model parameters of the proposed dynamic radiator model.

N_s	C_{Rad} [J/K]	H_w [kJ/(m ³ ·K)]	ϕ_N [W]	$\Delta t_{ar,N}$ [°C]	n
9	43254.3	4113.7	1873.7	42.5	1.32

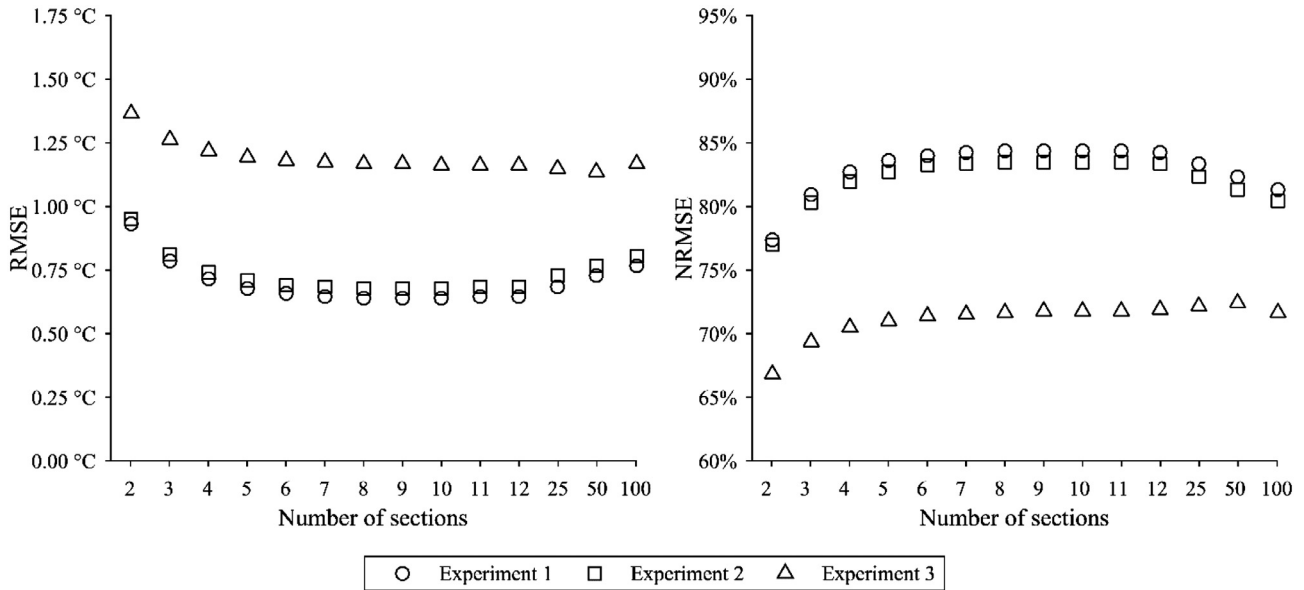


Fig. 7. RMSE and NRMSE values on validation data for radiator models calibrated based on the three distinct experiments with varying number of sections N_s .

structure, where the heat loss for each horizontal section is a function of the room air temperature. However, the temperature of the ambient air surrounding the radiator increases vertically, thus the model structure overestimates the heat loss in the top sections.

3.2. Performance of MPC schemes

The indoor air temperatures for the existing building in the simulated one-week period, using the constant setpoint tracking controller (reference) and the three MPC setups, respectively, are depicted in Fig. 9. The grey dashed lines indicate the thermal comfort bounds, and the bottom chart displays the historical time varying wholesale electricity prices. Compared to the reference controller, all the E-MPC schemes increased the space heating consumption and, consequently, increased the air temperatures in low price periods. Consequently, the thermal mass of the building constructions was charged and the heating consumption in the following high price periods was reduced. Overall, the trajectories depicted in Fig. 9 suggest that the three MPC setups resulted in similar space heating strategies.

It is noted that the simulations were only performed for a period of one week and for one specific apartment, which is why the specific absolute results cannot be used for generalizations on the effect of the MPC schemes. However, the observed tendencies are considered generalizable as they are consistent with previously obtained results investigating the performance of E-MPC [7,8,11].

The summarized results for the simulation week is presented in Table 4 and confirm that the three MPC setups achieved similar performance. Evaluation of the ability to achieve operational cost savings (Eq. (15)) showed that the three MPC setups achieved op-

erational cost savings of approx. 5% and 18% for the existing and retrofitted building, respectively. Furthermore, the ability to maintain an air temperature within the comfort bounds was evaluated as the number of degree hours where the air temperature violated the lower and upper temperature bounds. The performance was similar for all MPC setups, and the level of comfort violations was generally limited – a fact also indicated by Fig. 9. The reason for the minor comfort violations in setups a) and c), which solely relied on the control-model to predict the required space heating consumption, was the practically unavoidable building/control-model mismatch. In setup b), which relied on a low-level PI controller to track the setpoints specified by the MPC scheme, minor temperature over- and undershoots were observed when the low-level PI controller was switching between the upper and lower comfort bounds as setpoints.

The relative ability of the MPC setups to shift space heating consumption by exploiting the thermal mass as heat storage (Eq. (17)) is depicted in Figs. 10 and 11 for the existing and retrofitted building, respectively. A positive difference indicates a boosting period, where the room air temperature was increased to store heat, whereas a negative difference occurs at high price periods, where the heat storage was discharged. A negative difference of -100% indicates a period where the space heating was completely shut off. In general, the three MPC setups led to similar charging and discharging patterns.

The relative shifting potential was highest in the retrofitted building because of the lower reference heating consumption. The periods of complete heating shut-off were very limited in the existing building, whereas a total shut-off was possible for extended periods in the retrofitted building. Furthermore, Figs. 10 and

Table 4 Summarized simulation results.

		Energy	Operational cost	Cost savings	Comfort violations
Existing building	Reference	4.1 kWh/m ²	€ 12.0		0.4 °Ch
	Scenario (a)	4.3 kWh/m ²	€ 11.3	€ 0.7 (5.8%)	3.2 °Ch
	Scenario (b)	4.3 kWh/m ²	€ 11.3	€ 0.7 (5.8%)	3.7 °Ch
	Scenario (c)	4.4 kWh/m ²	€ 11.4	€ 0.6 (5.0%)	2.1 °Ch
Retrofitted building	Reference	1.4 kWh/m ²	€ 3.9		0.1 °Ch
	Scenario (a)	1.5 kWh/m ²	€ 3.2	€ 0.7 (18.0%)	2.3 °Ch
	Scenario (b)	1.5 kWh/m ²	€ 3.2	€ 0.7 (18.0%)	2.6 °Ch
	Scenario (c)	1.5 kWh/m ²	€ 3.2	€ 0.7 (18.0%)	1.6 °Ch

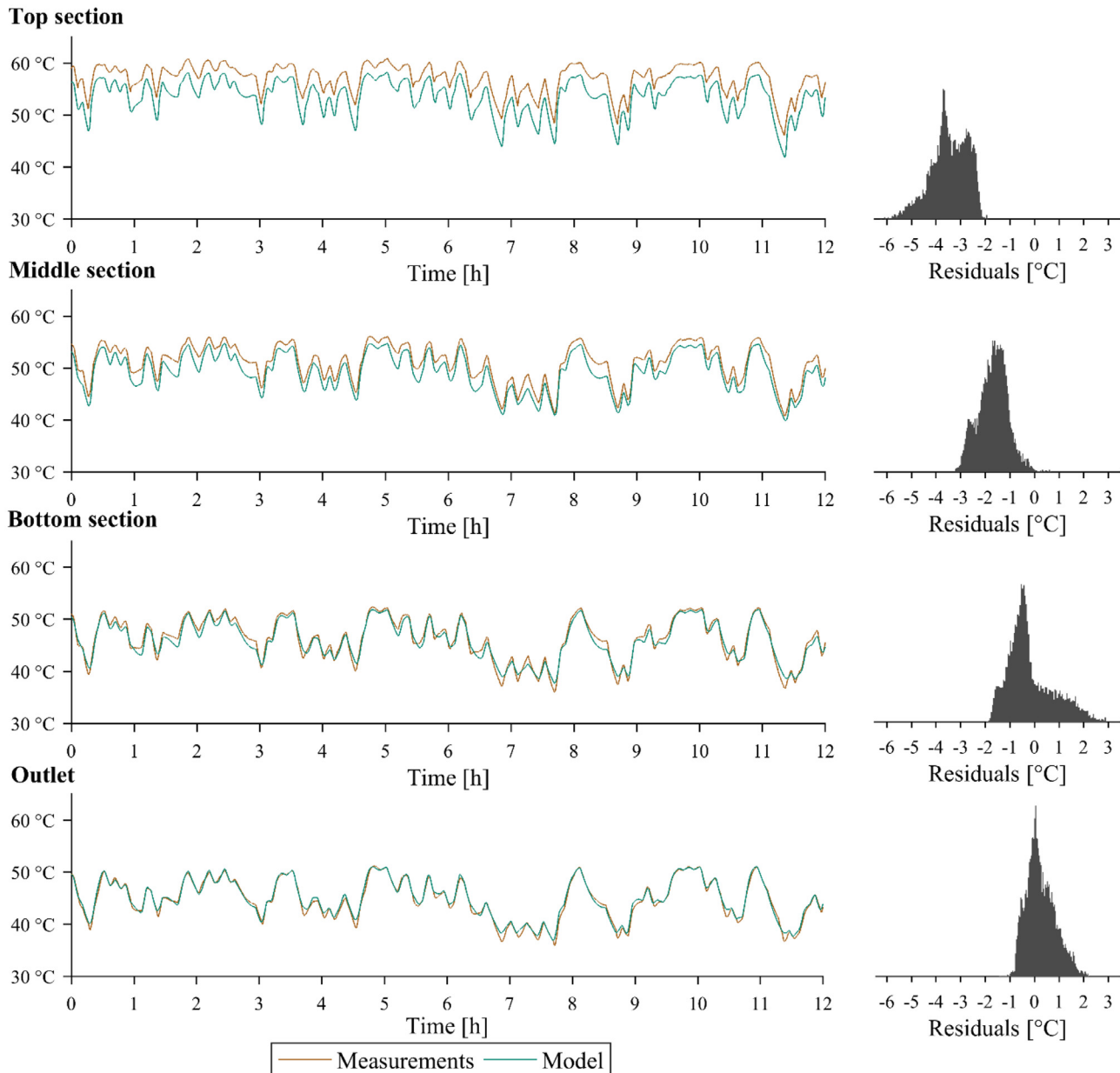


Fig. 8. Simulated system states compared to surface temperature measurements.

11 show that the temperature boosts resulted in space heating increases of up to approx. 100% and 300% compared to the reference controller for the existing and retrofitted building, respectively. For this to be possible, radiators have to be over-dimensioned when installed, which is typically the case in many existing Danish residential buildings in order to ensure fast response times and sufficient heating power given the worst-case weather conditions [30].

Fig. 12 displays the absolute shifting potential according to Eq. (16) for the existing and retrofitted building, respectively, using MPC setup (b). The simulation period was divided into six load shift events consisting of a charging and discharging period (see Eq. (18)). Overall, the existing building enabled the highest shifted consumption due to the generally higher reference consumption, whereas the retrofitted building enabled shifts over longer periods because of the increased storage efficiency. Information on the absolute charge and discharged heat in individual events is specified in Table 5 together with the shifting efficiency. In contrast to previous studies that used rule-based control to investigate the heat storage efficiency of thermal mass [9,31], the charging and dis-

Table 5
Specification of load shifting events.

		Charging	Discharging	η_{shifting}
Existing building	Event 1	108.1 Wh/m ²	-65.4 Wh/m ²	60.6%
	Event 2	86.8 Wh/m ²	-52.9 Wh/m ²	61.0%
	Event 3	102.8 Wh/m ²	-74.3 Wh/m ²	72.4%
	Event 4	79.7 Wh/m ²	-57.6 Wh/m ²	72.3%
	Event 5	88.5 Wh/m ²	-62.5 Wh/m ²	70.6%
	Event 6	79.4 Wh/m ²	-60.0 Wh/m ²	75.5%
Retrofitted building	Event 1	89.0 Wh/m ²	-57.9 Wh/m ²	65.1%
	Event 2	68.5 Wh/m ²	-53.3 Wh/m ²	77.9%
	Event 3	81.4 Wh/m ²	-69.3 Wh/m ²	85.1%
	Event 4	70.1 Wh/m ²	-56.6 Wh/m ²	80.7%
	Event 5	71.7 Wh/m ²	-57.7 Wh/m ²	80.5%
	Event 6	69.3 Wh/m ²	-70.4 Wh/m ²	101.5%

charging periods in this study varied in duration since the control was optimized based on the cost signal f .

As expected, the quantity of shifted consumption was slightly higher for the existing building; however, the shifting efficiency

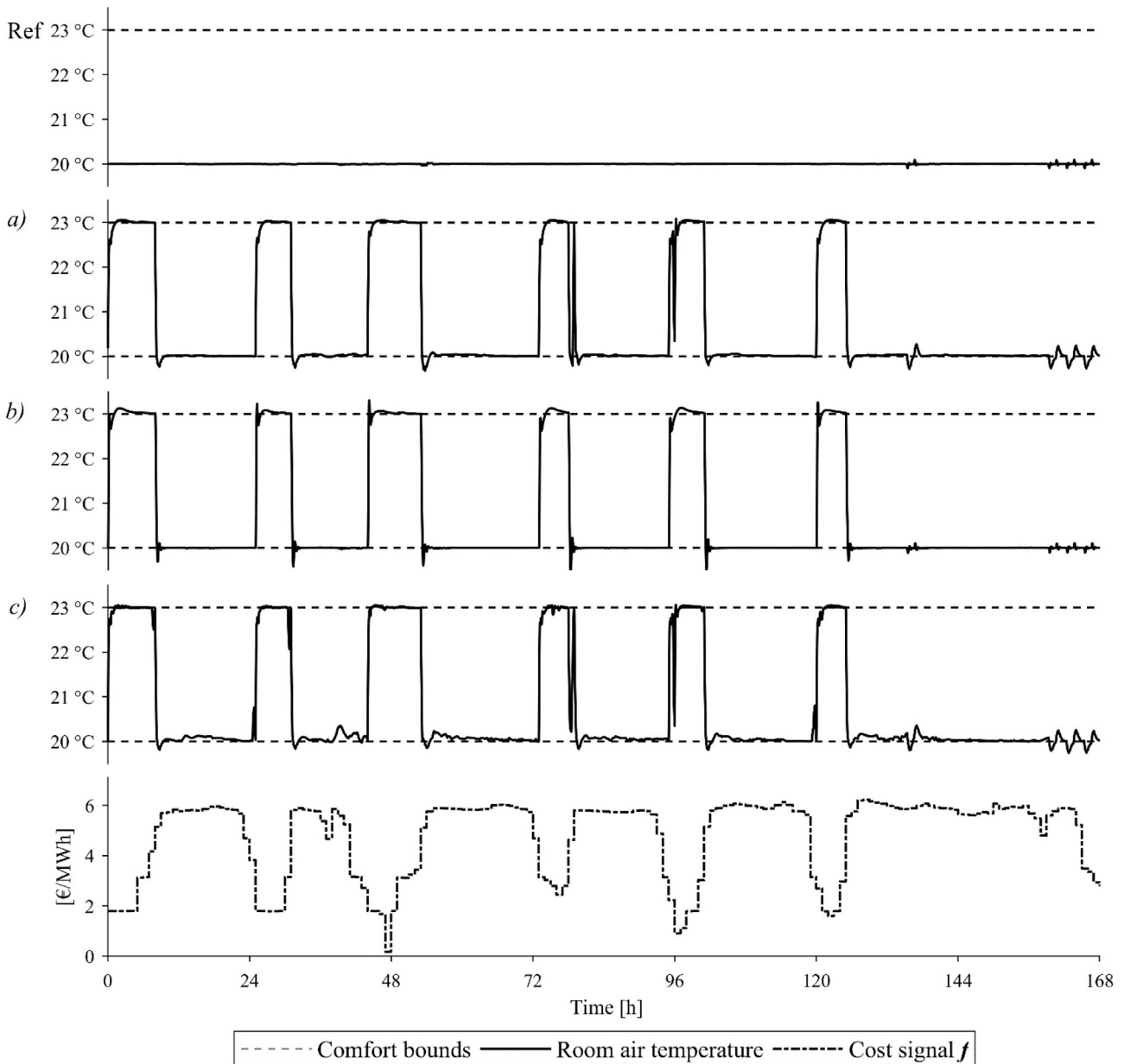


Fig. 9. One-week simulation results and associated cost signal.

was significantly higher for the retrofitted building. The efficiency of Event 6 was even above 100% since heat stored at previous events was not yet fully discharged coming into the event. This mechanism can also be observed in Fig. 11 where the relative consumption at the end of the fifth discharging period was still below zero before initiating charging period six. The observed shifted quantities and efficiencies are consistent with the results in [9].

4. Discussion

The results of this study showed very limited differences in performance between setups (a) and (b). This suggests that findings from previous studies using electrical baseboard heaters as in setup a), e.g. [7,8], also apply to buildings equipped with hydronic heating systems. Besides enabling a more broad generalization of previous research results, this equivalency also has a practical advantage. The simulation time for setup (c) significantly increased compared to setups (a) and (b) with a factor of up to 50. Based on

the findings of this study, it therefore seems practically reasonable that future simulation-based studies as well as real application of E-MPC for single-zone residential space heating rely on setup b). However, it may be necessary to include the dynamics of the radiator when operating multi-zone hydronic space heating systems or to investigate the dynamic response of the heating system.

Furthermore, in agreement with previous studies [7,8,9], the results suggest that the potential for shifting space heating consumption depends on the energy efficiency of the building envelope. The absolute potential for shifting energy on the short term was greater in the existing building because of the higher reference consumption, whereas the higher storage efficiency of the retrofitted building made it more suited for shifting loads over longer periods. Similarly, the retrofitted building allowed space heating to be completely shut off for multiple consecutive hours, while the existing building was incapable of sustaining comfortable temperatures without space heating. Despite these differences, the absolute loads shifted during the load shifting events were similar.

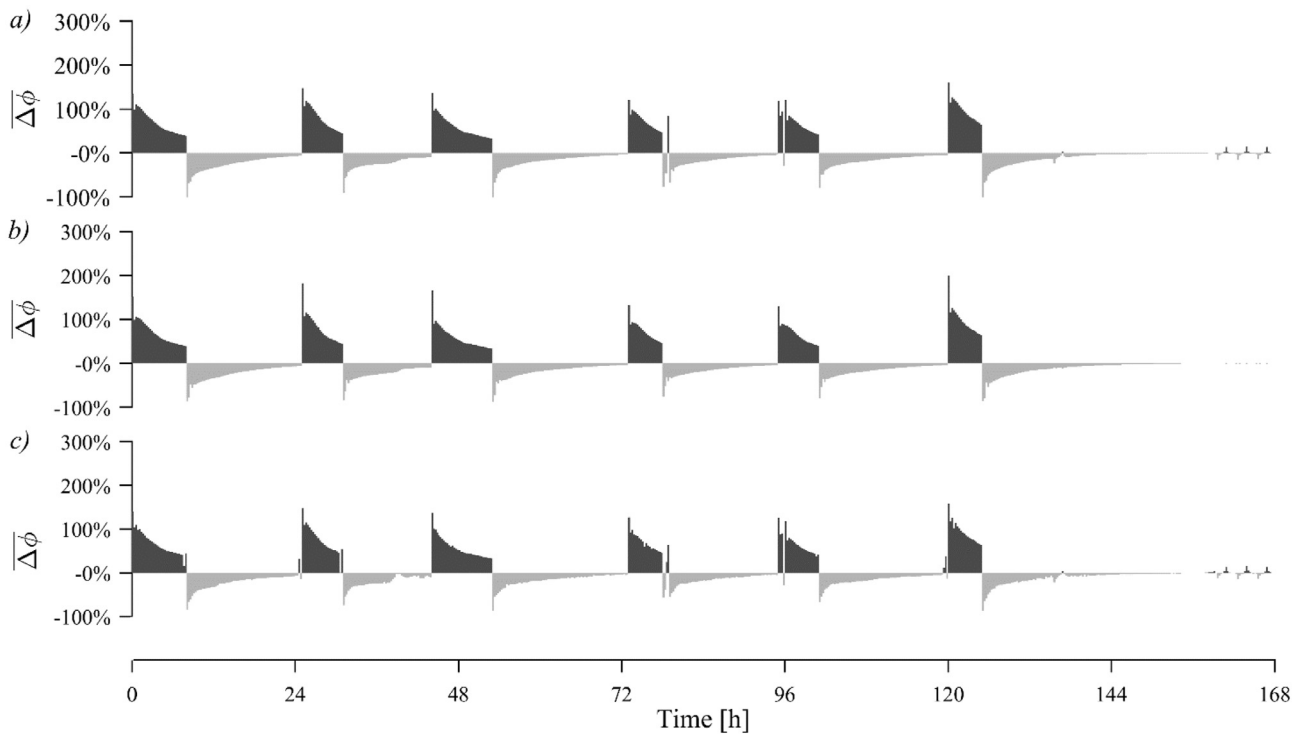


Fig. 10. Potential for exploiting the thermal mass as heat storage for the existing building.

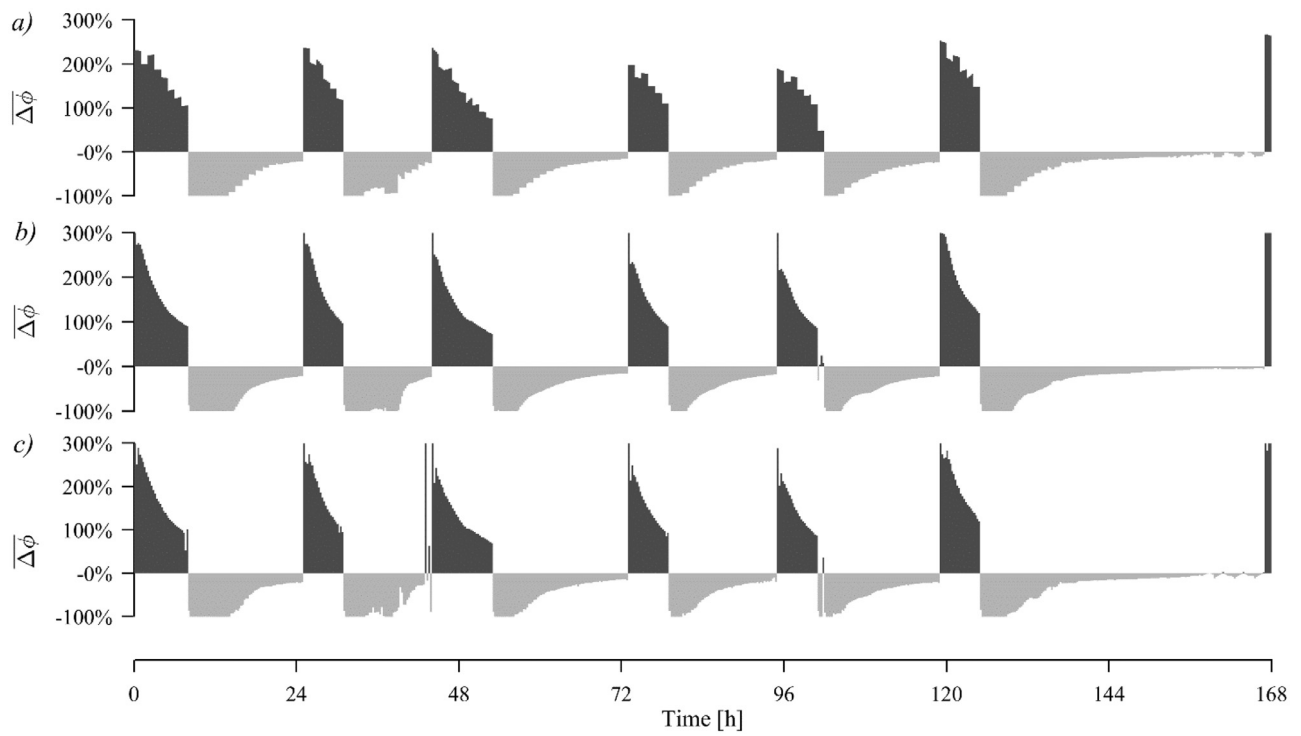


Fig. 11. Potential for exploiting the thermal mass as heat storage for the retrofitted building.



Fig. 12. Absolute shifting potential for the existing and retrofitted building using MPC setup (b).

5. Conclusion

This paper reported on the development of a reliable dynamic hydronic radiator model and an investigation of the effect of including the radiator dynamics in an associated MPC scheme for residential space heating with the objective to perform price-based demand response. Three MPC setups were defined: (a) a linear MPC controlling an electrical baseboard heater, (b) a two-level controller where a linear MPC calculated the heating setpoint for conventional PI-control of the hydronic radiator model, and (c) an N-MPC scheme that included the hydronic radiator in the control-model. The three MPC setups obtained similar simulation results, i.e. operational cost savings of approx. 5% and 18% in an existing and retrofitted building, respectively, while restricting the amount of thermal comfort violations to a limited extent. This suggest that the more practical two-level MPC implementation is preferable for real applications compared to the significantly more computational demanding N-MPC scheme for real applications.

The calibrated dynamic radiator model developed for this study was able to adequately simulate the behavior of the actual radiator when comparing measured experiment data with the states of the proposed dynamic model. As such, this paper also provides a reliable radiator model suitable for any simulation-based research study in which accurate representation of the dynamic behavior of hydronic radiators is desirable.

Acknowledgements

The authors gratefully acknowledge the support of this work from the project “READY.dk” financed by Energinet.dk (ForskEl) grant number [12305] and the project ‘Resource Efficient Cities Implementing Advanced Smart City Solutions’ (READY), financed by the 7th EU Framework Program (FP7-Energy project reference: 609127).

Appendix A

The complete system of non-linear ordinary differential equations of the hydronic radiator model.

$$C_{Rad} \cdot \frac{dt_1}{d\tau} = H_w \cdot q \cdot (t_{inlet} - t_1) \cdot N_S - \phi_N \cdot \left(\frac{t_1 - t_{room}}{\Delta t_{ar,N}} \right)^n \quad (A.1)$$

$$C_{Rad} \cdot \frac{dt_2}{d\tau} = H_w \cdot q \cdot (t_1 - t_2) \cdot N_S - \phi_N \cdot \left(\frac{t_2 - t_{room}}{\Delta t_{ar,N}} \right)^n \quad (A.2)$$

$$C_{Rad} \cdot \frac{dt_3}{d\tau} = H_w \cdot q \cdot (t_2 - t_3) \cdot N_S - \phi_N \cdot \left(\frac{t_3 - t_{room}}{\Delta t_{ar,N}} \right)^n \quad (A.3)$$

$$C_{Rad} \cdot \frac{dt_4}{d\tau} = H_w \cdot q \cdot (t_3 - t_4) \cdot N_S - \phi_N \cdot \left(\frac{t_4 - t_{room}}{\Delta t_{ar,N}} \right)^n \quad (A.4)$$

$$C_{Rad} \cdot \frac{dt_5}{d\tau} = H_w \cdot q \cdot (t_4 - t_5) \cdot N_S - \phi_N \cdot \left(\frac{t_5 - t_{room}}{\Delta t_{ar,N}} \right)^n \quad (A.5)$$

$$C_{Rad} \cdot \frac{dt_6}{d\tau} = H_w \cdot q \cdot (t_5 - t_6) \cdot N_S - \phi_N \cdot \left(\frac{t_6 - t_{room}}{\Delta t_{ar,N}} \right)^n \quad (A.6)$$

$$C_{Rad} \cdot \frac{dt_7}{d\tau} = H_w \cdot q \cdot (t_6 - t_7) \cdot N_S - \phi_N \cdot \left(\frac{t_7 - t_{room}}{\Delta t_{ar,N}} \right)^n \quad (A.7)$$

$$C_{Rad} \cdot \frac{dt_8}{d\tau} = H_w \cdot q \cdot (t_7 - t_8) \cdot N_S - \phi_N \cdot \left(\frac{t_8 - t_{room}}{\Delta t_{ar,N}} \right)^n \quad (A.8)$$

$$C_{Rad} \cdot \frac{dt_9}{d\tau} = H_w \cdot q \cdot (t_8 - t_9) \cdot N_S - \phi_N \cdot \left(\frac{t_9 - t_{room}}{\Delta t_{ar,N}} \right)^n \quad (A.9)$$

$$t_{outlet} = t_9 \quad (A.10)$$

References

- [1] S. Wang, X. Xue, C. Yan, Building power demand response methods toward smart grid, *HVAC&R Res.* 20 (6) (2014) 665–687.
- [2] E. Nyholm, S. Puranik, É. Mata, M. Odenberger, F. Johnsson, Demand response potential of electrical space heating in Swedish single-family dwellings, *Build. Environ.* 96 (2016) 270–282.
- [3] H. Lund, A.N. Andersen, P.A. Østergaard, B.V. Mathiesen, D. Connolly, From electricity smart grids to smart energy systems—A market operation based approach and understanding, *Energy* 42 (2012) 96–102.
- [4] J. Wang, H. Zhong, Z. Ma, Q. Xia, C. Kang, Review and prospect of integrated demand response in multi-energy system, *Appl. Energy* 202 (2017) 772–782.
- [5] M.D. Knudsen, S. Petersen, Model predictive control for demand response of domestic hot water preparation in ultra-low temperature district heating systems, *Energy Build.* 146 (2017) 55–64.
- [6] S. Stinner, K. Huchtemann, D. Müller, Quantifying the operational flexibility of building energy systems with thermal energy storages, *Appl. Energy* 181 (2016) 140–154.
- [7] T.H. Pedersen, R.E. Hedegaard, S. Petersen, Space heating demand response potential of retrofitted residential apartment blocks, *Energy Build.* 141 (2017) 158–166.
- [8] R.E. Hedegaard, T.H. Pedersen, S. Petersen, Multi-market demand response using economic model predictive control of space heating in residential buildings, *Energy Build.* 150 (2017) 253–261.
- [9] J. Le Dréau, P. Heiselberg, Energy flexibility of residential buildings using short term heat storage in the thermal mass, *Energy* 111 (2016) 991–1002.
- [10] J. Široký, F. Oldewurtel, J. Cigler, S. Privara, Experimental analysis of model predictive control for an energy efficient building heating system, *Appl. Energy* 88 (2011) 3079–3087.
- [11] M. Avci, M. Erkoç, A. Rahmani, S. Asfour, Model predictive HVAC load control in buildings using real-time electricity pricing, *Energy Build.* 60 (2013) 199–209.
- [12] G. Bianchini, M. Casini, A. Vicino, D. Zarrilli, Demand-response in building heating systems: A model predictive control approach, *Appl. Energy* 168 (2016) 159–170.
- [13] J. Kensby, A. Trüschel, J.-O. Dalenbäck, Potential of residential buildings as thermal energy storage in district heating systems—Results from a pilot test, *Appl. Energy* 137 (2015) 773–781.
- [14] M.A. Ahmed Awadelrahman, Y. Zong, H. Li, C. Agert, Economic model predictive control for hot water based heating systems in smart buildings, *Energy Power Eng.* 9 (2017) 112–119.
- [15] M. Wetter, Co-simulation of building energy and control systems with the building controls virtual test bed, *J. Build. Perform. Simu.* 3 (4) (2010) 1–19.
- [16] DL Radiators, "Radiatori Radel in Delonghi 2013".
- [17] L.H. Hansen, Stochastic Modelling of Central Heating Systems, IMM - DTU, Lyngby, 1997.
- [18] S. Holst, "TRNSYS-Models for radiator heating systems," München, 1996.
- [19] D. Risberg, M. Risberg, L. Westerlund, CFD modelling of radiators in buildings with user-defined wall functions, *Appl. Thermal Eng.* 94 (2016) 266–273.
- [20] Danfoss Heating Solutions, "Introduction to hydronic floor heating," 2010. <https://assets.danfoss.com/documents/DOC000086464411/DOC000086464411.pdf>.
- [21] H.A. Barker, GALOIS—A program for generating pseudo-random perturbation signals, 12th IFAC Symposium on System Identification (SYSID 2000), 2000.
- [22] M.W. Braun, D.E. Rivera, A. Stenman, W. Foslien, C. Hrenya, Multi-level pseudo-random signal design and "model-on-demand" estimation applied to non-linear identification of a RTP wafer reactor, American Control Conference, 1999.
- [23] EN 442-2:2014, Radiators and Convectors - Part 2: Test methods and Rating, CEN - European committee for standardization, Brussels, 2014.
- [24] F. Oldewurtel, A. Parisio, C.N. Jones, D. Gyalistras, M. Gweder, V. Stauch, B. Lehmann, M. Morari, Use of model predictive control and weather forecasts for energy efficient building climate control, *Energy Build.* 45 (2012) 15–27.
- [25] R.E. Kalman, A new approach to linear filtering and prediction problems, *J. Basic Eng.* 82 (1) (1960) 35–45.
- [26] T.H. Pedersen, M.D. Knudsen, R.E. Hedegaard, S. Petersen, Handling thermal comfort in economic model predictive control schemes for demand response, *Energy Procedia* (122) (2017) 985–990.
- [27] J.R. Dobbs, B.M. Hency, Model Predictive HVAC control with online occupancy model, *Energy Build.* 82 (2014) 675–684.
- [28] A. Acosta, A.I. González, J.M. Zamarreño, V. Álvarez, Energy savings and guaranteed thermal comfort in hotel rooms through nonlinear model predictive controllers, *Energy Build.* 129 (2016) 59–68 30.
- [29] T.H. Pedersen, R.E. Hedegaard, M.D. Knudsen, S. Petersen, Comparison of centralized and decentralized model predictive control in a building retrofit scenario, *Energy Procedia* 122 (2017) 979–984.
- [30] D.S. Østergaard, S. Svendsen, Theoretical overview of heating power and necessary heating supply temperatures in typical Danish single-family houses from the 1900s, *Energy Build.* 126 (2016) 375–383.
- [31] G. Reynders, J. Diriken, D. Saelens, Quantification method for the active demand response potential by structural storage in buildings, 14th International Conference of the International Building Performance Simulation Association, 2015.

**APPENDIX 3 PAPER: MODEL PREDICTIVE CONTROL OF
SPACE HEATING AND THE IMPACT OF TAXES ON DEMAND
RESPONSE: A SIMULATION STUDY (S3)**



AALBORG UNIVERSITY
DENMARK

Aalborg Universitet

CLIMA 2016 - proceedings of the 12th REHVA World Congress

Heiselberg, Per Kvols

Publication date:
2016

Document Version
Publisher's PDF, also known as Version of record

[Link to publication from Aalborg University](#)

Citation for published version (APA):
Heiselberg, P. K. (Ed.) (2016). CLIMA 2016 - proceedings of the 12th REHVA World Congress: volume 10. Aalborg: Aalborg University, Department of Civil Engineering.

General rights

Copyright and moral rights for the publications made accessible in the public portal are retained by the authors and/or other copyright owners and it is a condition of accessing publications that users recognise and abide by the legal requirements associated with these rights.

- ? Users may download and print one copy of any publication from the public portal for the purpose of private study or research.
- ? You may not further distribute the material or use it for any profit-making activity or commercial gain
- ? You may freely distribute the URL identifying the publication in the public portal ?

Take down policy

If you believe that this document breaches copyright please contact us at vbn@aub.aau.dk providing details, and we will remove access to the work immediately and investigate your claim.

Model Predictive Control of Space Heating and the Impact of Taxes on Demand Response: A Simulation Study

Michael Dahl Knudsen^{#1}, Rasmus Elbæk Hedegaard^{#2},
Theis Heidmann Pedersen^{#3}, Steffen Petersen^{#4}

*#Department of Engineering, Aarhus University
Inge Lehmanns Gade 10, 8000 Aarhus C, Denmark*

¹mdk@eng.au.dk, ²reh@eng.au.dk

³thp@eng.au.dk, ⁴stp@eng.au.dk

Abstract

Energy consumption for household HVAC systems constitutes a large demand response potential if it can be made flexible. One way of doing so is through a model predictive control (MPC) scheme that minimizes energy costs by shifting consumption according to a time-varying tariff. However, many studies on price-based demand response use tariffs with little or no taxes even though they often constitute a significant share of the total electricity price. This paper investigates the impact of taxes on the MPC-driven demand response potential for space heating. Simulations were conducted as co-simulations between EnergyPlus and MATLAB coupled by the Building Control Virtual Test Bed software. An economic MPC defined in MATLAB controls an electric radiator in a one-bedroom dormitory apartment. Three electricity tariffs with different taxes were tested as input to the MPC cost function to evaluate the effect on the DR potential: a tariff without taxes, a tariff with constant taxes and a tariff with variable taxes. The results indicated that taxes in general attenuate the load-flattening potential but reduced CO₂ emissions. Constant taxes were also found to reduce both the economic incentives of the end-consumer and the usage of wind power compared to a tariff without taxes while variable taxes did the opposite.

Keywords – *economic model predictive control; price-based demand response; space heating; taxes and levies;*

1. Introduction

As more and more intermittent renewable energy sources are introduced into the electric system it becomes increasingly difficult to rely solely on supply-side management to ensure grid stability. Price-based demand response (DR) is a demand-side management strategy that is often considered as a promising supplement to help keep balance in the electric system. The idea is to motivate consumers to change consumption pattern through varying electricity tariffs reflecting the state of the electric grid [2-4].

In the household sector, space heating represented approximately 68% of the total household energy consumption in the European Union [5]. Space heating therefore offers a great DR potential if this consumption can be made flexible. One possible approach to accomplish this is through an economic model predictive controller (E-MPC) that utilizes the thermal capacity of the building as an energy storage to be charged in periods with low energy prices and discharged when prices are high [6-10].

1.1 Related work and main objective

Many studies on price-based DR use the electricity spot price and ignore expenses associated with transportation of electricity, taxes and levies [6,8,11-13]. Other studies do recognize the importance of including all cost components but are often conducted in countries with a small share of taxes and levies such as Switzerland [1,7,9] where they represents 5.4% of the total tariff. In other countries such as Italy, Germany and Denmark taxes and levies represents the bulk of the total tariff [14-15] and this paper investigates how this affect the DR potential.

2. Simulation method

This study is based on co-simulations between an EnergyPlus model representing the true building [16] and an E-MPC controller defined in MATLAB [17]. The software environment Building Controls Virtual Test Bed handles the co-simulations [18-19].

A series of simulations have been carried out with different electricity tariffs to investigate the effects hereof. All simulations are performed for a simulation period from January 1 to February 14 and applies Danish electricity prices and system data from 2014 [20], and standard EnergyPlus weather data for Copenhagen [21].

2.1 EnergyPlus model

The simulated test case is a one-bedroom dorm located in Aarhus, Denmark, and its geometry is seen in Fig. 1.

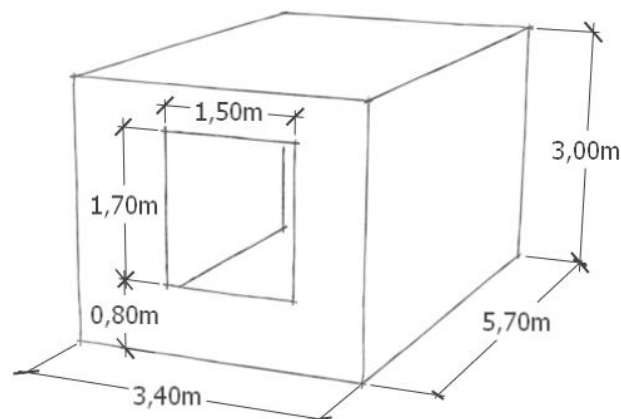


Figure 1. Geometry of the EnergyPlus model

There is an external south-facing wall with a window with a low-e glazing ($U=1.1 \text{ W}/(\text{m}^2\text{K})$, $g=0.63$). All other surfaces are internal and assumed to be adiabatic. Details regarding construction compositions are shown in Table 1. The dorm is equipped with a constant mechanical ventilation rate of 1.1 h^{-1} and has an infiltration rate of 0.05 h^{-1} . The heat source is an electric radiator and the heat power Φ is optimized by the E-MPC.

Table 1. Data for constructions used in the EnergyPlus model.

	Material	Thickness [m]	Resistance [$\text{m}^2\text{K}/\text{W}$]	Capacity [$\text{kJ}/(\text{m}^3\text{K})$]
External wall	concrete (ext.)	0.100	R=0.09	c=736
	insulation	0.250	R=6.76	c= 52
	concrete (int.)	0.200	R=0.18	c=736
Internal wall	concrete	0.180	R=0.16	c=736
Ceiling/ Floor	wood floor	0.025	R=0.17	c=991
	air space	0.050	R=0.10	
	concrete	0.220	R=0.20	c=736

2.2 Economic model predictive control

The control objective is to find the optimal heat sequence, $\bar{\Phi}_{OPT}$, defined as the heat sequence that minimize the linear cost function (1) subjected to various constraints (equations 1.a-1.e). The cost J represents the accumulated electricity cost over a prediction horizon of 72 hours and $p_x[k]$ is the electricity tariff in the k^{th} hour. Similar formulations and further details can be found in [6-10].

$$\min_{\Phi} J = \sum_{k=0}^{71} p_x[k] \cdot \Phi[k] \quad (1)$$

$$\text{s.t.} \quad \left. \begin{aligned} \bar{x}[k+1] &= \mathbf{A}\bar{x}[k] + \mathbf{B}\Phi[k] + \mathbf{E}\bar{d}[k] \\ T[k] &= \mathbf{C}\bar{x}[k] \end{aligned} \right\} \quad (1.a)$$

$$\bar{x}[0] = \hat{x}_{INI} \quad (1.b)$$

$$0 \leq \Phi[k] \leq 500 \text{ W} \quad (1.c)$$

$$21.6 \text{ }^\circ\text{C} \leq T[k] \leq 25.0 \text{ }^\circ\text{C} \quad (1.d)$$

$$-1.0 \frac{^\circ\text{C}}{\text{h}} \leq \frac{\Delta T[k]}{\Delta t} \leq 1.0 \frac{^\circ\text{C}}{\text{h}} \quad (1.e)$$

The first constraint (1.a) represents the system dynamics formulated as a linear state space system, where \bar{x} are the states of the system, Φ is the heat input, \bar{d} are the disturbances (ambient temperature and solar irradiation) and T is the room air temperature. **A**, **B**, **E** and **C** are black-box system matrices that captures the thermal dynamics of the EnergyPlus model and are determined via system identification (N4SID) [22]. Constraint (1.b) sets the initial state, (1.c) constrain the heat input according to the physical limitations of the radiator, (1.d) constrain room temperature and (1.e) constrain the rate of change of the room temperature.

The solution, $\bar{\Phi}_{OPT}$, is the optimal heat sequence over the entire horizon of 72 hours but only the first input, $\Phi[0]$, is applied. The problem is therefore solved again in the following hour – an approach known as the receding horizon procedure.

3. Construction of tariffs

The different tariffs that have been tested as input, p_x , in the objective function (1) were constructed according to the methodology described by Ulbig and Anderson [1]. However, this method is extended in this paper to also include variable taxes in one of the tested tariffs (see section 3.3).

All test-tariffs are exclusive of VAT but this has no effect on $\bar{\Phi}_{OPT}$. This is because the tariff inclusive of VAT, $p_{x,VAT}$, is calculated from the tariff exclusive of VAT, p_x , as follows:

$$p_{x,VAT} = f_{VAT} \cdot p_x \quad (2)$$

where f_{VAT} is a conversion factor (1.25 in Denmark). If we replaced p_x in (1) with the expression of $p_{x,VAT}$ in (2) we would simply get a new objective function similar to (1). The only difference is the constant f_{VAT} , which could be moved outside of the summation and therefore just scales J without changing $\bar{\Phi}_{OPT}$. Furthermore, the end-consumer also pays subscription fees but these are independent of Φ and would therefore be added as a constant term in (1). This term would not affect $\bar{\Phi}_{OPT}$ and is therefore omitted.

3.1 Baseline tariff (“Today’s tariff”)

The baseline tariff, p_{BASE} , is a constant tariff corresponding to the average tariff that Danish households paid in 2014 [15]. This tariff is comprised of four components:

$$p_{BASE} = c_{COM} + c_{TRA} + c_{EL_TAX} + c_{PSO} \quad (3)$$

where c_{COM} is the average commercial cost of electricity determined by the price on the Nordic spot market [23] plus expenses to the electricity supplier, c_{TRA} is the average cost due to transmission and distribution of electricity, c_{EL_TAX} is the average electricity tax and c_{PSO} is the average public

service obligations (PSO) levy. Table 2 shows the average values of these components in 2014 and their share of the total tariff.

Table 2. Components of the Danish electricity tariff in 2014 [15]

Component		Cost [DKK/MWh]	Share [%]
Spot	c_{COM}	352.8	30
Transportation	c_{TRA}	221.8	19
Tax*	c_{EL_TAX}	412.0	35
PSO	c_{PSO}	190.0	16
Total (excl. VAT)	p_{BASE}	1176.6	100

*The electricity tax for electric heating is lower than for other purposes.

3.2 Tariffs with constant taxes

Many studies on price-based DR apply the market spot price directly into the cost function but this is inappropriate as pointed out by Ulbig and Anderson [1] since the spot price does not represent the entire price. They therefore propose the following tariff:

$$p[k] = \frac{Spot[k]}{\overline{Spot}} \cdot c_{COM} + \frac{Load[k]}{\overline{Load}} \cdot c_{TRA} + c_{TAX} \quad (4)$$

where $Spot[k]$ is the spot price in the k^{th} hour, \overline{Spot} is the average spot price, $Load[k]$ is the grid load [20] in the k^{th} hour, \overline{Load} is the average grid load and c_{TAX} is taxes and levies. This way the commercial costs are scaled according to the current spot price, transportation costs are scaled according to the current grid load and taxes and levies are included as a constant term. It is important to realize that a constant electricity consumption under this tariff will result in the same yearly costs as under the constant tariff $c_{COM} + c_{TRA} + c_{TAX}$.

The studies that (to the knowledge of the authors) applies this method are all conducted for Switzerland where taxes and levies represents only 5.4% of the total tariff [1,9]. In many other countries, this percentage is significantly higher [14], e.g. 51% in Denmark (Table 2). To test the effect that taxes and levies have on the performance of the E-MPC the following tariffs are defined:

$$p_{NO_TAX}[k] = \frac{Spot[k]}{\overline{Spot}} \cdot c_{COM} + \frac{Load[k]}{\overline{Load}} \cdot c_{TRA} \quad (4.a)$$

$$p_{CON_TAX}[k] = \frac{Spot[k]}{\overline{Spot}} \cdot c_{COM} + \frac{Load[k]}{\overline{Load}} \cdot c_{TRA} + c_{EL_TAX} + c_{PSO} \quad (4.b)$$

where p_{NO_TAX} is a tariff without taxes and levies, and p_{CON_TAX} is a tariff that includes the Danish electricity tax and PSO levy. The difference in performance of the E-MPC under these two tariffs will show how taxes and levies can affect the DR potential.

3.3 Tariff with variable taxes

It seems natural to further develop (4) to also include variable taxes as follows:

$$p_{VAR_TAX}[k] = \frac{Spot[k]}{\overline{Spot}} \cdot c_{COM} + \frac{Load[k]}{\overline{Load}} \cdot c_{TRA} + \frac{CO_2[k]}{\overline{CO_2}} \cdot c_{EL_TAX} + f_{PSO}[k] \cdot c_{PSO} \quad (5)$$

where $CO_2[k]$ is the CO_2 intensity associated with the electricity production in the k^{th} hour, $\overline{CO_2}$ is the average CO_2 intensity, $f_{PSO}[k]$ is the PSO scaling factor in the k^{th} hour (to be explained). The electricity tax is thus scaled according to the CO_2 intensity which is aligned with the reasons for introducing electricity tax: to encourage a better usage of resources and to reduce pollution including CO_2 emissions [24]. Another intension of the electricity tax is to provide revenue for the state. For this purpose, it is an important property of the tariff that a constant electricity consumption results in the same yearly electricity tax as under a constant tax. The end-consumer is able to obtain a tax discount only if consumption is shifted to periods with a CO_2 intensity below average. Conversely, the end-consumer will get a price surcharge if electricity is used in periods with high CO_2 intensity.

The scaling of the PSO levy is more complicated but is also based on the intension of the levy: to cover a range of expenses such as subsidies for wind turbines, subsidies for decentralized heat and power plants and research activities etc. The subsidies for wind power represented 51% of the total PSO expenses in 2014 [25] and are paid as a supplement to the spot price. They decrease as the spot price increase [26] and are therefore high in periods with low market prices combined with a high wind power production. The detailed calculation of $f_{PSO}[k]$ is not included here but it is essentially constructed so that it scales the PSO component to be low in periods with high subsidies (see Fig. 2). This motivates the end-consumer to shift consumption towards periods with a combination of low market prices and a high production from wind turbines, thus reducing the need for subsidies.

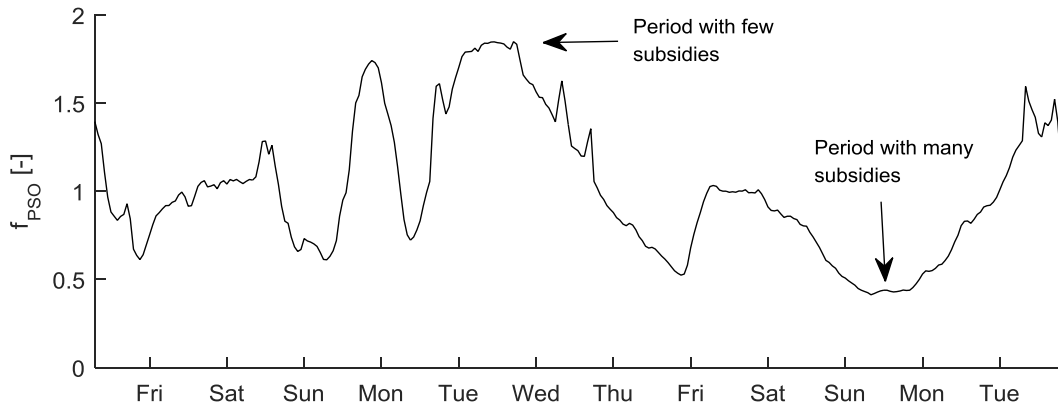


Figure 2. PSO Scaling factor as a function of time

4. Results

Fig. 3 is a time sample of the simulation results that visualize the behaviour of the E-MPC when exposed to the different tariffs. It appears that the tariff with no taxes gives rise to the most flexible behavior based on a visual inspection of the number of periods with heat-boosts that charge the thermal capacity of the building and hence increase the room temperature. The two tariffs with taxes seems to attenuate this behavior but less so for the tariff with variable taxes.

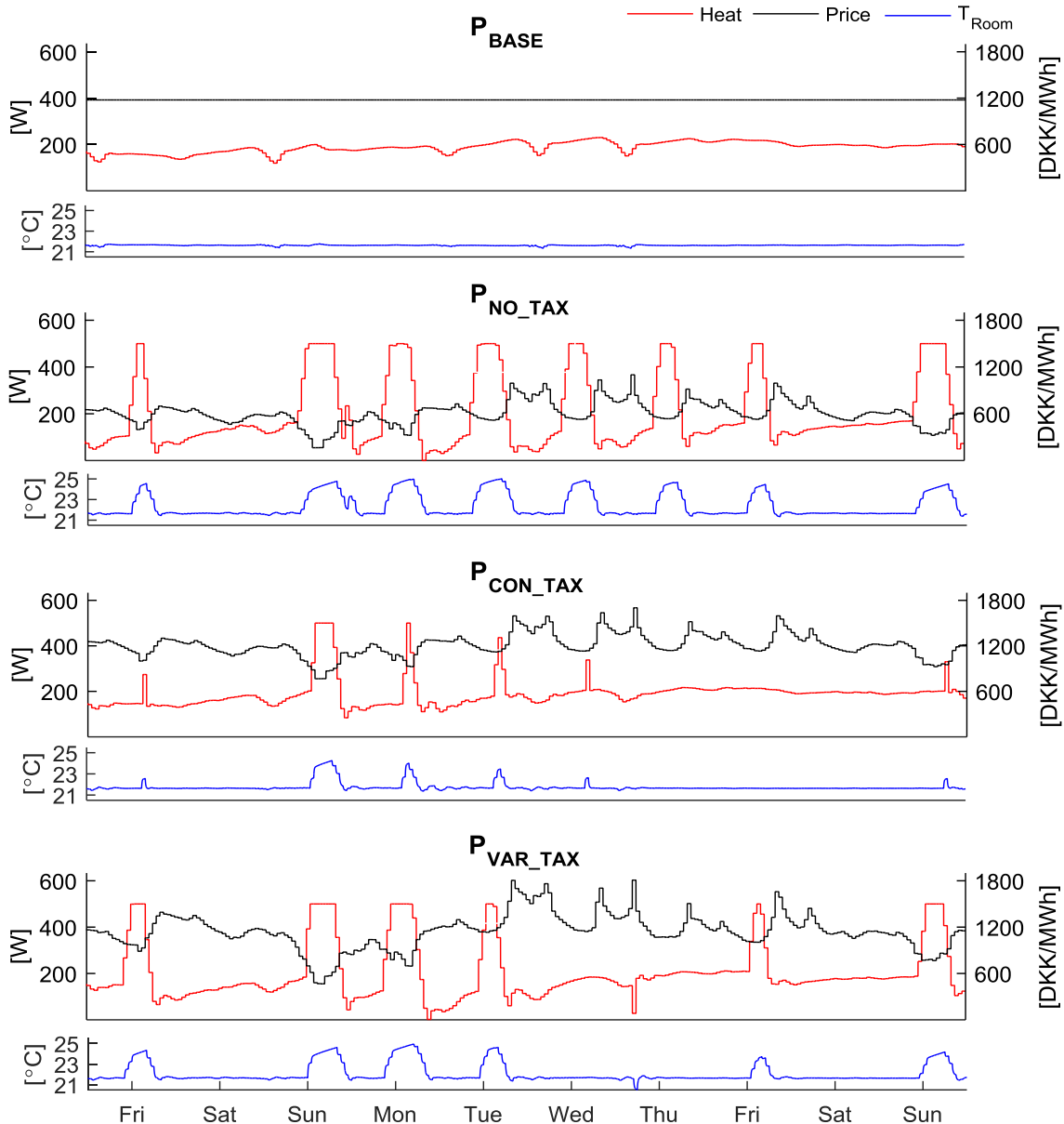


Figure 3. Time sample of the simulation results for the tested tariffs.

Fig. 4 depicts different performance indicators of the three test tariffs compared to the baseline tariff. The bar plot to the left shows that all tariffs resulted in an increased total electricity consumption (blue bar) especially the tariff with no tax, which is in line with the tendencies in Fig. 3. All three tariffs

also increased the usage of wind power but the tariff with variable taxes outperforms the others. Furthermore, the tariff without tax increased the usage of electricity from other sources than wind turbines (red bar) and increased the total CO₂ emissions (black bar). In contrast, both tariffs with taxes reduced the usage of non-wind generated electricity and CO₂ emissions but the variable taxing scheme proved most effective. The bar plot to the right in Fig. 4 shows how the tariffs managed to shift consumption to low load periods (9 PM–6 AM) from peak load periods (8 AM–12 PM & 5 PM–7 PM) and high load periods (the remaining periods). The tariff with no tax reduced consumption in peak and high load periods with 52% and 40%, respectively, and hence contributed significantly to flatten out the overall load in the electric grid. This load-flattening is reduced for the tariffs with taxes but less so for the tariff with variable taxes.

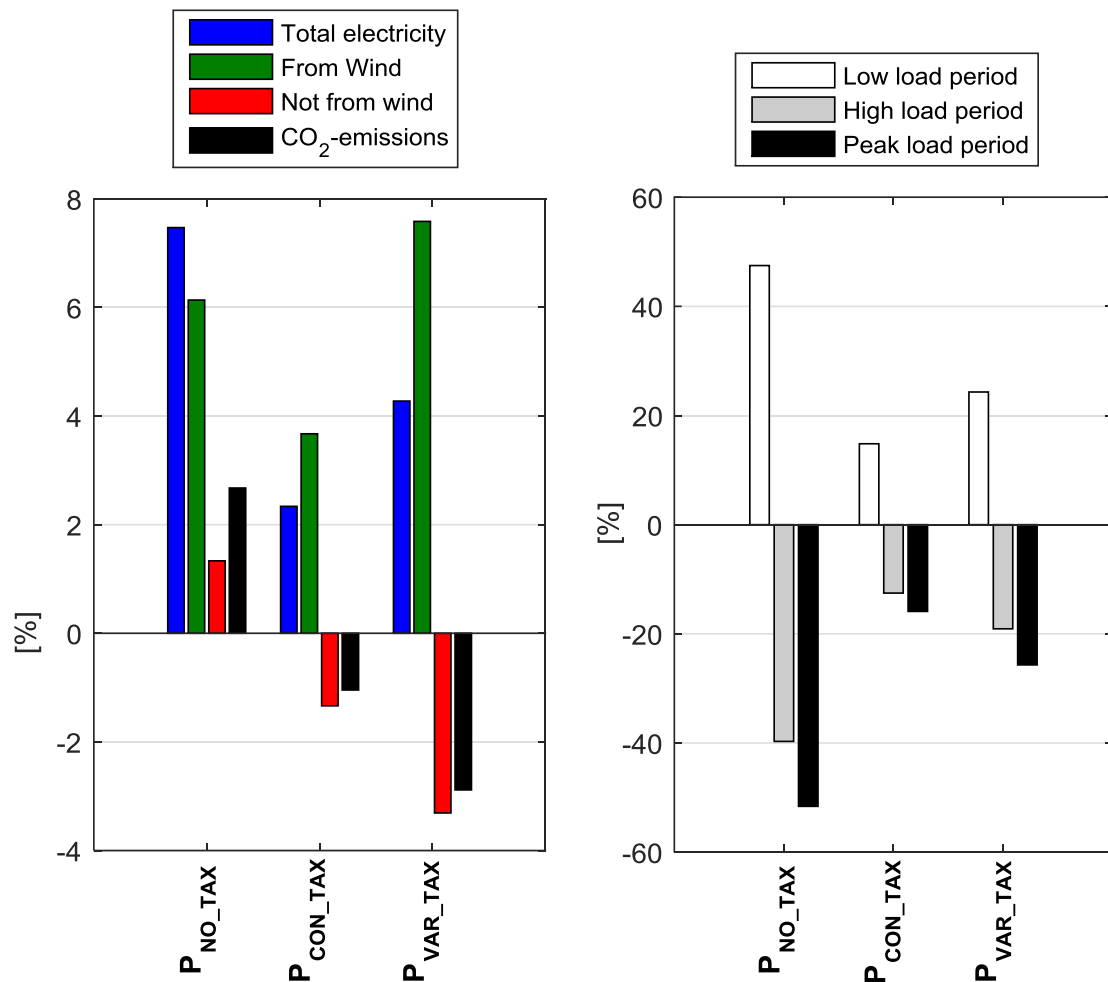


Fig. 4 Performance indicators for the tested tariffs evaluated in percentage w.r.t. the baseline tariff (3)

Finally, Table 3 shows the economic performance of the tariffs. The baseline costs are shown in absolute values while the other tariffs are shown relative to this. The tariff without taxes obtained savings on the spot and transport components and pays, of course, no tax or PSO. This gives a total

saving of 8.9% compared to the sum of the baseline spot and transport costs. The tariff with constant taxes obtained smaller savings on the spot and transport component, and end up paying more electricity tax and PSO levies due to the increased electricity consumption. The total saving is therefore only 1.6% compared to the total baseline cost. The tariff with variable taxes obtained savings on all components and end up with a total saving of 4.9%. Although the tariff without taxes obtained the largest saving in percentage the largest saving in absolute values is obtained by the tariff with variable taxes. The economic incentives are thus significantly reduced by constant taxes but increased when they are made variable.

Table 3. Economic performance. Baseline values are absolute and the others are relative to this.

	P_{BASE} [DKK]	P_{NO_TAX} [DKK]	P_{CON_TAX} [DKK]	P_{VAR_TAX} [DKK]
Com. (spot)	52.4	-6.1	-4.3	-5.2
Trans.	33.0	-1.5	-0.7	-0.7
Tax	61.2	-	1.4	-2.3
PSO	28.2	-	0.7	-0.3
Total	174.9	-7.6* (-8.9%)	-2.8 (-1.6%)	-8.6 (-4.9%)

*Compared to a baseline including only commercial and transportation costs.

5. Discussion and conclusion

The results presented in this study must be taken with some reservations. First of all, the simulations applied perfect forecasts of weather and electric grid data, which means that the obtained results should be considered as the performance bound. Secondly, the obtained results depended on a number of factors such as simulation period, building type and heating system, etc. Despite of these reservations, the authors expect that the following tendencies in general will hold: 1) taxes attenuate the load flattening potential but reduce CO₂ emissions, 2) variable taxes perform better than constant taxes on all performance indicators, and 3) constant taxes reduces the economic incentive of the end-customer while variable taxes increases the incentive.

Whether variable taxes should be introduced or not is a political decision. It might therefore be of political interest that variable taxes reduces the revenue for the state slightly but in return the pollution measured in CO₂ emissions is reduced, which is part of the intension of the tax. Furthermore, the PSO revenue is slightly reduced but in return the usage of electricity from wind turbines is significantly increased by variable taxes which would arguably lessen the need for subsidies.

Acknowledgment

The work presented in this paper was supported by The Danish Energy Agency project (no. 12019) - Virtual Power Plant for Smart Grid Ready Buildings (VPP4SGR) and Aarhus University, Denmark.

References

- [1] A.Ulbig and G.Andersson. Towards variable end-consumer electricity tariffs reflecting marginal costs: A benchmark tariff. *Energy Market Conference* 7 (June 2010) 23-25.
- [2] M.H.Albadi and E.F.El-Saadany. A summary of demand response in electricity markets. *Electronic Power Systems Research* 78(11) (November 2008) 1989-96.
- [3] N.O'Connell, P.Pinson, H.Madsen and M.O'Malley. Benefits and challenges of electrical demand response: A critical review. *Renewable and Sustainable Energy Reviews* 39 (November 2014) 686-99.
- [4] G.Strbac. Demand side management: Benefits and challenges *Energy Policy* 36(12) (December 2008) 4419-26.
- [5] European Environment Agency (EEA). Energy efficiency and energy consumption in the household sector. <http://www.eea.europa.eu> (2016).
- [6] R.Halvgaard, N.K.Poulsen, H.Madsen and J.B.Jørgensen. Economic Model Predictive Control for Building Climate Control in a Smart Grid. *Innovative Smart Grid Technologies* (January 2012) 1-6.
- [7] E.Vrettos, K.Lai, F.Oldewurtel and G.Andersson. Predictive Control of Buildings for Demand Response with Dynamic Day-ahead and Real-time Prices. *European Control Conference* (July 2013) 2527-34.
- [8] M.D.Knudsen and S.Petersen. Demand Response Potential of Model Predictive Control of Space Heating based on Price and CO₂ Intensity Signals. [Submitted to *Energy and Buildings*].
- [9] F.Oldewurtel, A.Ulbig, A.Parisio, G.Andersson and M.Morari. Reducing Peak Electricity Demand in Building Climate Control using Real-Time Pricing and Model Predictive Control. *IEEE Conference on Decision and Control* (December 2010) 1927-32.
- [10] D.Sturzenegger, D.Gyalistras, M.Gwerder, C.Sagerschnig, M.Morari and R.S. Smith. Model Predictive Climate Control of a Swiss Office Building: Implementation, Results, and Cost-Benefit Analysis. *IEEE Transactions on Control Systems Technology* 24(1) (2015) 1-12.
- [11] L.Schibuola, M.Scarpa and C.Tambani. Demand response management by means of heat pumps controlled via real time pricing. *Energy and Buildings* 90 (2015) 15-28.
- [12] M.Avcı, M.Erkoc, A.Rahmani and S.Asfour. Model predictive HVAC load control in buildings using real-time electricity pricing. *Energy and Buildings* 60 (2013) 199-209.
- [13] K.Paridari, A.Parisio, H.Sandberg and K.H.Johansson. Energy and CO₂ efficient scheduling of smart appliances in active houses equipped with batteries. *IEEE International Conference on Automation Science and Engineering* (August 2014) 623-9.
- [14] Eurostat, *Statistics Explained*, <http://ec.europa.eu/eurostat/statistics-explained> (2016)
- [15] Association of Danish Energy Companies. Electric Utility tariffs and electricity prices (Danish title: *Elforsyningsens tariffer & elpriser*) (2015).
- [16] US Department of Energy. *EnergyPlus* 8.1.0 Build 009 (December 2013).
- [17] The MathWorks, Inc. *MATLAB R2015a* (8.5.0.197613) (February 2015).
- [18] Lawrence Berkeley National Laboratory, *Building Controls Virtual Test Bed (BCVTB)* 1.5.0 (January 2015).
- [19] M.Wetter. Co-simulation of building energy and control systems with the Building Controls Virtual Test Bed. *Journal of Building Performance* 4(3) (September 2011) 185-203.
- [20] Energinet.dk. Introduction to download of market data. <http://www.energinet.dk/EN/El/Engrosmarked/Udtraek-af-markedsdata/Sider/Om-markedsdata.aspx> (2016).
- [21] US Department of Energy. *Energy Efficiency & Renewable Energy. EnergyPlus Weather Data – Copenhagen 061800 (IWEC)*. [https://energyplus.net/weather\(2016\)](https://energyplus.net/weather(2016)).
- [22] The MathWorks, Inc. *MATLAB R2015b, System Identification Toolbox* 9.2.
- [23] Nord Pool. *Day-Ahead Market Elspot*. <http://www.nordpoolspot.com> (2016).
- [24] SKAT (the Danish Tax Administration), *Den juridiske vejledning* 2015-2. <http://www.skat.dk/SKAT.aspx?oID=2061601&chk=211047> (2016).
- [25] Energinet.dk. *Specification af PSO-tariffen*. <http://www.energinet.dk> (2016).
- [26] Danish Energy Agency. *Oversigt over støtteregele*. <http://www.ens.dk> (2016).

**APPENDIX 4 PAPER: HANDLING STOCHASTIC OCCUPANCY
IN AN ECONOMIC MODEL PREDICTIVE CONTROL
FRAMEWORK FOR HEATING SYSTEM OPERATION IN
DWELLINGS (S4)**



AALBORG UNIVERSITY
DENMARK

Aalborg Universitet

CLIMA 2016 - proceedings of the 12th REHVA World Congress

Heiselberg, Per Kvols

Publication date:
2016

Document Version
Publisher's PDF, also known as Version of record

[Link to publication from Aalborg University](#)

Citation for published version (APA):
Heiselberg, P. K. (Ed.) (2016). CLIMA 2016 - proceedings of the 12th REHVA World Congress: volume 10. Aalborg: Aalborg University, Department of Civil Engineering.

General rights

Copyright and moral rights for the publications made accessible in the public portal are retained by the authors and/or other copyright owners and it is a condition of accessing publications that users recognise and abide by the legal requirements associated with these rights.

- ? Users may download and print one copy of any publication from the public portal for the purpose of private study or research.
- ? You may not further distribute the material or use it for any profit-making activity or commercial gain
- ? You may freely distribute the URL identifying the publication in the public portal ?

Take down policy

If you believe that this document breaches copyright please contact us at vbn@aub.aau.dk providing details, and we will remove access to the work immediately and investigate your claim.

Handling Stochastic Occupancy in an Economic Model Predictive Control Framework for Heating System Operation in Dwellings

Theis Heidmann Pedersen^{#1}, Michael Dahl Knudsen^{#2},
Rasmus Elbæk Hedegaard^{#3} and Steffen Petersen^{#4}

*#Department of Engineering, Aarhus University
Inge Lehmanns Gade 10, 8000 Aarhus C, Denmark*

¹thp@eng.au.dk, ²mdk@eng.au.dk, ³reh@eng.au.dk, ⁴stp@eng.au.dk

Abstract

This paper investigates the effect of integrating a proposed time inhomogeneous occupancy model in an Economic Model Predictive Control framework. Utilizing Model Predictive Control when planning the operation of the HVAC systems enables thermal conditioning based on information regarding the current occupancy and predictions of future occupancy. Performance evaluation of the proposed occupancy model is based on simulations of a one-bedroom apartment subject to stochastic occupancy derived from real-world CO₂ measurements. The simulation results suggest that an occupancy model with a sub-hourly temporal resolution reduces occupancy prediction errors compared to an hourly temporal resolution. The consequences of this are significantly reduces thermal comfort violations but only minor cost savings.

Keywords - Economic Model Predictive Control; Stochastic Occupancy; Occupancy Prediction; Markov Chain

1. Introduction

The thermal indoor climate of a building and, consequently, the need for heating, ventilation and air conditioning (HVAC) is highly affected by the internal heat gains generated by the metabolism of the occupants and their use of electrical equipment [1]. The common way to integrate occupancy information in HVAC control systems is to repeat a static 24-hour schedule. However, static schedules do not capture the stochastic nature of people, which may lead to uncomfortable thermal conditions or waste of energy because HVAC systems maintain thermal comfort in unoccupied building zones [2, 3]. One way to consider the stochastic nature of occupant presence in HVAC operation is to implement real-time occupancy detection, which has demonstrated to reduce energy consumption and uncomfortable thermal indoor climate conditions [4]. However, due to the thermal time-delay of the building first arrived occupants may experience uncomfortable thermal conditions. Furthermore, when awaiting the departure of the last occupant the thermal storage in the building mass is not fully exploited. The concept of Model Predictive Control (MPC) is able to accommodate this. MPC uses a model of the building dynamics together with predictions of the disturbances

acting on the building to optimize the HVAC operation by minimizing a cost function [5]. MPC is thus able to include information regarding the current occupancy and predictions of future occupancy for optimal HVAC operation.

The development of occupancy models with the objective to imitate realistic occupancy was first designed for building simulations tools [6, 7]. Page et al. [8] proposed a two-state time inhomogeneous Markov chain model, assuming that the probability of occupant presence satisfies a first order Markovian property, i.e. the future state at discrete time-step $k+1$ only depends on the current state at discrete time-step k . The assumption of a first-order Markovian property is also employed to model occupant presence patterns for employees in an office environment [9]. The model was defined as a generalized linear model based on a time inhomogeneous Markov chain, which captured the two-peak distribution of occupancy and demonstrated similar mean occupancy as the observations.

The integration of a Markov chain based occupancy model in a MPC framework has been proposed by Dobbs and Hency [10]. In their study, the integration of occupancy prediction yielded an energy saving potential of 31-44% compared to a baseline controller when considering very simple fabricated occupancy profiles. The same authors extended the methodology by implementing an automatic-trained Markov chain occupancy model, based on real occupancy data from an office building [4]. The proposed method uses fractional occupancy for each time-step to increase the precision of the occupancy prediction. However, a fraction of 0.5 (equivalent to 30 minutes with a time-step of 1 hour) do not inform whether the occupants stayed in the first or last part of the time-step or if the stays fluctuated throughout the time-step. The length of the occupancy period and the number of occupancy fluctuations has been shown to affect the MPC controller significantly [11], causing up to 25% difference on the total energy consumption.

1.1 Main Objective and Outline

This paper reports on a simulation-based investigation of the performance of an economic MPC which includes occupancy detection and predictions for optimal heating system operation of a one-bedroom apartment. The concept is similar to the one suggested by Dobbs and Hency [4] but the case is rather different. Furthermore, instead of using binary hourly values or hourly percentages of occupancy it is investigated whether an occupancy model with a sub-hourly temporal resolution improves the performance of the concept.

2. Markov Chain Occupancy Model

The occupancy model is a two-state first-order Markov chain model [8], which at every discrete time-step k yields a binary value of either $X_k=0$ or $X_k=1$ indicating vacancy or occupancy, respectively. The probability of continuing or changing state is dependent of the time of day k and the current state X_k and is collected in a time inhomogeneous right stochastic matrix (1). Since the sum

of each row is one, only estimates of p_{01} and p_{10} are required. It is assumed that the transition probabilities are periodic with a period of 24-hours but a distinction between workdays and weekends are made.

$$T_k = \begin{bmatrix} p_{00}(k) & p_{01}(k) \\ p_{10}(k) & p_{11}(k) \end{bmatrix} \quad (1)$$

The estimates of the transition probabilities follows a binomial distribution with two outcomes, where N is the total number of detections and N_s is the number of successes that indicates state transition (2).

$$f(N, N_s, \theta) = \binom{N}{N_s} \theta^{N_s} (1 - \theta)^{N - N_s} \quad (2)$$

If the total number of observations N and the number of successes N_s is known, the Maximum Likelihood (ML) estimate of θ is simply the proportion of N_s . The estimate of p_{01} only updates if the zone changes from vacant and p_{10} only changes if the zone was occupied. The initial estimate of the transition matrix entries is the identity matrix, implying that the best guess of the future state is the state in the current time-step, which has demonstrated satisfying results when used in a MPC framework [3]. The estimates of θ are updated at each observation instant as it is interconnected with real-time sensor-data based occupancy detections established by tracking the trajectory of CO₂-concentration measurements [12].

As the number of occupancy detections increases the importance of each observation decreases which may render the occupancy detection unable to adjust to changing occupancy usage. To investigate whether this affects the performance of the occupancy model a moving window is introduced which neglects observations that are older than the size of the moving window, i.e. enabling the occupancy model to maintain its flexibility and to adjust to changes in room usage.

2.1 Occupancy Prediction

Two methods are tested to evaluate which method makes the most reliable predictions of future occupancy: the Expected Occupancy (EO) or the Inverse Function Method (IFM) [8]. The expected occupancy is computed by the general setting of a time inhomogeneous Markov chain, hence $P(X_{k+r} = i | X_k = j)$ is determined by calculating the (j,i)'th entry of the matrix product $T_{k+1} \cdot T_{k+2} \cdot \dots \cdot T_{k+r}$, where T_k is the time inhomogeneous transition matrices at discrete time-step k . The expected occupancy is in general the best guess of the future occupancy; however, this method lacks the ability to handle stochastic occupancy. For instance, if the current state $X_k = 0$ and the transitions probabilities equals $p_{00} = 0.6$ and $p_{01} = 0.4$, the method of expected occupancy yields $X_{k+1} = 0$, i.e. neglecting the rather large 0.4 probability of $X_{k+1} = 1$. The IFM method is used to reproduce the stochastic nature of occupancy [8]. At each time-step, the transition probabilities are cumulated and a random number is drawn from a uniform distribution

determining the future state X_{k+1} . This approach tries to capture the stochastic nature of occupancy, with offset in the historical detections.

3. Economic MPC Formulation

The objective of the economic MPC controller (3) is to determine the optimal control input u for the heating system by minimizing the total operational cost for a finite future time horizon H based on predictions of the energy price f . At discrete time-step k the optimization problem is solved based on measurements of the current state, a model of the building dynamics, and predictions of the disturbances. The first control input of the optimized control plan is then applied to the building heating system. At next discrete time-step $k+1$ the optimization problem is solved again where a new measurement of the states is taken, and the prediction horizon is shifted by one time-step. This receding horizon approach introduces feedback to the system.

$$\min_{u_0 \dots u_H} \sum_{k=0}^H f_k \cdot u_k \quad (3a)$$

$$\text{s.t. } x_{k+1} = Ax_k + Bu_k + Ed_k \quad (3b)$$

$$y_k = Cx_k \quad (3c)$$

$$0 \leq u_k \leq P_{max} \quad (3d)$$

$$T_{min,k} \leq y_k \leq T_{max,k} \quad (3e)$$

The model of the building dynamics is defined as a discrete-time Linear Time Invariant (LTI) system described on state-space form (3b) with state matrix A , system states x_k , input matrix B , control inputs u_k , disturbance matrix E and disturbances d_k . The indoor air temperature (Ti) is the controllable system state y_k (3c) with output matrix C . The constraints on Ti is a function of the predicted occupancy and thus the requirement to maintain a comfortable thermal indoor climate when the room is occupied (3e). The control input is constrained by the maximum design power of the heating system (3d).

4. Simulation

To demonstrate the efficacy and to evaluate the difference between the occupancy prediction methods, simulations concerning the optimization of the operation of the heating system for a one-bedroom apartment were used. The one-bedroom apartment has a floor area of 3.4m x 5.7m, a room height of 3m and a south-facing window. It is located in a well-insulated new building designed to comply the Danish Building Regulation 2015 [13]. For further detailed information on the one-bedroom apartment, see [14].

The co-simulation tool Building Controls Virtual Test Bed (BCVTB) [15] was used to link an EnergyPlus model that represented the true apartment to

the economic MPC programmed in MATLAB. The state-space model of the building dynamics (3b) was established as a two-state grey-box model [16] discretized at a time-step of 60 seconds. Note that the importance of the building dynamics model and model-mismatch is not considered in this paper. The simulations were carried out for a period of 45 days using hourly historical weather data from Copenhagen, Denmark and Nord Pool Spot electric prices [17]. To ease the evaluation of the different approaches of occupancy prediction, perfect forecasts of the weather and electricity prices were assumed. A finite future time horizon H of 6 days was chosen to exploit the full potential of the thermal mass. The time-step for which a new control input was sent to the heating system (tsCI) varied between 30 or 60 minutes. The time-step of the occupancy model (tsOM) and the length of the moving window (MW) were varied to evaluate their importance. The temperature constraints were defined as 21°C - 24°C when occupied and 19°C-26°C when vacant. For workdays the static 24-hour schedule was defined as occupied from 00:00 to 08:00 and 17:00 to 00:00 and constantly occupied during weekends.

4.1 Real-World Occupancy Profiles

The simulations were performed for four different occupancy profiles that differed greatly due to the stochastic nature of the occupants. The occupancy profiles were established based on real-world CO₂-measurements from four apartments. The CO₂-measurements are transformed to binary occupancy schedules according to the method presented in [12] and assumed to be the actual occupancy (the ground truth). The total number of transitions from vacant to occupied, and the total time-of-use during the simulation period of 45 days for each apartment is listed in table 1.

Table 1 Inspection of real-world occupancy profiles

	Total number of transitions from vacant to occupied [times]	Total occupied time during the simulation period [hours]
Apartment 1	62	336.8
Apartment 2	80	589.1
Apartment 3	68	829.7
Apartment 4	49	728.7

Table 1 illustrates a significant difference between the four occupants and thus the need for an occupancy model that is able to handle stochastic occupancy.

Histograms of vacancy and occupancy intervals are displayed in Fig. 1. The histograms also emphasizes the divergent occupancy profiles for each apartment. It is remarked that for apartment 1 a bin for vacancy interval 10000-10050 minutes with probability 0.016 is omitted from the chart because of readability.

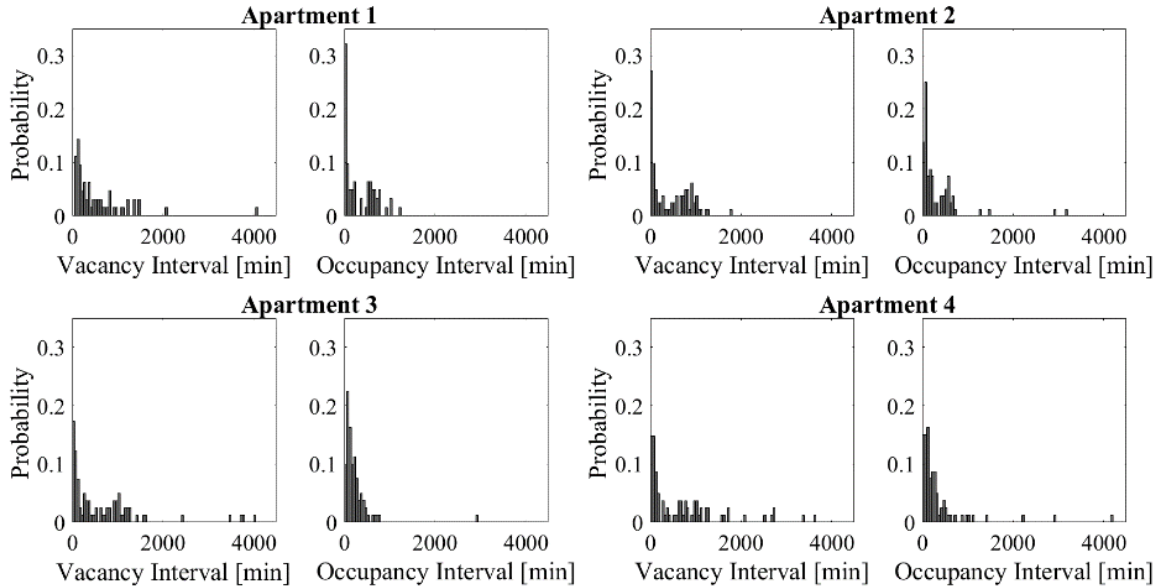


Fig. 1 Histograms of real-world occupancy profiles

5. Results and Discussion

First, the performance of the occupancy model is assessed. Secondly, the potential for achieving cost savings and reducing thermal discomfort is presented for the economic MPC controller where the influence of the occupancy model's temporal resolution and the impact of utilizing a moving window are investigated.

5.1 Occupancy Prediction

To assess the performance of the occupancy prediction methods EO and IFM, the mean absolute error (MAE) of the predictions was calculated. Fig. 2 displays the MAE for apartment 4 as a function of the future prediction time-step and for three occupancy model time-steps ts_{OM} . The charts indicate that the EO method leads to fewest predictions errors compared to IFM. Furthermore, Fig. 2 illustrates that the amount of false vacancies differs the most and that IFM generally underestimates periods of occupancy, potentially resulting in thermal comfort violations. Fig. 2 also shows that the EO method captures the anticipated periodicity of occupancy presence better.

Consistently for all four apartments, the EO method yields the most exact occupancy predictions. However, for apartment 2, which according to table 2 represents the most fluctuating occupant presence, the performance is very similar.

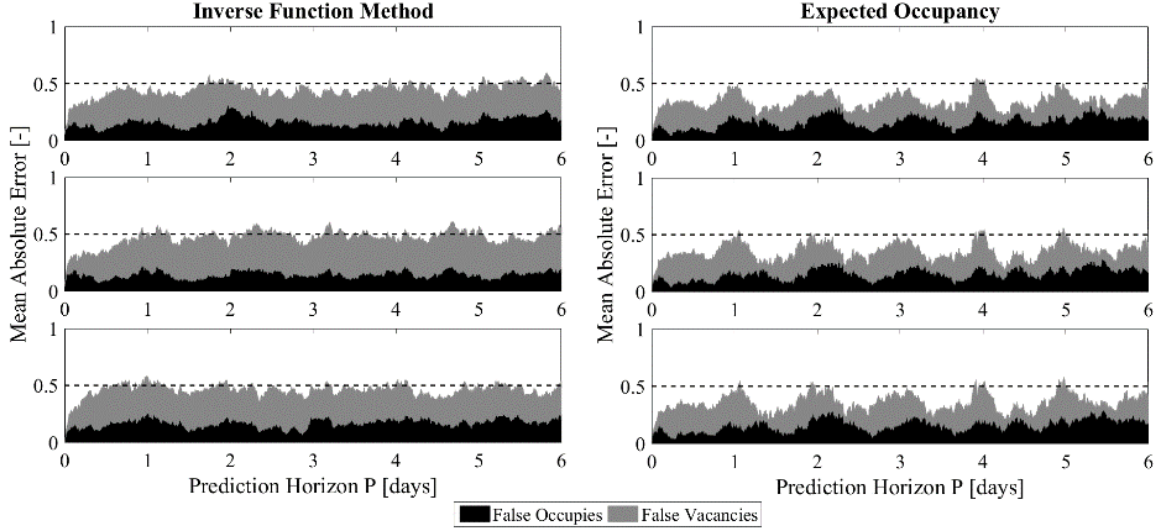


Fig. 2 Mean absolute prediction error. Top (a): tsOM = 60 min. Middle (b): tsOM = 15 min. Bottom (c): tsOM = 5 min.

The performance evaluations indicate that the IFM results in too fluctuating occupancy predictions. Analyzing the result for all four apartments showed that an occupancy model time-step of 15 minutes leads to the fewest predictions errors. The IFM is a stochastic method since it depends on a random number generator; thus, the prediction is one realization out of many. Therefore, five simulations using IFM is performed and the mean result is presented here.

5.2 Economic Model Predictive Control

The aim, when integrating an occupancy model, is to improve the performance compared to using static occupancy schedules; hence, results obtained with static schedules constitutes the performance benchmark. The deviation with respect to operational cost and thermal discomfort is calculated as stated in (4) and (5) respectively, and are displayed in Fig. 3.

$$\Delta \text{Operational Cost} = \frac{\int_0^P E \cdot f \, dt - \int_0^P E_{sch} \cdot f \, dt}{\int_0^P E_{sch} \cdot f \, dt} \quad (4)$$

where P is the total simulation period of 45 days, E is the energy use of the investigated method, f is the energy price and E_{sch} is the energy consumption using occupancy schedules.

$$\Delta \text{Thermal discomfort} = \frac{\int_0^P D_T \, dt - \int_0^P D_{T,sch} \, dt}{\int_0^P D_{T,sch} \, dt} \quad (5)$$

where D_T is the thermal discomfort of the investigated method and $D_{T,sch}$ is the thermal discomfort using static occupancy schedules. The thermal discomfort is the sum of violations of the lower and upper temperature bounds, for both occupied and vacant time-steps.

The *Performance Bound (PB)* constitutes the maximum theoretical savings potential, i.e. perfect occupancy predictions. A great potential for reducing thermal comfort violations is observed for all four apartments with a maximum reduction of approx. 85% (should be 100% if no model mismatch was present). The potential for operational cost savings is limited (maximum of approx. 4%).

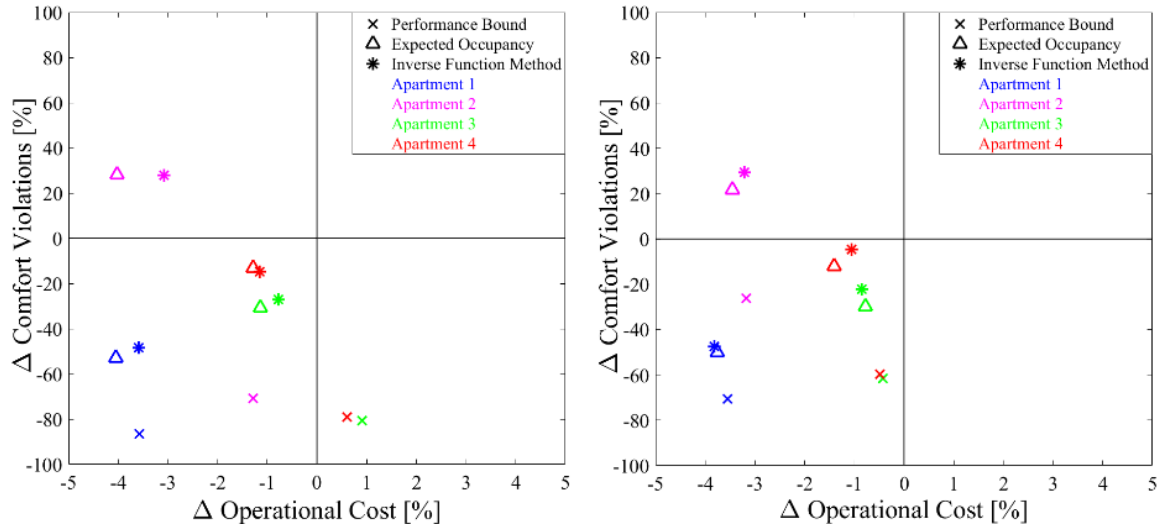


Fig. 3 Results with tsCI = 60 min and MW = 14 days.

Left (a): tsOM = 5 min. Right (b): tsOM = 60 min.

A maximum reduction of approx. 50% of thermal violations is obtained when integrating an occupancy model that utilizes either EO or IFM. Generally, EO is slightly better than IFM. For apartment 2 proper predictions of occupancy were not achieved causing approx. 30% increase of comfort violations compared to implementation of static schedules.

Fig. 3 also shows that the potential for cost savings and thermal discomfort reduction is affected by the temporal resolution of the occupancy model. To examine the importance of the occupancy model time-step closer, Fig. 4 (a) displays the relative savings potential compared to a temporal resolution of 60 minutes. Generally, a finer temporal resolution enables the occupancy models to handle more stochastic occupancy presence thus reducing thermal discomfort. However, Fig. 4 (a) stresses the same tendency as demonstrated in section 5.1, i.e. that a temporal resolution of 15 minutes yields the least occupancy prediction errors and therefore leads to fewer thermal comfort violations. To evaluate the importance of the moving window (MW), an occupancy model without a MW is taken as reference and the difference for a model with a MW length equal to 21 days and 14 days is illustrated in Fig. 4 (b). The results shows that applying a moving window and the length of the window affected the potential discomfort reduction. The results suggest that a length of 14 days was too short; hence, better performance was achieved with a length of 21 days. However, a clear tendency is difficult to observe and further investigations are necessary.

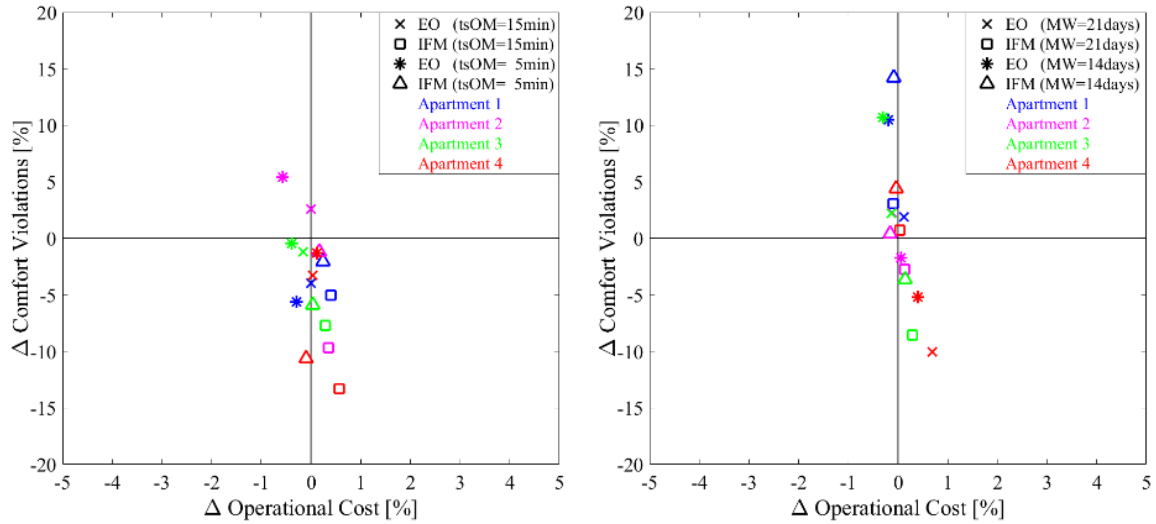


Fig. 4 Left (a): Importance of occupancy model time-step. $tsCI = 60$ min / $MW = 14$ days
Right (b) Importance of a moving window. $tsCI = 30$ min / $tsOM = 5$ min

6. Conclusion

The proposed occupancy model for handling stochastic occupancy in an economic model predictive control framework for heating system operation in dwellings demonstrated a capability to make reliable predictions of occupant presence for four apartments with very different occupant profiles. The performance evaluation suggests that a temporal resolution of 15 minutes leads to fewer prediction errors compared to an hourly temporal resolution. Furthermore, the results suggest that the EO method should be preferred compared to using IFM, because IFM provides too fluctuating occupancy schedules when used for HVAC control.

Results from test case simulations of the economic MPC framework including the proposed occupancy model suggest a potential for cost savings and thermal discomfort reduction compared to an economic MPC controller that utilizes static occupancy schedules. The results also indicate that an occupancy model with sub-hourly time-step achieves better performance than models with an hourly resolution. No clear impact of applying a moving window was observed. Future work include: i) Using an equivalent sub-hourly temporal resolution in the occupancy model and the optimization problem, thus enabling better handling of stochastic occupancy, but still only forwarding an hourly control input to the heating system by constraining the optimized control input to be equivalent for every hour. ii) Further investigations of the EO method. Currently, a transition probability of 0.5 is used to decide when a state transition is expected; however, this parameter can be increased to provide conservatism to the prediction of occupancy transition. iii) Applying the Markov chain transition probabilities in a stochastic optimization problem.

Acknowledgment

The authors gratefully acknowledge the support of this work through the project READY.DK financed by the Danish energy research and development program FORSKEL. Furthermore, the authors thank Grundfos Dormitory Lab for providing the CO₂ sensor data.

References

- [1] F. Haldi and D. Robinson, "The impact of occupants' behaviour on building energy demand," *Journal of Building Performance Simulation*, vol. 4, no. 4, pp. 323-338, 2011.
- [2] F. Oldewurtel, D. Sturznegger and M. Morari, "Importance of occupancy information for building climate control," *Applied Energy*, vol. 101, pp. 521-532, 2013.
- [3] S. Goyal, H. A. Ingley and P. Barooah, "Zone-Level Control Algorithms Based on Occupancy Information for Energy Efficient Buildings," in *American Control Conference*, Fairmont Queen Elisabeth, Montréal, Canada, 2012.
- [4] J. R. Dobbs and B. M. Hancey, "Model Predictive HVAC control with online occupancy model," *Energy and Buildings*, vol. 82, pp. 675-684, 2014.
- [5] M. Yudong, F. Borrelli, B. Hancey, B. Coffey, S. Bengea and P. Haves, "Model Predictive Control for the Operation of Building Cooling Systems," *IEEE Transactions on Control Systems Technology*, vol. 20, no. 3, pp. 796-803, 2011.
- [6] D. Wang, C. C. Federspiel and F. Rubenstein, "Modelling occupancy in single person offices," *Energy and Buildings*, vol. 37, pp. 121-126, 2005.
- [7] C. F. Reinhart, "Lightswitch-2002: a model for manual and automated control of electric lighting and blinds," *Solar Energy*, vol. 77, pp. 15-28, 2004.
- [8] J. Page, D. Robinson, N. Morel and J.-L. Scartezzini, "A generalised stochastic model for the simulation of occupant presence," *Energy and Buildings*, vol. 40, pp. 83-98, 2008.
- [9] P. D. Andersen, A. Iversen, H. Madsen and C. Rode, "Dynamic modeling of presence of occupants using inhomogeneous Markov chains," *Energy and Buildings*, vol. 69, pp. 213-223, 2014.
- [10] J. R. Dobbs and B. M. Hancey, "Predictive HVAC Control Using a Markov Occupancy Model," in *American Control Conference*, Portland, Oregon, USA, 2014.
- [11] S. Goyal, H. A. Ingley and P. Barooah, "Effect of Various Uncertainties on the Performance of Occupancy-Based Optimal Control of HVAC Zones," in *51st IEEE Conference on Decision and Control*, Maui, Hawaii, USA, 2012.
- [12] S. Petersen, T. H. Pedersen and K. U. Nielsen, "Method for room occupancy detection based on trajectory of sensor data. Part II: Method and results," *Energy and Buildings*, Submitted.
- [13] Trafik- og Byggestyrelsen, 20 01 2016. [Online]. Available: <http://byggningsreglementet.dk/>.
- [14] M. D. Knudsen and S. Petersen, "Demand Response Potential of Model Predictive Control of Space Heating based on Price and CO₂ Intensity Signals," *Energy and Buildings*, Submitted.
- [15] M. Wetter, "Co-simulation of building energy and control systems with the Building Controls Virtual Test Bed," *Journal of Building Performance Simulation*, pp. 1-19, 2010.
- [16] R. E. Hedegaard, T. H. Pedersen, M. D. Knudsen and S. Petersen, "Identifying a Comfortable Excitation Signal for Generating Statistics-Based Building Models for Model Predictive Control," in *CLIMA2016*, Aalborg, 2016.
- [17] Nord Pool, 20 01 2016. [Online]. Available: <http://www.nordpoolspot.com/>.

**APPENDIX 5 PAPER: COMPARISON OF CENTRALIZED AND
DECENTRALIZED MODEL PREDICTIVE CONTROL IN A
BUILDING RETROFIT SCENARIO (S5)**



Available online at www.sciencedirect.com

ScienceDirect

Energy Procedia 122 (2017) 979–984

Energy

Procedia

www.elsevier.com/locate/procedia

CISBAT 2017 International Conference – Future Buildings & Districts – Energy Efficiency from Nano to Urban Scale, CISBAT 2017 6-8 September 2017, Lausanne, Switzerland

Smart Buildings (Predictive & Neuro-Fuzzy Control)

Comparison of centralized and decentralized model predictive control in a building retrofit scenario

Theis Heidmann Pedersen^{a,*}, Rasmus Elbæk Hedegaard^a,
Michael Dahl Knudsen^a, Steffen Petersen^a

^a*Department of Engineering, Aarhus University, Inge Lehmanns Gade 10, 8000 Aarhus C, Denmark*

Abstract

Heat transfer between apartments can challenge the positive effects of applying model predictive control (MPC) in multi-apartment buildings. This paper reports on an investigation of how the performance of two different MPC approaches – centralized and decentralized – may be affected by non-insulated and insulated partition walls between apartments. The results suggest that ignoring inter-zonal thermal effects using the less complicated decentralized approach leads to insignificant performance reductions compared to the more complicated centralized approach – especially if partition walls are insulated.

© 2017 The Authors. Published by Elsevier Ltd.

Peer-review under responsibility of the scientific committee of the CISBAT 2017 International Conference – Future Buildings & Districts – Energy Efficiency from Nano to Urban Scale

Keywords: Model predictive control; Building retrofit; Energy flexibility; Residential space heating; Demand response

1. Introduction

Current studies have demonstrated that model predictive control (MPC) of building systems may increase energy efficiency and ensure thermal comfort. MPC schemes rely on a model of the building dynamics, measurements of the state of the building and forecasts of disturbances (e.g. weather and occupancy) to determine a sequence of optimal

* Corresponding author.

E-mail address: thp@eng.au.dk

control actions [1-3]. Several studies have applied MPC to optimize the operation of heating, ventilation and air conditioning (HVAC) systems and have achieved significant energy savings. Sourbron et al. [2] applied MPC to operate a heat pump in an office building equipped with thermo active building systems, which reduced the electricity consumption by 15% while ensuring thermal comfort. Goyal et al. [3] used MPC to operate an air-handling unit and achieved energy savings of 55-60% compared to a dual-maximum baseline control. In a simulation study, Oldewurtel et al. [1] compared MPC to conventional rule-based control for various building typologies and locations, and found that MPC, in most cases, reduced energy consumption while improving thermal comfort.

Several studies have also considered time-varying energy prices together with MPC to minimize the operational cost, i.e. economic model predictive control (E-MPC), to provide flexibility to the energy grid through demand response [4-7]. A simulation study by Avci et al. [4] used real time prices together with an E-MPC scheme to operate an AC unit in a single residence and reduced the energy consumption in peak-hours by 23.6% and operational cost with 13% compared to a baseline controller. Pedersen et al. [5] used an E-MPC scheme and day-ahead power market prices to investigate the demand response potential in an existing residential multi-apartment building before and after retrofitting the building envelope. Compared to a baseline PI controller, the simulation results suggested that the E-MPC scheme reduced the energy consumption in peak-hours in the existing and retrofitted building by approx. 7% and up to 47%, respectively, while ensuring thermal comfort.

For multi-zone buildings, centralized and decentralized thermal control schemes exist [5, 8, 9]. Centralized MPC schemes require a detailed building model that accounts for heat transfer between adjacent zones to determine the operation in all zones simultaneously. Decentralized MPC relies on a set of single-zone models that neglect inter-zonal heat transfer, leading to multiple detached optimization problems. In theory, decentralized control schemes return a sub-optimal solution compared to centralized MPC. To show this, Moroşan et al. [8] compared a conventional baseline controller with a decentralized and centralized MPC scheme, which achieved energy savings of 5.5% and 13.4%, respectively. However, the authors noted that the performance difference depends on the coupling degree between zones. Pedersen et al. [5] likewise found a minor performance difference between centralized and decentralized control structures when applying E-MPC.

In existing apartment buildings, the interior partition walls often consist of heavy materials with high conductivity, such as concrete. However, in a retrofit situation, where the energy efficiency of the building is increased, insulation is often added to the partition walls to reduce inter-zonal noise. Consequently, the conductivity of the wall is reduced, which may diminish any advantage of including inter-zonal thermal effects. The decentralized control approach may therefore be more practical since it does not require mapping of zone-adjacency during model establishment or exchange information between controlled zones during operation. This paper therefore investigates the performance difference between centralized and decentralized MPC in an apartment building without and with insulated partition walls.

2. Method

The third floor of an existing residential building located in Aarhus, Denmark, consisting of ten apartments and five stairwells was modelled in EnergyPlus (EP) and used to represent the actual building to be controlled. In addition to the existing building, a case with a retrofitted building envelope was considered. Information on geometry and thermal characteristics of the existing and retrofitted buildings are provided in ref. [5] (the retrofitted building is denoted retrofit8 in the reference). The existing partition walls between apartments were assumed to consist of 120 mm concrete while additional 100mm mineral wool and 13mm gypsum was added when insulating the walls.

The MPC scheme was implemented in MATLAB and used to operate the space heating (electrical baseload) of the EP model through co-simulation facilitated by the Building Controls Virtual Test Bed (BCVTB) [10]. The simulations were carried out for the period December 1, 2016 to February 28, 2017, which constitutes the coldest period of the heating season in Denmark, using an EP weather data file based on on-site weather measurements. To ease the interpretation of the results, internal gains originating from occupants and equipment were omitted and perfect weather forecasts were assumed.

2.1. Centralized and decentralized model predictive control

MPC is an optimization-based control scheme, which at each time step determines a sequence of optimal space heating control actions by minimization of a cost function based on an input weight vector c associated with the control actions. The problem (eq. 1a-1g) is solved for a finite prediction horizon N which, in this study, was set to 72 hours. The control actions are restricted by the maximum design power P_{max} of the heating system (eq. 1d), and eq. 1e and eq. 1f constrain the apartment air temperatures and the temperature rate of change, respectively. Specifications for input and state constraints are listed in Table 1. The control actions are communicated to the space heating system in a receding horizon approach, i.e. only the first control action is implemented and the procedure is then repeated at the next time step based on recent apartment air temperature measurements and updated disturbance forecasts [1].

$$\underset{u_{0|t}, \dots, u_{N|t}}{\text{minimize}} \quad J = \sum_{n=0}^{N-1} c_{n|t}^T \cdot u_{n|t} \tag{1a}$$

$$\text{subject to} \quad x_{n+1|t} = \mathbf{A}x_{n|t} + \mathbf{B}u_{n|t} + \mathbf{E}d_{n|t} \quad \forall n = 0, \dots, N-1 \tag{1b}$$

$$y_{n+1|t} = \mathbf{C}x_{n+1|t} \quad \forall n = 0, \dots, N-1 \tag{1c}$$

$$0 \leq u_{n|t} \leq P_{max} \quad \forall n = 0, \dots, N-1 \tag{1d}$$

$$T_{min,n|t} \leq y_{n+1|t} \leq T_{max,n|t} \quad \forall n = 0, \dots, N-1 \tag{1e}$$

$$\Delta T_{min,n|t} \leq \frac{y_{n+1|t} - y_{n|t}}{\Delta \tau} \leq \Delta T_{max,n|t} \quad \forall n = 0, \dots, N-1 \tag{1f}$$

$$x_{0|t} = x_t \tag{1g}$$

The MPC scheme requires a reduced-order model that adequately describes the thermodynamics of the building, e.g. grey-box models. Grey-box models are characterized by having a pre-specified model structure consisting of physically meaningful parameters that are estimated from measurement data through methods from the field of system identification [11]. In a multi-apartment building, the model represents an interconnected system of subsystems (corresponding to apartments), where the interactions occur due to conduction between apartments [12]. Identifying suitable multi-zone models for centralized control schemes, thus considering the thermal interactions, can be difficult and requires time-consuming experiments, planning and modeling [12, 13]. Decentralized control schemes neglect the interactions and treat the thermal influences between subsystems as external unknown disturbances, thus adequate models are easier to identify. In this study, a two-state grey-box apartment model was used, where the two states represent the lumped thermal capacity of the zone air and the constructions. The applied state space representation is given in (1b-1c) with state matrix \mathbf{A} , system states x for time step $t+n$ forecasted at time t , input matrix \mathbf{B} , control actions u , disturbance matrix \mathbf{E} , disturbances d , output matrix \mathbf{C} and output y (i.e. apartment air temperatures).

Table 1. Specification of input and state constraints

		Apt. 1	Apt. 2	Apt. 3	Apt. 4	Apt. 5	Apt. 6	Apt. 7	Apt. 8	Apt. 9	Apt. 10
Area	[m ²]	81	94	81	94	81	94	81	94	50	94
P _{max}	[W/m ²]	50	50	50	50	50	50	50	50	50	50
T _{min}	[°C]	20	22	20	22	20	22	20	22	20	22
T _{max}	[°C]	24	26	24	26	24	26	24	26	24	26
ΔT _{min}	[°C/h]	-2.1	-2.1	-2.1	-2.1	-2.1	-2.1	-2.1	-2.1	-2.1	-2.1
ΔT _{max}	[°C/h]	2.1	2.1	2.1	2.1	2.1	2.1	2.1	2.1	2.1	2.1

The centralized and decentralized MPC schemes were first evaluated in terms of their ability to track the lower comfort bounds, which constitutes the most energy efficient control approach. Secondly, the MPC schemes' ability to achieve end-user cost savings was assessed by considering time varying energy prices as input weights. Historical day-ahead power market prices for the simulation period were used, cleared for the bidding area western Denmark (DK1). For the sake of simplicity, taxation of electricity was omitted, thus results presented in absolute values are not directly comparable to actual costs paid by building owners.

3. Results and discussion

The ability of the centralized and decentralized MPC schemes to track the lower comfort bound for one week in apartment 9 in the retrofitted building, with and without insulated partition wall is displayed in Figure 1. For the building with existing partition walls, the centralized MPC scheme kept the air temperature close to the temperature set-point, whereas the decentralized MPC scheme overestimated the heating demand, leading to a positive temperature offset compared to the temperature set-point. The positive offset was caused by heat gains from adjacent apartments with higher temperature set-points (see Table 1). When insulating the partition walls, the heat exchange between adjacent apartments was reduced, resulting in a similar performance of the centralized and decentralized MPC schemes.

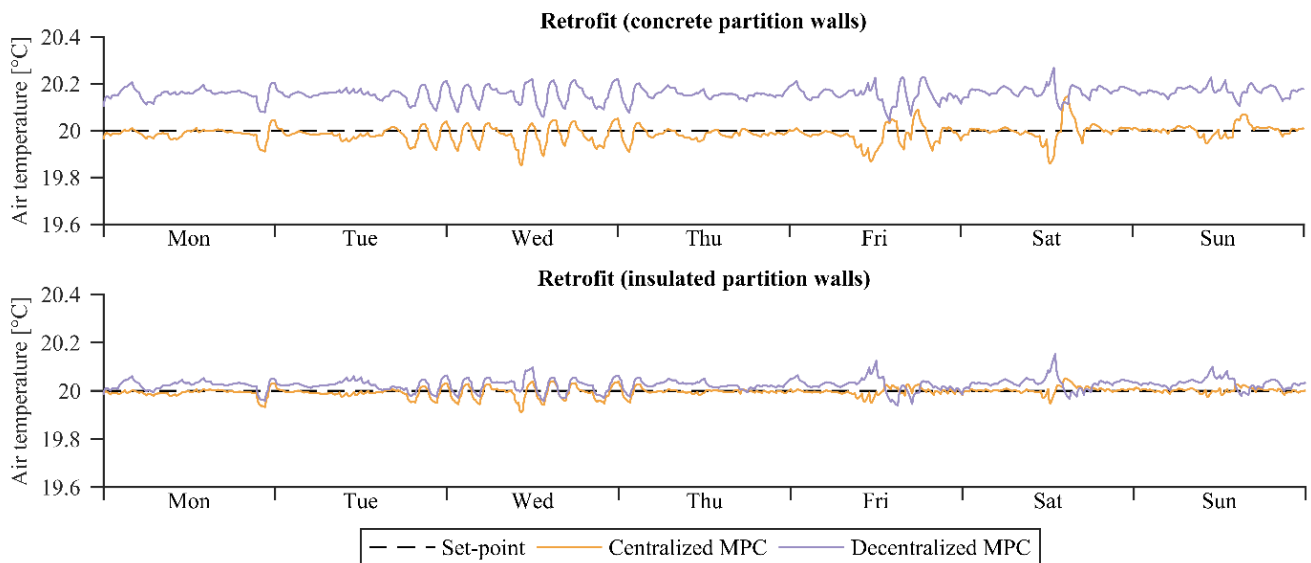


Figure 1. Simulation results of the room temperature in apt. 9 during one week.

The mean biased error (MBE) between the temperature set-points and the resulting air temperatures during the entire simulation period is specified in Table 2 (+ indicates insulated partition walls). The MBE supports the observations in Figure 1, where the decentralized MPC scheme in buildings with existing concrete partition walls led to positive and negative offsets for the apartments with a set-point of 20°C and 22°C, respectively. In the case with the insulated partition walls, the MBE for the two control schemes were very similar. In some apartments, the decentralized MPC scheme even achieved better results than centralized MPC, presumably because the required multi-apartment model was more difficult to identify than the single-apartment models, which led to a significant increase in the uncertainty of the parameter estimates [5].

Table 2. Mean biased error

Building	Control	Apt. 1	Apt. 2	Apt. 3	Apt. 4	Apt. 5	Apt. 6	Apt. 7	Apt. 8	Apt. 9	Apt. 10
Existing	Centralized	0.00	0.01	0.00	0.02	0.00	0.01	0.02	0.02	0.00	0.01
	Decentralized	0.06	-0.09	0.10	-0.07	0.12	-0.04	0.07	-0.07	0.12	-0.03
Existing+	Centralized	-0.01	0.03	-0.02	0.03	-0.01	0.01	-0.01	0.02	0.01	0.00
	Decentralized	0.01	-0.01	0.03	-0.01	0.03	-0.01	0.02	-0.01	0.03	0.00
Retrofit	Centralized	-0.01	0.03	-0.01	0.02	-0.02	0.02	-0.01	0.04	-0.02	0.00
	Decentralized	0.06	-0.09	0.10	-0.09	0.11	-0.05	0.06	-0.08	0.17	-0.05
Retrofit+	Centralized	-0.03	0.03	-0.02	0.02	-0.02	0.02	-0.04	0.03	0.00	-0.01
	Decentralized	0.00	-0.02	0.02	-0.02	0.02	-0.01	0.01	-0.02	0.03	-0.01

The mechanism of a conventional PI-controller and the E-MPC schemes using historical day-ahead prices during one week are displayed in Figure 2 for the retrofitted building with the existing partition walls and with insulated partition walls. In both cases, the conventional PI-controller maintained the air temperature close to the specified lower comfort set-point of 20°C at all times. The E-MPC schemes, however, exploited the structural thermal mass to reduce

the space heating consumption in high price periods by increasing the air temperature within the comfort bounds at times with low prices. Since the optimal control actions depend on the state of the building at any given time, direct comparison between the two control schemes at each time instance should be done carefully. However, in the case with the existing concrete partition walls, discrepancies between the two E-MPC schemes are clearly distinguishable on Thursday and Friday, where only the centralized E-MPC scheme increased the temperature. Furthermore, the temperature offset of the decentralized control scheme identified previously was also apparent in the case with the concrete partition walls. For the insulated partition walls, the control schemes led to almost identical operations.

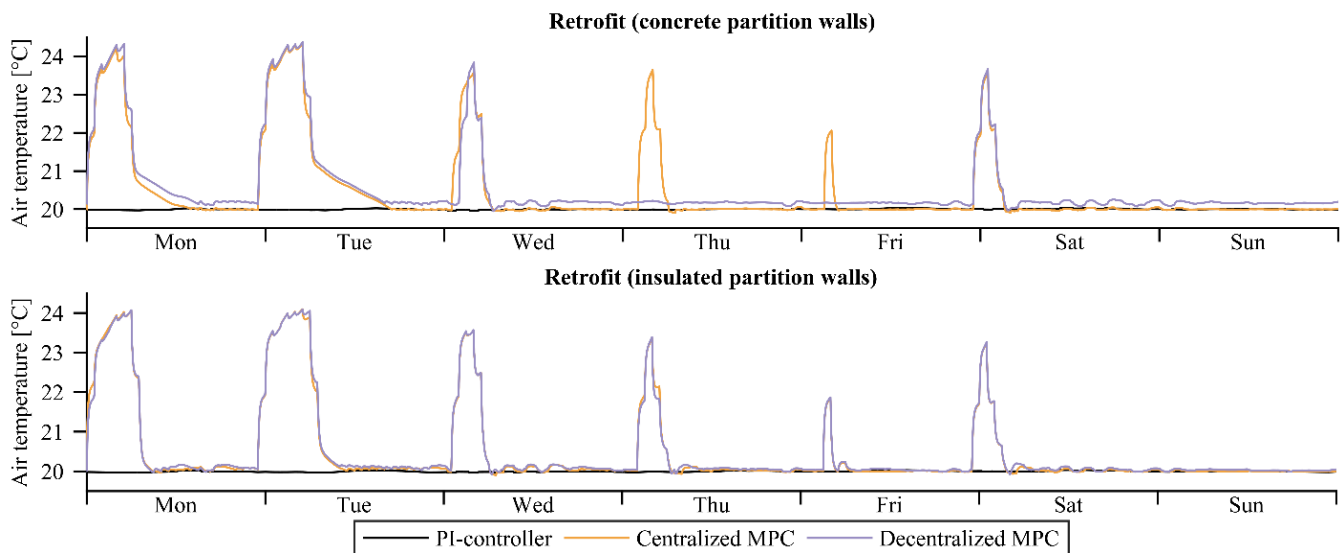


Figure 2. Simulation results of the room temperature in apt. 9 during one week using E-MPC.

Table 3 lists the total costs of each of the three control schemes (PI, centralized E-MPC and decentralized E-MPC) for the four building cases: before and after a general retrofit of the building envelope and with and without insulated partition walls. Furthermore, the total achieved cost savings and mean comfort violations compared to the PI-controller are specified. The standard deviations across the apartments are specified in the parentheses. The results suggest that centralized and decentralized E-MPC schemes achieved total cost savings similar to those of the PI controller. The decentralized control scheme, however, tended to distribute cost savings unevenly between the apartments in the scenarios without insulated partition walls. Further inspection of the simulation results indicated that this was due to lower achieved cost savings in the apartments with a lower comfort bound of 20°C; here, the E-MPC scheme planned the heating operation without considering the heat gains from adjacent apartments. This effect was significantly reduced in the scenarios with insulated partition walls. Furthermore, in the case with the insulated partition walls, the decentralized control scheme out-performed the centralized control scheme in terms of maintaining comfort, presumably because the multi-zone models are more challenging to identify.

Table 3. Summarized simulations results for all ten apartments

Building	Control	Total cost	Cost savings	Relative cost saving	Mean comfort violations
Existing	PI	€ 1040			89.7 (4.3) °Ch
	Centralized	€ 1010	€ 30 (0.66)	2.9%	18.1 (9.8) °Ch
	Decentralized	€ 1011	€ 29 (1.37)	2.8%	22.7 (9.4) °Ch
Existing+	PI	€ 1001			84.4 (2.9) °Ch
	Centralized	€ 977	€ 24 (0.42)	2.4%	15.9 (2.6) °Ch
	Decentralized	€ 979	€ 22 (0.50)	2.2%	11.2 (1.5) °Ch
Retrofit	PI	€ 327			43.9 (3.0) °Ch
	Centralized	€ 293	€ 34 (0.86)	10.4%	9.3 (8.7) °Ch
	Decentralized	€ 293	€ 34 (1.59)	10.4%	18.0 (8.7) °Ch
Retrofit+	PI	€ 323			38.5 (1.7) °Ch
	Centralized	€ 287	€ 36 (0.55)	11.1%	7.5 (3.0) °Ch
	Decentralized	€ 287	€ 36 (0.63)	11.1%	6.9 (2.2) °Ch

4. Conclusion

This paper reports on a simulation-based study of the performance differences between centralized and decentralized MPC schemes for optimal space heating operation in an existing and retrofitted multi-apartment building. The results of a 90-day simulation period showed that the decentralized MPC in buildings without insulated partition walls tended to result in a constant offset from the specified temperature set-point. Consequently, the achieved total cost savings for both schemes were found to be similar, but the decentralized control scheme failed to distribute the savings evenly across all apartments. Insulating the partition walls reduced the constant temperature offsets when applying the decentralized control scheme, which was reflected in the results. The decentralized control scheme was not only able to distribute cost savings evenly, but it also out-performed centralized control in terms of maintaining temperatures within the comfort bounds. This reversal in the optimal approach is likely caused by the fact that the advantages of centralized control diminish as insulation is added between zones, combined with the fact that the more complicated setup of the centralized control was more prone to uncertainty issues when identifying a building model for MPC.

Overall, the results suggest that decentralized control schemes can be applied in multi-apartment buildings, especially where partition walls are insulated for noise-reduction purposes. However, it is difficult to specify a general level of insulation, as the performance depends e.g. on the building, the modeling technique and the control purpose. Applying decentralized MPC also simplifies and reduces the time-consuming work involved when implementing MPC schemes. Furthermore, decentralized control schemes allow apartment owners to specify control objectives themselves, just as it allows for individual apartment owners to decide if and when to invest in advanced control.

Acknowledgements

The authors gratefully acknowledge the support of this work from the project “READY.dk” financed by the Danish energy research and development program ForskEl (grant number: 12305) and the project 'Resource Efficient Cities Implementing Advanced Smart City Solutions' (READY) financed by the 7th EU Framework Programme (FP7-Energy project reference: 609127).

References

- [1] F. Oldewurtel, A. Parisio, C. N. Jones, D. Gyalistras, M. Gweder, V. Stauch, B. Lehmann and M. Morari. Use of Model Predictive Control and Weather Forecasts for Energy Efficient Building Climate Control. *Energy Build.* 45 (2012) 15-27.
- [2] M. Sourbron, C. Verhelst and L. Helsén. Building models for model predictive control of office buildings with concrete core activation. *J. Build. Perform. Simul.* 6 (3) (2013) 175-198.
- [3] S. Goyal, H. A. Ingley and P. Barooah. Occupancy-based zone-climate control for energy-efficient buildings: Complexity vs. performance. *Appl. Energ.* 106 (2016) 209-221.
- [4] M. Avci, M. Erkoç, A. Rahmani and S. Asfour. Model predictive HVAC load control in buildings using real-time electricity pricing. *Energy Build.* 60 (2013) 199-209.
- [5] T. H. Pedersen, R. E. Hedegaard and S. Petersen. Space heating demand response potential of retrofitted residential apartment blocks. *Energy Build.* 141 (2017) 158-166.
- [6] M. D. Knudsen and S. Petersen. Demand response potential of model predictive control of Space heating based on price and carbon dioxide Intensity signals. *Energy Build.* 125 (2016) 196-204.
- [7] R. Halvgaard, N. K. Poulsen, H. Madsen and J. B. Jørgensen. Economic Model predictive Control for Building Climate Control in a Smart Grid. in *IEEE PES Innovative Smart Grid Technologies (ISGT)* (2012) 1-6, Washington, D.C., United States.
- [8] P.-D. Moroşan, R. Bourdais, D. Dumur and J. Buisson. Building temperature regulation using a distributed model predictive control. *Energy Build.* 42 (2010) 1445-1452.
- [9] V. Chandan and A. G. Alleyne. Decentralized Architectures for Thermal Control of Buildings. in *American Control Conference* (2012), Montreal, Canada.
- [10] M. Wetter. Co-simulation of building energy and control systems with the Building Controls Virtual Test Bed. *J. Build. Perform. Simul.* 3 (4) (2010) 1-19.
- [11] R. E. Hedegaard and S. Petersen. Evaluation of Grey-Box Model Parameter Estimates Intended for Thermal Characterization of Buildings. in *11th Nordic Symposium on Building Physics* (2017), Trondheim, Norway.
- [12] S. Goyal, C. Liao and P. Barooah. Identification of multi-zone building thermal interaction model from data. in *50th IEEE Conference on Decision and Control* (2011), Orlando, FL, USA.
- [13] C. Agbi, Z. Song and B. Krogh. Parameter Identifiability for Multi-Zone Building Models. in *51st IEEE conference on Decision and Control* (2012), Maui, Hawaii, USA.

APPENDIX 6 PAPER: HANDLING THERMAL COMFORT IN
ECONOMIC MODEL PREDICTIVE CONTROL SCHEMES FOR
DEMAND RESPONSE (S6)



Available online at www.sciencedirect.com

ScienceDirect

Energy Procedia 122 (2017) 985–990

Energy

Procedia

www.elsevier.com/locate/procedia

CISBAT 2017 International Conference – Future Buildings & Districts – Energy Efficiency from Nano to Urban Scale, CISBAT 2017 6-8 September 2017, Lausanne, Switzerland

Smart Buildings (Predictive & Neuro-Fuzzy Control)

Handling thermal comfort in economic model predictive control schemes for demand response

Theis Heidmann Pedersen^{a,*}, Michael Dahl Knudsen^a,
Rasmus Elbæk Hedegaard^a, Steffen Petersen^a

^a*Department of Engineering, Aarhus University, Inge Lehmanns Gade 10, 8000 Aarhus C, Denmark*

Abstract

Addressing thermal comfort is an important aspect of applying economic model predictive control (E-MPC) schemes with the objective to perform demand response (DR), e.g. minimize operational cost. This paper compares the performance of four E-MPC schemes using both single-objective and multi-objective formulations to address thermal comfort. It is difficult to proclaim the superior formulation as the notion of thermal comfort is a subjective matter. However, the single-objective problem formulation proposed in this paper contains a parameter, ϵ_{\max} , which describes the maximum acceptable deviations from the preferred indoor air temperature. This parameter can be regarded as a user-defined indicator of the acceptable deviations from the preferred temperature or, in other words, their ‘DR willingness’.

© 2017 The Authors. Published by Elsevier Ltd.

Peer-review under responsibility of the scientific committee of the CISBAT 2017 International Conference – Future Buildings & Districts – Energy Efficiency from Nano to Urban Scale

Keywords: Thermal comfort; Demand Response; Single objective optimization; Multi objective optimization; Economic model predictive control

* Corresponding author.

E-mail address: thp@eng.au.dk

1. Introduction

Economic model predictive control (E-MPC) of building energy systems is an optimization based control scheme that uses a model of the building thermodynamics, forecasts of disturbances and measurements of the building state to determine a sequence of optimal control actions. Applying E-MPC together with time-varying energy prices to minimize the space heating operational cost and perform demand response (DR) have been investigated in several studies [1-4]. These E-MPC schemes achieve economic benefits by using the thermal capacity of the structural mass as storage by charging and discharging it with the room heating system in periods with low or high prices, respectively. The schemes therefore result in fluctuating indoor temperatures, and it is therefore necessary to ensure that economic benefits are not violating the thermal comfort of the occupants.

A simple E-MPC formulation in this regard is to assume that occupants are comfortable as long as temperatures are within a predefined comfort band, e.g. defined by a preferred temperature and an acceptable deviation from it. Using this comfort formulation, several studies have suggested significant cost savings and DR potentials. Halvgaard et al. [5] minimized the operational cost of a heat pump and achieved cost savings of 25% compared to traditional control. Pedersen et al. [4] optimized the space heating operation in a multi-apartment building which, compared to a conventional PI-controller, achieved cost savings of up to 6% and reduced energy consumption in peak-hours with up to 47%. Vrettos et al. [1] applied E-MPC for heat pump operation and achieved cost savings of 18.4% compared to a rule-based controller. However, an E-MPC scheme using this comfort formulation will often result in the controller tracking either the upper or the lower boundary of the comfort band [4]. This behavior means that the air temperature rarely is equal to the preferred temperature specified by the occupants. Another shortcoming of this formulation is that the building has no downward flexibility to offer in periods where the lower comfort bound is tracked, i.e. it is not possible to reduce the space heating demand if this service is requested by the supply side [6].

Another approach to ensure comfort is to formulate a multi-objective optimization (MOO) problem, i.e. simultaneously minimize operational costs and thermal comfort violations [2, 7-10]. Avci et al. [2] used an E-MPC scheme to minimize energy consumption and penalize temperature deviations from the preferred temperature, and introduced a discomfort tolerance index to weigh the objectives. Compared to a baseline controller, the E-MPC scheme reduced operational cost with 13% while increasing the mean temperature with 0.15°C. Morales-Valdés et al. [8] evaluated several MOO formulations and suggested to include Fanger's predicted mean vote (PMV) index or predicted percentage dissatisfied (PPD) index in the cost function which, however, led to a nonlinear optimization problem. Therefore, Cigler et al. [7] proposed a convex approximation of the PMV index in the cost function. However, including the PMV index in the cost function relies on assumptions regarding clothing level and metabolic rate, as well as measurement of air speed, relative humidity and the mean radiant temperature. Furthermore, the performance reported in the above-mentioned MOO studies depends on the selection of the assigned relative weights which essentially vary in time as they depend on the building conditions.

Current studies address thermal comfort in E-MPC formulations very differently, which may affect the reported DR potentials. This paper therefore reports on a simulation-based study, where the performance of an E-MPC scheme using both single-objective and multi-objective formulations to address thermal comfort violations is investigated. The aim is to provide a quantitative performance assessment of the different formulations in terms of comfort violations and operational cost, and to discuss their practical implications.

2. Method

A residential building consisting of ten apartments and five stairwells located in Aarhus, Denmark, was chosen as test case. A detailed EnergyPlus (EP) model was used to represent the building to be controlled; information on geometry and thermal characteristics of the building are provided in ref. [4] in which the building is denoted retrofit8. Furthermore, 100mm insulation was added to the partitioning walls to minimize the effect of inter-zonal heat exchange and thereby allow for a decentralized control principle [11]. The E-MPC scheme was implemented in MATLAB and used to operate the space heating of the EP model through co-simulation facilitated by the Building Controls Virtual Test Bed (BCVTB) [12]. The simulations were carried out for the period December 1, 2016 to February 28, 2017, which constitutes the coldest period of the heating season in Denmark, using an EP weather file based on on-site weather measurements. Historical day-ahead power market prices (cleared for Western Denmark, DK1 region) from the simulation period were used. To ease the interpretation of the results, internal gains originating from occupants and equipment were omitted, and perfect weather and price forecasts were assumed.

2.1. Economic model predictive control

At each time step the E-MPC scheme (eq. 1a-1g) determines a sequence of optimal space heating control actions which minimize temperature deviations from the preferred temperature (j_1) and the operational costs (j_2) for a finite prediction horizon N (set to 72 hours in this study).

$$\begin{aligned}
 & \underset{\epsilon, u}{\text{minimize}} && \underbrace{\epsilon^T \mathbf{Q} \epsilon}_{j_1} + \underbrace{c^T u}_{j_2} && (1a) \\
 & \text{subject to} && x_{n+1} = \mathbf{A}x_n + \mathbf{B}u_n + \mathbf{E}d_n && \forall n = 0, \dots, N-1 && (1b) \\
 & && y_{n+1} = \mathbf{C}x_{n+1} && \forall n = 0, \dots, N-1 && (1c) \\
 & && \epsilon_{n+1} = T_{\text{preferred}} - y_{n+1} && \forall n = 0, \dots, N-1 && (1d) \\
 & && 0 \leq u_n \leq P_{\text{max}} && \forall n = 0, \dots, N-1 && (1e) \\
 & && T_{\text{min}} \leq y_{n+1} \leq T_{\text{max}} && \forall n = 0, \dots, N-1 && (1f) \\
 & && x_0 = x(0) && && (1g)
 \end{aligned}$$

where \mathbf{Q} is a time-invariant symmetric matrix with main diagonal elements and c is the time-varying day-ahead prices. A state space representation of the building’s thermodynamics is specified in eq. 1b and eq. 1c. The control actions are restricted by the maximum power P_{max} of the heating system (eq. 1e), and the defined thermal comfort band (eq. 1f), which may vary between the apartments as listed in Table 1. Recent measurements of the air temperature are used to update the current state of the building in eq. 1g with a Kalman Filter.

Table 1. Input and state constraints

	Apt. 1	Apt. 2	Apt. 3	Apt. 4	Apt. 5	Apt. 6	Apt. 7	Apt. 8	Apt. 9	Apt. 10
P_{max}	50 W/m ²									
$T_{\text{preferred}}$	20.5 °C	22.0 °C	21.5 °C	22.0 °C	20.5 °C	21.5 °C	21.0 °C	20.0 °C	22.0 °C	21.5 °C
T_{min}	19.5 °C	20.5 °C	20.5 °C	20.0 °C	19.0 °C	19.5 °C	19.0 °C	19.0 °C	20.5 °C	19.5 °C
T_{max}	21.5 °C	23.5 °C	22.5 °C	24.0 °C	22.0 °C	23.5 °C	23.0 °C	21.0 °C	23.5 °C	23.5 °C

Since the two objectives j_1 and j_2 are conflicting, there is generally no unique solution that optimizes both objectives simultaneously, which suggests that a useful approach to solving the MOO is that of Pareto optimality [13]. The set of Pareto optimal solutions, which from a mathematically point of view is equally acceptable, forms a Pareto front. The simplest method to obtain Pareto optimal solutions is convex combination of j_1 and j_2 , e.g. the weighted sum approach (as used in ref. [2, 7, 8]): $J = \lambda \cdot j_1 + (1-\lambda) \cdot j_2$, where $\lambda \in [0,1]$. Note that if $\lambda=1$ the control scheme is a traditional reference tracking control problem, whereas if $\lambda=0$ the control scheme is similar to the ones used in ref. [1, 4, 5]. However, as mentioned in the introduction, the performance of this approach depends significantly on the assigned relative weights which are difficult to choose when the Pareto front is steep or if the objective functions have very different ranges [13, 14]. Furthermore, thermal discomfort can be difficult to quantify since thermal comfort has no direct economic translation. To overcome this, Das and Dennis [13] proposed a normal boundary intersection (NBI) method to approximate the Pareto front with evenly distributed discrete solutions that are independent of weights between objectives (see Figure 1).

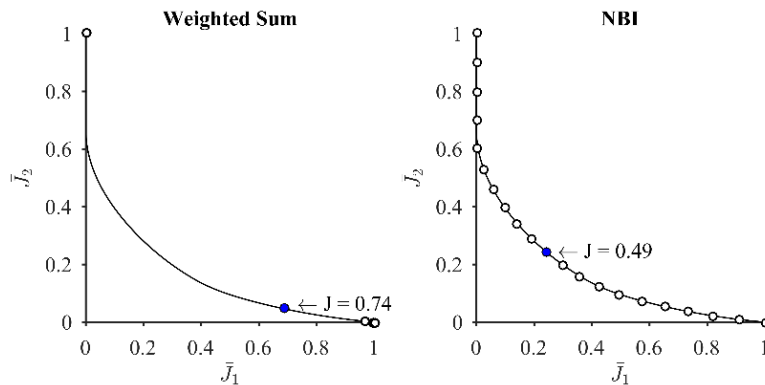


Figure 1. Normalized optimal Pareto solutions with λ increments of 0.05.

When the set of discrete Pareto solutions has been determined, several approaches exist to select and implement an agreeable trade-off between j_1 and j_2 [15]. In this study, the compromise solution is selected, which corresponds to the solution with the shortest Euclidean distance to the utopia point. The utopia point is, as the name suggests, an ideal solution when minimizing each objective independently. Figure 1 displays the results of the weighted sum and NBI methods for a scenario with two objectives with different ranges, and indicates that NBI is more resistant to ill-conditioned problems. The utopia point is origin, the solid line is the continuous Pareto front and the black and blue circles mark the obtained discrete Pareto solutions and the compromise solution, respectively.

Since an MOO problem is computationally demanding to solve compared to a single-objective optimization (SOO) problem, a SOO formulation is proposed which aims at imitating the behavior of MOO. The formulation builds on eq. 2a-2g. However, \mathbf{Q} is an appropriate sized matrix of zeros (i.e. only objective j_2 is effective). Furthermore, additional state constraints are specified as illustrated in Figure 2, describing the maximum acceptable temperature deviations within the prediction horizon using the parameter ϵ_{max} [°Ch] which is then a tuning parameter to indicate preference between thermal discomfort and operational cost minimization.

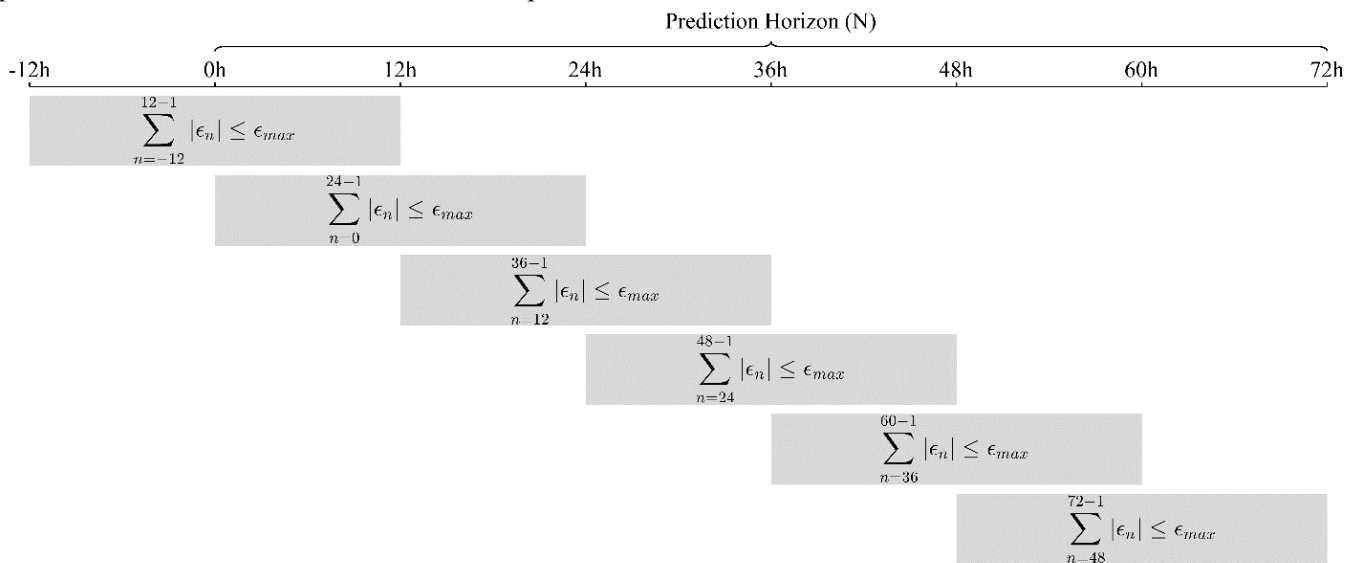


Figure 2. Principle of proposed additional six state constraints

3. Results and discussion

Simulation results obtained using the following four different E-MPC formulations have been evaluated with regard to their ability to reduce deviations from the preferred temperature (see Table 1) and to minimize operational costs:

- Single objective: Minimize temperature deviations from the preferred temperature.
- Single objective: Minimize operational costs.
- Multi objective: Compromise solution (see Figure 1) between temperature deviations and cost.
- Single objective: Minimize operational costs, but with additional state constraints (see Figure 2).

The objectives and constraints imposed in the four different control schemes vary as a result of the different formulations, thus rendering any direct comparison of results unfair from a mathematical point of view. The evaluation is therefore based on quantification of the four problem formulations on the achieved results. Figures 3a-d depict the indoor air temperature for a one week period in apartment 3 using the four E-MPC schemes with the time-varying energy prices c depicted at the bottom of Figure 3. Formulation a) ensured a temperature (solid line) close to the preferred temperature at all times, whereas the three other formulations utilized the thermal comfort band (dashed lines) to minimize operational cost. Formulation b) caused the E-MPC scheme to mainly track the lower and upper comfort bounds in order to exploit price fluctuations by charging and discharging the thermal capacity of the building. Formulation c) tracked the preferred temperature for the majority of the time, allowing deviations in temperature when prices encouraged it. The proposed formulation d) with $\epsilon_{max} = 9^\circ\text{Ch}$ exhibited similar behavior and DR-potential as c).

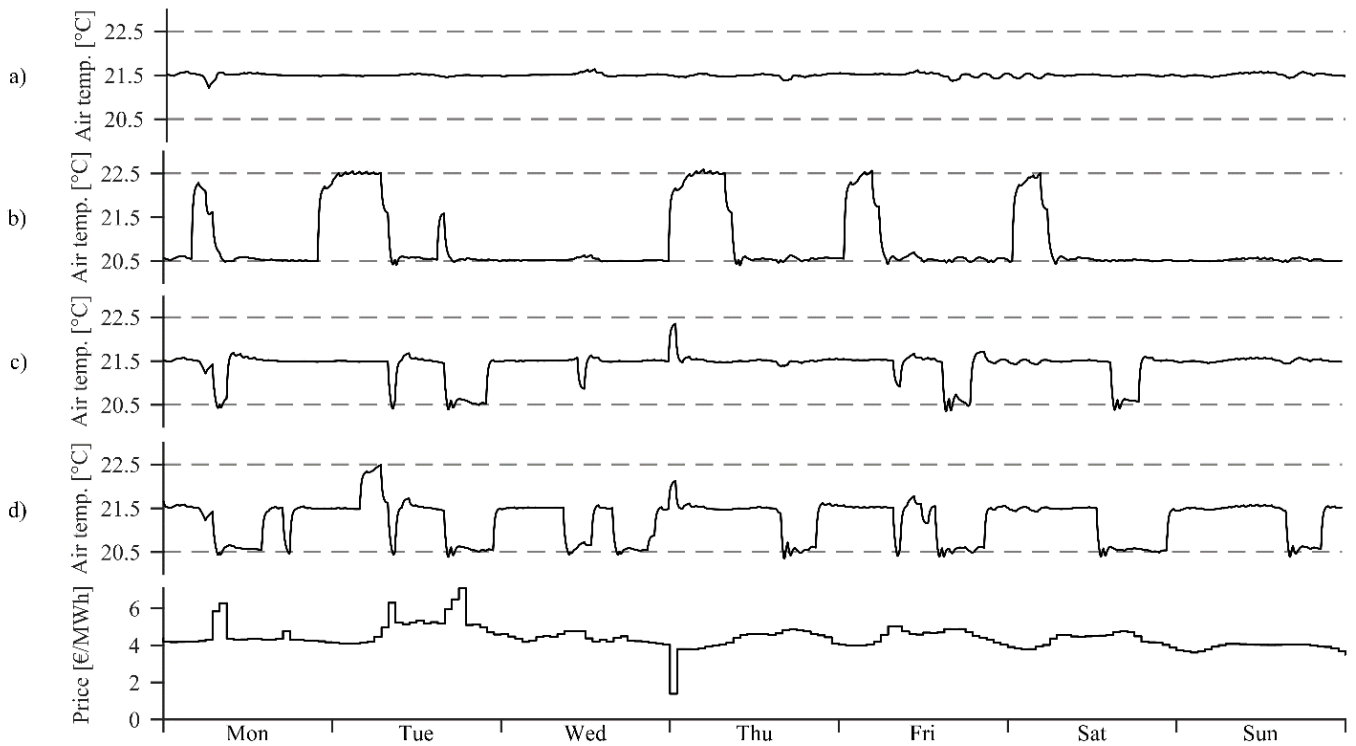


Figure 3. Mechanism of the four E-MPC schemes and the energy price during one week.

The normalized total operational cost during the entire 90-day simulation period as a function of the normalized average root-mean-square-error (RMSE) across the ten apartments is displayed in Figure 4 for the four formulations. The solutions obtained using problem formulations a), b) and c), respectively, are marked with “x” while solutions for formulation d) with different ϵ_{max} values are illustrated with “o” (displayed numbers are ϵ_{max}). Formulation a), which was a traditional set point tracking control problem, resulted in the lowest deviations from the preferred set point temperature but also the highest operational cost. Formulation b) achieved the lowest operational cost but also the highest RMSE. Formulation b) may therefore have overestimated the DR potential since occupants, in reality, may experience uncomfortable thermal conditions when tracking the lower comfort bound for long consecutive periods. Formulation c) demonstrated an acceptable compromise between the two objectives while formulation d) achieved similar performance as formulation c). Figure 4 indicates an almost convex combination of the two solutions a) and b) when choosing different values for ϵ_{max} , which could not be achieved by convex combination of the objectives (e.g. using the weighted sum approach) because of the different ranges of the objectives. Furthermore, formulation c) and d) enable downward flexibility, i.e. it is possible to reduce space heating if this service is sought by the grid.

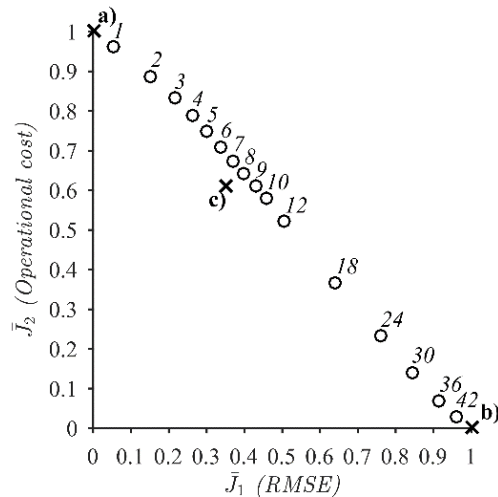


Figure 4. Normalized mean RMSE and total operational cost for all ten apartments.

4. Conclusion

This paper reports on a simulation-based study aimed at quantifying the performance of an E-MPC scheme using four different optimization problem formulations that handle thermal comfort in different ways. It is difficult to conclude which of the four formulations is preferable as it depends on whether – and how much – the occupants are willing to deviate from their preferred indoor air temperature to minimize operational cost through demand responses. However, the parameter ϵ_{\max} in the proposed single-objective problem formulation – a parameter describing the maximum acceptable deviations from the preferred indoor air temperature – could be communicated to occupants as a personal indicator for the acceptable tradeoff between deviations from the preferred temperature and cost savings or, in other words, their ‘DR willingness’.

Acknowledgements

The authors gratefully acknowledge the support of this work from the project “READY.dk” financed by the Danish energy research and development program ForskEl (grant number: 12305) and the project 'Resource Efficient Cities Implementing Advanced Smart City Solutions' (READY) financed by the 7th EU Framework Programme (FP7-Energy project reference: 609127).

References

- [1] E. Vrettos, K. Lai, F. Oldewurtel and G. Andersson. Predictive Control of Buildings for Demand Response with dynamic day-ahead and real-time prices. in Control Conference (ECC) (2013), Zürich.
- [2] M. Avci, M. Erkoç, A. Rahmani and S. Asfour. Model predictive HVAC load control in buildings using real-time electricity pricing. *Energy Build.* 60 (2013) 199-209.
- [3] M. D. Knudsen and S. Petersen. Demand response potential of model predictive control of Space heating based on price and carbon dioxide Intensity signals. *Energy Build.* 125 (2016) 196-204.
- [4] T. H. Pedersen, R. E. Hedegaard and S. Petersen. Space heating demand response potential of retrofitted residential apartment blocks. *Energy Build.* 141 (2017) 158-166.
- [5] R. Halvgaard, N. K. Poulsen, H. Madsen and J. B. Jørgensen. Economic Model predictive Control for Building Climate Control in a Smart Grid. in IEEE PES Innovative Smart Grid Technologies (ISGT). (2012) 1-6, Washington, D.C., United States.
- [6] R. E. Hedegaard, T. H. Pedersen and S. Petersen. Multi-market demand response using economic model predictive control of space heating in residential buildings. *Energy Build.*(2017), *in press*.
- [7] J. Cigler, S. Prívarová, Z. Váňa, E. Žáčková and L. Ferkl. Optimization of Predicted Mean Vost index within Model Predictive Control framework: Computationally tractable solution. *Energy Build.* 52 (2012) 39-49.
- [8] P. Moreles-Valdés, A. Flores-Tlacuahuac and V. M. Zavala. Analyzing the effects of comfort relaxation on energy demand flexibility of buildings: A multiobjective optimization approach. *Energy Build.* 85 (2014) 416-426.
- [9] M. Castilla, J. Álvarez, M. Berenguel, F. Rodríguez, J. Guzmán and M. Pérez. A comparison of thermal comfort predictive control strategies. *Energy Build.* 43 (2011) 2737-2746.
- [10] F. Ascione, N. Bianco, C. De Stasio and G. M. Mauro. Simulation-based model predictive control by the multi-objective optimization of building energy performance and thermal comfort. *Energy Build.* 111 (2016) 131-144.
- [11] T. H. Pedersen, R. E. Hedegaard, M. D. Knudsen and S. Petersen. Comparison of centralized and decentralized model predictive control in a building retrofit scenario. in CISBAT International Conference (2017), Lausanne, Switzerland, *submitted*.
- [12] M. Wetter. Co-simulation of building energy and control systems with the Building Controls Virtual Test Bed. *J. Build. Perform. Simul.* 3 (4) (2010) 1-19.
- [13] I. Das and J. E. Dennis. Normal-boundary intersection: A new method for generating the Pareto surface in nonlinear multicriteria optimization problems, *SIAM J. Optim.* 8 (3) (1998) 631-657.
- [14] A. Gambier. MPC and PID Control Based on Multi-objective Optimization. in American Control Conference (2008), Washington, USA.
- [15] V. M. Zavala. Real-Time Resolution of Conflicting Objectives in Building Energy Management: An Utopia-Tracking Approach. in Fifth National Conference of IBPSA-USA (2012), Madison, Wisconsin.

APPENDIX 7 PAPER: SYSTEM IDENTIFICATION OF THERMAL BUILDING MODELS FOR DEMAND RESPONSE – A PRACTICAL APPROACH (S7)



Available online at www.sciencedirect.com

ScienceDirect

Energy Procedia 122 (2017) 937–942

Energy

Procedia

www.elsevier.com/locate/procedia

CISBAT 2017 International Conference – Future Buildings & Districts – Energy Efficiency from Nano to Urban Scale, CISBAT 2017 6-8 September 2017, Lausanne, Switzerland

Smart Buildings (Predictive & Neuro-Fuzzy Control)

System identification of thermal building models for demand response – A practical approach

Michael D. Knudsen, Rasmus E. Hedegaard, Theis H. Pedersen, Steffen Petersen

Department of Engineering, Aarhus University, Inge Lehmannsgade 10, 8000 Aarhus C, Denmark

Abstract

Model predictive control is a promising control scheme to utilize space heating in buildings for price-based demand response. It is, however, crucial to have an adequate thermal model of the building in order to make this work. It is often very time-consuming to construct these models and common system identification approaches suggest experimental input signals that are difficult to obtain in practice, which often leads to thermal discomfort. This paper proposes an alternative approach where an initial model is identified from historical data and then later re-identified based on control input generated from a model predictive control using the initial model.

© 2017 The Authors. Published by Elsevier Ltd.

Peer-review under responsibility of the scientific committee of the CISBAT 2017 International Conference – Future Buildings & Districts – Energy Efficiency from Nano to Urban Scale

Keywords: Model predictive control; Black box models; System identification; Demand response, Space heating;

1. Introduction

Model predictive control (MPC) is a versatile control scheme applicable in a wide range of fields, which use a plant model to predict and optimize the future behavior of the dynamical system in question. Several studies have suggested that MPC of heating, ventilation and air-conditioning systems in buildings holds significant demand response potentials, see [1-3] to mention a few. A practical challenge when using MPC for building systems control is to

*Corresponding author. *Email address:* mdk@eng.au.dk

1876-6102 © 2017 The Authors. Published by Elsevier Ltd.

Peer-review under responsibility of the scientific committee of the CISBAT 2017 International Conference – Future Buildings & Districts – Energy Efficiency from Nano to Urban Scale

10.1016/j.egypro.2017.07.426

construct an adequate model of the building thermodynamics. Such models can be obtained through system identification techniques using measured data. It is often suggested to generate the training data using intrusive experiments, which aims to excite the dynamics, e.g. a pseudo random binary sequence (PRBS) [5-6]. A PRBS is periodic and deterministic with white noise-like properties [4]. Consequently, models can be fitted well at all frequencies, or a band-limited selection of frequencies, and have a low crest factor and high signal to noise ratio (SNR). However, it is often not possible or desirable in practice to generate a perfect PRBS for a space heating system. Baseboard heaters are often equipped with a thermostat with direct feedback (e.g. a P-regulator) that must be circumvented. This might be done by changing the thermostat setpoint according to the PRBS, but it is difficult to obtain an exact PRBS heat power input using a temperature setpoint without a risk of violating user thermal comfort.

To avoid week-long excitation experiments with high risk of user comfort violations before MPC can be applied, we propose that historical data already logged by the energy management system during standard heating system operation can be used to estimate an initial thermal building model. This initial model is likely to be of relatively poor quality since standard operation often uses a feedback controller (e.g. P-regulator) to ensure that the indoor temperature only have small deviations from the set point and therefore a low SNR. However, this drawback may be more than compensated by the fact that intrusive and costly experimentation can be avoided. The initial model generated from standard operation data can be applied directly in an MPC subjected to time-varying tariffs for a certain training period and then re-identified using the operation data obtained in the training period. This new data set will be more informative than the historical data, and it may result in a just-as-good – or even more suitable – model for MPC as a model based on a PRBS experiments since it have frequency content close to what could be expected when the space heating system is operated to minimize energy cost. This paper reports on a simulation-based study that aims to investigate whether the above-described proposal has the postulated benefits.

2. Method

The case building used in this study was a newly retrofitted two-bedroom apartment (75 m²) equipped with electrical baseboard heaters. The apartment was modelled in EnergyPlus (EP) and the heaters received control signals from MATLAB via the Building Controls Virtual Test Bed (BCVTB) [8] and it was therefore possible to apply MPC controllers (Section 2.2) and online system identification (Section 2.3). For further details regarding the model assumptions, see Pedersen et al [7].

2.1. State-space representation

It was assumed that the thermal dynamics of the EP case building could be approximated with sufficient accuracy by a low-order state-space model:

$$x[k + 1] = \mathbf{A}x[k] + \mathbf{B}u[k] + \mathbf{E}d[k] + w[k] \quad (1a)$$

$$y[k] = \mathbf{C}x[k] + v[k] \quad (1b)$$

The state matrix \mathbf{A} represents the dynamics of the system and describes how the states x evolve from time step k to $k+1$. The input matrix \mathbf{B} and the disturbance matrix \mathbf{E} describes how control inputs and uncontrollable (but measurable) disturbances are channeled to the states, respectively. The output matrix \mathbf{C} describes how the states are channeled to the output y while w and v are process and measurement noise, respectively. In this study, the system was treated as a black box and the states x does therefore not correspond to physical entities. The input u was heating power while the components of the disturbance d were external air temperature and solar irradiation. The time-varying internal heat load from two occupants was included in the EP model, but was assumed unmeasured and unpredictable to add realism to the simulations and was therefore included in the process noise term w . The measured output y was room air temperature and a white noise with standard deviation = 0.067 °C was imposed on the temperature sensor to further increase realism.

2.2. Model predictive control

In each hour, the MPC solved a mathematical program (Eq. 2a-2f) and determined hereby a sequence of electrical heating power actions that minimized the operational costs for a finite prediction horizon of 48 hours (Eq. 2a). The optimal solution had to respect system dynamics (Eq. 2b-c) as well as limitations on maximum radiator power (Eq. 2d) and acceptable room temperatures (Eq. 2e). Only the first control action $u[0]$ was implemented and the program solved the program again in the preceding hour but for a shifted time-horizon (receding horizon). The initial state x_0 was estimated to \hat{x}_{ini} by a Kalman filter incorporating noisy sensor feedback (Eq. 2f). Time-varying tariffs $c[k]$ were taken into account to allow for price-based demand response by shifting consumption from high- to low price periods.

$$\underset{u}{\text{minimize}} \quad J = \sum_{k=0}^{47} c[k] \cdot u[k] \quad (2a)$$

$$\text{subject to} \quad x[k+1] = Ax[k] + Bu[k] + Ed[k] \quad (2b)$$

$$y[k] = Cx[k] \quad (2c)$$

$$0 \leq u[k] \leq 1000 \text{ W} \quad (2d)$$

$$21 \text{ }^\circ\text{C} \leq y[k] \leq 24 \text{ }^\circ\text{C} \quad (2e)$$

$$x[0] = \hat{x}_{ini} \quad (2f)$$

2.3. System identification procedure

The matrices **A**, **B**, **E** and **C** were estimated using the N4SID subspace identification [4]. A number of design choices are available in subspace identification and it is out of the scope to go into any details thereon. The model order (i.e. number of states) was determined based on the logarithm of Hankel singular values [9]. The process does not involve cross validation and the whole dataset was used for training (i.e. no need for validation data). The identification procedure was fully automated and the model could therefore be re-identified continuously (i.e. every month) although this study only re-identifies a model once after 14 days.

The initial model was identified based on EP simulation data from October 1 to December 31, where the apartment was controlled by a P-regulator to track a set point of 21 °C. The initial model was used in the MPC for 14 days from January 1 to 14, generating a new data set used to identify a new model, which were used in the MPC for the remaining heating season of January 14 to April. The simulation results are presented in the following section and compared to results obtained by using the common approach of PRBS.

3. Results and discussion

Figure 1 (top) shows data logged from standard space heating operation with a P-regulator tracking a constant set point of 21 °C in a historic period from oct-jan. Notice that the measured room air temperature has high frequency fluctuations due to the imposed sensor noise. This data set was used to identify an initial state space second order model. This initial model was then used in the MPC for a period of 14 days. The generated heating input from this period and the resulting indoor air temperatures are shown in Figure 2 (top). The indoor air temperatures are within the predefined temperature range (Eq. 2e). This new dataset was used to identify a new second order model, which was used in the MPC for the rest of the heating season (end March). The performance of this approach was compared to a model generated from a PRBS experiment shown in Figure 2 (bottom). The PRBS input led to violations of the predefined temperature range in Eq. 2e.

Besides not violating the temperature range, the MPC-based excitation signal has the benefit of being negatively correlated with the energy tariffs (boosts temperature in low price periods) and as such, it is more cost-effective than the PRBS. In fact, the MPC-based signal reduces costs compared to a normal constant set point tracking P-regulator.

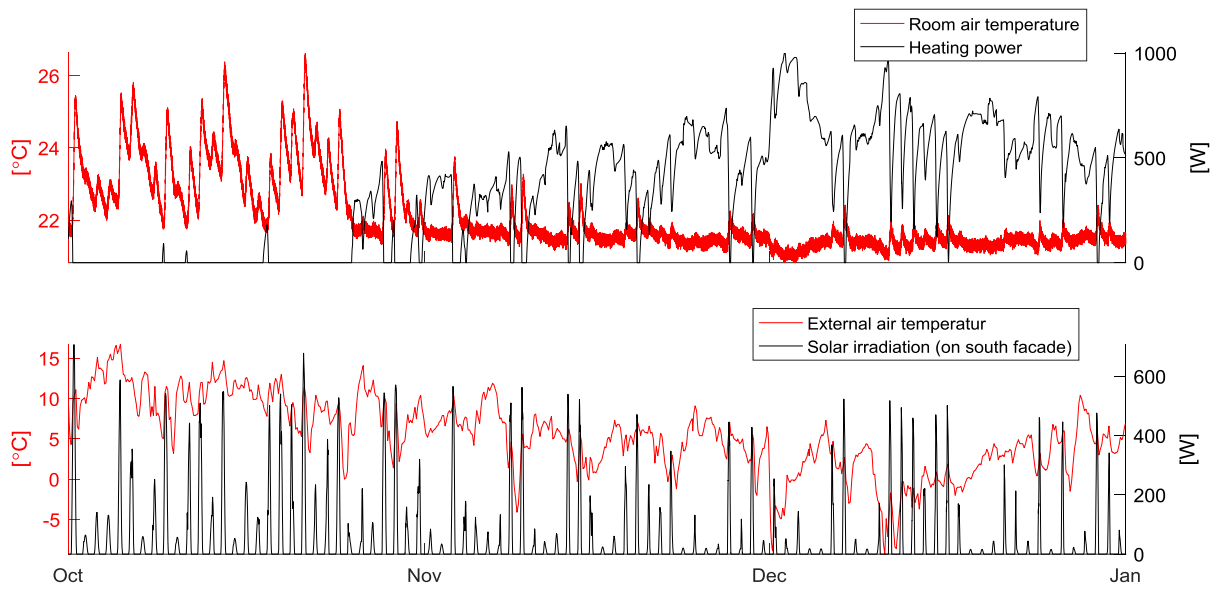


Figure 1. Historical data from normal operation.

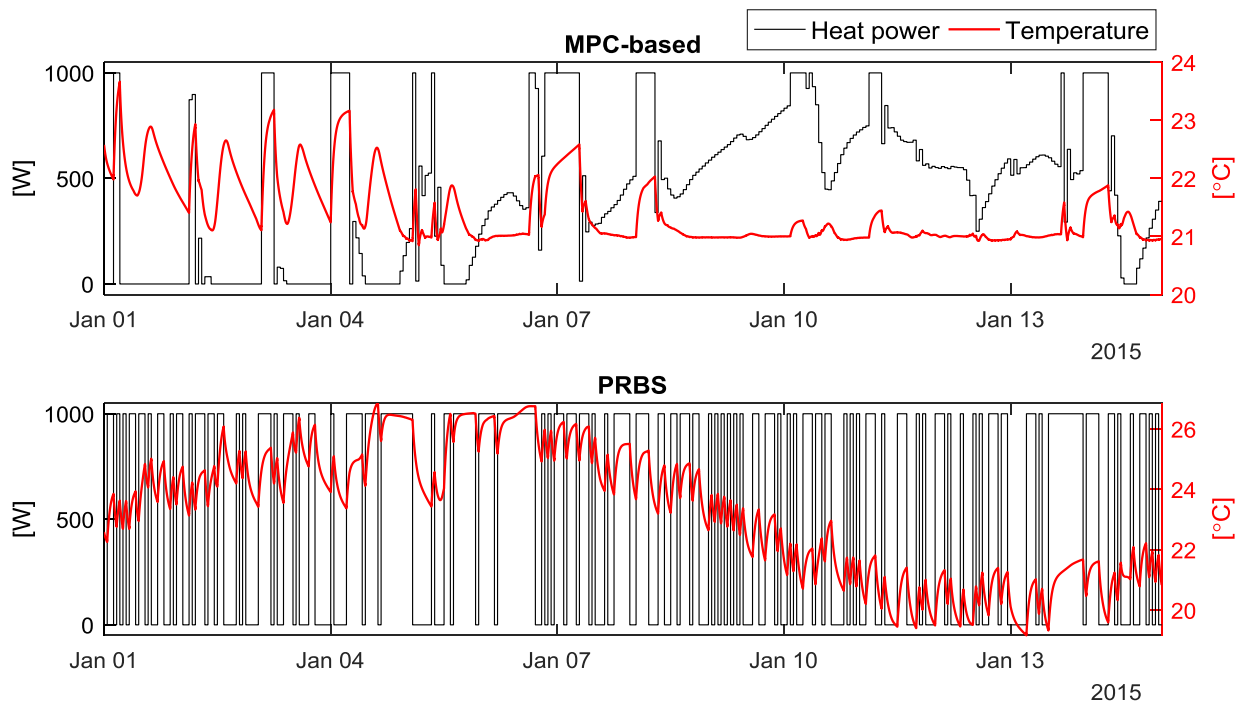


Figure 2. Heating power (black) in the training period when using PRBS and MPC generated heat input, respectively. The red curves show the resulting room temperatures.

Figure 3 depicts the one-step ahead prediction errors for the different models. For the MPC-based model, the errors to the left of the vertical dotted line are the errors for the initial model based on historical data while the errors to the right belong to the re-identified model based on MPC generated input. It clearly shows that the new model contains less prediction errors. For comparison, the bottom plot shows the prediction errors for the model based on PRBS input and they are seen to have errors of the same magnitude.

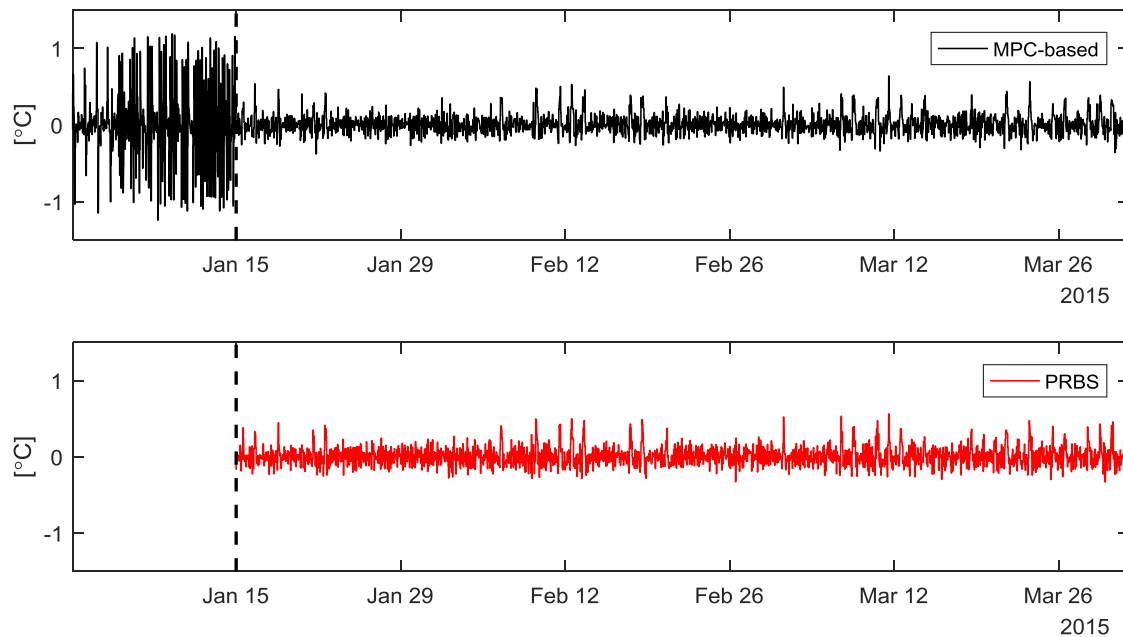


Figure 3. Top plot depicts the one-step ahead prediction errors for the MPC-based model before and after the re-identification (indicated with dotted vertical line). The bottom plot shows the one-step ahead prediction errors for the PRBS based model.

The MPC using a model based on the MPC generated input reduced energy costs by 13.7% compared to the baseline P-controller in the period January 15 to April. For comparison, the MPC using a PRBS based-model reduced costs by 13.5% and thus no significant difference in performance.

Conclusion

This paper proposes a method that avoids the use of dedicated excitation experiments, which often are regarded as mandatory to make sufficiently precise system identification of models for MPC of space heating systems. This paper presents simulation results suggesting that data from standard operation of the heating system can be used to identify an initial model with sufficient quality to be used by an economic MPC for a subsequent training period. Data from this training period can then be used to generate new control input that are informative enough to re-identify a model with qualities comparable to that of a PRBS based model. The benefits of this approach is that it does not require an intrusive experimental period with potential thermal discomfort and excessive energy costs. Furthermore, the perspective of this method is that re-identification of the building model can be done with an appropriate frequency to make it up-to-date with current conditions. Further studies are needed to investigate the benefits of a running re-identification of the model used for MPC of space heating systems.

Acknowledgements

The work presented in this paper was conducted as part of the REVALUE project financed by Innovation Fund Denmark. Furthermore, the authors express gratitude to the participants and the work done in the IEA-EBC Annex 67 on Energy Flexible Buildings. The second and third author gratefully acknowledges the funding from the project READY financed by the seventh EU Framework Program (FP7-Energy project reference: 609127) and the project READY.dk financed by the Danish energy research and development program ForskEl (grant number: 12305), respectively.

References

- [1] M.D. Knudsen and S. Petersen. Demand response potential of model predictive control of Space heating based on price and carbon dioxide Intensity signals. *Energy and Buildings* 125 (2016), pp. 196-204.
- [2] R. Halvgaard, N.K. Poulsen, H. Madsen, J.B. Jørgensen. Economic Model predictive Control for Building Climate Control in a Smart Grid. *Innovative Smart Grid Techn.* (2012), pp. 1-6.
- [3] E. Vrettos, K. Lai, F. Oldewurtel, G. Andersson. Predictive control of buildings for demand response with dynamic day-ahead and real-time prices. *Eur. Control Conf.* (2013), pp. 2527-34.
- [4] L. Ljung. *System Identification – Theory for the User*. 2nd ed. Prentice Hall PTR. 1999.
- [5] P. Bacher, H. Madsen. Identifying suitable models for the heat dynamics of buildings. *Energy and Buildings* 43 (2011), pp. 1511-22.
- [6] I. Hazyuk, C.Ghiaus, D.Penhuet. Optimal temperature control of intermittently heated buildings using Model Predictive Control: Part I – Building modeling. *Building and Environment* 51 (2012), pp. 379-87.
- [7] T.H. Pedersen, R.E. Hedegaard, S. Petersen. Space heating demand response potential of retrofitted residential apartment blocks. *Energy and Buildings* 141 (2017) pp. 158-66.
- [8] M. Wetter. Co-simulation of building energy and control systems with the Building Controls Virtual Test Bed. *Journal of Building Performance Simulation* (2010), pp. 1-19.
- [9] A.K. Tangirala. *Principles of System Identification: Theory and Practice*. CRC Press. 2015.

**APPENDIX 8 PAPER: URBAN-SCALE DYNAMIC BUILDING
ENERGY MODELING AND PREDICTION USING HIERARCHICAL
ARCHETYPES: A CASE STUDY OF TWO DANISH TOWNS (S8)**

Urban-scale dynamic building energy modeling and prediction using hierarchical archetypes: A case study of two Danish towns

Martin Heine Kristensen*, Rasmus Elbæk Hedegaard, Steffen Petersen
 Department of Engineering, Aarhus University, DK-8000 Aarhus, Denmark

* Corresponding author (mhk@eng.au.dk)

Introduction

It remains practically infeasible to gather all the required data inputs for physics-based urban building-by-building energy modelling (Reinhart and Davila, 2016). Simplifications may therefore be necessary, e.g. through archetype segregation of the building stock to reduce the task of data acquisition and calibration of uncertain parameters. The authors of this extended abstract recently proposed a novel hierarchical archetype calibration methodology that allows a robust probabilistic inference of unknown archetype input parameters for unseen buildings belonging to an archetype (Kristensen et al., 2018). The methodology has been proven fast and accurate for urban-scale predictions of aggregated building energy use under uncertainty.

In this contribution we demonstrate how hierarchically calibrated archetype models of Danish detached single-family houses (SFH's) can accurately predict the urban district heating energy use of unseen buildings in two different suburban towns. We end up by discussing the various practical applications of such urban models.

Methods

Data

Three-hourly district heating (DH) energy consumption data for 27,000 SFH's located in the municipality of Aarhus, Denmark, were coupled with six building-specific data fields from the Danish Building and Dwelling Register (BDR): 1) usage type, 2) construction year, 3) footprint, 4) number of floors, 5) basement and 6) attic area utilized for living/heated. The DH time series consisted of combined energy use for space heating and on-site domestic hot water (DHW) preparation.

Archetype segregation

The building stock was partitioned into nine SFH archetypes following the building stock segregation performed Danish Building Research institute as part of the European research project TABULA (Wittchen and Kragh, 2012). Only the construction year was used for segregation. The nine archetype age groups are shown in Table 1.

Building energy modeling

The DH energy use time series of each building was modeled using the hourly dynamic resistance-capacitance model of ISO 13790:2008 that treats each building as a single thermal zone, in combination with a

simple DHW consumption model. The only available and known data inputs were the footprint, number of floors, and the heated basement and attic area (besides basic climate data logged from a nearby weather station). All other inputs necessary to simulate the BEM were unknown at the level of individual buildings. A-priori probability density functions (PDF's) or fixed values were therefore given each uncertain input parameter at the level of archetypes to reflect historical data and educated guesses.

Hierarchical archetype calibration

The archetype calibration methodology proposed by (Kristensen et al., 2018) was applied to infer a-posteriori PDF's for six of the uncertain parameters per archetype: 1) window-floor ratio, 2) U-value of ext. walls/roof, 3) capacity of thermal mass, 4) infiltration airflow@50pa, 5) occupant density, and 6) room heating set point temperature. The methodology applies a Bayesian hierarchical formulation that binds training buildings together around a shared archetype estimate whereby the inference draw strength from all training building datasets simultaneously. The methodology allows training buildings that are very "likely" to dominate the inference of uncertain parameters, while outlying/unlikely buildings are given less weight – a process known as "shrinkage". Each archetype was trained on a sample of 35 randomly selected SFH's from the dataset, each with time series of three-hourly DH energy use of January 2017 (248 data points).

Urban case towns for prediction

Two suburban case towns were selected for validation of the urban-scale predictive capabilities of the archetype framework: 1) "DK-8250 Egå" and 2) "DK-8330 Beder" (Table 1). February 2017 (224 data points) was used for validation.

Table 1

Classification of case town buildings into nine archetypes.

Archetype partitioning	DK-8250 Egå	DK-8330 Beder
Arch. 1 (1851-1930)	105 (4.9%)	56 (8.1%)
Arch. 2 (1931-1950)	37 (1.7%)	43 (6.2%)
Arch. 3 (1951-1960)	74 (3.4%)	12 (1.7%)
Arch. 4 (1961-1972)	1166 (54.2%)	302 (43.8%)
Arch. 5 (1973-1978)	369 (17.1%)	83 (12.0%)
Arch. 6 (1979-1998)	226 (10.5%)	149 (21.6%)
Arch. 7 (1999-2006)	129 (6.0%)	37 (5.4%)
Arch. 8 (2007-2010)	21 (1.0%)	4 (0.6%)
Arch. 9 (2011-2015)	26 (1.2%)	4 (0.6%)
Total, n_b	2153 (100%)	690 (100%)

Results

The measured and simulated DH energy use of the two case towns is shown in Fig. 1 and measures of predictive performance are given in Table 2.

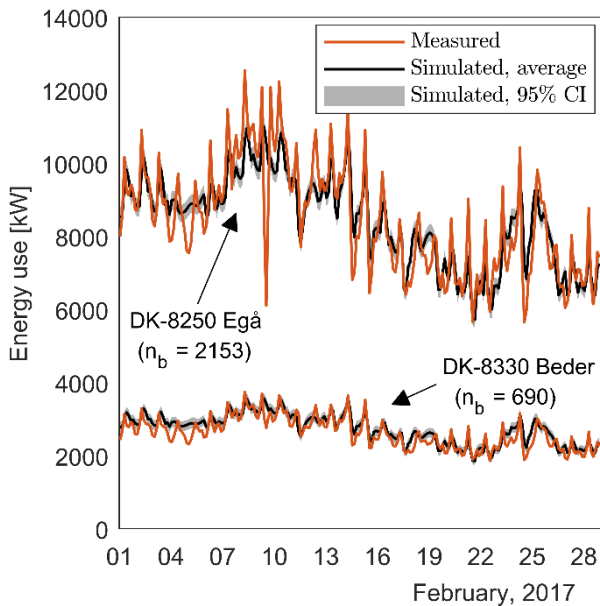


Fig. 1. Measured and simulated aggregated DH energy use (three-hourly) of two suburban towns, respectively. Simulated energy use consist of the 95% central posterior density region derived from aggregating 1000 random simulations from each of the individual building energy models. The average of the 1000 aggregated simulations is highlighted in black.

Table 2

Measures of predictive performance.

Metric	DK-8250 Egå	DK-8330 Beder
NMBE	0.4%	4.2%
MAPE	6.8%	7.2%
CVRMSE	9.0%	8.5%
R ²	74.0%	78.4%

The simulated energy use fit the measured energy use very well. The entire energy consumption of the validation period was predicted within a 4.2% error margin for both towns when measured with the normalized mean bias error (NMBE) metric. The accuracy of which individual data points (three-hourly values) were predicted was measured with the mean absolute percentage error (MAPE) metric to be within 7.2%. The coefficient of variation of the root mean squared error (CVRMSE) and the coefficient of determination (R²) measures the variability of the residuals and thus the explanatory power of the predictions. The two urban models explained approx. 74%-78% (R²-values) of the variability in the measured time series.

Discussion

Urban-scale models of this kind may allow city governments, utility companies, and other energy policy stakeholders that work on the urban scale of neighborhoods, cities, or even entire building stocks, to plan and predict

the effect of various energy efficiency measures and production strategies. The application of simple and publicly available building and property information as the only need-to-have input data about the buildings to be predicted (besides measured energy use datasets from a subsample of buildings for the initial archetype calibration) provides a flexible platform that can easily be expanded or further developed. Because the model structure is based on thermodynamic principles, it may also have use in investigating urban-scale effects on e.g. peak loads and overall energy use due to various interventions in the building stock, e.g. retrofitting, city densification or expansion, and building technologies for facilitating demand response programs.

The application of archetypes to represent the building stock is obviously a crude simplification of its true diversity. However, applying a probabilistic representation and calibration of the uncertain archetype parameters on the level of individual buildings through a hierarchical structure like in this study preserves much of the natural heterogeneity that defines the variability within archetypes. This preservation of heterogeneity is crucial for accurate predictions of new and unseen buildings from the archetypes.

The hierarchical archetype framework proves capable of predicting the aggregated energy use of buildings in larger urban areas with high accuracy as demonstrated for two suburban towns in this study. Although the framework remains to be implemented for other buildings than detached single-family dwellings in order to fully represent a true urban area with many different building types, we do not believe this to pose any difficulties for the framework. The temporal resolution of the predictions is in no way limited to three-hourly data points, but solely defined by the underlying physical model structure and quality of calibration data. Urban models of increasing temporal resolution will therefore be possible in the near future as the distribution of smart energy meters proceed to penetrate the market.

Acknowledgements

The authors would like to thank the district heating company in Aarhus, AffaldVarme Aarhus, for supplying the case data that serves to demonstrate the application of the proposed calibration framework. The work was funded by the 7th EU Framework Programme (FP7-Energy project “READY”, project reference: 609127).

References

- Kristensen, M. H., Hedegaard, R. E., and Petersen, S. (2018). Hierarchical calibration of archetypes for urban building energy modeling. *Energy and Buildings [In Press, Available online]*.
- Reinhart, C. F. and Davila, C. C. (2016). Urban building energy modeling – A review of a nascent field. *Building and Environment* 97, 196–202.
- Wittchen, K. B. and Kragh, J. (2012). SBi 2012:01 Danish building typologies – Participation in the TABULA project. Technical report, Danish Building Research Institute, Aalborg University.